5th INTERNATIONAL CONFERENCE

MNF 2016

Micro and Nano Flows

BOOK OF ABSTRACTS

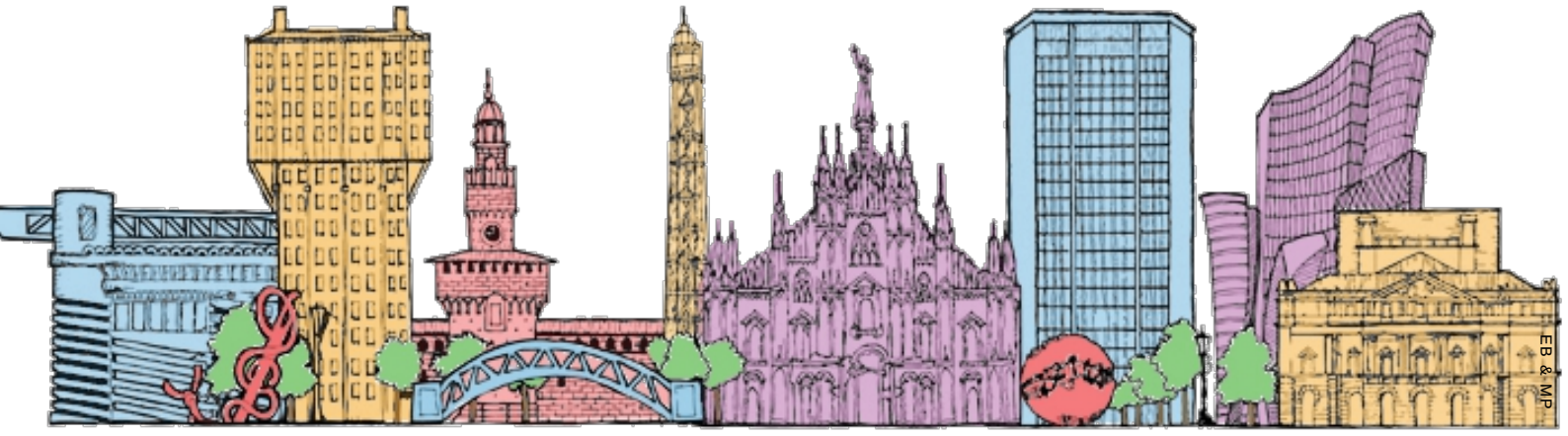

11-14 September 2016, Milan, Italy

POLITECNICO MILANO 1863

Brunel University London

www.mnf2016.com

ORGANIZATION

Conference Committee

Chair	**T.G. Karayiannis** *Brunel University London, UK*
	J. Brandner *Karlsruhe Inst. of Technology, Germany*
	S. Garimella *Georgia Institute of Technology, USA*
	D. Papageorgiou *Imperial College, UK*
	A. Redaelli *Politecnico di Milano, Italy*
	Y. Takata *Kyushu University, Japan*
	J. Xu *North China Electric Power University, China*
Scientific Secretary	**C.S. König** *Brunel University London, UK*

Local Organizing Committee

Chair:	**F. Inzoli** *Politecnico di Milano, Italy*
	G. Dubini *Politecnico di Milano, Italy*
	R. Mereu *Politecnico di Milano, Italy*
	R. Osellame *Politecnico di Milano, Italy*
	G. Passoni *Politecnico di Milano, Italy*
	A. Redaelli *Politecnico di Milano, Italy*
Scientific Secretary	**E. Bianchi** *Politecnico di Milano, Italy*
	M. Piergiovanni *Politecnico di Milano, Italy*

Under the patronage of

Gold Sponsors

ANSYS®

COMSOL

Silver Sponsors

nanoscribe

DANTEC DYNAMICS

Springer

FLUIGENT
MICROFLUIDICS MADE EASY™

Under the patronage of:

POLITECNICO
MILANO 1863

Brunel University London

European Society of Biomechanics

UIT
Unione Italiana Termofluidodinamica

heat transfer society

energy institute

Process Intensification Network

HEXAG
HEAT EXCHANGER ACTION GROUP

LCN
LONDON CENTRE FOR NANOTECHNOLOGY

Institution of MECHANICAL ENGINEERS

The International NanoScience Community
www.nanopaprika.eu
"Spicy world of NanoScience"

VENUE

Politecnico di Milano

The conference will be held in the ***Politecnico di Milano***, Italy, which is one of the world's leading universities for science and engineering. The conference will take place in the university's central campus, the Milano Città Studi, which is located close to the heart of Milan. Milan is renowned to be a city of culture, design and fashion and is home to numerous museums and galleries and the famous opera house, La Scala.

Building number 3:

- Keynote lectures are held in ***De Donato room***
- Sponsor booths and coffee breaks are located in the courtyard

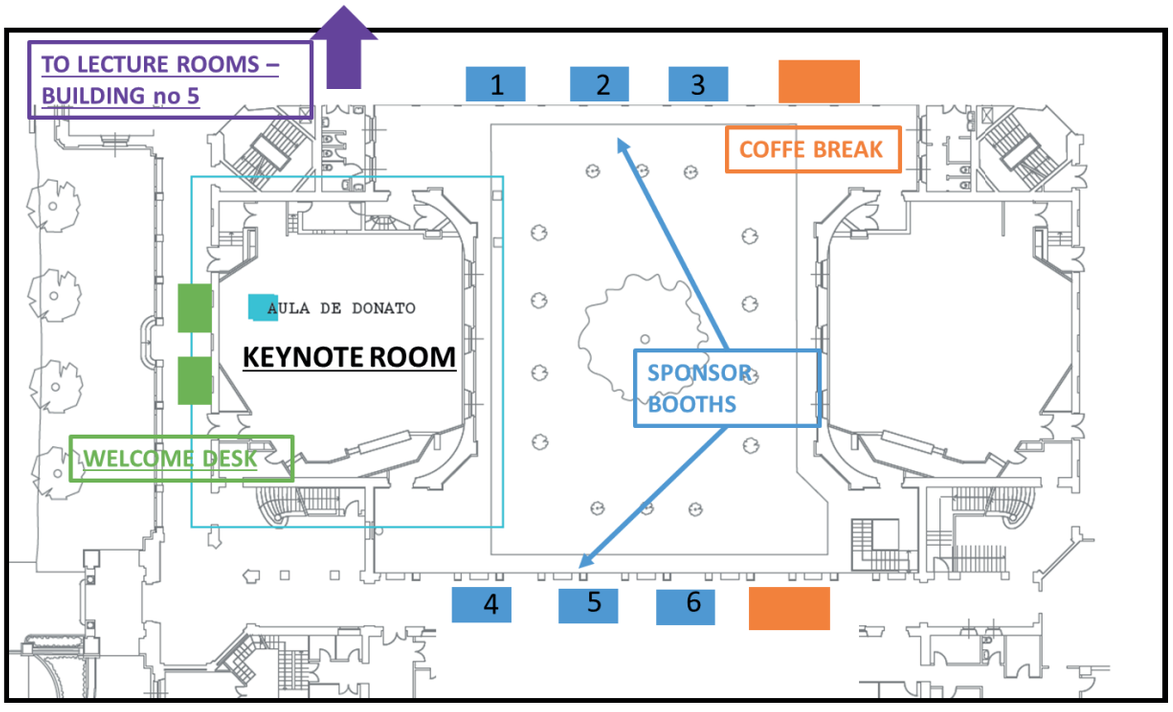

Building number 5:

- Scientific sessions are held in ***Castigliano, Beltrami and C.0.1 rooms*** (ground floor)
- Lunch will be served outside, in the gazebo area

VENUE

Castello Sforzesco

Sforza Castle (Italian: ***Castello Sforzesco***) is a castle in Milan, built in the 15th century by Francesco Sforza, Duke of Milan, on the remains of a 14th-century fortification. Later renovated and enlarged, in the 16th and 17th centuries it was one of the largest citadels in Europe. Extensively rebuilt by Luca Beltrami in 1891–1905, it now houses several of the city's museums and art collections.

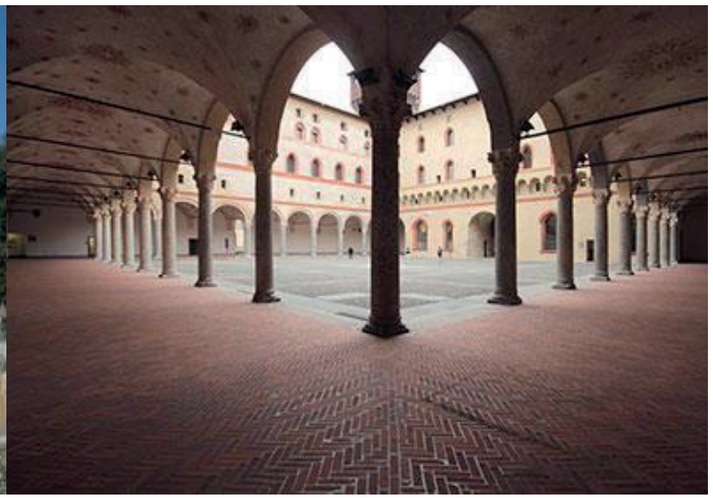

The gala dinner will take place in the wonderful ***Courtyard of Arms.***
On the side facing the Carmine gate, stand the remnants of a by-gone age: stone sarcophagi from the late Roman period (3rd - 4th century AD), fragments of statues and archaeological artefacts. On the opposite side of the courtyard is the Spanish hospital, while, moving towards the Ducal courtyard one comes upon the moat surrounding the medieval walls, known as the dead moat.

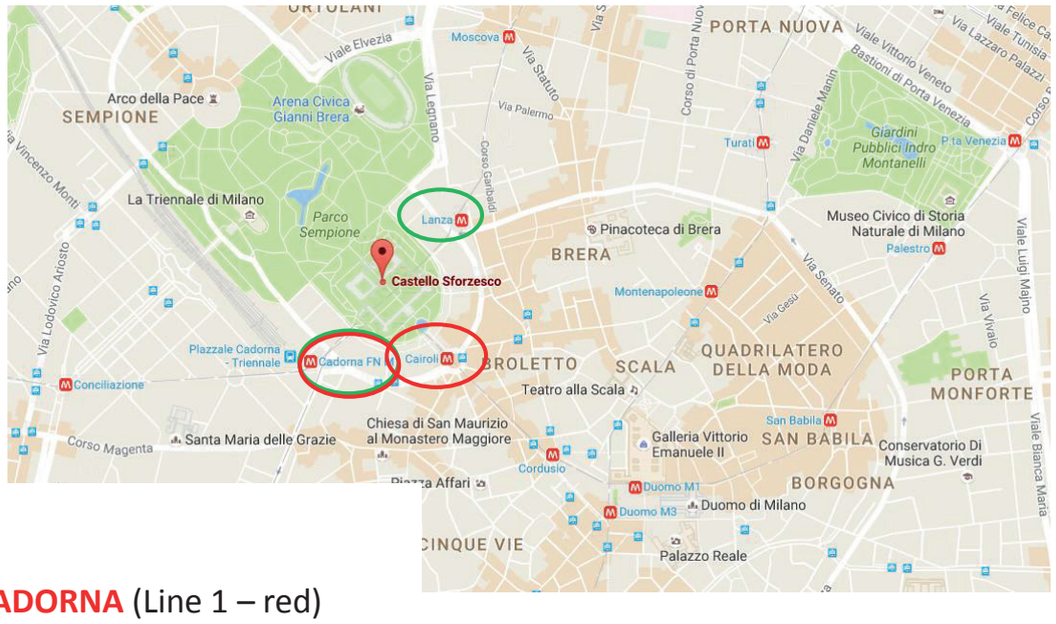

How to reach:
Metro Station:
CAIROLI and CADORNA (Line 1 – red)
LANZA and CADORNA (Line 2 – green)

GENERAL INFO

Arriving at PoliMi

Metro Station: **PIOLA**
(Line 2 - green)

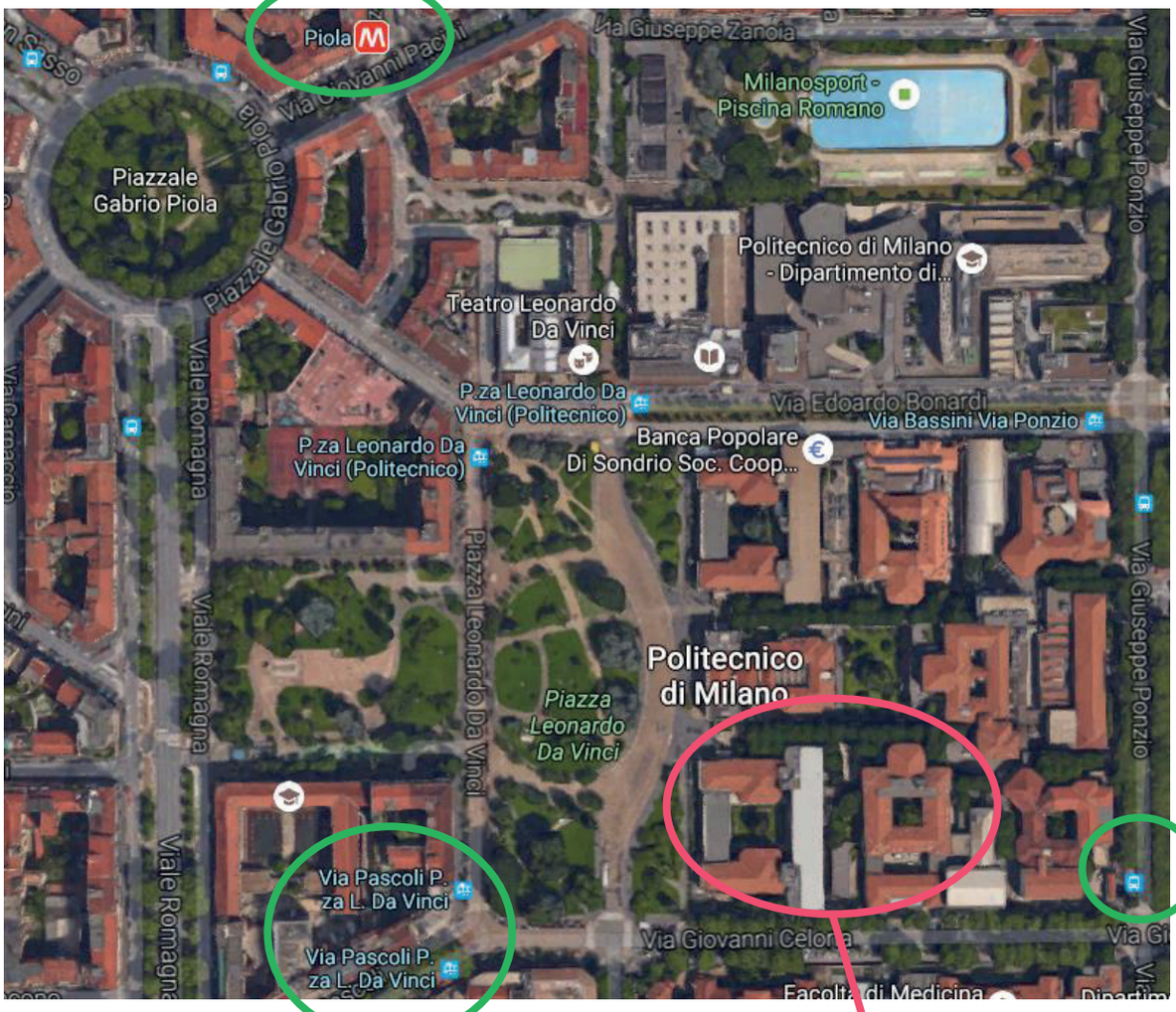

Tram number **23** and **33**

Trolley bus number **93**

MNF2016: Buildings number 3 & 5

Enter the gate (right side) and the Welcome Desk will be on your right, under the portico

Session Overview

	Day 0 - 11 Sept. 2016		
18:00 - 21:00	***Welcome reception***		

	Day 1 - 12 Sept. 2016		
7:45 - 9:00	***Users Registrations***		
			ROOM De Donato
9:15 - 9:50	***Welcome addresses***	- Rector of Politecnico - Deputy VC (Research), Brunel - Chair	Professor Giovanni Azzone Professor Goeff Rodgers Professor Tassos Karayiannis
9:50 - 10:20	***Keynote lecture***	Professor Srinivas Garimella	
10:20 - 10:50	***Coffee break***		
	ROOM S.0.2	***ROOM S.0.3***	***ROOM S.0.4***
10:50 - 12:50	***BIO1*** - *Lab-on a-chip 1*	***MP1*** - *Liquid-liquid, droplets*	***SP1*** - *experimental*
12:50 - 13:35	***Lunch break***		
			ROOM De Donato
13:35 - 14:05	***Keynote lecture***	Dr. Pietro Asinari	
14:05 - 14:25	***Sponsor Presentation 1***	Andrea Arensi, M.Eng. - ANSYS	
14:30 - 16:10	***BIO2*** - *Lab-on-a-chip 2*	***MP2*** - *Bubbles, droplet & solids 1*	***SP2*** - *Modelling 1*
16:10 - 16:30	***Coffee break***		
16:30 - 18:10	***BIO3*** - *Lab-on-a-chip 3*	***MP3*** *Bubbles, droplet & solids 2*	***SP3*** - *Applications*

	Day 2 - 13 Sept. 2016		
08:00 - 09:00	***Users Registrations***		
09:00 - 09:30	***Keynote lecture*** Prof Gian Luca Morini		***ROOM De Donato***
	ROOM S.0.2	***ROOM S.0.3***	***ROOM S.0.4***
09:35 - 10:55	***BIO4*** *- Lab-on-a-chip 4*	***MP4*** *- Heat transfer*	***SP4*** *- Modelling 2*
10:55 - 11:15	***Coffee break***		
11:15 - 12:55	***BIO5*** *- Lab-on-a-chip 5*	***MP5*** *- Condensation 1*	***SP5*** *- Modelling 3 & Heat Transfer 1*
12:55 - 13:40	***Lunch break***		
13:40 - 14:10	***Keynote lecture*** Professor Roger D. Kamm		***ROOM De Donato***
14:10 - 14:30	***Sponsor Presentation 2*** Beatrice Carasi, M.Eng - COMSOL		
14:35 - 16:15	***BIO6*** *– Lab-on-a-chip 6 & Biomedical 1*	***MP7*** *- Boiling 1*	***MP6*** *- Modelling 1 & Condensation 2*
16:15 - 16:35	***Coffee break***		
16:35 - 17:55	***BIO7*** *- Biomedical 2*	***MP8*** *- Boiling 2*	***SP6*** *- Heat transfer 2*
19:45	***Conference dinner - Castello Sforzesco***		

	Day 3 - 14 Sept. 2016		
08:30 - 09:00	***Users Registrations***		
09:00 - 09:30	***Keynote lecture*** Professor Carlotta Guiducci		***ROOM De Donato***
	ROOM S.0.2	***ROOM S.0.3***	***ROOM S.0.4***
09:35 - 11:15	***BIO8*** *-Complex flows & suspensions in microsystems (Special Session)*	***MP9*** *– Modelling 2*	***NNF1*** *- Nanofluids 1*
11:15 - 11:35	***Coffee break***		
11:35 - 12:55	***BIO9*** *- Lab-on-a-chip 7*	***MP10*** *- Visualisation/experimental*	***NNF2*** *- Nanofluids 2*
12:55 - 13:40	***Lunch break***		
13:40 - 14:10	***Keynote lecture*** Professor Vladimir V. Kuznetsov		***ROOM De Donato***
14:15 - 15:55	***BIO10*** *- Applications*	***MF11*** *- Boiling 3*	***SP7*** *- Heat transfer 3*
16:00 - 16:10	Conference closure & farewell		
16:10	***Farewell Coffee break***		

Scientific Programme

SCAN THE QR CODE TO DOWNLOAD THE PROGRAMME OF THE CONFERENCE AND THE PROCEEDINGS

Day 0 – Sunday 11 Sept. 2016

18:00 – 21:00 Welcome reception and registration – (Room: Aula Magna)

Day 1 – Monday 12 Sept. 2016

7:45 – 9:00 Registration

9: 15 Welcome addresses (Room De Donato)

Professor Marco Ricotti (Rector's delegate for Research of Politecnico di Milano),

Professor Goeff Rodgers (Deputy Vice-Chancellor-Research-, Brunel University)

Professor Tassos Karayiannis (Chair)

9:50 Keynote lecture (Room De Donato): **Professor Srinivas Garimella "Convective condensation at small scales: Experimental and analytical advances"**
Session Chair: Prof. F. Inzoli

10:20 Coffee break

10:50 – 12:30	**BIO1 - Lab-on a-chip 1 - Session Chair: Prof. S. Balabani**	**Room S.0.2**
MICROFLUIDIC-ENABLED SCREENING OF KIDNEY ORGANOGENESIS Mr. Nick Glass, Dr. Minoru Takasato, Ms. Pei Xuan Er, Prof. Melissa Little, Prof. Ernst Wolvetang, **Prof. Justin Cooper-White**		ID. 172
MICRO-SCALE ENGINEERED SCAR-LIKE TISSUES AS IN VITRO MODEL TO INVESTIGATE FIBROBLAST PROLIFERATION AND PHENOTYPE SWITCH TYPICAL OF A WOUND HEALING PROCESS Ms. Chiara Conficconi, Ms. Marta Lemme, Dr. Paola Occhetta, **Dr. Giulia Cerino**, Ms. Roberta Visone, Mr. Emanuele Gaudiello, Dr. Marija Plodinec, Prof. Alberto Redaelli, Dr. Marco Rasponi, Dr. Anna Marsano		ID. 126
HIGH-THROUGHPUT PRE-CONCENTRATION FOR BACTERIA USING ACOUSTOFLUIDIC CHIP **Dr. Yan-yu Chen**, Dr. Sha Xiong, Prof. Ai-Qun Liu		ID. 232
A MICROSCALE BIOMIMETRIC PLATFORM FOR GENERATION AND ELECTRO-MECHANICAL STIMULATION OF 3D CARDIAC CONSTRUCTS **Ms. Roberta Visone**, Dr. Paola Occhetta, Mr. Giuseppe Talo', Dr. Matteo Moretti, Dr. Marco Rasponi		ID. 73

LAB-ON-A-CHIP MICROFLUIDIC PLATFORMS TO MONITOR THE SHEAR-INDUCED THROMBOTIC RISK IN BLOOD CONTACTING DEVICES — ID. 64
Ms. Annalisa Dimasi, Dr. Filippo Consolo, Dr. Marco Rasponi, Prof. Gianfranco B Fiore, Dr. Lorenzo Valerio, Dr. Federico Pappalardo, Prof. Danny Bluestein, Dr. Marvin J Slepian, **Prof. Alberto Redaelli**

10:50 – 12:50	**MP1 - Liquid-liquid, droplets - Session Chair: Prof. R. Osellame**	**Room S.0.3**

SCALE-OUT OF LIQUID-LIQUID FLOWS IN SMALL CHANNELS — ID. 167
Mr. Eduardo Garciadiego Ortega, Dr. Dimitrios Tsaoulidis, Prof. Panagiota Angeli

VISCOSITY INFLUENCE ON FLOW PATTERN MAP OF IMMISCIBLE LIQUID-LIQUID FLOW IN A T-SHAPED MICROCHANNEL — ID. 43
Ms. Anna Yagodnitsyna, Mr. Alexander Kovalev, Dr. Artur Bilsky

MEASUREMENTS OF MICRO-MUSHROOM PATTERNS IN A MAGNETIC MICROMIXER — ID. 196
Dr. Gökhan Ergin

ASPHALTENE AGGREGATION AND DEPOSITION IN TRANSPARENT T-SHAPED MICRO-CHANNEL — ID. 206
Dr. Afshin Goharzadeh, Mr. Yougong Zhuang, Dr. Yit Fatt Yap

PLUG FORMATION IN A MICROCHANNEL IN TWO-PHASE FLOWS WITH NON-NEWTONIAN LIQUIDS — ID. 98
Ms. Evangelia Roumpea, Dr. Maxime Chinaud, Prof. Panagiota Angeli

DYNAMIC MOTION OF DROPLETS ON SLIPPERY LUBRICANT-IMPREGNATED SURFACES WITH MICRO TEXTURES — ID. 69
Ms. Jingxian Zhang, Dr. Zhaohui Yao, Dr. Pengfei Hao, Dr. Bing Bao

10:50 – 12:30	**SP1 – Experimental - Session Chair: Prof. D. Emerson**	**Room S.0.4**

THE EFFECT OF ASYMMETRY ON MICROMIXING IN CURVILINEAR MICROCHANNELS — ID. 89
Mr. Sarp Akgönül, Ms. Arzu Ozbey, Mr. Mehrdad Karimzadehkhouei, Prof. Ali Kosar

FLOW CONFIGURATIONS IN A Y SPLITTING-JUNCTION MICROCHANNEL — ID. 59
Prof. Giovanni Paolo Romano, Dr. Marco Pecorario,

WALL SHEAR STRESS MEASUREMENT IN MICRO-CHANNEL — ID. 33
Dr. Zhaohui Yao

EXPERIMENTAL INVESTIGATION OF SUPERSONIC TWO-DIMENSIONAL FREE MICROJETS — ID. 195
Dr. Vladimir Aniskin

VELOCITY MEASUREMENTS IN AN OMEGA-MICROMIXER USING STEREO-MICROPIV — ID. 211
Dr. Gökhan Ergin

12:50 Lunch break

13:35 Keynote lecture (Room De Donato): **Prof. Pietro Asinari "Multiscale Simulation of Nanofluids for Solar Thermal Energy"**
Session Chair: Prof. T. Karayiannis

14:05 Sponsor Presentation 1 (Room De Donato): **Andrea Arensi M.Eng. (ANSYS)**
"CAE Simulation Platform for product development"

14:30 – 16:10 BIO2 - Lab-on a-chip 2 - Session Chair: Prof. A. Redaelli — Room S.0.2

CHARACTERISATION OF MICROFLUIDIC SYSTEMS USING OPTICAL METHODS AT DYNAMIC FLOW RATES — ID. 36
Mr Joerg Schroeter , Mr. Lino Del Bianco , Dr. Christian Damiani, Prof. Stephan Klein, Prof. Bodo Nestler

3D FEM DISSIPATION MODEL OF SUSPENDED MICRO CHANNEL RESONATORS — ID. 83
Ms. Annalisa De Pastina, Dr. Andrea Fani, Prof. François Gallaire, Prof. Luis Guillermo Villanueva

HIGH-THROUGHPUT MICROFLUIDIC PLATFORM FOR GUIDING MESENCHYMAL STROMAL CELL PERFUSED MICROMASSES TOWARDS CHONDROGENIC DIFFERENTIATION — ID. 74
Dr. Paola Occhetta, Dr. Andrea Barbero, Dr. Marco Rasponi, Prof. Ivan Martin

ON-CHIP MAGNETIC PLATFORM FOR SINGLE-PARTICLE MANIPULATION WITH INTEGRATED ELECTRICAL FEEDBACK — ID. 128
Mr. Marco Monticelli, **Dr. Daniela Petti**, Dr. Edoardo Albisetti, Prof. Riccardo Bertacco

DYNAMICS OF CELL-FREE LAYER FORMATION AFTER ARTERIOLAR BIFURCATIONS AND ITS PHYSIOLOGICAL EFFECTS — ID. 51
Mr Yan Cheng Ng, Dr Bumseok Namgung, Prof Sangho Kim

14:30 – 16:10 MP2 - Bubbles, droplet & solids 1 - Session Chair: Prof. Y. Yan — Room S.0.3

INVESTIGATION OF ELASTICITY IN MICROMIXING OF LOW VISCOSITY EMULSIONS — ID. 219
Dr. Valentina Preziosi, Dr. Giovanna Tomaiuolo, Prof. Sergio Caserta, Prof. Stefano Guido

MICROFLUIDIC CHARACTERISATION OF ULTRALOW INTERFACIAL TENSION DROPLETS BY THERMAL CAPILLARY WAVE ANALYSIS — ID. 200
Dr. Guido Bolognesi, Mr. Yuki Saito, Dr. Arwen I. I. Tyler, Dr. Andrew D. Ward, Prof. Colin D. Bain, Dr. Oscar Ces

TRAINS OF PARTICLES IN FINITE-REYNOLDS-NUMBER MICRO SQUARE FLOW — ID. 40
Mr. Yanfeng Gao, Mrs. Pascale Magaud, Prof. Lucien Baldas, Mrs. Christine Lafforgue, Mrs. Micheline Abbas, Prof. Stéphane COLIN

A NOVEL CHIP DESIGN WITH SIDE-CHANNEL PRE-ALIGNMENT FOR PARTICLE SORTING — ID. 231
Dr. Sha Xiong, Prof. Ai-Qun Liu, Dr. Yan-yu Chen

EXPERIMENTAL ANALYSIS OF DROPLET FORMATION IN A MICRO CROSS-JUNCTION — ID. 210
Mr. Behnam Rostami, Prof. Beatrice Pulvirenti, Mr. Giacomo Puccetti, Prof. Gian Luca Morini

14:30 – 16:10 SP2 – Modelling 1 - Session Chair: Dr. S. Lorenzani — Room S.0.4

MIXING THROUGH VORTEX SHEDDING IN A MICROFLUIDIC CHANNEL: A NUMERICAL SIMULATION STUDY — ID. 87
Mr. Nitin Mythreya, **Mr. Venkat Subba Rao**, Dr. Aravinda Raghavan, Dr. Meenakshi Viswanathan

PRESSURE DROP ANALYSIS IN A RECTANGULAR MICROCHANNEL WITH STAGGERED ARRANGEMENTS OF CYLINDRICAL MICRO PIN FINS — ID. 143
Mr. Ali Mohammadi, Prof. Ali Kosar

MODELLING ANALYSIS OF MASS TRANSPORT IN POLYMER ELECTROLYTE FUEL CELLS POROUS MEDIA WITH THE AID OF COMPUTATIONAL FLUID DYNAMICS — ID. 65
Dr. Andrea Baricci, Dr. Riccardo Mereu, Mr. Mirko Messaggi, Dr. Matteo Zago, Prof. Fabio Inzoli, Prof. Andrea Casalegno

NUMERICAL AND EXPERIMENTAL INVESTIGATION OF THE LEVITATION AND FLOW CREATED BY ULTRASONIC FIELDS IN NARROW GAPS — ID. 76
Mr Marcus Schmidt, Mr Kai Saalbach, Prof Peter Reinke, Mr Tom Beckmann, Dr Jens Twiefel

ACCELERATING A MULTISCALE FLUIDIC MODEL WITH GAUSSIAN PROCESSES — ID. 183
Dr David Stephenson, Dr James Kermode, Prof Duncan Lockerby

16:10 Coffee break

16:30 – 17:50	**BIO3 - Lab-on a-chip 3 - Session Chair: Prof. C. Koenig**	**Room S.0.2**

FLUID DYNAMIC MODELING OF A SIZE-BASED SORTER LAB-ON-CHIP FOR THE INERTIAL TRAPPING OF CIRCULATING TUMOR CELLS — ID. 155
Ms. Annalisa Volpe, Mr. Antonio Ancona, Prof. Giuseppe Pascazio,

MICRO-CHIP FOR SINGLE CELL ISOLATION WITH LASER-INDUCED FORWARD TRANSFER — ID. 124
Dr. Yu Deng, Prof. Zhongning Guo, Mr. Wensheng Hong, Mr. Wenhao Mai, Mr. Ruilin Zhang

SPACE-TIME CHROMATOGRAPHY OF MESOSCOPIC SUSPENDED OBJECTS IN PERIODICALLY PATTERNED MICROFLUIDIC DEVICES — ID. 118
Prof. Stefano Cerbelli, Prof. Massimiliano Giona

CYCLIC UNIAXIAL STRAIN ON 3D MICROCONSTRUCTS: A NOVEL HEART-ON-A-CHIP PLATFORM FOR THE GENERATION OF FUNCTIONAL CARDIAC MICROTISSUES — ID. 149
Dr. Anna Marsano, Dr. Chiara Conficconi, Ms. Marta Lemme, Dr. Paola Occhetta, Mr. Emanuele Gaudiello, Dr. Emiliano Votta, Dr. Giulia Cerino, Prof. Alberto Redaelli, **Dr. Marco Rasponi**

16:30 – 18:10	**MP3 - Bubbles, droplet & solids 2 - Session Chair: Dr. F.G. Ergin**	**Room S.0.3**

LIGHT ACTUATED MICRO DROPLET EJECTION FOR 3D PRINTING — ID. 27
Prof. Christophe Moser, Mr. Paul Delrot. Dr. Miguel Modesto, Prof. Demetria Psaltis,

ROLE OF VISCOELASTICITY IN DROPLET FORMATION INSIDE A MICROFLUIDIC T-JUNCTION — ID. 100
Mr. Enrico Chiarello, Prof. Giampaolo Mistura, Dr. Matteo Pierno, Prof. Mauro Sbragaglia

DROP MOTION INDUCED BY VERTICAL VIBRATIONS — ID. 49
Mr. Paolo Sartori, Ms. Silvia Varagnolo, Dr. Matteo Pierno, Prof. Giampaolo Mistura, Dr. Francesco Magaletti, Prof. Carlo Massimo Casciola

ACOUSTOTHERMAL HEATING FOR DROPLET MANIPULATION — ID. 57
Mr. Jinsoo Park, Mr. Jin Ho Jung, Mr. Byung Hang Ha, Mr. Ghulam Destgeer, Mr. Husnain Ahmed, Dr. Hyung Jin Sung

TWO-PHASE FLOW IN T – JUNCTION MICROCHANNELS — ID. 119
Dr. Davide Caprini, Dr. Giorgia Sinibaldi, Dr. Mauro Chinappi, Prof. Luca Marino, Prof. Carlo Massimo Casciola,

16:30 – 17:30	**SP3 – Applications - Session Chair: Dr. P. Hao**	**Room S.0.4**

HEAT TRANSFER OPTIMIZATION IN COMPACT AIR HEAT EXCHANGER — ID. 202
Dr Tomasz Muszynski, Dr Slawomir Koziel

FABRICATION OF NANOPOROUS MEMBRANES THROUGH SILICON TEMPLATES : TWO DIFFERENT APPROACHES — ID. 197
Mr Stefano Varricchio, Dr Niccoló Piacentini, Dr Arnaud Bertsch, Prof Philippe Renaud

MAGNETIC NANOFLUIDS HELP IMPROVE THE EFFICIENCY OF SOLAR THERMAL COLLECTOR — ID. 237
Prof Yuying Yan

Day 2 - 13 Sept. 2016

8:00 – 9:00 Registration

9:00 Keynote lecture (Room De Donato): **Prof Gian Luca Morini "The challenge to measure single-phase convective heat transfer coefficients in microchannels"**

Session Chair: Prof. A. Redaelli

9:35 – 10:55	**BIO4 - Lab-on-a-chip 4 - Session Chair: Prof. C. Guiducci**	**Room S.0.2**
FLOW AND MASS TRANSFER OPTIMIZATION IN A BIOTHERAPEUTIC PURIFICATION DEVICE BASED ON NANOFIBRE MATERIAL **Dr. Cesar Augusto Cortes Quiroz**, Dr. Alice R. Mazzer, Dr. Iwan Roberts, Dr. Oliver Hardick, Dr. Daniel Bracewell		ID. 166
A MICROFLUIDIC DEVICE FOR STUDYING DRUG TRANSPORT THROUGH ENDOTHELIAL BLOOD BRAIN BARRIER CELLS MONOLAYERS **Mr. Giovanni Stefano Ugolini**, Dr. Marco Rasponi, Prof. Alberto Redaelli		ID. 55
AN INTEGRATED MICROFLUIDIC DIGITAL PCR SYSTEM FOR ALGINATE DROPLET FORMATION, EFFICIENT DIRECT PCR AMPLIFICATION AND IMAGING **Ms. Lijun Li**, Dr. Linfen Yu, Dr. Tianzhun Wu		ID. 178
DESIGN AND PROCESS OPTIMIZATION IN MICROFLUIDIC DEVICES FOR DNA AMPLIFICATION Mrs. Ioanna Kefala, **Mr. Vasileios Papadopoulos**, Mrs. Georgia Kaprou, Dr. George Kokkoris, Dr. Angeliki Tserepi		ID. 146

09:35 – 10:55	**MP4 – Heat transfer - Session Chair: Dr. T. Muszynski**	**Room S.0.3**
EXPERIMENTAL STUDY OF THE EFFECT OF AN ELECTRICAL FIELD ON A LIQUID VAPOR INTERFACE IN A NARROW CHANNEL **Mr. Baptiste Blaineau**, Dr. Sébastien Dutour, Dr.Thierry Callegari, Dr. Pascal Lavieille, Dr. Marc Miscevic, Dr. Stéphane Blanco, Dr. Yves Bertin		ID 131
SIMULATIONS OF MICROSCALE WATER FLOWS IN A SQUARED LID CAVITY UNDER FREEZING CONDITIONS USING ENERGY **Dr. Toru Yamada**, Dr. Erik Johansson, Prof. Jinliang Yuan, Dr. Shinji Tamano, Prof. Yohei Morinishi, Prof. Bengt Sunden		ID 66
COMPARISON OF WORKING FLUID COMBINATIONS IN A MICROCHANNEL MEMBRANE ABSORBER **Prof. Mercedes de Vega**, Prof. María Venegas, Prof. Néstor García-Hernando		ID 54
IMPROVEMENT OF THERMOSYPHON PERFORMANCE BY WALL WETTABILITY MODIFICATION **Dr. Rafał Andrzejczyk**, Dr. Tomasz Muszynski		ID 204

9:35 – 10:55	**SP4 – Modelling 2 - Session Chair: Prof. G. L. Morini**	**Room S.0.4**
INFLUENCE OF THE BOUNDARY CONDITIONS ON THE DAMPING FORCES EXERTED BY GAS MIXTURES IN HIGH-FREQUENCY MEMS DEVICES **Dr. Silvia Lorenzani**		ID. 58
NON-EQUILIBRIUM EFFECTS ON STEADY FLOW PAST A STATIONARY CIRCULAR MICRO-CYLINDER **Dr. Xiaojun Gu**, Prof. David Emerson		ID. 109
ANALYSIS AND DESIGN OF A NEW MICROPUMP DOABLE WITH A SIMPLE MICRO-FABRICATION PROCESS **Prof. Raffaele Ardito**, Dr. Emanuele Bertarelli, Prof. Alberto Corigliano, Dr. Marco Ferrera		ID. 145

NON-EQUILIBRIUM DYNAMICS OF DENSE GAS UNDER TIGHT CONFINEMENT — ID. 41
Dr Lei Wu

10:55 Coffee break

11:15 – 12:35	**BIO5 - Lab-on-a-chip 5 - Session Chair: Prof. J. Cooper-White**	**Room S.0.2**

MEASUREMENT OF MOLECULAR DIFFUSION IN THE VICINITY OF LIQUID-SOLID INTERFACE BY TOTAL INTERNAL REFLECTION RAMAN IMAGING — ID. 194
Mr. Masaharu Kinoshita, Mr. Tetsuro Tateishi, Dr. Reiko Kuriyama, Prof. Yohei Sato

HYDRODYNAMIC STRUCTURES TO IMPROVE CELL CAPTURING IN MICROCHANNELS — ID. 23
Dr. Elena Bianchi, Ms. Monica Piergiovanni, Mr. Matteo De Gennaro, Dr. Simone Bersini, Ms. Mara Gilardi, Dr. Chiara Arrigoni, Ms. Junko Enomoto, Prof. Junji Fukuda, Dr. Alfonso Gautieri, Dr. Matteo Moretti, Prof. Gabriele Dubini

SIMULATION OF BIO-PARTICLE SEPARATION USING INERTIAL MICROFLUIDICS IN A SPIRAL MICROCHANNEL FOR BIOMEDICAL APPLICATIONS — ID. 209
Mr. Reza Rasooli, Mr. Onur Kaan Karaoğlu, **Dr. Barbaros Cetin**

MAGNETIC ARTIFICIAL CILIA FABRICATED IN AN OUT-OF-CLEANROOM ROLL-PULLING PROCESS GENERATE SIGNIFICANT MICROFLUIDIC PUMPING — ID. 11
Dr. Ye Wang, Dr. Ruth Cardinaels, Prof. Patrick Anderson, **Prof. Jaap den Toonder**

11:15 – 12:55	**MP5 – Condensation 1 - Session Chair: R. Andrzejczyk**	**Room S.0.3**

NANO-PCMS FOR ENHANCED THERMAL ENERGY STORAGE APPLICATIONS — ID 163
Dr. Laura Colla, Dr. Laura Fedele, Dr. Simone Mancin, Dr. Sergio Bobbo, Dr. Michela Arfé, **Dr. Davide Ercole**, Prof. Oronzio Manca

STEADY STATE AND TRANSIENT NUMERICAL SIMULATIONS OF CONDENSATION IN SMALL DIAMETER CHANNELS — ID 140
Mr. Paolo Toninelli, Dr. Stefano Bortolin, Mr. Marco Azzolin, Prof. Davide Del Col

HIGH PRESSURE CONDENSING REFRIGERANT FLOWS THROUGH MICROCHANNELS PART 1: PRESSURE DROP MODELS — ID 213
Dr. Brendon Keinath, **Prof. Srinivas Garimella**

HIGH PRESSURE CONDENSING REFRIGERANT FLOWS THROUGH MICROCHANNELS PART 2: HEAT TRANSFER MODELS — ID 214
Dr. Brendon Keinath, **Prof. Srinivas Garimella**

PERFORMANCE OF SHELL-AND-TUBE CONDENSER WITH MINICHANNELS FOR THE MICRO DOMESTIC ORC — ID 104
Dr. Jan Wajs, **Prof. Dariusz Mikielewicz**, Ms. Blanka Jakubowska

11:15 – 12:55	**SP5 - Modelling 3 & Heat Transfer 1 - Session Chair: Prof. R. Ardito**	**Room S.0.4**

TRANSIENT DYNAMICS OF ELASTIC HELE-SHAW CELL DUE TO EXTERNAL FORCES WITH APPLICATION TO IMPACT MITIGATION — ID. 92
Mr. Arie Tulchinsky, Prof. Amir Gat

NUMERICAL MODELLING OF ELECTRO-OSMOTIC FLOW IN POROUS MICRO-CHANNELS — ID. 39
Ms. Simona Di Fraia, Prof. Nicola Massarotti, Prof. Perumal Nithiarasu

HEAT TRANSFER ENHANCEMENT IN COUNTER-FLOW-HEAT-EXCHANGER FOR USE IN MICROFABRICATED JOULE-THOMSON CRYOCOOLER — ID. 21
Mr. Leonid Fraiman

STRUCTURAL OPTIMIZATION OF MICROJET ARRAY COOLING SYSTEM — ID. 201
Dr. Tomasz Muszynski, Prof. Dariusz Mikielewicz

PARAMETRIZATION STUDY OF THE THERMALLY DRIVEN RAREFIED FLOW BETWEEN SAW-TOOTH LIKE SURFACES — ID. 148
Mr Giorgos Tatsios, Prof Dimitris Valougeorgis, Dr Jie Chen, Prof Lucien Baldas, Prof Stéphane Colin, Prof Stefan Stefanov

12:55 Lunch break

13:40 Keynote lecture (Room De Donato): **Prof Roger D. Kamm "Microfluidic Models of Metastatic Cancer"**

Session Chair: Prof. G. Dubini

14:10 Sponsor presentation 2 (Room De Donato): **Beatrice Carasi (COMSOL) "Modeling Microfluidic Devices in COMSOL Multiphysics"**

14:35 – 16:15	**BIO6 - Lab-on-a-chip 6 & Biomedical 1 - Session Chair: Dr. M. Rasponi**	**Room S.0.2**

DEVELOPMENT OF "EVANESCENT WAVE FOR A CHIP" FOR DISTRIBUTION MEASUREMENTS OF PHYSICAL QUANTITIES IN THE VICINITY OF LIQUID-SOLID INTERFACE — ID. 193
Mr. Atsuhisa Uchigasaki, Ms. Maho Urushidani, Prof. Yohei Sato

ACTIVE MICRO-MIXER FOR BIOMEDICAL APPLICATIONS — ID. 223
Dr. Simone Ferrari, Prof. Gabriele Dubini, **Prof. Luca Cortelezzi**

THE EFFECT OF RBC STIFFNESS ON MICROHEMODYNAMICS — ID. 168
Mr. Andreas Passos, Dr. Stavroula Balabani

CHARACTERISTICS OF RED BLOOD CELL PERFUSION IN MICROFLUIDIC MODELS OF PULMONARY CAPILLARY NETWORKS — ID. 32
Mrs. Hagit Stauber, Dr. Dan Waisman, Prof. Netanel Korin, Prof. Josue Sznitman

LOCAL AGGREGATION CHARACTERISTICS OF MICROSCALE BLOOD FLOWS — ID. 169
Dr. Efstathios Kaliviotis, Dr. Stavroula Balabani, Dr. Joseph Sherwood

14:35 – 16:15	**MP7 – Boiling 1 - Session Chair: Dr. S. Gedupudi**	**Room S.0.3**

DYNAMICS OF DROPLETS EVAPORATING ON STRUCTURED SURFACES — ID 179
Dr. Gail Duursma, **Dr. Coinneach Dover**, Mr. Nathan West, Dr. John Christy, Prof. Khellil Sefiane

TRANSIENT FLOW BOILING LOCAL HEAT TRANSFER IN A MULTI-MICROCHANNEL EVAPORATOR UNDER A HEAT FLUX DISTURBANCE — ID 224
Mr. Houxue Huang, Dr. Nicolas Lamaison, Prof. John Thome

TEM STUDY ON PHASE CHANGE IN A NANO LIQUID CELL — ID 199
Ms. Yoko Tomo, Prof. Koji Takahashi, Dr. Takashi Nishiyama, Mr. Tatsuya Ikuta, Prof. Yasuyuki Takata

EXPERIMENTAL INVESTIGATION OF THERMAL PERFORMANCE OF ALUMINUM-GROOVED MICRO HEAT PIPES — ID 190
Mr. Hossein Alijani, **Dr. Barbaros Cetin**, Prof. Zafer Dursunkaya

GRAPHENE POWDER PROCESSING FOR WATER SOLAR DISTILLATION USING NANOFLUIDS — ID 235
Dr. Nadhira Laidani, Dr. Francesca Marchetti, Dr. Hafeez Ullah, Prof. Marina Scarpa, Dr. Cecilia Maestri, Prof. Said Makhlouf, Dr. Gloria Gottardi, Dr. Ruben Bartali, Dr. Victor Micheli

14:35– 16:15 MP6 - Modelling 1 & Condensation 2 - Session Chair: Prof. D. Del Col	Room S.0.4
MASS TRANSFER CHARACTERIZATION OF CHEMICAL ABSORPTION OF CO2 IN MICROCHANNEL ABSORBERS **Mr. Ziqiang Yang**, Dr. Tariq Saeed Khan, Dr. Mohamed Alshehhi, Dr. Yasser Al Wahedi	ID. 13
NANOSTRUCTURED COATINGS FOR WATER/SURFACE SLIP: A MOLECULAR DYNAMICS APPROACH **DR. SRINIVASA RAMISETTI**, DR. MATTHEW BORG, PROF. DUNCAN LOCKERBY, PROF. JASON REESE	ID. 37
GROWTH AND DEWETTING OF CONDENSATION MICRODROPLETS ON SUPERHYDROPHOBIC SURFACES WITH TWO-TIER ROGHNESS **DR. PENGFEI HAO**	ID. 68
R1234YF CONDENSATION INSIDE A HORIZONTAL 3.4 MM ID MICROFIN TUBE **DR ANDREA DIANI**, PROF. ALBERTO CAVALLINI, PROF. LUISA ROSSETTO	ID. 173
ACCURATE AND INEXPENSIVE THERMAL TIME-OF-FLIGHT SENSOR FOR MEASURING REFRIGERANT FLOW IN MINICHANNELS **MS. ALLISON MAHVI**, MR. BACHIR EL FIL, PROF. SRINIVAS GARIMELLA	ID. 212

16:15 Coffee break

16:35 – 17:55 BIO7 - Biomedical 2 - Session Chair: Dr. E. Kaliviotis	Room S.0.2
IN-VITRO M-PIV IN CONTRACTING LYMPHATIC VESSELS **Dr. Konstantinos Margaris**, Dr. Zhanna Nepiyushchikh, Prof. James Moore, Jr., Dr. Dave Zawiejia, Dr. Richard Black	ID. 72
CFD MODEL OF MOUSE LIVER MICROCIRCULATION BASED ON A 3D RECONSTRUCTION **Ms. Monica Piergiovanni**, Dr. Elena Bianchi, Ms. Lucia Ganzer, Ms. Giada Capitani, Ms. Irene Li Piani, Prof. Matteo Iannacone, Prof. Luca G. Guidotti, Prof. Gabriele Dubini	ID. 137
μ-PARTICLE IMAGE VELOCIMETRY AND COMPUTATIONAL FLUID DYNAMIC STUDY OF CELL SEEDING WITHIN A 3D POROUS SCAFFOLD **Dr. Ana Campos**, Mr. Tommaso Grossi, Dr. Elena Bianchi, Prof. Gabriele Dubini, Prof. Damien Lacroix	ID. 48
FLOW MIXING AND DISPERSION PHENOMENA IN LUNG-INSPIRED MICROFLUIDIC STRUCTURES Dr. Rami Fishler, **Prof. Josue Sznitman**	ID. 31

16:35– 17:55 MP8 – Boiling 2 - Session Chair: Dr.A. MirzaGheitaghy	Room S.0.3
INVESTIGATION ON THE BUBBLE CUSHION DURING CONTACTLESS BOILING IN MICRO-EVAPORATORS **Dr. Cor Rops**, Ms. Joy Huiberts, Mr. Giel Priems, Prof. Cees Geld	ID 77
TRANSITION FROM SUBCOOLED TO SATURATED FLOW BOILING ON THE BASIS OF ENERGY DISSIPATION BALANCE IN MINICHANNELS **Prof. Dariusz Mikielewicz**, Prof. Jaroslaw Mikielewicz	ID 82
POOL BOILING ENHANCEMENT ON NANOSTRUCTURED COPPER OXIDE SURFACES PREPARED BY WET CHEMICAL METHOD WITH VARIOUS HYDROPHILICITY **Mr. Amir MirzaGheytaghi**, Ms. Shahrzad Tabatabaei, Dr. Hamid Saffari	ID 186

1-D MODELLING OF PRESSURE FLUCTUATION AND FLOW REVERSAL DURING FLOW BOILING IN A MICRO-CHANNEL WITH VAPOUR VENTING MEMBRANE — ID 129
Mr. Ahmed Mohiuddin, Dr. Sateesh Gedupudi

16:35 – 17:55	**SP6 - Heat transfer 2 - Session Chair: Prof. D. Emerson**	**Room S.0.4**

EVALUATION OF HEAT LOSSES IN COUNTER FLOW MICRO HEAT EXCHANGERS — ID. 42
Mr. Anatoly Parahovnik, Dr. Nir Tzabar, Prof. Gilad Yossifon

HIGH PERFORMANCE TUBULAR HEAT EXCHANGER WITH MICROJET HEAT TRANSFER ENHANCEMENT — ID. 86
Dr. Jan Wajs, Prof. Dariusz Mikielewicz, **Dr. Elzbieta Fornalik-Wajs**, Mr. Michał Bajor

HEAT TRANSFER ENHANCEMENT IN MICROJET HEAT EXCHANGER — ID. 203
Dr. Tomasz Muszynski, Dr. Rafał Andrzejczyk

ENHANCEMENT OF HEAT TRANSFER CHARACTERISTICS OF MICROCHANNEL HEAT SINK WITH MICRO-RIBS TO INDUCE LONGITUDINAL VORTICES — ID. 30
Prof. Yeong-Ley Tsay, Prof. Jen-chieh Cheng

Starting at 19:45 - Conference dinner (Castello Sforzesco)

Day 3 - 14 Sept. 2016

8:30 – 9:00 Registration

9:00 Keynote lecture (Room De Donato): **Prof. Carlotta Guiducci "Advancements in electrical-based techniques on chip for single-cell level analytics"**

Session Chair: Dr. E. Bianchi

09:35 – 11:15	**BIO8 -Complex flows & suspensions in microsystems (Special Session) - Session Chair: Prof. R. D. Kamm**	**Room S.0.2**

THE ROLE OF VON WILLEBRAND FACTOR AND PLATELET MARGINATION IN THEIR ADHESION — ID. 95
Mr Masoud Hoore, Dr Kathrin Müller, Dr Dmitry Fedosov, Prof Gerhard Gompper

ANALYZING A SINGLE DEFORMABLE CELL IN AN INCLINED CENTRIFUGE MICROSCOPE: A NUMERICAL STUDY — ID. 217
Mr Arash Alizad Banaei, Dr Jean-Christophe Loiseau, Prof Luca Brandt, Dr Suguru Miyauchi, Prof Toshiyuki Hayase

DEFORMABILITY AND SIZE BASED CAPSULE SORTING — ID. 216
Ms Doriane Vesperini, Ms Nadège Munier, Ms Pauline Maire, Dr Anne-virginie Salsac, Dr Anne Le Goff

HIGH-ACCURACY PARTICLE SIZING IN SHEATH LESS MICROFLUIDIC IMPEDANCE CYTOMETRY — ID. 185
Dr Federica Caselli, Prof Paolo Bisegna

STUDY OF THE PHASE SEPARATION EFFECT IN CAPILLARY-SIZE MICRO-CHANNELS — ID. 208
Mr Adlan Merlo, Dr Paul Duru, Dr Sylvie Lorthois

9:35– 11:15	MP9 – Modelling 2 - Session Chair: Prof. P. Asinari	Room S.0.3

CFD SIMULATION OF PRECIPITATION IN SOLVENT-DISPLACEMENT PROCESSES — ID. 61
Mr Matteo Rizzotto, Mr Mattia Sponchini, Prof Davide Moscatelli, Prof Renato Rota, Prof Valentina Busini

DETERMINING TRANSPORT PROPERTIES BY MOLECULAR DYNAMICS — ID. 221
Dr Angelo Damone

PRESSURE DROP MODELLING IN GAS CHANNELS OF POLYMER ELECTROLYTE FUEL CELLS — ID. 56
Dr Zan Wu, Prof Matin Andersson, **Prof Benqt Sunden**

HYBRID NUMERICAL SIMULATIONS OF DIGITAL ROCK FROM PORE SCALE TO DARCY SCALE — ID. 236
Dr Moussa Tembely, Dr. Ali Alsumaiti, Dr Khurshed Rahimov, Dr Mohamed Soufiane Jouini

SIMULATION OF R134A FLOW BOILING IN MICROCHANNELS — ID 233
Dr. Rahim Jafari

9:35 – 11:15	Nanofluids 1 - Session Chair: Dr. R. Mereu	Room S.0.4

DIAMAGNETIC NANOFLUID BEHAVIOUR IN THE STRONG MAGNETIC FIELD — ID. 93
Mrs Aleksandra Roszko, **Dr Elzbieta Fornalik-Wajs**, Prof Sasa Kenjeres

NUMERICAL STUDY OF NATURAL CONVECTION FOR AL2O3 AND CUO NANOFLUIDS INSIDE DIFFERENT ENCLOSURES — ID. 96
Dr Sahar Abbood, Dr Zan Wu, **Prof Bengt Sunden**

DOES PARTICLE SIZE MATTER IN NANOFLUIDS' THERMAL PROPERTIES? — ID. 97
Dr Michael Frank, Prof Dimitris Drikakis

A NOVEL DE-NOISING SCHEME FOR EFFECTIVE EXTRACTION OF ENSEMBLE SOLUTION FROM NANO/MICROFLUID SIMULATIONS — ID. 218
Dr Malgorzata Zimon, Dr Robert Prosser, Prof David Emerson

ATOMICALLY CONTROLLED ELECTROCHEMICAL REACTION FOR COST-EFFECTIVE AND HIGH-THROUGHPUT FABRICATION OF NANOPORES IN 2D MATERIALS — ID. 222
Dr Gianpaolo Turri, Prof Aleksandra Radenovic, **Dr Ke Liu**

11:15 Coffee break

11:35 – 12:55	BIO9 –Lab on a chip 7 - Session Chair: Dr. P. Occhetta	Room S.0.2

MICROFLUIDIC DEVICE FOR HIGH THROUGHPUT SPIM ON CHIP — ID. 60
Dr Petra Paiè, Dr Francesca Bragheri, Prof Andrea Bassi, Dr Roberto Osellame

INTEGRATED TEMPERATURE CONTROL SYSTEM FOR MICROFLUIDIC CULTURE OF NEMATODES — ID. 116
Ms Maria Cristina Letizia, Mr Matteo Cornaglia, Prof Martin Gijs

HIGHLY DEFORMABLE HYDROGEL NANOFILAMENTS IN POISEUILLE FLOW — ID. 35
Ms Sylwia Pawłowska, Dr Filippo Pierini

THREAD-BASED MICROFLUIDICS: SPONTANEOUS CAPILLARY FLOW IN HOMOGENEOUS AND HETEROGENEOUS MICROFIBER BUNDLES — ID. 176
Prof Kenneth Brakke, Mr David Gosselin, Dr Erwin Berthier, **Dr Jean Berthier**

11:35 – 12:55	**MP10 – Visualisation/Experimental - Session Chair: Prof. V. Kuznetsov**	**Room S.0.3**

INFLUENCE OF THE SHAPE OF AN ORIFICE ENTRANCE ON THE FLOW PATTERN AND DROPLET DEFORMATION DURING HIGH-PRESSURE HOMOGENISATION — ID. 102
Ms. Ariane Bisten, Prof Heike P Schuchmann

ENERGETIC EFFICIENCY OF MIXING IN A MICRO-FLUIDIZED BED — ID. 80
Dr Vladimir Zivkovic, Ms Nadia Ridge, Prof Mark Biggs

NANOMANIPULATING AND SENSING SINGLE PARTICLES INTERACTIONS WITH COMBINED ATOMIC FORCE MICROSCOPY OPTICAL TWEEZERS (AFM/OT) — ID. 25
Dr Filippo Pierini, Mr Krzysztof Zembrzycki, Dr Paweł Nakielski, Ms Sylwia Pawłowska, Prof Tomasz Aleksander Kowalewski

GOLD NANOPARTICLE SYNTHESIS IN GAS-LIQUID-LIQUID FLOW IN A MICROCHANNEL — ID. 110
Dr Nikolay Cherkasov, Prof Evgeny Rebrov

11:35 – 12:55	**Nanofluids 2 - Session Chair: Prof. F. Inzoli**	**Room S.0.4**

EFFECT OF INLET TEMPERATURE ON CONVECTIVE HEAT TRANSFER OF GAMMA-AL2O3/WATER NANOFLUID IN MICROTUBE — ID. 90
Mr Mehrdad Karimzadehkhouei, Ms Arzu Ozbey, Mr Sarp Akgönül, **Mr Ali Mohammadi**, Dr Kursat Sendur, Prof M. Pinar Menguc, Prof Ali Kosar

COOLING PROCESS OF NANOFLUID IN A CAVITY SUBMITTED TO NON-ISOTHERMAL HEATING — ID. 181
Dr Ismail Arroub, Prof Ahmed Bahlaoui, Prof Abdelghani Raji, Prof Mohamed Hasnaoui, Prof Mohamed Naïmi

CHARACTERISTICS OF FLUID FLOW AND HEAT TRANSFER OF NANOFLUID FLOW IN MICROCHANNELS WITH MICROMIXERS — ID. 16
Prof Mohammad Hemmat Esfe, Prof Wei-Mon Yan, **Mr Chung-Hao Kao**

NANOFLUID FLOW AND HEAT TRANSFER IN BOUNDARY LAYERS AT SMALL NANOPARTICLE VOLUME FRACTION — ID. 26
Prof Joseph Liu, Mr Mark Fuller, Ms Ling Ka Wu, Mr Alexander Czulak, Mr Alexander G. Kithes, Mr Collin J. Felten

12:55 Lunch break

13:40 Keynote lecture (Room De Donato): **Prof. Vladimir V. Kuznetsov**

"Fundamental Issues Related to Flow Boiling and Two-Phase Flow Patterns in Microchannels - Experimental Challenges and Opportunities"

Session Chair: Dr. R. Mereu

14:15 – 15:35	**BIO10 – Applications - Session Chair: Dr. Y. Deng**	**Room S.0.2**

SPONTANEOUS CAPILLARY FLOW LIMIT IN DIVERGING OPEN U-GROOVES AND SUSPENDED CHANNELS — ID. 175

Dr Jean Berthier, Prof Kenneth Brakke, Mr David Gosselin, Dr Fabrice Navarro, Dr Erwin Berthier

DYNAMIC MODELLING OF MICROFLUIDIC NETWORKS USING WAVE DIGITAL FILTERS — ID. 120
Dr Alberto Bernardini, Dr Elena Bianchi, Ms Monica Piergiovanni, Prof Augusto Sarti, Prof Gabriele Dubini

ELECTROOSMOTIC FLOW THROUGH AN A-HEMOLYSIN NANOPORE — ID. 113
Mrs Emma Letizia Bonome, Dr Fabio Cecconi, **Dr Mauro Chinappi**

INTERACTION EFFECTS OF MICRO/NANOPARTICLES ON TARGETED MAGNETIC-PARTICLE DELIVERY IN A BLOOD MICROVESSEL — ID. 105
Prof Huei Chu Weng, Mr Cheng-hung Cheng

14:15 – 15:55 MP11 – Boiling 3 - Session Chair: Prof. S. Garimella — **Room S.0.3**

1-D MODELLING OF THE INFLUENCE OF NUCLEATION FREQUENCY ON PRESSURE FLUCTUATIONS AND FLOW REVERSAL DURING FLOW BOILING IN RECTANGULAR MICRO-CHANNELS — ID. 139
Mr. Mahesh Kurup, **Dr Sateesh Gedupudi**

EVAPORATION AND BOILING IN NARROW GAP — ID. 125
Prof Mitsushiro Matsumoto, Mr Keita Ogawa, Mr Yuichi Yasumoto

EXPERIMENTAL INVESTIGATION OF FLUID FLOW AND HEAT TRANSFER OF FLOW BOILING IN MINICHANNELS AT HIGH REDUCED PRESSURE — ID. 99
Mr Alexander Belyaev, Prof. Alexey Dedov, Prof Alexander Komov, Prof Alexander Varava

PERFORMANCE OF A MICRO SCALE INTEGRATED THERMAL MANAGEMENT SYSTEM — ID. 12
Dr Mohamed Mahmoud, Prof Tassos Karayiannis

EFFECT OF NANOSTRUCTURE IN MICROPOROUS SURFACES ON POOL BOILING AUGMENTATION — ID. 187
Mr Amir MirzaGheytaghi, Dr Hamid Saffari, Prof Guo Qi Zhang

14:15 – 15:35 SP7 - Heat transfer 3 - Session Chair: Prof. D. Mikielewicz — **Room S.0.4**

MEASUREMENT OF THERMAL TRANSPIRATION FLOW THROUGH A MICROTUBE — ID. 147
Dr Jie Chen, **Dr Marcos Rojas-Cardenas**, Dr Lucien Baldas, Prof Stéphane Colin, Dr Christine Barrot

HEAT TRANSFER INTENSIFICATION IN VERTICAL SHELL -AND COIL HEAT EXCHANGERS; EXERGY AND NTU ANALYSIS — ID. 205
Dr Rafał Andrzejczyk, Dr Tomasz Muszynski

FLUID FLOW AND HEAT TRANSFER OF A NON-NEWTONIAN FLUID IN A MICRO -ANNULUS IN THE PRESENCE OF VISCOUS DISSIPATION — ID. 152
Prof Marco Lorenzini, Prof Irene Dapra, Prof Giambattista Scarpi

ELECTROCHEMICAL MODELLING AND SIMULATION OF LITHIUM-ION BATTERY COOLING — ID. 114
Dr Angelo Greco, Prof Xi Jiang

16:00 Conference closure & farewell (Room De Donato)

16:10 Farewell Coffee break

KEYNOTE SPEAKERS

Prof. Roger D. Kamm

is the Cecil and Ida Green Distinguished Professor of Biological and Mechanical Engineering at MIT and Director of the NSF Science and Technology Center for Emergent Behaviors of Integrated Cellular Systems. A primary objective of Kamm's research group has been the application of fundamental concepts in fluid and solid mechanics to better understand essential biological and physiological phenomena. His lab focuses on the molecular mechanisms of cellular force sensation, and the development of new microfluidic technologies for vascularized engineered tissues and models of metastatic cancer. Kamm is the recipient of numerous awards including the ASME Lissner Award and the Europen Society of Biomechanics Huiskes Medal. He was elected to be a member of the Institute of Medicine in 2010.

Prof. Pietro Asinari

received his B.S. and M.S. (summa cum laude) in Mechanical Engineering in 2001 and his Ph.D. in Energetics in 2005 from Politecnico di Torino. In 2005, he won the ENI Award. He is the Director of the Multi-Scale Modeling Laboratory - SMaLL - (www.polito.it/small) and Associate Professor of Applied Physics. He is member of the operational management board of the European Materials Modelling Council - EMMC - (http://emmc.info) and operational team manager of the working group on discrete modelling of materials. He is member of the International Scientific Committee of the International Conference for Mesoscopic Methods in Engineering and Science (ICMMES) and member of the Editorial Board of the international journal Computation. He is the Principal Investigator of many projects on materials modeling (including THERMALSKIN and NANOBRIDGE). Since 2002, he has (co-) authored over 70 publications (54 peer-reviewed articles, 34 as senior author) about multi-scale modelling in nanotechnology and biotechnology.

KEYNOTE SPEAKERS

Prof. Jürgen J. Brandner

read Chemistry at the University of Heidelberg and Electrical Engineering at the University of Karlsruhe. In 2003 he obtained his Doctorate in Mechanical Engineering at the University of Karlsruhe, followed by his Habilitation in Process Engineering at the Technical University of Dresden in 2008. He is a scientist at the Karlsruhe Institute of Technology (KIT) since 1996 and is currently head of the Process Technology Department (PTE) of the Institute for Micro Process Engineering (IMVT). In 2009 the Technical University of Dresden bestowed him the Linde Award for the Best Habilitation Thesis. In both, 2014 and 2015 he was awarded the “NEULAND” Innovation Award by KIT. Jürgen’s research interest include miniaturization and process intensification, fluid flow at micro scale including heat and mass transfer, improvement of heat transfer, phase transition processes, integrated sensors and actuators, in-situ measurement methods, process development and transfer into application

Prof. Vladimir V. Kuznetsov

is the Head of the Department of Thermophysics of Multiphase Systems at the Kutateladze Institute of Thermophysics of Siberian Branch of Russian Academy of Sciences, Russia since 2002. He is Professor of the Faculty of Physics of Novosibirsk State University since 1995. His work focuses on fundamental studies of thermal and fluid transport phenomena with phase change at microscales and nanoscales, gas-liquid flow and flow boiling heat transfer in micro/minichannels, explosive evaporation in microsystems, nanofluid flow in porous media, catalytic reactions in microscale. It covers the development of microcooling systems, compact evaporators and condensers, microreactors for hydrogen production. Prof. Kuznetsov received his Ph.D. in 1978 and the degree of Doctor of Science in 1995 at Kutateladze Institute of Thermophysics, Russia. He is the author of about 260 journal and conference publications and of two books related to modelling of microflow with phase change. He is a member of National Committee for Heat and Mass Transfer of the Russian Academy of Sciences and the editorial board for Journal of Engineering Thermophysics.

KEYNOTE SPEAKERS

Prof. Carlotta Guiducci

joined EPFL in 2009 as an assistant professor with the Institute of Bioengineering and the Institute of Electrical Engineering, holding the swissUp foundation Chair. She received her Ph.D. degree in Electrical Engineering from University of Bologna. She was a visiting scientist at Minatech, Grenoble (France) and ParisTech (ESPCI). She is the recipient of the Intel Early Career Faculty Award for her contribution in the field of label-free biosensors and 3D integration of biochips.

Her work on integrated microsystems for bioanalytics and an interview on the role of Semiconductors in personalized medicine have been featured in “IET Electronics Letters” in 2012. In 2013, she has been invited by Nature Methods to comment on the novel pH-based electronic solutions for quantitative PCR

Prof. Gian Luca Morini

is Full Professor of Applied Thermal Engineering at the Alma Mater Studiorum Università di Bologna since 2002, where he directs the Applied Thermal Engineering & Microfluidics Laboratory of the Department of Industrial Engineering of the University of Bologna. He received his Ph.D. in Nuclear Engineering at University of Bologna, Italy in 1995 and he is currently member of the Board of Professors of the Ph. D. School in Mechanical Engineering of the same University. His main research interests lie in microscale heat transfer, forced convection, energy efficient buildings and renewable energy sources. He is author of 150 technical papers in the areas of heat transfer, micro heat exchangers, heating and cooling systems. He is member of many international scientific organizations like UIT (Italian Union of Thermal Fluid-dynamics), the EUROTHERM Committee, the Scientific Committee of the Société Hydrotechnique de France (SHF), the Scientific Council of International Center of Heat and Mass Transfer (ICHMT) and the Assembly of the World Conference (AWC) on Experimental Heat Transfer, Fluid Mechanics, and Thermodynamics. He has been Guest Editor for a series of Special issues on Microfluidics appeared in the following journals: Experimental Heat Transfer, Microfluidics & Nanofluidics, Microsystems Technologies, Bio-Microfluidics and L’Houille Blanche. Prof. Morini is co-Chair with Prof. Stephane Colin and Dr. J.J. Brandner of the European Conference on Microfluidics (mFlu) and he hosted the first edition of this series of Conference at Bologna in December, 2008.

KEYNOTE SPEAKERS

Prof. Srinivas Garimella

is the Hightower Chair in Engineering and Director of the Sustainable Thermal Systems Laboratory at Georgia Institute of Technology. He received M. S. and Ph.D. degrees from The Ohio State University, and a Bachelor's degree from the Indian Institute of Technology, Kanpur. He has held prior positions as Research Scientist at Battelle Memorial Institute, Senior Engineer at General Motors Corp., and Associate Professor at Western Michigan University and Iowa State University. He is a Fellow of the American Society of Mechanical Engineers, past Associate Editor of the ASME Journal of Heat Transfer, and Editor of the International Journal of Air-conditioning and Refrigeration. He has also served as Associate Editor of the ASME Journal of Energy Resources Technology, and Past Chair of the Advanced Energy Systems Division of ASME. He was an Associate Editor of the ASHRAE HVAC&R Research Journal and Chair of the ASHRAE Technical Committee on Absorption and Heat Operated Machines, and was on the ASHRAE Research Administration Committee. He held the William and Virginia Binger Associate Professorship of Mechanical Engineering at ISU from 1999-2001. He has mentored over 70 graduate students, with his research resulting in over 225 archival journal and conference publications, a textbook on Heat Transfer and Fluid Flow in Minichannels and Microchannels (2nd Ed., Elsevier 2014), and a book on Condensation Heat Transfer (World Scientific Publishing, 2015.) He has been awarded eight patents. He is the recipient of the NSF CAREER Award (1999), the ASHRAE New Investigator Award (1998), the SAE Ralph E. Teetor Educational Award for Engineering Educators (1998), and was the Iowa State University Miller Faculty Fellow (1999-2000) and Woodruff Faculty Fellow (2003-2008) at Georgia Tech. He received the ASME Award for Outstanding Research Contributions in the Field of Two-Phase Flow and Condensation in Microchannels, 2012. He also received the Thomas French Distinguished Educator Achievement Award (2008) from The Ohio State University, and the Zeigler Outstanding Educator Award (2012) at Georgia Tech.

ABSTRACTS

5th Micro and Nano Flows Conference
Milan, Italy, 11-14 September 2016

Numerical And Experimental Study Of Microdrops Manipulation By Fluidic Oscillator Device

Tawfiq CHEKIFI [1,*], Brahim DENNAI [1] and Rachid KHELFAOUI [1]

* Corresponding author: Tel.: +213 (0) 49 81 55 81/91; Fax: +213 (0) 49 81 52 44; Email: chekifi.tawfiq@gmail.com
1 ENERGARID Laboratory, University of Bechar, B. P. 417, 08000 Bechar, Algeria

Keywords: Microdrops, Fluidic Oscillator, CFD modeling and VOF (volume-of-fluid method).

Microdrops have been one of the most important branches in microfluidic science, Microfluidic oscillators were obtained from wall attachment microfluidic amplifiers using a feedback loop from the outputs to the control inputs [1], [2] have experimentally investigated the effects of the dimensions of the jet nozzle and feedback channel on the oscillatory frequency of water. In this work, we based on a feedback fluidic oscillator studied by [2], we perform numerical CFD study on the influence of hydrodynamics and physical parameters on the production of microdrops and its flow-separation, for that, we use the typical geometry, which includes double T-junction connected by a fluidic oscillator in order to produce simultaneous microdrops of oil on water. The generation of microdrops is computed by volume-of-fluid method (VOF). We investigated the microdrops frequencies as function of the difference of applied pressure (ΔP) and interfacial tension, flow oscillations of microdrops were triggered by the Coanda effect on jet flow, physical analysis of simulation results is also presented. The computational results show that the difference of applied pressure (ΔP) on T-junction and interfacial tension have a significant effect on the microdrops oscillatory frequency and its selection.

.

ID 3

5th Micro and Nano Flows Conference
Milan,Italy, 11-14 September 2016

Facile Synthesis, Characterization, Magnetic Properties, Catalytic Activity and enhanced heat capacity of Some $MFe_{2-x}Lu_xO_4$ (M = Zn, Cu, Co and Lu = La, Ce) Nanostructures

Mehdi Rahimi-Nasrabadi*,[1], Ali Sobhani-Nasab[2]

*Corresponding author: Tel.: ++98 9122585077; Fax: ++98 2177104930; Email: rahiminasrabadi@gmail.com
[1]Nano-Science Center, Imam Hossein University, Tehran, Iran
[2]Institute of Nano Science and Nano Technology, University of Kashan, Kashan, Iran

Keywords: Ferrite, Lu^{3+}-doped, Nanostructures, Catalyst, Nanofluid, Heat capacity, Phase change material

Lu^{3+} doped MFe_2O_4 (M = Zn, Co and Lu = La, Ce) nanostructures were prepared by the two-step sol gel method in the presence of $M(NO_3)_2$, $Fe(NO_3)_3{\cdot}9H_2O$, and $Lu(NO_3)_3$ in an aqueous solution. Besides, the effect of different type of surfactants such as SDS, CTAB, PVA, oleic acid, and PVP on the morphology and particle size of final product was investigated. Furthermore, the effect of Lu^{3+} dope on the magnetic properties of MFe_2O_4 nanostructures was investigated. VSM results demonstrated the dope concentration play an important role on the magnetic properties of final products. The products were characterized by XRD, SEM, EDX, VSM, TEM, UV-visible, and EDS. Nano- $LuMFe_2O_4$ as an efficient and green catalyst has been used in a cycloaddition reaction for the preparation of tetrazoles. This method provides several advantages including easy work-up, excellent yields, short reaction times, recoverability of the catalyst, and little catalyst loading. Furthermore, Nano-$LuMFe_2O_4$ nanoparticles have been used for preparation of novel nano-enhanced phase change materials (NePCMs). Nano-$LuMFe_2O_4$ and paraffin were selected as nano material and phase change material (PCM), respectively. The results showed that the heat capacity of nano-enhanced phase change materials was increased by the doping of nano- $LuMFe_2O_4$.

Introduction: Ferrites, i.e., ferrimagnetic cubic spinels possess the combined properties of magnetic materials and insulators. The important structural, electrical and magnetic properties of these spinels, are responsible for their applications in various fields. The properties of ferrites are affected by the type of the substitution and microstructure [1]. Spinel-type ferrites with the general formula MFe_2O_4 (M is a divalent metal cation) are very important materials because of their dielectric and magnetic properties [2]. The electric and magnetic properties, such as resistivity, initial permeability, and saturation magnetization, can be controlled by substitution of trivalent ions (RE) in the host spinel lattice [3]. The nano-enhanced phase change materials (NePCMs) were recently introduced, for improving thermal energy storage by increasing heat conductivity [4]. Recent investigations showed that specific heat capacity of PCM could also be enhanced by doping small amount of nanoparticles. The enhanced heat capacity of PCMs would directly improve their thermal energy storage performance [5].

Experimental

Heat capacity measurement: The specific heat of the samples was measured by sapphire method. For each sample, an empty pan, the pan with the reference material, and the same pan with the sample material were subjected to the appropriate temperature cycles and the heat transfer was recorded by the instrument. Then the heat capacity can be calculated based on the true value of heat capacity of sapphire.

Results and Discussion

The XRD pattern of the MFe_2O_4 in presence of Lu^{3+} doped were investigated. For example, the XRD pattern indicates the formation of pure orthorhombic phase of $ZnFe_{2-x}La_xO_4$ nanostructures (JCPDS No. 88-0639), with the calculated cell parameter of a = 5.5203 Å, b=7.8142 Å, and c= 5.5390 Å. The lattice parameter of pure $ZnFe_2O_4$ is found to be equal to 8.4465 Å which is in good accordance with the standard value of 8.4465Å (JCPDS No. 79-1150).

Energy dispersive X-ray microanalysis (EDX) technique used for the chemical characterization of nanostructures. All EDX spectrums show presence of appropriate elements with correct constant. FT-IR analysis was performed to identify the presence of certain functional groups in the nanostructures and confirm the purity of it. The diffused reflectance spectrum of the as-prepared nanostructures were investigated. The fundamental absorption edge in most semiconductors follows the exponential law. Using the absorption data the band gap was estimated by Tauc's relationship.

To investigate the effect of Lu^{3+} on magnetic properties of MFe_2O_4 nanostructures, their hysteresis loops were measured by VSM. For example, it is observed that M_s of the $ZnFe_2O_4$ nanostructures increased with the added of La^{3+}content to x = 0.05 ($ZnFe_{2-x}La_xO_4$). Hence, the Ms of $ZnFe_{2-x}La_xO_4$ nanostructures depends on the distribution of Fe^{3+} ions among tetrahedral and octahedral lattice sites, because both $La^{3+}$and Zn^{2+} ions are non-magnetic in nature.

Since, surfactants have significant effect on the morphology and particle size of final products; therefore, the effect of several surfactants such as SDS, CTAB, PVA, oleic acid, and PVP on the morphology and particle size of final product was investigated. It was revealed that the morphology and particle size of final products were changed with change in surfactants. Also, TEM images with different magnifications were taken.

Catalytic activity of $LuMFe_2O_4$ nanoparticles: Catalytic activity of $LuMFe_2O_4$ nanoparticles in cycloaddition reaction of nitriles with sodium azide for the synthesis of 5-substituted 1H-tetrazoles was investigated. In order to study the effect of catalyst particle size on the reaction parameters, synthesis reaction was carried out in identical conditions using $LuMFe_2O_4$ with severals different average particle sizes. The results show that $LuMFe_2O_4$ nanoparticles could catalyze the [2 + 3] cyclo-addition reaction of nitriles with sodium azide to form 5-substited 1H tetrazoles in DMF media. On the other hand, our finding showed that the catalyst particle size has main effect on the reaction rate.

Enthalpy of Fusion and heat capacity of NePCMs: The DSC curves of pure paraffin and NePCMs with different volume fraction of nanoparticles was investigated. The results shows that the heat flow curves were changed by the doping of nanoparticles. The heat capacity of the pure paraffin and NePCMs was investigated. The results shows that the heat capacity of PCM was essentially increased by mixind $LuMFe_2O_4$ nanoparticles into paraffin.

References:

[1] A.M. Samy, H.M. EI-Sayed, A.A. Sattar, Phys. Stat. Sol. (a) 200 (2003) 401–406.
[2] S.F. Yan, W. Ling, E.L. Zhou, J. Cryst. Growth 273 (2004) 226-231.
[3] S.E. Jacobo, S. Dubalde, H.R. Bertorello, J. Magn. Magn.Mater. 2253 (2004) 272-276.
[4] J.M. Khodadadi, S.F. Hosseinizadeh, Int. Commun. Heat Mass Transfer 34 (2007) 534–543.
[5] L. Zhichao, Z. Qiang, W. Gaohui, International Journal of Heat and Mass Transfer 80 (2015) 653–659.

5th Micro and Nano Flows Conference
Milan, Italy, 11-14 September 2016

Miniaturization and Process Intensification - smaller means better?

Juergen J. BRANDNER [1,*]

* Corresponding author: Tel.: ++49 (0)721 608 23963; Fax: ++49 (0)721 608 23186; Email: juergen.brandner@kit.edu
1 Karlsruhe Institute of Technology, Institute for Micro Process Engineering, Hermann-von-Helmholtz-Platz 1, D-76344 Eggenstein-Leopoldshafen

Keywords: Process Intensification, Miniaturization, Micro, Heat Transfer, Mass Transfer

Depletion of natural resources combined with the extending footprint of mankind has led to a shift in importance of research and development topics. Emphasis is now focused on resource efficiency as a primary objective. This is directly connected to intensification of processes in terms of resource consumption, yield, selectivity and economic output. The European Roadmap of Process Intensification [1] identifies several measures, amongst which miniaturization is named to be a very promising one.

It is a well-known fact that minimization of heat and mass transfer resistances lead to tremendous increase in the related transport capacities. Thus, miniaturized devices will play a key role in future industrial applications and transport systems as well as in the re-design of existing processes that directly impact on the daily life of citizens, ranging from industrial technologies to personal equipment.

However, there are significant gaps in the fundamental knowledge-base for both mass and heat transfer processes in the micro scale. Current research is primarily focused on phase transition or multi-phase flows, with less attention paid to single-phase gas flows. Liquid flows in microscale are considered to be understood and well described.

Measurement systems with sufficiently high temporal and spatial resolution to clarify phenomena in micro scale are in many cases not available, and modelling of such processes is exceptionally challenging. Because of this, pre-calculation and design of miniaturized devices is often based on trial-and-error. Thus, very often it is not possible to predict whether a process really can gain advantages from miniaturized equipment or suffer by the disadvantages. In terms of industrial processes, this leads to the situation that application of miniaturized equipment is a risk very often not taken.

Almost all parts of technology are influenced by miniaturization concerns. At the moment, the highest visible impact is to see on information technology and electronics. Nowhere else is the need to miniaturize, compact and intensify processes as high as here, dealing with huge volumes and high flows of information. Other technological topics are naturally not so much influenced, e.g. architecture. However, even here impacts are to see, since the development of miniaturized LED light has opened new opportunities for architectural design. Another example for the use of miniaturized systems is not so prominent but the most common one: the exhaust gas catalyst system for combustion engines is based on mini- or microscale channels serving as catalytically active ducts for the combustion exhaust gases.

It has to be carefully decided for which application miniaturization is a real advantage, just transforms into a new technology without major advantages or disadvantages, or may be even reducing efficiency of processes. The publication presented here will focus on applications of miniaturized devices in process engineering. Thus, considerations on heat transfer and mass transfer as well as some other technological aspects linked to these will be the primary content.

The basic principle behind intensification of thermal and chemical processes is the enhancement of transport processes by minimization of transport distances as well as reduction of transport resistances. Therefore, it is not necessary to have always microstructures inside devices, it is also suitable to miniaturize and structure the fluid streams, bring them close together and take advantage from this. Heat transfer as well as mass transport are strongly promoted by the small distances, thus, heat transfer time as well as mixing time can reach millisecond or even microsecond range. Besides, in most cases miniaturization in process engineering is linked to modularization, which allows combine different functionalities more easily than with conventionally sized equipment. This leads to a unique situation: While combination of different tasks in macro scale equipment runs on the time scale (residence time in each device has to be kept according to the limitations of the device vessel to reach reasonable effects), the modular micro scale equipment can be combined on a local scale by separating single parts of the process to optimized miniaturized devices and combining them to form the complete process. The enhancement in heat and mass transfer is high, thus, optimum conditions can be reached much more easily than with conventional sized devices [2], [3]. However, there are some major issues to be taken into account, which in many cases prevent the application of microscale devices to processes. Amongst those is the unknown long-term behavior, but also problems with fouling, cleaning and overall efficiency, taking heat transfer, mass transfer and pressure losses into account.

[1] European and Community (2014). "Process Intensification Roadmap." from http://efce.info/Working+Parties/Process+Intensification/Discussion+Forum/EUROPIN.html.
[2] Kockmann, N. (2006). Micro Process Engineering: Fundamentals, Devices, Fabrication, And Applications, Wiley-VCH.
[3] Hessel, V., A. Renken, et al. (2009). Micro Process Engineering: A Comprehensive Handbook, John Wiley & Sons.

5th Micro and Nano Flows Conference
Milan, Italy, 11-14 September 2016

Microfluidic Models of Metastatic Cancer

Roger D. KAMM [1,*]

* Corresponding author: Tel.: +01 617-253-5330; Email: rdkamm@mit.edu
1 Departments of Biological Engineering and Mechanical Engineering, Massachusetts Institute of Technology, USA

Keywords: Microfluidics, Cancer, Disease Models, 3D Cell Culture

Over the past 10 years, our ability to realistically model the critical biological steps in disease have dramatically improved, due in large part to the advances in microfluidic technologies. In particular, the capabilities to create realistic 3D microenvironments, including microvascular perfusion, have led to in vitro models for disease that offer considerable advantages over in vivo experiments. In this talk, I will present some recent advances in modeling the successive stages of metastatic cancer, especially in the context of immunotherapies and organ-specific models of metastasis.

1 Setting the Stage

Cancer metastasis progresses through a cascade of events, beginning with the separation of tumor cells from the primary tumor into the surrounding tissue where they experience changes in matrix stiffness, interstitial flows, and biochemical signaling, all of which influence their ability to migrate away from the tumor, either individually or in clusters. In order to create a secondary tumor in a remote organ, the cells need to gain access to the circulatory system, which they do either via the lymphatics or by direct intravasation into a small local blood vessel. There, they are convected by the blood flow first to the lung, and subsequently to other the organs of the body. Due to their size, tumor cells become lodged in the smallest capillaries, where they can either become activated to escape into the surrounding tissue, grossly deform in order to pass through, or succumb to the actions of blood shear stress or interactions with other circulating cells in the blood. Escape from the vasculature poses a challenge due to the tight junctions of the vascular wall. Cancer cells escape, however, by extravasating: sending projections between neighboring endothelial cells, adhering to the subendothelial matrix, and pulling themselves through by acto-myosin contractions. Once in the local tissue, they then can revert to a non-migratory phenotype, begin to proliferate and establish a secondary tumor.

2 The Role of Microfluidics

Historically, cancer metastasis been studied primarily in animal models, due to the critical need for multiple cell types, the essential role of the vasculature, and the 3D nature of the tissues involved in each stage. Microfluidic technologies can effectively be brought to bear in this situation, however, and their application has led to a variety of models that incorporate many of these key features, either singly or in combination. Subsequently, this work has begun to provide new insights into disease progression. Included among these are models of:

(1) Dispersion of cells from a primary tumor, either in empty matrix or in the presence of macrophages [1].
(2) Migration through matrix under the influence of interstitial flow [2].
(3) Migration through ECM in the presence of macrophages [3].
(4) Intravasation from tissue across an intact endothelium [4].
(5) Adhesion to an endothelial monolayer under shear flow conditions [5].
(6) Extravasation across an intact monolayer either into empty matrix or cell-seeded matrix to mimic a particular organ [6].

3 Organ-Specific Models

It is well-known that specific tumors have a propensity to metastasize to particular organs, yet the causes for this are virtually unknown. Our group has begun to probe this issue by seeding organ-specific cells into matrix. For example, we find that breast cancer calls home preferentially to matrix containing MSC-derived osteoblasts over a muscle-mimicking tissue containing a myoblast cell line. We further demonstrated that one of the factors responsible for the low rates of extravasation to muscle is adenosine, which binds to the A_3 adenosine receptor on the breast cancer cells.

4 Models of Immunotherapy

Tremendous interest has developed in the use of the body's own immune system to treat cancer, both primary and metastatic, yet these treatments tend not to be universally effective, and current methods to identify the responsive subpopulation have met with only limited success. Microfluidic models may be useful in identifying the response of a particular patient by introducing patient-derived samples taken from biopsy into a device and using this to screen for effective therapies. Alternatively, microfluidic models can be used to better understand the role of engineered immune cells such at T-cells or NK-cells, and to test for their efficacy in 3D, organ-specific environments, using microfluidics to recapitulate aspects of the in vivo condition.

5 References

[1] Aref AR, Huang RY-J, Yu W, Chua K-N, et al.. Integr Biol (Camb). 2013 Feb;5(2):381-9.
[2] Polacheck WJ, German AE, Mammoto A, Ingber DE, Kamm RD. Proc Natl Acad Sci USA. 2014 Feb 18;111(7):2447-52.
[3] Bai J, Adriani G, Dang TM, Tu TY, Penny HL, Wong SC, Kamm RD, Thiery JP. Oncotarget. 2015 Jul 30.
[4] Zervantonakis IK, Hughes-Alford SK, Charest JL, Condeelis JS, Gertler FB, Kamm RD. Proc Natl Acad Sci U S A. 2012 Aug 21;109(34):13515-20.
[5] Chen MB, Whisler JA, Jeon JS, Kamm RD. Integr Biol (Camb). 2013 5(10):1262-71.
[6] Jeon JS, Bersini, S; Gilardi, M; Dubini, G; Charest, JL; Moretti, M; Kamm, RD; Proc Natl Acad Sci USA, pp. 201417115, 2014

Magnetic Artificial Cilia Fabricated in an Out-of-Cleanroom Roll-Pulling Process Generate Significant Microfluidic Pumping

Ye WANG[1,2,*], Ruth CARDINAELS[1], Patrick ANDERSON[1], Jaap den TOONDER[1]

* Corresponding author: Tel.: +31 (0) 40 247 3647; Email: y.wang2@tue.nl
1: Eindhoven University of Technology, 5600 MB, Eindhoven, the Netherlands
2: Dutch Polymer Institute DPI, Eindhoven, the Netherlands

Keywords: Microfluidics, Artificial Cilia, Pumping, Out-of-Cleanroom Fabrication

In recent years, a novel class of bio-inspired micro-actuators known as artificial cilia (ArtC) has drawn a lot of interest because of their potential applications in microfluidics. They can be made to respond to various stimuli, such as electric field, light and magnetic field, and some of them have been shown to produce effective fluid pumping and mixing.[1] However, the fabrication techniques adopted in making those functional artificial cilia involve either microfabrication techniques under cleanroom conditions, or using expensive sacrificial materials as moulds. As a result, effective but expensive prototypes were made and they have little prospect to be used in commercial applications. Previously we have reported two techniques to produce ArtC in out-of-cleanroom settings.[2, 3] However the methods are not suitable for large scale production. Here we report a novel out-of-cleanroom fabrication method, which produces magnetic ArtC in a continuous manner without cleanroom requirement. The resulting ArtC can be used for generating microfluidic pumping with external magnetic actuation.

An in-house-developed rolling setup was used to fabricate artificial cilia (Fig. 1a). The setup features a synchronized movement and an adjustable gap between the aluminum roll and the substrate holder. A poly(dimethylsiloxane) (PDMS) film with micropillars (Fig. 1b) is attached to the roll. A substrate covered by a 200 μm thick liquid PDMS based precursor film containing iron particles travels beneath the roll and filaments are pulled out by the micropillars. These filaments reach a certain critical length before breaking, creating ArtC on the substrate. Silica nanoparticles and a polyethylene oxide/PDMS block copolymer were added into the precursor to give the mixture a yield stress, which is crucial for the formed artificial cilia to resist collapsing after their formation, and they make the process more robust as the curing of the ArtC can be delayed. A pair of vertically aligned electromagnetic poles is fixed above and below the moving parts to provide a magnetic field during fabrication for the vertical alignment of the ArtC. As a result, cone shaped slender artificial cilia with a length of about 300 μm and an aspect ratio of about 10 were created (Fig. 1c).

We integrated the ArtC into a recirculation microfluidic chip made of PDMS to characterise their flow generation capacity. A rotating magnet was placed underneath the cilia with its rotation axis at an offset with respect to the centre of the cilia chamber. This way, a time-dependent magnetic field was generated that actuated the cilia to perform a tilted conical motion, which generates a net fluid flow in the chip. The flow speed was then characterised by tracking freely buoyant particles in the fluid. As shown in Fig. 1d, at an actuation frequency of 20 Hz, a flow speed over 120 μm/s was created in the flow chip.

References

[1] J. M. den Toonder and P. R. Onck. *Trends in Biotechnology*, 31(2):85–91, 2013.

[2] Y. Wang, Y. Gao, H. Wyss, P. Anderson, and J. den Toonder. *Lab on a chip*, 13(17):3360–6, 2013.

[3] Y. Wang, Y. Gao, H. M. Wyss, P. D. Anderson, and J. M. J. den Toonder. *Microfluidics and Nanofluidics*, 18(2):167–174, 2014.

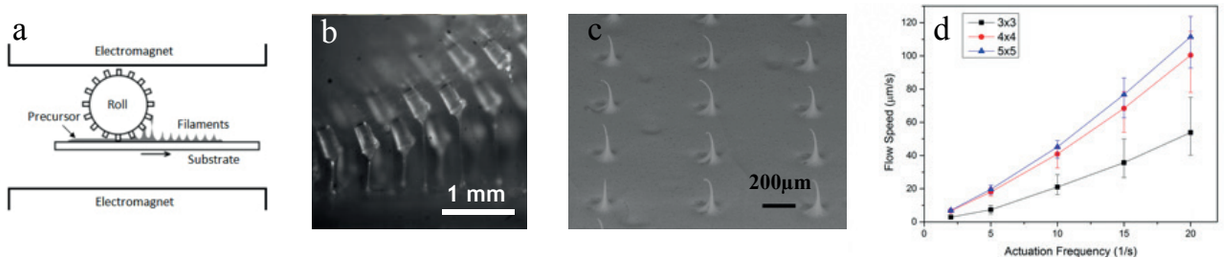

Figure 1 (a) Schematic of the roll-pulling setup; (b) liquid filaments being pulled out from the precursor film by micropillars, captured by high speed imaging; (c) micrograph of the resulting artificial cilia; (d) flow speed generated by artificial cilia in a microfludic device actuated using a rotating external magnetic field.

5th Micro and Nano Flows Conference
Milan, Italy, 11-14 September 2016

Performance of a Micro Scale Integrated Thermal Management System

Tassos G. KARAYIANNIS [1,*], Mohamed M. Mahmoud [1,2]

* Corresponding author: Tel.: ++44 (0)1895 267132; Fax: ++44 (0)1895 256392; Email: tassos.karayiannis@brunel.ac.uk
1: College of Engineering, Design and Physical Sciences, Brunel University London, UK
2: Faculty of Engineering, Zagazig University, Egypt, mohamed.mahmoud@brunel.ac.uk, mbasuny@zu.edu.eg

Keywords: Microchannels, Flow boiling, System Integration

The design, commissioning and thermal performance of an integrated small scale cooling system incorporating a micro-channel evaporator and condenser are presented in this paper. Existing models and correlations predicting the thermo-fluid performance of the evaporator and condenser were first reviewed. The final correlations used in the design of the micro heat exchangers and their limitations will be discussed in the paper.

The new facility can test flow boiling and condensation in micro-channels as well as overall system performance. The evaporator and condenser were instrumented to allow their performance to be recorded (and hence later optimised) prior to investigating the overall system performance. The evaporator consisted of 50 rectangular channels 0.3 mm wide, 1.0 mm high and 0.1 mm in fin thickness. It was made of oxygen free copper by CNC machining with overall dimensions of 51×26 mm of which 25×20 mm is a heated footprint area. The evaporator was designed with a semi-circular inlet and outlet manifolds with a transparent top cover for flow visualization. The condenser was made of oxygen free copper by CNC machining and consisted of 90 rectangular channels of 0.4 mm wide, 1 mm high, 0.1 mm separating wall thickness, 160 mm long and 45 mm wide. The inlet and outlet manifolds were also semi-circular. A wide range of heat and mass fluxes was examined. Flow patterns, flow instability, heat transfer and pressure drop results will be presented and discussed. The overall system performance will also be presented. Subsequently, the manifolds were re-designed to assess the effect of inlet and outlet manifold design on flow reversal and instability.

ID 13

5th Micro and Nano Flows Conference
Milan, Italy, 11-14 September 2016

MASS TRANSFER CHARACTERIZATION OF CHEMICAL ABSORPTION OF CO_2 IN MICROCHANNEL ABSORBERS

Ziqiang Yang[1,*], Tariq S. Khan[1], Mohamed Saeed AlShehhi[1], Yasser Fowad AlWahedi[2]

* Corresponding author: Tel.: +971 (0)56 491 4231; Email: ziyang@pi.ac.ae
1 Department of Mechanical Engineering, The Petroleum Institute P.O. Box 2533, Abu Dhabi, United Arab Emirates
2 Department of Chemical Engineering, The Petroleum Institute P.O. Box 2533, Abu Dhabi, United Arab Emirates

Keywords: CO_2, diethanolamine, absorption, microchannel, absorber.

CO_2 absorption using amine solution can be significantly enhanced in micro reactors that offer high surface area per unit volume. In this work, chemical absorption of 10v% CO_2 mixed with N_2 into 20w% diethanolamine in water was investigated in a microchannel with circular cross-section. Absorption efficiency, mass transfer coefficient and CO_2 loading were studied here by varying the phase super velocity, channel length, diameter and temperature. The experimental results showed that liquid side volumetric mass transfer coefficient increased with gas and liquid phase super velocity in slug flow regime and achieved its maximum value in the slug-annular flow and churn flow regime. An empirical correlation of CO_2 loading was proposed based on the Reynolds number, configuration of microchannel and the temperature. The predicted values of CO_2 loading agreed well with the experimental data. The values of mass transfer coefficient in this study are multiple orders of magnitude higher than those in convectional gas-liquid absorption system.

Multiscale Simulation of Nanofluids for Solar Thermal Energy

Annalisa CARDELLINI [1], Matteo FASANO [1], Matteo MORCIANO [1], Eliodoro CHIAVAZZO [1], Pietro ASINARI [1,*]

* Corresponding author: Tel.: +39 011 0904434; Fax: +39 011 0904499; Email: pietro.asinari@polito.it
[1] Multi-scale Modelling Laboratory (SMaLL), Department of Energy, Politecnico di Torino, Italy

Keywords: Nanofluids, Nano-colloids, Solar Thermal Energy, Coarse-Grained Molecular Dynamics (CGMD) Simulations

Volumetric solar receivers are showing promising efficiencies as compared to traditional collectors. Many colloidal nano-suspensions (nanofluids) with enhanced optical and thermal transport properties have been investigated to directly absorb the solar radiation. However, a rational design of nanofluids for solar applications is still missing due to their multiscale nature. Here, a multiscale Coarse-Grained (CG) approach applied to nanofluids for volumetric solar receivers is introduced. By means of molecular dynamics simulations, the pair Potential of Mean Forces (pPMF) between nanoparticles is evaluated. As an exemplificative case, a couple of uncharged, alumina nanoparticles in water is considered. These results are the first steps to implement the CG force field and thus multiscale model for solar nanofluids, which may facilitate the translation of nanofluid technology from lab- to large-scale industrial production.

1 Introduction

An alternative concept for solar thermal collectors is the volumetric solar receiver, which is based on nanofluids directly absorbing the incident radiation [1]. The addition of nanoparticles to traditional fluids can drastically enhance their optical properties and improve their thermophysical performances, leading to highly efficient volumetric solar receivers. However, the multiscale nature of nanofluids makes difficult to relating nanoscale characteristics with resulting macroscopic properties. In particular, the complex mechanism of nanoparticle clustering is one of the main responsible of nanofluids stability and thus effective properties. Due to the nanoscale effects involved in nanofluids, multiscale simulation methods are needed to guide their rational design. The Coarse-Grained (CG) approach is a modelling technique able to bridge Molecular Dynamics (MD) simulations from atomistic scale to mesoscale [2]. The basic idea of coarse graining is to combine several atoms into homogeneous groups (CG beads), which interact each other by means of bonded and non-bonded interaction potentials. Here, a suitable bottom-up CG model for nanofluids is employed for directly evaluating the pPMF from MD simulations. In particular, a couple of alumina nanoparticles solvated in water is chosen as an exemplificative building block for nanofluids with solar applications.

2 Methods and Results

To evaluate the pPMF between suspended $\boldsymbol{\alpha - Al_2O_3}$ nanoparticles (NPs) in water, MD simulations are carried out. The following steps describe the adopted protocol ("pulling procedure"). First, the atomistic model of each $\boldsymbol{\alpha - Al_2O_3}$ NP is prepared by defining the particle geometry and atomistic force field. Specifically, 2 nm alumina spheres are hydrogenated by adding OH terminal groups on the surface. All bonds, angles and dihedral within the NP core are modeled with a harmonic potential; instead, Lennard-Jones and Coulomb potentials are imposed for mimicking non-bonded interactions. The CLAYFF force field is adopted to distributing partial charges on the NP surface, which is neutral overall [3].

Second, two alumina nanoparticles are considered. The NPs couple is placed in a water box (22x8x8 nm) and, after energy minimization, the whole system is equilibrated at T=300 K and p=1 bar. In the first configuration, the distance between NPs center of mass (com) is set to 2 nm. Then, by restraining one particle while pulling the second one along a reaction coordinate r, a series of configurations is generated. Each configuration, which corresponds to a precise separation distance between the NPs, is taken into account for an independent 2 ns MD simulation.

Third, the pPMF is calculated by numerically integrating the interacting forces between the NPs. Results show that the minimum energy between NPs is achieved at the shortest com distance. The MD results are then compared with the DLVO theory [4]. Since we are dealing with uncharged nanoparticles, only the attractive contribution of the DLVO model is considered.

3 Conclusions

Flocculation in colloidal systems is one of the most critical aspects in the use of nanofluids for volumetric solar receivers. Here, the pair Potential of Mean Forces between two alumina nanoparticles in water is evaluated by means of MD simulations. The results show and confirm the adhesion energy between particles. The reason of such attractive interaction is mainly attributed to the London-Van der Waals forces. However, the attractive Coulomb contribution between OH groups on NPs surface should be also considered.

A complete CG model able to study nanoparticle clustering is defined by including the effects of water adsorbed at solid-liquid interface [5], nanoparticle surface charge and solution pH.

Acknowledgements: NANO-BRIDGE project (PRIN 2012) and CINECA (COGRAINS).

References

[1] Moradi A, *et al.* Carbon-nanohorn based nanofluids for a direct absorption solar collector for civil application. *J. Nano. Nanotech.* 2015;15:3488-3495.
[2] Villa A, *et al.* Self-assembling dipeptides: including solvent degrees of freedom in a coarse-grained model, *Phys. Chem. Chem. Phys.* 2009;11(12): 2068-76.
[3] Cygan RT, Liang J-J, and Kalinichev AG. Molecular models of hydroxide, oxyhydroxide, and clay phases and the development of a general force field. *J. Phys. Chem. B* 2004; 108.4:1255-1266.
[4] Hamaker HC. The London—van der Waals attraction between spherical particles. *Physica* 1937;4.10:1058-1072.
[5] Chiavazzo E, *et al.* Scaling behaviour for the water transport in nanoconfined geometries. *Nat. comm.* 2014;5.

5th Micro and Nano Flows Conference
Milan, Italy, 11-14 September 2016

Characteristics of Fluid Flow and Heat Transfer of Nanofluid Flow in Microchannels with Micromixers

Mohammad HEMMAT ESFE[1], Wei-Mon YAN[2,*] and Chung-Hao KAO[2]

* Corresponding author: Tel.: +886-972909259; Fax: +886-2-27314919; Email: wmyan@ntut.edu.tw
[1] Department of Mechanical Engineering, Faculty of Engineering, Najafabad Branch, Islamic Azad University, Najafabad, Isfahan, Iran
[2] Department of Energy and Refrigerating Air-Conditioning Engineering, National Taipei University of Technology, Taipei 10608, Taiwan

Keywords: Micromixer, Baffle, Microchannel, Nanofluid, Heat transfer

Convective heat transfer in a microchannel is a very effective method for the thermal control micro electronic device because of the high surface area to volume ratio of these channels. Therefore, the ability to remove heat from the high heat flux region becomes an important factor in designing microsystem. A very different application of nanofluids could be in modern medicine, where for example nanodrugs are mixed in microchannels for controlled delivery with bio-MEMS. In such application, rapid completely mixing of fluid is required. Microchannel flows, due to very low flow rate, are characterized by very low Reynolds number. Owing to the predominantly laminar flow, it is difficult to achieve effective mixing fluids. If the mixing is obtained primarily by a diffusion mechanism, then fast mixing becomes impossible. Hence, microfluidic mixing is a very challenging problem because it requires fast and efficient mixing of low diffusivity fluids.

The schematic of geometry considered in this work is shown in Fig. 1. The microchannel consists of two plates with the distance of L and the length of S (=13L). Four baffles with heights of e_1, e_2, e_3 and e_4 , respectively, are placed inside the channel. The distance of baffles from the beginning of the channel are shown in Fig. 1. The baffles are assumed adiabatic with zero thickness in the numerical simulation. The steady, laminar flow of nanofluid, enters the microchannel with uinform velocity u_o and temperature T_o. The microchannel is kept at contant wall temperature T_w.

The governing equations with the associated boundary conditions are numerically solved using the finite volume method. The thermophysical properties such as thermal conductivity and viscosity are solved concurrently with flow, temperature in whole solution domain. On the control volume faces these properties are averaged linearly using the calculated values on the grids. To ensure the accuracy as well as the consistency of numerical results, several grids have been submitted to an extensive testing procedure for each of the cases considered.

The effects of Reynolds numbers Re_f and nanoparticle volume fraction φ in a microchannel with baffles on flow patterns are showed in Fig. 2. It is clear in Fig. 2 that there is a recirculation zone downstream of baffles. The recirculation zone increases with Reynolds number Re_f and decreases with nanoparticle volume fraction φ. For a given Re_f, the viscosity of nanofluid increases with increasing the nanoparticle volume fraction and the size of recirculation zone decreases.

In this work, the characteristics of heat transfer and fluid flow of Al_2O_3 /water nanofluid in two dimensional parallel plate microchannel with four micromixers have been numerically studied for nanoparticle volume fractions of φ = 0, φ = 4% and base fluid Reynolds numbers of Re_f = 5, 20, and 50. The effects of baffle distances and baffle heights were investigated in details. Results show that there is a recirculation zone downstream of the baffles. The size of this zone increases with Reynolds number and decreases with nanoparticles volume fraction. It is observed that the influence of nanoparticle volume fraction on vortex size is weaker at low Reynolds numbers. Additionally, the presence of baffles would affect the local heat transfer and wall shear stress distributions. The influence increases with increasing the Reynolds number and number of baffles.

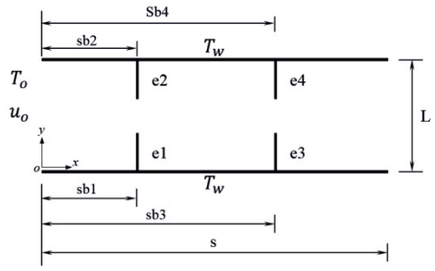

Fig. 1 Geometrical configuration

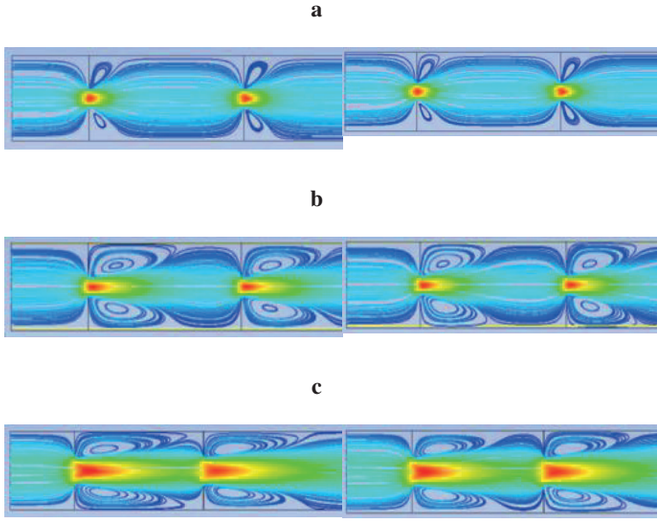

Fig. 2 Effects of Re_f on flow patterns with φ = 0 (left column), φ = 0.04 (right column), sb_1=sb_2= L, sb_3=sb_4=3L, e_1=e_2=e_3=e_4=0.4L. (a) Re_f=5, (b) Re_f=20, (c) Re_f=50

ID 17

Onset of convection in a porous medium layer saturated with a nanofluid using Walters B fluid

J.C. Umavathi and Maurizio Sasso
Department of Engineering, University of Sannio, Piazza Roma 21, 82100 Benevento, Italy

Email: drumavathi@rediffmail.com

Abstract
The onset of nanofluid convection in a Walters B fluid saturated horizontal porous layer is studied with thermal conductivity and viscosity dependent on the nanoparticle volume fraction. Nanofluid incorporates the effects of Brownian motion along with thermophoresis and a Darcy model has been used for the porous medium. The nanofluid is assumed to be diluted and this enables the porous medium to be treated as a weakly heterogeneous medium with variation in the vertical direction of conductivity and viscosity. In addition the thermal energy equation includes regular diffusion and cross diffusion terms. A normal mode technique has been used for the linear stability analysis, while for nonlinear analysis, a minimal representation of the truncated Fourier series representation involving only two terms has been used. The effects of various governing parameters such as the concentration Rayleigh number, Lewis number, modified diffusivity ratio, Soret and Dufour parameters, Solutal Rayleigh number, elastic parameter, modified Prandtl number, viscosity ratio and conductivity ratio on the stationary and oscillatory convections are presented graphically. For steady finite amplitude motions, the heat and mass transport is also brought out. We also study the effect of time on transient Nusselt number and Sherwood number which is found to be oscillatory when time is small. However, when time becomes very large, the transient Nusselt and transient Sherwood values approaches to their steady state values.

5th Micro and Nano Flows Conference
Milan, Italy, 11-14 September 2016

Heat transfer enhancement in counter-flow-heat-exchanger for use in microfabricated Joule-Thomson cryocooler

Leonid Fraiman[1], Anatoly Parahovnik[1], Gilad Yossifon[1,*]

* Corresponding author: yossifon@technion.ac.il
[1] Faculty of Mechanical Engineering, Technion-Israel Institute of Technology

Keywords: Micro-channels, Micro-pillars, Gas flow, Heat exchangers

This study presents heat transfer enhancement in micro fabricated counter flow heat exchanger (Fig. 1), using nitrogen gas as working fluid. The heat exchanger is designed to be part of a Joule Thomson cryocooler [1]. Cylindrical pillars, for constructional strength enhancement, were integrated within the rectangular microchannels at both high and low pressure and temperature streams. Heat exchanger performance were predicted by spreadsheet calculations (Fig. 2) using empirical correlations for heat transfer coefficient by Metzger [2] and pressure drop by Jacob [3]. Geometry optimization of microchannel height and pillar diameter was made to minimize pressure drop (Fig. 3) and maximize heat transfer (Fig.4). Pressure losses are very important since pressure defines temperature at saturation state, for cryocooler usage. Special attention was given to scaling [4] and axial conduction [5] effects. In addition to the heat transfer problem a parametric study was conducted to examine the structural strength of the device. Optimal heat exchangers will be then fabricated and experimentally tested with their performance compared against the computation predictions.

References

[1] Cryocooler, www.wikipedia.com, 2015.
[2] Metzger D. E, "Developing heat transfer in rectangular ducts with staggered arrays of short pin fins", Trans. ASME, vol. 104, p. 700-706, 1982.
[3] Jakob, M. "Heat Transfer and Flow Resistance in Cross Flow of Gases over Tube Banks," Trans. ASME, vol. 60, p. 384, 1938.
[4] P. Rosa, T.G. Karayiannis, M.W. Collins, Single-phase heat transfer in microchannels the importance of scaling effects, Applied Thermal Engineering (2009).
[5] Maranzana G. et al., "Mini and micro-channels: influence of axial conduction in the walls", International Journal of Heat and Mass Transfer 47 (2004) 3993-4004.

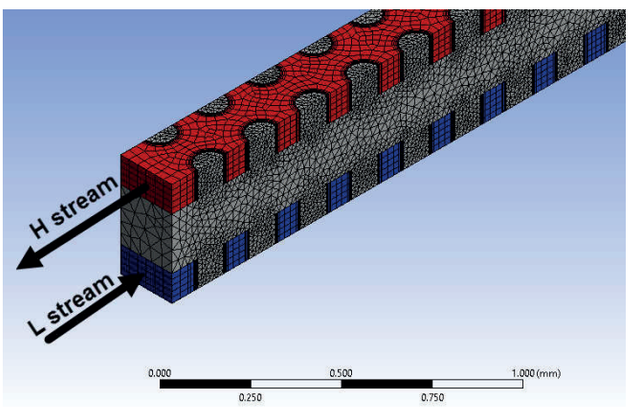

Fig 1 – A periodic slice of the simulated counter flow heat exchanger.

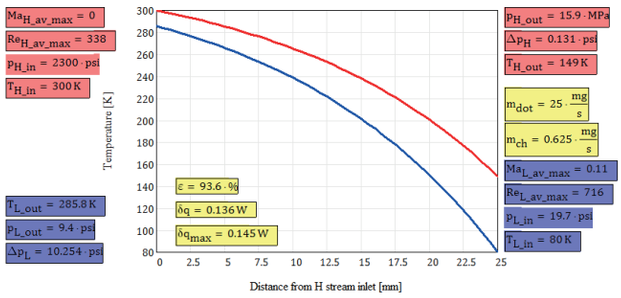

Fig 2 – Temperature distribution along HE length.

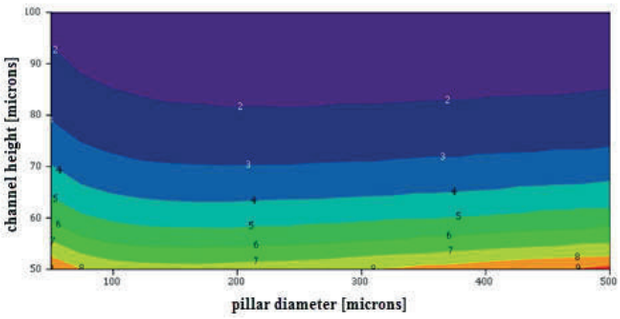

Fig 3 – Pressure [psi] drop characteristic map, as a function of low pressure stream channel geometry.

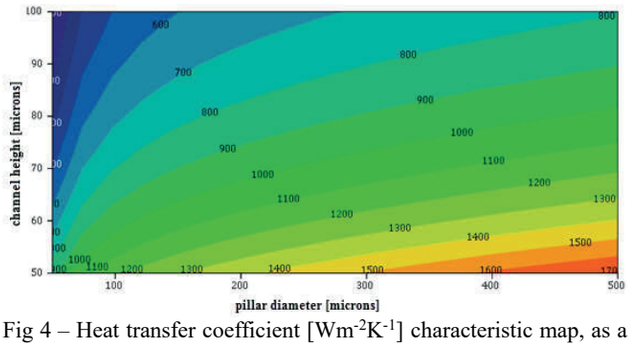

Fig 4 – Heat transfer coefficient [$Wm^{-2}K^{-1}$] characteristic map, as a function of channel geometry.

5th Micro and Nano Flows Conference
Milan, Italy, 11-14 September 2016

Hydrodynamic structures to improve cell capturing in microchannels

Elena BIANCHI [1*], Monica PIERGIOVANNI [1], Matteo DE GENNARO[1], Simone BERSINI [2], Mara GILARDI [2], Chiara ARRIGONI [2], Junko ENOMOTO [3], Junji FUKUDA [3], Alfonso GAUTIERI [4], Matteo MORETTI [2], Gabriele DUBINI [2]

* Corresponding author: Tel.: ++39 (0)22399 4317; Fax: ++39 (0)22399 4293; Email: elena1.bianchi@polimi.it
1 Laboratory of Biological Structures Mechanics - CMIC, Politecnico di Milano, Milano, IT
2 IRCCS Istituto Ortopedico Galeazzi, Milano, IT
3 Yokohama National University, JP
4 Dipartimento di Elettronica, Informazione e Bioingegneria - DEIB, Politecnico di Milano, Milano, IT

Keywords: Cellular assays, Lab on Chip, Cell sorting, Hydrodynamic structures

1. Introduction

Precise selection of specific cell subtypes is of fundamental importance for different areas, such as cell based therapies, especially if the cell type of interest is rare in the source sample. In case of stem cell separation several strategies for cell sorting from heterogeneous cell populations have been investigated in the literature [1-3], proposing methods for the extraction, based on cell size or cell biochemical affinity. Among these methods cell selection based on selective adhesion of target cells to a specific coated surface is the most efficient approach, but it could be very time-costing. A microfluidic approach to this selection method can improve the efficiency of the separation, reducing the operative time needed to efficiently induce cells to get in contact to the coated surface. The role of hydrodynamic structures in patterning laminar flows, especially the herring-bone shape like structures, has been investigated in the literature as mixing generators (Stroock in 2002 [4]) and considered to be powerful means to tune cell trajectories in microfluidic channels [5] and improve cell adhesion rate [6]. In this work we have designed a microfluidic channel, patterned on one surface with herringbone inspired hydrodynamic structures in order to improve the selective adhesion of mesenchymal stem cells from a biological multicellular source sample.

2. Materials and Methods

A single channel, fed by a syringe pump, has been designed in order to evaluate the efficacy of these hydrodynamic structures in capturing cells target by selective adhesion on a coated internal surface. Computational Fluid Dynamic CFD modeling (ANSYS Fluent 16 Canonsburg, PA) on a unit channel segment (periodic boundaries to represent a repetitive pattern) has been performed to evaluate the effect of the structures geometrical parameters on the streamlines deviation and on the cells trajectories.

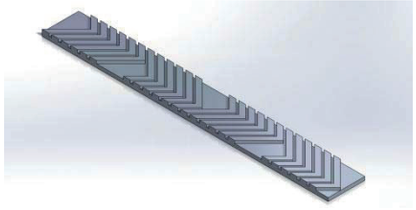

Fig.1 Geometrical model of a hydrodynamic structures in a channel portion

Hydrodynamic structures are located on the top surface of the microchannel (width 1 – 2 mm, height 150 – 400 µm) and protrude inside the channel for about a half of the total height.

The investigated geometries differ in angles (60° – 90°), step and specific width of the cavities. Streamlines and particles tracking analyses (12 µm ∅, rigid spheres,) were useful to understand how much each geometrical and flow parameters are able to tune the mixing and to induce the cells to get repetitively in contact with coated surface. Selected geometries are ready to be fabricated by soft lithography in order to evaluate their performance in increasing selective capturing of cells on a target surface where a specific aptamer will be immobilized.

3. Results

CFD models allows for the evaluation of the efficacy of singular geometries in fluid recirculation and in inducing fluid/particles to get in touch with the coated surface (Fig.2). Is then possible the estimation of the number of consecutive channel units necessary to

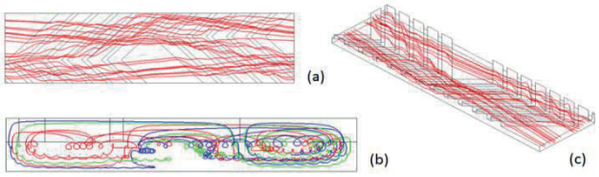

Fig.2 Streamlines of flow inside a modelled channel (a)(c) View from the top and 3D view, (b) view from the inlet: each color represents a single streamline, randomly selected, for 10 geometrical unit channel length. Each streamline is alternatively induced to move down to the target surface and then up into the hydrodynamic structures.

obtain a set degree of fluid recirculation (>90% of streamlines passed at a distance < 5 µm from the surface), able to capture the majority of the rare target cells contained in the cellular sample. Experimental investigations will evaluate the efficacy of patterned channels in capturing target cells with respect to rectangular section microchannels.

4. Acknowledgements

This work has been supported by Fondazione Cariplo, grant no.2013-0766.

5. References

[1]B. Zhu and S. K. Murthy, "Stem cell separation technologies," *Current Opinion in Chemical Engineering,* vol. 2, pp. 3-7, 2013.

[2]Z. Gudleviciene, *et al.*, "Quick and effective method of bone marrow mesenchymal stem cell extraction," in *Open Medicine* vol. 10, ed, 2015.

[3]S. Otsuru, *et al.*, "Improved isolation and expansion of bone marrow mesenchymal stromal cells using a novel marrow filter device.," *Cytotherapy,* vol. 15, p. 8, 2013.

[4]A. D. Stroock, *et al.*, "Chaotic Mixer for Microchannels," *Science,* vol. 295, p. 5, 2002.

[5]T. P. Forbes and J. G. Kralj, "Engineering and analysis of surface interactions in a microfluidic herringbone micromixer," *Lab on a Chip,* vol. 12, pp. 2634-2637, 2012.

[6]S. L. Stott, *et al.*, "Isolation of circulating tumor cells using a microvortex-generating herringbone-chip," *Proceedings of the National Academy of Sciences,* vol. 107, pp. 18392-18397, 2010.

5th Micro and Nano Flows Conference
Milan, Italy, 11-14 September 2016

Droplet formation in microfluidic double-T-junction devices

Ich-Long NGO [1], Sang W. JOO [1], Chan BYON [1*]

* Corresponding author: Tel.: ++82 (0)53 810 2452; Fax: ++82 (0)53 810 4627; Email: cbyon@ynu.ac.kr
1 School of Mechanical Engineering, Yeungnam University, Korea

Keywords: Microfluidics, double-T-junction, droplet

The understanding of underlying physics of the ADF phenomenon is useful for many applications, including nanoparticle synthesis with different concentrations, hydrogel bead generation, and cell transplantation in biomedical therapy. In this study, the droplet formation in microfluidic double-T- junction is investigated numerically, based on volume of fluid method. The effects of capillary number, volume fraction, and viscosity ratio on the droplet formation characteristics are considered. Based on an extensive numerical result, parametric condition for having the preferred alternating droplet formation (ADF) regime is explored, and physical reason responsible for ADF formation is suggested. The numerical results indicate that the ADF is shifted toward lower capillary numbers when the channel width ratio is less than unity. The alternating droplet size is shown to increase with the increase of channel width ratio. The droplet formation in MFDTD depends significantly on the viscosity ratio, and the droplet size in ADF decreases with the increase of the viscosity ratio.

5th Micro and Nano Flows Conference
Milan, Italy, 11-14 September 2016

Nanomanipulating and sensing single particles interactions with combined atomic force microscopy optical tweezers (AFM/OT)

Filippo PIERINI*, Krzysztof ZEMBRZYCKI, Paweł NAKIELSKI, Sylwia PAWŁOWSKA, Tomasz Aleksander KOWALEWSKI

* Corresponding author: Tel.: (+48)228261281; Fax: (+48)-228269815; Email: fpierini@ippt.pan.pl
Department of Mechanics and Physics of Fluids, Institute of Fundamental Technological Research, Polish Academy of Sciences, Warsaw, Poland

Keywords: Atomic force microscopy/optical tweezers, Nanomanipulation, Single particles analysis, Interaction force measurement, DLVO theory

Materials containing suspended micro- or nanoparticles serve a wide variety of purposes and they are used in several applications. In all the colloid system applications it is necessary to maintain the particles well dispersed and to avoid the formation of aggregates. It is for this reason that it is absolutely necessary to know the particle-particle interaction forces at the nanoscale.

The equilibrium state and the hydrodynamic properties of colloid systems in aqueous medium are affected by several environmental parameters. The addition of salt influences stability of colloids [1]. An explanation for this fact was given by the Derjaguin-Landau-Verwey-Overbeek (DLVO) theory, describing the surface charges at interfaces. This theory assumes that the interaction force between two particles is due to the sum of the electrostatic double-layer repulsion and the van der Waals attraction [2].

In order to study the effects of surrounding liquid properties on the stability of single particles from a new point of view, we have designed, developed and calibrated a combined atomic force microscopy/optical tweezers apparatus (Figure 1) [3]. This high resolution imaging instrument is capable to confine micro- and nanomaterial and to quantify force in the femtonewton scale.

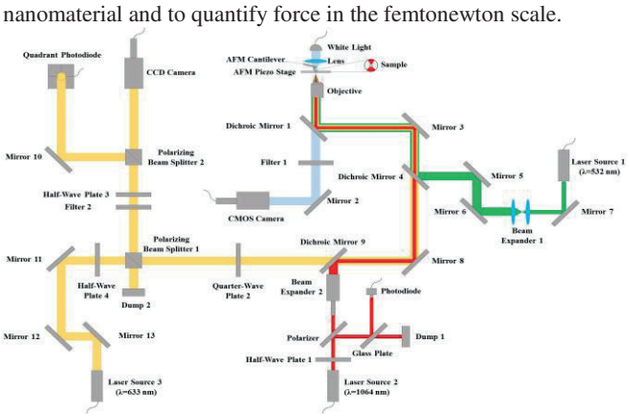

Figure 1. A sketch showing the scheme of atomic force microscopy and optical tweezers (AFM/OT) setup.

Moreover, one of the most interesting applications of the proposed apparatus is to use optical tweezers in order to manipulate single objects (e.g. nanomaterials and cells). The main achievement of the optical trapping nanomanipulation is to develop a selective nanomaterials sorting process with the aim to purify samples and to study the properties of single selected nano-objects. Nanomanipulation can also be useful to organize, assemble and locate complex hierarchical structures composed through optical tweezers manipulation.

In the first experiment, the AFM/OT system (Figure 2) was used to isolate a 1.0 μm polystyrene particles into a microfluidic well using the dragging force of the trapping laser. Subsequently, a custom-made AFM colloidal probe cantilever in which a single

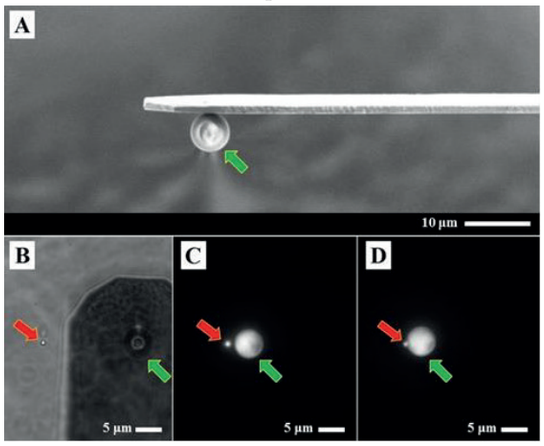

Figure 2. A SEM micrograph of the 5.5 polystyrene particle mounted on the tipless AFM cantilever using AFM as a manipulator (A). A 1.0 μm polystyrene particle was trapped a few micrometers from the cantilever (B), then the probe was translated in the trapped particle direction (C) and finally the particle glued to the cantilever approached the surface of the trapped particle (D).

fluorescent 5.5 μm particle was glued to the end of a tip-less AFM cantilever was used to quantify the interaction force between two polystyrene particles.

The experiment was carried out by approaching the trapped particle with the AFM particle probe at a constant velocity (200 nm/s) in pure water and recording the optical tweezers output signals with the resolution of ±100 fN. The same experiment was repeated in 10^{-5} M and 10^{-3} M KCl solutions in that order. The obtained data (Figure 3) confirm that the behavior of colloidal systems observed experimentally agrees with the theoretical predictions. In pure water, long range attraction is clearly measured, whereas small short range repulsions are still not strong enough to overcome the attractive component in the analyzed range.

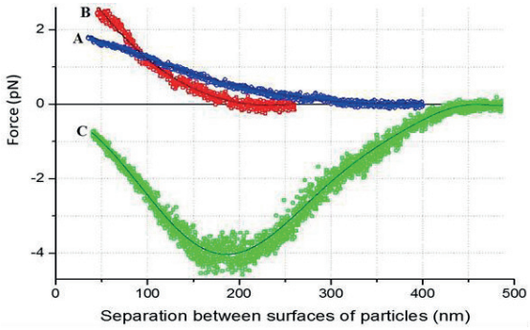

Figure 3. Force as a function of the relative distance between a single pair of polystyrene particles. The interaction force were collected varying KCl concentration: 10^{-3} M (blue circles; A), 10^{-5} M (red squares; B) and pure water (green triangles; C) at pH 7.

A completely different behavior is observed in presence of KCl, where no final attractive forces act in the analyzed range, while repulsive forces that grow exponentially with decreasing particle-particle distance are visible. In all the studied systems, no interaction forces between the polystyrene particles could be observed at distances exceeding 450 nm.

Another experiment was carried out in order to create a multi-particles structure, allowed us to prove the AFM/OT instrument capability of acting as a nanomanipulator and to scan the produced structure with the AFM probe at the same time, generating a high resolution image of the manipulated sample. In this case, the trapping laser was used as a high precision nanomanipulator while the AFM cantilever guarantees the capability to visualize the treated sample zone with high resolution.

Five polystyrene particles were maneuvered and isolated from the colloidal system, then the selected particles were individually confined in a clean water microfluidic well and dragged to the glassy bottom of the channel in order to form a perfectly aligned straight line structure. The force exerted by the trapping laser is strong enough to push the particles to the glass wall and the adhesion effects allow to immobilize the particles to the substrate.

The AFM/ OT system was used to collect AFM topographies of the area selected for conducting the experiment before and after the particle deposition (Figure 4) as well as the surface of the single dragged particles.

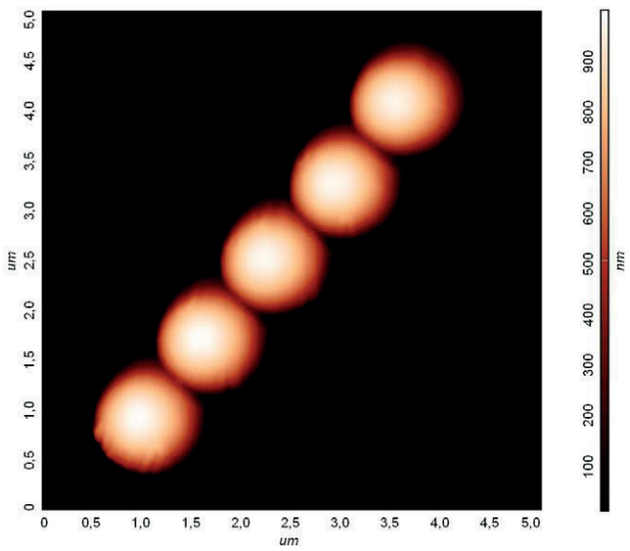

Figure 4. Topography image of the produced polystyrene particles structured immobilized onto the substrate obtained in tapping mode AFM.

This experiment allows to study the surface properties of the particles and substrates taking into consideration one single particle–surface interaction and to study such single events to characterize locally the studied materials.

Concluding, the obtained experimental results confirm the applicability of our combined system to study single particles interaction forces. It is shown that the polystyrene particles colloid systems are more stable in a 10^{-3} M KCl solution, than a 10^{-5} M KCl solution and that is, in turn, more stable than the same system in water. Furthermore, we have proved the instrument capability to manipulate single polystyrene particles and simultaneously study the sample surface properties by using the hybrid double probe AFM/OT system.

References

[1] C. Chassagne et al., *Colloids Surf. A*, 440, 208 - 216, 2014.
[2] J. A. Marotoet al., *Colloid. Polym. Sci.*, 276 453 - 458, 1998.
[3] F. Pierini et al., *Meas. Sci. Technol.*, 27, 25904 - 25915, 2016.

Project was funded by NCN grant no. 2011/03/B/ST8/05481.

Nanofluid Flow and Heat Transfer in Boundary Layers at Small Nanoparticle Volume Fraction

Joseph T. C. Liu[1;2;]*, Mark E. Fuller[2], Ka Ling Wu[2], Alexander Czulak[2], Alexander G. Kithes[2], Collin J. Felten[2]

* Corresponding author: Tel.: +401 8632654; Fax: +401 8639028; Email: joseph_liu@brown.edu

[1]Department of the Mechanics and Physics of Fluids
Institute for Fundamental Technological Research, Polish Academy of Sciences
02-106 Warsaw, Poland

[2]School of Engineering EN2760 and the Center for Fluid Mechanics
Brown University, Providence, Rhode Island 02912, USA

Keywords: nanofluids, heat transfer enhancement, nanoparticles, boundary layers

Abstract A continuum description of the leading edge region of boundary layers in a nanofluid is performed, where heat transfer enhancement is known experimentally to be enhanced. Expansions are performed for small nanoparticle volume fraction in a perturbation theory. Thermophysical properties from mixture theory (mix) are used to compare theoretical results for a zero volume flux, solid wall with that of experiments (for alumina, in entrance region of micro channels or tubes). The theory underestimates the experimental enhancement, one possibility if due to the (mix) properties used. We then turn to using results from prevailing molecular dynamics (MD) calculation of thermophysical properties, which is available only for gold nanoparticles and compare with results from (mix) thermophysical properties for the same gold nanoparticles (for which experiments are not available). It is found that(mix) properties drastically underestimates heat transfer enhancement, while the shear stress enhanced and hence necessary increase in pumping power, is considerably larger than the realizable heat transfer. The (MD) properties gave comparable shear stress and heat transfer enhancement, while both are at much larger magnitudes compared to the (mix) results. It would be interesting to perform experiments for gold-nanofluids as well as broaden molecular dynamics computations of theromophysical properties of many other useful nanofluids.

1. Introduction

Continuum description of nanofluids [1], following the formalisms of Bird, et al. [2] is applied to the Rayleigh-Stokes approximation of developing boundary layers [3] in an attempt to explain the high heat transfer enhancement observed [4],[5] in the entrance region of tubes and channels at small nanoparticle volume fraction. The present paper considers the full boundary layer problem accompanied by the perturbation procedure for small volume fraction. The zeroth order problem is the known Blasius momentum and Pohlhausen heat transfer problems. The first order perturbation velocity and temperature functions are transformed to similarity form using the Blasius similarity variable. Lead by way of the Rayleigh-Stokes solution [3], we identify the competing roles played by enhanced thermal conductivity and by inertia and obtain surface heat transfer rates and skin friction for alumina (mix) and compared to experiments [4],[5]; and using (mix) and (MD) properties for gold nanofluid and compare the heat transfer and skin friction results from both.

2. The case for zero nanoparticle volume flux at solid wall

In the zero wall flux case, according to the volume flux diffusion equation in absence of thermal diffusion and zero sources in the interior, the volume fraction is constant and equal to that in the free stream across the entire boundary layer. The first order momentum and thermal energy equations simplify to, in similarity variable the forms,

$$f_1''' + \frac{1}{2}(f_0 f_1'' + f_1 f_0'') = \left((\mu^*)'_{\phi=0} - (\rho^*)'_{\phi=0}\right)\frac{1}{2} f_0 f_0''$$

$$f_1(0) = f_1'(0) = 0,\ f_1'(\infty) = 0$$

and

$$\theta_1'' + \frac{\mathrm{Pr}_f}{2}(f_0\theta_1' + f_1\theta_0') = \left((k^*)'_{\phi=0} - (\rho^* c^*)'_{\phi=0}\right)\frac{\mathrm{Pr}_f}{2} f_0\theta_0'$$

$$\theta_1(0) = \theta_1(\infty) = 0$$

where Pr_f is the base fluid Prandtl number; f_1 , θ_1 are the respective first order stream and temperature functions similar to that of the respective zeroth Blasius and Pohlhausen functions denoted by subscript 0. Rescaling the streamfunction $F_1 = f_1 \Big/ \left((\mu^*)'_{\phi=0} - (\rho^*)'_{\phi=0}\right)$,

$$F_1''' + \frac{1}{2}(f_0 F_1'' + F_1 f_0'') = \frac{1}{2} f_0 f_0''$$

$$F_1(0) = F_1'(0) = 0,\ F_1'(\infty) = 0$$

which now can be solved as a "universal function" independent of thermophysical properties.

The thermophysical properties, in dimensionless form, normalized by that of the base fluid is written as linear functions of the volume fraction, with the slopes denoted by primed quantities at zero volume fraction

$$\rho^* = \rho/\rho_f = 1 + \phi_\infty (\rho^*)'_{\phi=0}\Phi_1 + \vartheta(\phi_\infty^2)$$

$$\rho^* c^* = \rho c/\rho_f c_f = 1 + \phi_\infty (\rho^* c^*)'_{\phi=0}\Phi_1 + \vartheta(\phi_\infty^2)$$

$$\mu^* = \mu/\mu_f = 1 + \phi_\infty (\mu^*)'_{\phi=0}\Phi_1 + \vartheta(\phi_\infty^2)$$

$$k^* = k/k_f = 1 + \phi_\infty (k^*)'_{\phi=0}\Phi_1 + \vartheta(\phi_\infty^2)$$

Two property cases are calculated for comparisons: one for alumina and the use of (mix) properties for the nanofluid density and heat capacity and transport properties prevalently used in the literature attributed to Einstein and to Maxwell [6], [7], and measured in [4]. Experiments in the entrance region for alumina Wen & Ding [6] and Jung, et al. [7] are available for comparison,

but no molecular dynamics property results are available. The second is for gold nanofluids, for which (mix) and prevalently used transport properties as basis for comparison with recent molecular dynamics property results [8], [9]:

Alumina(mix): $(\rho^*)'_{\phi=0,mix} = 2.89$, $(\rho^* c^*)'_{\phi=0,mix} = -0.18$,
$(\mu^*)'_{\phi=0,Einstein} = 2.5$, $(k^*)'_{\phi=0,W\&D} \cong 6$

Gold/Water(mix): $(\rho^*)'_{\phi=0,mix} = 18.3$, $(\rho^* c^*)'_{\phi=0,mix} = -0.40$,
$(\mu^*)'_{\phi=0,Einstein} = 2.5$, $(k^*)'_{\phi=0,Maxwell} = 3$

Gold/Water(MD): $(\rho^*)'_{\phi=0,MD} = 18.7$, $(\rho^* c^*)'_{\phi=0,MD} \cong -2.37$,
$(\mu^*)'_{\phi=0,MD} = 10$, $(k^*)'_{\phi=0,MD} = 20$.

Subscripts W&D refer to measurements of Wen & Ding [6]. The molecular dynamics results used in estimating the viscosity and thermal conductivity are found in [8].

The profile functions of the velocity and temperature are solved for the above parameters and will be fully discussed at MNF2016 (due to limit of space here). We concentrate on the heat transfer and skin friction enhancement results here. Denoting the wall condition by the subscript 0, the Newtonian shear stress at the wall is

$$\tau_0 = \left(\mu \frac{\partial u}{\partial y}\right)_0 = \mu_f \mu_0^* u_\infty \sqrt{u_\infty / \nu_f x}\, f''(0)$$

Inserting the perturbation representations, to first order in ϕ_∞, the ratio of nanofluid shear stress enhancement to that of base fluid is

$$\tau^* - 1 = \phi_\infty \left[(\mu^*)'_{\phi=0} + f_1''(0)/f_0''(0)\right] = \phi_\infty (\tau^*)'_{\phi=0}$$

where $\tau^* = \tau_0 / \tau_{0,f}$ and the base fluid shear stress is $\tau_{0,f} = \mu_f u_\infty \sqrt{u_\infty / \nu_f x}\, f_0''(0)$. The slope $(\tau^*)'_{\phi=0}$ requires the input of transport property and the solution of the boundary layer similarity solutions up to the first order.

The general surface heat transfer rate at the wall would include the heat transfer owing to diffusion currents

$$q_0 = -\left(k \frac{\partial T}{\partial y}\right)_0 - \left(\rho_p D \frac{\partial \phi}{\partial y} h_p\right)_0$$

For a solid wall for which there is zero flux of nanoparticles across the wall, the solution is $\Phi_1 = \phi / \phi_\infty = 1$ throughout the diffusion layer. The heat transfer at the wall is thus accomplished by heat conduction alone. Using the representation of nanofluid thermal conductivity and the perturbation representations, we obtain the enhanced the heat transfer rate relative to the base fluid, to first order in ϕ_∞

$$q^* - 1 = \phi_\infty \left[(k^*)'_0 + \theta_1'(0)/\theta_0'(0)\right] = \phi_\infty (q^*)'_{\phi=0}$$

where the surface heat transfer rate is normalized by that of the base fluid

$$q^* = q_0 / q_{0,f},\ q_{0,f} = k_f (T_0 - T_\infty)\theta_0'(0)\sqrt{u_\infty / \nu_f x}$$

The results in the rise in shear stress and hear transfer enhancement are presented in the following table, for the three cases discussed.

	alumina(mix)	gold/water(mix)	gold/water (MD)
$(q^*)'_{\phi=0}$	3.98	4.44	13.90
$(\tau^*)'_{\phi=0}$	2.70	10.40	14.35

The detailed comparison with experiments in alumina [4],[5], which will be shown and discussed at the conference, indicate that the mixture and "conventional" thermophysical properties consistently underestimates the heat transfer enhancement from that of experiments. (MD calculation of thermophysical properties for alumina is not available). Although there are no experiments performed with gold nanoparticles, there exist (MD) calculations [8],[9] of properties. The results here indicate that mixture approach and conventional use of Einstein and Maxwell viscosity and thermal conductivity relations considerably underestimates the skin friction rise and enhanced heat transfer compared to molecular dynamics results for thermophysical properties, as the slopes in the above table indicate. Use of molecular dynamics approach to thermophysical properties results in appreciably enhanced heat transfer and skin friction but they are at the same relative level of enhancement.

3. Concluding remarks

It is found that the use of molecular dynamics properties considerably increased the heat transfer enhancement relative to results using "conventional" properties. Furthermore, heat transfer enhancement is comparable to the enhanced skin friction rise, whereas using conventionally obtained properties the enhanced skin friction rise is ominously larger than the heat transfer enhanced for gold nanoparticles. To fully appreciate the potential in the use of nanofluids in heat transfer enhancement, further molecular dynamics computations of properties of nanofluids, including transport properties, accompanied by careful laboratory experiments on velocity and temperature profiles are unavoidable.

References

[1] J. Buongiorno, Convective transport in nanofluids. ASME Journal Heat Transfer, Volume 128, 240-250 (2006) (doi:10.1063/1.3245330)

[2] R.B. Bird, W.E. Stewart, and E.N. Lightfoot, Transport Phenomena, 2nd edn. Hoboken, N.J.:Wiley. (2001)

[3] J.T.C. Liu, On the anomalous laminar heat transfer intensification in developing region of nanofluid flow in channels or tubes. Proceedings of the Royal Society A, Volume 468, 2383-2398 (2012) (doi: 10.1098/rspa.2011.0671)

[4] D. Wen and Y. Ding, Experimental investigation into convective heat transfer of nanofluids at the entrance region under laminar flow conditions. International Journal of Heat and Mass Transfer, Volume 47, 5181-5188 (2004) (doi:10.1016/j.ijheatmasstransfer.2004.07.012)

[5] J.-Y. Jung, H.-S. Oh and H.-Y. Kwak, Forced convective heat transfer of nanofluids in microchannels. International Journal of Heat and Mass Transfer, Volume 52, 466-472 (2009) (doi:10.1016/j.ijheatmasstransfer.2008.03.033)

[6] J. Buongiorno, et al., A benchmark study on the thermal conductivity of nanofluids. Journal of Applied Physics, Volume 106, 094312 (2009) (doi:10.1063/1.3245330)

[7] D.C. Venerus, Viscosity measurements on colloidal dispersions (nanofluids) for heat transfer applications. Applied Rheology, Volume 20, 44582-1 - 44582-7 (2010)

[8] Puliti, G. Properties of Gold-Water Nanofluids Using Molecular Dynamics. PhD Thesis, Univ. Notre Dame (2012)

[9] S. Paolucci and G. Puliti, Properties of nanofluids. Heat Transfer Enhancement with Nanofluids (V. Bianco, O. Manca, S. Nardini and K. Vafai, Eds.) N.Y.: CRC. Pp. 1-44 (2015)

ID 27

5th Micro and Nano Flows Conference
Milan, Italy, 11-14 September 2016

Light actuated micro droplet ejection for 3D printing

Paul Delrot [1], Christophe Moser [*1]

* Corresponding author: Tel.: ++41 (0)21 693 6110; Email: Christophe.moser@epfl.ch
[1] Laboratory of Applied Photonics Devices, MicroEngineering Department, Ecole Polytechnique Fédérale de Lausanne, Switzerland

Keywords: Micro-droplets, Capillary, Light actuation, 3D printing, Bubbles

We investigate light actuated micro droplet ejection from a capillary as a mean to 3D print high-resolution transparent structures. This is accomplished by focusing light from a pulsed nanosecond laser in a liquid-filled glass capillary. The acoustic wave generated is able to eject droplets thanks to a flow-focusing phenomenon [1]. This effect was shown by a Dutch group in 2012 for the generation of highly focused supersonic jets [2]. Here, this technique was implemented for the generation of low-velocity micro-droplets of low and high viscosity (0.6-148 mPa.s). We investigated parameters such as the viscosity of the fluid, the capillary diameter, the meniscus contact angle and the pulse energy on the ejection speed, the droplet(s) size and the printing accuracy.
Several ejection regimes were demonstrated depending on the pulse energy and liquid viscosity. Single micro-droplets of photopolymer inks were generated with a diameter less than 20% that of the nozzle for the least viscous liquid. Two-dimensional patterns were printed with a good controllability and consequently cured, which opens up new possibilities for the additive manufacturing of microstructures.

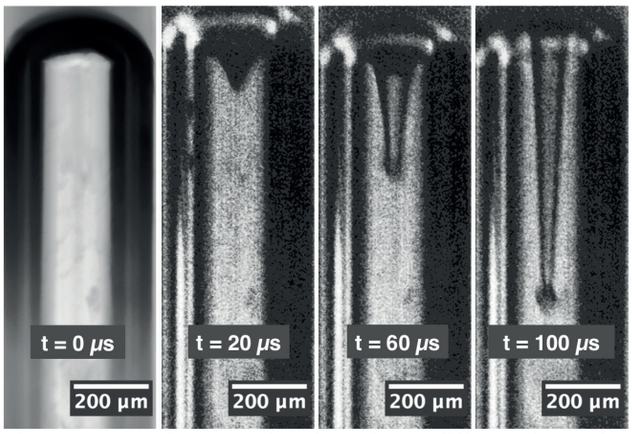

Figure 1 – Droplet generation dynamics at different times after laser firing, the capillary walls corresponds to the lateral sides of each picture.

References

[1] I. R. Peters, Y. Tagawa, N. Oudalov, C. Sun, A. Prosperetti, D. Lohse, and D. van der Meer, "Highly focused supersonic microjets: numerical simulations," *Journal of Fluid Mechanics*, vol. 719, pp. 587–605, Mar. 2013.

[2] Y. Tagawa, N. Oudalov, C. W. Visser, I. R. Peters, D. van der Meer, C. Sun, A. Prosperetti, and D. Lohse, "Highly Focused Supersonic Microjets," *Phys. Rev. X*, vol. 2, no. 3, p. 031002, Jul. 2012.

5th Micro and Nano Flows Conference
Milan, Italy, 11-14 September 2016

Enhancement of Heat Transfer Characteristics of Microchannel Heat Sink with Micro-Ribs to Induce Longitudinal Vortices

Jen-Chieh Cheng, Yeong-Ley Tsay*, Xin-Xian Dong and Zih-Cian Yan

* Corresponding author: Tel.: +886-958196676; Fax: +886-5-6312415; Email: yltsay@nfu.edu.tw
Department of Aeronautical Engineering, National Formosa University, Yunlin 63208, Taiwan

Keywords: Microchannel, Micro-ribs, Longitudinal vortex, Heat transfer

The heat flux of integrated chips has become more and more vast due to the requirements of increasing output power and decreasing volume for the chips. If the heat flux can not be removed effectively, the temperature of electric chip would rise to relatively high, and consequently reduce the performance of respective systems. The microchannel heat sink is considered to be the one of effective methods for the electric chip cooling. The main purpose of this study is to investigate the cooling performance enhancement for the microchannel heat sink by utilizing longitudinal vortex generator.

The physical system under consideration is a 10 mm x 10 mm x 1 mm silicon substrate. The microchannels in the substrate have a width of 142 μm and a height of 500 μm. The bottom surface of heat sink is subjected to constant heat flux. Liquid water is used as the coolant. The inclined ribs with 50 μm in thickness are designed onto the channel walls to induce the longitudinal vortices for the liquid water flow. The governing equations with the associated boundary conditions for the conjugate conduction-forced convection heat transfer in silicon-based microchannel heat sink are solved by the QUICK and SIMPLE techniques. The numerical simulation is rigorously performed. The effects of grid arrangement are carefully verified. In addition, the results of limiting cases without vortex generator are validated with available results of relevant articles. Through these program tests, the proposed numerical scheme is considered to be appropriate for the present study.

Figure 1 represents the variations of the three-dimensional path lines in the microchannels for the cases without and with ribs. A comparison on the path lines in Figs. 1（a）－（c）reveals that the ribs could induce helical-shaped advective motion in the main stream flowing direction. Figure 2 shows effects of different configuration and number of ribs on the hot spot temperatures of heat sink. It is noted that, for the case with ribs on both bottom and up channel walls, the maximum reduction in hot spot temperature of thy system could be up to 41 %.

This study investigate numerically the heat transfer enhancement of microchannel heat sink by constructing ribs onto channel walls. The results indicate that the 45° ribs could induce strongly the longitudinal vortices. The heat transfer enhancement is more effective for situation with ribs on bottom channel wall as N ＜20. While it becomes better for situation with ribs both on bottom and up channel walls as N ＞20. The maximum reduction in hot spot temperature can be up to 41 %.

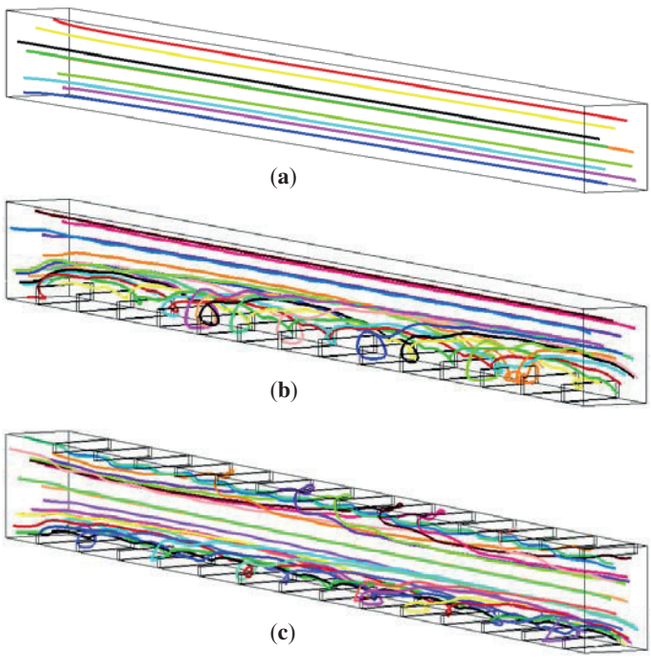

Fig. 1. Distributions of path lines, （a）without rib, （b）ribs on bottom channel wall, （c）ribs on bottom and up channel walls.

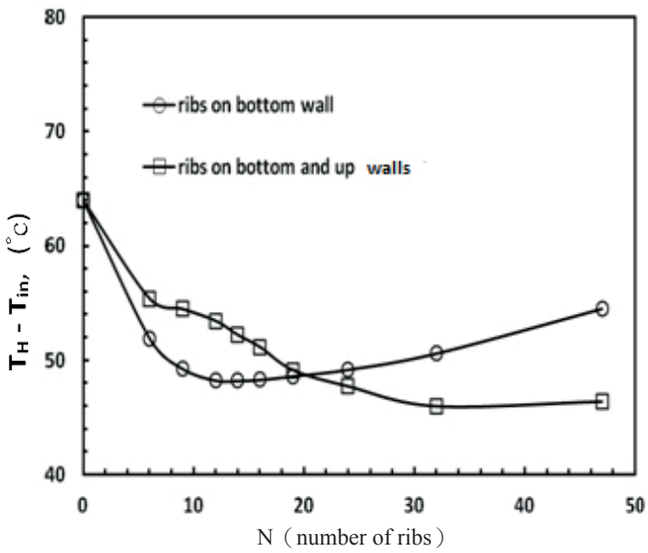

Fig. 2. Variations of hot spot temperatures for cases with different rib numbers.

5th Micro and Nano Flows Conference
Milan, Italy, 11-14 September 2016

Flow mixing and dispersion phenomena in lung-inspired microfluidic structures

Rami Fishler[1] and Josué Sznitman[1,*]

* Corresponding author: Tel.: +972(4)8295678; Email: sznitman@bm.technion.ac.il
Department of Biomedical Engineering, Technion - Istrael Institute of Technology, Haifa, Israel.

Keywords: convective mixing, lung flows, dispersion phenomena, wall motions, pumping, tree structures

Respiratory flows in the deep sub-millimeter alveolated regions of the lungs are widely acknowledged to give rise to irreversibility as a result of convective mixing that occurs between residual and inhaled air [1]. Seminal flow visualizations in excised rats [2] have qualitatively revealed the existence of recirculating, vortex-like flows inside alveoli and the ensuing stretch-and-fold flow patterns characteristic of chaotic mixing phenomena at low Reynolds number (Re~10^{-3} to 1). Despite such progress, *in situ* experiments remain not only delicate to conduct in real lungs, they have also come short of providing robust and quantitative experimental platforms for time-resolved acinar flow diagnostics.

Pumping-like flow phenomena in the pulmonary acinus resulting from breathing motions have been widely studied in numerical models, with geometries ranging from single alveoli [3] and alveolated ducts [4] to more complex bifurcating tree structures [5]. In contrast, few if any experimental setups have addressed the mixing characteristics of such physiological processes directly at the acinar scale. To explore the underlying mechanisms governing convective acinar mixing, we have leveraged modern microfabrication capabilities to devise some of the first biomimetically-inspired prototypes of pulmonary acinar networks at true scale using microfluidics [6, 7]. In particular, to better understand and characterize the nature of such irreversible low Reynold number flows of the lung depths, and thereby possibly harness their mixing capabilities for microfluidic devices, we experimentally study hydrodynamic dispersion phenomena inside microfluidic acinar tree structures consisting of alveolated ducts (Fig. 1). At the heart of the matter, we investigate how the coupling between alveolated channel networks and intrinsic, yet inhomogeneous (i.e. not self-similar), wall motions govern net convective mixing over cumulative breathing cycles.

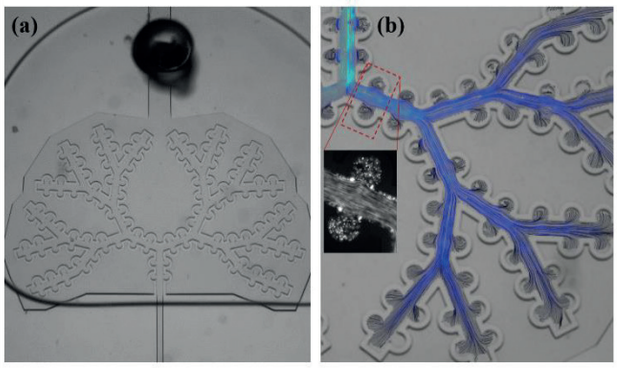

Figure 1: Microfluidic model of acinar airways. The breathing tree is constructed of thin and elastic PDMS walls that separate the alveolated airways from the surrounding chambers (side and top). Walls are periodically deformed by changing the pressure within the chambers. (b) Instantaneous flow visualization in branches (qualitative color-coding according to flow magnitude from cool to dark). Inset: fluorescent particles within alveoli and the duct. In (a) and (b) ducts are ~120 um wide.

Our microfluidic devices are constructed of thin, flexible elastomer (i.e. PDMS) walls where acinar channels are cyclically deformed by altering the pressure inside liquid-filled chambers that surround the top and sides of the branching structure (Fig. 1a). In turn, devices are capable of rhythmically pumping fluid into and out of the channels that mimic respiratory breathing motions (i.e. frequency, volume displacements, etc.). At the individual alveolar scale, quantitative flow visualization (Fig. 1b) is first performed by tracking over multiple flow cycles liquid-suspended fluorescent polystyrene tracer micro-particles using fluorescent microscopy. Irreversible flow phenomena are then investigated by tracking Lagrangian particle trajectories, and constructing mean velocity maps that correspond to the distance between the initial and final position of each particle during a full flow cycle [3]; such information coincides with the net convective drift the fluid will experience as a result of convective mixing In a next step, we assess the extent of dispersion on the scale of the branching network by tracking a bolus of seeded particles that originates initially from a narrow zone near the first generation of the device [4]. Finally, we demonstrate the applicability of such bifurcating tree structures for micromixing applications by sequentially feeding the device with fluorescent beads of two different colors.

1. Sznitman J. Respiratory microflows in the pulmonary acinus. (2013) *J. Biomech.* 46: 284-298.
2. Tsuda *et al.* (2002) Chaotic mixing deep in the lung. *PNAS* 99: 10173-10178.
3. Kumar *et al.* (2011) Steady streaming: a key mixing mechanism in low-Reynolds-number acinar flows. *Phys Fluids* 23: 041902.
4. Hofemeier *et al.* (2014) The role of respiratory flow asynchrony on convective mixing in the pulmonary acinus. *Fluid Dynamics Research* 46: 041407.
5. Ma and Darquenne (2012) Aerosol bolus dispersion in acinar airways—influence of gravity and airway asymmetry. *J. Applied Physiology* 113: 442-450.
6. Fishler *et al.* (2013). Acinus-on-chip: a microfluidic platform for pulmonary acinar flows. *J. Biomech.* 46: 2817-2823.
7. Fishler *et al.* (2015). Particle dynamics and deposition in true-scale pulmonary acinar models. *Sci. Rep.* 5: 14071.

5th Micro and Nano Flows Conference
Milan, Italy, 11-14 September 2016

Characteristics of Red Blood Cell Perfusion in Microfluidic Models of Pulmonary Capillary Networks

Hagit STAUBER[1,*], Dan WAISMAN[2,3], and Josué SZNITMAN[1]

* Corresponding author: Tel.: +972 (0)77 8871876; Fax: +972 (0)4 8294599; Email: stauber@campus.technion.ac.il
1: Department of Biomedical Engineering, Technion- Israel Institute of Technology, Haifa, Israel
2: Department of Neonatology, Carmel Medical Center, Haifa, Israel
3: Faculty of Medicine, – Technion- Israel Institute of Technology Haifa, Israel

Keywords: Microfluidics, Red Blood Cells, Blood Perfusion, Pulmonary Capillaries, Microcirculation

Blood is a biphasic fluid, composed of plasma and cells, mainly red blood cells (RBCs) that constitute ~99% of the cell phase. Given their high deformability, both the shape and transport of RBCs are influenced by the scale and morphology of the blood vessels in which they flow. Most noticeably, in the microcirculation where vessels are <300 µm in diameter, the migration of RBCs to the vessel center leads to a cell-free layer near the wall; a phenomenon known as the *Fahraeus-Lindqvist* effect [1]. Other examples include the *pathway effect* in arterioles where the redistribution of RBCs at bifurcations gives rise to plasma skimming and cell screening in daughter vessels [2]. In the smallest capillaries (~5 µm wide), RBCs are known to flow in a single file. Yet, in many organs, microcirculatory flows are not characterized by single isolated vessels or bifurcations solely, but rather by intricate networks that bring together the above and where the characteristic length scales for local flow remain similar to the size of a RBC.

The pulmonary capillary networks (PCNs) represent a prime example of such physiological systems; these organ-specific

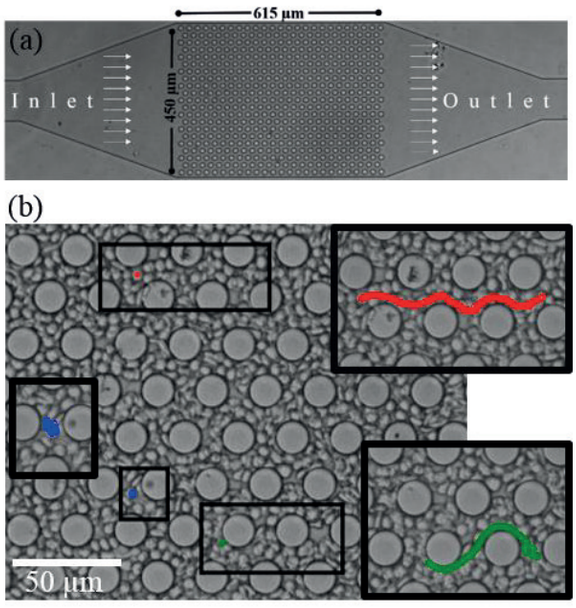

Fig.1: (a) Microfluidic sheet flow model representative of the pulmonary capillary networks (PCNs). (b) Instantaneous snapshot of RBCs flowing across networks of circular posts. Inset: Examples of representative RBC trajectories in free motion (red), partially (green) and completely trapped (blue).

capillaries wrap around the smallest units of the lungs, i.e. alveoli, with vessels that exhibit lengths and diameters of nearly the same size [3], i.e. ranging between ~3-10 µm. Seminal descriptions of such capillary flows include the classic "sheet flow model" [4], where PCNs are constructed of repeating lattices made of posts and capillary flow exists in the area available between them. Early investigations, however, have been limited to scaled-up experimental setups using Newtonian fluids, and thus came short of capturing physiological dynamics of RBCs in such micro-networks.

With the advent of microfluidics, we revisit in experiments the original “sheet flow model” to bridge our understanding of RBC perfusion dynamics in anatomically-inspired models of PCNs, at one-to-one scale. Our microfluidic devices (Fig. 1a) are composed of a base lattice with inter-distances between posts in the range of ~5-10 µm and where the entire lattice extends over a surface area capturing ~2-5 alveoli. Using a pressure-driven setup and high-speed image acquisition, we investigate the characteristics of RBC perfusion across such networks. Specifically, we implement tracking velocimetry techniques to extract Lagrangian data on their motion and trajectories, including instantaneous velocities (Fig. 1b). Together, such measurements let us construct a statistical description of RBC perfusion directly at the microscale as well as information regarding RBC dispersion through the networks. In addition, we investigate the relationship between pressure drop and bulk RBC flow, as a function of the network porosity (i.e. dependent on the size of the lattice and interspaces).

Overall, our efforts are aimed at establishing a robust yet attractive *in vitro* platform to deliver physiologically-inspired true-scale quantitative characteristics of the pulmonary ACN microcirculation.

---

[1] R. Fåhræus and T. Lindqvist, The viscosity of the blood in narrow capillary tubes, *Am. J. Physiol. -- Leg. Content*, vol. 96, no. 3, pp. 562–568, 1931.

[2] A. R. Pries, T. W. Secomb, and P. Gaehtgens, Biophysical aspects of blood flow in the microvasculature, *Cardiovasc. Res.*, vol. 32, no. 4, pp. 654–667, Oct. 1996.

[3] F. Y. Zhuang, M. R. T. Yen, Y. C. Fung, and S. S. Sobin, How many pulmonary alveoli are supplied by a single arteriole and drained by a single venule? *Microvasc. Res.*, vol. 29, no. 1, pp. 18–31, 1985.

[4] Y. C. Fung and S. S. Sobin, Theory of sheet flow in lung alveoli, *J. Appl. Physiol.*, vol. 26, no. 4, pp. 472–488, 1969.

5th Micro and Nano Flows Conference
Milan, Italy, 11-14 September 2016

Wall Shear Stress Measurement in Micro-channel

Zhaohui YAO*, Pengfei HAO, Qiming GE

* Corresponding author: Tel.: ++86 (10)6277 2558; Email: yaozh@tsinghua.edu.cn
Department of Engineering Mechanics, Tsinghua University, Beijing, 100084, China

Keywords: Micro-channel; Shear Stress; Sensor; Compressibility

A micro sensor based on heat transfer principles that can measure the wall shear stress inside the micro channel is designed and fabricated by using silicon micromachining techniques. Calibration of the wall shear stress sensor was conducted and the wall shear stress measurements of the air flow in micro-channel under various pressure differences were performed. The experimental results demonstrated that the gas compressibility cannot be ignored in the micro channel even for low speed of the gas flow, which is quite different from the gas flow in the normal scale.

1 Introduction

The micro-electro-mechanical-system (MEMS)-based shear stress sensor emerged with the development of photolithographic techniques. Compared with the conventional thermal shear-stress sensor, MEMS-based thermal shear sensors are miniaturized (~200 μm in dimensions) to allow maximal spatial resolution, minimal power consumption and negligible flow interference, and they can be batch-fabricated inexpensively [1-3].

However, the previous shear stress sensors are usually used for external flow field measurements. In the present work, a micro sensor based on heat transfer principles that can measure shear stress inside a micro channel is designed and fabricated by using silicon micromachining techniques.

2 Operating Principles

The thermal sensor benefits from the fact that the heat transfer from a sufficiently small heated surface depends only on the flow characteristics in the viscous region of the boundary layer.

The rate of heat loss from a thermal film to the surrounding flow depends on the velocity profile in the boundary layer, so the flow shear stress can be deduced from the heat loss rate of the thermal film. The thermal film is connected in an arm of an electric bridge, so the heat loss rate of the thermal film can be known by measuring its electric resistance change. In this paper, the wall shear stress in a micro channel is obtained from the electric resistance change of the thermal film.

Under ohmic heating, the input power is related to the driving current and the sensor electric resistance. One part of the input power is transferred to the flow and the rest is lost through the substrate, the balance equation is expressed as [2]

$$i^2 R / \Delta T = A\tau^{1/3} + B \quad (1)$$

where i is the driving current through the thermal film and R is its electric resistance (Thus i2R stands for the input power.), ΔT is the temperature difference between the thermal film and the flow, and τ is the shear stress above the thermal film. A and B are two constants that need to be calibrated through experiments.

3 Fabrication and Testing

The fabrication of the micro-channel is based on silicon micromachining techniques which are categorized into bulk micromachining and surface micromachining [4]. The micro-channel carrying shear stress sensor involved in this paper is fabricated by using this combined method.

The micromachining fabrication process is illustrated in Figure 1. The material includes a 350-micron thick silicon wafer and Pyrex. First, a 100-nanometer silicon oxide layer is grown on the silicon wafer as a stress relieving layer (Figure 2.a). Second, a 150-nanometer silicon nitride layer is deposited by low temperature chemical vapor deposition (LTCVD) (Figure 2.b). This silicon nitride layer acts as a barrier layer for bulk etching due to its low etching rate in KOH. Third, the location and shape of the micro channel is defined on the front face of the wafer by photolithography and then etched by inductively coupled plasma (ICP) (Figure 2.c). Fourth, the ends of the micro channel are etched on the back side of the wafer by KOH anisotropic etching to form the entrance and exit for working media (Figure. 2.d). The etching is performed in 33wt% KOH solutions at 850C. Ultrasonic waves are added to the bath continuously. Their power and duration depend on the thickness and adulteration of the wafer. Last, a Ti/Pt (300A/2000A) film is sputtered on the Pyrex and then the Pyrex is packaged with the silicon wafer by using anodic bonding. The micro channel fabricated in this paper is 4 centimeter long, 1000 microns wide and 8 microns high. The thermal film is 15 microns wide, 2300 angstroms thick and 800 microns long. It is made of Ti/Pt alloy.

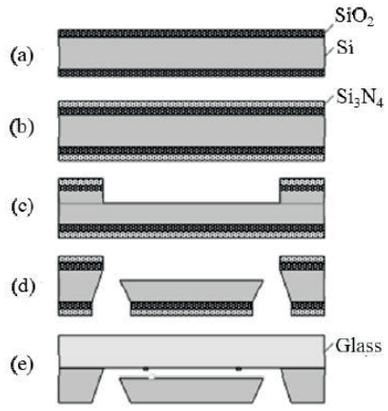

Figure 1 Micromachining fabrication process of micro channel carrying shear stress sensor

The heat-insulating property of the shear stress sensor is evaluated. Results of voltage-current (V-I) measurements conducted in still air are obtained. In the present work, the temperature coefficient of resistance (TCR) was obtained by heating the sensor silicon wafer in a water tank in which the temperature can be adjusted and maintained to be constant. To obtain TCR, we use the relation that $R=R_0(1+\alpha(T-T_0))$ to fit the data where α is the TCR. Here reference temperature T_0 is 0 ºC. A resistor has a typical positive TCR value of approximately 0.206%/ºC. Furthermore, using the data from V-I curves and the known TCR of the resistors, we can deduce the relationship between resistor temperature and power inputs.

The time constant can be determined by superimposing a small signal into the Et terminal of the circuit. When a step current passes through the resistor, the transient voltage response is used to

deduce the time constant. Using constant current mode circuit, the measured time constant of the shear stress sensor is on the order of several hundred microseconds. Figure 2 exhibits the results under various overheat ratios. Overheat ratio is an important parameter for the operation of a thermal-principle-based WSS sensor. Because of self-heating, a sensing element has a greater working temperature (T) than ambient (T_0). The temperature overheat ratio, α_T, is defined by $\alpha_T=(T-T_0)/T_0$. Figure 2 indicates that the shear stress sensor in this work has a time constant of nearly 400μs. That is, the response frequency is 2.5 kHz. In this work, the time averaged shear stress is studied. Thus this time constant can meet the experimental requirements.

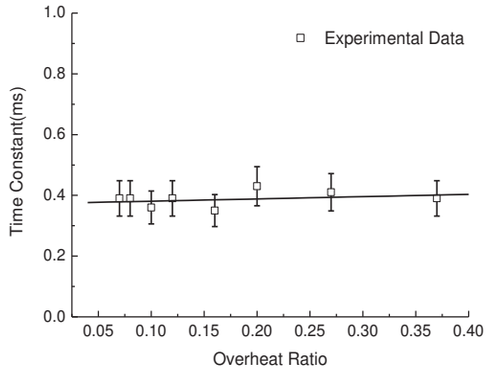

Figure 3. Time constant of shear stress sensor under various overheat ratios

In the experiment, the resistance of the thermal film is about 70Ω. According to the maximum work temperature (370K) and the frequency bandwidth (100 kHz) of the circuit, the voltage output by the heat noise is about 0.38μV, so the heat noise can be ignored in the experiment.

4 Experiment, Calibration and Discussion

The measurement set-up for shear stress in micro channels is presented in Figure 3.

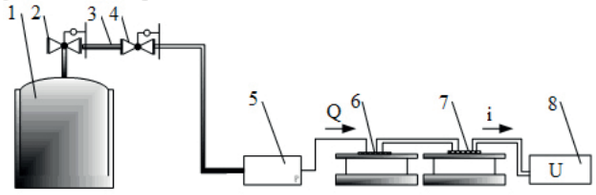

1. Air Chamber
2. Filter & relief valve I
3. Pipeline
4. Filter & relief valve II
5. Manometer
6. Silicon wafer with microchannels
7. Printed circuit board
8. Thermal decoder

Figure 3 Measurement set-up for micro channel

In this set-up, the thermal film is working at the overheat ratio of 0.37 and the pressure differences between inlet and outlet range from 10kPa to 400kPa. Since the flow characteristics in a micro channel exhibit incompressibility under low pressure differences, the coefficients A and B in equation (1) are calibrated by the theoretical solution [5] of incompressible flow on a rectangular cross-section with the inlet and outlet pressure differences under 50kPa. In the calibration, first the voltages V on the thermal film at different inlet and outlet pressure differences are measured, then the currents I, resistances R, and temperature differences ΔT are obtained. By the wall shear stress equation and balance equation, the coefficients A and B in equation (2) are found to be 26.56×10^{-3} and 3.24×10^{-3}, respectively.

Shear stress with the pressure differences ranging between 50kPa to 400kPa is obtained by equation (1) with the calibrated coefficients and the voltages on the thermal film. Figure 4 shows the experimental results compared with the theoretical data and simulated data. The dash line stands for the incompressible theoretical solutions, the red star for the experimental results, and the solid line is for the results of simulation which three-dimensional (3D) compressible Navier-Stokes equations were employed for the above micro-channel. Under lower pressure differences (especially <50kPa), the wall shear stress exhibits a linear increment. This validates the calibrating method used in the present work. Under higher pressure differences, however, both results of the simulation and the experiment indicate that the wall shear stress gradually deviates from the incompressible theoretical solutions as the pressure difference increases. The relationship between the wall shear stresses and pressure differences is no longer linear under high pressure differences and the flow field in a micro channel appears compressible. The experimental results are coincided with the 3D compressible simulation results and reveal these compressible phenomena. It verified the reliability of our developed micro wall shear stress sensor.

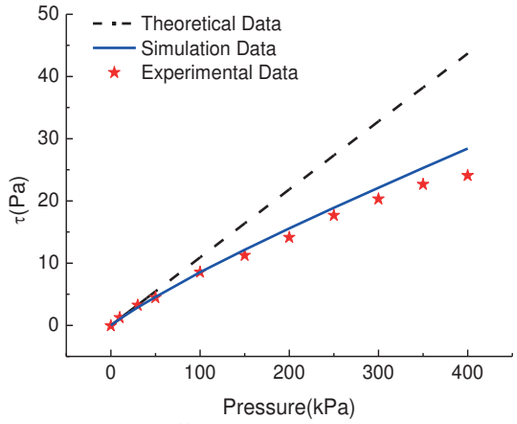

Figure 4. Pressure difference vs. wall shear stress (Measurement point at 1.2cm from entrance)

5 Conclusions

Measurement of shear stress in micro scale is a challenge task due to the small size and energy consumption. In this paper, a micro sensor that can be used to measure the wall shear stress in a micro channel has been developed. The sensor is set up on the bottom of a micro channel and operates on heat transfer principles. Calibration has been conducted and wall shear stress versus pressure difference in micro-channel has been measured. The experimental result of the wall shear stress in the micro channel demonstrates that in a micro channel, compressibility cannot be ignored even for low speed gas, which is quite different from the situation in a normal scale flow. Moreover, this type of the shear stress sensor can be fabricated in the other micro-fluidic systems to measure the internal flow field in the micro-fluidics.

Acknowledgments

The project was supported by the National Science Foundation of China with grant number 11272176.

References

[1] N. J. Allen, D. B. Sims-Williams and D. Wood, J. Micromech. Microeng., 2012, 22, 074007.
[2] A. N. Menendez, B. R. Ramaprian,. J. Fluid Mech., 1985, 161:139-159.
[3] V. Lijo, H. D. Kim, T. Setoguchi, Int. J. of Heat and Mass Transfer, 2012,55(4), 701-709.
[4] J. B. Huang, F. K. Jiang, Y. C. Tai, C.M. Ho, Measurement Science and Technology, 1999,10(8): 687-696.
[5] F. M. White, Viscous Fluid Flow, 3rd ed., McGraw-Hill, New York 2006

5th Micro and Nano Flows Conference
Milan, Italy, 11-14 September 2016

Highly Deformable Hydrogel Nanofilaments in Poiseuille Flow

Sylwia PAWŁOWSKA*, Paweł NAKIELSKI, Filippo PIERINI, Krzysztof ZEMBRZYCKI, Tomasz Aleksander KOWALEWSKI

* Corresponding author: Tel.: +48 22 826 12 81 ext. 330; Fax: +48 22 8269815; Email: spaw@ippt.pan.pl
Institute of Fundamental Technological Research, Polish Academy of Sciences, Poland

Keywords: Hydrogel Nanofilaments, Bending Dynamics, Poiseuille Flow, Electrospinning

The flow of deformable objects has non-Newtonian character, strongly influencing its short time response at microscopic level. Under the flow this objects are oriented, deformed and coiled leading to a microscopic variation of the transport properties. The microscopic structure as well as the microscopic response depends on both the nature of the suspended objects and geometry of the flow. Theoretical assumptions, especially in the field of polymer physics, use coarse-grained models to study the folding process of nucleic acids and proteins. However to describe this phenomenon on a molecular scale it is still limited to very small length and time scales. In these scales it is very difficult (or impossible) to find answers to basic questions about the potential effects of interactions or complex hydrodynamic behaviour of long biological molecules. Introduction of microscale model for elastic properties allow for precise optical measurements and the use of a simple hydrodynamic models that allow for the description of dynamic of elastic bio-objects such as DNA or protein [1-2]. Classical methods of analysing flow properties, based on general microscopic observations are not sufficient for generating quantitative data for the future modelling. In addition, it is very difficult to directly model of microbial processes that require complex molecular interactions. Migration of fibres or other long objects in Poiseuille flow is one of the fundamental problems of modern lab-on-chip thermodynamics Moreover, this is important in a variety of biological, medical and industrial contexts, such as Brownian dynamics of proteins, DNA or biological polymers, cell movement, movement of microbes or drugs delivery.

A comprehensive understanding of the dynamics of individual polymer objects is crucial for their further applications [3-4].
The present study is based on the idea that highly deformable polymeric nanofilaments, produced by electrospining technique, can easily travel in crowed environments of body fluids and biological tissues. Hydrogel nanofilaments, prepared by NIPAAm and cross-linker BIS-AAm in defined proportions, are placed in a microchannel, and then treated with a laminar flow. Geometry and dimension of nanofilaments (contour length from a few to several tens of microns and diameter around 100 nm) and mechanical properties (persistence length) are well-defined. Study of bending dynamic of nanofilaments moving in the flow is carried out using fluorescence microscope. Pulsatile flow, generated by precise micro pumps, causes the coiling and the uncoiling of the analyzed filaments. This procedure is designed to simulate intercellular flows. Study of this behavior can help to determine the impact that the conformational changes are periodic movements. In order to perform an in depth analysis the flow profile in the channel was determine.
The results are useful for the verification of the theoretical models of biological and physical phenomena responsible for the dynamics of the bending of long bio-objects (proteins, DNA). Furthermore, the obtained results help to understand the link between the microscopic structure of the very flexible nanofilaments and the macroscopic flow properties opening the possibility to design nano-objects transported by body fluids for targeted drug release or local tissue regeneration.

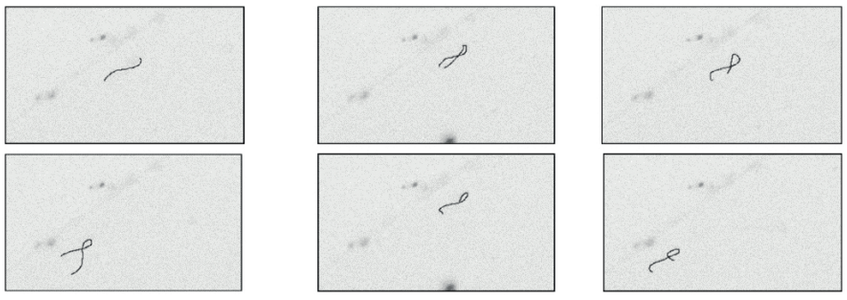

Fig.1. Sequence of image of a single flexible nanofilament (diameter 100 nm, contour length 25 μm) conveyed by Poiseuille flow.

References

[1] Nakielski, P., Pawlowska, S., Pierini, F., Liwinska, V., Hejduk, P., Zembrzycki, K., E. Zabost, E., Kowalewski, T.A., Hydrogel nanofilaments via core-shell electrospinning, *PLOS ONE* 10(6), 2015.
[2] Słowicka, A.M., Ekiel-Jeżewska, M.L., Sadlej, K., Wajnryb, E., Dynamics of fibers in a wide microchannel, *J. of Chemical Physics* 136, 044904, 2012.
[3] Sadlej, K., Wajnryb, E., Ekiel-Jezewska, M.L., Lamparska, D., Kowalewski, T.A., Dynamics of nanofibres conveyed by low Reynolds number flow in a microchannel, *Int. J. Heat Fluid Flow* 31, pp. 996–1004, 2010.
[4] Mai D.J., Brockman C., Schroeder C.M., Microfluidic systems for single DNA dynamics, *Soft Matter* 8, 10560-10572, 2012.

Project was funded by NCN grant no. 2011/03/B/ST8/05481 and NCN Preludium grant.

5th Micro and Nano Flows Conference
Milan, Italy, 11-14 September 2016

ID 36

Characterisation of microfluidic systems using optical methods at dynamic flow rates

Joerg SCHROETER [1,*], Lino DEL BIANCO [1], Christian DAMIANI, Stephan KLEIN, Bodo NESTLER [1]

* Corresponding author: Tel.: ++49 (0)451 300 5511; Fax: ++49 (0)451 300 5512; Email: joerg.schroeter@fh-luebeck.de
1 Medical Sensors and Devices Laboratory, University of Applied Sciences Luebeck, GER

Keywords: Micro Flow, Sensors, Flow Pulse, Step Response, Pumps

1 Introduction

In medical applications fast changing flows are common. Flow adjustments during infusion therapy lead to significant flow deviations. In complex flow systems, flow and concentrations of drugs are often different from expected values [1]. To control microfluidic devices or intelligent systems, suitable actuators and corresponding sensors are required. To investigate and furthermore control complex flow systems a measuring technique to characterise the dynamic limitations of conventional flow meters is required. Thermal flow meters were e.g. delivered with high sample rates. But the thermal transfer properties and the inertia of the sensor channel influence the dynamic response to a flow change. In addition, the fluidic resistance of the flow sensors often dominates a micro fluidic system. Further challenges are high dynamic flow changes with accurately defined volumes. These are generated e.g. by valves or the pulsatile portion of micro pumps. For this purpose sensors with sample rates in the range of milliseconds are needed to determine the demanded volumes.
For manufacturers of micro flow sensors and systems such as micro dosing units, analysis units (lab on chip systems) and infusion devices (drug delivery) a measurement technique will be provided, to qualify their products. The optical method should cover a wide range of clinical relevant flow rates (50 nl/ min to 2 ml/ min) and change rates up to 15 ml/s^2.

2 Methods

Thermal flow measuring methods have to be calibrated to every specific liquid and its properties (heat conductivity, heat capacity). Differential pressure sensors are inappropriate for flow measurements of liquids with different viscosities. On the other hand optical methods are independent of physical properties of the liquid. Front-tracking is a method developed to measure very low flows down to 5 nl/min [2]. The *volumetric change* inside a cylindrical geometry could be measured with high precision by monitoring the displacement of the liquid front and the related time. Two methods were applied.

- High precision capillaries (0.15 mm to 1 mm inner diameter) in combination with a telecentric lens and a high speed camera were used to examine smaller flows between 50 nl/min and 500 µl/min at sample rates up to 5 kHz (5000 fps), Figure 1. Acquisition times between 2 and 60 s are possible. Uncertainty calculations and traceable calibrations of the key components were described in [2, 3].
- The setup for larger flows consisted of a high precision glass syringe and a laser displacement sensor, Figure 2. It was used to examine flows between 100 µl/ min and 50 ml/ min at sample rates up to 49.02 kHz.

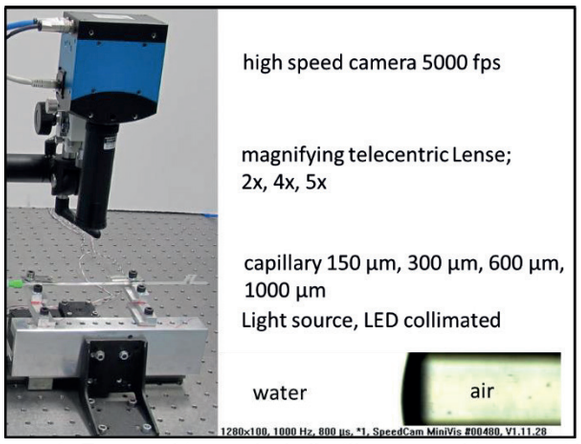

Figure 1: Front-tracking method: Capillary in combination with a high speed camera

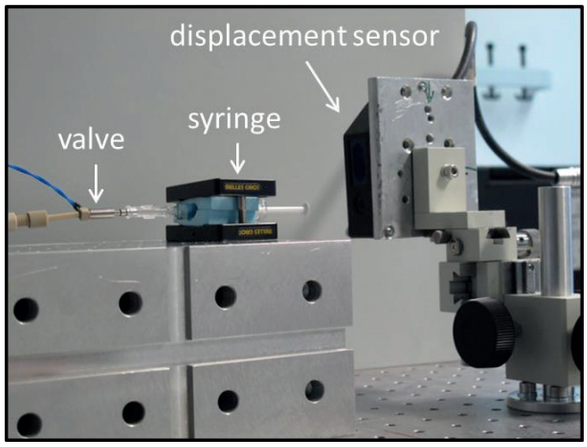

Figure 2: Front-tracking method: syringe in combination with a displacement sensor

The volumetric flow Q was determined by the displacement Δx of the liquid front during Δt and the radius R of the capillary/ syringe.

$$Q = \frac{\Delta x}{\Delta t}\,\pi\,R^2 \qquad (1)$$

3 Results

The two concepts were realised and tested. Both setups were mounted on an optical table to reduce the interference of the environment. The capillaries and syringes were calibrated. The influence of the measuring tools to the investigated flow systems were examined and characterised. The limitations of the flow meters were determined.

As applications the dynamic behaviour of different types of micro pumps, micro valves and some marketable thermal flow sensors were tested.

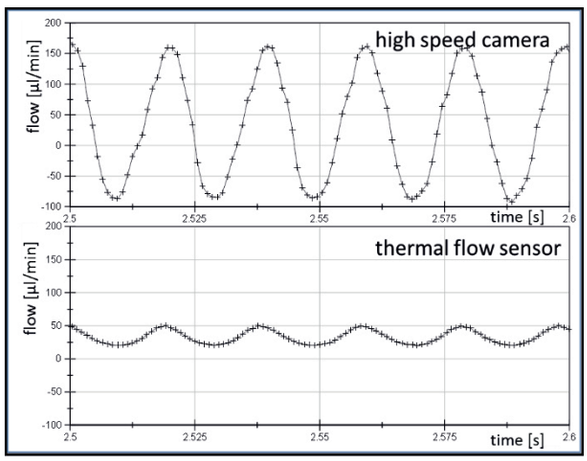

Figure 3: Volumetric flow of a piezo actuated micro membrane pump (operating frequency: f=50 Hz), measured with the optical method (top diagram) and a thermal flow sensor (bottom diagram).

For example: A piezo actuated micro membrane pump, operated at 50 Hz, was examined by connecting it to a thermal flow sensor and the first optical method (capillary and high speed camera). With the optical system an approximately harmonic flow, oscillating between -90 µl/min and 160 µl/min (250 µl/min amplitude pp) with a mean flow of 32 µl/min was measured. The thermal sensor measured a harmonic flow with the correct frequency and the same mean flow, too. Compared to the optical system, shown in Figure 3, the displayed amplitude was much lower, only 28 µl/min pp.

4 Conclusion

The presented optical flow metering methods are appropriate to characterise dynamic properties of microfluidic systems. They are also suitable to investigate the dynamic behaviour of clinical or medical devices like syringe pumps, micro pumps, implantable infusion pumps or flow sensors based on thermal- or differential pressure-methods, etc.

References

[1] R. A. Snijder, M. K. Konings, P. Lucas et al., Flow variability and its physical causes in infusion technology: a systematic review of in vitro measurement and modelling studies, Biomed ENG- Biomed Tech 2015; 60: 277-300

[2] M. Ahrens, St. Klein, B. Nestler et al., Design and uncertainty assessment of a setup for calibration of microfluidic devices down to 5 nl min^{-1}, Meas. Sci. Technol. 25 (2014) 015301

[3] M. Ahrens, B. Nestler, S. Klein, H. T. Petter and C. Damiani, An experimental setup for traceable measurement and calibration of liquid flow rates down to 5 nl/min, Biomed ENG- Biomed Tech 2015; 60: 337-345.

Nanostructured Coatings for Water/Surface Slip: A Molecular Dynamics Approach

Srinivasa B. Ramisetti [1,*], Matthew K. BORG [1], Duncan A. LOCKERBY [2], Jason M. REESE [1]

* Corresponding author: Tel.: ++44 (0)131 651 7071; Email: s.ramisetti@ed.ac.uk
1 School of Engineering, University of Edinburgh, UK
2 School of Engineering, University of Warwick, UK

Keywords: Molecular Dynamics, Slip, Skin Friction, Drag Reduction, Carbon Nanotubes, Nanofluidics

Introduction

The fundamental understanding of wetting and liquid slippage over solid surfaces is important for several engineering applications. For instance, marine coatings that produce low skin-friction could increase the fuel efficiency of ships. The role of the surface structure down to the nanoscale is important in determining the liquid slip [1]. In this work, we present the results of investigations using molecular dynamics (MD) to calculate the slip over surface coatings with different nano-structured features.

Method

Figure 1 shows an example of a typical MD simulation considered in this work; all our simulations are performed using mdFOAM [2].

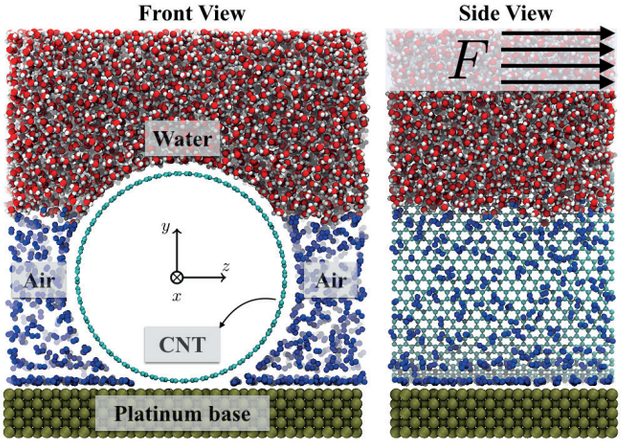

Figure 1: Simulation of water flow over a CNT and air coating on a platinum base. Left: front view, Right: side view.

A no-slip FCC platinum surface, which mimics a marine hull surface, is considered as the base surface on which a nanostructured coating is applied. Our simulations are to measure the slip length of water (at 300 K and 1 bar) over various surface coatings, relative to the base surface. While the standard approach would be to prescribe a fixed velocity at the top water layer in the simulations, we find that when dealing with surface coatings and relative slip velocity measurements it is more effective to apply a fixed shear stress. The shear stress $\tau_{xy} = 0.7$ MPa is chosen to be large enough to provide good ensemble statistics but low enough to give a linear stress/strain response. The shear stress is converted into a force F that is applied to the equations of motion of molecules within a forcing region (see Fig.1, right). When a steady-state flow is obtained, the flow velocity <v> at a reference height H from the surface is measured over 4 ns. The slip length relative to the substrate is then calculated using $\eta = \mu < v > /\tau_{xy} - H$, where μ is the dynamic viscosity of water.

Results

Our method is first validated by calculating the slip length η for the flow of water over a pristine graphene coating; when comparing our results with previous MD studies [3] we obtain a similar value of the slip length. We then test different surface coatings of single

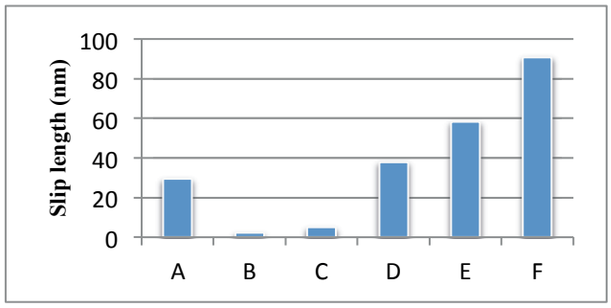

Figure 2: Slip lengths (nm) for (A) graphene, (B,C) CNT only, and (D,E,F) CNT-air coatings. CNTs of radii 0.7 nm and 2 nm are used in case B and cases C,D,E,F, respectively. D,E,F are placed in ascending order of air/water interface area.

wall carbon nanotubes (CNTs, aligned longitudinally to the water flow) on a platinum base surface, as well as introduce a nitrogen gas layer between the CNTs (see Fig. 1). While CNTs normally have low friction characteristics close to those of graphene, the interstitial gas helps to (a) reduce the overall solid-liquid interfacial interactions and (b) to shield the water from the platinum surface. The slip lengths calculated for the different cases considered in this work are shown in Fig. 2. For a CNT of 4 nm diameter, slip lengths of 90 nm and 4.9 nm are found in the Cassie and Wenzel states respectively. The slip length as a function of air/water interface area is qualitatively in agreement with other theoretical predictions [4].

Conclusion

Non-equilibrium molecular dynamics simulations are a useful tool for characterizing and comparing the slip properties of different nanostructured surface coatings. Our results for super-hydrophobic coatings of horizontally-aligned CNTs on a platinum substrate show that i) the effective slip of CNT-only coatings increases with the CNT radius and ii) the presence of trapped air pockets between the CNTs interfaces enhances the relative slip length.

References

[1] Liu et al. ACS Appl. Mater. Interfaces, 5 (18): 8907–8914, 2013.
[2] Macpherson et al. Mol. Simul, 34 (1): 97-115, 2008.
[3] Kannam et al. J. Chem. Phys, 135(14): 144701, 2011.
[4] Ybert et al. Phys. Fluids, Vol. 19, 2007.

5th Micro and Nano Flows Conference
Milan, Italy, 11-14 September 2016

Numerical modelling of electro-osmotic flow in porous micro-channels

Simona DI FRAIA [1,*], Nicola MASSAROTTI [1], Perumal NITHIARASU [2]

* Corresponding author: Tel.: ++39 347 2542201; Email: simona.difraia@uniparthenope.it
[1] Dipartimento di Ingegneria, Università degli Studi di Napoli "Parthenope", Napoli, Italy
[2] Biomedical Engineering and Rheology Group, Zienkiewicz Centre for Computational Engineering, Swansea University, Swansea SA2 8PP, United-Kingdom

Keywords: Electro-osmosis, Porous materials, Microscopic approach, CBS.

The aim of the present work is to present a model that has been developed as a tool for the analysis and design of porous Electro–Osmotic Flow (EOF) driven systems. The Navier–Stokes (NS) equations for microscopic heat transfer and fluid flow, together with the Poisson–Boltzmann and Laplace equations, have been used to numerically model EOF through porous media at the pores level.

1 Theoretical background

Electroosmotic driven flow phenomena have broad applications in various branches of engineering and technology, such as biomedical, geophysical, energy and chemical. Electro kinetic effects have been widely exploited in micro– and nano–fluidic devices: the most common applications concern pumping and capillary electrochromatography, and recently EOF systems have also been employed for dehumidification and regeneration of desiccant structures.

The principle of EOF driven systems is the following. When a solid surface is in contact with an electrolytic solution, it becomes charged: the ions distribution changes with the formation of a high concentration region, called Electrical Double Layer (EDL). If the electrolytic solution is subjected to an external electric field, the ions of the EDL move, dragging the near ions with them. While in flow through channel applications only the channel surface is taken into account for EOF, in porous media systems the contribution of charged solid particles should also be considered.

Many experimental and numerical studies have been carried out to analyse electroosmotic flow in micro– and nano–channels and recently, the behaviour of Non–Newtonian fluids under EOF has also been investigated, but only a very small number of students have been attempted on EOF in porous media [1]. Several simplifying hypotheses have been considered in modelling EOF in porous media: in the past decades most of the authors have just considered the charge of the channel walls and neglected the charge of solid particles [2], both in the equation governing the internal potential and in the momentum equation. Recently, some authors have considered the contributions of solid particles to EOF: some of them have employed a microscopic approach and solved the problem with Lattice Boltzmann Method (LBM) [3, 4]; others have used the generalized model for porous media and added a source term in the momentum equation depending on the charge density of porous medium and the applied electrical field, but used the internal potential equation for standard channel flows [2, 5]. Since the literature is full of conflicting models, the aim of this work is to present a comprehensive Finite Element Method (FEM) modelling approach to EOF in porous media in order to assess the influence of solid particles charge.

2 Methods

The study has been carried out by using a microscopic approach, in which the porous medium is represented by different assemblies of cylinders [6]. The equations used to model the electrokinetic effects responsible for EOF are Laplace equation for external applied potential and Poisson–Boltzmann equation for the EDL potential. Fluid flow and heat transfer through the porous medium have been analysed through the NS equations. The equations governing the electrical field have been decoupled and solved separately from the NS equations and their effect has been implemented into the source term of the momentum equation. The set of fluid flow and heat transfer equations has been solved by using a fully explicit artificial compressibility–based CBS (Characteristic Based Split) scheme [7].

A porous two-dimensional rectangular channel characterised by an aspect ratio equal to 10 has been considered for the simulations. This work will help in assessing the contributions of solid charged particles on the microscopic flow so that an effective macroscopic approach can be formulated.

References

[1] Li, B., Zhou, W.N., Yan, Y.Y., Tian, C., Evaluation of electro-osmotic pumping effect on microporous media flow, Applied Thermal Engineering 60, 449–455, 2013.

[2] Scales, N., Modelling electroosmotic and pressure-driven flow in porous media for microfluidic applications, Master thesis, Carleton University, Canada, 2004.

[3] Wang, M., Wang, J., Chen, S., Pana, N., Electrokinetic pumping effects of charged porous media in microchannels using the lattice Poisson–Boltzmann method, Journal of Colloid and Interface Science 304, 246–253, 2006.

[4] Li, B., Zhou, W., Yan, Y, Han, Z., Ren, L., Numerical Modelling of Electroosmotic Driven Flow in Nanoporous Media by Lattice Boltzmann Method, Journal of Bionic Engineering 10 (1), 2013.

[5] Tang, G.H., Ye, P.X., Tao, W.Q., Pressure-driven and electroosmotic non-Newtonian flows through microporous media via lattice Boltzmann method, Journal of Non-Newtonian Fluid Mechanics 165, 1536–1542, 2010.

[6] Massarotti, N., Nithiarasu, P., Carotenuto, A., Microscopic and macroscopic approach for natural convection in enclosures filled with fluid saturated porous medium, International Journal of Numerical Methods for Heat & Fluid Flow 13 (7), pp. 862–886, 2003.

[7] Nithiarasu, P., An efficient artificial compressibility (AC) scheme based on the characteristic based split (CBS) method for incompressible flows, Int. Journal for Numerical Methods in Engineering 56, 1815–45, 2003.

5th Micro and Nano Flows Conference
Milan, Italy, 11-14 September 2016

Trains of Particles in Finite-Reynolds-number Micro Square Flow

Yanfeng GAO [1], Pascale MAGAUD [1,*], Lucien BALDAS [1], Christine LAFFORGUE [2], Micheline ABBAS [3], Philippe SCHMITZ [2], Stéphane COLIN [1]

* Corresponding author: Tel.: +33 (0) 5 61 17 11 02; Fax: +33 (0) 5 61 17 10 80; Email: pascale.magaud@insa-toulouse.fr
1 Université Fédérale Toulouse Midi-Pyrénées; CNRS FRE 3687; Institut Clément Ader, 3 Rue Caroline Aigle, F-31400 Toulouse, France
2 Université Fédérale Toulouse Midi-Pyrénées; INSA, UPS, INP; LISBP, 135 Avenue de Rangueil, F-31077 Toulouse, France
INRA, UMR792 Ingénierie des Systèmes Biologiques et des Procédés, F-31400 Toulouse, France
CNRS, UMR5504, F-31400 Toulouse, France
3 Université Fédérale Toulouse Midi-Pyrénées; INPT, UPS; Laboratoire de Génie Chimique, 4 Allée Emile Monso, 31432 Toulouse, France

Keywords: Microfluidics, Inertial Focusing, Train of Particles, Square Channels, Moderate Re

Controlling the transport of particles in flowing suspensions at micro-scale level is of interest in a number of contexts such as the development of miniaturized and up to care analytical devices (in bio-engineering, for medicine foodborne detection…) and polymer engineering. However, the seemingly simple question, "How are microscopic particles transported in a given flow?" can rarely be answered up to date due to the high complexity of the situations encountered in most of the applications. In square wall-bounded flows in micro-channels, neutrally buoyant spherical particles are known to migrate laterally and concentrate at specific equilibrium positions located in the channel center at low flow inertia, and at the four centers of the channel faces at moderate Reynolds numbers Re. Because these equilibrium positions depend on particle size, the migration phenomenon in square channel is a promising way for particle concentration and/or separation and the development of low cost separation devices. In the course of investigating the Reynolds number dependence of this migration, it is shown that the spherical particles are found to align in the direction of flow and form evenly spaced train (as shown in Fig. 1).

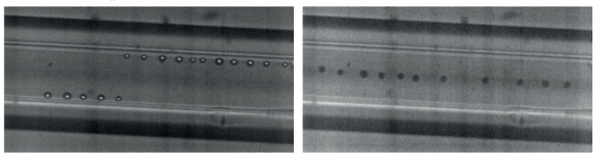

Fig. 1. Trains of spherical particles with a diameter of 8.7 µm observed in a micro square channel $80 \times 80\ \mu m^2$ at Re = 210

This longitudinally particle ordering has already been observed by Matas [1] in pipe flow, Humphry [2] and Kahkeshani [3] in rectangular channels. Given the interest in the application of inertial focusing approaches for concentrating and/or separating particles, there is a need to better understand the formation of the trains, their robustness and the way in which particles arrange in case of bi-dispersed suspensions.

To address this objective, experiments have been conducted. *In situ* visualization of the flowing particles is performed by classical microscopy (the experimental setup has been previously detailed [4]). Obtained images are post-processed and trains are identified. Parameters such as fraction of particles in trains and separation distance between nearby particles in a same train have been extracted and analyzed in function of Reynolds number, particle to channel-size ratio and volume fraction.

Preliminary results seem to show that trains occur at finite Reynolds number when particles have reached their equilibrium positions near the channel walls. The percentage of the particles included in trains increases with Re and concentration, whereas the separation distance depends only on Re, regardless of the concentration.

Experiments are still in progress in the case of bi-dispersed suspensions.

References

[1] Matas J P, Glezer V, Guazzelli É, et al. Trains of particles in finite-Reynolds-number pipe flow. Physics of Fluids, 16(11): 4192-4195 (2004).

[2] Humphry K J, Kulkarni P M, Weitz D A, et al. Axial and lateral particle ordering in finite Reynolds number channel flows. Physics of Fluids, 22(8): 081703 (2010).

[3] Kahkeshani S, Haddadi H, Di Carlo D. Preferred interparticle spacings in trains of particles in inertial microchannel flows. Journal of Fluid Mechanics, 786: R3 (2016).

[4] Abbas M, Magaud P, Gao Y, et al. Migration of finite sized particles in a laminar square channel flow from low to high Reynolds numbers. Physics of Fluids, 26(12): 123301 (2014).

5th Micro and Nano Flows Conference
Milan, Italy, 11-14 September 2016

Non-equilibrium dynamics of dense gas under tight confinement

Lei WU[1,*]

* Corresponding author: Email: lei.wu.100@strath.ac.uk
1 James Weir Fluids Laboratory, Department of Mechanical and Aerospace Engineering, University of Strathclyde, Glasgow G1 1XJ, UK

Abstract

Poiseuille flow of rarefied gas has received much attention, due to the development of micro/nano-electromechanical systems and the shale gas revolution in US. It's mass flow rate is a key parameter in the generalized Reynolds equation to describe gas-film lubrication problems, as well as in the upscaling methods to predict the gas permeability of the ultra-tight shale strata. While the Boltzmann equation is a fundamental model for gas dynamics at low pressure, its applicability to a typical shale gas production scenario is problematic, because the Boltzmann equation is derived under the assumption that the molecular mean free path is much larger than the molecular dimension, but this is not the case for large gas pressures.

The force-driven Poiseuille flow of dense gases between two parallel plates is investigated through the numerical solution of the Enskog equation. We focus on the competition between the mean free path λ, the channel width L, and the disc diameter σ. For elastic collisions between hard discs, the mass flow rate in the hydrodynamic limit increases with L/σ for a fixed Knudsen number (defined as $Kn=\lambda/L$), but is always smaller than that predicted by the Boltzmann equation. Under ultra-tight confinement the famous Knudsen minimum disappears, and the mass flow rate increases with Kn, which is larger than that of the Boltzmann equation in the free-molecular flow regime: the smaller the L/σ the larger the mass flow rate. In the transitional flow regime, however, the variation of the mass flow rate with L/σ is not monotonic when Kn is fixed.

Keywords: Rarefied gas dynamics, Dense gas, Enskog equation, Poiseuille flow

Evaluation of heat losses in counter flow micro heat exchangers

Anatoly Parahovnik [1,2],Nir Tzabar[2], Gilad Yossifon [1]

[1] *Faculty of Mechanical Engineering Technion-Israel Institute of Technology, Technion city 32000, Israel*
[2] *Rafael, Haifa, 3102102 Israel*

Keywords: Micro Channels, Recuperative Heat Exchanger, Gas Micro Flow, MEMS Fabricated

A gas to gas counter flow micro Heat Exchanger (HE) made of an array of microchannels and fabricated using a combination of Silicon and glass wafers is studied, Fig.1. A divergence of the experimental results from the classical heat exchanger theory is observed due to discernible axial conduction effects, Fig.2. Hence, device performance was evaluated using a modified NTU approach that includes also non-negligible axial conduction effects due to the extremely low heat fluxes inside the heat exchanger. This along with proper boundary conditions for the heat equation within the separating wall enables to evaluate the heat losses to the environment. The standard NTU [1] approach assuming: steady state, constant physical properties, negligible axial conduction and insulated heat exchanger is extended to account for axial conduction through the separating wall [2]

$$-\frac{d\theta_h}{dX}+\nu\cdot\frac{d\theta_c}{dX}+\frac{\lambda}{\mu}\cdot\frac{d^2\theta_w}{dX^2}=0 \qquad (1)$$

Herein, the dimensionless temperature θ, and length X are defined as

$$\theta_i=\frac{T_i-T_{h,in}}{T_{h,in}-T_{c,in}}\,,X=\frac{L}{x} \qquad (2)$$

where L is the total length of the heat exchanger, h and c stands for hot and cold streams and suffix in symbolize the value at the inlet of the device. The dimensionless values in equation 1 are

$$\nu=\frac{(\dot{m}c_p)_c}{(\dot{m}c_p)_h},\mu=\frac{(\dot{m}c_p)_c}{(\dot{m}c_p)_{min}}\;;\quad\lambda=\frac{k\cdot A_w}{L\cdot(\dot{m}c_p)_{min}} \qquad (3)$$

Where A_w is wall cross section,$\dot{m}$ is the mass flux, C_p is the specific heat of the gas and k is the coefficient of thermal conduction of the separating wall. Since we cannot neglect the heat losses from the ends of the separating wall made of Silicon, the common thermal insulation boundary conditions are replaced by temperature boundary conditions with some relations to the stream temperatures at the ends. This resulted in fair agreement with experimental.

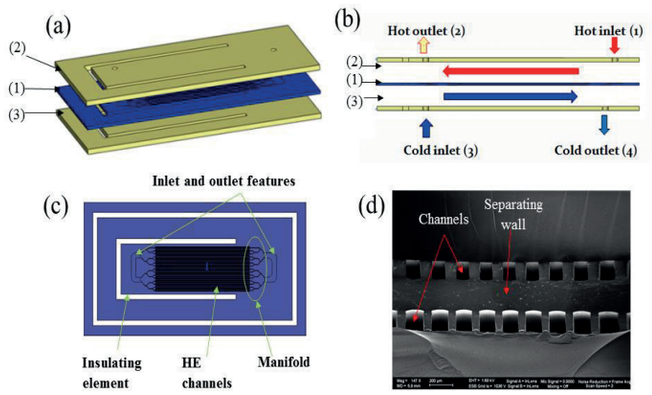

Figure 1 – Examined Heat exchange, the figure presents the construction of the HE (a), flow configuration inside the examined chip (b), different etched elements in the silicon piece (c) and SEM micrograph of HE cross section (d). In the last figure it can be seen that the separating wall thickness isn't negligible.

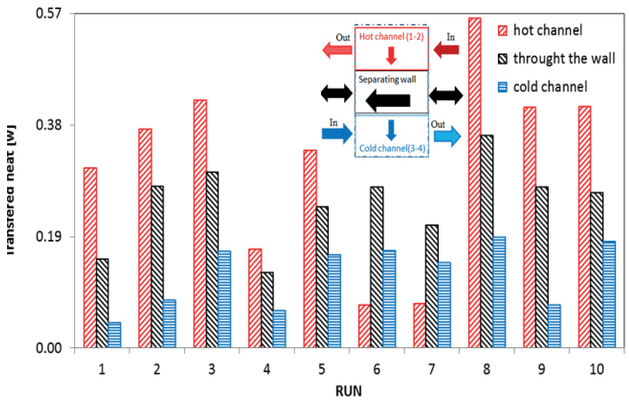

Figure 2 – Amount of heat transferred inside the HE at different experimental conditions (X axis present different experiments), it can be seen that the heat transferred through the wall is significant and can't be neglected

References

[1] Frank p. Incropera, David p. Dewitt, Theodore L. Bergman, Adrienne S. Lavine Fundamentals of heat and mass transfer, sixth edition.

[2] P.G.Kroeger, Performance Deterioration in high effectivness heat exchanger due to axial heat conduction effects,, Advances in Cryogenic Engineering Vol.12 ,1967, pp 363-372.

5th Micro and Nano Flows Conference
Milan, Italy, 11-14 September 2016

Viscosity Influence On Flow Pattern Map Of Immiscible Liquid-Liquid Flow In A T-Shaped Microchannel

Anna A. YAGODNITSYNA [1, 2, *], Alexander V. KOVALEV [1, 2], Artur V. BILSKY [1, 2]

* Corresponding author: Tel.: +7 (383) 335 66 84; Fax: +7 (383) 335 66 84; Email: yagodnitsinaAA@gmail.com
1 Kutateladze Institute of Thermophysics, Novosibirsk, Russia
2 Novosibirsk State University, Novosibirsk, Russia

Abstract Visualization of flow patterns for three sets of immiscible liquids with different physical properties was done for a broad range of Weber numbers. A new flow pattern with steady wavy interface was found. A parameter for flow pattern maps generalization was proposed. For typical flow regimes micro-PIV measurements in water and kerosene phases were carried out.

Keywords: Immiscible liquid-liquid flow, T-shaped microchannel, Flow pattern

1. Introduction

In last decade microreactors have become alternative to traditional reactors in chemical industry and biotechnology. Channels with submillimeter hydraulic diameter have extremely large surface to volume ratio which leads to intensification of heat and mass transfer. Besides that microreactors have such advantages as small volume of reacting fluids and better reaction control. Flows of immiscible liquids in microchannels are important for different kinds of technical applications such as microreactors in chemistry, bioMEMS devices, extraction reactions, emulsions production etc. In the present paper experimental investigation of immiscible liquids flow in a T-shaped microchannel was carried out.

2. Results

A flow of tree sets of immiscible liquids in a rectangular microchannel with T-junction made of SU-8 material was studied. Liquid-liquid sets were kerosene – water; paraffin oil – water; paraffin oil – castor oil. The size of inlet channels was 200x200 μm, the size of outlet channel was 200x400 μm. We used high speed camera (pco.1200 hs) and inverted microscope (Zeiss Axio Oberver.Z1) with 5x magnification to visualize flow patterns and interfacial dynamics. The flow of liquids was controlled by KDS Gemini 88 double syringe pump. Density, viscosity, interfacial tension and contact angles of all liquids were measured directly prior experiments.

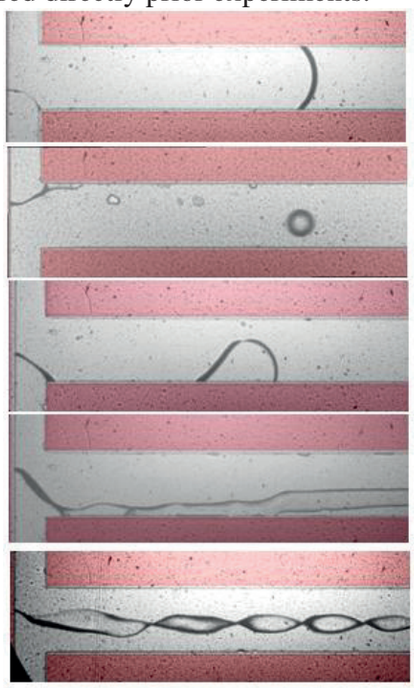

Figure 1: Typical flow patterns for kerosene and water near the T-junction. From top to bottom: plug flow, droplet flow, slug flow, rivulet flow and parallel flow with steady wavy interface.

For water-kerosene flow we observed following flow patterns: plug flow (water in kerosene), slug flow (for both liquids), droplet flow (water in kerosene), rivulet flow (for both liquids) and parallel flow (Fig.1). It is important to notice that we didn't observe annular flow because of low contact angle of both liquids. High surface wettability was the reason for occurrence of slug flow for both liquids and rivulet flow instead of annular flow. New flow pattern of parallel flow with steady wavy interface was found. Flow visualization of paraffin oil – water and paraffin oil – castor oil gave similar flow patterns.

As flow visualization was done we derived flow map using Weber number of both liquids (Fig. 2). The flow map was different from that obtained by [1]. So we can conclude that Weber number is not the only parameter which defines flow regime. Comparison of flow maps for all liquid sets showed that those were similar to each other but pattern transition was on different Weber numbers. In order to take into account fluid viscosity we constructed new flow maps based on Weber number multiplied by liquid viscosity (Fig.2). After that flow maps coincided with each other.

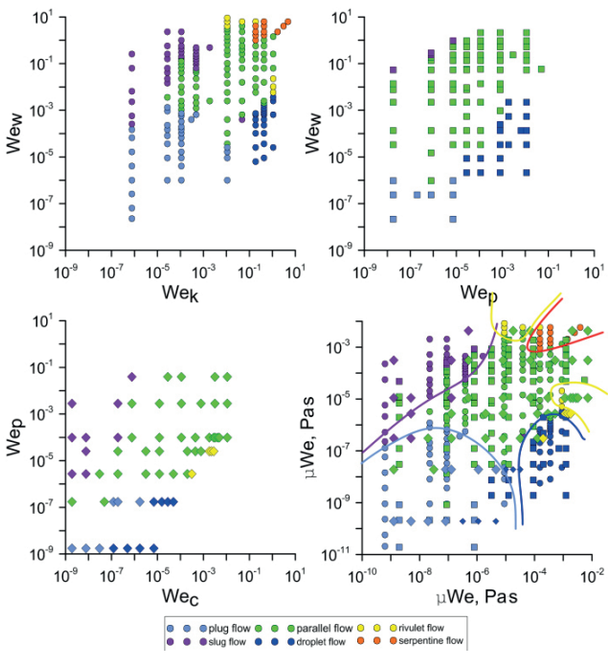

Figure 2: Flow pattern maps for kerosene-water (top left), paraffin oil-water (top right), paraffin oil – castor oil (bottom left). Modified joint flow map for all liquid systems (bottom right).

For typical flow regimes we made micro-PIV measurements for water and kerosene in order to evaluate convective flows inside both phases which are important for microreactors development and optimization (Fig. 3).

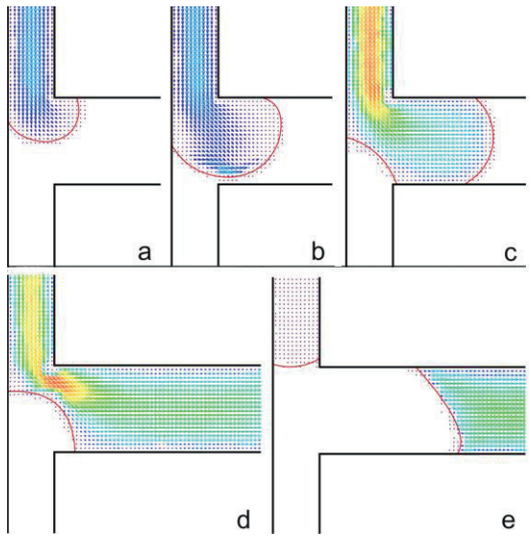

Figure 3: Instantaneous velocity fields in central plane of the channel in different phases of water plug formation.

3. Conclusion

For three sets of immiscible liquids flow patterns in a broad range of Weber numbers were obtained. Flow regimes include those of interfacial tension and inertia forces domination. Fluids chosen have different physical properties. For all of three liquid sets flow pattern maps based on Weber numbers were drawn. To combine all flow pattern map into one we offer to use new parameter – Weber number multiplied by liquid viscosity. Flow map using this parameter gave a good agreement between different liquid sets.

Acknowledgments

This work was supported by a grant from the Russian Science Foundation (project Nr. 16-19-10519).

References

1. Zhao Y., Chen G., Yuan Q. (2006) Liquid-liquid two-phase flow patterns in a rectangular microchannel, AIChE Journal, 52, Issue 12, pp. 4052–4060.

Photothermal Conversion Performance of Gold Nanoparticle Dispersion in Different Wavelength

Hui Zhang [1,*], Hui-Jiuan Chen [2], Xiaoze Du [1], Dongsheng WEN [3]

* Corresponding author: Tel.: ++86 (10)61773372; Email: huizhang@ncepu.edu.cn
1 School of Energy and Power, North China Electric Power University, China
2 SYSU-CMU Shunde International Joint Research Institute, Shunde, China
3 School of Chemical and Process Engineering, University of Leeds, UK

Keywords: Gold, Nanoparticles, Photo-thermal conversion, Extinction coefficient

The photothermal conversion performance of the gold nanoparticle dispersion was investigated in the different wavelength sections. Characteristics in a single wavelength are different with that in the whole solar spectrum. The relationship between the photothermal conversion efficiency and extinction coefficient is not proportional. Characteristics in

1 Introduction

Nanoparticle-based direct absorbing solar energy collector (DASC) employs nanoparticles to convert light energy into thermal energy directly. Comparing to conventional solar thermal collectors, nanoparticles absorb solar energy directly within the fluid volume. Such an idea transfers the surface heat transfer limitation associated with conventional solar collectors into a volumetric absorption phenomenon. An optimized DASC system could not only simplifying the conventional system, i.e. replacing metal pipes with transparent glass tubes, but also increasing the absorption efficiency by engineering the absorption spectrum at the nanoscale.[1-4]

Gold nanoparticles (GNPs) were found to have remarkable performance in improving the photothermal conversion efficiency of the base fluid at very low particle concentrations. And the photothermal conversion efficiency increases with the particle concentration but in a non-linear fashion. On the other hand, the extinction coefficient is a key factor to show the wavelength-selective absorbing feature and absorption ability of nanoparticles on solar energy. However our previous study showed the extinction coefficient don't represent the real photo-thermal energy conversion process[5-6]. On the base of the photothermal conversion experiment in whole spectrum, the experiment research is about the photothermal conversion performance of GNPs in a single wavelength.

2 Experiment Setup

In this work, gold nanoparticle dispersions are formulated through simultaneous production and dispersion of nanoparticles in situ. GNPs were synthesized by the citrate reduction method with the aid of ultrasonification for particle morphology control [7]. Five slices of filters (410, 520, 710, 860, 1064nm) were used to study the photothermal conversion performance of GNPs within a narrow wavelength, and other three slices of filters were utilized to form three wide-wavelength irradiation which were only in the ultraviolet, the visible and the infrared section. Gold nanoparticle mass concentration is 0.0028% (1.5ppm) in all experiments.

A solar simulator (Newport Co. Oriel Xenon Arc lamp) was used as the light source. As the filter allows only a narrow wavelength of the light passing, the ouput power of the sun simulator is increased into 0.2W/cm2 (the sun light is about 0.1W/cm2) to gain clearly the temperature variation. The experiment system is showed in Fig.1.

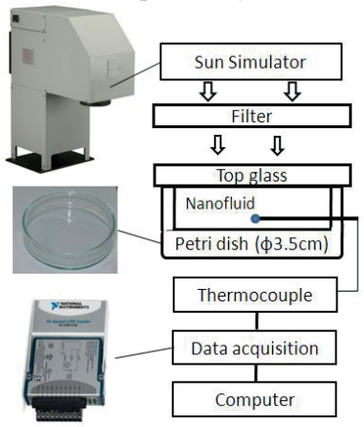

Figure 1 Schematic illustration of the experimental system

3 References

[1]Lenert A. and Wang E. N., Optimization of nanofluid volumetric receivers for solar thermal energy conversion, Solar Energy, 86(2012):253-265.

[2]Otanicar T. P., Phelan P. E. and Golden J. S., Optical properties of liquids for direct absorption solar thermal energy systems, Solar Energy, 83(2009):969-977.

[3]Taylor R.A., et al., Nanofluid optical property characterization: towards efficient direct absorption solar collectors, Nanoscale Research Letters 2011, 6:225.

[4]Becker J., et al. The Optimal aspect ratio of gold nanorods for plasmonic bio-sensing, Plasmonics, 2010(5):161-167.

[5]Zhang H; Chen H-J; Du X; Wen D Photothermal conversion characteristics of gold nanoparticle dispersions. Solar Energy, 100(2014):141-147.

[6]Zhang H; Chen H-J; Du X; Lin G; Wen D Dependence of photothermal conversion characteristics on different nanoparticle dispersions. Journal of Nanoscience and Nanotechnology, 15(2015):3055-3060.

[7]Chen HJ and Wen DS, Ultrasonic-aided fabrication of gold nanofluids, Nanoscale Research Letter, 2011, 6:198.

5th Micro and Nano Flows Conference
Milan, Italy, 11-14 September 2016

µ-Particle Image Velocimetry and Computational Fluid Dynamic Study of Cell Seeding within a 3D Porous Scaffold

Ana Campos Marin[1]*, Tommaso Grossi[2], Elena Bianchi[2], Gabriele Dubini[2], Damien Lacroix[1]

* Corresponding author: Tel.: ++44 (0) 114 2226072; Email: a.camposmarin@sheffield.ac.uk
1 Insigneo Institute for in silico medicine, Department of Mechanical Engineering, University of Sheffield, UK
2 Laboratory of Biological Structure Mechanics, Department of Chemistry, Materials and Chemical Engineering, Politecnico di Milano, Italy

Keywords: Microfluidics, CFD, µPIV, Scaffold

Introduction

Cell seeding of 3D scaffolds is a critical step in tissue engineering since it precedes all steps in tissue formation. It is desirable to obtain homogeneously distributed cells throughout the entire structure and high cell seeding efficiency since donor cells can be limited. The combination of 3D interconnected porous structures with fluid dynamic based bioreactors can enhance such cell seeding outcomes [1]. So, it is important to optimise key parameters involved in cell seeding in vitro experiments such as perfusion flow rate in order to obtain the most suitable mechanical environment for cell adhesion. The goal of this study is to develop a Computational Fluid Dynamics (CFD) model able to predict cell seeding efficiency. A new experimental approach using a micro Particle Image Velocimetry (µPIV) system is presented in combination with CFD simulations to explore and predict the local fluid dynamics and cell motion inside a 3D scaffold.

Methods

A commercial PCL scaffold from 3D Biotek with 300 µm pore size was trimmed and placed inside a microfluidic PDMS chamber with square channel profile (3x1x40 mm3). The chamber was located on the stage of an inverted microscope and 1 µm diameter red fluorescent polystyrene microspheres diluted in distilled water were infused using a syringe pump with a constant flow rate. The flow media was illuminated using Nd:YAG 532 nm laser and the reflected light from the tracer particles was captured in double frame images. Images were imported in Insight 3G and divided in sub-regions where local velocity vectors were calculated by statistical methods. To study cell motion, MG63 cells were labelled with orange CMTMR fluorescent dye (Life Technologies) and suspended in culture media. Transient flow rate was applied while single frame images were captured and after that evaluated in ImageJ. CFD simulations using Ansys Fluent were performed replicating the experimental conditions. Incompressible Newtonian fluid with viscosity of 1x10-3 Pa×s and no-slip condition were adopted. The fluid volume was meshed around the µCT-based scaffold geometry with 10 million tetrahedral elements. To calculate cell motion, cells were simulated as a discrete phase of microsphere particles that move along the fluid volume in a Lagrangian formulation.

Results

µPIV and CFD velocity profiles agree well showing that fluid velocities are higher at the center of the pores and decrease towards the fibers. Values extracted from both profiles show a difference less than 12% at the center of the pore however near the fibers µPIV values are higher (Figure 1). Cells both in CFD and µPIV follow the fluid streamlines, higher cell velocities and frequency of cells passing are found at the center of the pores (Figure 2).

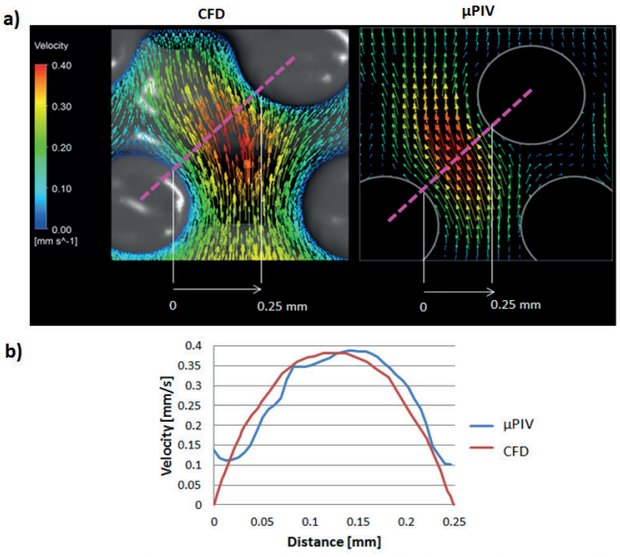

Figure 1 a) Velocity vectors calculated with CFD and µPIV inside the scaffold. b) Velocity values extracted from the pink line in a).

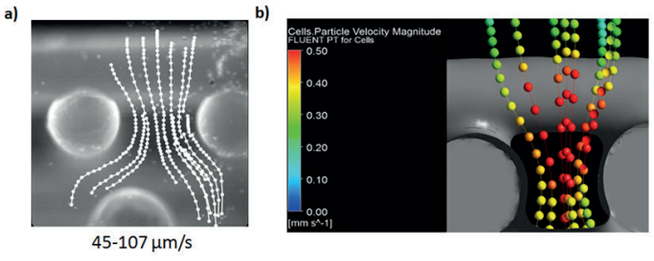

Figure 2 Cell path tracked with µPIV (a) and CFD (b).

Discussion

Despite the fact that cells reach all regions inside the scaffold, they mainly follow streamlines without intercepting the fibers. For this reason, low cell seeding efficiency is expected as found in the cell seeding CFD model. This suggests new configurations should be developed to aid cells to collide with scaffold substrate. This study shows an experimental approach that permits to investigate cell seeding inside a 3D scaffold and a computational model able to predict local fluid dynamics and seeding efficiency.

References

(1) Melchels FPW et al, Acta biomater, 6:4208–17, 2010.

Acknowledgments

Financial support from European Research Council (258321) and the European Society of Biomechanics Mobility Award

5th Micro and Nano Flows Conference
Milan, Italy, 11-14 September 2016

Drop Motion Induced by Vertical Vibrations

Paolo SARTORI [1], Silvia VARAGNOLO [1], Matteo PIERNO [1], Giampaolo MISTURA [1,*], Francesco MAGALETTI [2], Carlo Massimo CASCIOLA [2]

* Corresponding author: Email: giampaolo.mistura@unipd.it
1 CNISM and Dipartimento di Fisica e Astronomia "G.Galilei", Università degli Studi di Padova, Italy
2 Dipartimento di Ingegneria Meccanica e Aerospaziale, Università La Sapienza, Italy

Keywords: Moving Drops, Drop Actuation, Vertical Vibrations

The manipulation of small (micro-/nano-liter scale) discrete amount of liquid is a subject of great interest for applications in many fields, from chemical synthesis to biological analysis. We can distinguish mainly two branches of Microfluidics dealing with the actuation of droplets: two-phase flows in closed micro-channels [1] and sessile drops motion on open surfaces [2]. Focusing on the latter, recently it has been demonstrated the possibility of moving sessile droplets by means of vibrations of the substrate [3-4].

We have studied the one-dimensional motion of few microliters liquid drops on a PMMA inclined plate subject to vertical sinusoidal oscillation ranging from 30 Hz to 120 Hz [5]. The liquids comprised distilled water and different aqueous solutions of glycerol, ethanol and isopropanol spanning the range 1–39 $mm^2\ s^{-1}$ in kinematic viscosities and 40–72 mNm^{-1} in surface tension. Because of contact angle hysteresis, at sufficiently low oscillating amplitudes, the drops are always pinned to the surface. Vibrating the plate above a certain amplitude yields sliding of the drop. Further increasing the oscillating amplitude drives the drop upward against gravity (Figure 1). In the case of the most hydrophilic aqueous solutions, this motion is not observed and the drop only slides downward. Images taken with a fast camera show that the drop profile evolves in a different way during sliding and climbing. This dynamics is due to the asymmetric variations of the front and rear contact angles with respect to the advancing and receding values. In particular, the climbing drop experiences a much bigger variation in its profile during an oscillating period.

Complementary numerical simulations of 2D drops based on a diffuse interface approach confirm the experimental findings. The overall qualitative behavior is reproduced suggesting that the contact line pinning due to contact angle hysteresis is not necessary to explain the drop climbing.

We are currently further investigating these phenomena in the case of non-Newtonian fluids, such as Xanthan or polyacrylamide aqueous solutions [6].

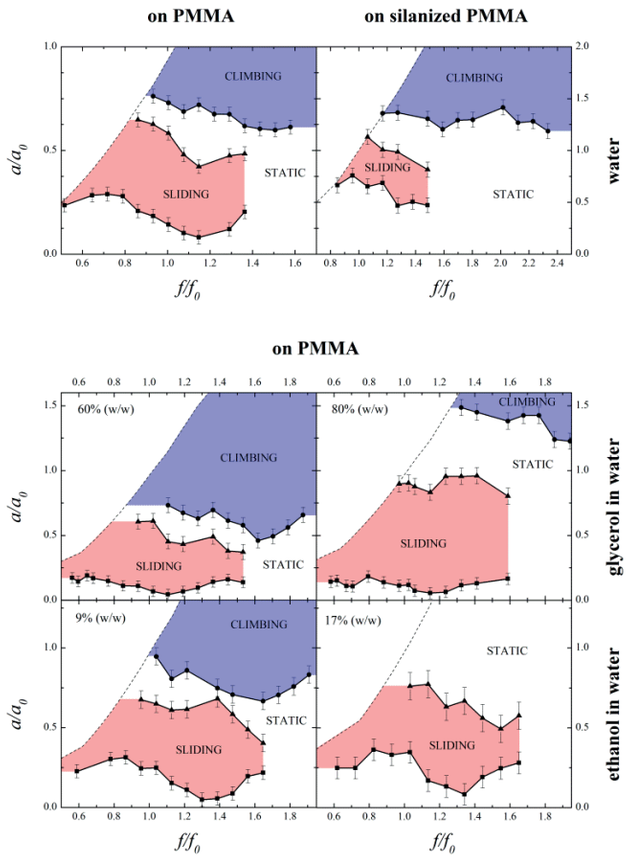

Figure 1. Dynamical phase diagrams of drops of different aqueous solutions corresponding to a volume V=2 μL and a plate inclination α=30°. The normalization factors are the resonance frequency f_0 of the drop's rocking mode corresponding to a supported drop vibrated in a direction parallel to the substrate and the corresponding acceleration a_0 with an amplitude given by $V^{1/3}$: a0=241 m/s2 and f0=70 Hz for water on PMMA and a0=110 m/s2 and f0=47 Hz for water on silanized PMMA. For the other liquids they are comprised in the ranges a0=117-173 m/s2 and f0= 48-59 Hz.

[1] S.-Y. Teh, R. Lin, L.-H. Hung, A. P. Lee, Lab Chip 8 (2008) 198-220
[2] F. Mugele, J.-C. Baret, J. Phys.: Condens. Matter 17 (2005) R705–R774 (2005)
[3] P. Brunet, J. Eggers, R. D. Deegan, Phys. Rev. Lett. 99 (2007) 144501
[4] X. Noblin, R. Kofman, F. Celestini, Phys. Rev. Lett. 102 (2009) 194504
[5] P. Sartori, D. Quagliati, S. Varagnolo, M. Pierno, G. Mistura, F. Magaletti, C. M. Casciola, New J. Phys. 17 (2015) 113017
[6] S. Varagnolo, G. Mistura, M. Pierno, M. Sbragaglia, Eur. Phys. J. E 38 (2015) 126

5th Micro and Nano Flows Conference
Milan, Italy, 11-14 September 2016

Dynamics of Cell-free Layer Formation after Arteriolar Bifurcations and its Physiological Effects

Yan Cheng NG [1,2], Bumseok NAMGUNG [2], Sangho KIM [1,2,3,*]

* Corresponding author: Tel.: +65 6516 6713; Fax: +65 6872 3069; Email: bieks@nus.edu.sg
1: NUS Graduate School for Integrative Sciences and Engineering, National University of Singapore, Singapore
2: Department of Biomedical Engineering, National University of Singapore, Singapore
3: Department of Surgery, National University of Singapore, Singapore

Keywords: Microcirculation, Bifurcation, Red blood cell, Aggregation, Hemodynamics

The arteriolar microvasculature provides a large area that allows the exchange of substances between the blood stream and surrounding tissues. Ramification of these vessels can contribute to the temporal switching of red blood cells (RBCs) at the bifurcations, which in turn leads to spatial heterogeneity of perfusion at the junction [1]. Moreover, RBCs tend to migrate axially towards the flow center in microcirculations, resulting in the formation of a cell-free plasma layer (CFL) which can be promoted by RBC aggregation [2]. Consequently, a disproportionate amount of CFL and RBCs entering the daughter microvessels could manifest to the heterogeneous distribution of hematocrit in microvascular networks [3]. In this study, we investigated the formation of CFL from 2 to 6 vessel-diameter (2D-6D) downstream of arteriolar bifurcations in the rat cremaster muscle (Fig. 1) under reduced flow conditions (pseudoshear rates = 9.3 ± 1.8 s^{-1}). Concomitantly, we extended our previously developed two-dimensional transient diffusion model to illustrate the potential impact of the hemodynamics on the physiological functions of arterioles by numerically predicting the bioavailability of nitric oxide (NO), oxygen (O_2) and soluble guanylyl cyclase (sGC) activity in the arterioles which influences the vascular tone.

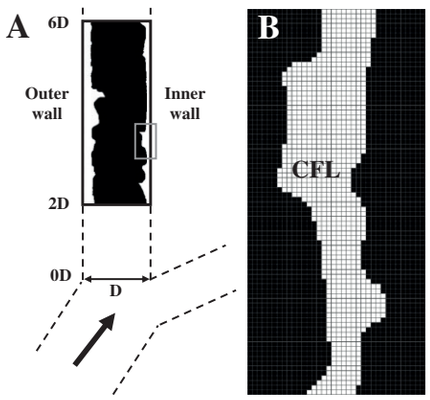

Figure 1 A: Schematic of a typical arteriolar bifurcation with the region of interest at the larger daughter vessel. **B**: Two dimensional cell-free layer (CFL) measurement from an in vivo image. The CFL region was highlighted with white grid boxes, and the each grid box has a size of 0.42 μm by 0.42 μm.

Our experimental results showed that an asymmetric formation of CFL width along the vessel walls was evident up to 6D from the bifurcating point. RBC aggregation preferentially augmented the development of CFL widths along the outer wall after the bifurcation but did not to seem enhance the recovery of flow asymmetry significantly. Additionally, our numerical prediction of NO/O_2 concentrations (Fig. 2) and sGC activity revealed that vasoactivity might not occur uniformly along the arteriole within an inter-bifurcation distance, in particular under reduced flow and aggregating conditions. This illustrates that the contribution of asymmetric CFL widths on the heterogeneity of NO/O_2 concentrations and sGC activity could propagate in the entire arteriolar network.

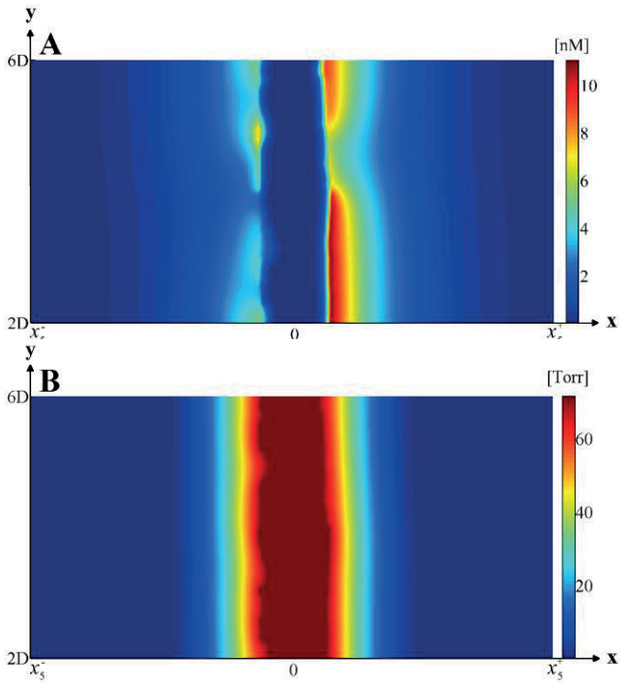

Figure 2 Instantaneous spatial distribution of NO (**A**) and P_{O2} (**B**) in hyper-aggregating condition.

References

[1] Butcher et al., 2013. Blunted temporal activity of microvascular perfusion heterogeneity in metabolic syndrome: a new attractor for peripheral vascular disease? *American journal of physiology Heart and circulatory physiology* 304: H547-558.

[2] Goldsmith, 1986. The Microcirculatory Society Eugene M. Landis Award Lecture. The Microrheology of Human Blood. *Microvascular Research*. 31, 121–142.

[3] Pries et al., 1989. Red cell distribution at microvascular bifurcations. *Microvascular Research* 38, 81-101.

5th Micro and Nano Flows Conference
Milan, Italy, 11-14 September 2016

Comparison of working fluid combinations in a microchannel membrane absorber

Mercedes de VEGA [1,2*], María VENEGAS [1,2,3], Néstor GARCÍA-HERNANDO [1,2]

* Corresponding author: Tel.: +34 (1)6248464; Email: mdevega@ing.uc3m.es
1 ISE Research Group, Department of Thermal and Fluids Engineering, Universidad Carlos III de Madrid, Avda. Universidad 30, 28911 Leganés, Madrid, Spain
2 GTA Research Group, Department of Thermal and Fluids Engineering, Universidad Carlos III de Madrid, Avda. Universidad 30, 28911 Leganés, Madrid, Spain
3 Associated Research Unit CSIC-Universidad Carlos III de Madrid, Spain

Keywords: microchannel, absorption, microporous membrane

With the aim of reducing the size and increasing the energy efficiency of absorption chillers, the use of microporous membrane technology in these systems is at present under study. In particular, the simulation of an absorber using porous fibers for the heat and mass transfer between the solution and the vapor phase is considered in the present work. The performance of the microchannel absorber is evaluated for three different solutions-refrigerant pairs: LiBr-H2O, LiCl-H2O and LiNO3-NH3.

1 Micro absorber

The absorber is one of the most performance limiting and volume demanding components of absorption systems. The main challenge in designing and operating these devices is to maximize the mass transfer rate by getting as much interfacial area as possible, minimizing the overall size. This can be achieved using membrane contactors in microchannel heat exchangers. The new technology used here has already been presented for LiBr-H2O and H2O- NH3 pairs [1, 2, 3, 4], but to our best knowledge, there are no studies considering the LiCl-H2O and LiNO3-NH3 solution-refrigerant pairs. In the proposed absorber, the refrigerant vapor (in the present study, water or ammonia) passes the membrane and is absorbed by the solution (LiBr-H2O, LiCl-H2O and LiNO3-NH3) flowing inside constrained flow passages. The vapor pressure difference across the membrane is the driving force for vapor transfer. If the partial pressure of the vapor inside the solution is less than the vapor pressure, it is absorbed at the interface between solution and vapor.

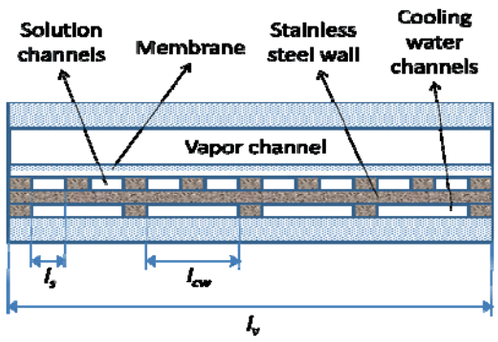

Figure 1: Plate and frame micro absorber

The configuration considered for the absorber in the present study is shown in Fig. 1. It is a plate-and-frame membrane module consisting of a vapor channel, the contact membrane, the solution and cooling water channels separated by a stainless steel wall. The dimensions of the microchannels are: 150µm height and 1.5 mm width. The absorber is discretized in differential elements. Using the inlet conditions, the variables at the outlet of the element are calculated.

2 Heat and mass transfer models

Our model is based in the dusty-gas model, for the vapour mass transfer through the membrane, and the film theory: the heat and mass transfer equations are described in terms of the corresponding mass and heat transfer coefficients. The global mass and heat transfer resistances are evaluated using correlations for heat and mass transfer in microchannels from the literature, applied to each of the solutions considered in the present study. These equations are combined with the global energy and mass balances to predict the performance of the absorber. The properties of each solution pair have been evaluated using data reported on the literature. The resulting system of equations is solved using Engineering Equation Solver software, EES™, as in [5].

3 Results

The performance of the absorber working with the three different solutions is evaluated. The ratio of cooling effect to absorber volume is used as a comparison parameter. This value along the channels of the micro-absorber is shown in figure 2 for the three solutions, working at a vapor temperature of 7ºC.

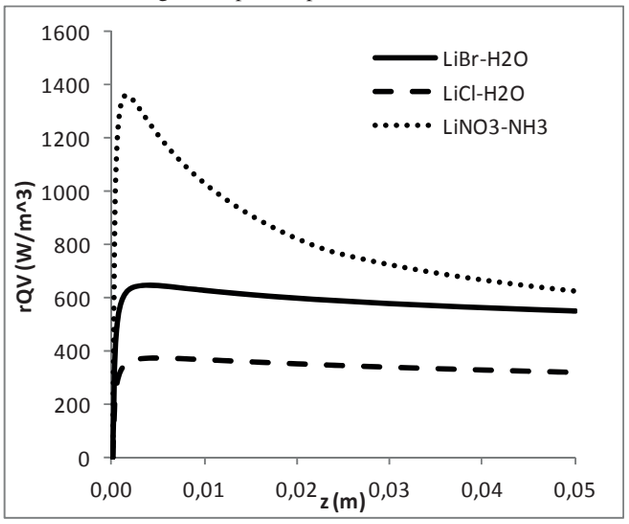

Figure 2: Cooling to volume ratio (vapor temperature 7ºC)

The higher performance has been found for the LiNO3-NH3 solution. This solution presents higher mass diffusion coefficient than the LiBr-H2O and the LiCl-H2O solutions.
For a vapor temperature of 10ºC, the results are shown in figure 3.

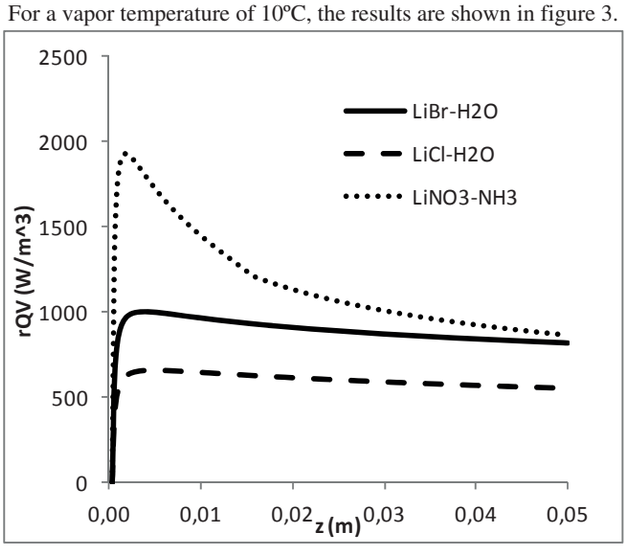

Figure 3: Cooling to volume ratio (vapor temperature 10ºC)

It is clearly seen, that the higher the vapor temperature, the higher the cooling effect as the pressure driving potential increases.
If the length of the micro-absorber is 5cm, this ratio is around 900W/m^3 for a vapor temperature of 10ºC, for the LiNO3-NH3 and LiBr-H2O solutions. For the LiCl-H2O, this value is equal to 550W/m^3. In all the cases, these parameters result larger than the ones found in conventional absorbers.

References

[1] Ali, A.H.H., 2010, "Design of a compact absorber with hydrophobic membrane contactor at the liquid-vapor interface for lithium bromide-water absorption chillers", Applied energy 87 pp. 1112-1121.
[2] Yu, D., Chung, J., Moghaddam, S., 2013, "Absorption characteristics of lithium bromide (LiBr) solution constrained by superhydrophobic nanofibrous structures", Int. J. Heat and Mass Transf. 63 pp. 82-90.
[3] de Vega, M., Venegas, M., García-Hernando, N., Ruiz-Rivas, U., 2015, "Performance evaluation of H2O-LiBr absorber operating with microporous membrane technology", 1st Thermal and Fluid Engineering Summer Conference, TFESC, NY, USA
[4] Schaal, F., Weimer, T., Hasse, H., 2008, "Membrane Contactors for Absorption Refrigeration," *International Sorption Heat Pump Conference*, Seoul, Korea
[5] M. Venegas, M. de Vega, N. García-Hernando, U. Ruiz-Rivas, "A simple model to predict the performance of a H2O–LiBr absorber operating with a microporous membrane", Energy 96 pp. 383-393.

5th Micro and Nano Flows Conference
Milan, Italy, 11-14 September 2016

A microfluidic device for studying drug transport through endothelial Blood Brain Barrier cells monolayers

Giovanni Stefano Ugolini[1], Marco Rasponi[1], Alberto Redaelli[1]

[1]Department of Electronics, Information and Bioengineering, Politecnico di Milano, Milan. Italy

Keywords: Blood Brain Barrier, Microdevice, TEER, endothelial cells

Introduction

The Blood Brain Barrier (BBB) is a functional biological structure of the Central Nervous System (CNS) that separates the vascular compartment of the brain from the cerebral parenchyma. Particularly tight junctions between endothelial cells protect the CNS tissue from undesirable molecules and small organism flowing in the blood [1]. This, however, leads also to an impeded transport of drug molecules and treatments from the bloodstream to the brain. Engineering a controlled strategy to selectively deliver molecules across the BBB is a key objective of brain research, with the goal of improving and finding treatments for pathologies such as Alzheimer's and Parkinson's disease, brain infections and brain cancer [2].

Developing *in vitro* models of the BBB represents a key step towards the optimization and discovery of effective ways to cross the BBB and deliver therapies. The most common mimicking strategy is the use of two-chamber cell culture systems: by seeding endothelial cells on top of a filter membrane and reaching confluence, the transport of drug candidates is evaluated at the bottom of the filter, in a collecting chamber. An increase in Trans-Endothelial Electrical Resistance (TEER) is the standard technique for monitoring endothelial barrier formation and is usually performed with commercial voltohmeters.

In this work, we developed and tested a microfluidic device as an *in vitro* model of the BBB: the main advantage of employing micron-scale devices is the reduced amounts of cells, reagents and candidate drug molecules to be employed in experiments.

Materials and Methods

Microdevice fabrication. Silicon master molds are fabricated by standard SU-8 photolithography on clean silicon wafers. The microfluidic device is fabricated in polydimethylsiloxane (PDMS) and polycarbonate (PC): a PC porous membrane is included between two PDMS fluidic layers realized through replica molding of PDMS on the silicon molds. The top layer features a seeding chamber for endothelial cells seeding and the bottom layer features a collecting chamber for transport molecules collection. In both upper and lower layers, side channels are present for insertion of four total electrodes: two Ag/AgCl electrodes (one in each layer) and two Platinum electrodes (one in each layer). This setup allows a four-point measure of the electrical resistance across the PC membrane.

Cell culture Devices were sterilized in ethanol overnight, coated with fibronectin and subsequently seeded with murine brain endothelial cells (Br-Bend5). TEER recordings were performed every 24h. After 5 days of culture, cells were fixed and probed for antibodies against V-Cadherin and Claudin to assess tight junction formation. A fluorescence analysis of FITC-labeled 40kDa Dextran transport was also carried out.

Results and Discussion

The devices showed high biocompatibility with cell cultures successfully performed for up to 7 days. Cells cultured in the microdevices were positive for tight junctional markers (V-Cadherin, Claudin). Injection of FITC-labeled 40kDa dextran in the upper chamber resulted in free transport to the lower chamber only in control conditions. After 5 days of culture, the Br-Bend5 monolayer was able to block the transport of 40 kDa dextran. This further demonstrates the formation of a functional barrier that hinders transport of small molecules.

The embedded electrical system for TEER measurement was also tested: the results obtained show a slight increase of the TEER in cultured devices with respect to control devices (no cells seeded) especially at day 5. However, the measurement resulted affected by noise and by an increasing drift also in control devices. This is in line with recent communications underlining the difficulty of translating the TEER measurement system from macro-scale to micro-scale platforms due to small channels and high electrical resistances [3].

Conclusions

We designed and developed a microdevice for transport studies across endothelial BBB monolayers. The device features a PC porous membrane for cell seeding in an upper chamber, and a lower chamber collecting the transported molecules. Side electrodes also allow monitoring of TEER during culture. A preliminary validation was carried out with murine endothelial BBB cells and resulted in cells forming a functional barrier to small molecules and increasing the resistance measured by the embedded TEER measurement system.

References:

[1] Weiss, *et al.,* 2009. The blood-brain barrier in brain homeostasis and neurological diseases. *Biochimica et biophysica acta.* 1788 (4). 842-57

[2] Pardridge, 2012. Drug transport across the blood–brain barrier. *Journal of Cerebral Blood Flow & Metabolism.* 32 (11). 1959-72

[3] Odijk, *et al.,* 2015. Measuring direct current trans-epithelial electrical resistance in organ-on-a-chip microsystems. *Lab Chip*. 15(3). 745-52.

ID 56

Pressure Drop Modelling in Gas Channels of Polymer Electrolyte Fuel Cells

Zan WU *, Martin ANDERSSON, Bengt SUNDEN

* Corresponding author: Tel.: +46 (0)46 2228604; Fax: +46 (0)46 2224717; Email: zan.wu@energy.lth.se
Department of Energy Sciences, Lund University, Lund, Sweden

Abstract The two-phase pressure drop characteristics in gas channels of Polymer Electrolyte Fuel Cells (PEFCs) are modelled in this work for different flow patterns. The two-phase flow in gas channels of PEFCs has its special features: (1) combination of reactant gas, water vapor and liquid water, (2) flow in micro/minichannels, (3) reactant consumption, (4) condensation from water vapor, (5) continuous water introduction from reaction and (6) flow pattern transitions. Therefore, previous two-phase pressure drop correlations, primarily for gas-liquid adiabatic flow, are unable to capture the pressure drop of the gas channels accurately. In general, there are three main two-phase flow patterns in the gas channels, i.e., slug flow, film flow and droplet flow. Flow-pattern based and segmented pressure drop modelling along the gas channels is generalized. The new predictive tool presents improved accuracy in pressure drop estimation for different current densities and stoichiometric ratios.

Keywords: Pressure drop, Two-phase flow, Polymer electrolyte fuel cell, Flow pattern

1. Introduction

The use of clean-fuel and pollutant-free PEFCs, which convert chemical energy released during the electrochemical reaction of hydrogen and oxygen directly into electricity, still has substantial momentum for future sustainable and renewable energy conversion systems. Liquid water from the reaction is transported through the gas diffusion layers (GDLs) into the gas channels. Water management is a central issue for PEFCs because a perfect amount of water is required in PEFCs, for example, for membrane hydration. The flow and hydrodynamics in gas channels are important to maintain a delicate water balance. This work will focus on the flow pressure drop in gas channels, which is of relevance for the reactant pumping power and the cell performance.

Single-phase pressure drop in micro/minichannels is well understood and predictive methods for conventional channels are still applicable for micro/minichannels if the surface roughness and entrance effects are correctly realized. However, the pressure drop prediction for two-phase flow is more complex and pressure drop correlations for conventional channels are not applicable any more, or only applicable within a limited range. Compared to adiabatic gas-liquid two-phase flow in microchannels, the two-phase flow in gas channels of PEFCs has its special features: (1) combination of reactant gas, water vapor and liquid water, (2) reactant consumption, (3) water vapor condensation, (4) continuous water introduction from reaction and (5) flow pattern transitions. As pressure drop for two-phase flow is closely coupled with flow patterns, flow-pattern based methods need to be developed to provide a relatively general and reliable prediction.

2. Flow Patterns in Gas Channels

Due to continuous water introduction from the GDLs and possible water condensation from water vapor, the flow in gas channels may experience different flow patterns, e.g., single-phase gas flow, droplet flow (also called mist flow), film flow (also called annular flow) and slug flow. Hussaini and Wang [1] firstly observed all these flow patterns in an operating fuel cell and developed a flow pattern map. In the droplet flow, small water droplets flow at the same velocity as the gas flow. The film flow indicates that liquid flows on the channel walls and gas flows in the core. The slug flow means large liquid plugs (longer than the channel diameter) with large gas slugs in between. In this work, the flow pattern map of Hussaini and Wang [1], which can also capture the experimental data of See [2], is used to determine the flow patterns. It should be noted that within a PEFC, the microchannels have

three solid walls and one porous wall (the gas channel/GDL interface) with significant different wall characteristics.

3. Pressure drop modelling

There are two concepts for two-phase frictional pressure drop modelling: homogeneous flow modelling and separated flow modelling. In the homogeneous flow modelling, the two-phase mixture is assumed as a pseudo single phase flow by using averaged viscosity and density values. The average density is given by

$$\rho_{\mathrm{TP}} = \left(\frac{x}{\rho_{\mathrm{g}}} + \frac{1-x}{\rho_{\mathrm{l}}} \right)^{-1} \quad (1)$$

There are different two-phase viscosity models, e.g., the Dukler et al. model [3]. Different viscosity models might give a large difference in prediction of the frictional pressure drop. In the droplet flow pattern in gas channels of PEFCs, the small droplets flow at the same velocity as the gas, i.e., zero slip velocity. Therefore, the homogeneous model can be used to calculate the pressure drop in the droplet flow pattern.

In the separated flow modelling, the two-phase frictional pressure drop is estimated based on the pressure drop of one phase multiplied by the two-phase frictional multiplier.

$$\left(\frac{dP}{dz} \right)_{\mathrm{TP}} = \phi_{\mathrm{g}}^2 \left(\frac{dP}{dz} \right)_{\mathrm{l}} \quad (2)$$

Chisholm [4] introduced a Chisholm parameter to define the two-phase frictional multiplier as

$$\phi_{\mathrm{g}}^2 = 1 + CX + X^2 \quad (3)$$

where X is the Martinelli parameter. The above equation was modified by Zhang et al. [5] considering non-uniform water introduction from GDL,

$$\phi_{\mathrm{g}}^2 = 1 + \frac{1}{2}CX + \frac{1}{3}X^2 \quad (4)$$

Various modifications of the Chisholm parameter C were presented in the literature to match the experimental data. Specific to gas channels in PEFCs, Grimm et al. [6] correlated the value of C as a function of the quality ratio, as given below

$$C = 0.0856 u_{\mathrm{l}}^{-1.202} \left(\frac{x}{1-x} \right)^{\left[0.004 u_{\mathrm{l}}^{-0.526} \right]} \quad (5)$$

where x and u_{l} indicate the gas flow quality and the liquid superficial velocity, respectively. Anderson et al. [7] proposed C as a function of current density (i, mA cm^{-2})

$$C = 5 + 12.2 \exp\left(\frac{82}{i} \right) \quad (6)$$

As the slip velocity in the film flow and slug flow patterns in gas channels is not zero, separated flow models need to be used.

Therefore, a flow-pattern based pressure drop model is proposed in this work. Firstly, flow patterns in gas channels will be identified by the Hussaini and Wang [1] flow pattern map. Then, specific to gas channels in PEFCs, different models need to be used for subsections of different flow patterns, e.g., single-phase correlations for gas flow, homogeneous flow modelling for droplet flow and separated flow models for film flow and slug flow patterns. Property variations might be neglected for small temperature differences. Each flow pattern might be segmented into several control volumes considering the variation of the water introduction along the length of the gas channels, i.e., the variations of the liquid and gas superficial velocities. The Darcy law will be used to calculate the velocity for each phase.

The total frictional pressure drop calculated by the above model will be compared with literature data and possible modifications of the Chisholm parameter C might be realized for better pressure drop estimations.

References

[1] I.S. Hussaini, C.Y. Wang, J. Power Sources 187 (2009) 444-451.
[2] E. See, M.S. Thesis, Rochester Institute of Technology, 2013.
[3] A.E. Dukler, M. Wicks, R.G. Cleveland, AICHE J. 10 (1964) 38-51.
[4] D. Chisholm, Int. J. Heat Mass Transf. 10 (1967) 1767-1778.
[5] L. Zhang, H.T. Bi, D.P. Wilkinson, J. Stumper, H. Wang, J. Power Sources 183 (2008) 643-660.
[6] M. Grimm, E.J. See, S.G. Kandlikar, Int. J. Hydrogen Energy 37 (2012) 12489-12503.
[7] R. Anderson, E. Eggleton, L. Zhang, Int. J. Hydrogen Energy 40 (2015) 1173-1185.

5th Micro and Nano Flows Conference
Milan, Italy, 11-14 September 2016

Acoustothermal heaters for thermochromic point-of-care displays

Jinsoo PARK[1], Byung Hang HA[1], Ghulam DESTGEER[1], Jin Ho JUNG[1], and Hyung Jin SUNG[1,*]

* Corresponding author: Tel.: +82 (42) 350 3027; Fax: +82 (42) 350 3296; Email: hjsung@kaist.ac.kr
1 Department of Mechanical Engineering, KAIST, Deajeon, Korea

Keywords: Thermochromism, Point-of-care displays, Acoustothermal heater, Surface acoustic wave

Over the last few decades, surface acoustic waves (SAWs) have been extensively utilized in diverse fields including microfluidics and telecommunication. Recently, we extended the applications of SAWs to acoustothermal heating toward continuous flow PCR [1] and one-shot high-resolution melting analysis [2]. Here we introduce disposable thermochromic point-of-care (POC) displays with acoustothermal heating, taking advantage of its spatiotemporal controllability. In POC diagnostics, the test results should be unambiguously displayed to prevent misinterpretation [3]. To meet the needs for POC displays, various types of thermochromic displays have been developed [4, 5]. Thermochromism refers to a reversible change of colors depending of temperature. Compared to the previously reported thermochromic displays, the proposed displays with acoustothermal heaters have significant advantages. First, the heaters and displays can be separated, leading to disposable display, a decrease in cost and an increase in flexibility of display contents. Second, the acoustothermal heaters can be spatiotemporally controlled with time-division multiplexed (TDM) AC signals, allowing fast and accurate control of display without an additional driver circuit.

As illustrated in Fig. 1(a), a typical SAW system is composed of a piezoelectric substrate ($LiNbO_3$, LN) and an interdigital transducer (IDT) deposited on the LN substrate. When AC signals with a frequency (f_{AC}) corresponding to c_s/λ (sound velocity of LN/IDT spacing), IDT resonates and thus produces SAWs bidirectionally. When a viscoelastic material (PDMS) is loaded on the IDT/LN substrate, SAWs are converted into longitudinal waves (LWs) and attenuated by viscoelastic damping, generating heat. The thermochromic display system comprises the acoustothermal heating element composed of the LN substrate, IDT, and this PDMS membrane and the thermochromic display element composed of an adhesive paper where information is pre-programmed and an thermochromic film that changes its color from black to translucent at the critical temperature (40°C), as in Fig. 1(b). When the thermal energy transformed from the acoustic energy of SAWs is transferred to the thermochromic film of the display element, display contents concealed under the film is exposed. As mentioned earlier, the acoustothermal heater can be spatio-temporally controlled with TDM AC signals. As in Fig. 2(a), when TDM AC signals with frequencies of f_1 and f_2 with a time interval (τ) of 0.0001 s are applied to the acoustothermal heater array with resonant frequencies of f_1, f_2, and f_3 (Fig. 2(b)), the corresponding IDTs resonate thereby heating up the display deposited on the heater, causing a selective heating and displaying as in Fig. 2(c). The inherent limitation that only pre-programmed information can be displayed can be addressed with a 3×3 acoustothermal heater array with 9 resonant frequencies (Fig. 3(a)). The alphabets 'A' and 'T' and numeric digits '1' and '2' are displayed in Figs. 3(b) and (c), respectively. More results will be presented in the full paper including colorimetric gradient displays and level displays. In summary, we introduce acoustothermal heaters with TDM AC signals and their application to disposable thermochromic POC displays.

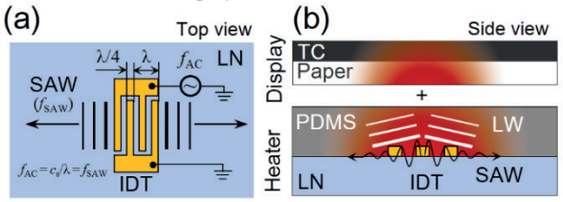

Figure 1. (a) Principles of SAWs; **(b)** Schematics of thermochromic displays with acoustothermal heaters.

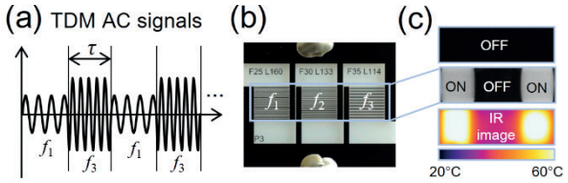

Figure 2. (a) TDM AC signals; **(b)** A 1×3 acoustothermal heater array; **(c)** Photos and IR images of thermochromic displays.

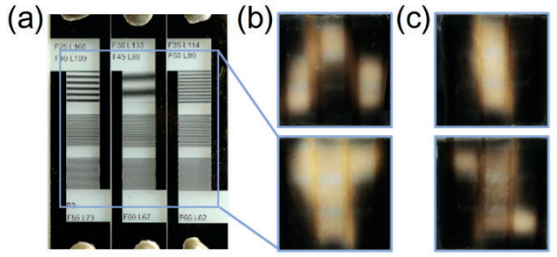

Figure 3. (a) A 3×3 acoustothermal heater array; **(b)** Alphabet displays of 'A' and 'T'; **(c)** Numeric digit displays of '1' and '2'.

References

[1] B. H. Ha, K. S. Lee, G. Destgeer, J. Park, J. S. Choung, J. H. Jung, et al., "Acoustothermal heating of polydimethylsiloxane microfluidic system," Sci Rep, vol. 5, p. 11851, 2015.

[2] B. H. Ha, J. Park, G. Destgeer, J. H. Jung, and H. J. Sung, "Generation of Dynamic Free-Form Temperature Gradients in a Disposable Microchip," Anal Chem, 2015.

[3] P. Yager, T. Edwards, E. Fu, K. Helton, K. Nelson, M. R. Tam, et al., "Microfluidic diagnostic technologies for global public health," Nature, vol. 442, pp. 412-8, 2006.

[4] A. C. Siegel, S. T. Phillips, B. J. Wiley, and G. M. Whitesides, "Thin, lightweight, foldable thermochromic displays on paper," Lab Chip, vol. 9, pp. 2775-81, 2009.

[5] H. Shin, B. Yoon, I. S. Park, and J. M. Kim, "An electrothermochromic paper display based on colorimetrically reversible polydiacetylenes," Nanotechnology, vol. 25, p. 094011, 2014.

ID 58

5nd Micro and Nano Flows Conference
Milan, Italy, 11-14 September 2016

Influence of the boundary conditions on the damping forces exerted by gas mixtures in high-frequency MEMS devices

Silvia LORENZANI [1,*]

* Corresponding author: Tel.: ++39 (0)2 23994566; Fax: ++39 (0)2 23994568; Email: silvia.lorenzani@polimi.it
1 Dipartimento di Matematica, Politecnico di Milano, Italy

Keywords: MEMS devices, gas mixtures, damping forces, Boltzmann equation

Micro-electro-mechanical systems devices vibrating at high frequencies (RF MEMS) (ranging from 1 MHz to 60 GHz) have been identified as a technology that has the potential to provide a major impact on existing RF architectures. In particular, the development of integrated silicon-based micromechanical resonators with high frequencies can have a great impact on the future of wireless communication systems [1], [2]. The high quality factors maintained by RF disk resonators at atmospheric pressure indicate the potential of these microdevices for several applications and implementation without the need for expensive vacuum packaging.

So far, in all the works where a mechanical analysis of RF MEMS has been reported, it was stressed that these devices are able to maintain high quality factors even at atmospheric pressure due to their much higher stiffness in comparison to other types of resonators vibrating at low frequencies. Low-frequency MEMS devices are normally operated at very low pressure in order to minimize the damping due to the internal friction of the gas (viscous damping).

When MEMS devices vibrate at relatively high frequencies, gas compressibility and inertial forces lead then to another damping mechanism which is related to the propagation of sound waves generated by high-frequency oscillating micro-structures.

Very recently, it has been proved in [3] for a single-component gas that sound waves propagating between the micro-device walls induce a resonant/antiresonant response of the system due to the constructive/destructive interference occurring between the incident and reflected sound waves. The occurrence of an antiresonance is particularly important since if the device is operated close to the corresponding frequency, the damping due to the gas is considerably reduced. Since gas resonances take place for each value of the rarefaction parameter (inverse Knudsen number), the RF MEMS devices can perform well also at atmospheric pressure.

In this frame, it is important to analyze not only the damping forces exerted by single-component gases but also those exerted by gas mixtures, since during the wafer bonding process a mixture of noble gases (like Ar, Kr or Ne) and getterable gases (like N2, O2 or CO2) is usually backfilled into the MEMS sensor package to set its operating pressure ('backfilling process').

In the current investigation, we extend the previous analysis carried out for a single species gas [3] to a gas mixture, by using the linearized Boltzmann equation based on a simplified kinetic model of BGK-type [4].

General boundary conditions of Maxwell's type [5] have been considered in order to take into account bounding surfaces with different physical structures.

References

[1] Pourkamali, S., Hao, Z., Ayazi, F. (2004). VHF single crystal silicon capacitive elliptic bulk-mode disk resonators-Part II: Implementation and characterization.
Journal of Microelectromechanical Systems, 13, 1054-1062.

[2] Clark, J. R., Hsu, W.-T., Abdelmoneum, M.A., Nguyen, C. T.-C. (2005). High-Q UHF micromechanical radial-contour mode disk resonators.
Journal of Microelectromechanical Systems, 14, 1298-1310.

[3] Desvillettes, L., Lorenzani, S. (2012). Sound wave resonances in micro-electro-mechanical systems devices vibrating at high frequencies according to the kinetic theory of gases.
*Phys. Fluids, 24**, 092001*-**24.**

[4] Groppi, M., Spiga, G. (2004). A Bhatnagar-Gross-Krook-type approach for chemically reacting gas mixtures.
Phys. Fluids, 16, 4273-4284.

[5] Cercignani, C. (1988). The Boltzmann equation and its applications. Springer, New York.

5th Micro and Nano Flows Conference
Milan, Italy, 11-14 September 2016

Flow configurations in a Y Splitting-Junction Microchannel

Marco PECORARIO, Giovanni P. ROMANO *

* Corresponding author: Tel.: ++39/0644585913; Fax: ++39/0644585250; Email: giampaolo.romano@uniroma1.it
Dept. Mechanical & Aerospace Engineering, University La Sapienza, Roma, Italy

Keywords: Micro Flow, Micromixer, Y Junction, Reynolds number, microPIV

In the present work, the flow field in a splitting-junction micro channel with Y shape, which can be employed as micro-heat-exchanger and micro-mixer, is investigated experimentally using mPIV (micro Particle Image Velocimetry). The angular divergence in the Y splitting is changed as also the Reynolds number in order to investigate the instantaneous and mean flow configurations which are more suitable for applications.

1 Introduction

The use of micro-devices is nowadays widely increasing due to the relevant advantages in efficiency when compared to their macro counterparts. This led to several applications in the field of Biomedicine and Bio-Engineering, in Sensors, Control and Automation and in Energy Engineering. Considering the latter, the devices which are usually employed in this field are micro-heat-exchangers, micro-mixers and micro-pumps (Laser & Santiago 2004, Kallio 2010). Specifically, it is challenging to design those systems at micro-scales ensuring net momentum (or temperature) diffusion with passive methods, i.e. using only changes in geometry or inserting external elements in the flow.
In micro-channel flows, an effective simple possibility to increase diffusion is to add a Y splitting section and then recombining the two branches in an inverse Y junction. However, the effect of the angular divergence and convergence also in relation to Reynolds number is not entirely investigated. Thus, the aim of the present experimental work is to investigate the effect of the Y section angle and of the flow velocity (Reynolds number) in the resulting flow configuration, in order to optimize the design of micro-heat-exchangers and micro-mixing devices.

2 Device and set-up specifications

The test section consists of a channel with rectangular cross-section (height = 0.4 mm, width = 4 mm) followed by a splitting section with two possible angles, 30é and 45é and again by a junction with angles respectively of 45é and 30é.

An example of the test section is given in Figure 1. The measurements have been performed in a range of velocities from 0.01 m/s to 0.1 m/s, thus resulting a maximum Reynolds number around 50. A 50 mm focal lens objective is used with multiple extension tubes up to 48 mm. High resolution images of the region upstream of the splitting section, of the two branches and of the junction are acquired by a high speed video-camera (up to 2000 frames/s at the maximum spatial resolution of 1024½1024 pixels) and stored on a PC. The water flow is seeded with hollow glass spherical tracers with diameters between 5mm and 10 mm, which are injected in the flow using a syringe pump. Two consecutive frames are analyzed in order to determine the flow tracer displacements using the micro Particle Image Velocimetry (mPIV) technique. An example of result on the instantaneous flow field is presented in Figure 2. The data are obtained from two consecutive images as that in Figure 1 by applying iterative cross-correlation algorithms, using 32*32 pixel final sub-windows. The velocity vectors are clearly seen without major spurious data. About 1000 frame couples are acquired in each condition to derive mean and rms fields.

3 Results

In Figure 3, examples of the resulting mean vector fields for the Y junction region are presented for two converging angles at the same Reynolds number (around 40). It is clearly observed that the two configurations are rather different, the one with the smallest angles (around 30é) showing a velocity defect at the centerline persisting further downstream in comparison to the other (angle equal to 45é). Thus, the maximum velocity at the centerline is smaller for the small angle compared to the other (by about 10% to 20% depending on the Reynolds number) and the velocity profile is flatter. This is also observed in Figure 4 in which the color plots of the horizontal velocity component are presented for the two conditions.

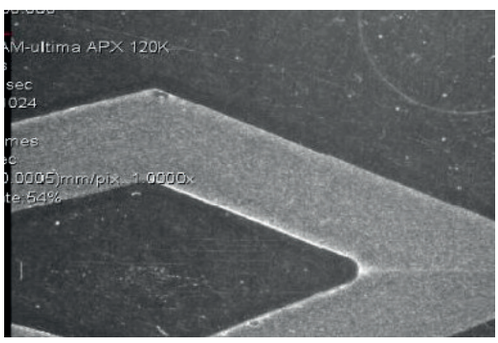

Figure 1. Detail of the Y channel junction as acquired by the camera.

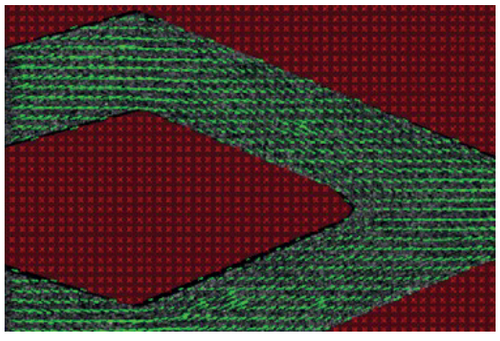

Figure 2. Instantaneous flow vector field derived from image in Figure 1.

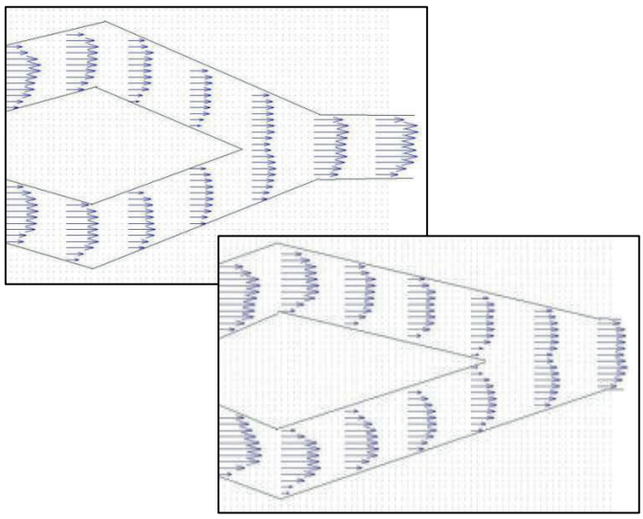

Figure 3. Vector fields in the Y channel junction for angles equal to 45é (on the left) and 30é (on the right) at a Reynolds number equal to 40.

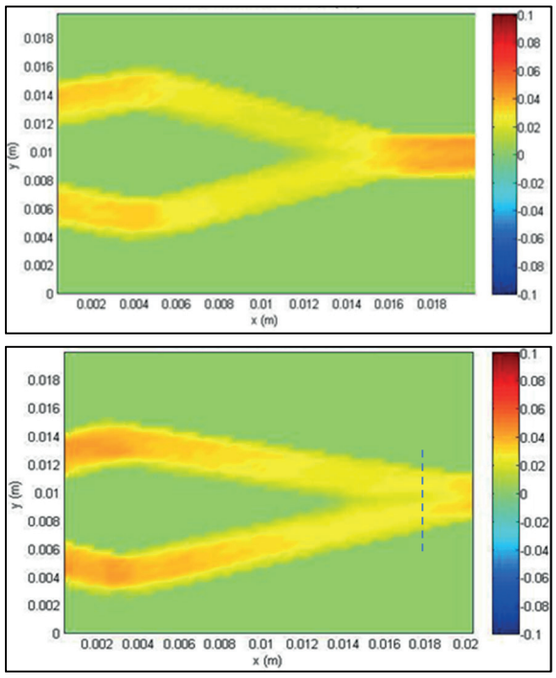

Figure 4. Horizontal velocity component in the Y channel junction for angles equal to 45é (at the top) and 30é (at the bottom) at a Reynolds number equal to 40. Velocity scale in m/s.

For the second configuration, the velocity is recovered further downstream in comparison to the first, thus indicating that a large splitting angle at the inlet of the bifurcation followed by a small junction angle seems to produce a better mixing in comparison to the opposite.

This is verified by considering the average velocity fluctuations as measured by rms values, presented in Figure 5 for the horizontal velocity component. In the figure, it is observed that the maximum intensity of fluctuations is always lower than 10% (1/10th of the maximum velocity), but in the second configuration this level is higher, i.e. about 20% even in the splitting section. Moreover, in comparing the fluctuation levels after the junction with those at the inlet, it is observed that in the first configuration the increment is limited to 2%, whereas in the second it raises to (5-10)%.

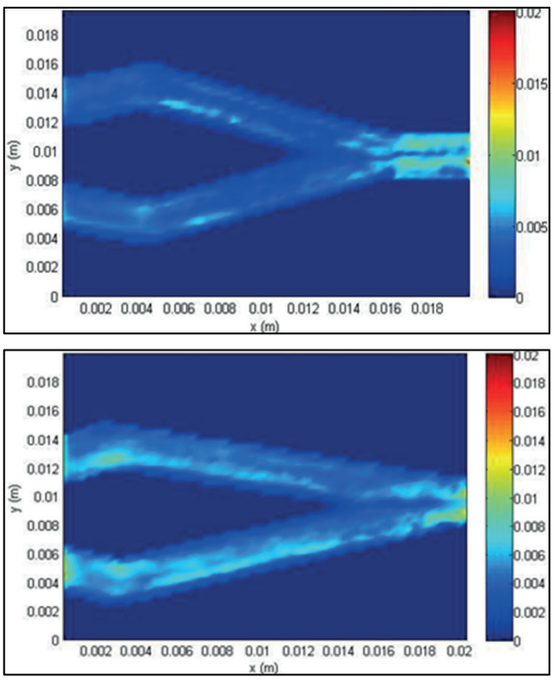

Figure 5. Root mean square fluctuations of horizontal velocity component in the Y channel junction for angles equal to 45é (at the top) and 30é (at the bottom) at a Reynolds number equal to 40. Velocity scale in m/s.

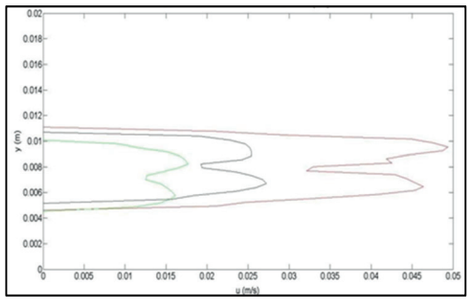

Figure 6. Horizontal velocity component profiles in the Y channel junction for an angle equal to 30é at Reynolds numbers around 13 (green), 23 (blue) and 40 (red). The profile is taken along the dotted line of Figure 4.

The dependence on the Reynolds number of these results is also related to the specific geometry. For example, for the second configuration, in Figure 6 the velocity profiles at the outlet (the dotted line in Figure 4) for four different flow rates are compared. In this case, the basic configuration is very similar and there seems to be a low Reynolds number dependence, whereas for the first condition the dependence is much more high due to the higher converging angle (not shown).

References

ST Wereley and CD Meinhart, `Recent Advances in Micro-Particle Image Velocimetry_, Annual Review of Fluid Mech., pp. 561-563, 2010.

TA Ameel, RO Warrington, RS Wegeng and MK Drost, `Miniaturization technologies applied to energy systems_, Energy Conversion and Management, Vol. 38, pp. 978-979, 1997.

GS Nuno Leal and V Semiao, `Determination of microchannels geometric parameters using micro-PIV_, Chemical Engineering Research and Design. Vol. 87, 2009.

5th Micro and Nano Flows Conference
Milan, Italy, 11-14 September 2016

Microfluidic device for high throughput SPIM on chip

Petra PAIE'[1,*], Francesca BRAGHERI[2], Andrea BASSI[1] , Roberto OSELLAME[2]

* Corresponding author: Email: petra.paie@mail.polimi.it
1Dipartimento di Fisica, Politecnico di Milano, Piazza Leonardo da Vinci 32, 20133 Milano, Italy
2Istituto di Fotonica e Nanotecnologie, CNR, Piazza Leonardo da Vinci 32, 20133 Milano, Italy

Keywords: Microfluidic, optofluidic, fluorescence microscopy

Selective Plane Illumination Microscopy (SPIM) is a powerful microscopy technique that permits to obtain 3D reconstruction of biological samples, in a noninvasive way, by optical sectioning. Specific and dedicated setups are often needed, moreover the sample positioning and alignment is time consuming and prevents the use of this method for a statistical relevant number of specimens. Here we propose an innovative microfluidic device, with a footprint of few mm^3, which is capable to upgrade a standard microscope to a SPIM one, and capable to analyze up to 30 samples/minute.

SPIM on chip

SPIMis a powerful microscopy technique that optically sections a sample illuminating it with a light sheet [1]. The fluorescence signal is orthogonally collected with a microscope objective. Sample translation or rotation is required to capture the signal from all the distinct slices that constitute the sample and that are needed for the reconstruction of the 3D image. Bulk set up and specific instrumentation is needed to perform this measurement, moreover the manual sample positioning in the middle of a water filled sample chamber has to be accurate and perfectly aligned with respect to the light sheet and to the collection objective. This procedure can last up to several minutes. Here we present a compact microfluidic device that integrates light sheet formation and sample translation in the same platform, permitting to continuously analyze distinct specimens, without the need of manual positioning or alignment. This device is capable to speed up the measure, making possible for the first time the SPIM acquisition of large sample populations in a reasonable amount of time.

The device fabrication in a fused silica substrate is made possible by the FLICE technique, which is Femtosecond Laser Irradiation followed by Chemical Etching. This is a two-step fabrication approach, where the device is first irradiated by a focused femtosecond laser beam that locally modifies the material in correspondence of the focal region. Then the substrate is exposed to an ultrasonic bath of Hydrofluoric acid (HF) solution, which selectively attacks the irradiated regions, leading to the microchannel formation [2-4]. The 3D capabilities of this technique are fundamental in developing the SPIM on chip layout.

The device geometry is reported in figure 1, where it is possible to note the presence of the microfluidic lens, which is used to obtain the light sheet and the sample channel. The sample flows in the microfluidic network where it is intercepted by the light sheet and sectioned with no manual positioning or alignment needed. The signal is collected with an external microscope objective, while the cylindrical lens that produces the light sheet is fabricated in the chip with an optimized design to reduce the impact of spherical aberrations, which would reduce the quality of the light sheet and consequently the resolution of the SPIM image.

This device has been validated with fixed cellular spheroids, which

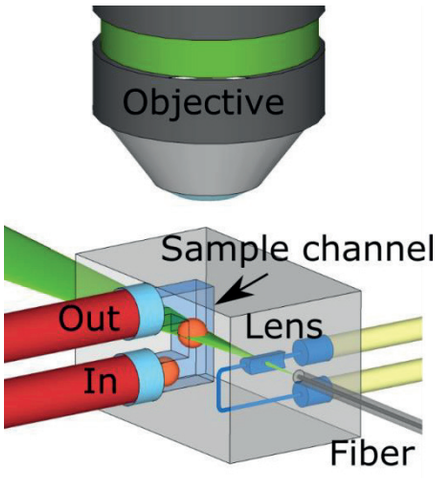

Figure 1 Schematic design of the SPIM on chip device.

are spherical cell aggregates with a few hundreds micrometer size. The validation demonstrated the capability of this device to obtain 3D reconstruction of the sample with very good subcellular resolution. Moreover, by increasing the sample flow rate and using a fast camera, we have been able to process up to 30 samples/minute.

This is a very promising device, with many innovative features. Not only it permits to upgrade a standard microscope to a SPIM one, just placing this device on its plate, but also it facilitates the SPIM acquisition, which can now be performed by non-expert end-users. High throughput acquisition is demonstrated, opening SPIM microscopy to new interesting applications.

References

1. Huisken, J., Swoger, J., Del Bene, F., Wittbrodt, J., & Stelzer, E.H., Optical Sectioning Deep Inside Live Embryos by Selective Plane Illumination Microscopy, *Science* **305**, 1007-1009 (2004).
2. Osellame, R., Hoekstra, H. J., Cerullo, G., Pollnau, M. Femtosecond laser microstructuring: an enabling tool for optofluidic lab-on-chips. *Laser & Photonics Reviews* **5**, 442-463 (2011).
3. Gattass, R. & Mazur, E., Femtosecond laser micromachining in transparent materials *Nature Photon.* **2**, 219 (2008).
4. Paiè, P., et al. Straightforward 3D hydrodynamic focusing in femtosecond laser fabricated microfluidic channels. *Lab on a Chip*, ***14***(11), 1826-1833. (2014).

5th Micro and Nano Flows Conference
Milan, Italy, 11-14 September 2016

CFD simulation of precipitation in solvent-displacement processes

Matteo RIZZOTTO [1], Mattia SPONCHIONI [1], Davide MOSCATELLI [1], Renato ROTA [1], Valentina BUSINI [1,*]

* Corresponding author: Tel.: +39 0223993186; Fax: +39 0223993180; Email: valentina.busini@polimi.it
1 Department of Chemistry, Materials and Chemical Engineering "G. Natta", Politecnico di Milano, IT

Abstract Polymer nanoparticles have been proved as nanocarriers for controlled drug delivery, due to their tunable properties and their low toxicity. A very important parameter for nanoparticles is their Particle Size Distribution (PSD), because it influences some key properties such as particle surface area and rheology. In this work a comparison between experimental data and a computational fluid dynamics (CFD) model for precipitation of polycaprolactone nanoparticles via solvent-displacement is presented. The model is implemented in ANSYS Fluent, where particle formation is determined by the description of classical nucleation, molecular growth, and aggregation. Results show good agreement with experimental data, proving the suitability of the CFD approach in this type of problems.

Keywords: Precipitation, Population balance, Computational fluid dynamics, T-reactor

1. Introduction

Polymer nanoparticles (NPs) have been largely studied in recent literature because they owe multiple degrees of freedom like tunable degradability and hydrophobicity, size, surface charge and form in which they can be produced (such as particles or capsules) [1].
Accordingly, polymer NPs show interesting applications in several fields, such as controlled drug delivery. An important characteristic of the polymer NPs used for biomedical applications is their Particle Size Distribution (PSD) which has to be as narrow as possible to effectively deliver the drug to the target [2].
Most of the methods used to produce NPs involve the mixing of two or more liquid streams, as for instance in the solvent displacement process, which is also known as nanoflash precipitation [1]. To obtain a narrow PSD through nanoflash precipitation it is necessary to suitably tune the operating conditions in order to favor the particles nucleation process with respect to the molecular growth process, which can be obtained by improving the mixing efficiency.
A very high mixing rate can be achieved using a T-reactor, where two liquid flows are mixed in a T-shaped junction.

2. Material and methods

In this work, a small PTFE cylindrical chamber of 1 cm of diameter and 1 cm of length with an axial perforation of 1 mm diameter and a radial one of 500 μm was used. In this reactor, the injection of different fluids from the radial duct with a suitable velocity provides the mixing of the two solutions in a very short time, therefore allowing for obtaining the required narrow PSD. A sketch of the reactor is shown in Fig. 1.

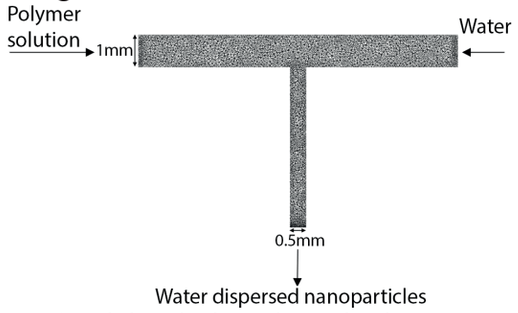

Fig. 1. Mixing device schematization.

Using this reactor, polycaprolactone (PCL, Mw 14kDa) NPs were produced by feeding the reactor with a solution of PCL in acetone from

one side and water from the other side (see Figure 1). Both these solutions were loaded in syringe pumps and injected radially in the device at the same flow rate (1 mL/min). PCL was synthesized using ring opening polymerization (ROP) using stannous octoate as catalyst and benzyl alcohol as initiator in a mole ratio of 1:123 with respect to the caprolactone monomer, as reported in literature [3]. In order to study the influence of PCL concentration on nanoparticles size, different PCL solution concentrations were used in this work. NPs produced with different operating conditions were characterized through dynamic light scattering (DLS) using a Malvern Zetasizer Nano ZS analyzer.

The T-reactor was then simulated through CFD modeling (in particular, the ANSYS Fluent 15 code was used in this work [4]) coupled with the population balance tool embedded in the software for the determination of particles distribution and the description of nucleation, particles growth, and aggregation phenomena. Due to the saturation levels achieved during the simulations, only homogeneous primary nucleation was considered. As stated in the classic theory [5], the nucleation rate was implemented as follows:

$$J(S)=\frac{2D}{d^5}\,exp\left(-\frac{16\pi\gamma^3\tilde{v}^2}{3k_B^3T^3(ln\,S)^2}\right) \qquad (1)$$

Where D is the mass diffusivity of PCL, d is its molecular volume, γ is the interfacial tension between PCL NPs and the solution, $\tilde{v}$ is the PCL molecular volume, k_B is the Boltzmann constant, T is the temperature, and S is the saturation ratio, respectively.

Considering the size of the obtained particles (i.e., lower than 1 μm) the process can be assumed as diffusion-controlled and the growth rate can be expressed as follows:

$$G(S,L)=\frac{2ShDM_w c_{s,eq}}{L\rho}(S-1) \qquad (2)$$

Where Sh is the Sherwood number (equal to two), L is the particle size, $c_{s,eq}$ is the PCL solubility, and ρ is the PCL density, respectively.

Nucleation rate and growth rate were implemented in Fluent via UDF, whereas for the aggregation kernel the embedded free molecular model was used.

The adjustable parameters strictly related to the investigated system (surface tension, solubility, etc…) were either derived from suitable literature models when available or tuned on the experimental data [6].

3. Results and conclusions

As shown in Fig. 2 the trend of both experimental data and Fluent results is the same; the value of the mean diameter increases with the increasing of the initial PCL concentration, thus validating the CFD model.

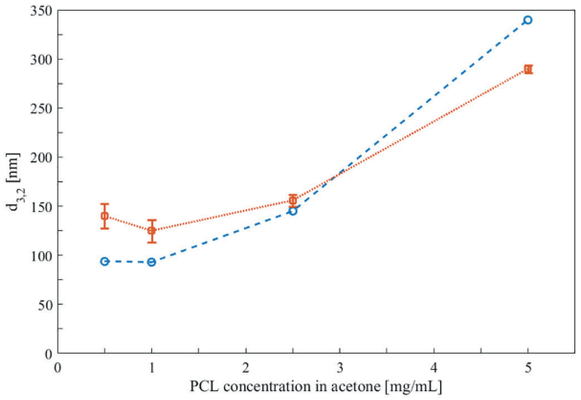

Fig. 2. Comparison of the Sauter diameter $d_{3,2}$ at the T-reactor outlet between experimental data (□) and Fluent prediction (○).

[1] Kamaly, N., et al., Targeted polymeric therapeutic nanoparticles: design, development and clinical translation. Chem. Soc. Rev., 2012. 41(7): p. 2971-3010.

[2] Alexis, F., et al., Factors Affecting the Clearance and Biodistribution of Polymeric Nanoparticles. Mol. Pharm., 2008. 5(4): p. 505-515.

[3] Labet M., Thielemans W., Synthesis of Polycaprolactone: a review. Chem. Soc. Rev., 2009. 38(12): p. 3484-3504.

[4] ANSYS Inc., ANSYS Fluent 15 User's guide. In Canonsburg, PA, USA, 2014.

[5] Mersmann A., Crystallization and precipitation, Chem. Eng. Process., 1999. 38(4-6): p. 345-353.

[6] Lince F., et al., J. Colloid Interface Sci., 2008, 322(2): p. 505–515

5th Micro and Nano Flows Conference
Milan, Italy, 11-14 September 2016

Characteristic of fluid flow in porous media with different open porosity

Tao Lin , Liang Gong *, Minghai Xu

* Corresponding author: Email: lgong@upc.edu.cn
Shandong Province Key Laboratory of Oil&gas Storage and Transportation Safety
China University of Petroleum (East China), Qingdao, Shandong, PRC. 266580

Keywords: Porous Media, IPT, QSGS, Block Structured Lattice Boltzmann Method, Darcy Law

Fluid flow in porous media is considered complex flow, which finds wide application in the fields of reservoir development, environmental protection, and chemical process. Therefore, it has important research significance. Fluid flow in porous media of different porosity and boundary conditions is studied in this paper. The porous media is constructed using Image Processing Technology (IPT) and Quartet Structure Generation Set (QSGS). (shown in Fig. 1). Under different porosity of porous media and pressure drop condition, fluid flow in a two dimensional channel partially filled with porous media is simulated using the block structured lattice Boltzmann method (shown in Fig. 2) on pore scale. As shown in Fig. 3, the block structured lattice Boltzmann method can successfully simulate complex flow in porous media. Furthermore, the detailed information of fluid flow in porous structure can be fully obtained. As shown in Fig. 4, within the scope of pressure drop conditions studied, the Darcy law remains valid. The relation between flux, permeability and porosity under different pressure drop is further studied. Fig. 5, shows that the flux increases with increasing porosity in both (a) and (b) under every pressure drop condition. Fig. 6, shows that the flux in porous media constructed with IPT is higher than that in porous model constructed using QSGS with the same porosity under the same pressure drop. From Fig. 7 shows that the permeability increases with increasing porosity in both (a) and (b) under every pressure drop condition. It also shows that the permeability does not vary much with changing pressure drop. In Fig. 8, we can see that the permeability of porous media constructed with IPT is higher than that of porous media of the same porosity but constructed with QSGS. Below conclusions can be drawn:

(1) The block structured lattice Boltzmann method can successfully simulate complex flow in porous media. Furthermore, the detailed information of fluid flow in porous media can be obtained.

(2) Within the scope of pressure drop conditions in study, the Darcy law remains valid.

(3) Under every pressure drop condition, both the flux and the permeability of porous media increase with increasing porosity, regardless of construction method being IPT or QSGS.

(4) With the same porosity, both the flux and the permeability models constructed by IPT are greater than those of models constructed using QSGS.

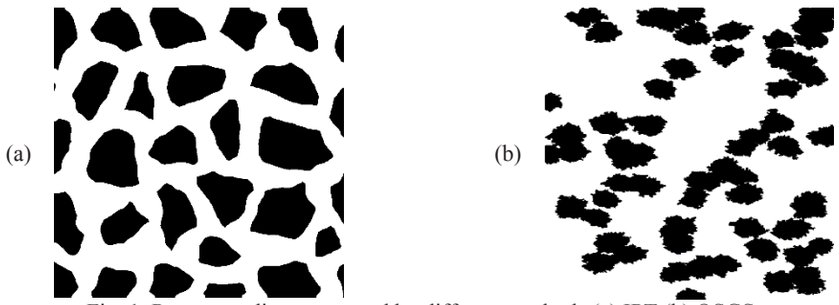

Fig. 1. Porous media constructed by different methods (a) IPT (b) QSGS

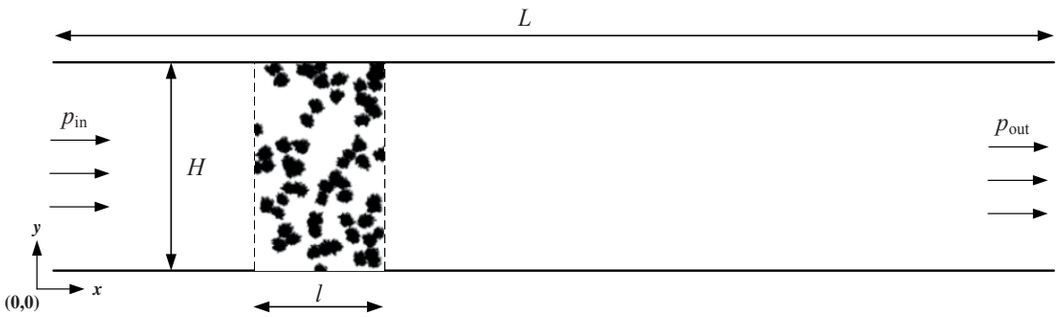

Fig. 2. Schematic diagram of the channel with porous media

The work was supported by the National Natural Science Foundation of China (51276199) and Fundamental Research Funds for the Central Universities (No. 14CX05027A, 15CX05037A).

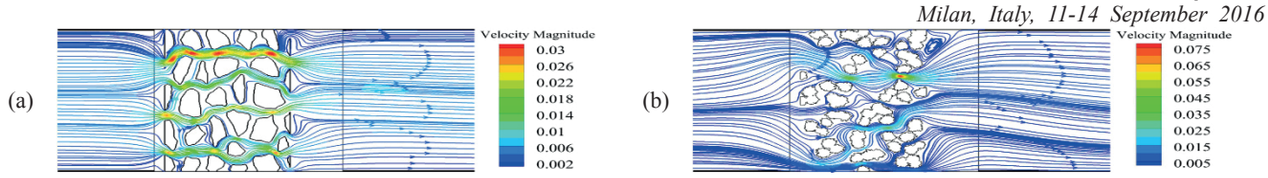

Fig. 3. Streamlines in porous media constructed by different methods (a) IPT (b) QSGS

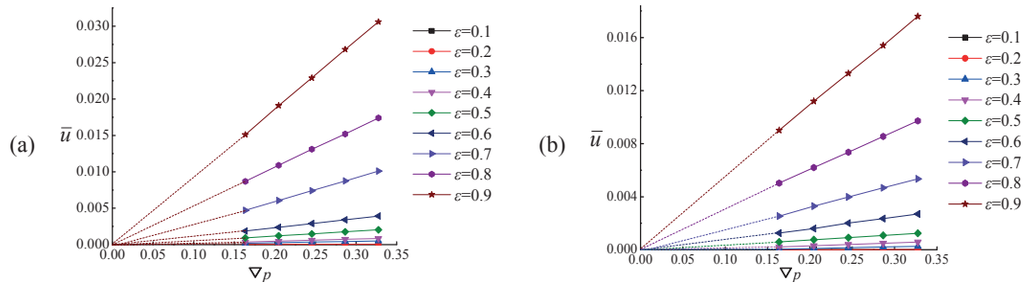

Fig. 4. The relation between mean velocity and the pressure gradient (a) IPT (b) QSGS

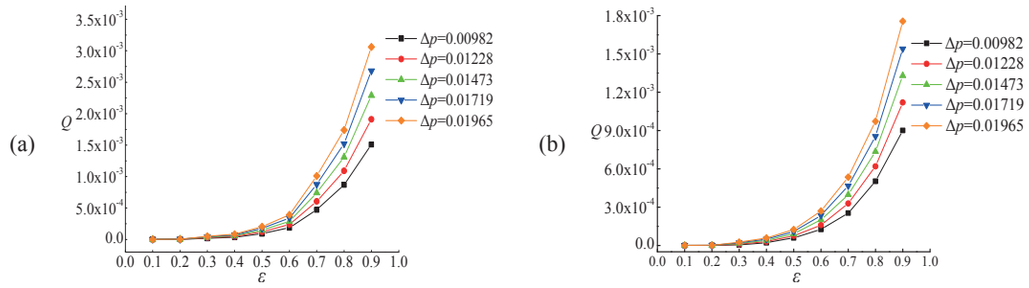

Fig. 5. The relation between the flux and the porosity (a) IPT (b) QSGS

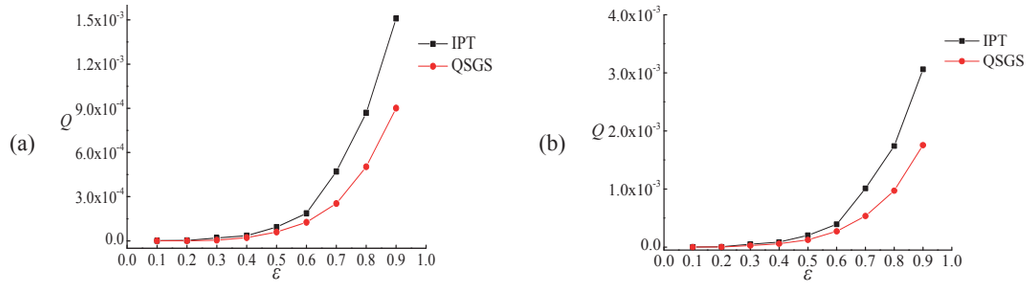

Fig. 6. The comparison of the flux between IPT and QSGS (a) Δp=0.00982 (b) Δp=0.01965

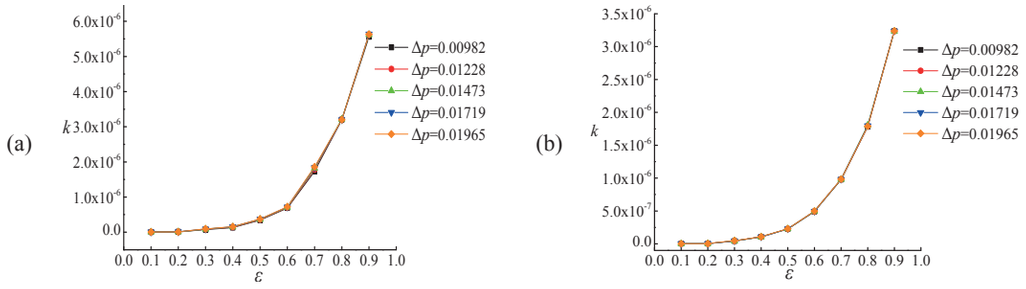

Fig. 7. The relation between the permeability and the porosity (a) IPT (b) QSGS

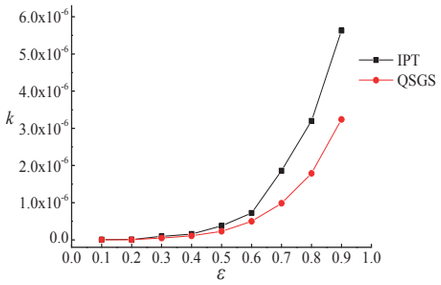

Fig. 8. The comparison of the permeability between IPT and QSGS

ID 63

5th Micro and Nano Flows Conference
Milan, Italy, 11-14 September 2016

New Approach for Mitigating Velocity and Temperature Non-Uniformity in Parallel Channel Microchannel Heat Sink

Vikas Yadav, Ritunesh Kumar [1,*]

* Corresponding author: Tel.: (+91) 7324 240734; Fax: (+91) 7324 240761; Email: ritunesh@iiti.ac.in
1: Mechanical Engineering Department, Indian Institute of Technology Indore, MP, India

Keywords: Microchannels, Heat Sink, Maldistribution, Non-Uniform, Nusselt Number,

Parallel channel MCHSs suffer from the problem of non-uniform flow (flow maldistribution) across channels. Flow maldistribution causes non-uniform velocity profile, which gives rise in non-uniform temperature profile due to unequal heat transfer from parallel microchannels. However, ideally it is desired that entire heat sink base should be at the same temperature in order to avoid problem of localized overheating. In the present single phase heat transfer study, effect of liquid flow mal-distribution on parallel channel (15 channels) MCHS has been studied numerically using water as working fluid. The entire heat sink has been taken as computational domain; three-dimensional governing equations for both fluid flow and energy transfer have been solved by finite volume method. The non-uniformity of velocity and temperature profile; caused due to flow maldistribution have been computed by finding average velocity and average temperature across each parallel microchannel. A novel liquid distributor design, bifurcating the inlet fluid flow into two liquid inlet lines; opening at inlet plenum has been proposed. Velocity and temperature distribution results of newly proposed design have been analyzed and compared with conventional design MCHS. Proposed design is found to effectively reduce temperature and velocity maldistribution in the parallel MCHS. The effect of Reynolds number on velocity maldistribution and temperature distribution has also been investigated in the current study.

Lab-on-a-Chip microfluidic platforms to monitor the shear-induced thrombotic risk in blood contacting devices

Annalisa DIMASI [1,*], Filippo CONSOLO [1], Marco RASPONI [1], Gianfranco B. FIORE [1], Lorenzo VALERIO [1,2], Federico PAPPALARDO [2], Danny BLUESTEIN [3], Marvin J. SLEPIAN [4], Alberto REDAELLI [1]

* Corresponding author: Tel.: +39 022399 4142; Fax: +39 022399 3360; Email: annalisa.dimasi@polimi.it
1 Department of Electronics, Information and Bioengineering, Politecnico di Milano, Milano IT
2 Department of Anesthesia and Intensive Care, IRCCS San Raffaele Scientific Institute, Milano IT
3 Department of Biomedical Engineering, Stony Brook University, Stony Brook (NY) USA
4 Department of Medicine and Biomedical Engineering, University of Arizona, Tucson (AZ) USA

Keywords: shear-induced thrombosis, platelet activation, PDMS microfluidics, blood contacting devices

Introduction

Blood contacting devices (BCD) such as ventricular assist devices (VADs), are widely used in the clinics to manage patients with heart failure. The fluid dynamic conditions in such devices can cause blood cell trauma and reaction such as hemolysis and platelet sensitization due to non-physiological shear stress patterns [1]. Shear-induced thrombosis due to platelet activation (PA) can cause device failure and serious post-implant complications for the patients. Flow-based assays allow to evaluate the shear-induced thrombotic risk *in vitro*. However, standard flow-based assays require large volumes of sample and reagents and do not allow high-throughput experiments. Furthermore, "hyper-shear" conditions and fast dynamics of shear stress patterns cannot be replicated in viscometer-based devices. As opposed, microfluidic technology can overcome these limitations and provide novel flow-based assays in which realistic flow patterns happening in BCDs can be replicated in a miniaturized microfluidic device.

Materials and Methods

In a recent numerical study [2], our group demonstrated the feasibility of designing microfluidic channels that replicate shear stress patterns experienced by platelets in VADs. Here, the same approach was used to design microfluidic channels (Fig. 1, left panel) that replicate a relevant shear stress pattern of the Heart Assist V (MicroMed Technology Inc., USA) VAD (Fig. 1, right panel). PDMS microfluidic platforms were fabricated through standard soft-lithography (Fig. 2, right panel).

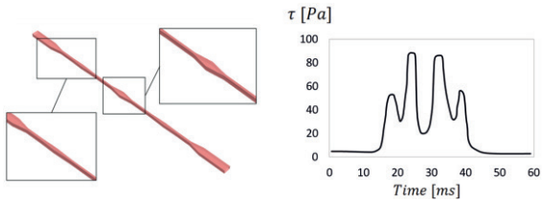

Figure 1. Design of the emulating microfluidic channel (left panel) and dynamic shear stress patterns (right panel).

In vitro tests of PA were performed by using the platelet activity state (PAS) assay [3]. Blood was withdrawn from healthy adult volunteers. Gel-filtered platelets (GFP) were collected after blood centrifugation and subsequent gel-column filtration of platelet rich plasma.

Experiments were conducted by flowing the GFP sample through the microfluidic platforms by means of two synchronized syringe pumps connected to the two inlet ports of the microfluidic device. The syringe pumps worked in a reciprocating mode allowing to flow the sample alternatively in two directions through the device. At different time points (corresponding to 4, 40 and 72 passages through the emulating channels) GFP was collected and tested for PA through the PAS assay.

Results

PAS values obtained in the *in vitro* tests are shown in Fig. 2 (right panel). Results are normalized with respect to a positive control obtained by sonicating the GFP sample. The 0 time point corresponds to the baseline PAS level of non-stimulated GFP samples. An increasing trend of activation was observed between 0 and 40 passages, while a quasi-plateau behaviour was observed from 40 to 72 passages, suggesting that a limit of platelet activation was reached at longer exposure time. This result is in accordance with the model of PA in stenosed vessels proposed by Boreda and co-authors [4] that would predict a non-linear trend of PA with respect to exposure time.

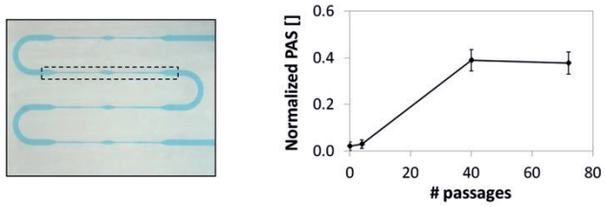

Figure 2. Microfluidic platform filled with stained water with the single emulating channel highlighted (left panle). Results of the *in vitro* tests of PA (right panel).

Conclusions

The study demonstrated the feasibility of using microfluidic platforms to perform shear-induced tests of PA under dynamic and VAD-like shear flow conditions. The shear-induced thrombogenic potential of a platform emulating a representative shear stress pattern of the HA5 VAD was characterized. In future experiments, *on chip* tests of PA will be performed and shear stress patterns of different devices will be compared. Platforms will be also used to test the effect of different anti-platelet drugs.

References

[1] G. Girdhar and D. Bluestein, Expert Rev Med Devices 5(2): 167-181 (2008)
[2] A. Dimasi et al, Biomed Microdevices, In Press.
[3] D. Bluestein et al, J Biomech 46(2):338-344 (2013).
[4] R. Boreda et al, J Vasc Invest 1:26-37 (1995).

5th Micro and Nano Flows Conference
Milan, Italy, 11-14 September 2016

Modelling analysis of mass transport in polymer electrolyte fuel cells porous media with the aid of computational fluid dynamics

Andrea BARICCI*, Riccardo MEREU, Mirko MESSAGGI, Matteo ZAGO, Fabio INZOLI, Andrea CASALEGNO

* Corresponding author: Tel.: ++39 0223993840; E-mail: andrea.baricci@polimi.it
Department of Energy, Politecnico di Milano, IT

Keywords: Polymer fuel cells, mass transport, Knudsen, Stefan-Maxwell

Polymer electrolyte membrane fuel cells (PEMFC) are electrochemical devices that directly convert the chemical energy of hydrogen into electricity. PEMFC devices have been long investigated for applications in the automotive industry, thanks to their intrinsic characteristics of high power density, virtually zero direct emission of pollutants and fast start-up. Nevertheless this technology is still facing some issues hindering widespread diffusion, among which the availability of distributed hydrogen infrastructure and the cost of PEMFC stacks [1]. Economic analysis of PEMFC indicates that a significant part of the cost is due to the use of precious metals in the electrodes. State-of-Art catalyst layer (CL), in fact, uses Platinum or Platinum alloys to promote the sluggish electrochemical oxygen reduction reaction (ORR) that takes place at the cathode:

$$1/2\,O_2 + 2H^+ + 2e^- \rightarrow H_2O$$

The reduction of Platinum loading is one of the major objectives of PEMFC research, but a tough task to achieve, since State-of-Art low Platinum CLs suffer sluggish oxygen transport that significantly impacts system power density [2]. Mass transport resistance in PEMFC is the resultant of several components, at least: convection in channel distributors, molecular diffusion in porous media, Knudsen diffusion in the CL macro-pores and transport into primary catalyst pores flooded by electrolyte.

The scope of this work is to get insights into the mass transport phenomena taking place in H_2-PEMFC. The methodology is a modelling analysis based on a commercial computational fluid dynamics (CFD) code to interpret experimental data.

1 Modelling

A model of PEMFC has been developed in ANSYS Fluent environment. The geometry of the model is reported in Figure 1. The polymer membrane guarantees ionic contact and electric insulation between anode and cathode electrodes. Anode and cathode electrodes are both composed of the CL (approximately 10 µm thick) and the gas diffusion layer (GDL), that is a 175 µm thick porous layer that guarantees even distribution of reactants over CL and electrical contact. A square channel on each side distributes reactants and removes the produced water.

The following physical phenomena are implemented in the model, with respect to mass transfer analysis:

1. Molecular diffusion with Stefan-Maxwell equation to consider multicomponent diffusion;
2. Knudsen diffusion in the approximately 50 nm pores of the CL;
3. Flooded agglomerate model (FAM) to account for oxygen transport in the electrolyte flooded pores of the CL;
4. Water transport across the electrolyte membrane, regulated by electroosmotic drag and diffusion;
5. Laminar flow in the channel distributors.

Modelling of polarization curves and electrochemical impedance spectra (EIS) is carried out in the present work.

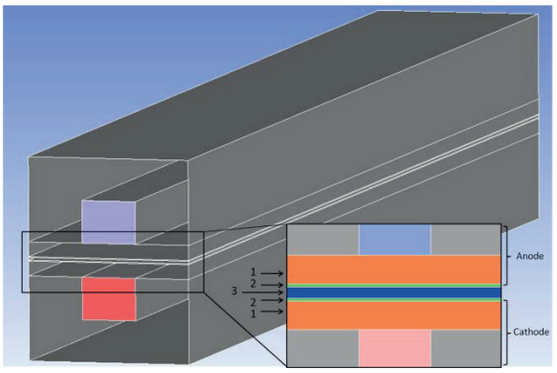

Fig. 1. View of the PEMFC domain. 1) Gas diffusion layer, 2) catalyst layer, 3) polymer membrane.

2 Experimental

Experiments have been carried out on commercial membrane electrode assembly (MEA). Polarization curves and EIS have been performed in H_2/O_2 and H_2/Air configuration. Additional tests have been carried out at low oxygen concentration (5%) with different dilutants (N_2 or He) to get further information on mass transport mechanisms. Electrochemical active surface has been estimated by cyclic voltammetry.

3 Results

The preliminary results are reported, while a detailed validation of the model is in progress. The analysis of mass transport carried out in the present work indicates that there is a dominant Knudsen effect in the CL that hinders mass transport. Simulation of EIS is also carried out to get further insights into the oxygen transport mechanisms and the impact on performance.

Comparison of CFD results with simplified 1D and 2D models is also performed, evidencing experimental cases where the use of reduced models is appropriate.

References

[1] U.S. Driving Research and Innovation for Vehicle efficiency and Energy sustainability Partnership, *Fuel Cell Technical Roadmap* (2013)

[2] N. Nonoyama, S. Okazaki, A. Z. Weber, Y. Ikogi, T. Yoshida, Journal of The Electrochemical Society (2011) 158 : B416-B423.

Simulations of microscale water flows in a squared lid cavity under freezing conditions using energy conserving dissipative particle dynamics

Toru YAMADA [1,*], Erik O. JOHANSSON [2], Jinliang YUAN[2], Shinji TAMANO[1], Yohei MORINISHI[1] and Bengt SUNDÉN[2]

* Corresponding author: Tel.: +81 (0)52 7357183; Fax: +81 (0)52 7355442; Email: yamada.toru@nitech.ac.jp
1 Graduate School of Engineering, Nagoya Institute of Technology, Gokisocho, Showa-ku, Nagoya, 466-8555, JAPAN
2 Department of Energy Sciences, Lund University, P.O. Box 118, SE221-00, Lund, SWEDEN

Abstract Energy conserving dissipative particle dynamics (DPDe) simulations are carried out to study the water flows in a squared lid-cavity when the bottom wall temperature is set as the temperature below the freezing point. The DPDe model employed in the present study has the ability to experience the water/ice phase transitions. The simulations are performed in a two-dimensional solution domain where the DPDe particles representing water are randomly distributed. The domain is surrounded by solid walls with the bounce back boundary condition where a constant velocity is applied only at the top wall. The temperature boundary condition at the side walls are considered to be either isothermal or adiabatic. A set of the water flow simulations with freezing conditions are implemented and the effect of ice layer on the velocity profile in the domain is discussed.

Keywords: Microscale, Water flow, Squared lid cavity, Freezing condition, Energy conserving dissipative particle dynamics

1. Introduction

Liquid experiences a phase change, or phase transition, when its temperature becomes below a certain temperature. This phenomenon is called freezing. The freezing phenomena at the nano/micro-scales has become a topic of significant interest because of its importance for several engineering applications, such as proton exchange membrane fuel cells (PEMFCs) experiencing a crucial performance degradation under freezing conditions due to the ice formation. Since it is very difficult to conduct experimental measurements at the nano/micro-scales, numerical simulations have been utilized to better understand the details of the phenomena at such small scales.

We currently performed a set of simulations using energy conserving dissipative particle dynamics (DPDe) method to study the water freezing phenomenon in a microscale parallel-plate channel. This study showed a difference between the DPDe simulation and the analytical study [1]. In the present study, the water flows under a freezing condition in a squared lid cavity is investigated using the DPDe method and the effect of ice layer on the velocity profile in the domain is discussed.

2. Methodology

The DPDe method is a coarse-grained version of molecular dynamics. This method was introduced by Español who ensured the energy conservation of the DPD method by adding the energy equation [2]. It is on the basis of pair-wise momentum and energy interactions with surrounding particles. The water temperature dependent properties and its freezing phenomenon was modeled by employing the models introduced by Li et al. [3] and Willemsen et al. [4], respectively. The details of these model and the original DPDe method [2] are not shown here but can be found elsewhere [1-4].

A set of the DPDe simulations is performed in a two-dimensional solution domain having a length of $L = 40$ on a side, of which the schematic is shown in figure 1. The DPDe particles representing water are randomly distributed in the domain with the number density $\rho = 4$. The domain is surrounded by solid walls with the bounce back boundary condition where a constant velocity, U, is applied only at the top wall.

The bottom wall has a constant temperature $T_1 = 0.85$ which is below the freezing temperature,

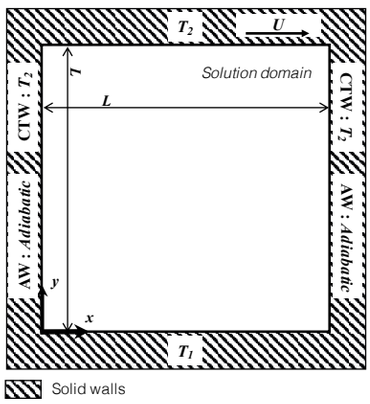

Figure 1. Schematic of the solution domain.

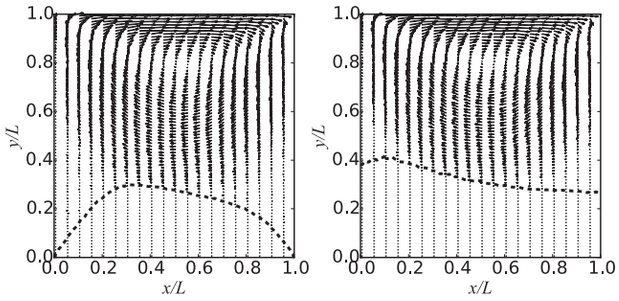

(a) IW case (b) AW case

Figure 2. Velocity vectors in the solution domain. (Dashed line: Ice-water interface)

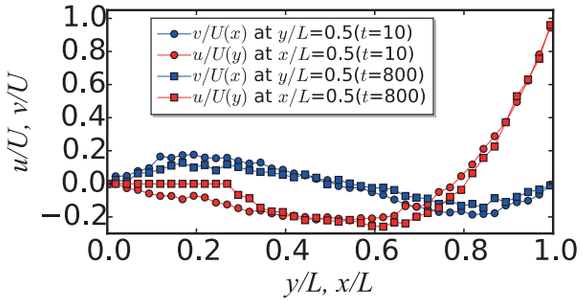

(a) IW case

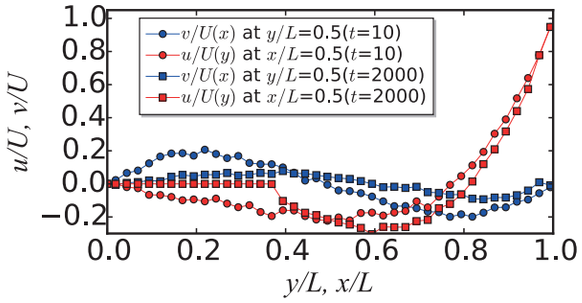

(b) AW case

Figure 3. u/U and v/U profiles at y/L, $x/L = 0.5$.

$T_f = 0.91$ [1]. The temperature of the top wall, T_2, is set to be constant at 0.95. There are two simulation cases: One has the side walls with the constant temperature, T_2, (IW) while the other case has adiabatic side walls (AW). The constant wall velocity, U, is set as 3.25 in such a way that the Reynolds number becomes 10.

According to the dimension analysis introduced by Li et al. [4], the unit length in the DPDe scale corresponds to 11 nm that leads to L = 440 nm. Also, the temperatures, T_f, T_1 and T_2 are calculated to be 0, -18 and 12℃, respectively.

For all the simulation cases, the velocity field is first equilibrated with T_2, and then T_1 was applied at the bottom wall, at which the time was set to be zero ($t = 0$).

3. Results and discussion

Figure 2 shows the velocity vectors in the solution domain when the growth of the ice layer stopped for (a) IW and (b) AW cases, respectively. As can be seen in this figure, ice layer is formed on the lower side of the domain for both cases. It is observed that there is a difference in the layer shape between the two cases due to the difference in temperature boundary condition. Accordingly, a moderate distinction in the velocity distribution between the two cases is observed.

In order to further investigate the difference in velocity field between the two cases, the velocity profiles in the middle of the solution domain in both x- and y-directions are plotted in Figure 3, where u and v denote the local velocity in x- and y-directions, respectively. Fig.3(a) presents the change in the profiles as time advances for the IW case. As can be seen in this figure, there is not distinct change in the u/U and v/U profiles between t = 10 and 800. Thus, it seems that the ice layer does not affect the flow in the cavity for this case. In the meanwhile, Fig.3(b) shows a visible difference between t = 10 and 2000 for the AW case. This is obviously due to the ice layer. However, it is still unsure what is dominating factor influencing the velocity profiles, which will be further investigated in the future research.

4. Conclusions

In this study, a set of DPDe simulations were performed for the microscale squared lid-cavity flows under a freezing condition. The results showed that the effect of ice layer formed on the bottom wall arose for the adiabatic side-wall case where the constant temperatures, 0.95 and 0.85, were set on top and bottom walls, respectively.

Acknowledgement:
A part of this work was financially supported by JSPS KAKENHI (Grant number: 16K18014)

References:

[1] Johansson, E. O., Yamada, T., Sundén, B., Yuan, J., 2016. Modeling mesoscopic solidification using dissipative particle dynamics. Int. J. Therm. Sci., 101, 207-216.

[2] Español, P., 1997. Dissipative particle dynamics with energy conservation. *EPL*, 40(6), 631.

[3] Li, Z., Tang, Y. H., Lei, H., Caswell, B., Karniadakis, G. E., 2014. Energy-conserving dissipative particle dynamics with temperature-dependent properties. J. Comput. Phys., *265*, 113-127.

[4] Willemsen, S. M., Hoefsloot, H. C. J., Visser, D. C., Hamersma, P. J., Iedema, P. D., 2000. Modelling phase change with dissipative particle dynamics using a consistent boundary condition. J. Comput. Phys., 162(2), 385-394.

5th Micro and Nano Flows Conference
Milan, Italy, 11-14 September 2016

Growth and Dewetting of Condensation Microdroplets on Superhydrophobic Surfaces with Two-tier Roghness

Pengfei Hao,* Zhaohui Yao, Cunjing Lv, Xiwen Zhang and Feng He

* Corresponding author: Tel.: 86 (10)62787470; Email: haopf@tsinghua.edu.cn
Department of Engineering Mechanics, Tsinghua University, Beijing 100084, China

Keywords: Dewetting, Superhydrophobic, Condensation, Microdroplet, Laplace pressure

Abstract

Condensation of water vapor is an everyday phenomenon which plays an important role in power generation, thermal management, chemical processing and water harvesting. Realizing dewetting of droplets spontaneously on solid rough surfaces is quite challenging, it is becoming a key research topic in many practical applications which require highly efficient removal of liquid. This article focuses on growing and dewetting of microdroplets on superhydrophobic substrates owning two-tier (micro and nano) roughness under condensation situation. A moist ambient environment are employed, which allowing a systematical study of growth processes, wetting transitions, as well as jumping behaviors of condensation microdroplets by using optical microscopy.

We report spontaneous dewetting of condensed microdroplets ($\leqslant$ 10 μm) on superhydrophobic substrates owing to excellent superhydrophobicity at the nanoscale and the geometrical topologies at the microscle. Moreover, three dewetting modes are observed. We not only develop a theoretical expression which can be utilized to predict the Laplace pressure of the droplet with no fitting parameters, but also construct an explicit model which links the critical size of the droplet, and the spacing and height of the micropillars. Our experimental and theoretical results indicate that further decreased value of Laplace pressure on the top side of the individual droplet leads to instability, and subsequently a surprising spontaneous dewetting without any external force. We further reveal that the spacing of the micropillars is essential for determining the critical size of the droplet for dewetting. We have to emphasize that the contact angle hysteresis of the material/structure systems plays an essential role accounting for the motion of the droplets, only if it is further suppressed and overcome, the spontaneous dewetting can be realized effectively. Thus, the design of devices with not only highly efficient removal of water but also highly enhanced heat transfer performance in real applications can be inspired by our ideas.

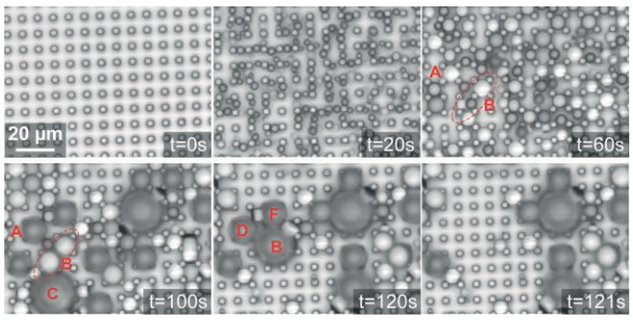

FIG.1. Dropwise condensation on one of the two-tier substrates, which corresponds to L = 3 μm, S = 4.5 μm and H = 5 μm. Droplets with lighter color means a direct contact on the substrate among the neighboring pillars. On the contrary, droplets with darker color means a non-contact with the substrate, in other words, such droplets attach the side or on the top of the micropillars.

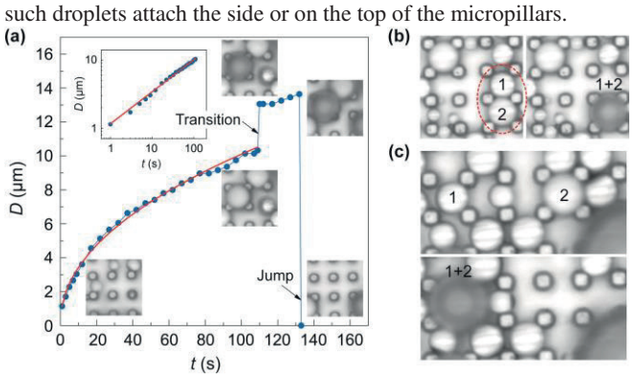

FIG. 2. Three types of wetting transition modes on the two-tier substrates (L = 3 μm, S = 4.5 μm and H = 5 μm). (a) *Mode – 1:* Time evolution of the diameter of an individual droplet during condensation (blue squares), in which the growth rate is scaled as $D \sim t^{0.47}$ (the red line). The insert covers $t \leq$ 109 s in log-log graph. The inserted frames along the growing processes correspond t = 20 s, 109 s, 110 s, 133 s and 134 s, respectively. There are a wetting transition at t = 109s and a jump at t = 133s. (b) *Mode – 2:* A wetting transition results from merging of two isolated droplet marked as 1 and 2. (c) *Mode – 3:* A wetting transition results from a flying droplet from other place, i.e. droplet-2.

Dynamic motion of Droplets on Slippery Lubricant-Impregnated Surfaces with Micro Textures

Jingxian ZHANG [1], Zhaohui YAO[1,*], Pengfei HAO[1], Bing BAO[2], Yanlin SONG[2]

* Corresponding author: Tel.: ++86 10 6277 2558; Email: yaozh@tsinghua.edu.cn
1 Department of Engineering Mechanics, Tsinghua University, P.R. China
2 Institute of Chemistry, Chinese Academy of Sciences, P.R. China

Keywords: Lubricant-Impregnated Surfaces, droplet motion, micro textures, slip velocity

I. Introduction

Inspired by Nepenthes pitcher plants, Lubricant-impregnated surfaces are surfaces with lubricant infused in the textures which forms a slippery interfaces. With excellent super-slippery and robust properties, lubricant-impregnated surfaces have wide potential practical applications such as self-cleaning, drag reduction and antifouling.

In this paper, droplets motions on six different slippery lubricant-impregnated surfaces are investigated. The surfaces are PDM surface with no textures, surface with micro-pillar textures and surface with micro hole textures, denoted as SmoothS, MPS and MHS respectively.

II. Experimental setup

Measured by microscope, the morphologies of the surfaces are shown in Fig.1.

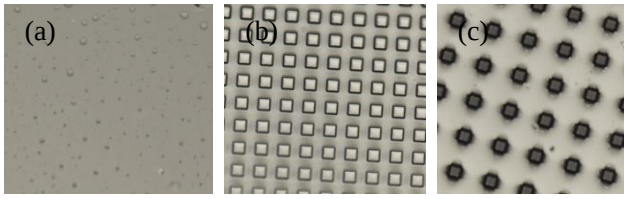

Fig. 1. Microscope images of lubricant-impregnated surfaces with (a) no textures, (b) micro-pillar textures, (c) micro holes.

Each lubricant-impregnated surface is immersed into silicone oil sufficiently, and then dipped into deionized water to remove the excessive silicone oil. To testing the stability of the surfaces, they are rinsed under the tap for 5 minutes, and marked as SmoothS', MPS' and MHS' respectively. Detailed properties of the surfaces are shown in Table 1. In Table 1, a is the length of the pillar/hole, s is the space between two pillars/holes, and h is the height of the textures.

Contact angle and sliding angle were measured by contact angle meter (JC2000CD1), with a 10μL water droplet.

As shown in Table 1, the contact angle of the SmoothS, MPS and MHS surface are quite close (about 97°). This indicates that a layer of oil is on the surface, and the contact angles are mainly influenced by the contact angle between water and silicon oil. When the oil layer is removed (i.e., surfaces rinsed under the tap), the contact angles became different and the MPS surface has the largest contact angle. For the sliding angle, the surfaces with an oil layer (MPS surface and SmoothS surface) have quite lower sliding angle than others, which is between 5~15°. The MPS surface has the lowest sliding angle before and after the rinse, which indicates that the prompt microstructures will enhance the slippery property and make it lasts longer. Meanwhile, the sliding angle of the MHS surface is even larger than the SmoothS, which means the micro textures may have bad effect on the slippery property too.

Table 1. Properties of the surfaces

Surface	Textures	Textures' Size	Contact Angle	Sliding Angle
Common PDMS	--	--	88.9±1.0°	--
SmoothS	--	--	96.2±0.6°	14°
SmoothS'	--	--	92.3±4.3°	40°
MPS	Micropillar	a=18μm, s = 14μm, h=20μm	97.7±0.6°	9°
MPS'	Micropillar	a=18μm, s = 14μm, h=20μm	129±3.1°	30°
MHS	microhole	a=20μm, s = 30μm, h=20μm	97.1±0.8°	70°
MHS'	microhole	a=20μm, s = 30μm, h=20μm	88.3±3.2°	--

To investigate the detailed motion of the droplet on these surfaces, Particle Image Velocimetry (PIV) technology was used to capture the internal velocity distribution of water droplets on different lubricant-impregnated surfaces, as shown in Fig. 2. The rotating base (marked as 1 in Fig. 2) is fixed at 10 degrees, which is a typical slipping angle for MPS and MHS surfaces.

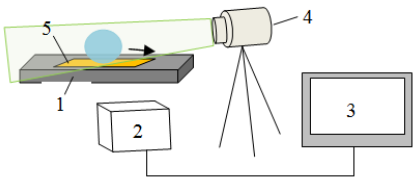

1:Adjustable rotating base; 2:High speed CCD; 3:Calculation system; 4:Laser source; 5:surface to test

Fig. 2. Measurement of droplet rolling on surface by PIV

III. Results and Discussion

Velocity fields for a common PDMS surface and six lubricant-impregnated surfaces are calculated and shown in Fig. 3, together with their PIV images. The base angle was fixed at the sliding angle for each surface. For the surface with no sliding effect (common PDMS and MHS'), the base angle was fixed at 30° (same as the sliding angle of MPS').Comparing with the one with

no lubricant infused, higher sliding velocity under the same base angle was observed on the lubricant-impregnated surfaces.

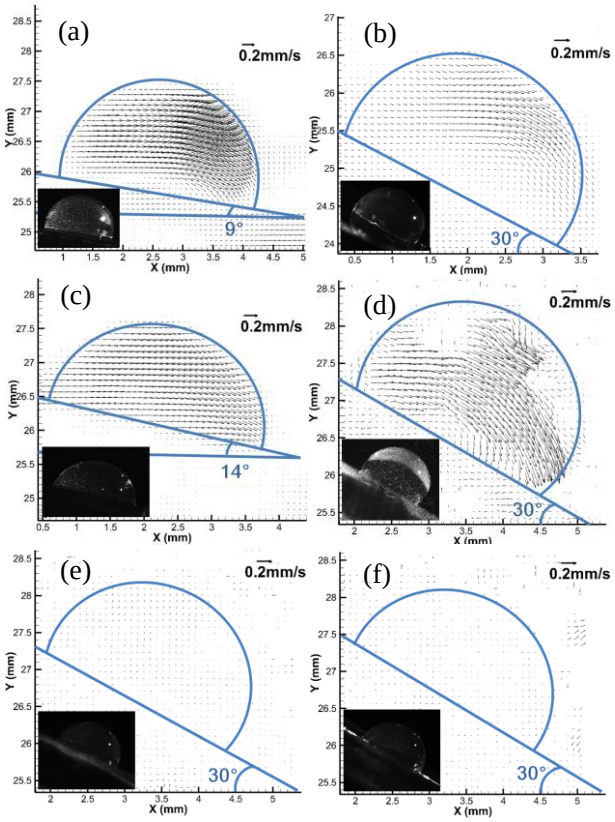

Fig. 3. Velocity fields for different surfaces. (a) SmoothS surface (b) SmoothS' surface (c)MPS surface (d) MPS' surface (e) MHS/MHS' surface (f) common PDMS surface

As shown in Fig. 3, the vectors inside the droplet in Fig.3 (b) (c) (d) are relatively uniform (compare with Fig.3 (a)), and are parallel to the base surface. These means the droplet is sliding on the lubricant-impregnated surface with a slip velocity on the base surface, which is quite different from the rolling motion of the droplet on a superhydrophobic surface.

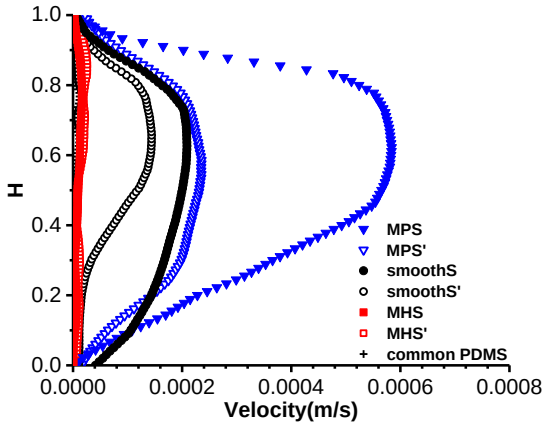

Fig. 4. Velocity distributions on the droplet's centerline for different surfaces

Figure 4 shows the velocity distributions on the droplet's centerline for different surfaces. The velocity of the MPS surface is much larger than other surfaces, and after the rinse, the MPS' surface still has slippery performance. This result is consistent with what observed in the slip angle measurement. The micro-pillar structures can improve the slippery property and stability of the lubricant-impregnated surface.

IV. Conclusion

Large slips were observed on the lubricant-impregnated surfaces. The mechanism of the differences in the droplet motion is linked with the state on the interface. For a lubricant-impregnated surface with proper micro textures, a thin layer of lubricant is sustained on the interface, which can bring excellent slippery properties. In our experiment, lubricant-impregnated surface with micro pillars has the best slippery performance while the one with micro holes has the worst slippery performance. Micro textures on the surfaces have effects on the morphology of the lubricant droplets, which can affect the slip on the interface a lot.

Foundation: National Natural Science Foundation of China (No. 11272176)

References

1 A. Lafuma and D. Quéré Slipperhy pre-suffused surfaces. A Letter Journal Exploring the Frontiers of Physics, 2011,96, 56001.

2 Tak-Sing Wong, Sung Hoon Kang, Sindy K. Y. Tang, Elizabeth J. Smythe, Benjamin D. Hatton, Alison Grinthal and Joanna Aizenberg. Bioinspired self-repairing slippery surfaces with pressure-stable omniphobicity. Nature, 2011, 477, 443-447

3 Brian R. Solomon, Karim S. Khalil and Kripa K. Varanasi. Drag Reduction using Lubricant-Impregnated Surfaces in Viscous Laminar Flow. Langmuir, 2014, 30, 10970-10976.

5th Micro and Nano Flows Conference
Milan, Italy, 11-14 September 2016

ID 72

In-Vitro μ-PIV in contracting lymphatic vessels

Konstantinos N. MARGARIS,[1,*] Zhanna NEPIYUSHCHIKH,[2] James MOORE Jr,[3] Dave C. ZAWIEJA[4] and Richard A. BLACK[1]

* Corresponding author: Email: kmargaris@gmail.com
1: Department of Biomedical Engineering, University of Strathclyde, UK
2: The George W. Woodruff School of Mechanical Engineering, Georgia Institute of Technology, USA
3: Department of Bioengineering, Imperial College, UK
4: Texas A&M Health Science Centre, Texas A&M University, USA

Abstract The present paper describes the application of the time-resolved micro-Particle Image Velocimetry (PIV) technique for resolving the two-dimensional flow field at the mid-plane of isolated contracting mesenteric rat lymphatic vessels *in vitro*. The aim was to develop an experimental protocol for accurately estimating flow parameters with high spatial and temporal resolution. A custom light source was developed, utilising high-power light-emitting diodes (LEDs), as well as associated control and image processing software. Image analysis was performed with PIV cross-correlation algorithms and was facilitated by custom vessel wall detection algorithms. Flow velocity, flow rate and shear stresses were estimated following analysis of the raw images; additionally, the dynamic pressure was estimated allowing for extraction of pressure volume curves. The results demonstrated the successful application of the micro-PIV technique in lymphatic vessels and yielded quantitative data on their contractile behaviour not previously reported.

Keywords: Lymph Flow, Micro-PIV, Microfluidics, LED, Physiological Flows

1. Introduction

The vessels of the lymphatic system exhibit vasomotion, that is, periodic distension or constriction of the vessel wall in response to fluidic and/or chemical stimuli. The active contraction of these vessels generates flow by displacing fluid through a series of non-return valves [1].

The scope of this work was to interrogate the flow field in lymphatic vessels during their active contraction *in vitro* using the time-resolved micro-Particle Image Velocimetry (μ-PIV) method [2, 3], with the aim of establishing flow rates, wall shear stresses and other derived quantities of interest within those vessels. Previous attempts to study flow in lymphatic vessels relied on cells as flow tracers, which necessitated certain assumptions on the nature of the velocity profile [4]. Moreover, those studies assumed that the radial wall motion is negligible compared to the axial fluid velocity, which has implications when resolving the instantaneous flow field within these vessels. The present μ-PIV apparatus was based around a custom LED light source capable of resolving the 2D velocity field without the need for such assumptions.

2. Materials & Methods

Rat mesenteric lymphatic vessels were isolated from adult rats. The vessels were placed in a vessel chamber in an albumin-enriched physiologic solution. Two reservoirs were used to adjust the input and output pressures. The flow was seeded with neutrally buoyant mono-disperse polystyrene micro-particles 1 μm in diameter.

The vessels were illuminated by a single, high-power LED source via fibre-optic cable and the μ-PIV optics configured to capture the flow field in the mid-plane of the vessel (Fig. 1). The minimum period between light pulses was of the order of 5 μs.

A series of images at 20x magnification was acquired with the aid of a high-speed

CMOS camera. Synchronization of camera and light source was achieved with LabVIEW software and a multifunction DAQ device.

The images were processed using a PIV cross-correlation algorithm in Matlab R2012b using the open-source toolbox PIVlab [4]. Custom edge-detection algorithms were implemented to locate the vessel wall.

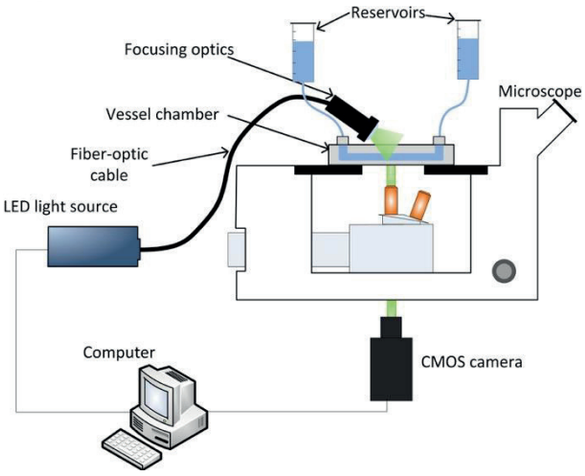

Figure 1: Experimental setup

3. Results

The system proved to be capable of resolving flows throughout successive contraction cycles, revealing some insights into the relationship between lymphatic vessel contraction, volumetric flow and wall shear stress. An example of a velocity flow field is shown in Figure 2, from which data the corresponding Pressure-Volume relationships during vessel contraction may be obtained.

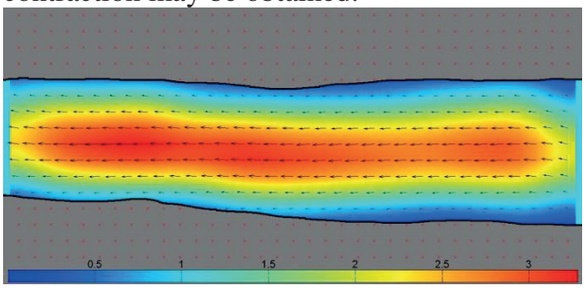

Figure 2: Velocity flow field (scale in mm/s)

The results challenge the assumptions of Hagen-Poiseuille velocity profile and negligible wall radial velocity. Finally, speculation that recirculation occurs around lymphatic valves has now been confirmed quantitatively.

4. Conclusions

This study demonstrates, for the first time, the ability of the micro-PIV system to resolve the flow field in collecting lymphatic vessels and valves during contraction *in vitro*. Unlike previous results, the method employed here yields detailed quantitative information about the flow field without any assumptions having to be made *a priori*, including fluid velocity, pressure distribution and wall shear stresses. Moreover, the system may be adapted for use *in situ* or *ex vivo*, provided sufficient optical access is available and a suitable route of particle administration is identified.

Although micro-PIV is used primarily for fluid flow measurements, optical-based systems such as the one developed here may be employed for cell trafficking studies or tracing fluorescently-tagged macro-molecules of physiological importance with minor modification.

5. References

[1] K. N. Margaris and R. A. Black, “Modelling the lymphatic system: challenges and opportunities”, J. R. Soc. Interface, vol 9(69), 2012, pp 601-612

[2] M. Raffel et al., “Particle Image Velocimetry: A practical guide”, 2007, 2nd ed, Springer

[3] K. N. Margaris et al., “Microparticle image velocimetry approach to flow measurements in isolated contracting lymphatic vessels”, J. Biomed. Opt., vol 21(2), 2016, pp 025002

[4] Thielicke, W. and Stamhuis, E. J. (2014): PIVlab - Time-Resolved Digital Particle Image Velocimetry Tool for MATLAB (version: 1.32)

5th Micro and Nano Flows Conference
Milan, Italy, 11-14 September 2016

A MICROSCALE BIOMIMETIC PLATFORM FOR GENERATION AND ELECTRO-MECHANICAL STIMULATION OF 3D CARDIAC CONSTRUCTS

Roberta VISONE[1,*], Paola OCCHETTA[1,2], Matteo MORETTI[3], Marco RASPONI[1]

* Corresponding author: Tel.: ++39 (02)23993327; Fax: ++39 (02)2399 3360; Email: roberta.visone@polimi.it
1 Department of Electronics, Information and Bioengineering, Polytechnic University of Milan, Italy
2 Department of Biomedicine, University Hospital Basel, Switzerland
3 Cell and Tissue Engineering Lab, IRCCS Istituto Ortopedico Galeazzi, Italy

Keywords: electrical stimulation, mechanical stimulation, cardiac maturation, biomimetic platform

The understanding of basic mechanisms involved in cell differentiation and tissue generation and maturation remains a great challenge in the field of tissue engineering [1]. In vitro cardiac models therefore are potent tools to investigate in an economically sustainable way stem cell regulatory mechanism of cardiac differentiation and mature myocardium tissue development [2]. In this regards, we present an innovative micro-bioreactor designed to provide cells with a controlled biomimetic environment that allows the culture of three-dimensional cardiac constructs under biochemical, electrical and mechanical stimulations.

Materials and Methods

The biomimetic platform consists of three different functional elements: (i) a culture chamber divided in a central channel for 3D cell-laden hydrogel confinement between two arrays of posts and lateral media channels; (ii) a pressure-actuated compartment, providing constructs with a cyclic mechanical compression; and (iii) a couple of stainless-steel (120µm in diameter) electrodes.
The micro-bioreactor design was optimized through finite element (FE) modeling, in terms of electric fields distribution and current density intensity. The platform was experimentally characterized by recording the electric current flowing between electrodes in both mono and biphasic stimulating waves (5V/cm amplitude, 2ms duration, frequency 1Hz).
Preliminary cellular validation was performed culturing human bone marrow stromal cells (hBMSCs) embedded in fibrin gel under electrical stimulation with biphasic waves (0.6V/3V amplitude, 2ms duration, 1Hz), evaluating cellular viability and preferential orientation. Furthermore, to investigate the ability of the platform on guiding tissue maturation, we are currently studying the effect of mechanical and electrical stimulation on neonatal rat cardiomyocytes (NRCMs).

Results

The configuration of the micro-bioreactor provides cell-laden hydrogels with a highly controlled biomimetic environment. FE analysis indeed demonstrated that constructs are subjected to uniform electric field and current density, being about 5V/cm and 60mA/cm respectively. Such results were confirmed by experimental characterization, showing that the platform allowed transmitting correctly the electric significant signals for cardiac development, allowing for long-term stimulations. The electrical system, entirely integrated in the platform during the fabrication process, could also be exploited to pace culturing constructs with the aim to evaluate maturation level and beating performances.
BMSCs cultured up to seven days showed high viability under electrical stimulation and started to exhibit a preferential orientation coherent with electric field direction (Fig 1).

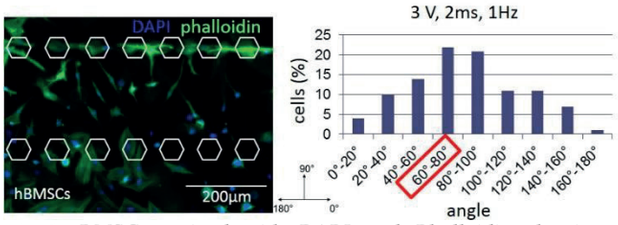

***Fig 1**: BMSCs stained with DAPI and Phalloidin showing a preferential orientation along the applied electric field.*

Preliminary results on NRCMs showed positive effects on constructs in terms of electrical connections (Cx43), spontaneous and synchronous beating, and expression of proteins characterizing cardiac maturation (Myosin Light Chain2, Sarcomeric-α-Actinin) (Fig 2).

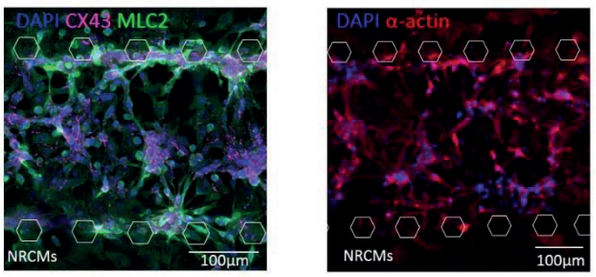

***Fig 2**: NRCMs expressing Cx-43, MLC2 and α-Actin as a result of cardiac construct maturation, achieved both in term of electrical connections and at cellular level.*

Conclusion

The micro-bioreactor allows the evaluation of biochemical, mechanical and electrical stimulation effects, alone or in their combinations, on guiding stem cells differentiation towards a cardiac phenotype and on inducing cardiac tissue maturation. Considering its peculiar ability to combine a 3D microenvironment with electro-mechanical stimuli, the platform represents a promising tool for generation of 3D human cardiac micro-tissues in vitro models, enabling to study cardiac response to *in vivo*-like stimulations and in perspective to conduct preclinical drug screening, possibly on a disease' patient specific basis [3].

References

[1] Parsa H. et al., Adv Drug Deliv Rev., 2015
[2] Uzel S. et al., Prog Biophys Mol Biol, 2014
[3] Vunjak Novakovic G. et al., Cold Spring Harb Perspect Med, 2014

5th Micro and Nano Flows Conference
Milan, Italy, 11-14 September 2016

High-Throughput Microfluidic Platform for Guiding Mesenchymal Stromal Cell Micromasses Towards Stable Chondrogenic Differentiation

Paola OCCHETTA [1,*], Andrea BARBERO [1], Marco RASPONI [2], Ivan MARTIN[1]

* Corresponding author: Tel.: ++41 (0)61 2653898; Email: Paola.Occhetta@usb.ch
1 Departments of Surgery and of Biomedicine, University Hospital Basel, University of Basel, Switzerland
2 Department of Electronics, Information and Bioengineering, Politecnico di Milano, Milano, Italy

Keywords: Microfluidics, 3D Cell Culture, Mesenchymal Stem Cell, High-Throughput, Organ on Chip

Introduction

Cartilage is a tissue with poor intrinsic regeneration capacity. Human bone marrow-derived mesenchymal stromal cells (hBM-MSCs) constitute a promising cellular source to treat chondral defects, due to their readily availability, intrinsic tissue-repair capacity and immunomodulatory effects. However, the translation of hBM-MSC-based tissue engineering (TE) approaches into clinical practice is still limited by a poor control over stable chondrogenic differentiation of hBM-MSCs [1]. Deep efforts have been recently focused in elucidating the right sequence of instructive factors able to sequentially guide hBM-MSCs towards a stable chondrogenic phenotype. To accomplish this requirement, the development of reliable and physiologically relevant *in vitro* models is mandatory to screen the effect of key morpho-regulatory factors on hBM-MSCs commitment. Towards this aim, organ-on-chip technologies and microfluidics hold great potentialities for the generation and analysis of cartilaginous "proto-tissues" models *in vitro,* directly integrating high-throughput screening and live imaging capabilities.
In this study, we exploit a high-throughput microfluidic platform as a tool for screening the combinatory role of specific pathways inhibitors/enhancers in stabilizing the chodrogenic phenotype of hBM-MSCs.

Materials and methods

A microfluidic platform, designed to generate and culture 3D stem/progenitor cells as perfused micromasses (PMMs) [2], was exploited as *in vitro* model to study hBM-MSCs chondrogenesis.

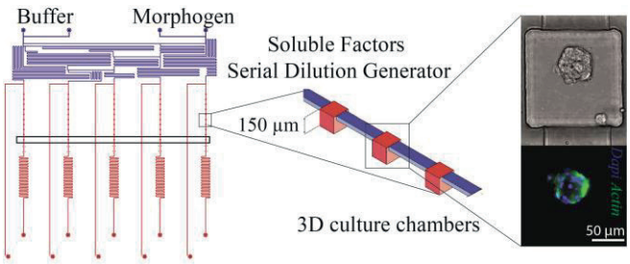

Fig 1. *Microfluidic platform for modeling hBM-MSCs chondrogenesis in vitro, integrating high-throughput screening and live imaging capabilities.*

The platform consists of a serial dilution generator (SDG, blue in Fig.1) and a 3D culture region (red in Fig.1). Patterns of different combinations/concentrations of morphogens are generated through the SDG and delivered to downstream culture units, each comprised of 10 cubic microchambers (side 150µm). Two different SDG layouts were exploited: a logarithmic configuration to screen soluble factors over a wide concentration range, and a linear layout for finer tunings within narrower concentration windows.
Primary hBM-MSCs were seeded within the microfluidic platform as previously described [2]. Upon seeding, hBM-MSCs entrapped within the microchambers were cultured under mild perfusion of serum free medium supplemented with specific morphogens.

Results and discussion

Within few hours from the seeding, hBM-MSCs generated spherical micromasses (77±15cells, Φ=56.2±3.9µm) by undergoing spontaneous condensation. Interestingly, the presence of TGFβ (10ng/ml) from the beginning of the culture was demonstrated to be mandatory for the achievement of a robust and compact cell condensation, as depicted in Fig.2a.

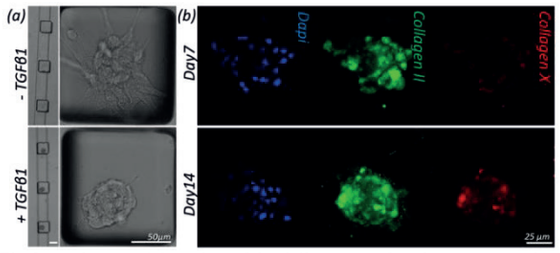

Fig 2. *(a) hBM-MSCs cultured for 24hours, in the absence or in the presence of TGFβ1 (10ng/ml). (b) Expression of collagen type-I and –X within hBM-MSCs PMMS cultured up to 14days in TGFβ1-based medium.*

Investigation on hBM-MSCs PMMs chondrogenic potential were then directed culturing them under perfusion of TGFβ1-based medium. Immunofluorescent analyses demonstrated overtime up-regulation of collagen type-II from day7 to day14. After two weeks, expression of collagen type-X, an early marker of hypertrophy, was also detected, confirming that hBM-MSCs chondrogenic state is only transiently present under traditional culture conditions (Fig.2b). Investigations are ongoing within this platform to assess the combinatory role of specific pathways inhibitors/enhancers in stabilizing the obtained chodrogenic state of hBM-MSCs.

Conclusions

We exploited a novel microfluidic platform for 3D stem cell micromasses culture as *in vitro* models of chondrogenesis. This "cartilage-on-chip" platform enables a high-throughput exposure of hBM-MSCs proto-tissues to exogenous factors and is compatible to live cell imaging and monitoring. It thus represents a powerful *in vitro* tool towards the definition of robust approaches for stable cartilaginous tissue regeneration.

References

[1] Pelttari et al., *ARTHRITIS & RHEUMATISM*, 2006
[2] Occhetta et al., *Scientific Reports*, 2015

ID 76

Numerical and experimental investigation of the levitation and flow created by ultrasonic fields in narrow gaps

Marcus SCHMIDT [1,*], Peter REINKE[1], Tom BECKMANN[1],
Kai-Alexander SAALBACH [2], Joerg WALLASCHEK[2], Jens TWIEFEL[2], Fushi BAI[2]

* Corresponding author: Tel.: ++49 (0)551 3705333; Fax: ++49 (0)551 3705200101;
Email: marcus.schmidt@hawk-hhg.de
1 Faculty of Natural Sciences and Technology, HAWK HHG, Goettingen, Germany
1 Institute of Dynamics and Vibration Research, Leibniz University, Hannover, Germany

Abstract Ultrasonic levitation is used in applications such as in the field of engineering, chemistry and medicine. In addition to the magnetic and electrodynamic levitation the acoustic or ultrasonic levitation is more and more used in technical applications. Levitation refers to a technique that describes a steady, non-contact positioning of solids and liquids. It is well understood if the carrying fluid is a gas. This work deals with the investigation of the applicability to liquids. Usually, the necessary load capacity is generated by means of standing waves in the carrier fluid. The principle of standing waves works very well for wide gap ranges. If the gap between the ultrasonic horn and the body decreases, a steady pressure field ceases to exist. The levitation mechanism is then based on the inertia effects of a liquid film under the influence of a pressure field. Here, the gap size is in the range of a few micrometers or in a range where the small gap theory applies like for example in journal bearings. Hence, a modified Reynolds equation can be formulated to describe the fluid dynamics. Again, solutions have been presented by various authors for ultrasonic levitation in gaseous media based on the small gap analogy. The work on hand expands this approach and shows the application for ultrasonic levitation in liquids and narrow gaps. The article presents the theoretical analysis of hydrodynamics compared to the numerical CFD simulation and an experiment. The numerical results include images of complex flow structures and pressure distributions in the gap. In summary, the numerical model expands the scope for the numerical simulation of flows in small gaps under the influence of ultrasound excitation.

Keywords: Ultrasonic, Levitation, CFD

1. Introduction

For small gap width the levitation mechanism is based on the inertia effects of a liquid film under the influence of a pressure field. Figure 1 illustrates the schematic setup.

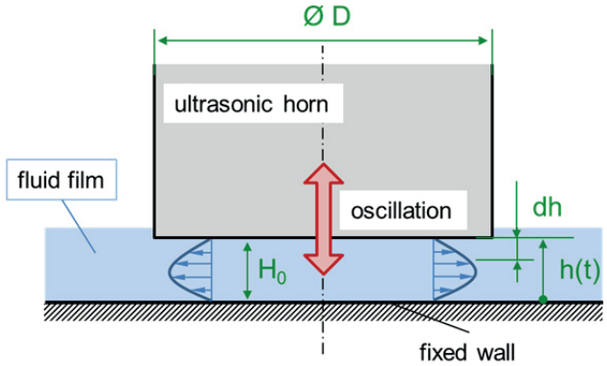

Fig. 1: Schematic system configuration

The clearance between ultrasonic horn tip (diameter D) and the fixed wall is defined by H_0. The gap is fully filled with water. The horn tip is oscillating with a defined frequency and amplitude which results in a time-depending gap width $h(t)$. Furthermore, the combination of frequency and amplitude together with the small gap width can lead to cavitation in the gap region.

2. Experimental and numerical setup

Figure 2 shows a photography of the experiment. The ultrasonic horn is submerged in water, and the clearance H_0 between the tip end of the horn and the top surface of the fixed wall is varied from 0.01 mm to 0.75 mm by means of a linear motion guide for accurate positioning. The distance between the tip end

of the horn and water surface is always 10 mm. The outer diameter D of the horn is 28 mm at the tip end. The transducer is operated at resonance frequency of approximate 22 kHz. The standoff distance is measured with an LVDT sensor. For force measurements a scale is placed underneath the glass vessel.

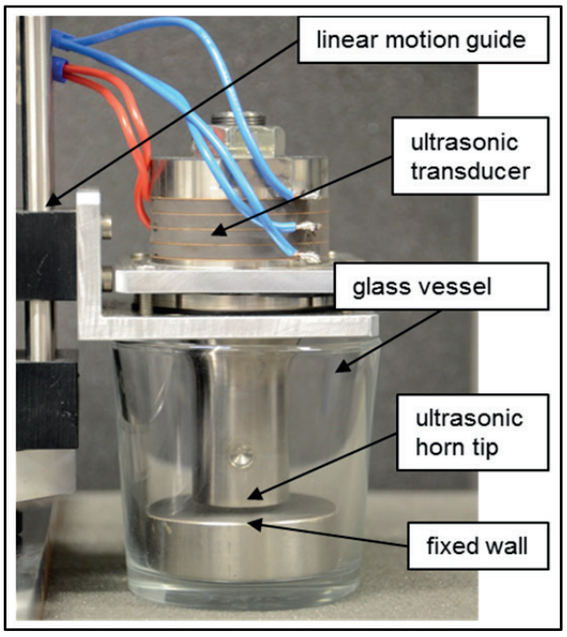

Fig. 2: Experimental setup

The numerical simulations were performed using the software OpenFOAM. The numerical code is based on the finite-volume method and solves the compressible, transient Navier-Stokes equations together with the continuity equation.

$$\frac{\partial \rho \mathbf{u}}{\partial t} + \rho(\nabla \mathbf{u}\mathbf{u}) = -\nabla p \; + \nabla(\mu \, \nabla \, \mathbf{u}) \qquad (1)$$

$$\frac{\partial \rho}{\partial t} + \nabla \cdot (\rho \mathbf{u}) = 0 \qquad (2)$$

A homogeneous equilibrium model with a two-phase mixture approach including a barotropic equation of state is applied to describe both, a second phase and the phase change. The relation of pressure and density is formulated by eq. (3) and the volume fraction γ of the two phases is calculated by eq. (4):

$$\frac{D\rho}{Dt} = \Psi \frac{Dp}{Dt} \qquad (3) \qquad \gamma = \frac{\rho - \rho_l}{\rho_v - \rho_l} \quad , \qquad (4)$$

where ρ is the mixture density, Ψ is the compressibility, p the pressure and ρ_v, ρ_l the liquid and vapour saturation density.

Fig. 3 shows the volume mesh of the fluid film between the ultrasonic horn and the fixed wall. An axis-symmetrical model is appropriate to describing the geometry under investigation most efficiently.

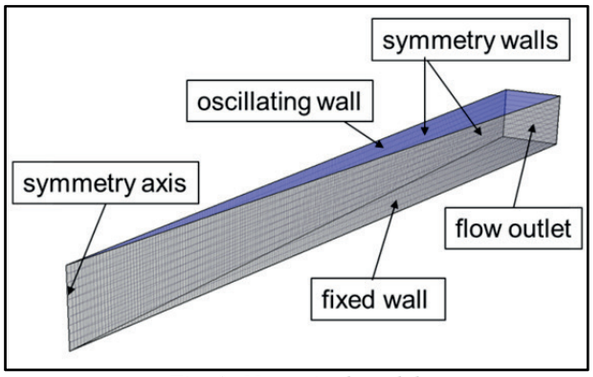

Fig. 3: Numerical model

3. Results

The Fig. 4 displays the comparison of numerical simulation results and measurement data obtained by the experiment. The curves show the force acting on the fixed wall opposite to the ultrasonic horn vs. the gap width. The applied amplitude (peak to peak) is 7.9 µm. For a moderate gap from 0.75 to 0.1 mm both the calculated and measured forces are in close proximity to zero. If the gap is less than 0.1 mm, the acting force increases significantly.

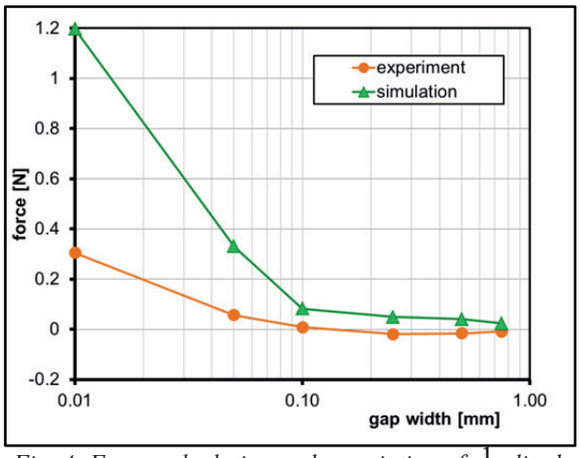

Fig. 4: Force calculation under variation of amplitude and gap width

The work on hand shows the application for ultrasonic levitation in liquids and narrow gaps.

5th Micro and Nano Flows Conference
Milan, Italy, 11-14 September 2016

ID 77

Investigation on the bubble cushion during contactless boiling in micro-evaporators

Cor M. ROPS [1,*], Joy HUIBERTS [1], Giel J.M. PRIEMS [2], Cees W.M. v.d. GELD [3]

* Corresponding author; Tel.: +31 88 866 6335; Email: cor.rops@tno.nl
1 Equipment for Additive Manufacturing, TNO Technical Sciences, The Netherlands
2 Department of Mechanical Engineering, Eindhoven university of Technology, The Netherlands
3 Department of Chemical Engineering & Chemistry, Eindhoven university of Technology, The Netherlands

Abstract In the miniaturisation of two-phase heat exchangers, micro-evaporators and micro reactors tremendous progress has been made. However, the benefits do not always overtake the concerns. Of course, decreasing the channel diameter leads to an increased surface-to-volume ratio and higher heat transfer. Next to shorter residence times, this miniaturisation leads to light-weight, compact and disposable equipment. But most often the reliability of the system is a big showstopper. Therefore, for a successful application design extra attention must be paid to minimise the fouling of the system. A novel strategy to enhance the system stability and to reduce fouling is the creation of a thin gas blanket between the wall and the fluid is presented, so-called "contact-less boiling". This bubble cushion of heated gas limits direct contact of liquid and wall and reduces the explosive growth rate of the vapour bubbles. Earlier studies showed indirectly the presence of such a layer, in this study first visualisations have been made of the existence of this bubble cushion.

Keywords: Flow boiling, Inverted annular flow, Heat transfer, System reliability.

1. Introduction

Through the last decades fascinating progress has been made in the miniaturisation of two-phase heat exchangers, micro-evaporators and micro reactors. However, the pros not always appear to outweigh the cons. Of course, decreasing the channel diameter leads to an increased surface-to-volume ratio and higher heat transfer. Next to shorter residence times, this miniaturisation leads to light-weight, compact and disposable equipment. But the reliability of the systems is often the showstopper. For a successful application design extra attention must be paid to fouling and thermo-mechanical management of the system. In addition, some physical processes occur that limit the performance. These issues are addressed in the present study that utilizes so-called "contactless boiling" as a cure in a way described shortly.

In micro-channels, the importance of the capillary forces is high as compared to body forces and inertia, which causes a high probability of channel blockage [1]. Even explosive vapour bubble growth [2] with large pressure fluctuations [3] and flow instabilities [4] is observed. Fouling is obviously determined by the deposition and entrainment rates of particles at the wall. The heated wall of a micro-evaporator may act as a catalyst leading to fouling accumulation and undesired chemical reactions. This causes uncontrolled behaviour of the micro evaporator over time [5].

A novel strategy to enhance the system stability and to reduce fouling is the creation of a thin gas blanket between the wall and the fluid. This bubble cushion limits direct contact of liquid and wall and reduces the explosive growth rate of the vapour bubbles. Combined thermal and pressure measurements in a porous conical channel gave indications for the existence of a bubble cushion [6]. The present study reports our initial findings on the existence and stability of this bubble cushion in a dedicated visualization test set-up.

2. Bubble cushion stability

The stability of the bubble cushion relates to its ability to withstand any detachment and sliding forces. The main attaching forces of a gas bubble is the surface tension force at the contact line [7].

$$F_{\text{attach}} = \left[\pi D_{contact}\sigma \sin\theta\right]_{surf.tension}$$

The main intrinsic detachment forces are the

buoyancy and the pressure excess over the bubble contact area [7].

$$F_{\text{detach}} = \left[\left(\rho_{liq}-\rho_{gas}\right)gV_{bub}\right]_{buoyancy} + \left[\frac{4\sigma}{D_{bub}}\tfrac{1}{4}\pi D_{contact}^{2}\right]_{contact.pres}$$

The above mentioned forces are normal to the wall. A gas bubble can remain attached by adjusting its shape such that the attaching forces compensate the detaching forces. Since the bubble is pinned to the cavities of the porous wall, its contact line is fixed. A force balance is obtained by changing the contact angle (Fig 1).

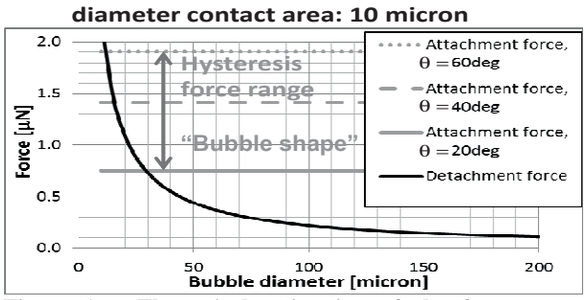

Figure 1 – Theoretical estimation of the force range induced by bubble shape; A measure for the bubble cushion stability.

It is reasonable to assume that a similar shape adjustment allows to compensate for parallel or sliding detachment forces of the same order of magnitude. A typical force obtained by shape adjustment for small bubbles (order 10µm) is in the order of 1 µN. This corresponds to several mbar pressure variation over the small bubble.

3 Experimental setup

The test set-up to visualize the bubble cushion consists of a porous block with on top a thick glass cover, in which a 2.0x1.5mm^2 flow channel is made, and with a pressurized air chamber underneath (Fig. 2).

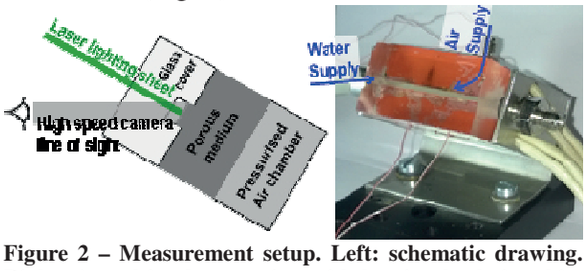

Figure 2 – Measurement setup. Left: schematic drawing. Right: Actual implementation with heating leads in white on the right.

Air is pushed through the porous wall to create the bubble cushion. The other three walls allow visualization. With a thin laser sheet and a high-speed camera (10 000fps) the bubbles at the wall are visualized.

4 Results and discussion

By changing the air pressure in the pressurized chamber the size of the bubbles at the porous wall is controlled (Fig. 3). If the air chamber is at atmospheric conditions some small bubbles are still observed in the form of immobile white dots. Without overpressure no bubbles are observed (photograph at -0.4 barg). At 1.0 barg overpressure some big leakage bubbles spoiled the visualization occasionally.

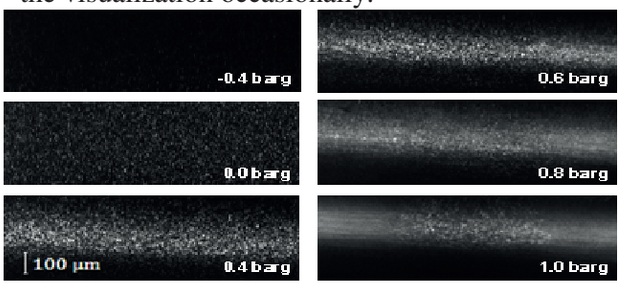

Figure 3 – Visualization of bubble cushion for various air pressures inside the pressurized air chamber.

The observed bubble size ranges from 10µm to 30µm, depending on the overpressure applied in the air chamber. This corresponds nicely to the size estimated from the heat transfer reduction in the round porous channel experiment [6]. Further results will be presented and analysed.

References

[1] C.M. Rops, L.F.G. Geers, J. Westerweel, 2008, Explosive bubble growth during flow boiling in micro-channels, Proceedings of 5th European Thermal-Sciences Conference, Eindhoven, The Netherlands.

[2] L. Zhang et al. , 2005, Phase change phenomena in silicon microchannels, Int. j. of heat and mass transfer, 48, 1572-1582.

[3] J.E. Kennedy et al. , 2000, The onset of flow instability in uniformly heated horizontal microchannels, J. of Heat Transfer, 122(1), 118-125.

[4] S.G. Kandlikar, 2004, Heat transfer mechanisms during flow boiling in microchannels, J. of heat transfer, 126, 8-16.

[5] J.F. Perry, 2008, Fouling in silicon microchannel designs used for IC chip cooling and its mitigation, Dissertation, Rochester Institute of Tech.

[6] C. M. Rops, G.J. Oosterbaan, C.W.M. Geld, 2014, Once-through contactless flow boiling in a micro evaporator, Interfacial Phenomena and Heat Transfer, 2(3), 265–271.

[7] C.W.M. Geld, 2007, The dynamics of a boiling bubble before and after detachment, Heat Mass Transfer, Special Issue, DOI 10.1007/s00231-007-0254-7.

Energetic Efficiency of Mixing in a Micro-Fluidized Bed

Vladimir ZIVKOVIC[1*], Nadia RIDGE[2], Mark J. BIGGS[2,3]

* Corresponding author: Tel.: ++44 (0)191 2084865; Fax: ++44 (0) 191 208 5292; Email: vladimir.zivkovic@ncl.ac.uk
1 School of Chemical Engineering and Advanced Materials, Newcastle University, Newcastle, UK
2 School of Chemical Engineering, The University of Adelaide, Adelaide, Australia
3 School of Science, Loughborough University, Loughborough, UK

Abstract The micro-fluidized bed represents a novel means of significantly enhancing mixing and mass and heat transfer under the low Reynolds number flows that dominate in microfluidic devices. This study experimentally evaluates the mixing performance of a micro-fluidized bed and the efficiency improvements it affords over the equivalent particle-free system. The dye dilution technique coupled with standard top-view image analysis was used to characterize the mixing in a 400 x 175 μm^2 polydimethylsiloxane (PDMS) Y-shaped microchannel. The mixing performance is strongly affected by the bed voidage with the optimal operating voidage of around 0.8, at which the energy efficiency of mixing is maximized. Overall, the micro-fluidized bed can provide mixing efficiencies up to four times greater than those in the particle-free channel.

Keywords: Fluidization; Mixing efficiency; Micro-fluidized bed; Micro-mixer; Process intensification.

1. Introduction

Chemical micro-process technologies are a relatively new concept in chemical engineering considered to be a promising way of achieving process intensification [1]. Mixing is an essential part in chemical processing influencing overall performance of such technologies. However, a flow in micro-devices is almost universally laminar and transport is dominated by molecular diffusion which limits mixing at micro-scale. Many micro-mixer technologies have been developed to overcome this limit and to achieve good mixing within reasonable time and length scales [2, 3]. Ultimately, all proposed micro-mixing methods lead to increase in the pressure drop (energy consumption), so one should take both mixing quality and energy consumption into consideration when selecting a micro-mixer.

The micro-fluidized bed (μFB) [4-6], which is essentially fluidization of micro-particles in sub-centimeter bed, can provide enhancement of mixing, mass and heat transfer for micro-devices due to chaotic motion of fluidized particles. This study experimentally evaluated the mixing performance of a micro-fluidized bed showing good potential for application in microfluidics and micro-process technologies context.

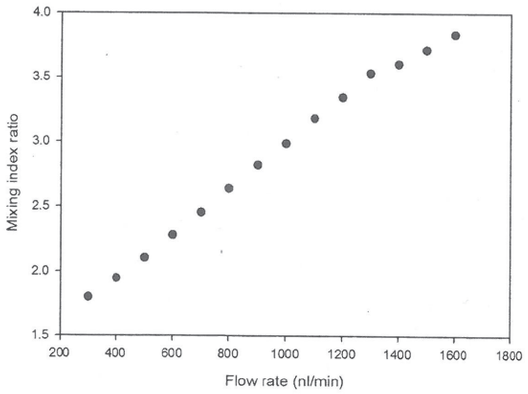

Fig. 1. Ratio of μFB and Y-mixer mixing index at different volumetric flow rates. The fluidized particles were 30 μm glass spheres.

2. Results and discussion

We used a mixing index [3], defined as the ratio of variances of mixed and un-mixed state images, to characterize the mixing quality in a 400 x 175 μm^2 polydimethylsiloxane (PDMS) Y-shaped microchannel. Fig. 1 shows that the

micro-fluidized bed was found to yield up to a four times improvement in mixing quality compared with the particle free channel (Y-mixer) in a creeping flow regime (Re number between 0.01 and 0.1).

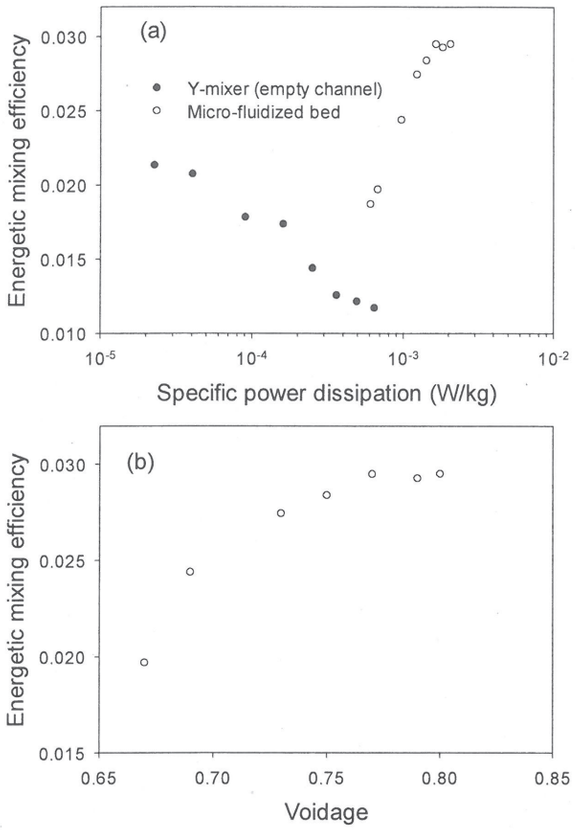

Fig 2. Energetic mixing efficiency as a function of (a) specific power dissipation and (b) fluidized bed voidage.

Kockmann *et al.* [7] introduced the mixing effectiveness factor taking into account both mixing quality and power consumption to evaluate micro-mixers. Our results (not shown here) indicate that micro-fluidized bed at lower flow rates (voidage) is not as effective as an empty channel, but at higher flow rates it can offer up to four times larger mixing effectiveness factors. Furthermore, we calculated the energetic efficiency of mixing as used by Falk and Commenge [8] for micro-mixer comparison. Although only about 2-3 percent of the total power input is effectively used for mixing, similar to other types of complex micro-mixer [8] and indeed in previous study on mixing in μFB [9], direct comparison with empty channel (Y-mixer) shows again up to 4 times larger energy efficiency at similar specific power consumptions as shown in Fig. 2a.

However, Fig. 2b shows that the voidage is critical in performance of μFB mixer with energy efficiency comparable to Y-mixer at lower voidage at the same power dissipation as already implied by the mixing effectiveness results. The optimum voidage for operation of the micro-fluidized bed is found to be around 0.8, in agreement with prediction, $\varepsilon_{max}=n/(n-1)$, from macroscopic fluidized beds experiments [10] as the Richardson-Zaki exponent is $n \approx 5$ in our case [4, 5]. In conclusion, μFBs have potential in the process intensification context but the operating voidage is crucial on its energy efficiency performances.

References

[1] V. Hessel, J.C. Schouten, A. Renken, J.-i. Yoshida, Micro process engineering: a comprehensive handbook, John Wiley & Sons 2009.

[2] V. Hessel, H. Löwe, F. Schönfeld, Micromixers - a review on passive and active mixing principles, Chem. Eng. Sci., 60 (2005) 2479-2501.

[3] N.-T. Nguyen, Micromixers: fundamentals, design and fabrication, William Andrew2011.

[4] V. Zivkovic, M.J. Biggs, Z.T. Alwahabi, Experimental study of a liquid fluidization in a microfluidic channel, AIChE J., 59 (2013) 361-364.

[5] V. Zivkovic, M.N. Kashani, M.J. Biggs, Experimental and theoretical study of a micro-fluidized bed, AIP Conference Proceedings, 1542 (2013) 93-96.

[6] V. Zivkovic, M.J. Biggs, On importance of surface forces in a microfluidic fluidized bed, Chem. Eng. Sci., 126 (2015) 143-149.

[7] N. Kockmann, T. Kiefer, M. Engler, P. Woias, Convective mixing and chemical reactions in microchannels with high flow rates, Sensors and Actuators B: Chemical, 117 (2006) 495-508.

[8] L. Falk, J.M. Commenge, Performance comparison of micromixers, Chem. Eng. Sci., 65 (2010) 405-411.

[9] E. Doroodchi, M. Sathe, G. Evans, B. Moghtaderi, Liquid–liquid mixing using micro-fluidised beds, Chem. Eng. Res. Des., 91 (2013) 2235-2242.

[10] N. Epstein, Liquid-solids fluidization, in: W.-c. Yang (Ed.) Handbook of fluidization and fluid-particle systems, CRC Press, New York, USA, 2003, pp. 705-764.

ID 82

5th Micro and Nano Flows Conference
Milan, Italy, 11-14 September 2016

Transition from Subcooled to Saturated Flow Boiling on the Basis of Energy Dissipation Balance in Minichannels

Dariusz MIKIELEWICZ [1,*], Jarosław MIKIELEWICZ [2]

* Corresponding author: Tel.: +48 583472254; Fax: +48 3472816; Email: Dariusz.Mikielewicz@pg.gda.pl
1: Department of Energy and Industrial Apparatus, Gdansk University of Technology, Poland
2: Institute of Fluid-Flow Machinery PAS, Gdansk, Poland

Keywords: Subcooled flow boiling, Saturated flow boiling, Dissipation energy, Modelling

The subcooled flow boiling for a long time is perceived as one of the most effective ways of removal of large heat fluxes due to a large temperature difference and presence of boiling in the flow. The phenomenon found application in various areas of technology where efficient cooling is required. An example of such application is nuclear reactor cooling, cooling of neutron generators used in treatment of tumors, testing of materials, cooling of electronic equipment or cooling of gas turbine nozzles. Understanding of the physics of local boiling in subcooled liquids flowing inside heated channels is still unsatisfactory. A number of papers in the literature are devoted this issue but the complexity of the process makes the analysis of the issue very challenging. Numerous models have been developed to predict the heat transfer rate during subcooled flow boiling. These models can be generally divided into two categories: purely empirical correlations for heat flux calculations or the formulas based on mechanistic models. The empirical models express the wall heat flux or partitioning of the wall heat flux. Empirical correlations for heat transfer coefficient are used for expressing a particular wall heat flux partitioning. Such correlations, on the other hand, are generally limited to particular flow conditions. Hence empirical correlations do not include modeling of the heat transfer mechanisms. On the other hand, the mechanistic models can determine particular heat flux components individually. Usually two main aspects of the problem are studied, firstly, the inception of subcooled boiling and its distance from the inlet of the channel and, secondly, heat transfer from the wall to fluid. Hence empirical correlations for wall heat flux partitioning can only provide information regarding how the wall heat flux is to be partitioned. They cannot be used for the prediction of the wall heat flux itself. The mechanistic models, on the other hand, which are based on the relevant heat transfer mechanisms occurring during the boiling process, have the capability for individual determination of each of the relevant heat flux components. Hence the mechanistic models can be used for both the prediction of the wall heat flux and the partitioning of the wall heat flux between the liquid and vapor phases. An excellent review of literature on the topic of empirical correlations for heat flux, empirical correlation for partitioning of wall heat flux and mechanistic models for prediction of wall heat flux and partitioning can be found in Warrier and Dhir [1].

The objective of the present work is to devise a model for calculation of the convective part of heat transfer coefficient in subcooled flow boiling developed on the basis of energy dissipation in the flow. The approach belongs to the group of mechanistic approaches to determination of the contribution of convective heat transfer in subcooled flow boiling. The resultant model is a modification to the saturation flow boiling developed earlier by the authors, presented in detail in [2-3]. In addition the heat flux due to evaporation has been determined. In the original approach the heat transfer coefficient in the saturated flow boiling was devised in terms of the simpler modes of heat transfer namely the single phase heat transfer and pool boiling heat transfer as well as a two-phase flow multiplier, which is a distinct feature of the model. The beginning of the process of flow boiling modeling was referenced to the forced convection value in the liquid only flow. Such approach is not physically correct, as the boiling process starts not from the equilibrium quality equal zero, but earlier when the bubble nucleation is developing on the wall. Therefore the model presented in the following attempts to determine the reference heat transfer coefficient for the saturated flow boiling in terms of the value taking into account the subcooled flow conditions. In authors previous papers [2-3], concerning saturated flow boiling, we used the heat transfer coefficient for the liquid single-phase flow as a reference level, due to the lack of the appropriate model for heat transfer coefficient for the subcooled flow boiling. Therefore that issue was a fundamental weakness of the model developed in earlier approaches. The purpose of present investigation is to fullfil this drawback.

References

1. G.R. Warrier, V.K. Dhir, Heat Transfer and Wall Heat Flux Partitioning During Subcooled Flow Nucleate Boiling—A Review, Journal of Heat Transfer, vol. 128, 1243-1256, 2006.
2. Mikielewicz J., “Semi-empirical method of determining the heat transfer coefficient for subcooled saturated boiling in a channel”, *Int. J. Heat Transfer*, vol. 17, pp. 1129-1134, 1973.
3. Mikielewicz D., “A new method for determination of flow boiling heat transfer coefficient in conventional diameter channels and minichannels”, *Heat Transfer Engineering*, vol. 31, No. 4, pp. 276-287, 2010.

ID 83

3D FEM dissipation model of suspended micro channel resonators

Annalisa DE PASTINA [1,*,♠], Andrea FANI [2,♠], François GALLAIRE [3], Luis Guillermo VILLANUEVA [1]

* Corresponding author: Tel.: ++41 (0)216930908; Email:annalisa.depastina@epfl.ch
1 Institute of Microengineering, École Polytechnique Fédérale de Lausanne, Switzerland
2 Dipartimento di Scienze e Tecnologie Aerospaziali, Politecnico di Milano, Italy
3 Institute of Mechanical Engineering, École Polytechnique Fédérale de Lausanne, Switzerland
♠ These authors contributed equally to this work.

Abstract Suspended micro channel resonators (SMCs) consist of hollow resonant structures containing an embedded u-shaped micro fluidic channel. The confinement of the fluid inside the resonator allows real time detection of liquid compounds in air or in vacuum, while the device quality factor remains almost unaffected. Quality factor of conventional cantilevers immersed in fluid monotonically decreases as the fluid viscosity increases. On the other hand SMCs exhibit a *non-monotonic* energy dissipation as the fluid viscosity is increased or decreased. In this work we present a fully three dimensional modal analysis of the fluid structure interaction (FSI) problem to predict the quality factor dependence on fluid properties. The reliability of our model is demonstrated through literature comparison of analytical model and experimental results.

Keywords: Biosensors, Suspended microchannel resonator, Microfluidics, Dissipation, Fluid-structure interaction, FEM, ALE

1. Introduction

Nanomechanical resonators have demonstrated great capabilities in life-science label-free sensing applications, such as detection of viruses and single molecules [1]. Frequency stability and high quality factor are both fundamental to optimize the device performances. Operating with biological samples usually involves immersing the resonator in a liquid environment, which yields a deterioration of the device sensing performances due to a coupling between the mechanical resonant structure and the surrounding viscous fluid. This, in turn, decreases the quality factor of the resonator by several orders of magnitude, and also affects its resonance frequency. An alternative approach is the use of suspended microchannel resonators (SMRs) [2], which consist of hollow resonant structures containing an embedded u-shaped micro fluidic channel. The fluid is thus confined inside the resonator, allowing for real time detection of liquid compounds while the device quality factor remains almost unaffected. Quality factors up to 15000 have been demonstrated and a mass sensitivity of 1 attogram (10^{-18} g) in 1 kHz bandwidth has been achieved [3].

In this work we focus on the fluidic contribute to the dissipation of SMRs as a function of fluid properties, in particular viscosity. Theoretical studies and experimental results have shown that these devices present a *non-monotonic* energy dissipation as the fluid viscosity is increased or decreased [4]

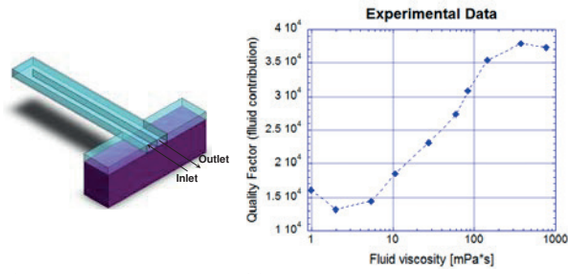

a) b)

Fig. 1.a) Schematic of SMCs device. The u-shaped microfluidic channel is embedded in the cantilever. b) Experimental data showing the non-monotonic dependence of the quality factor on the fluid viscosity [4]. Only the fluid contribution is shown.

As shown in Fig. 1.b), the quality factor reverses its trend twice as the viscosity increases, revealing alternating regimes of increasing and decreasing dissipation. This is in contrast with conventional cantilevers immersed in fluid, where the quality factor monotonically decreases as the fluid viscosity increases. The reason of this behavior stems

from the shearing of the fluid on the microchannel walls due to inertial effects of the viscous boundary layer at the fluid-solid interface.

2. FEM Model

In order to study the properties of the beam resonator we carry out a fully three dimensional modal analysis of the fluid structure interaction (FSI) problem. We use the Arbitrary Lagrangian Eulerian formulation to tackle the coupled problem and in particular we derive a linearized version of the equations assuming small perturbations. The viscous effects of the fluid are retained in the analysis. Therefore, it is possible to accurately compute the quality factor of the beam from the damping ratio obtained within the modal analysis. The device under exam is a silicon cantilever 210 µm long, 12 µm thick and 33 µm wide. The suspended microfluidic channel, centered on the neutral axis of the resonator, is 8 µm thick and spans the entire length of the cantilever. The quality factor for the first mode of resonance is simulated for several viscous compressible fluids. In order to take into account the contribution of the viscous boundary layer to the damping, a mesh refinement in proximity of the micro-channel walls is performed.

3. Results and discussion

In this paper we investigate the effect of dynamic viscosity on the quality factor of a suspended micro-channel resonator. The reliability of our model is demonstrated through a comparison with theoretical and experimental results found in literature [4, 5]. We vary the viscosity up to 60 mPa·s, taking into account the fluid compressibility.

Our FEM model is in good agreement with experimental data and exhibits a more accurate fit compared to the analytical model already proposed by Sader et al. [4, 5]. In addition, the FEM model allows to predict and calculate not only the resonator quality factor and frequency, but also fluidic properties such as bulk modulus and bulk viscosity.

Future work will be done to complete the validation of the model at higher viscosities, up to 1000 mPa·s. At high viscosity regimes the inertial effects are minimum and the flow induced by the beam oscillation is dominated by the fluid viscous contribute. Also, the viscous boundary layers at the top and the bottom walls of the channel overlap, requiring a finer discretization of the fluidic volume which results in a higher computational cost.

Upon validation across a wider range of viscosities, the FEM model will be used as a tool to investigate the properties of non-newtonian fluids in the MHz frequency range.

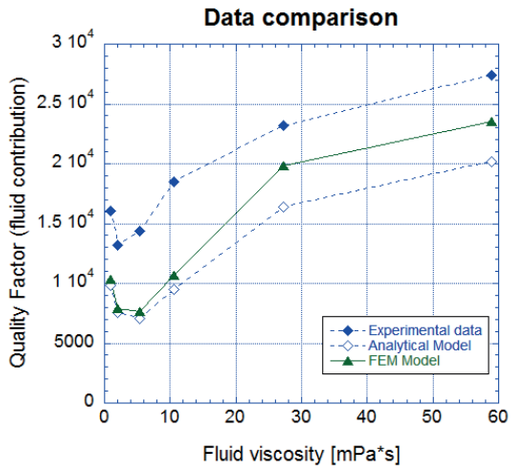

Fig. 2: Comparison between FEM model, experimental measurements and analytical data [4, 5]. The FEM model gives a good prediction of the fluid contribution to the quality factor in function of the fluid viscosity, up to 60 mPa·s.

References:

[1] J. Tamayo, P. M. Kosaka, J. J. Ruz, A. San Paulo, and M. Calleja, "Biosensors based on nanomechanical systems," *Chemical Society Reviews,* vol. 42, pp. 1287-1311, 2013.

[2] T. P. Burg and S. R. Manalis, "Suspended microchannel resonators for biomolecular detection," *Applied Physics Letters,* vol. 83, pp. 2698-2700, Sep 2003.

[3] T. P. Burg, M. Godin, S. M. Knudsen, W. Shen, G. Carlson, J. S. Foster, *et al.*, "Weighing of biomolecules, single cells and single nanoparticles in fluid," *Nature,* vol. 446, pp. 1066-1069, Apr 2007.

[4] T. P. Burg, J. E. Sader, and S. R. Manalis, "Nonmonotonic Energy Dissipation in Microfluidic Resonators," *Physical Review Letters,* vol. 102, p. 4, Jun 2009.

[5] J. E. Sader, J. Lee, and S. R. Manalis, "Energy dissipation in microfluidic beam resonators: Dependence on mode number," *Journal of Applied Physics,* vol. 108, Dec 1 2010.

ID 85

Inertial Microfluidics for Focusing and Sorting of Microparticles by Size in Curvilinear Microchannels

Arzu ÖZBEY [1], Mehrdad KARIMZADEHKHOUEI [1], Sarp AKGÖNÜL [1], Devrim GÖZÜAÇIK [2], Ali KOŞAR[1,*]

* Corresponding author: Tel.: 90 (216) 483 9621 ; Fax: +90 (216) 483 9550; Email: kosara@sabanciuniv.edu
1 Faculty of Engineering and Natural Science, Mechatronics Engineering Program, Sabanci University, Istanbul, Turkey
2 Faculty of Engineering and Natural Science, Biological Sciences and Bioengineering Program

Abstract Focusing behavior of 15 µm and 20 µm fluorescent polystyrene microparticles were examined over a broad range of channel Reynolds numbers. The effect of curvature on particle focusing and separation was also carefully assessed by measuring particle migration either towards or away from center of the curvature as Reynolds number increased. The goal of this study is further analyzing the decoupled effects of inertial forces and dean drag forces on microparticles of different sizes in curvilinear microchannels with a rectangular cross section geometry.

Keywords: Inertial Microfluidics, Particle Focusing, Particle Separation

1. Introduction

Focusing microparticles using microfluidic systems has been essential in efficient separating, encounting and detecting. A passive, continuous and size-dependent focusing phenomenon called "inertial microfluidics", which takes the advantage of hydrodynamic forces, is implemented in this study to sort the microbeads (Amini et al., 2014; Carlo, 2009; Di Carlo et al., 2007; Kuntaegowdanahalli and Bhagat, 2009). In this work, we have developed continuous, high throughput, label-free and parallelizable size based particle separation in a specific symmetrical curved channel. Our design allows occupying the same footprint as straight channels, which makes parallelization possible with sufficiently parallel optical detection integration as well as achieving high efficiency similar to spiral channels. This feature is also useful for ultra-high throughput applications such as flow cytometers with the advantages of reducing cost and size.

2. Experimental Setup

PDMS microchannels were fabricated using the Soft Lithography technique. For each experiment, fluorescently labelled particles were diluted in DI water (0.01 % wt) and particle suspensions were filled in a 60 mL plastic syringe and injected into the microfluidics device at flow rates ranging from 100 to 3000 µl/min using a syringe pump.
The device is mounted on an inverted phase contrast microscope (Olympus IX72) equipped with a (12-bit) charge coupled device camera. ImageJ software was used for image processing.

2. Results and Discussion

A typical PDMS microfluidics chip consists of one microchannel design with one inlet, and three outlets with a diameter of 1 mm each.

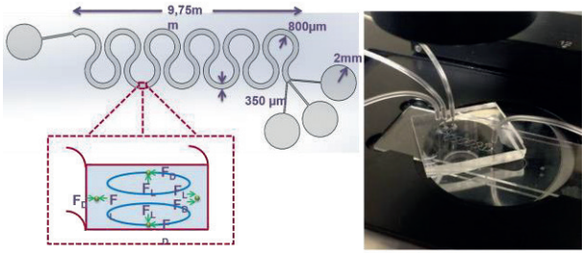

Fig. 1. Microchannel dimensions and decouple effect of inertial and dean drag forces on particles (left) Experimental setup (right)

The height of the microchannel is 91 µm, while the width and radius of curvature are 350 µm × 800 µm, respectively. The whole chip comprised of 11 curvilinear geometries, each having the radius of curvature of 800 µm with an angle of curvature of 280 degrees. The total chip length was 9.75 mm. An illustration of the device is provided in the Fig. 1.

At low Re_C numbers, no focusing line has been observed, and particles are in uniform alignment throughout the microchannel. Increasing Re_C number results in formation of single focusing line at the centerline along the microchannels. With a further increase in Re_C number, a transverse motion of particle stream is observed. Our results show that transverse motion of particle stream can be seen at lower flow rates for 15 µm particles (Fig. 2). The central steak of 15 µm particles shifts towards to the channel wall, while the steak of 20 µm particles is still close to the centerline at Re_C ~ 140 (Fig. 3). Taking the advantage of this behavior, at optimum Re_C numbers (140-150), efficient separation can be achieved.

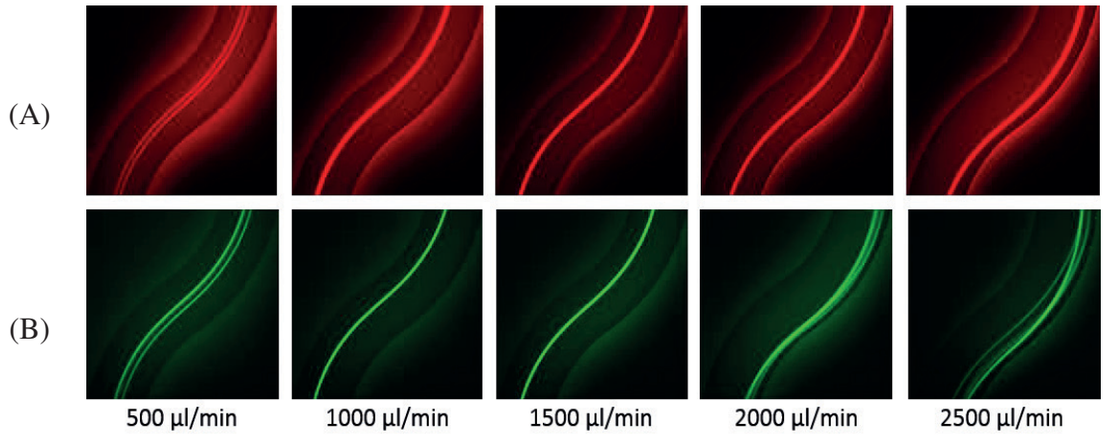

Fig. 2. Microparticle focusing behavior in microchannel with different Flow Rates in transition region (A) 20 µm particles (B) 15 µm particles

As the angle of the curvature increases, the dean flow becomes stronger so that the intensity of the secondary flow proportionally depends on the angle of the curvature. Accordingly, a sudden rotational change (between the inner and outer wall) leads to a better separation efficiency rather than serpentine channels where the angle of curvature is 180°. Due to the sudden change in the channel curvature (inner wall rearranges as the outer wall), the direction of dean vortices change so that particle location is disturbed as the particles move through to centerline from the outer wall.

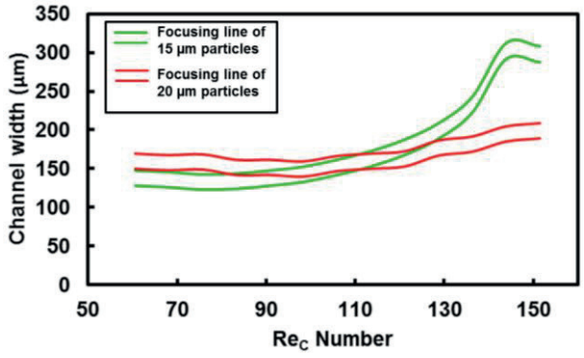

Fig. 3. Particle streak position lines of 15 µm and 20 µm particles for different channel Re numbers in transition region.

Our results show that focusing of particles at a single equilibrium position can be obtained through a sufficiently augmented curvature angle and separation capability for 15 and 20 micron particles is high at Re_C ~140-150.

References

Amini, H., Lee, W., Carlo, D. Di, 2014. Inertial microfluidic physics. Lab Chip.

Carlo, D. Di, 2009. Inertial microfluidics. Lab Chip.

Di Carlo, D., Irimia, D., Tompkins, R.G., Toner, M., 2007. Continuous inertial focusing, ordering, and separation of particles in microchannels. Proc. Natl. Acad. Sci. U. S. A. 104, 18892–7.

Kuntaegowdanahalli, S., Bhagat, A., 2009. Inertial microfluidics for continuous particle separation in spiral microchannels. Lab Chip.

5th Micro and Nano Flows Conference
Milan, Italy, 11-14 September 2016

High Performance Tubular Heat Exchanger with Microjet Heat Transfer Enhancement

Jan WAJS [1,*], Dariusz MIKIELEWICZ [1], Elzbieta FORNALIK-WAJS [2], Michal BAJOR [1]

* Corresponding author: Tel.: +48 583472830; Fax: +48 3472816; Email: janwajs@pg.gda.pl
1: Department of Energy and Industrial Apparatus, Gdansk University of Technology, Poland
2: Department of Fundamental Research in Energy Engineering, AGH University of Science and Technology, Poland

Keywords: Microjets Technology, Heat Transfer Intensification, Heat Exchangers

It is observed that the demand for energy is increasing every year, therefore in parallel to the technological development, new or rather at least better ways of energy use are scrutinised. Efficient heat production and distribution are very important from the economical and natural resources depletion point of view. Therefore an extensive research and developments have been pursuit in the area of heat transfer intensification over the past couple of decades. It is even more pronounced nowadays as we can observe the tendency of miniaturization in every aspect of life, especially in technical applications. Hence the problems of high heat fluxes removal are of great significance. This is the reason why this new challenges require high efficiency system components, especially highly efficient and compact heat exchangers. It is known that in the case of recuperators the convective heat transfer coefficients on both sides of partition are the most crucial in determination of the overall heat transfer and directly influence their capacity. It is also important to bear in mind that the overall heat transfer coefficient is always lower than the lowest value between both mentioned convective heat transfer coefficients. Therefore a special care has to be exercised to the heat transfer conditions on the weaker side of partition.

In literature numerous descriptions of heat transfer intensification techniques can be found [1]. Generally speaking all methods can be divided into active (requiring additional energy), passive (no additional energy, but the intensification is attained by surface extension or introduction of surface modifications) and combined (parallel application of active and passive methods or various passive ones). Due to the requirement of additional energy in the case of active methods, they are very often applied in the phase change processes, however their control is rather difficult. In the case of passive methods of heat transfer intensification the effect can be obtained by surface extension (e.g. fins) or by increasing the convective heat transfer coefficient (e.g. flow turbulization).

Among the heat transfer enhancement techniques the implementation of microjets technology into the recuperators can be regarded as innovative. In effect application of such method ensures significantly higher values of heat transfer coefficients as the consequence of generated fluid microstreams impinging on the heat transfer partition, separating hot and cold fluids. Laminar fluid film on the partition is locally disturbed by mentioned fluid streams. It is especially very attractive for the system, in which the heat is transferred between gas and liquid, gas and condensing vapor or gas and boiling liquid. On the gas side the values of heat transfer coefficient are significantly lower, limiting the efficiency of recuperation. That, due to the microjets can be improved. Microjet heat exchangers feature high performance, especially at low media flow rates and low temperature differences between them.

In the paper the original cylindrical heat exchanger with microjets is introduced. Its novel construction is an “in-house” patented design [2]. The systematic experimental analysis of the prototype heat exchanger will be described especially from the point of view of such parameters as the heat transfer effectiveness, heat transfer rates, overall heat transfer coefficients and pressure drop. The heat transfer coefficients were determined on the basis of the Wilson plot method [3], which is the most suitable for heat exchangers of complex geometry.

The thermal-hydraulic characteristics of novel heat exchanger were compared with the prototype plate microjet heat exchanger (patented design developed by Plata [4]) as well as commercially available typical plate heat exchanger. The direct comparison of the thermal and flow characteristics between mentioned units was possible due to the assurance of equivalent conditions during the experiment. Equivalent conditions mean the same volumetric flow rates and the same media temperatures at the inlet of heat exchangers in the corresponding measurements’ series. The comparison was done for the single-phase convective heat transfer in the water-water and water-ethanol configuration. Presented results showed high performance of the discussed microjet heat exchanger.

In subsequent studies the heat exchanger design will be optimized with respect to the length of nozzles. In Authors’ opinion the novel construction is a good proposal for broadly defined thermal engineering applications.

References

[1] Kreith F. at. al. (1999). Heat and mass transfer, Mechanical engineering handbook, CRC Press LLC.
[2] Wajs J., Mikielewicz D., Fornalik-Wajs E. (2013). Microjet heat exchanger of cylindrical geometry, dedicated both to the general applications and heat recovery from low temperature waste energy sources. Patent application P.404601 (in Polish).
[3] Fernandez-Seara, J., Uhia, F.J., Sieres, J., Campo, A. (2007). A general review of the Wilson plot method and its modifications to determine convection coefficients in heat exchange devices, Applied Thermal Engineering, vol. 27, pp. 2745-2757.
[4] Plata M. (2009). Fluid microject system, World patent, WO 2009095896 20090806.

5th Micro and Nano Flows Conference
Milan, Italy, 11-14 September 2016

Mixing through Vortex Shedding in a Microfluidic Channel: A numerical simulation study

Yadlapalli Venkata Nitin Mythreya, Yammani Venkat Subba Rao, R Aravinda Narayanan and V. Meenakshi*

* Corresponding author: Email: meenakshi@hyderabad.bits-pilani.ac.in
Department of Physics, Birla Institute of Technology and Science, Pilani- Hyderabad Campus, Hyderabad – 500078, Telangana State, India.

Keywords: Microfluidics, Micromixing, Water drop obstacles, Lab on a chip, Point of care devices

With an aim to enhance the mixing of two fluids in a microfluidic channel, we have designed Y type micromixers with various obstacles capable of mixing at low Reynolds numbers which also includes a novel design of an obstacle shaped like a water droplet to break-up and combine fluid flows. The flow field is numerically simulated using the COMSOL multiphysics software by incorporating the obstacle in a Y type micromixer. The main result is that, for a Reynolds number between 4 and 400, vortex shedding phenomenon is observed: vortices of variable strengths are generated and distributed across the channel resulting in more contact area between the fluids (Fig. 1 and Fig. 2 are representative).

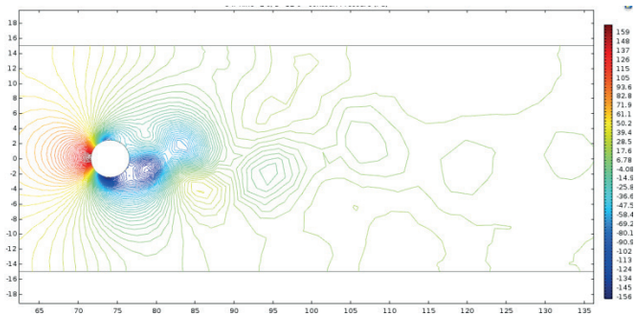

Fig. 1. Vortex shedding in Y Channel with cylindrical Obstacle

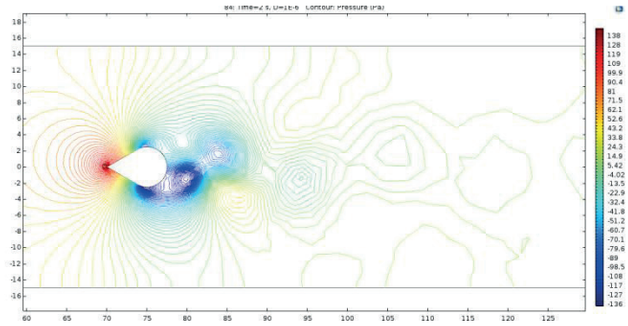

Fig. 2. Vortex shedding in Y Channel with water drop obstacle

5th Micro and Nano Flows Conference
Milan, Italy, 11-14 September 2016

The Effect of Asymmetry on Micromixing in Curvilinear Microchannels

Sarp AKGÖNÜL[1], Arzu ÖZBEY [1], Mehrdad KARIMZADEHKHOUEI [1], Bartu DEMİRSOY[1], Devrim GOZUACİK[2], Ali KOŞAR[1,*]

* Corresponding author: Tel.: 90 (216) 483 9621; Fax: +90 (216) 483 9550; Email: kosara@sabanciuniv.edu

1 Faculty of Engineering and Natural Science, Mechatronics Engineering Program, Sabanci University, Istanbul, Turkey

2 Faculty of Engineering and Natural Science, Biological Sciences, Genetics and Bioengineering Program, Sabanci University, Istanbul, Turkey

Abstract. The aim of this study is to compare contribution of Dean Vortices to the efficiency of micromixing in curvilinear microchannels with and without width shift using varying flow rates. While micromixing of Phenolphthalein and Sodium hydroxide (NaOH) in 70 wt% ethanol solution was investigated at various Reynolds and Dean Numbers. Due to curvilinearity and width shift, sudden changes in the direction and magnitude of Dean Vortices generate enhanced mixing with a safer and contamination free platform offering high mixing capabilities for the biochemical and pharmaceutical industry.

Keywords: Advection mixing, Chaotic mixing, Passive micromixer, Dean Vortices, Curved Microchannels

1. Introduction

Genetic analysis, biochemistry analysis, chemical synthesis are some of many applications, in which micromixing devices find applications (Vilkner et al.,2004). Considering microfluidic devices, active micromixers may have the upper hand in mixing effectiveness compared to passive micromixers. As the literature indicates, active micromixers may reduce the mixing length (Junghun Cha et al., 2006). However, the simplicity of passive micromixer fabrication processes combined with good efficiency and room for potential improvement in the field shifts the passive ones toward the center of attention. The experiments were conducted in this study to reveal whether the asymmetry in width improves or hinders the efficiency of a passive micromixer, which will offer some insight for future studies and applications.

2. Experimental Setup

Soft Lithography technique was used to fabricate the PDMS microchannels illustrated in Fig.1. The experiments were conducted with two transparent 70 wt% ethanol/water solutions of Phenolphthalein and Sodium hydroxide (NaOH) because while they are transparent in aqueous solutions their mixture results in a fuchsia color giving an opportunity to visualize the mixing efficiency even with a monochrome camera. Solutions were filled in two 60 mL plastic syringes and injected into the curvilinear micromixer

device at flow rates varying from 100 to 3000 µl/min using a syringe pump. Visualization of the experiment was carried on an inverted phase contrast microscope (Leica DM IL LED) equipped with a 12 bit Phantom High Speed Camera V 310. Image processing was done with ImageJ software.

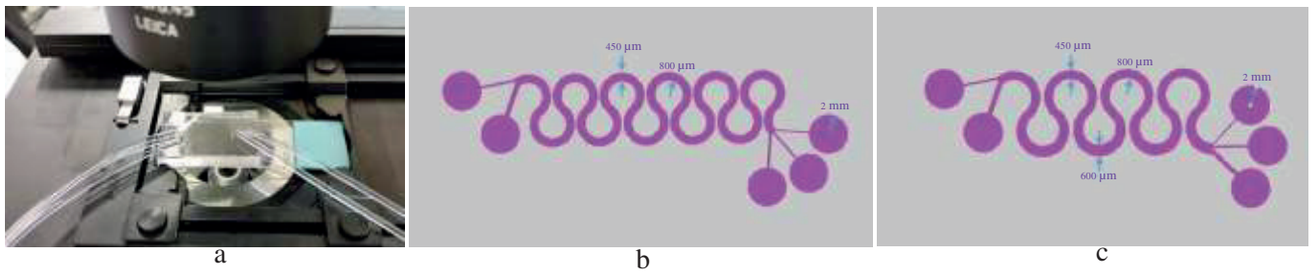

Fig. 1. Experimental setup (a) and schematic of the devices with symmetrical (b) and asymmetrical (c) width

3. Results and Discussion

Two microchannel configurations were considered in the experiments, one having an asymmetry in width of 450-600 µm and one having width of 450 µm. Asymmetrical channel has a height of 87 µm and the reference channel has a height of 88 µm. The radius of curvature of the channels is 800 µm. The novelty of this study lies in the analysis of the asymmetry with microchips having an angle of curvature of 280 degrees. width result in a better mixing performance compared to ones with a constant width. The comparison was made visualizing near the outlet to better assess the mixing efficiency in a stabilized stream.Black regions refer to fully mixed regions. As the color intensity goes to white, the mixing ratio gradually decreases to zero. The data show that for the given flow rates, the asymmetrical micromixer with a smooth width shift from 450 to 600 µm surpasses the micromixer with the constant width of 450 µm at every turn.

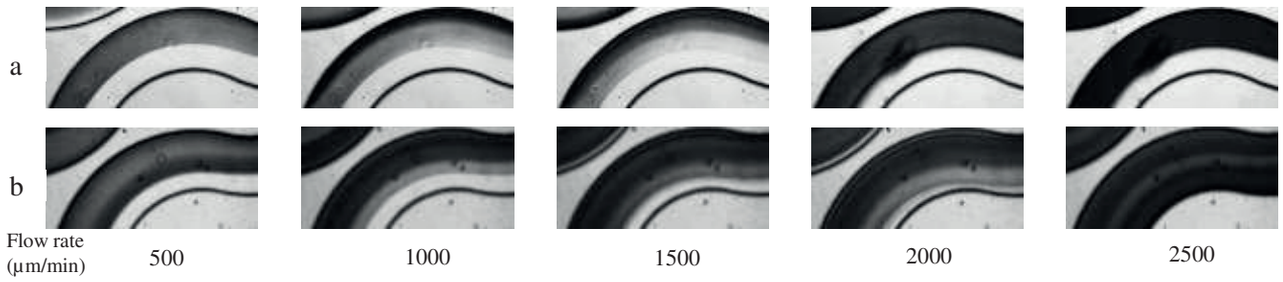

Fig. 2. Visualisation of the mixing for varying flow rates for symmetrical (a) and asymmetrical (b)

For both micromixers, the curvilinear geometry introduces Dean Vortices, which play the essential role in mixing. As the flow rate increases Dean Force dominates the flow, while the sudden change in curve direction alters the direction of the Dean Vortices resulting in an effective micromixing. As can be seen from Fig.2, experimental data indicate that curved passive micromixers with asymmetrical

References

Vilkner, T., Janasek, D., & Manz, A., 2004. Micro total analysis systems. Recent developments. *Analytical chemistry*, *76*(12), 3373-3386.

Cha, J., Kim, J., Ryu, S. K., Park, J., Jeong, Y., Park, S., ... & Chun, K. (2006). A highly efficient 3D micromixer using soft PDMS bonding. *Journal of Micromechanics and Microengineering*, *16*(9), 1778.

ID 90

Effect of Inlet Temperature on Convective Heat Transfer of gamma-Al_2O_3/Water Nanofluids in a Microtube

Mehrdad KARIMZADEHKHOUEI [1], Arzu ÖZBEY [1], Sarp AKGÖNÜL [1]
Kürşat ŞENDUR [1], M. Pınar MENGÜÇ [2], Ali KOŞAR [1,*]

* Corresponding author: Tel.: ++90 (0)216 4839621; Fax: ++90 (0)216 4839550
Email: kosara@sabanciuniv.edu
1 Faculty of Engineering and Natural Sciences, Mechatronics Engineering
Sabanci University Istanbul, Turkey
2 Department of Mechanical Engineering, Ozyegin University Istanbul, Turkey

Abstract. Important parameters affecting single- and two-phase heat transfer of nanofluids are shape, material and average diameter of nanoparticles, fraction ratio and stability of nanofluid, surface roughness and fluid inlet temperature. In this study, the effect of inlet temperature of water based alumina nanofluids is investigated at a mass fraction of 0.1% for hydrodynamically developed and thermally developing laminar flows with Reynolds numbers of 650, 1000 and 1300, in a microtube.

Keywords: Convective Heat Transfer, Nanofluid, Laminar Flow, Microtube, Inlet Temperature

1. Introduction

Nanofluids are the dispersions of the nanoparticles having the average diameter of 1-100 nm in convectional liquids, such as water, ethylene glycol, engine oil, refrigerants and/or proper mixture of mentioned base fluids (Choi and Eastman, 1995).

There are already many studies on nanofluids in many applications. For example, Naraki et al. in their experimental study on car radiator by CuO/water nanofluids investigated the effect fraction ratio and nanofluid inlet temperature (Naraki et al., 2013). According to their results, increasing the fraction ratio up to 0.4 vol.% leads to an overall enhancement in heat transfer and conversely, increasing the nanofluid inlet temperature from 50°C to 80°C had a negative effect on heat transfer. In Ravisankar et al. study on tractor radiator, the same trend was observed (Ravisankar et al., 2015).

In our previous study (Karimzadehkhouei et al., 2015), convective heat transfer coefficients of water based gamma-Al2O3 nanofluids was investigated at the same constant inlet temperature. In this study, the effect of inlet temperature was investigated for a weight fraction of 0.1% of for Reynolds numbers of 650, 1000 and 1300.

2. Experimental Setup and Nanofluid Preparation

The experimental test setup, shown in Fig. 1, consists of a syringe pump, microtube with inner and outer diameters of 889 and 1067 micrometer, respectively, heated length of 11.5 cm and 4 K-type thermocouples located at different locations. Local heat transfer coefficients were calculated at different Reynolds numbers, heat fluxes and fluid inlet temperatures.

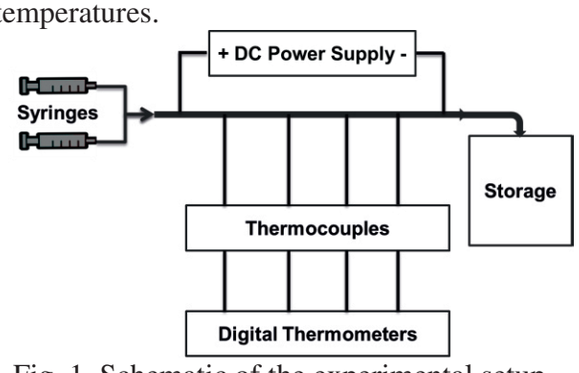

Fig. 1. Schematic of the experimental setup.

Spherical γ-Al_2O_3 nanoparticles with an average diameter of 20 nm were added to the distilled water (DI), for preparing the nanofluids. A weight fraction ratio of 0.1%

was achieved by adding nanoparticles to a mixture of base fluid and SDS as surfactant with concentration of 2500ppm and by performing sonication and stirring for at least an hour.

3. Results, Discussion and Conclusion

According to the initial results, shown in Fig. 2a, at a lower Reynolds number, 650, and lower heat flux, 117 kW/m^2, a small increase in heat transfer of nanofluid (NF) in comparison to pure water can be seen at the entrance of test section by increasing the fluid inlet temperature from 19 to 31ºC, which may be explained by the increase in the nanofluid conductivity. However, this difference decreases longitudinally, which could be as a consequence of nanoparticle agglomeration during heating at a lower flow rate. At higher Reynolds numbers, it can be observed that coefficients are remain the same or deteriorated relative to the pure base fluid results, as the fluid inlet temperature increased to 31ºC (Figs. 2b-c).

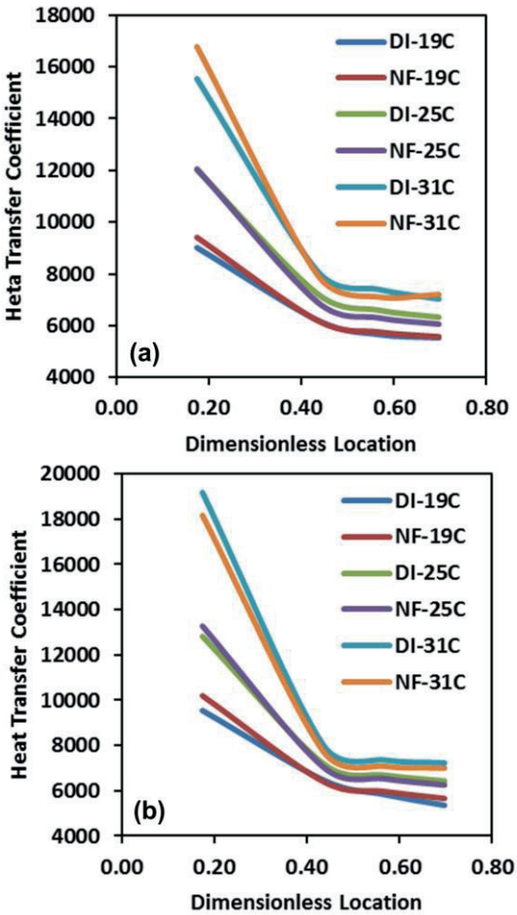

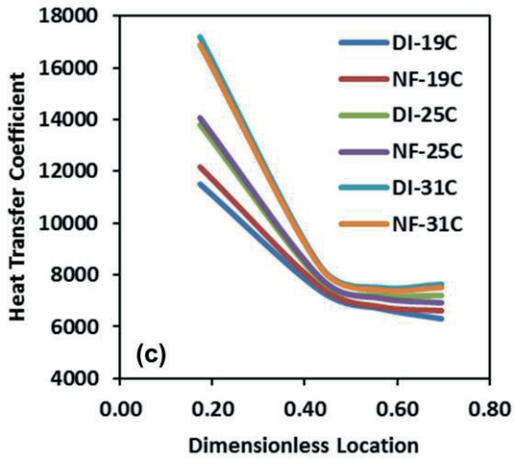

Fig. 2. Local heat transfer coefficients of nanofluids and pure water for Reynolds number and heat fluxes of: a) 650, 117, b) 1000, 117 and c) 1300, 176 kW/m^2, respectively.

In conclusion, according to the results, local heat transfer of nanofluids deteriorates relative to the base fluid with the increasing the fluid inlet temperature from 19 to 31ºC, which is in good agreement with the literature (Naraki et al., 2013; Ravisankar et al., 2015), while the opposite is true for low flow rates. More studies are needed for fully understanding the effect of nanofluid concentration and Reynolds number at higher inlet temperatures.

References

Choi, S.U.S., Eastman, J.A., 1995. Enhancing thermal conductivity of fluids with nanoparticles. No. ANL/MSD/CP-84938; CONF-951135-29.

Karimzadehkhouei, M., Yalcin, S.E., Şendur, K., Pınar Mengüç, M., Koşar, A., 2015. Pressure drop and heat transfer characteristics of nanofluids in horizontal microtubes under thermally developing flow conditions. Exp. Therm. Fluid Sci. 67, 37–47.

Naraki, M., Peyghambarzadeh, S.M., Hashemabadi, S.H., Vermahmoudi, Y., 2013. Parametric study of overall heat transfer coefficient of CuO/water nanofluids in a car radiator. Int. J. Therm. Sci. 66, 82–90.

Ravisankar, R., Venkatachalapathy, V.S.K., Alagumurthy, N., 2015. Thermal Performance Improvement of Tractor Radiator Using CuO/Water Nanofluid. Heat Transf. Res.

ID 91

5th Micro and Nano Flows Conference
Milan, Italy, 11-14 September 2016

Thermal-Optical Modeling of a Photothermal Spectroscopy Approach for Paper-Based Diagnostics

David G. GASPERINO [1,*], Kevin P. NICHOLS [2]

* Corresponding author: Tel.: ++001 (425) 247 2147; Email: dgasperino@intven.com
1 Intellectual Ventures Laboratory, 14360 SE Eastgate Way, Bellevue, WA 98007, USA

Keywords: Photothermal spectroscopy, Lateral Flow Immnoassay, Optical Monte Carlo, Finite Element Method

1. Purpose

Point of care diagnostics aimed at low-resource settings need to be relatively simple, robust and low-cost. The most commonly-used diagnostic platform in these settings for the detection of non-nucleic acid chemical biomarkers are lateral flow assays (LFAs). These tests are easy to administer, low-cost, require only small volumes of patient sample for operation, and can generate a visual result in less than 30 minutes. While LFAs have proven highly effective for *Plasmodium falciparum* – a malaria parasite - case management, their relatively high limit of detection makes them unable to diagnose asymptomatic carriers [1]. Mechanistically, this means that while there are signal particles at the LFA test line, there are not enough of them to generate a signal visible to the human eye. To get around this limitation, a variety of LFA reader technologies have been developed to identify the presence of signal particles at the LFA test line at concentrations below the visual threshold of the human eye. One technology in particular exploits the optical absorption properties of LFA signal particles composed of colloidal gold by illuminating the particles at the test line with laser light emitted at the particles' plasmonic resonance frequency [2]. This approach has the potential to generate a signal distinguishable from the background signal when the concentration of colloidal gold particles at the LFA test line is significantly lower than the visual threshold concentration. In this presentation, we describe efforts to characterize the performance limitations and opportunities of this method using a model system that couples the output from optical Monte Carlo (OMC) simulations to a finite element model for simulating the absorptive heating effects of the colloidal gold nanoparticles on an LFA strip during laser illumination.

2. Methods

The transfer of optical energy to thermal energy within the LFA is a complex process due to the absorptive properties of the gold signal particles and the multilayered nature of LFA's, where each layer has unique optical absorption and scattering characteristics. A desire to understand the limits of performance of the laser illumination approach amongst this complexity motivated the creation of a first-principles computational model that couples and simulates optical and thermal phenomena. The model simulates light propagation and absorption within the LFA materials using an established Monte Carlo approach, and heat transfer due to optical absorption and thermal/convective transport using COMSOL Multiphysics (see Figure 3). The resulting model enables the efficient exploration of important questions about the performance capabilities of the laser illumination approach, and enables the exploration of 'what if' scenarios that would otherwise take significant time to explore at the bench top.

3. Results

To be filled-in when we receive internal approval for publication, by 12/11/2015.

4. Conclusions

To be filled-in when we receive internal approval for publication, by 12/11/2015.

References

[1] "Malaria rapid diagnostic test performance: results of WHO product testing of malaria RDTs: round 5 (2013)," WHO, Geneva, 2014.
[2] Z. Qin, W. C. Chan, D. R. Boulware, T. Akkin, E. K. Butler and J. C. Bischof, "Significantly improved analytical sensitivity of lateral flow immunoassays by using thermal contrast," Angewandte Chemie, vol. 18, pp. 4434-4437, 2012.

5th Micro and Nano Flows Conference
Milan, Italy, 11-14 September 2016

Transient Dynamics of Elastic Hele-Shaw Cell Due to External Forces with Application to Impact Mitigation

Arie TULCHINSKY, Amir D. GAT*

* Corresponding author: amirgat@technion.ac.il
Faculty of Mechanical Engineering, Technion – Israel Institute of technology, Haifa, Israel

Abstract We study the transient dynamics of a viscous liquid contained in a narrow gap between a rigid surface and a parallel elastic plate. The elastic plate is deformed due to an externally applied time-varying pressure-field. We model the flow-field via the lubrication approximation and the plate deformation by the Kirchhoff-Love plate theory. We obtain a self-similarity solution for the case of an external point impulse acting on the elastic plate. We examine a distributed external pressure, spatially uniform and linearly increasing with time, acting on the elastic plate over a finite region and during a finite time period, similar to the viscous-elastic interaction time-scale. The interaction between elasticity and viscosity is shown to reduce by order of magnitude the pressure within the Hele-Shaw cell compared with the externally applied pressure, thus suggesting such configurations may be used for impact mitigation.

Keywords: Lubrication approximation, Fluid-Solid-Interaction

1. Dynamics due to external point impulse

We study the transient dynamics of a viscous liquid contained in a narrow gap between a rigid surface and a parallel elastic plate. The elastic plate is deformed due to an external time-varying pressure-field applied perpendicular to the plate. We focus on configuration consisting of a shallow geometry, small ratio of transverse plate deformations to viscous film height, small Womersley number, negligible solid inertia and negligible membrane effects. Under the assumptions given, the upper elastic plate dynamics are governed by the Kirchhoff-Love equation and the viscous liquid by the lubrication approximation. Normalizing and combining the equations together with the no-slip and no penetration boundary conditions, we obtain a governing equation in terms of the pressure P

$$\frac{\partial P}{\partial T} - \nabla^6 P = \frac{\partial P_e}{\partial T} \tag{1}$$

where P_e is the external pressure. We focus on the viscous-elastic time scale, where there is no effect from the boundaries, thus prescribing $P(\boldsymbol{X} \to \infty) \to 0$.

We utilize the Green function for (1), in its Fourier integral form, and the symmetry of the transformation argument, thus converting it into a Hankel integral. We Express the Bessel function in a series form and integrate to obtain a closed form self-similar expression

$$G = \frac{\Psi(\eta)}{T^{\frac{1}{3}}}, \qquad \eta = \frac{|\boldsymbol{X}|}{6T^{\frac{1}{6}}}, \tag{2}$$

$$\Psi(\eta) = \frac{1}{12\pi}\begin{bmatrix} \Gamma\left(\frac{1}{3}\right) & {}_0F_4\left(\frac{1}{3},\frac{2}{3},\frac{2}{3},1,-\eta^6\right) \\ -9\eta^2\Gamma\left(\frac{2}{3}\right) & {}_0F_4\left(\frac{2}{3},1,\frac{4}{3},\frac{4}{3},-\eta^6\right) \\ +\frac{81}{4}\eta^4 & {}_0F_4\left(\frac{4}{3},\frac{4}{3},\frac{5}{3},\frac{5}{3},-\eta^6\right) \end{bmatrix}.$$

While the function presented can be used by convolution to obtain a general solution, more insight may be obtained from a solution for the case of $P_e = \delta(\boldsymbol{X})\delta(T)$. This may be achieved without convolution by applying a time derivative on the green function equation to obtain an equation equivalent to (1). Thus, the pressure-field due to a unit point impulse is

$$G_p = \frac{\partial G_p}{\partial T} \tag{3}$$

2. Impact mitigation and response dynamics to external pressures

We examine an external pressure, evenly distributed on a disk of radius L_e, linearly increasing in magnitude with respect to time until T_e and than decreases linearly until vanishing at $2T_e$, with a total impulse of 1. Convolving the external pressure with G_p, denoting $\eta_{L_e} = \frac{L_e}{6T^{1/6}}$ and dividing by P_e yields the ratio of pressures at

the center for $T \le T_e$

$$\frac{P(\boldsymbol{X}=0,T)}{P_e(T)} = \eta_{L_e}^6 \, G_{\{2,7\}}^{\{4,1\}}\left(\eta_{L_e}^6\right) \qquad (4)$$

where $G_{\{2,7\}}^{\{4,1\}}$ is the Meijer G-function. Eq. (4) is presented in Fig. 1a. Three distinct periods are evident: I. An initial period, $2.5 \le \eta_{L_e} < \infty$, where the fluidic pressure closely follows the external pressure, II. The interval, $0.5 \le \eta_{L_e} \le 2.5$, shows small oscillations of the pressure ratio going from mitigation to amplification and vise versa, and III. The period $0 \le \eta_{L_e} \le 0.5$ where mitigation occurs and grows with time.

Fig. 1b shows the ratio of pressures at the time where maximal external pressure is reached (i.e. T_e). From Fig. 1b, it is evident that for any width of external pressure L_e, mitigation may be achieved if the application time is sufficiently long. Specifically, for the case of $L_e = 0.1$, mitigation of more than 90\% is obtained for external pressures applied over the period of $2T_e = 10^{-3}$ or greater.

3. Experimental Verification

Experiments were conducted to illustrate and verify some of the theoretical results. The experimental setup (see Fig. 1a) consists of a 5mm width Polyurethane rubber plate floating over a 6mm silicon-oil film. The center of the plate is deformed due to application of a linear actuator connected to a load cell measuring the force applied on the elastic plate. The radial deformation profile created during force application is sampled by a laser profilometer. The theoretical deformation is obtained by convolution of the external force measurements.The radial location of the minimal radius measured by the laser profilometer was estimated by correlation to the analytic solution as r=20mm. No other fitting parameters are used and good agreement between the analytical results and experimental data is evident (see Fig. 2b).

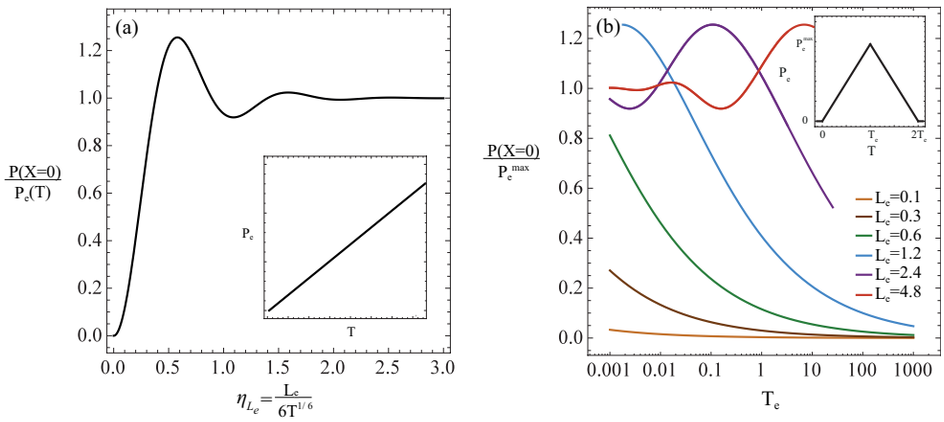

*Figure 1. The liquid pressure at **X**=0] divided by the external pressure during application period as a function of the non-dimensional parameter η_{L_e} (a), and the time maximal magnitude of external pressure is reached T_e (b).*

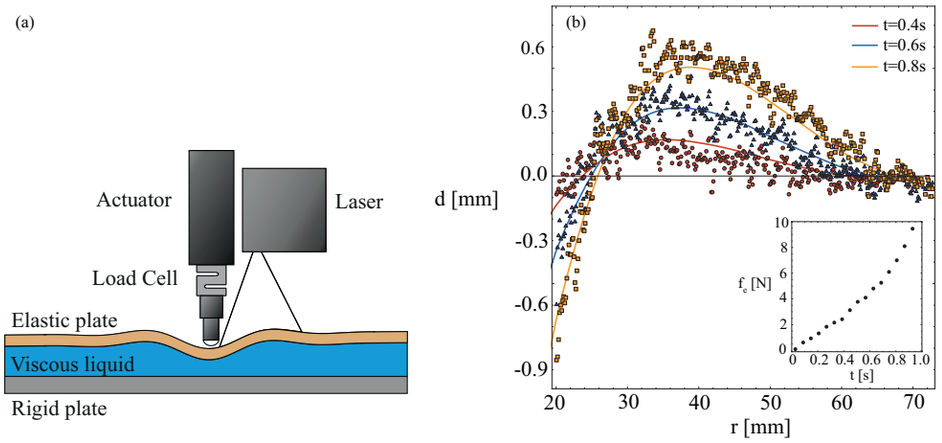

Figure 2. (a) (a) Illustration of the experimental setup. (b) Experimental (markers) and theoretical (smooth lines) deformation d vs. r at t=0.4s (red), t=0.6s (blue) and t=0.8s (yellow), during the application of the external force f_e. The insert in part (b) shows force measurements f_e vs. time t.

5th Micro and Nano Flows Conference
Milan, Italy, 11-14 September 2016

Diamagnetic nanofluid behaviour in the strong magnetic field

Aleksandra Roszko[1], Elzbieta Fornalik-Wajs[1,*], Sasa Kenjeres[2] and Janusz S. Szmyd[1]

* Corresponding author: Tel.: +48 12 617 2663; Email: elaf@agh.edu.pl
1: Department of Fundamental Research in Energy Engineering, AGH University of Science and Technology, Krakow, Poland
2: Department of Chemical Engineering, Delft University of Technology, The Netherlands

Keywords: Nanofluid, Thermo-magnetic convection, Diamagnetics, Spectral analysis, Nusselt number

1 Motivation and research concept

The nanofluids become a study subject of many research groups due to their properties and possible applications, e.g. heating of the buildings, solar absorption, energy storage, industrial cooling applications, friction reduction, nanodrug delivery, transportation, etc. [1]. Their properties differ from the common fluids, therefore they can be applied to improve existent processes and also in new areas. One of the possible applications is related to the heat transfer intensification [2]. Going toward the higher heat fluxes transfer the nanofluids appeared as the promising working fluid due to changes of base fluid physical properties. The Authors goal is to verify if the magnetic field will improve transfer of the high heat fluxes by the low concentration nanofluids. To obtain this aim the experimental analysis of nanofluid fundamental behavior under the influence of magnetic field was undertaken. The studies seem to be promising, taking into account the heat transfer control by magnetic field in the case of one-phase paramagnetic fluids [3-4]. Some of the previous results regarding the nanofluids behaviour in the magnetic field were published in [5].

2 Experimental procedure

Experimental cubical enclosure was located in the superconducting magnet (able to generate magnetic gradients about 900 T^2/m) test section. The strong magnetic gradients can change the flow of weakly magnetic fluids, therefore, the specific location of the enclosure was chosen in accordance with their maxima. Temperature of heated and cooled copper walls was measured by six thermocouples, whereas the temperature of fluid was measured by thermocouples placed inside the enclosure in the vicinity of wall. Examined fluids were nanofluids with base fluid (distilled water) containing Cu/CuO nanoparticles of 40-60 nm diameter. The concentrations of nanofluids were 0.0112, 0.056 and 0.112 vol.%, which correspond with 0.1, 0.5 and 1 mas.%, respectively. The working fluids had diamagnetic properties and in consequence the interaction of gravitational and magnetic buoyancy forces was, in each case, very complex. The analysis of heat transfer and flow structure were done with utilization of the recorded temperature signals. Two aspects were investigated: how the (1) heat transfer and (2) flow structure changed in the applied conditions. For these purposes the Nusselt number and Fast Fourier Transform analyses were performed.

The nanofluids are the media, which are very difficult to handle during the experiment. The difficulties start from the preparation step, are going through their opaqueness and are finalizing in their stability. The first and last problems were solved, however the opaqueness is one of the major obstacles. Therefore, the analysis method was based on the temperature measurement signal, its fluctuation. Passive scalar spectra in the isotropic and anisotropic form in the turbulent fluid flow with the power law was shown in [6]. Such analysis would define the range of characteristic flow type appearance (i.e. inertial-convective or viscous-convection ranges). It is valuable information, because it helped to indicate if the magnetic field had an influence on the flow or not, even if it would not be directly measured. Reorganization of the flow structure would be taken as a proof of such influence.

From the other point of view the FFT method helped to analyze the flow due to the appearance of periodic structures. The impact of magnetic field manifested through the changes of frequency or strength of such structures. The most important for future applications analyzed aspects was the heat transfer enhancement as the result of magnetic field operation, estimated by the Nusselt number.

3 Results

Various examples of spectral and heat transfer analysis were presented. The reorganization of the flow due to the magnetic field action was found. However, there was no clear tendency that higher concentration showed higher impact of magnetic field. The same conclusions could be pointed out for the heat transfer analysis.

It was found that interpretation of heat transfer data is very difficult due to the complex forces system. The experimental analysis will be continued to obtain the description of analyzed aspects and answer the question, if the heat transfer phenomena is the result of only structure reorganization or also fluid properties.

4 References

[1] Yu W, Xie H. A Review on Nanofluids: Preparation, Stability Mechanisms, and Applications. *J Nanomater*. 2012;2012:1-17.

[2] Kakaç S, Pramuanjaroenkij A. Review of convective heat transfer enhancement with nanofluids. *Int J Heat Mass Transf*. 2009;52(13-14):3187-3196.

[3] Wrobel W, Fornalik-Wajs E, Szmyd JS. Experimental and numerical analysis of thermo-magnetic convection in a vertical annular enclosure. *Int J Heat Fluid Flow*. 2010;31(6):1019-1031.

[4] Kenjereš S, Pyrda L, Fornalik-Wajs E, Szmyd JS. Numerical and Experimental Study of Rayleigh–Bénard–Kelvin Convection. *Flow, Turbul Combust*. 2013;92(1-2):371-393.

[5] Roszko A, Fornalik-Wajs E. Potential of low concentration nanofluids in heat transfer, *Acta Innovations*, 2015;16:48–55,

[6] Elperin T, Kleeorin N, Rogachevskii I. Isotropic and anisotropic spectra of passive scalar fluctuations in turbulent fluid flow. *Phys Rev E*. 1996;53(4):3431-3441.

ID 94

5th Micro and Nano Flows Conference
Milan, Italy, 11-14 September 2016

Deformation and Breakup of a Non-Newtonian Droplet in a Shear Flow

Haihu LIU [1,*], Ningning WANG [1]

* Corresponding author: Tel.: ++86 (0)136 30283538; Email: haihu.liu@xjtu.edu.cn
1 School of Energy and Power Engineering, Xi'an Jiaotong University, China

Keywords: Lattice Boltzmann method, Droplet deformation and breakup, Non-Newtonian fluid, Critical capillary number, Geometry confinement

Abstract

This study focuses on the dynamical behavior of a droplet immersed in a matrix liquid subject to a simple shear flow. Theoretical and phenomenological models are able to predict the droplet deformation assuming that both fluids are Newtonian in the steady state. However, the droplet shape and orientation can be quantified by numerical methods without this limitation. In this work a multiple-relaxation-time (MRT) lattice Boltzmann method, which uses a forcing term and a recoloring algorithm to realize the interfacial tension effect and phase separation respectively, is developed to simulate the deformation and breakup of a three-dimensional droplet of non-Newtonian power-law fluid in a Newtonian matrix fluid when subjected to a simple shear flow. This method is first validated against the theoretical predictions, experimental and numerical data available in literature by the simulations of the droplet deformation and breakup for the power-law index n=1, i.e., Newtonian fluid. It is then used to systematically study the impact of capillary number, viscosity of the matrix fluid, and the geometry confinement on the deformation and breakup of the non-Newtonian droplet over a wide range of power-law index ($0.2<n<2$). We find that the non-Newtonian effects can significantly affect the droplet dynamical behavior, thus quantitatively modifying the dependence of the deformation parameter and the orientation angle on the capillary number, viscosity of the matrix fluid, and the confinement ratio. In addition, the phase diagrams that describe the dependence of the critical capillary number (above which the droplet breakup occurs) on the confinement ratio are established for both shear-thinning and shear-thickening droplets, and their results are quantitatively compared.

5th Micro and Nano Flows Conference
Milan, Italy, 11-14 September 2016

The Role of von Willebrand Factor and Platelet Margination in their Adhesion

Masoud HOORE, Kathrin MÜLLER, Dmitry A. FEDOSOV*, Gerhard GOMPPER

* Corresponding author: Tel.: +49-2461-612972; Fax: +49-2461-613180; Email: d.fedosov@fz-juelich.de
Institute of Complex Systems and Institute for Advanced Simulation, Forschungszentrum Jülich, 52425 Jülich, Germany

Keywords: blood flow, haemostasis, catch-slip bond, membrane model, mesoscopic modeling, smoothed dissipative particle dynamics

In order to stop bleeding, platelets adhere to the site of injury and plug the opening. Platelet adhesion is mediated by various factors and proteins, including von Willebrand factor (VWF). VWF molecules are long chains, which comprise a number of VWF dimers bound to each other [1]. The conformation of VWF polymer is such that in the absence of shear stress, the polymer is globular, thus hiding adhesive sites of VWF A1-domain to platelet Glycoprotein Ib or collagen. When VWF is under sufficient shear stress, the chain opens up, as illustrated in Figure 1, making the interaction of the A1-domain with Glycoprotein Ib or collagen possible.

In case of an injury, VWF A1 and A3 domains bind to collagen in the extracellular matrix of the endothelium and become immobilized [2]. Furthermore, blood flow exerts shear stress onto bound VWFs such that the polymers stretch. Consequently, the platelet Glycoprotein receptors can bind to the A1 domains of VWFs. Binding of platelets to the immobilized VWFs reduces their velocities to much lower values than those in blood flow [3] and leads to their firm adhesion to an injured wall. This process is called primary haemostasis.

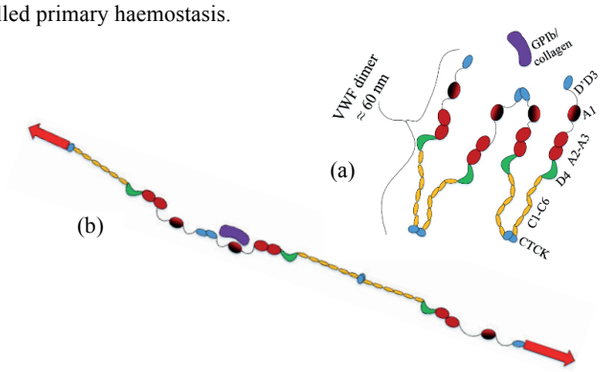

Figure1. Schematic of VWF dimeric structure; the domains of each monomer are specified in the image. (a) No shear stress is applied. (b) If shear stress is applied on the polymer, it expands and exposes its adhesive sites to GPIbα.

The adhesive bond between the VWF A1-domain and GPIbα has two equilibrium states with respect to an applied force [4], which implies a catch-bond behavior for these interactions. This means that by increasing the force on the bond, the bond exhibits a longer lifetime. Considering the conformation-dependent activity of VWF polymers and their catch-slip bond nature, we show using blood-flow simulations that the VWF-platelet adhesion depends critically on flow conditions. Thus, when a system of VWFs and platelets is under strong enough shear flow, VWFs stretch and a VWF-platelet network can be formed (see Fig. 2). As the shear rate increases, the network grows and the bonds become stronger. Interestingly, when the shear flow is stopped, the bonds disappear and the network dissolves in the solvent fluid. This reversible adhesion has been experimentally observed in Ref. [5].

Under blood flow conditions, VWF and platelets migrate towards vessel walls through a process called margination. The margination phenomenon has been experimentally found for platelets [2], and results in a higher concentration of platelets near the wall in comparison to that in the bulk of blood flow. This migration effect is mediated by red blood cells, which fill the center of the vessel, leaving a thin red-blood-cell free layer near the wall, and force platelets into that layer [2, 6]. In our computational study, we also find that VWF polymers marginate similar to platelets, which leads to a more efficient wall adhesion. Another advantage of VWF margination for the hemostatic process, which we find in simulations, is that VWF is able to stretch at lower shear rates in the red-blood-cell free layer in comparison to its stretching in a bulk fluid. This occurs due to the effect of quasi-confinement of marginated VWFs between the vessel wall and the central column of flowing red blood cells.

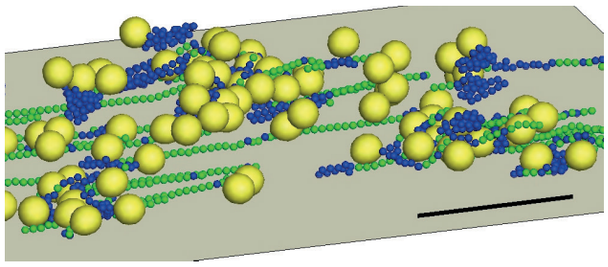

Figure2. Primary haemostasis is affected by platelet and VWF margination and the shear stress exerted on VWFs by blood flow.

Acknowledgements

M.H. and K.M. are thankful for the support by the DFG Research Unit FOR 1543 SHENC - Shear Flow Regulation in Hemostasis. D.A.F. acknowledges funding by the Alexander von Humboldt Foundation. We also gratefully acknowledge a CPU time grant by the Jülich Supercomputing Center.

References

[1] Springer T.A., Blood, 124(9):1412--1425, 2014
[2] Reininger A.J., Haemophilia, 14(s5):11--26, 2008
[3] Savage B. et al., Cell, 84(2):289—297, 1996
[4] Kim J. et al., Nature, 466(7309):992--995, 2010
[5] Chen H. et al, Nature comm, 4:1333, 2013
[6] Müller K. et al,. Scien rep, 4, 2014

ID 96

Numerical study of natural convection for Al_2O_3 and CuO nanofluids inside different enclosures

Sahar A. Abbood, Zan Wu, Bengt Sundén*
Department of Energy Sciences, Lund University, P.O. Box 118, Lund SE-22100, Sweden
**Corresponding author, e-mail: bengt.sunden@energy.lth.se*

Abstract In this study steady-state natural convection for Al_2O_3 and CuO nanofluids inside different enclosures are numerically investigated. Natural convection is concerned due to a temperature difference between hot and cold surfaces. Rectangular and curved enclosures are investigated. The Boussinesq approximation is used to form the governing equations and the commercial software package ANSYS Fluent version 14.0 is used to numerically solve the governing equations. The temperature profiles and flow patterns for different cases are studied. Heat transfer coefficients for various Rayleigh numbers are presented for the enclosures with different nanofluid concentrations. The nanoparticles enhance the heat transfer. The heat transfer enhancement increases with increase in nanoparticle concentration. A new curved enclosure is suggested to provide highest heat transfer.

Keywords: Natural Convection, Numerical, Nanoparticles, Enclosures

1. Introduction

Natural convection heat transfer is widely investigated due to its importance in many engineering applications such as electronic devices, heat exchangers, MEMS devices and solar collectors [1]. Markatos and Pericleous [2] presented a computational method for laminar and turbulent natural convection in a square cavity. The results established new correlations for Nusselt and Rayliegh numbers. An inclined square cavity of air natural convection was studied by Kuper et al. [3]. The study included laminar and turbulent flows for different angles between 0 °-180 ° and different heating conditions. For turbulent flow the standard k-ε model was applied. The results showed that Nusselt number depends on the orientation of the cavity. Ref. [4] numerically studied steady laminar convection in rectangular enclosures heated from below and cooled from above. The aspect ratio in the model was changed between 0.66 and 8 and Rayleigh numbers varied between 10^3 and 10^6. Dimensionless correlations were obtained for heat transfer rates.

Nanotechnology is a new topic to enhance heat transfer by using nanoparticles in the base fluid. Many applications nowadays used this technique which is aimed to enhance the thermal conductivity of the fluid [5]. An experimental study [6] was performed to study fluids with nano-sized solid particles inside a horizontal cylinder heated from one end and cooled from the other. The results showed that the deterioration is dependent on concentration, material and geometry of particles. This study shed light on the nanoparticles and more investigations have to be done to understand the physical phenomenon. A numerical study [7] analyzed the effects of inclination angle of 0°-120° on natural convection in enclosures filled with Cu-water nanofluid. The finite-volume method was used to solve the governing equations. The results showed that increasing copper nanoparticle concentrations enhanced heat transfer with respect to the base fluid but the effect of these particles on Nusselt number was more pronounced at lower Ra values than at higher Ra values. An experimental study was performed by [8] to study natural convection heat transfer for vertical square enclosures of different sizes with Al_2O_3 nanoparticle concentrations ranging from 0.1% - 4% dispersed in water. The results showed enhancement in heat transfer about 18% at a low nanoparticle concentration of 0.1 %. Another study was performed by [9] using the SIMPLE-C algorithm to solve the governing equations. The study investigated natural convection in square enclosures differentially heated at the sides using alumina-water nanofluids with temperature dependent physical properties. The volume fractions of the nanofluid ranged from 0 to 6%. The heat transfer was enhanced with increasing nanoparticles till an optimal value. The present work aims to study steady-state natural convection for two different nanoparticles inside different enclosures.

2. Numerical method

The Boussinesq approximation was used to form the governing equations and the finite volume based solver ANSYS Fluent 14.0 was used to

numerically solve the steady-state continuity, momentum and energy equations for Newtonian fluids. The model of the two-dimensional curved enclosure was shown in Fig. 1. The curved bottom surface is the hot surface while the other three sides of the enclosure are cold surfaces.

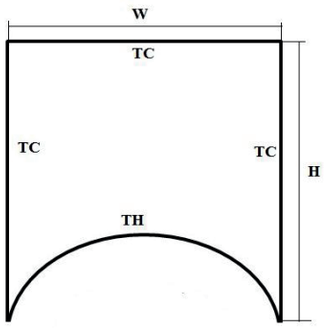

Fig. 1 Schematic of the enclosure with a curved heat source.

The density, specific heat, thermal expansion coefficient, thermal conductivity and viscosity of the nanofluids were calculated by the following equations:

$$\rho_{nf} = (1-\varphi)\rho_f + \varphi\rho_s \qquad (1)$$

$$(\rho c_p)_{nf} = (1-\phi)(\rho c_p)_f + \phi(\rho c_p)_p \qquad (2)$$

$$(\rho\beta)_{nf} = (1-\phi)(\rho\beta)_f + \phi(\rho\beta)_p \qquad (3)$$

$$\frac{k_{nf}}{k_f} = \frac{k_s + 2k_f - 2\varphi(k_f - k_s)}{k_s + 2k_f + \varphi(k_f - k_s)} \qquad (4)$$

$$\mu_{nf} = \frac{\mu_f}{(1-\varphi)^{2.5}} \qquad (5)$$

The present numerical model was validated by comparing the results with numerical results of Khnafer et al. [10] and experimental results of Krane and Jesse [11] for the case of Ra = 10^5 and Pr = 0.7 at constant physical properties, as shown in Fig. 2.

3. Results and discussions

The numerical results focus on the effects of the curvature ratio of the hot curved surface and different nanoparticles on natural convection heat transfer at different Ra numbers. Figure 3 shows temperature contours for water (base fluid) at Ra = 10^5 and constant thermo-physical properties except the density. It can be seen that thermal gradients are significant near the hot curved surface. The mushroom temperature contours indicate strong buoyancy effect. The effects of the curved surface and different nanoparticle materials and concentrations will be investigated.

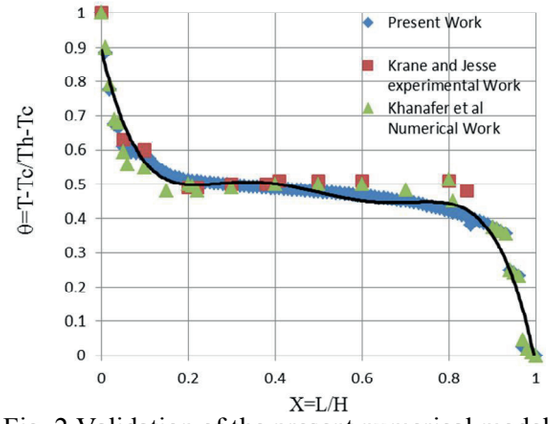

Fig. 2 Validation of the present numerical model.

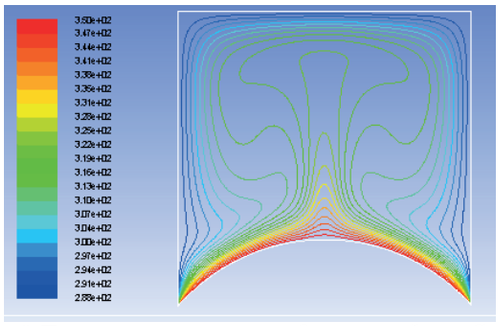

Fig. 3 Temperature contours for water (base fluid) at Ra and constant fluid properties except density.

References

[1] Bejan, A., Convective Heat transfer, 2nd ed. Wiley.
[2]Markatos, N.C., Pericleous, K.A., Int. J. Heat Mass Transf. 27(1984)755-772.
[3]Kuper R.A., Van Der Meer T., Hoogendoom R.A. et al., Int. J. Heat Mass Transf. 36(1993)2899-2911.
[4]Corcion M., Int. J. Therm. Sci. 42(2003)199-208.
[5]Wu Z., Wang L., Sunden B., Appl. Therm. Eng. 60(2013)266-274
[6]Putra N., Roetzel W., Das S.K., Heat Mass Transfer 39(2003)775-782.
[7]Abu-Nada E., Oztop H.F., Int. J. Heat Fluid Flow 30(2009)669-678.
[8]Ho C.J., Liu W.K., Chang Y.S., Lin C.C., Int. J. Therm. Sci. 49(2010)1345-1353.
[9]Cianfrini M., Corcione M., Quintino A., Therm. Sci. 19(2015)591-608.
[10]Khanafer K., Vafai K., Lightstone M., Int. J. Heat Mass Transf. 46(2003)3639-3653.
[11]Krane R., Jessee J., Proc 1st ASME- JSME Therm. Eng. Joint Conf. 1(1983)323-329.

5th Micro and Nano Flows Conference
Milan, Italy, 11-14 September 2016

Does particle size matter in nanofluids' thermal properties?

Michael Frank [1], Dimitris Drikakis [1,*]

* Corresponding author: Tel.: ++44 141 548 4849; Email: dimitris.drikakis@strath.ac.uk
[1] University of Strathclyde, UK

Keywords: nanofluids, particle, size, thermal, conductivity

Nanofluids are suspensions of solid particles with nanometre-sized diameters within a fluid medium. Their academic interest is continuously increasing due to their use across a wide range of industrial applications, ranging from biomedicine (e.g. drug delivery systems) to cooling applications [1].

A large body of experimental work has shown that even a tiny percentage of particles can significantly enhance the heat transfer capacity of a fluid [2, 3]. This renders nanofluids excellent candidates for thermal management, an important area for high demanding applications where overheating of circuits is becoming a limiting factor. However, due to their fluid nature, the behaviour and properties of nanofluids are not well described by methods used for solid-composites. Studies have found that in many instances, such "classical" models significantly underestimate the thermal conductivity of nanofluids. A number of theoretical studies speculate on the possible physical mechanisms that give rise to this enhanced thermal conductivity and propose models to bridge the gap between experiment and theory. Despite all the efforts, there is a lack of consensus with respect to the physical characteristics of nanofluids that result to these unpredictable effects. An example of such a disagreement is in the dependence of the thermal conductivity on the particle size: some believe that larger particles increase the heat capacitance of the fluid [4] while some believe that smaller ones provide this advantage [5].

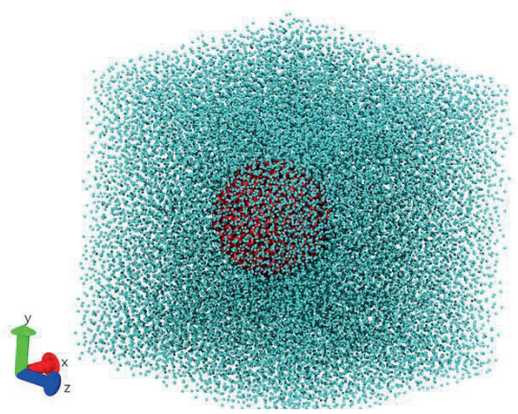

Figure 1 Schematic of the MD model of the nanofluid with a copper particle (red) suspended in liquid argon (green)

In this study we computationally investigate the effect of the particle diameter on the thermal properties of a nanofluid. Molecular Dynamics (MD) simulations are employed to study the system in question at an atomic resolution. The model consists of a copper particle suspended in a Lennard-Jones (LJ) fluid (Figure 1). Periodic boundary conditions are used in all dimensions in order to emulate a bulk nanofluid with nanoparticles spread uniformly across its volume. We investigate the particle size dependence of the nanofluid by changing the particle diameter across different cases. In order to keep the volume fraction constant, the size of the periodic simulation box also varied accordingly.

Our findings show that, if all other parameters are kept constant, the size of the particle has no effect on the thermal conductivity. In fact, we believe that for a uniformly dispersed nanofluid, the thermal conductivity is simply a function of the volume fraction. However, we believe that in the absence of any surfactants, where the particles are free to agglomerate, the particle size (as well as other parameters) can have some effect on the thermal properties of the nanofluid.

Bibliography

[1] K. V. Wong and O. De Leon, "Applications of nanofluids: current and future," *Advances in Mechanical Engineering,* vol. 2, p. 519659, 2010.

[2] J. Eastman, S. Choi, S. Li, W. Yu and L. Thompson, "Anomalously increased effective thermal conductivities of ethylene glycol-based nanofluids containing copper nanoparticles," *Applied Physics Letters,* vol. 78, no. 6, pp. 718-720, 2001.

[3] S. Choi, Z. Zhang, W. Yu, F. Lockwood and E. Grulke, "Anomalous thermal conductivity enhancement in nanotube suspensions," *Applied physics letters,* vol. 79, no. 14, pp. 2252-2254, 2001.

[4] M. P. Beck, Y. Yuan, P. Warrier and A. S. Teja, "The effect of particle size on the thermal conductivity of alumina nanofluids," *Journal of Nanoparticle Research,* vol. 11, no. 5, pp. 1129-1136, 2009.

[5] S. H. Kim, S. R. Choi and D. Kim, "Thermal conductivity of metal-oxide nanofluids: particle size dependence and effect of laser irradiation," *Journal of Heat Transfer,* vol. 129, no. 3, pp. 298-307, 2007.

5th Micro and Nano Flows Conference
Milan, Italy, 11-14 September 2016

Plug formation in a microchannel in two-phase flows with non-Newtonian liquids

Evangelia ROUMPEA, Maxime CHINAUD, Panagiota ANGELI*

* Corresponding author: Email: p.angeli@ucl.ac.uk
Department of Chemical Engineering, University College London, Torrington Place, London WC1E 7JE, UK

Keywords: non-Newtonian, Microchannel, PIV, Plug formation

1 Introduction

The demand for sustainable and efficient continuous processing makes micro-fluidic devices an attractive option. Two-phase flow chemical operations in microchannels offer significant advantages compared to large-scale processes, such as lower sample consumption, increased safety and high surface-to-volume ratio. However, most studies are limited to Newtonian fluids although fluids with non-Newtonian rheology are very common industrially, including catalytic polymerization reactions, food processing and enhanced oil recovery [1-2].

The present work investigates the dynamics of plug formation of a non-Newtonian shear-thinning aqueous solution and a Newtonian organic fluid in a circular, glass microchannel. The effects of the flow rates and the viscosity of the aqueous phase on the hydrodynamic characteristics and the velocity fields are studied using a two-colour micro-PIV system.

2 Experimental setup

Two aqueous glycerol solutions containing xanthan gum (1000 and 2000 ppm) are used as the non-Newtonian fluids while silicone oil (Sigma-Aldrich) is the Newtonian phase. Two oils with different viscosities, 5 and 155 cSt have been considered. The corresponding Newtonian aqueous solution is also used for reference and comparison. All runs are carried out in a circular glass microchannel (Dolomite® microfluidics) with inner diameter 200 μm at different combinations of flow rates of the two phases, that varied in the range of 0.01-0.1 ml/min.

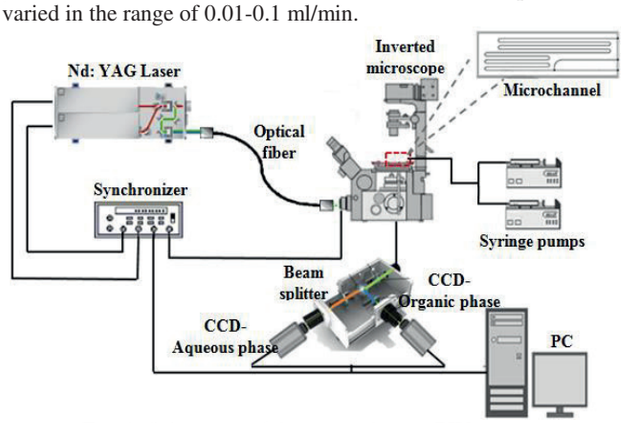

Fig. 1: Schematic of the two-colour μ-PIV system.

Using separate syringe pumps (KDS®), the two immiscible fluids are introduced in the microchannel via a T-junction. In the two-colour micro-PIV experiments (Fig. 1) the aqueous phase is seeded with 1 μm carboxylate-modified microspheres FluoSpheres® with orange fluorescent colour (540/560 nm) whereas the organic phase is seeded with 1 μm blue polystyrene microspheres particles Fluoro-Max® (350/440 nm). The illumination is achieved with a UV double pulsed Nd:YAG laser (Litron Lasers®) and the light emitted from the seeded fluids in the test section is led from the microscope to a beam splitter (Andor® Technology). Each wavelength of the emitted light is led subsequently to a separate CCD camera. Both cameras are connected to a laser pulse synchronizer TSI® and a PC. Image processing software (Insight 4G, TSI®) is used for extracting information from the acquired video images. The flow is also visualized using a high speed CCD camera and a light source for the illumination of the test section.

3 Results

Under the specific experimental conditions, the organic 5 cSt Newotnian phase always forms the dispersed plugs irrespective of the side branch of the T-junction used to introduce it in the main channel. In the case of the viscous oil 155 cSt, the phase continuity is inversed and the aqueous non-Newotnian phase forms the plugs whereas the organic phase is now the continuous one.

During the plug formation different stages of detachment can be observed [3]. For the same stage of breakage, the effect of shear-thinning behaviour is presented in Fig. 2. The dynamics of filament breakage change depending on the amount of xanthan gum and the rheology of the aqueous phase. For the 2000 ppm non-Newtonian solution case, the break-up point has moved further downstream compared to the less dense solution and the breakage time is longer.

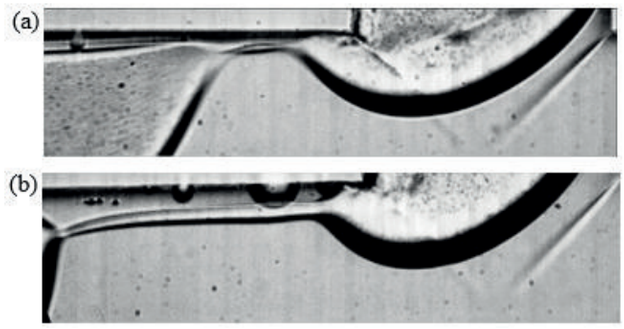

Fig. 2: Dynamics of filament breakage for 155 cSt silicone oil and (a) Newtonian aqueous phase (b) non-Newtonian aqueous phase, 2000 ppm.

4 References

[1] Salim, A., Fourar, M., Pironon, J., Sausse, J., 2008. Oil–water two-phase flow in microchannels: flow patterns and pressure drop measurements. *Can. J. Chem. Eng*. 86, 978–988.

[2] Tang, G., Lu, Y., Zhang, S., Wang, F., Tao, W., 2012. Experimental investigation of non-Newtonian liquid flow in microchannels. Journal of non-Newtonian Fluid Mechanics. 174, 21-29.

[3] Garstecki P., Fuerstman MJ., Stone HA., Whitesides GM., 2006. Formation of droplets and bubbles in a microfluidic T-junction—scaling and mechanism of break-up. Lab on a Chip 6(3): 437-446.

5th Micro and Nano Flows Conference
Milan, Italy, 11-14 September 2016

EXPERIMENTAL INVESTIGATION OF FLUID FLOW AND HEAT TRANSFER OF FLOW BOILING IN MINICHANNELS AT HIGH REDUCED PRESSURE

Alexander V. BELYAEV, Aleksey V. DEDOB *, Alexander T. KOMOV, Alexander N. VARAVA

* Corresponding author: Tel.: +10 (903)7895756; Email: dedovav@mpei.ru
National Research University "MPEI", Moscow, Krasnokazarmennaya, 14

Keywords: Flow boiling, Hydrodynamics, Heat transfer, High reduced pressure

This work presents experimental results of fluid flow and heat transfer of flow boiling in minichannels at high reduced pressures. The relevance of this study is determined by the growing interest to miniaturized heat exchangers in various fields of industry.

In minichannels of $0.2 < d \leq 3$ mm peculiarities resulting from the characteristic scale of the phenomena taking place in boiling flow and the linear scale of the channel may take place. Two-phase flow regimes become dominant in understanding of heat transfer mechanism. Heat transfer found with the common formulas for regular channels does not agree with experimental data well, if at all. Thus a need for new methods to determine heat transfer arises. A lot of experimental works is available in literature at the moment; however, the data in most of them was obtained for low and moderate reduced pressures. Moreover, the calculation methods proposed by the authors have empirical nature and are only suitable to describe the cases close to those of the authors.

The aim of this work is experimental confirmation of hypothesis that at high reduced pressures two-phase flow regimes in minichannels become similar to macrochannel ones. In that case, heat transfer in minichannels could be predicted by common correlations used for macrochannels.

This paper describes an experimental setup and reports experimental heat transfer data. Experiments on the hydrodynamics and heat transfer of R113 and RC318 in two vertical channels with diameter of 1.36 and 0.95 mm and length of 200 and 100 mm respectively have been performed. The hydraulic loop of the experimental setup allows to maintain stable flow parameters at the channel inlet at pressures up to 2.7 MPa and temperatures up to 200 ºC. The measured parameters in the experiment were the following: mass flow rate, pressure and temperature at the inlet and outlet of the test section, electric heating power, temperature of the wall in six cross-sections along the length of the minichannel. The measurements were carried out using an automated data acquisition system.

The experiments were carried out for 195 regimes, in which inlet pressure to critical pressure ratio (reduced pressure p_r) was $p/p_{cr} \cong 0.15 \div 0.9$, mass velocity ranges were between 1000 and 4600 kg/(m^{2}s), and inlet temperatures from 50 to 180 ºC. For each regime with fixed parameters the maximum possible heating power value was applied, being limited either by the maximum output of the power supply, occurrence of dryout, or the wall temperature exceeding 350 ºC. Fig. 1 and 2 show an example of raw data.

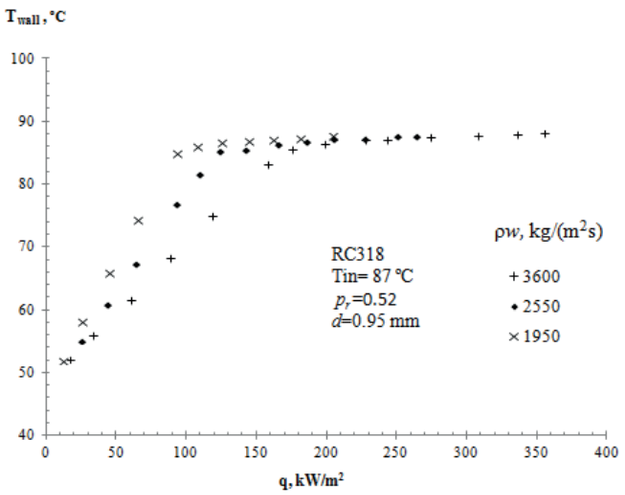

Fig.1 Wall temperature versus heat flux

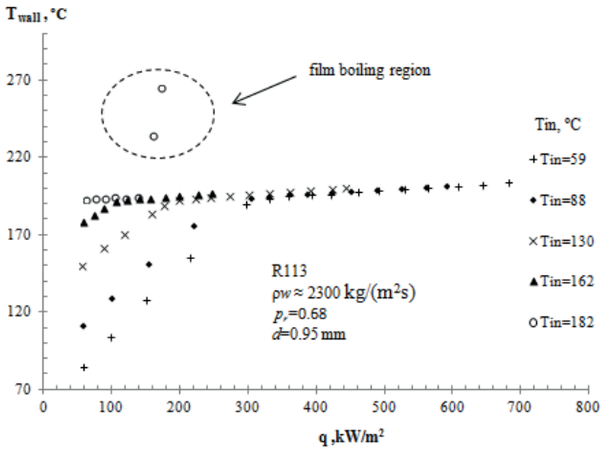

Fig.2 Wall temperature versus heat flux

5th Micro and Nano Flows Conference
Milan, Italy, 11-14 September 2016

Role of viscoelasticity in droplet formation inside a microfluidic T-junction

Enrico CHIARELLO[1], Matteo PIERNO[1], Giampaolo MISTURA[1,*], Mauro SBRAGAGLIA[2]

* Corresponding author: Tel.: +39-049-8277020; Fax: +39-049-8277003; Email: giampaolo.mistura@unipd.it
1: Dipartimento di Fisica e Astronomia “G. Galilei”, Università di Padova, Padova, Italy
2: Dipartimento di Fisica, Università di Roma "Tor Vergata", Roma, Italy

Keywords: droplet microfluidics, T-junction; squeezing regime, non-Newtonian fluids

The progressive break-up of a fluid thread into a number of small drops [1] is a rich physical phenomenon which impacts many applications [2,3]. In particular, droplet-based microfluidic devices have gained a considerable deal of attention, due to their importance in studies that require high throughput control over droplet size. Common droplet generator designs used in these devices are T-shaped geometries [4-6] and flow-focusing devices [7–9]. With a few exceptions [10–12], previous research has been mainly restricted to Newtonian fluids. However, the processing of biological fluids with high molecular weight macromolecules inevitably results in considering a non-Newtonian viscoelastic behaviour. Consistently, the use of viscoelastic liquids in flow-focusing devices [10,11] or T-junction geometries [12] has recently been taken into account, but needs further investigation.

Here we investigate the role of viscoelasticity in droplet formation in a microfluidic T-junction, where newtonian oil droplets are dispersed in non-newtonian aqueous polymer solutions of Polyacrylamide and Xanthan, which display normal stress effects and shear-thinning respectively, at different concentrations in the semidilute regime [13]. Numerical simulations with lattice Boltzmann [14] are performed on the same system, enabling us to visualize the stress distribution in the viscoelastic continuous phase.

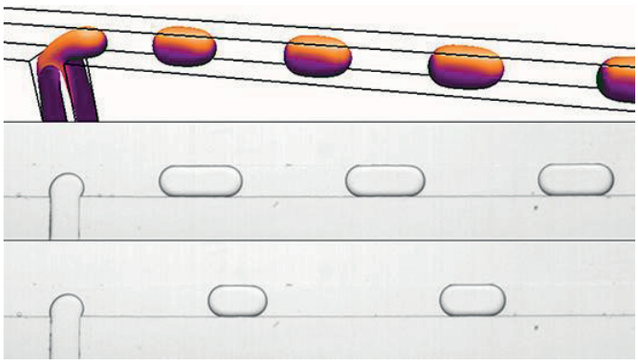

Figure 1. Top: numerical LBM simulation of droplet formation in the T-Junction geometry. Middle-Bottom: micrographs of droplets produced in the experimental T-Junction.

References

[1] J. Eggers, Rev. Mod. Phys. 69 (1997) 865 .

[2] G.F. Christopher, S.L. Anna, J Phys D Appl Phys 40 (2007) R319.

[3] S. Teh, R. Lin, L. Hung, A. Lee, Lab. Chip 8 (2008) 198.

[4] M.D. Menech, P. Garstecki, F. Jousse, H.A. Stone, Jour. Fluid. Mech. 595 (2008) 141.

[5] M.D. Menech, Phys. Rev. E 73 (2006) 031505.

[6] E. Piccin, D. Ferraro, P. Sartori, E. Chiarello, M. Pierno, G. Mistura, Sensors and Actuators B. 196 (2014) 525–531.

[7] H. Liu, Y. Zhang, J. Appl. Phys. 106 (2009) 034906.

[8] H. Liu, Y. Zhang, Physics of Fluids 23 (2011) 082101.

[9] L. Derzsi, M. Kasprzyk, J.P. Plog, P. Garstecki, Phys. Fluids 25 (2013) 092001.

[10] P.E. Arratia, J.P. Gollub, D.J. Durian, Phys. Rev. E 77 (2008) 036309.

[11] B. Steinhaus, A.Q. Shen, R. Sureshkumar, Phys. Fluids 19 (2007) 073103.

[12] J. Husny, J. Cooper-White, J. Non-Newton. Fluid Mech. 137 (2006) 121.

[13] E. Chiarello, L. Derzsi, M. Pierno, G. Mistura, E. Piccin, Micromachines 6 (2015) 1825-1835.

[14] A. Gupta, M. Sbragaglia, A. Scagliarini, Journal of Computational Physics 291 (2015) 177–197

5th Micro and Nano Flows Conference
Milan, Italy, 11-14 September 2016

Influence of the shape of an orifice entrance on the flow pattern and droplet deformation during high-pressure homogenisation

Ariane BISTEN [1,*], Heike P. SCHUCHMANN [1]

* Corresponding author: Tel.: ++49 (0)721 608 43785; Fax: ++49 (0)721 608 45967; Email: ariane.bisten@kit.edu
1 Institute of Process Engineering in Life Sciences, Section I: Food Process Engineering, Karlsruhe Institute of Technology, Germany

Keywords: Micro Flow Pattern, High-Pressure Homogenisation, Micro-PIV, Emulsification

High-pressure homogenisation is a commonly used process in life sciences e.g. APIs are stabilised in emulsions. In homogenisation, compressed raw emulsions are relaxed through narrow disruption units and as a result the droplet size is reduced. Adjusting or changing droplet size distributions in a process is often based on empirical knowledge, because droplet break-up is influenced by the flow pattern in the disruption unit. The flow pattern before, in and after the disruption unit lead to elongation, shear, turbulence and cavitation. Understanding the forces which influence the droplet size and size distribution is consequently essential to improve performance and areas of application of high-pressure homogenizers.

Because of transitional and turbulent flow regimes and the microscale of the disruption unit, measuring the flow conditions in a high-pressure homogenizer is challenging. Intrusive measurement methods change the flow immensely regarding the physical dimensions of the disruption units from about 100 - 500 µm. A relatively new measurement method to determine flow regimes is Micro Particle-Image-Velocimetry (µPIV). This is an optical, non intrusive measurement method, which was already used by our research group to measure the flow regimes in a modified optical accessible disruption unit (Kelemen et al. 2014; Kelemen et al. 2015). Here, the disruption unit is positioned on top of the channel (see Fig. 1, a) and not in the middle of the channel like in commonly used disruption units. This design enabled measurements inside the disruption unit.

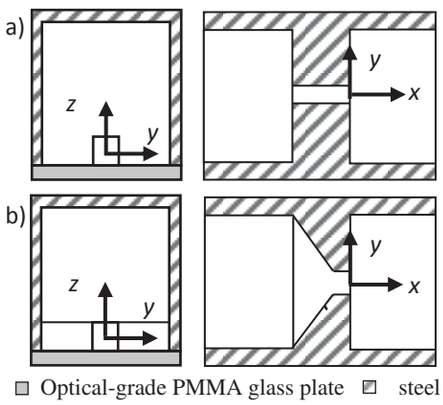

Fig. 1: Shape and position of disruption units with a) sharp edged entrance and b) conical entrance

The shape of the entrance of disruption units was varied was varied in previous works and it was shown that the resulting droplet size was influenced by the shape of the entrance (Aguilar et al. 2004; Freudig 2004). In this experiments only the resulting droplet size distribution was measured. To understand the resulting changes the local flow pattern needs to be investigated. First measurements of local flow pattern during high-pressure homogenization were performed in a modified disruption unit with a sharp edged entrance (see Fig. 1, a) (Kelemen et al. 2014). To investigate the effect of the shape of the entrance further the characterisation of local flow pattern in conical and sharp edged disruption units is essential.

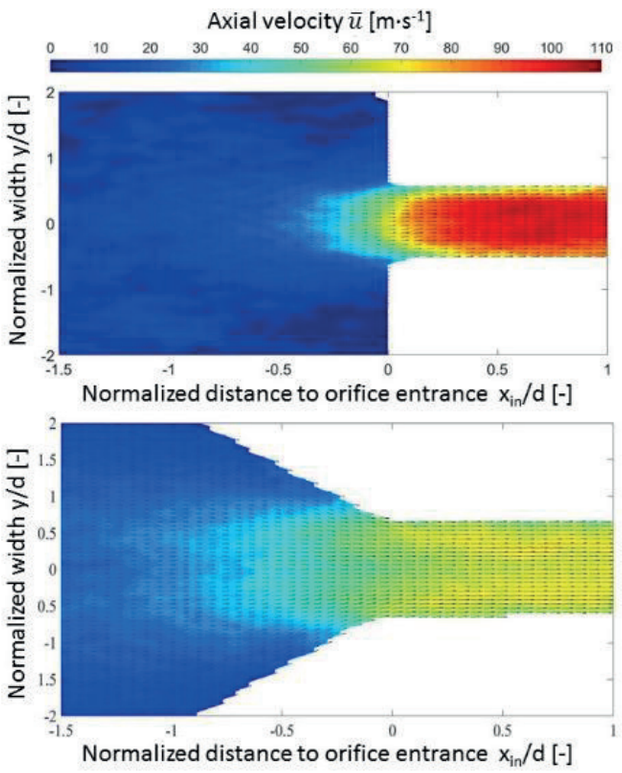

Fig. 2: Velocity contours of the disruption units at z = 0 mm and at a Reynolds number Re ≈ 1000 for sharp edged entrance (top) and conical entrance (bottom)

In this work the design of the disruption unit is adjusted to investigate the effect of conical entrances in disruption units on the local flow pattern (see Fig. 1, b). Additionally, it also gets closer to the designs used in industrial application. The change of the shape of the disruption unit leads to a different flow pattern in front of and in the disruption unit. The calculated stress profiles (shear stress and elongation) from the conical also differ from the sharp edged disruption unit. We will compare the measured velocities (velocity distributions and fluctuations of the local velocities) with

the results of the already established modified disruption unit (see Fig. 2). The comparison of the flow pattern in the conical and the sharp edge disruption unit will give indication on the resulting local stresses which lead to droplet break-up.

Additionally to the flow measurements the deformation of the droplets at the entrance and in the disruption unit is visualized and the resulting droplet size distribution is measured for both disruption units. Shear stresses influence the droplet deformation and break-up in laminar flow only until a certain viscosity ratio between disperse phase and continuous phase. Therefore the viscosity ratio is varied to change the influence of shear stresses accordingly. The comparison of the flow pattern in the conical and the sharp edge disruption unit will give indication on the resulting local stresses which lead to droplet break-up. Therefore the experiments are based on the same conditions (Reynolds-number, viscosity of disperse phase and continuous phase, droplet size of the raw emulsion).

Combining the results of visualized droplets and final droplet size distribution with the flow measurements the efficiency of the disruption units can be evaluated and the influence on droplet break-up can be determined.

References

Aguilar FA, Freudig B, Schuchmann HP (2004) Herstellen von Emulsionen in Hochdruckhomogenisatoren mit modifizierten Lochblenden. Chemie Ingenieur Technik 76(4):396–399. doi: 10.1002/cite.200403375

Freudig B (2004) Herstellen von Emulsionen und Homogenisieren von Milch in modifizierten Lochblenden, Universität Karlsruhe (TH)

Kelemen K, Crowther FE, Cierpka C, Hecht LL, Kähler CJ, Schuchmann HP (2014) Investigations on the characterization of laminar and transitional flow conditions after high pressure homogenization orifices. Microfluidics and Nanofluidics 18(4):599–612. doi: 10.1007/s10404-014-1457-0

Kelemen K, Gepperth S, Koch R, Bauer H, Schuchmann HP (2015) On the visualization of droplet deformation and breakup during high-pressure homogenization. Microfluidics and Nanofluidics 19(5):1139–1158. doi: 10.1007/s10404-015-1631-z

5th Micro and Nano Flows Conference
Milan, Italy, 11-14 September 2016

Performance of Shell-and-Tube Condenser with Minichannels for the Micro Domestic ORC

Jan WAJS [1,*], Dariusz MIKIELEWICZ [1], Blanka JAKUBOWSKA [1]

* Corresponding author: Tel.: +48 583472830; Fax: +48 3472816; Email: janwajs@pg.gda.pl
1: Department of Energy and Industrial Apparatus, Gdansk University of Technology, Poland

Keywords: Minichannels, Heat Exchangers, condensation, micro-CHP

In recent years there is observed a tendency to increase the importance of so called dispersed generation, based on the local energy sources and also the working systems utilizing both the fossil fuels and the renewable energy resources. Generation of electricity on a small domestic scale together with production of heat can be obtained through the technologies like the gas engine units, micro gas turbines, fuel cells with efficient electrolysis, Stirling engines or the ORC systems. All of them are mentioned in the EU directive 2012/27/EU for cogenerative production of heat and electricity. Considering mentioned technologies and their development, the ORC system seems to be the closest to implementation. However, it should be pointed out that practical realization of the organic Rankine cycle (ORC) in a micro-scale (the electrical power production below 10 kWe) is still kind of technical challenge. Such unit must be equipped with small size turbine or expansion machine and high efficient and compact heat exchangers (evaporator, condenser). This is the reason why the novel constructions of recuperators or enhancement mechanisms are looked for. The mini or microchannels based heat exchangers are very efficient therefore their utilization in such applications.

The Authors are developing the idea of cogeneration boiler for the household applications. A demonstration prototype micro-CHP unit based on the ORC technology was developed [1]. The system consists of the vapour module (with ethanol as a working fluid) coupled with the commercial gas boiler, which is available on the market and used in many houses. The idea of such system is to produce electricity for household demand or for selling it to electric grid – in such situation the system user will became the prosumer. Investigations showed that the boiler with a thermal power of 25 kW was able to provide the saturated/superheated steam of ethanol at proper conditions needed in the ORC system and it can be utilized as a heat source in the domestic micro-CHP. The tested system could produce electricity in the amount of 1 kW_e [2].

In the paper, the original compact shell-and-tube heat exchanger with circular minichannels of in-house design and manufacture is presented as the unit for the domestic micro power plant investigations as well as other future technical applications. It was equipped with turbulizing baffles inside the jacket. Heat exchange surface of the heat exchanger was 0.4 m^2. The outer jacket was made of a pipe having an inner diameter of 67 mm. The jacket's input constitutes a hexagonal arrangement of 103 pipes of the active length of 310 mm, an inner diameter of 2 mm and a wall thickness of 1 mm. All the components of the heat exchanger were made of stainless austenitic chromium-nickel steel. During the test the prototype construction served as the condenser cooled by water with ethanol as a working fluid.

Condensation of etanol vapour was accomplished by means of two methods, namely based on the empirical model due to Shah [3] and semi-empirical model due to Mikielewicz [4]. The correlation due to Shah is a widely known and approved model for calculations of heat transfer in conventional size channels, and is also performing well in predictions of heat transfer coefficient in minichannels. On the other hand the model due to Mikielewicz accounts additionally for the non-adiabatic effects in convective heat transfer coefficient. The obtained results are in a very good consistency.

References

[1] Mikielewicz D., Wajs J., Mikielewicz J. (2014). Gas boiler as a heat source for a domestic micro-CHP, Journal of Power Technologies, vol. 94, no. 4, pp. 317-322.

[2] Wajs J., Mikielewicz D., Woźnowska M.. (2015). Cogeneration gas boiler – investigations of prototype, Instal, No 12 (in print).

[3] Shah M.M. (1979). A general correlation for heat transfer during film condensation inside pipes, Int. Journal of Heat and Mass Transfer, vol. 22, pp. 547-556.

[4]Mikielewicz D., Andrzejczyk R., Wajs J., Mikielewicz J. (2012). A general method for calculation of two-phase flow pressure drop in flow boiling and flow condensation. ECI 8th International Conference on Boiling and Condensation Heat Transfer, 3-7 June 2012, Lausanne, Switzerland.

5th Micro and Nano Flows Conference
Milan, Italy, 11-14 September 2016

ID 105

Interaction Effects of Micro/Nanoparticles on Targeted Magnetic-Particle Delivery in a Blood Microvessel

Huei Chu WENG [1,*], Cheng-Hung CHENG [1]

* Corresponding author: Tel.: +886-3-265-4311; Fax: +886-3-265-4399; Email: hcweng@cycu.edu.tw
1 Department of Mechanical Engineering, Chung Yuan Christian University, Taoyuan, Taiwan

Abstract When the size of a human blood vessel gets smaller down to micrometers, the microflow behavior of blood with micro/nanoparticles (including red blood cells, white blood cells, platelets, and magnetic nanoparticles) would become a more important issue. It is desirable to understand the role of the collision and friction between micro/nanoparticles and between micro/nanoparticles and vessel wall in blood flow with magnetic nanoparticles at the microscale. In this study, the influence of particle interaction on targeted magnetic-particle delivery in a blood microvessel under different magnetic field gradients is investigated. The fully developed analytical solutions are presented for the blood flow with magnetite nanoparticles in a microtube at state of body temperature. Results reveal that the role of the collision and friction is dominated by the interaction between particles and vessel wall surface. The interaction effect of particles is to reduce fluid velocity and volume flow rate. Moreover, increasing the magnetic field gradient and particle volume fraction could enhance the effect.

Keywords: Magnetic-Particle Delivery, Biomedical Magnetic Fluids, Particle Interaction, Nanoparticles and Microparticles

1. Introduction

Recent advances in nanotechnology have led to reductions in scale of artificial things. Fluids with magnetic nanoscale artificial things could be designed to exhibit novel and improved mechanical, thermal, chemical, magnetic, optical, electronic, and biological properties. Weng [1] performed an analysis for the effects of magnetic-particle concentration and magnetic field gradient on the blood flow in a blood vessel. However, when the blood vessel size gets smaller down to micrometers in human body, e.g. arteriole, capillary, and venule, the blood flow at the microscale would become a more important issue.

In this study, an analysis of the interaction effects of micro/nanoparticles on the flow in a blood microvessel before targeted magnetic particles arrive at their destination under different magnetic field gradients is conducted, so as to examine how particle interaction affects the targeted magnetic-particle delivery (TMPD) behavior.

2. Analytical Solutions

Consider a flow of blood of magnetic artificial-particle concentration φ and natural-particle concentration $\hat{\varphi}$ through a microtube under the dimensionless magnetic field gradient ΔH. Let R denote the dimensionless position from the axis of the microtube. If the aspect ratio of the tube is sufficiently large and the magnetization attains its saturation value, then the fully developed flow prevails in the microtube and has velocity and flow rate analytical solutions:

$$U(R) = \frac{2(1+\varphi\Delta H)(1-R^2)}{\left((1-(\varphi+\hat{\varphi}))^{\frac{-5}{2}\varepsilon}\right)\left(1+\frac{3}{2}\varphi\varepsilon_m\right)} \quad (1)$$

$$\dot{Q} = \frac{(1+\varphi\Delta H)}{\left((1-(\varphi+\hat{\varphi}))^{\frac{-5}{2}\varepsilon}\right)\left(1+\frac{3}{2}\varphi\varepsilon_m\right)} \quad (2)$$

where ε and ε_m are two viscosity correction factors that characterize interaction effects [2].

3. Results and Discussion

Following the physical properties of blood with magnetite nanoparticles (at state of body temperature) used in Weng [1], the analytical results are shown and the discussion based on these results is made. The collision and friction between micro/nanoparticles and vessel wall could be found to dominate the role as a major interaction for a sufficiently small vessel size and to result in a dramatic increase in effective viscosity (unshown here due to article length). In figure 1, we plot the variations of the velocity U with the position parameter R for different values of the correction factors ε (unshown) and ε_m at zero magnetic field gradient ($\Delta H = 0$). It is found that both the increases in ε and ε_m lead to a reduction in U. In figure 2, we plot the influence of the magnetic field gradient ΔH on the flow rate $\dot{Q}$ at different values of ε (unshown) and ε_m. It is obvious that the presence of particles leads to the decreases in flow rate. Such a particle interaction effect can be magnified by increasing the magnetic field gradient and particle volume fraction (unshown).

4. Conclusions

A study has been made on the particle interaction effects on targeted magnetic-particle delivery (TMPD) in a blood microvessel. Results showed that the collision and friction between micro/nanoparticles and vessel wall surface dominates the major role. The presence of magnetic nanoparticles was found to increase the flow, but the interaction between particles and vessel wall surface was found to be a flow retardation effect. The particle interaction results in a reduced velocity and therefore a decrease in flow rate. The particle interaction effect can be magnified by increased magnetic driving force and particle concentration.

The results help us to understand the TMPD behavior in a blood microvessel and benefit the designs of bio-functional magnetofluidic device.

Acknowledgments

The authors would like to acknowledge financial support from the Ministry of Science and Technology of Taiwan under Grant No. MOST 104-2221-E-033-045.

References

[1] Weng, H. C., 2013, "Hydrodynamic Modeling of Targeted Magnetic-Particle Delivery in a Blood Vessel," *J. Biomech. Eng. - Trans. ASME*, Vol. 135, p. 034504.

[2] Lo, K. J. and Weng, H. C., 2015, "Convective Heat Transfer of Magnetic Nanofluids in a Microtube," *Smart Sci.*, Vol. 3, pp. 56-64.

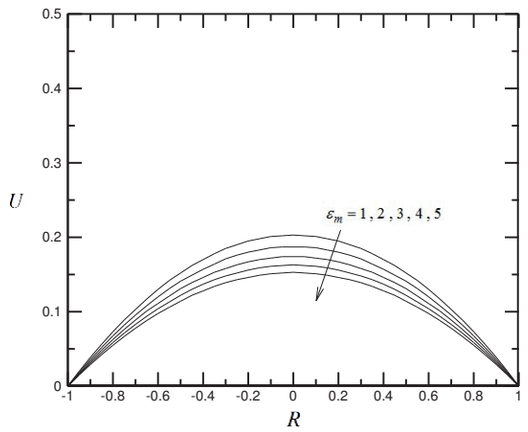

Figure 1. Velocity distribution $U(R)$ for different values of the correction factor ε_m with the magnetic field gradient $\Delta H = 0$.

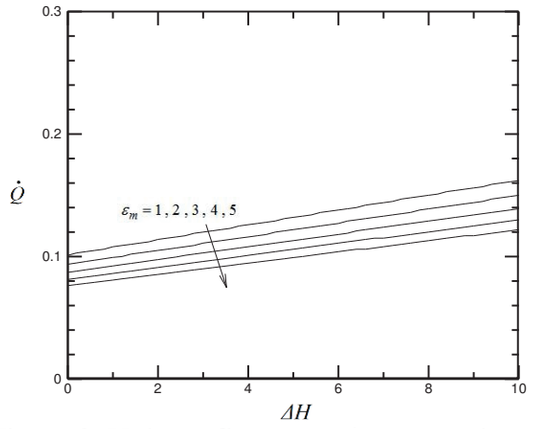

Figure 2. Volume flow rate $\dot{Q}$ versus the magnetic field gradient ΔH for different values of the correction factor ε_m.

Numerical Simulation of Micro cavity Flow Using Perturbation Theory

Mohammad S. KHALILI [1,*], Mohsen SAGHAFIAN [1], Ahmad SEDAGHAT [1], Ebrahim SHIRANI [1]

* Corresponding author: Tel.: ++98 (0)372 4525206; Email: ms.khalili@me.iut.ac.ir
1: Department of Mechanical Engineering, Isfahan University of Technology, Iran
saghafian@cc.iut.ac.ir, sedaghat@cc.iut.ac.ir, eshirani@cc.iut.ac.ir

Keywords: Micro Flow, Perturbation Method, Slip Flow, Micropoiseuille, Microcouette, Microcavity

1 Introduction and Perturbation Method

A new method for modeling of micro flows is presented in this research. First, the continuum equations of fluid dynamics are developed by using perturbation expansions of the velocity, pressure, density and temperature fields:

$$\phi = \phi_0 + Kn\,\phi_1 + Kn^2\,\phi_2 + Kn^3\,\phi_3 + O(Kn^4) \qquad (1)$$
$$\phi = u, v, w,\ p,\ \rho, T$$

Where the no-slip fields are denoted by $\phi_0(\boldsymbol{x},t)$, and corrections to the fields due to different orders of Kn dependence are denoted by $\phi_i(\boldsymbol{x},t)$ (i=1, 2, ...), and also slip fields are denoted by $\phi(\boldsymbol{x},t)$. Subsequently, different orders of equations in dependence of Knudsen number are obtained. Required boundary conditions for solving each order of these equations are obtained by substitution of the perturbation expansions into the general boundary conditions for velocity slip and temperature jump [1].

2 Development, Discretization and Solution Algorithm

In the present work, we use three-term perturbation expansions and reach to three order of equations O(1), O(Kn), O(Kn^2) and their boundary conditions. In fact, the equations of O(1) are the no-slip Navier-Stokes equations. Also, the equations of O(Kn) and O(Kn^2) govern the required corrections due to the velocity slip and temperature jump. This set of equations is discretized in two-dimensional state on a staggered grid using the finite volume method.

Total algorithm of solution includes three steps: The first step is solution of the O(1) equations with the O(1) boundary conditions. The second step is solution of the O(Kn) equations with the O(Kn) boundary conditions. This step's boundary conditions are obtained by fitting the first step's fields on the walls. The third step of algorithm is solution of the O(Kn^2) equations with the O(Kn^2) boundary conditions. This step's boundary conditions are also obtained by fitting the first and second step's fields on the walls. A three-part computer program has been produced for solving the set of discretized equations. Each part of this code, solve one order of the equations with the SIMPLE algorithm.

3 Some Micro Flows, Results and Conclusions

At First, incompressible slip micropoiseuille and microcouette flows are solved either analytically or numerically using the perturbation method. Good agreement is found between analytical and numerical results. In Both case, numerical results of the perturbation method deviate from its analytical results by increasing the Knudsen number. This reveals that more corrections are needed in the perturbation method by increasing the Knudsen number. Instead, by combination of two slip coefficients and the two-correction perturbation method, it can be easily used this method in the higher Knudsen numbers.

Also, a shear-driven microcavity flow with slip is investigated and its results are compared with those by the DSMC approach [2]. Good agreement is found between the results of two approaches, except near the upper corners of the cavity. At this problem, we also try to evaluate different researcher's slip coefficients [3] and probably to propose more accurate slip coefficients.

For Argon gas flow in a lid-driven microcavity with a unit aspect ratio (The channel length and height L=H=1.288μm, at T_0=298K and P_0=1atm, σ_v=1, U_{lid}=28.934 m/s, Re=2.913, Ma=0.09, Kn=0.05 and uniform staggered grid 60×60), Schematic diagram of the problem and Nondimensional velocity profiles along the centreline of the cavity are shown in Fig. 1 and in Fig. 2.

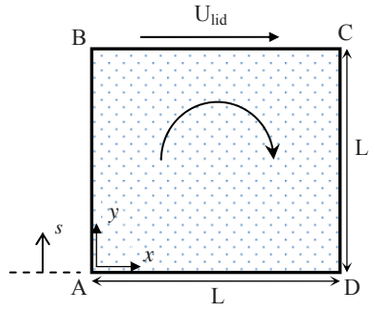

Figure 1. Schematic diagram of the microcavity.

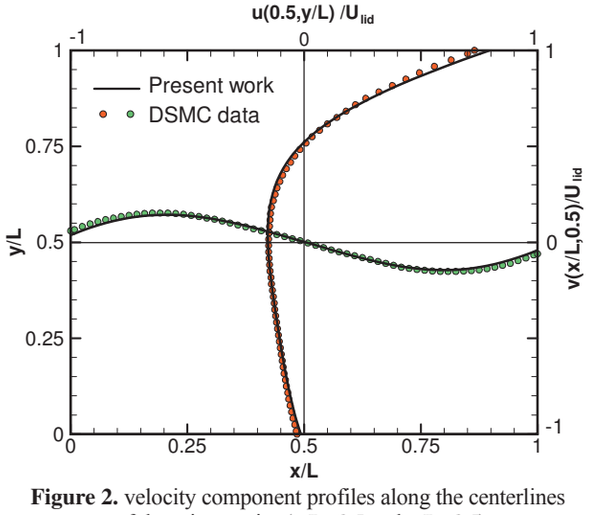

Figure 2. velocity component profiles along the centerlines of the microcavity (*x/L=0.5* and *y/L=0.5*).

4 Some References

[1] Karniadakis, G., Beskok, A. and Aluru, N., 2005. Microflows and Nanoflows- fundamentals and simulation. SpringerScience and Business Media, Inc., New York.

[2] Mizzi, S., Emerson, D. R. and Stefanov, S. K., 2007. Effects of rarefaction on Cavity flow in the slip regime. Journal of Computational and Theoretical Nanoscience, 4(4), 817-822.

[3] Zhang, W. M., Meng, G. and Wei, X., 2012. A review on slip models for gas microflows. Microfluidics and Nanofluidics, 13, 845-882, ISSN 1613-4982.

Condensation of FC72 in Microchannels

Lei CHAI [1], Jie SUN [1, 2], Nan HUA [1, 3], Rong Ji XU [1, 4], Yong Xin LIU [1], Tian Yi SONG [1, 5, 6], Guang Xu YU [7], Hua Sheng WANG [1,*] John W ROSE [1,*]

* Corresponding author: Tel.: ++44 (0)2078 827921; Email: h.s.wang@qmul.ac.uk
1 School of Engineering and Materials Science, Queen Mary University of London, UK
2 Institute of Engineering Thermophysics, Chinese Academy of Sciences, China
3 Faculty of Material and Engineering, Guangdong University of Technology, China
4 Beijing Engineering Research Center of Sustainable Energy and Buildings，Beijing University of Civil Engineering and Architecture, China
5 Institute of Chemical Engineering, Dalian University of Technology, China
6 Luoyang Longhua Heat Transfer & Energy Conservation Co. Ltd., China
7 DENSO Marston Ltd., UK

Keywords: Microchannels, Condensation, FC72, Inverse calculation, Experimentation

ABSTRACT

New heat-transfer measurements are reported for condensation of FC72 in microchannels. The test section comprised a cooper block made in two halves with lapped interfaces (see Figs. 1 and 2). Six parallel microchannels (1.5 mm deep x 1.0 mm wide) were machined in the mating surface of the lower block. The length of the microchannels was 540 mm. The upper and lower blocks housed each housed 49 thermocouples in small holes (0.6 mm diameter) spaced through the blocks at 7 locations in the flow direction. Each block was cooled along its outer surface by water in counter flow.

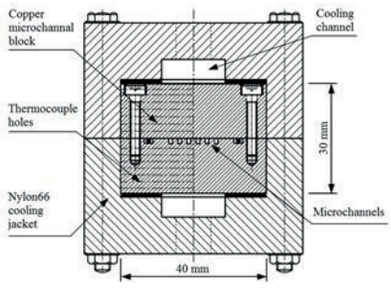

Fig. 1 Section through test section

The heat flux from the interface to the upper and lower blocks and the temperature at the interface were determined by an inverse solution of the conduction equation (see Yu et al. [1]). These were used to determine the heat flux and surface temperature distributions along the channels and hence local heat-transfer coefficient and local quality. The Figure 3 shows typical measured temperatures through the blocks.

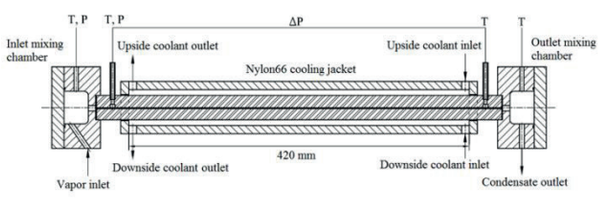

Fig. 2 Details of the test section geometry

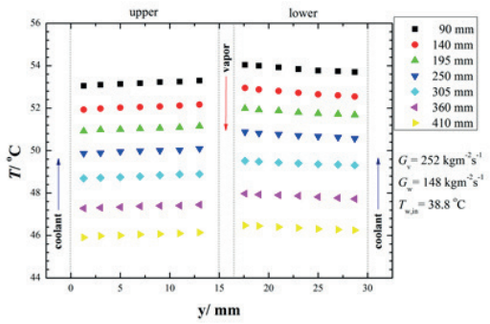

Fig. 3 Specimen temperature distributions in test block. Symbols denote distance from channel inlet. Positions of thermocouple junctions measured from upper surface (left side is upper half of the test block).

The results are compared with recent measurements of Kim and Mudawar [2] for FC72 and with correlations based on data for R134a and with a Nusselt-based theory which assumes laminar annular flow.

REFERENCES

[1] Yu, G. X., Sun, J., Wang, H. S., Wen, P. H., Rose, J. W., 2014. Meshless inverse method to determine temperature and heat flux at boundaries for 2D steady-state heat conduction problems. *Exp. Therm. Fluid Sci*. **52**, 156-163.

[2] Kim, S-M., Mudawar, I., 2012. Flow condensation in parallel micro-channels – Part 2: Heat transfer results and correlation technique. *Int. J. Heat Mass Transfer* **55**, 984-994.

5th Micro and Nano Flows Conference
Milan, Italy, 11-14 September 2016

Non-equilibrium effects on steady flow past a stationary circular micro-cylinder

Xiao-Jun. GU [1,*], David R. EMERSON[1]

* Corresponding author: Tel.: ++44 (0)1925 603663; Fax: ++44 (0)1925 603634; Email: xiaojun.gu@stfc.ac.uk
[1]Scientific Computing Department, STFC Daresbury Laboratory, Warrington WA4 4AD, UK

Keywords: Micro Flow, Cylinder, Rarefied Gas, Knudsen Number, Drag Coefficient

Flow past a stationary circular cylinder is a classical problem in fluid mechanics. Although the geometric configuration is relatively simple, the physics associated with the flow around the cylinder is rich [1]. As a consequence, the problem has been extensively studied experimentally and computationally [2-6]. In the continuum regime, the flow characteristics depend solely on the Reynolds number, Re. When $0 < Re \le 4$, the flow is attached to the cylinder and symmetric. As Re increases and exceeds ~4, the steady separation forms a pair of symmetric contra-rotating vortices behind the cylinder. The fluid in these vortices circulates continuously, not moving downstream. These eddies get bigger with increasing Re. For flow with $Re > 40$, the wake downstream of the cylinder becomes unsteady. In micro-electro-mechanical systems (MEMS), the Reynolds number is usually low and below this critical value. However, for gas flows in MEMS, non-equilibrium effects need to be considered as the gas molecules collide with solid walls more often than among themselves to reach to the equilibrium state.

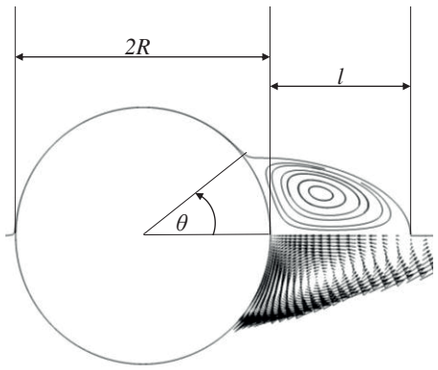

Figure 1. The computed twin vortices behind a stationary cylinder by the R26 moment equations, represented by streamlines and velocity vectors, for $Re = 20$ and $Kn = 0.05$.

The extent of the non-equilibrium or rarefaction is measured by the Knudsen number, Kn, the ratio of the molecular mean free path, λ, to the characteristic length of the geometry, i.e. the diameter of the cylinder, D, in the present study. When $Kn < 0.1$, i.e. in the slip regime, the Navier-Stokes-Fourier (NSF) equations coupled with appropriate velocity-slip and temperature-jump wall boundary conditions may predict certain main features of the flow. When the Knudsen number is greater than 0.1, in the *transition* regime, usually kinetic theory is required to study the flow details. The Boltzmann equation [7] and the direct simulation Monte Carlo (DSMC) [8] are the main kinetic methods used to simulate non-equilibrium gas flow. However, they are computationally expensive, particularly for flows at low speed in the early transition regime. Despite great efforts being made to overcome the numerical difficulties and computing costs, solutions using the Boltzmann equation or DSMC are still too difficult to be widely used in practical engineering applications. Alternative approaches are being developed that aim to alleviate the difficulties in kinetic theory but are accurate enough for engineering design.

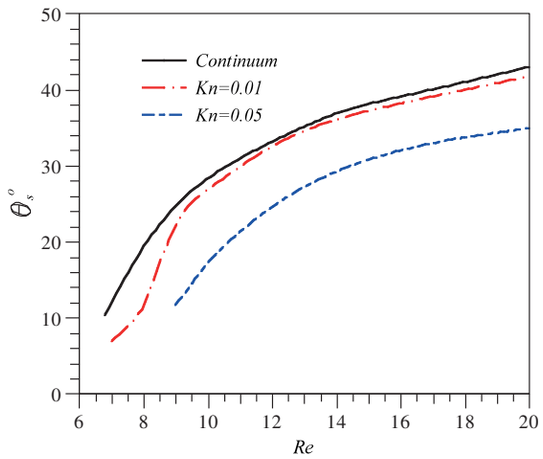

Figure 2. The separation angle, θ_s, predicted by the R26 moment equations for $Kn = 0.01$ and 0.05 in comparison with the continuum solution with the NSF equations.

Extending hydro-thermal-dynamics into the transition regime is one of the most promising approaches [9]. The method of moments, which was originally proposed by Grad [10] as an approximate solution procedure to the Boltzmann equation, is currently being developed to bridge the gap between the hydro-thermal-dynamics and kinetic theory. In this approach, the Boltzmann equation is satisfied in a certain average sense rather than at the molecular distribution function level. How far the hydro-thermal-dynamics should be extended, i.e. how many moments should be used, largely depend on the flow regime. It was found [11-13] that the regularized 13 moment equations (R13) are not adequate enough to capture the Knudsen layer in Kramers' problem and the regularized 26 moment equations (R26) are required to accurately reproduce the velocity defect found with kinetic data. However, both the R13 and R26 equation models can capture many non-equilibrium phenomena produced by kinetic theory, such as the tangential heat flux in planar Couette flow and the bimodal temperature profile in planar force-driven Poiseuille flow in the early transition regime with different accuracy [14-17].

Not many studies have been carried on the non-equilibrium effects on the flow past a stationary circular cylinder. The velocity slip on the wall and the Knudsen layer close to the wall alters the flow characteristics around the cylinder. In the present study, we investigate, with the method of moments, the effects of non-equilibrium on the onset of flow separation; the location of the separation point; the size of the attached eddies, and drag coefficients, for $Re < 20$.

Shown in Fig. 1 is the wake behind a stationary cylinder with a radius equal to R. The flow starts to separate from the cylinder wall at an angle of θ_s. and forms a wake of length, l. The predicted values of the separation angle for different values of Re and two Knudsen numbers, 0.01 and 0.05, in comparison with the continuum solution, are presented in Fig. 2. The flow separation first appears at a Reynolds number just below 7 for the continuum flow, which is consistent with the early numerical study by Dennis and Chang [6]. When the value of Re increases, the separation point moves upstream, so the separation angle is increased. For a gas with $Kn = 0.01$, the flow starts to separate at a similar Reynolds number as the continuum flow but with a smaller angle. As the Reynolds number increases, the value θ_s increases and approaches to the continuum. At $Kn = 0.05$, the separation Reynolds number increases to 9 and the separation angle is much smaller than in the continuum, as indicated in Fig. 2. When the Knudsen number is above 0.1 and the Reynolds number is under 20, no flow separation is predicted.

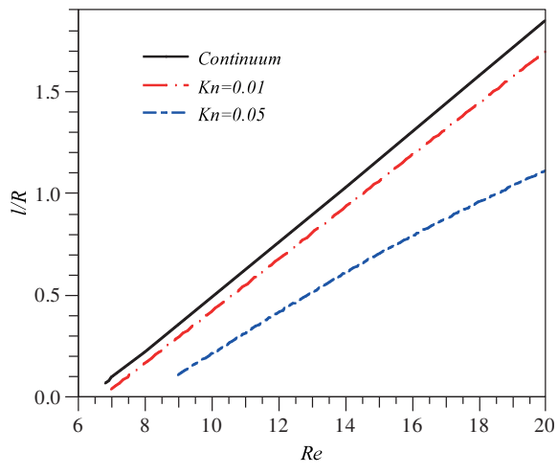

Figure 3. Normalized wake length at $Kn = 0.01$ and 0.05 in comparison with the continuum.

The rarefaction effect on the wake length is shown in Fig. 3. The wake length increases approximately linearly with the Reynolds number, but reduces significantly with an increase in Kn. At $Re = 20$ and $Kn = 0.05$, the wake length is only 60% of the continuum at the same Reynolds number.

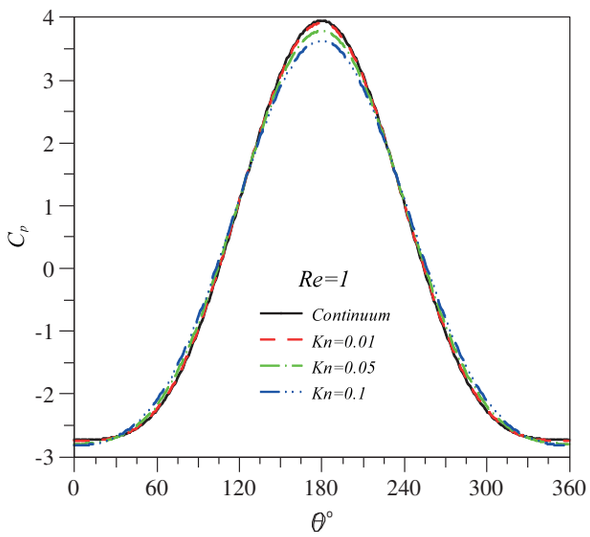

Figure 4. Pressure coefficient on the cylinder surface at $Re = 1$ and $Kn = 0.01$, 0.05 and 0.1 in comparison with the continuum.

Curves of the pressure coefficient, C_p, on the cylinder surface at $Re = 1$ and different values of Kn are given in Fig. 4. In comparison with the continuum, the pressure at the front and the rear of the cylinder drops as the Knudsen number increases while the pressure along the side of the cylinder increases. The resultant rarefaction effect on the flow past a cylinder is reflected in the change of the drag coefficient, C_D, in Fig. 5. As the value of Kn increases from 0 at the continuum to 0.1 at the early transition regime, the drag coefficient is reduced 7% for a flow with $Re = 1$.

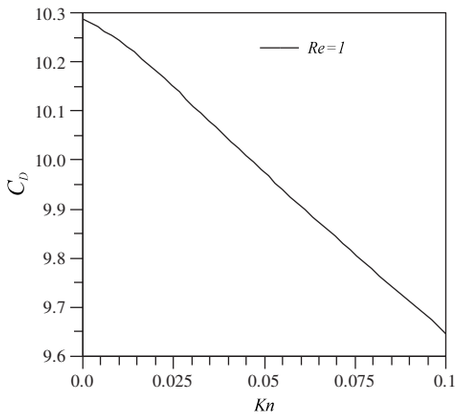

Figure 5. Drag coefficient against the Knudsen number at $Re = 1$.

Acknowledgements This work was supported by the Hartree Centre and the United Kingdom Engineering and Physical Sciences Research Council (EPSRC) under grants EP/N016602/1 and EP/K038427/1.

References

[1] Zdravkovich, M., Flow around Circular Cylinders, vol. 1, Oxford Science Publication, 1997.
[2] Tritton, D.J., J. Fluid Mech., 6:574, 1959.
[3] Son, J. S. and Hanratty T. J., J. Fluid Mech. 35:360, 1969.
[4] Fornberg, B., J. Fluid Mech. 98:819 , 1980.
[5] Sen, S., Mittal, S. and Biswas, G., J.Fluid Mech. 620:89, 2009.
[6] Dennis, S. C. R. and Chang G.-Z., J Fluid Mech 40:471, 1970.
[7] Cercignani, C., The Boltzmann Equation and Its Applications. Springer, New York, 1988.
[8] Bird, G., Molecular Gas Dynamics and the Direct Simulation of Gas Flows. Clarendon Press, Oxford, 1994.
[9] Struchtrup, H., 2005. Macroscopic Transport Equations for Rarefied Gas Flows. Springer, Berlin.
[10] Grad, H., Pure Appl. Math. 2:331, 1949.
[11] Young, J. B., Int. J. of Heat and Mass Transfer 54:2902, 2011.
[12] Gu, X. J., Emerson, D. R. and Tang, G., Phys. Rev. E 81, 016313, 2010.
[13] Gu, X. J. and Emerson, D. R., Phys. Rev. E 89, 063020, 2014.
[14] Gu, X. J. and Emerson, D. R., J. Fluids Mech. 636:117, 2009.
[15] Taheri, P. and Struchtrup, H., 2009. Phys. Rev. E 80, 066317, 2009.
[16] Taheri, P., Torrilhon, M. and Struchtrup, H., Phys. Fluids, 21, 017102, 2009.

Gold nanoparticle synthesis in gas-liquid-liquid flow in a microchannel

Nikolay Cherkasov[1], Evgeny V. Rebrov[1,2*]

* Corresponding author: Tel.: +44(0)2476 5 22202; Email: e.rebrov@warwick.ac.uk
[1] School of Engineering, University of Warwick, Coventry, CV4 7AL, UK
[2] Department of Biotechnology and Chemistry, Tver State Technical University, 22 Nab. A. Nikitina, Tver, 170026, Russia
Keywords: Microfluidics, Residence time distribution, Nanoparticle synthesis, Gas-Liquid-liquid

1 Introduction

Microreactors offer a number of advantages to address economic and environmental problems of large-scale production. In particular, small dimensions of microreactor channels provide very quick mixing via diffusion. High surface to volume ratio results in fast heat and mass transfer. These properties provide substantial decrease in the by-product formation in many reactions such as highly exothermic organic reactions or quick reduction of metal nanoparticles. Moreover, microreactors substantially increase process safety because only a minute amount of reactants is released in case of a reactor rupture.

Safety advantages are particularly important for gas-liquid reactions where high pressure gas provides a substantial hazard in conventional batch reactor systems. For such systems, Taylor flow consisting of alternating slugs of gas and liquid phases is particularly important because it provides efficient mixing and high gas-liquid contact area, orders of magnitude higher than in conventional reactors. An additional advantage of Taylor flow is full isolation of liquid slugs resulting in zero-dispersion residence time distribution (RTD). These conditions can be observed for a limited number of gas-liquid systems and many liquid-liquid systems. The main factor here is the formation of a thin liquid film at the channel walls between the slugs. In the latter case, liquid interexchange results in a broad RTD.

Applications of gas-liquid Taylor flow are, however, limited because the formation of solid phase during the reaction may result in particle sedimentation on the reactor walls. Once reactor walls contain nuclei of the forming solid phase, growth and nucleation processes are affected resulting in poor reproducibility. This type of photochemical reactions is even more sensitive because deposition of solid phase on the reactor walls decreases solution exposure and the product yield. To avoid these problems, it is advisable to introduce the third immiscible phase to prevent the formation of solid deposits on the reactor walls. The aim of the current work is to study hydrodynamics and RTD in a gas-water-oil flow in a circular microchannel. The data obtained were used in a photochemical synthesis of gold nanoparticles with the size control by changing O_2 content in the gas phase.

2 Experimental

The experimental study has been performed in a 0.50 mm id FEP tubing connected via an X-joint to a set of syringe pumps (Nemesis) with (i) deionised water, and/or a solution of 8 mg mL^{-1} methylene blue dye in water, (ii) silicone oil (viscosity: 350 cP), and (iii) to a gas line. The gases (N_2 and O_2) were fed with mass flow controllers. The flow patterns in the inlet and outlet sections of the reactor were observed with a microscope (Olympus) connected to a video camera. In the RTD experiments, the solution of methylene blue dye was introduced as a step (or pulse) function under various flow conditions and the concentration of dye in the flow was determined by the image analysis. The residence time distribution was determined by deconvolution of the outlet concentration profile. The synthesis of gold nanoparticles has been performed in the aqueous phase using a 1 mM solution of $AuCl_3$, 20 mM irgacure-2959 photoinitiator and a capping agent polyvinylpyrrolidone with the monomer concentration of 20 mM.

3 Results and Discussion

The flow regime map has been studied for a range of water, oil and gas flow rates of 1-200 L min^{-1}. Several flow regimes observed are presented in Fig. 1a. The most importantly, in a wide range of flow rates, gas-aqueous slugs were observed with a layer of oil at the channel walls. The RTD experiments confirmed that there is no interexchange of aqueous phase between the slugs because of the presence of a hydrophobic oil film on the channel walls.

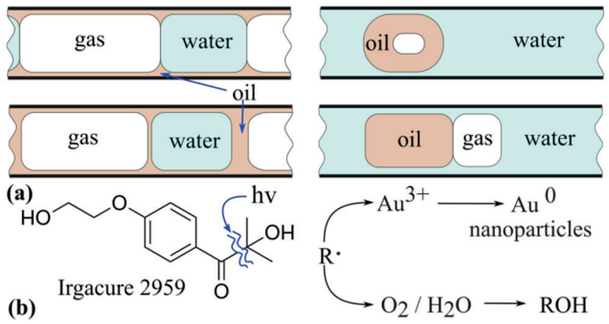

Fig. 1. (a) Flow regimes in the gas-water-oil three-phase flow, (b) scheme of photochemical gold nanoparticle synthesis with radical consumption competition between Au^{3+} and O_2.

The photochemical synthesis of gold nanoparticles has been performed in the presence of irgacure-2959 photoinitiator which generates radicals under UV light. The exact control of the oxygen concentration (by changing the O_2 and N_2 flow rates) in the gas phase allows to adjust the amount of the radicals needed to reduce the gold precursors and therefore to control the size of the obtained Au nanoparticles (Fig. 1b). The developed method provides a facile way for the synthesis of gold nanoparticles with controlled dimensions of 2-20 nm. The long-term stability studies showed that there was no gold deposition on the reactor walls for a period of 3 h, while without the oil phase substantial amounts of gold were deposited onto the channel walls within 15 min of operation.

Acknowledgements
The authors are grateful to the European Research Council (ERC) project 279867 and the Russian Science Foundation, 15-13-20015.

ID 112

5th Micro and Nano Flows Conference
Milan, Italy, 11-14 September 2016

Enhancement of Electroosmotic flow in a micro/nano-channel through patterned slip strips

Simanta De *, Somnath Bhattacharyya

* Corresponding author: Tel.: +91 3222 282275; Email: Simanta.de@gmail.com
Department of Mathematics, Indian Institute of Technology Kharagpur, Kharagpur 721302, India

Keywords: Electroosmotic Flow, Grooved Channel, Nano Channel, Poisson-Nernst-Planck Equations

The flow through micro/nano-channels is receiving increasing attention with the rapid development of micro- and nanotechnologies. Electroosmosis is found to be the most suitable mechanism to drive fluids in such cases. In recent years, several studies on enhancement of electroosmotic flow (EOF) in micro-channels have been made. Superhydrophobic surfaces are widely adopted for reducing the flow resistance in microfluidic channels.

We present a study on EOF in a channel whose walls are patterned with periodically arranged patches of hydrodynamic slippage. The no-slip portions of the wall are assumed to have a constant ζ-potential or charge density and an induced ζ-potential may develop along the slip strips. The hydrophobic surfaces are formed by considering wall-mounted grooved filled with dielectric uncharged liquid. Thus, the electric charge along the slippery surfaces can be mobile. We have also considered uncharged superhydrophobic strips. The induced surface charge along the hydrophobic walls is obtained by solving the electric field equation inside the groove along with suitable matching conditions at the liquid-liquid interface. The flow enhancement factor E_f, representing the average velocity through the hydrophobic channel scaled by the average velocity through a plane channel with uniform zeta potential, is determined for a wide range of intrinsic parameters values. While it has been shown that under the assumption of thin-Debye layer values of E_f close to 1 should be expected for EOF along a hydrophobic surface, a substantial flow enhancement is found when the Debye length is in the order of the channel height. This study may provide guidelines to design nano-channels in order to maximize the electroosmotic flow rate.

Mathematical Model

We consider electroosmotic flow of an incompressible Newtonian fluid through a long grooved channel of height H. The grooves are arranged in a periodic manner of periodicity L. All grooves are filled with nonelectrolyte fluid. The shift between the periodic patterns of the grooves at the upper and lower wall is denoting by δ. A uniform electric field E_0 is imposed parallel to the x-axis. The grooves wall is considered to be uncharged and the channel wall carries an electrostatic surface charge density.

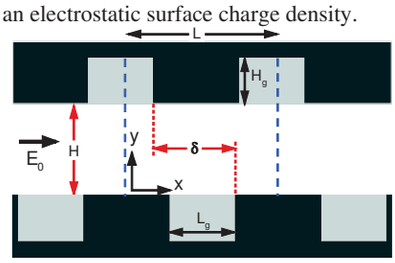

Fig 1: Schematic of the model geometry. The computational domain is in-between the blue dashed lines.

The non-dimensional sets of equations to describe the electroosmotic flow inside the channel are

$$Re(\boldsymbol{u}\cdot\nabla)\boldsymbol{u}+\nabla p-\nabla^2\boldsymbol{u}+\frac{(\kappa H)^2}{\Lambda}\rho_e\nabla\phi=0$$
$$\nabla\cdot\boldsymbol{u}=0,\qquad \nabla^2\phi=-(\kappa H)^2\rho_e$$
$$Pe_j\left(\boldsymbol{u}\cdot\nabla n_j\right)-\nabla^2 n_j-z_j\left(\nabla n_j\cdot\nabla\phi\right)+(\kappa H)^2 z_j n_j\rho_e=0$$

The non-dimensional sets of equations to describe the fluid flow inside the grooves are

$$\rho_r Re(\tilde{\boldsymbol{u}}\cdot\nabla)\tilde{\boldsymbol{u}}+\nabla\tilde{p}-\mu_r\nabla^2\tilde{\boldsymbol{u}}=0$$
$$\nabla\cdot\tilde{\boldsymbol{u}}=0,\qquad \nabla^2\tilde{\phi}=0$$

The non-dimensional parameters governing the electroosmosis are the Reynolds number $Re=\rho U_{HS}H/\mu$, the Peclet number $Pe_j=U_{HS}H/D_j$, the Debye-Huckel parameter κH, the scaled electric field $\Lambda=E_0H/\phi_0$, $\rho_r=\tilde{\rho}/\rho$ and $\mu_r=\tilde{\mu}/\mu$. Here ρ and μ are the density and the viscosity of the medium, respectively. Here $\sim$ denotes the quantities inside the grooves.

A periodic boundary condition is imposed at the inlet and outlet of the domain of interest and a non-slip boundary condition is imposed along the groove walls.

On the channel wall: $\boldsymbol{u}=0$, $\left(\nabla n_j+z_j n_j\nabla\phi\right)\cdot\boldsymbol{n}=0$, $\frac{\partial\phi}{\partial\boldsymbol{n}}=-(\kappa H)\sigma$

At the liquid-liquid interfaces: $\boldsymbol{u}\cdot\boldsymbol{n}=\tilde{\boldsymbol{u}}\cdot\boldsymbol{n}=0$, $\boldsymbol{u}\cdot\boldsymbol{t}=\tilde{\boldsymbol{u}}\cdot\boldsymbol{t}$, $\frac{\partial\boldsymbol{u}}{\partial\boldsymbol{n}}+\frac{1}{\Lambda}\frac{\partial\phi}{\partial\boldsymbol{t}}\frac{\partial\phi}{\partial\boldsymbol{n}}=\mu_r\frac{\partial\tilde{\boldsymbol{u}}}{\partial\boldsymbol{n}}$, $\phi=\tilde{\phi}$, $\frac{\partial\phi}{\partial\boldsymbol{n}}=\varepsilon_r\frac{\partial\tilde{\phi}}{\partial\boldsymbol{n}}$, $\left(\nabla n_j+z_j n_j\nabla\phi\right)\cdot\boldsymbol{n}=0$,

here $\boldsymbol{n}$ and $\boldsymbol{t}$ are the unit normal and tangential vector to the wall or interface.

The governing equations are solved numerically through a control volume approach over a staggered grid arrangement. The discretized equations are solved through the pressure-correction based iterative SIMPLE (Semi-Implicit Method for pressure-Linked Equations) algorithm.

Results and Discussion

A parametric study is conducted to analyze how E_f depends on the Debye layer thickness, the channel width, the spatial period of the surface patterns, the relative shift between the patterns at the top and bottom wall, and the relative extension of the no-slip and the slip patches. An induced charge density at the gas-liquid interface develops which depends on the permittivity ratio, Debye length and applied electric field.

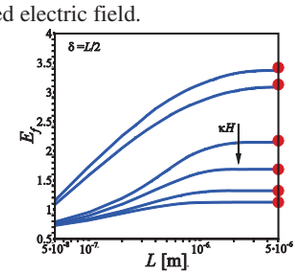

Fig 2: Flow enhancement factor as a function of L, with κH =0.5, 1, 2, 3, 5, 10 and σ =3.6× 10^{-4} C/m^2.

5th Micro and Nano Flows Conference
Milan, Italy, 11-14 September 2016

ID 113

Electroosmotic flow through an α-hemolysin nanopore

Emma Letizia BONOME [1], Fabio CECCONI [2], Mauro CHINAPPI [3,*]

* Corresponding author: Email: mauro.chinappi@iit.it
1 Dipartimento di Ingegneria Meccanica e Aerospaziale, Sapienza, Università di Roma, Italia
2 Istituto dei Sistemi Complessi UoS Sapienza, CNR, Roma, Italia
3 Center for Life Nano Science@Sapienza, Istituto Italiano di Tecnoloria, Roma, Italia

Keywords: Nanopores, Electrohydrodynamics, Electroosmosis, Molecular Dynamics Simulations

---

The determination of structures and sequences of macromolecules is a key element in modern biology and medicine. High-throughput DNA (and RNA) sequencing and mass spectrometry are currently producing a huge quantity of data paving the way to innovative approaches with potential applications ranging from personalized therapies to evolutionary biology.
A relevant innovation in the biomolecule sensing is the employment of nanopore based devices for the analysis of macromolecules at a single molecule level [1-2]. In a nanopore sensor the interaction between the macromolecule and the pore alters the ionic current flowing through a single pore that separates two chambers containing an electrolyte solution. The typical signal in a nanopore based devices is a multilevel current trace where the baseline level corresponds to no macromolecule inside the pore and each of the other levels corresponds to a specific interaction between the pore and the macromolecule, such as the presence of a specific monomer inside the pore. Although the method is quite simple, only recently, important developments in nanotechnology allowed the rescaling of the principle down to the nanoscale enabling, for instance, the development of a nanopore based DNA sequencer [1].

In this framework, a fundamental nanofluidic issue is the characterization of the open pore current level (i.e. the baseline signal when no molecules occupies the pore). Although the electrolyte solution is globally neutral, the nanopore typically presents a surface charge that alters the ion distribution in the neighborhood of the pore. In addition, positive and negative ions have different hydration shells the behavior of which is strongly altered by the nanoconfinement. All these circumstances result in a complex electro-hydrodynamical problem. In general, the unbalance between positive and negative ions distribution and the difference in ionic mobilities under confinement, give raise to an electroosmotic flow [3] that is supposed to have a strong impact on the dynamics of the macromolecule capture by the pore and to its eventual translocation [3-4]. In addition, the electrical system response in not Ohmic [3,6].

In this contribution, we characterize the water and the ion flows through a nanopore. In particular, we studied the α-hemolysin [5] pore (the widely employed biological nanopores for sensing devices) via molecular dynamics simulations where all the components of the system are modelled at atomic level. We explored the electro-hydrodynamical response of the system for different ionic concentrations and applied potentials. Our simulations provide a first extensive set of data at atomic scale that clarify the role of electroosmotic flow in α-hemolysin based nanopore sensing devices.

Acknowledgments: This research used the computational resource of the PRACE project 2014112673 (TGCC Curie, France).

References

[1] Mikheyev, Alexander S., and Mandy MY Tin. "A first look at the Oxford Nanopore MinION sequencer." Molecular ecology resources 14.6 (2014): 1097-1102.
[2] Cressiot, Benjamin, et al. "Focus on protein unfolding through nanopores." BioNanoScience 4.2 (2014): 111-118.
[3] Piguet, Fabien, et al. "Electroosmosis through α-Hemolysin That Depends on Alkali Cation Type." The Journal of Physical Chemistry Letters 5.24 (2014): 4362-4367.
[4] Mereuta, Loredana, et al. "Slowing down single-molecule trafficking through a protein nanopore reveals intermediates for peptide translocation." Scientific reports 4 (2014).
[5] Song, Langzhou, et al. "Structure of staphylococcal α-hemolysin, a heptameric transmembrane pore." Science 274.5294 (1996): 1859-1865. 8/10
[6] Bhattacharya, Swati, et al. "Rectification of the current in α-Hemolysin pore depends on the cation type: the alkali series probed by molecular dynamics simulations and experiments." The Journal of Physical Chemistry C 115.10 (2011): 4255-4264.

ID 114

5th Micro and Nano Flows Conference
Milan, Italy, 11-14 September 2016

Electrochemical Modelling and Simulation of Lithium-ion Battery Cooling

Angelo GRECO, Xi JIANG *

* Corresponding author: Tel.: ++44 (0)1524 592439; Fax: ++44 (0)1524 381707; Email: x.jiang@lancaster.ac.uk
[2] Department of Engineering, Lancaster University, UK

Keywords: Battery, Cooling, Electrochemistry, Modelling

Batteries are important storage devices for electrical energy with numerous applications. For instance, electrical and hybrid electrical vehicles are alternatives in the global effort of reducing the carbon dioxide emissions from the transport sector. Batteries are normally used as the power source for these vehicles, and the high power requirement has made the lithium-ion (Li-ion) battery the best candidate. However, the performance of Li-ion battery is limited by temperature during the discharge/charge processes, despite its high capacity and energy density. Temperature affects the reliability, safety, and efficiency of the battery. Besides, the temperature uniformity is important in order to avoid thermal runaway and hotspots, leading to short circuit in the battery module.

An efficient battery thermal management system (BTMS) is required in order to maintain the battery temperature between 20ºC and 40ºC, which is the required temperature range for the operation of Li-ion batteries. Moreover, to avoid any short circuit leading potentially to destroy the battery, an even temperature distribution must be achieved in the battery module and pack. For achieving a uniform temperature distribution, the temperature difference from cell to cell and module to module should be normally within 5ºC. The development of BTMS for Li-ion batteries is a challenging task, involving a number of coupled processes.

The thermal behaviour of the battery is strongly coupled to the electrochemical process, which can be investigated by high-fidelity numerical modelling and simulation. Numerical simulation of the thermal behaviour of Li-ion battery cell during discharge/charge has to account for the coupling between heat and mass transfer of particles at a micro scale level with the description of the battery cell temperature at the macro level. In the meantime, simplifications such as reduced dimensionality are always needed and advantageous for the modelling of BTMS for engineering applications.

In this study, an electrochemistry model (average model) is coupled to a thermal model, in order to calculate the heat generation of the battery cell from low to relatively high discharge rates. This model takes into account the heat and mass transfer of the Li-ion particles in the solid and solution phases through the different electrodes.

The heat and mass transfer at the micro scale level, in the solution and solid phase are solved with the addition of a one-dimensional (1D) model using the nodal network method [1]. These models are validated against analytical solution which can reduce the computational time of the electrochemistry model while allowing for non-linear and temperature dependent diffusion coefficients.

Advanced passive cooling technologies such as phase change material (PCM) enhanced by a graphite matrix structure has been shown to be effective in battery cooling [2]. As a novel cooling method, PCM/compressed expanded natural graphite (CENG) composite presents favourable mechanical properties and chemical inertness. Besides, various shapes can be easily molded from expanded graphite powders. The compression process during the manufacture of the graphite matrix can also lead to directional conductivities for effective heat transfer. Li-ion battery cooling using a PCM/CENG composite is investigated in this study, for a cylindrical battery cell. The impact of this cooling method on the heat generation based on electrochemistry is also studied with different PCM/CENG design parameters and geometries.

The analysis of the temperature distributions of three-dimensional battery models has shown that a two-dimensional (2D) model and one-dimensional model are sufficient to describe the transient temperature rise for a battery module and battery cell, respectively. In consequence, a 2D cell-centred finite volume code for unstructured meshes and a 1D computational model are developed with additions of the electrochemistry and the phase change. Furthermore, comparisons between the predictions from different analytical and computational tools and open-source packages were carried out, and close agreements have been observed.

References

[1] Greco, A., Cao, D., Jiang, X. and Yang, H., A theoretical and computational study of lithium-ion battery thermal management for electric vehicles using heat pipes. *Journal of Power Sources* 257: 344-355 (2014).

[2] Greco, A., Jiang, X. and Cao, D., An investigation of lithium-ion battery thermal management using paraffin/porous-graphite matrix composite. *Journal of Power Sources* 278: 50–68 (2015).

5th Micro and Nano Flows Conference
Milan, Italy, 11-14 September 2016

Integrated temperature control system for microfluidic culture of nematodes

Maria Cristina LETIZIA [1,*], Matteo CORNAGLIA [1], Martin GIJS [1]

* Corresponding author: Tel.: +41216937766; Email: mariacristina.letizia@epfl.ch
1: Laboratory of Microsystems, Ecole Polytechnique Fédérale de Lausanne, Switzerland

Keywords: Temperature controller, Heat transfer, Microfluidics, Lab-on-chip, *C. elegans*, Heat-shock response

We describe the development of a temperature control system integrated in a microfluidic platform dedicated to on-chip culture of the nematode *C. elegans*. The system allows to setting precise temperature conditions for *C. elegans* development and maintenance.

Traditionally, *C. elegans* is cultured on Nematode Growth Medium (NGM) plates, which are kept in thermal incubators at a temperature between 16 °C and 25 °C [1]. Interestingly, it was shown that *C. elegans* grows 2.1 times faster at 25 °C than at 16 °C, and 1.3 times faster at 20 °C than at 16 °C, suggesting that *C. elegans* development time and lifespan are strongly dependent on environmental conditions [1]. In addition, temperature control is crucial when studying *C. elegans* stress response. Specifically, the *C. elegans* heat-shock pathway is used as a model for complex disease pathways in humans [2]. In this type of experiments, NGM plates are heated up in an oven at 35 °C for 2 h, after which the plates are returned to the basal temperature (16 °C - 25 °C). Therefore temperature setting evidently has to be well controlled for performing reproducible experiments.

Recently, *C. elegans* research has been particularly impacted by microfluidics and many platforms for easy worm handling and manipulation have been proposed in replacement of otherwise manual, laborious and time-consuming protocols [3]. However, a fully-integrated microfluidic setup provided with a temperature controller is still missing, making experiments less reproducible, as susceptible to room temperature variations over time. Moreover, heat-shock experiments cannot be performed, unless moving the microfluidic chip in a dedicated oven when needed [2], which is not ideal and requires again human intervention.

Our solution consists in a temperature control system that is fully integrated in a microfluidic platform (see Figure 1a). A thermoelectric (Peltier) module is used to set the temperature. The polydimethylsiloxane (PDMS) - glass microfluidic chip and the aluminum thermalization frame are both in contact with the Peltier module. A thermally insulating frame prevents thermal dissipation and holds the microfluidic chip on the microscope stage. The full stack is provided with a central aperture, in order to allow light transmission through the microfluidic chip and enable transmission microscopy imaging. A temperature sensor is placed in contact with the glass slide of the microfluidic chip and measures the temperature experienced by the worms in the microfluidic channels. Such signal is given as input to a proportional integrative derivative (PID) controller, which controls the electrical power supplied to the Peltier module in a closed-loop configuration.

We tested the performance of the setup, by first characterizing its response to different constant cooling electrical powers. Starting from an ambient temperature (T_{ext}), the system is cooled down to a specific equilibrium temperature (T_{eq}), set by the equilibrium between thermoelectric cooling and heat convection in the surrounding air. As Figure 1b shows, starting from T_{ext} of 24 °C, the chip can reach a T_{eq} up to 10 °C, showing a clear dependence of T_{eq} on the electrical power. The dynamics of heat exchange was studied by normalizing such curves with respect to T_{ext} and T_{eq}, and was confirmed by a time-dependent simulation via the Finite Element Method (FEM). The measured temperature decreases exponentially and reaches T_{eq} in ~10 min. Because of the geometry of the system, the spatial temperature distribution is not constant throughout the chip area, as observed via measurements at different points of the glass surface and confirmed by FEM simulations (Figure 1c). However, for worm culture experiments in the 16 °C - 25 °C range, this difference is minor and perfectly acceptable.

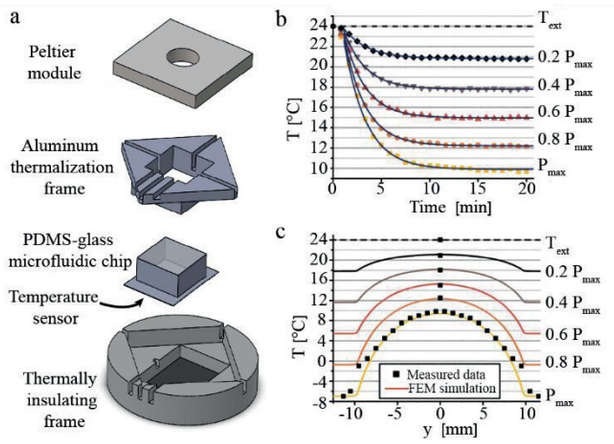

Figure 1. (a) *Schematic representation of the main components of the temperature control system.* (b) *Experimental characterization of the device performance when cooling from a T_{ext} of 24 °C with different heating powers defined as function of the maximum electrical power P_{max} used.* (c) *Spatial temperature distribution across the chip area, both experimentally measured and simulated via FEM.*

Thanks to our control system, the temperature experienced by worms in the microfluidic chamber can be precisely set. *C. elegans* lifespan experiments at a determined temperature are now in progress, as well as heat-shock stimulation experiments, enabled by controlling both the strength and the duration of the heat stimulus.

[1] Stiernagle, T. (2006). Maintenance of *C. elegans*. WormBook : The Online Review of *C. elegans* Biology, 1–11
[2] Rodriguez, M. et al. (2013). Worms under stress : *C. elegans* stress response and its relevance to complex human disease and aging. Trends in Genetics, 29(6), 367–374.
[3] Sivagnanam, V. and Gijs, M.A.M. (2013). Exploring living multicellular organisms, organs, and tissues using microfluidic systems. Chem. Rev. 113, 3214−3247.

5th Micro and Nano Flows Conference
Milan, Italy, 11-14 September 2016

ID 118

Space-time chromatography of mesoscopic suspended objects in periodically patterned microfluidic devices

Stefano CERBELLI[1,*] and Massimiliano GIONA[1]

* Corresponding author: Tel.: ++39(0)644585339; Email: stefano.cerbelli@uniroma1.it
1 Dipartimento di Ingegneria Chimica Materiali Ambiente, Sapienza Università di Roma, IT

Keywords: Size-based Separation, Mobility, Dispersion, Periodic Media, Microfluidics

---

An intense research activity, both experimental and theoretical/numerical, has been put forward in the last decade to characterize transport of mesoscopic suspended objects entrained in a laminar microflow and subject to a spatially periodic pattern of forces. Such forces can arise from a variety of sources such as solid impermeable obstacles, focused laser beams, electrostatic potentials. In most applications (e.g.~Deterministic Lateral Displacement [1], optical tweezers [2], Brownian ratchets [3]), the interaction with the large-scale drive and the periodic landscape of forces is exploited for the size-based separation of multidisperse populations of particles, as particles of different characteristic dimension experience different force field while flowing through the periodic pattern. The possibility of predicting the flow structure to any desired degree of accuracy, ultimately afforded by the prevailing laminar character of the flow in microfluidic equipment, makes these types of separation devices competitive with well established separation techniques such as SEC chromatography or gel electrophoresis. This is because the resolution of SEC or gel electrophoretic columns is unavoidably hindered by the unchecked dispersion ensuing from the synergistic interaction of mean field convection, Brownian diffusion, and the disordered structure of the medium hosting particle transport. Notwithstanding the great potential allowed by the ordered geometry of microfluidic periodically-patterned separation equipment, much is yet to understand as regards the interplay between the deterministic and stochastic components of particle motion, both in terms of mean displacement of the particle swarm, and of the fluctuation-driven dispersion of particles about the center of mass of the swarm. In general terms, it is becoming more and more clear that the large-scale outcome of the small scale interaction between particle convection and thermal fluctuations is equivalent to an effective advection-diffusion process

$$\partial C/\partial t = -U_e \cdot \nabla C + D_e \cdot \nabla^2 C \qquad (1)$$

where C is a locally averaged particle number density, U_e is an constant effective vector velocity, and $D_e = \left(\left(d_{ij} \right) \right)$ is a spatially homogeneous second-order effective dispersion tensor. Both the effective velocity and the effective dispersion depend markedly and non-trivially on the geometry of the force lattice, on the structure and intensity of the entraining laminar flow, and on the bare particle diffusivity. Most of the research effort has been focused on understanding how the average particle velocity is affected by the particle size for a fixed device geometry and assigned overall flowrate of the entraining fluid. In turn, the knowledge gained from a wealth of studies ensuing from this research line has been exploited to design tailored devices which can perform high-resolution separation of target particle size from a mixture of suspended particles of different characteristic dimension [4]. In most implementations of the process, steady-state conditions are typically enforced, where a mixture particles of different features (e.g. size, electric charge) released in a focused stream at the inlet of the device migrate at different angles with respect to the average flow stream. Thus, from the standpoint of the effective transport template expressed by Eq. (1), these steady-state operating devices are based on the dependence of *the direction* of U_e on particle features. In this work, we explore the possibility of performing a combined space-time chromatography, operated under unsteady transport conditions, *where both the direction and the magnitude (mobility) of the average velocity contribute to particle separation*. A thorough analysis of the dispersion process and its dependence on particle features is also carried out. We show that the combination of this two pieces of information, one about the mean motion, the other about particle dispersion can improve the use of the separation equipment for analytical purposes, i.e. when the characterization of the size distribution of an unknown mixture of particles is being dealt with. Specifically, we show the existence of conditions where the occurrence of enhanced dispersion regimes is anti-correlated with particle mobility. In this case, the use of transient space-time chromatography allows to single out ranges of particle size that would not be possible to identify while performing a conventional continuous steady state separation.

References

[1] Huang L., Cox E., Austin R., Sturm J. (2004) Continuous particle separation through deterministic lateral displacement. *Science* **304**:987–990.

[2] Jonas A., Zemanek P. (2008) Light at work: the use of optical forces for particle maipulation, sorting, and analysis. *Electrophoresis* **29**:4813–4851

[3] Hanggi P., Marchesoni F. (2009) Artificial Brownian motors: controlling transport on the nanoscale. *Rev Mod Phys* **81**:387–442

[4] Cerbelli S., Garofalo F., Giona M. (2015) Effective dispersion and separation resolution in continuous particle fractionation, *Microfluidics and Nanofluidics*, **19**:1035-1046

5th Micro and Nano Flows Conference
Milan, Italy, 11-14 September 2016

Two-phase flow in T – junction microchannels

Davide Caprini[1], Giorgia Sinibaldi[1,*], Mauro Chinappi[2], Luca Marino[1], Carlo M. Casciola[1]

* Corresponding author: Tel.: ++39 06-44585735; Email: sinibaldi.giorgia@gmail.com
1 Mechanical and Aerospace Department, University of Rome La Sapienza",Italy
2 Italian Institute of Technology, Center for Life Nano Science, Italy

Keywords: Micro Flow, Two-Phase flows, Bubble generation, Pumps, Energy

Two-phase flows in microdevices received a noticeable attention in the last decade. Bubbles occur in several technological applications, such as polymer de-volatilization process, two-phase micromixing, biochemical reactions and heat exchange. Moreover, it is well known that the study on the effect of surface wettability on the gas-liquid two phase flow characteristics in micro-channels with hydraulic diameters smaller than 1mm is required.

We present an experimental and numerical analysis of bubbles generation and fluid transport in T- junction microfluidic systems. Possible links to commercial lab-on-chip and rapid prototyping technology multilayer lab-on-chip are evaluated.

The liquid phase is controlled by a syringe pump (PHD Ultra-Harvard). In the inlet forcing gas phase a pressure pump (Mitos P-pump, dolomite microfluidics) is used to control pressure accurately. Moreover a flow meter (Mitos Flowrate sensor) is adopted to control the gas phase flow rate.

Images are recorded with a Photron FastCam mini UX100 connected to an inverted microscope (Zeiss Observer Z1). The liquid flow rates and gas pressures are investigated to explore different regimes of bubbles production. A particular attention was paid to the unstable flow regimes, where the bubbles flow does not present a stationary behaviour. In addition different flow regimes have been investigated to evaluated the effects of the characteristic parameters which drives the phenomenon.

The first results benchmark the Capillary number *Ca* effect on shape and size of the produced bubbles and the *Ca* threashould value to obtain stable and stationary bubbles flow was evaluated and compared with published results. A comparison of the main quantities obtained in our experiments against experimental data [1,2] is provided.

As an example of the carried out analysis, we report a set of photographs showing the bubble generation.

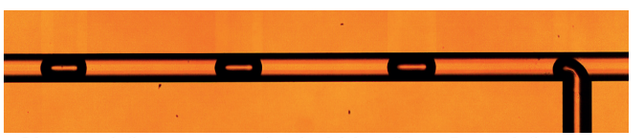

Observed flow pattern for bubbles flow. Liquid flow rate Q_l= 20 μL/min, pressure of gas set at 900 mbar

Observed flow pattern for bubbles flow. Liquid flow rate Q_l= 3 μL/min, pressure of gas set at 335 mbar

Observed flow pattern for bubbles flow. Liquid flow rate Q_l= 20 μL/min, pressure of gas set at 1000 mbar

Detail of the bubble formation at two different time steps. Liquid flow rate Q_l= 20 μL/min, pressure of gas set at 1000 mbar

References

[1] P. Garstecki et al., *Formation of droplets and bubbles in a microfluidic T-junction-scaling and mechanism of break-up,* Lab Chip, 2006, **6,** 437-446.

[2] T. Cuabaud et al., *Bubble dispenser in microfluidic devices,* Phys. Rev E, 2005, **72,** 037302.

Support from grant ERC-2013-ADG 339446 is gratefully acknowledged

Dynamic Modelling of Microfluidic Networks using Wave Digital Filters

Alberto BERNARDINI [1,*], Elena BIANCHI [2], Monica PIERGIOVANNI [2], Augusto SARTI [1], Gabriele DUBINI [2]

* Corresponding author: Tel.: 3484982848 Email: alberto.bernardini@polimi.it
1 Dipartimento di Elettronica, Informazione e Bioingegneria, Politecnico di Milano, Italy
2 Laboratory of Biological Structures Mechanics - CMIC, Politecnico di Milano, Italy

Keywords: Microcirculation, Lab-On-a-Chip, Wave Digital Filters, Dynamic Hydraulic Resistance

Lab-On-a-Chip (LOC) devices and Micro Total Analysis Systems characterized by Microfluidic Networks (MNs) are of great interest in many biological, chemical or pharmaceutical applications [1]. The design of intricate MNs is a very hard task, as an accurate modelling of local flows requires the use of Computational Fluid Dynamics (CFD) analyses. In these cases CFD-based simulation tools turn out to be quite complex and time-demanding. However, the behavior of hydraulic circuits with laminar flows may be suitably described using electric networks, according to the Hagen-Poiseuille's law [2]. The electrical analogy maps the volumetric flow rate into a current, the pressure into a voltage and the hydraulic resistance into an electric resistance. In the literature on microfluidics and LOC the use of offline circuit simulation tools such as SPICE is quite widespread [3], as it simplifies the simulation of complex multi-component networks. It is worth noticing, however, that SPICE-like tools do not allow real time interaction with the virtual model. This means that the virtual model parameters of the MN are difficult to be adjusted during the simulation according to the actual variations of the physical variables (e.g. flow rate, hydraulic resistance). For these purposes we would need interactive models which "follow" the dynamics of the physical system.

In this work we do a first step toward a possible solution to these issues. We introduce a method based on Wave Digital Filters (WDFs) [4] for modelling, analyzing and controlling MNs in an interactive fashion. WDFs allow modelling electric circuits through lumped structures. Using classical Kirchhoff port variables (voltage and current), electric networks turn out to be described by systems of implicit equations. WDFs, on the other hand, employ *wave* port variables (incident wave and reflected wave), which can be obtained from Kirchhoff variables using a simple linear transformation. Making use of such *wave* port variables, it is possible to derive explicit models of analog circuits, characterized by circuit elements represented by blocks, which are connected to each other through input-output relations. WDFs exhibit high stability and excellent energetic properties; the balance of energy is constant over time, just as it happens in physical phenomena, and the matrices that implement topological connections are inherently energy-transparent. Thanks to their virtues WDFs are ideal for implementing physical models with low computational cost and they allow the user to change the model parameters interacting with the system in real time. For these reasons they have been extensively used for emulating analog circuits in Virtual Analog applications [5] or for modelling mechanical and acoustical systems through electric equivalents in sound synthesis applications [6]. We propose employing WDFs also for modelling MNs, when describing the hydraulic circuit through electric equivalents is possible. Not only WDFs ensure all the advantages of SPICE-like tools in the design phase, but they allow considering the virtual model of the MN as part of the final system enforcing the control over the MN and increasing the ability of the LOC device. In fact, using a layer of sensors and actuators between the MN and the virtual model, it is possible both to constantly update the model parameters and impose changes to the physical variables according to the feedbacks from the MN to the virtual model itself.

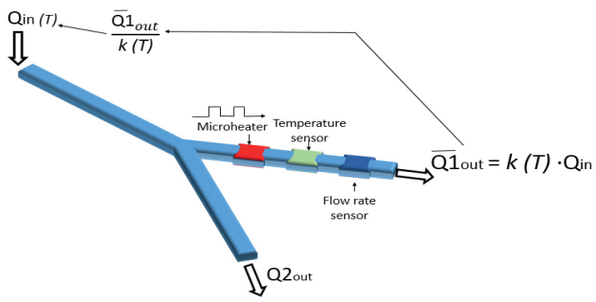

Fig.1 Simulated MNt: Q_{in} is the inlet flow rate, Q_{1out} and Q_{2out} are the outlet flow rates. The splitting of the flow between out channels 1 and 2 varies according to $Q_{1out} = k(T)\ Q_{in}$, where $k()$ is a function of temperature T, which is affected by the microheater. The system is set to balance Q_{in} in order to reach the target value of Q_{1out}.

In this paper we propose a proof of concept of the application of this method to a MN. We consider the very simple MN depicted in Fig. 1; a main channel connected to other two parallel channels of the same length and alimented by a syringe pump. We place a microheater and a temperature sensor in one of the two parallel channels of the MN. Through the microheater, we can vary the local temperature and change the viscosity of the fluid, which consequently affects the hydraulic resistance within the channel. Through the sensor we can update the equivalent electric resistance of the virtual model, thus effectively closing the control loop. This way we derive a simple system for controlling the flow rate at the inlet of the system and reaching a target flow rate in the actuated channel. In order to validate our system, we accurately simulate the described system using CFD-based software and we compare the resulting data to the outputs of a virtual model based on WDFs.

References

[1] J. West, M. Becker, S. Tombrink and A. Manz, "Micro total analysis systems: latest achievements", Anal. Chem., 2008, 80, 4403–4419.
[2] K. W. Oh, K. Lee, B. Ahn, and E. P. Furlani, "Design of pressure-driven microfluidic networks using electric circuit analogy", Lab Chip, 2012, 12, 515–545.
[3] S.Yang, A. Undar and J. D. Zahn, "A microfluidic device for continuous, real time blood plasma separation", Lab Chip, 2006, 6, 871–880.
[4] A. Fettweis, "Wave digital filters: Theory and practice," Proc. IEEE ,vol. 74, no. 2, pp. 270–327, Feb. 1986.
[5] G. De Sanctis and A. Sarti, "Virtual analog modeling in the wave-digital domain," IEEE Trans. Audio, Speech, Lang. Process., vol. 18, no. 4, pp. 715–727, May 2010.
[6] V. Välimäki, J. Pakarinen, C Erkut, and M. Karjalainen, "Discrete time modeling of music instruments," Rep. Prog. Phys., vol. 69, pp. 1–78, Jan. 2006.

5th Micro and Nano Flows Conference
Milan,Italy, 11-14 September 2016

Micro-chip for Single Cell Isolation with Laser-induced Forward Transfer

Yu Deng [1,*], Zhongning Guo [1],Wensheng Hong[1], Wenhao Mai[1], Ruiling Zhang[1]

* Corresponding author: Tel.: ++86 (0)2039322412; Fax: ++86 (0)2039322413; Email: yu.deng@mail2.gdut.edu.cn
1 School of Electromechanical Engineering, Guangdong University of Technology, UK

Keywords: Single cell isolation, Microchip, Heat, laser induced forward transfer

A target cell with viability is crucial for single cell research. The isolated cell can be used for homogenous culture as well as for gene and protein express analyses. Recently, Florescence-activated cell sorting (FACS)[1]and Magnetic-activated cell sorting (MACS)[2] are the most employed method for cell separation. However, both of them are limited for necessary of samples with small amount of cells. Meanwhile, micro fluidics is prototyped for isolating individual cell with hydrodynamic flow based on the properties of cell, like size[3,4], stiffness[5] and adhesion[6]. However, none of the mention method is capable to obtain a valid single cell. From our previous study[7], we have separated an individual cell of interest with laser induced forward transfer and it shows the necessary to keep the cell in a well control environment with the purpose of cell viability. In this report, a micro-chip with micro resistance heating is presented to keep the cell in the condition of 37 celsium degree and 100% humiditye during the isolation procedure. With this chip, the survival ratio of separated cell goes up to 96% from 70%. It optimized the laser induced forward transfer process and offers promising possibility to separate an interesting cell.

References

[1] Pasut, Alessandra, Paul Oleynik, and Michael A. Rudnicki. "Isolation of muscle stem cells by fluorescence activated cell sorting cytometry." Myogenesis. Humana Press, 2012. 53-64.

[2] Bucar, Sara, et al. "DNA fragmentation in human sperm after magnetic-activated cell sorting." Journal of assisted reproduction and genetics 32.1 (2015): 147-154.

[3] Song, Seungjeong, et al. "A continuous-flow microfluidic syringe filter for size-based cell sorting." Lab on a Chip 15.5 (2015): 1250-1254.

[4] Kralj, Jason G., et al. "Continuous dielectrophoretic size-based particle sorting." Analytical chemistry 78.14 (2006): 5019-5025.

[5] Hirose, Yuki, et al. "A new stiffness evaluation toward high speed cell sorter." Robotics and Automation (ICRA), 2010 IEEE International Conference on. IEEE, 2010.

[6] Guillaume-Gentil, Orane, Tomaso Zambelli, and Julia A. Vorholt. "Isolation of single mammalian cells from adherent cultures by fluidic force microscopy." Lab on a Chip 14.2 (2014): 402-414.

[7] Yu Deng. "Research on process and mechanism of laser induced single cell transfer." Guangdong University of Technology (2015)

ID 125

Evaporation and Boiling in Narrow Gap

Mitsuhiro MATSUMOTO [1,*], Keita OGAWA [1], Yuichi YASUMOTO [1]

* Corresponding author: Tel.: +81-75-383-3655; Email: matsumoto@kues.kyoto-u.ac.jp
1 Department of Mechanical Engineering and Science, Kyoto University, Japan

Abstract In order to investigate a cleansing process of oil-immersed laminated metal plates with solvent vapor, we have done visualization experiments of evaporation of liquid, which is confined between solid plates. Water, ethanol, and several other organic solvents were used as test liquids, each of which is sandwiched between a normal glass plate and a sand-blasted one, horizontally placed in a vacuum chamber, and monitored by irradiation of a planar LED backlight. Under a reduced pressure of typically 3-10 kPa at room temperature, the liquid was observed to evaporate from the plate edge. As evaporation proceeds, complicated branching patterns appear. Rapid motions of liquid front are occasionally observed, which are supposed to be two-dimensional flush boiling and may play an important role in the cleansing process. The boiling behavior was found to strongly depend on the surface roughness. When the plates are not clamped, the top plate shows occasional jumping motion, corresponding to the flush boiling. The surface roughness strongly affects the jumping.

Keywords: Evaporation, Boiling, Wettability, Pattern Formation, Condensation Coefficient

1. Introduction

This study focuses on the cleaning mechanism of laminated steel plates used as metal cores in various types of electric transformers. The cores are normally immersed in insulating mineral oils. In their disposal, it takes much time and cost to wash the remaining oil away. Until 1970s, polychlorinated biphenyls (PCBs) were widely used as an ingredient, the use of which is now banned worldwide due to their high toxicity. Thus the ways of safe and cost-effective disposal process are demanded.

A method of vapor washing with organic solvents has been recently proposed [1]; under sufficiently high temperature (typically 150~250 ℃) and reduced pressure conditions, the insulating mineral oil between the core plates is gradually replaced by the solvent vapor and easily washed away. To understand the mechanism and optimize the process in view of time and energy consumption, it is essential to investigate the fluid dynamics in such narrow gaps in more details. For that purpose, we have tried to visualize the behavior of fluid phase change using model systems [2-4].

2. Experimental Setup

2.1 Model System

To visualize the dynamics of fluids in narrow gaps, we use four working liquids, ion-exchanged water, ethanol, acetone, and heptane; they are colorless and sufficiently volatile under room temperature. To optically observe the fluid dynamics in gaps, we adopt transparent glass plates instead of metallic ones. Two types of commercially available glass plate are used; one is float glass with

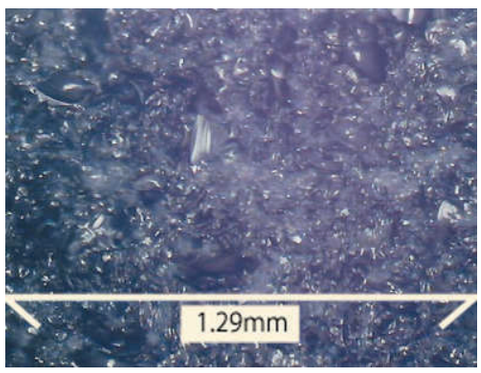

Fig. 1 Microscope image of sand-blasted glass surface.

smooth surface, another sand-blasted one. The surface image of the latter taken with an optical microscope is shown in Fig. 1.

When liquid fills the gap between the float glass plate and the sand-blasted one, the system is almost completely transparent; as the evaporation proceeds and the gap is getting dried, it becomes opaque due to diffusive scattering of light, thus the drying process will be easily monitored.

The surface of the float glass is very smooth, while the sand-blasted one is rough. The roughness of sand-blasted plate is typically $20\sim50$ μm, which is coincidentally the same order of magnitude as typical metal plates used in transformers in industrial use. The sand-blasted glass is highly wettable to water and organic solvents; for example, the contact angle of ethanol on the float glass is $\sim18°$, while that on the sand-blasted one is almost zero.

2.2 Visualization System

A schematic setup is shown in Fig. 2. The vacuum chamber is made of transparent acrylic resin ($200 \times 200 \times 200$ mm^3), inside of which glass plates sandwiching the test liquid are horizontally placed with simple zigs. The area size of the glass plate is 100×100 mm^2 with 5 mm thickness. The plates are illuminated with a white-type LED diffuse light source. The chamber is depressurized with a rotary vacuum pump (48 L/min). The inside pressure is monitored with a digital differential pressure gauge.

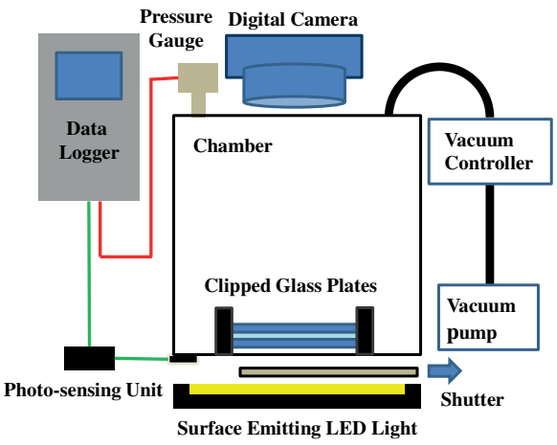

Fig. 2 Schematic view of the experimental setup. The shutter and the photo-sensing unit are used to synchronize the data acquisition.

All experiments reported in this paper were done at room temperature, although we are planning to develop a new chamber system with a temperature control unit.

3. Results and Discussion

Two cases are investigated separately; (1) evaporation in a clamped plate system, where pattern formation and occasional flush boiling are observed, and (2) evaporation in a unclamped system, where the top plate is seen to jump due to the boiling.

3.1 Clamped System

Typical examples of the observed image during evaporation are shown in Figs. 3-5. The obtained grey-scale images can be categorized typically into three regions with different brightness. At the initial stages, the gap between the glass plates is (almost) completely filled with liquid, thus most of the incident light passes the gap without scattering, which corresponds to the brightest region. At the later stages, empty gaps randomly scatter the incident light, which should be the darkest region. In between, we found the third area, half-dark region. Considering the high wettability of glass plates, this half-dark region is considered to be a “semi-dried” area where thin liquid film spreads on the plate surface.

Branching pattern of semi-dried region appears, as shown in Fig. 4 (b); this is especially noticeable for ethanol. We suppose that some hydrodynamic instability brings this branching, similarly to the fingering in a Hele-Shaw cell [5]. The patterns during the evaporation vary with experimental conditions, such as the working fluids and the surface roughness; dissolved gas also affects the phenomenon.

The area of the three regions (brightest, darkest, and in-between) is evaluated with a simple image processing technique; examples are shown in Fig. 6 for the ethanol case. Based on this analysis we can evaluate the liquid content V_L in the gap, with assumption that the gap is completely filled with the liquid in

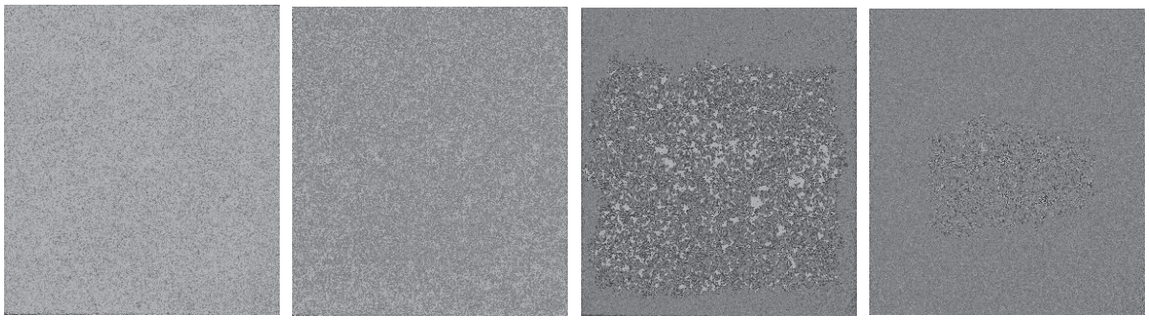

(a) 100 s (b) 200 s (c) 400 s (d) 700 s

Fig. 3 Examples of the obtained image during the evaporation process; water case.

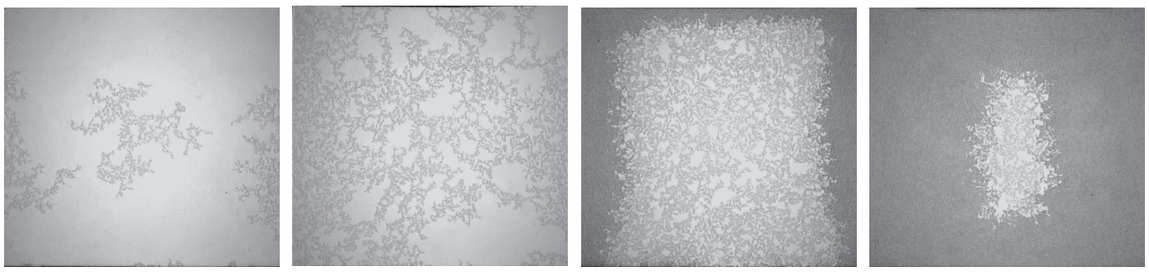

(a) 55 s (b) 60 s (c) 90 s (d) 130 s

Fig. 4 Similar to Fig. 3 for ethanol case.

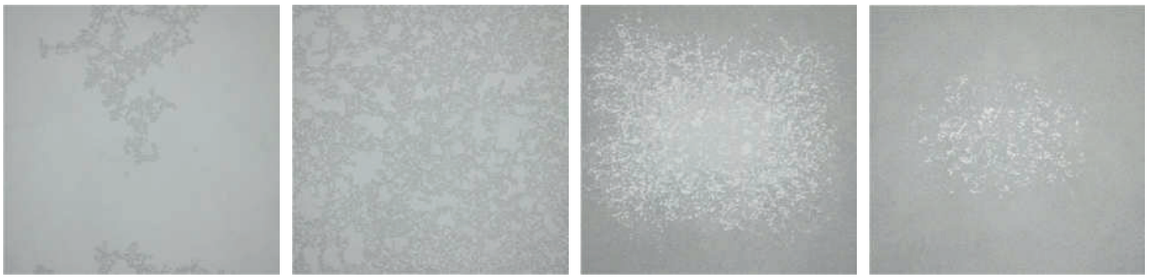

(a) 17 s (b) 29 s (c) 36 s (d) 38 s

Fig. 5 Similar to Fig.3 for acetone case.

the wet region and that the amount of liquid in the semi-dried region is negligible. The results are shown in Fig. 7, with the evaporation rate $\frac{dV_L}{dt}$.

As shown in Fig. 8, we occasionally observed abrupt and rapid deformation of the wet region, which is supposed to be flush boiling in quasi two dimensions. During the "boiling," the propagation of the region boundary becomes as fast as 50 mm/s, in contrast to the typical evaporating speed of (i.e., propagation of branching pattern) of 0.1-0.5 mm/s. This phenomenon of rapid phase change should play an important role in the oil retrieve process in transformer cores.

3.2 Unclamped System

For practical reasons of the cleansing process of laminated metal cores, we are interested in the "flush boiling" observed in the clamped system. To investigate its kinetics, we have done experiments with unclamped

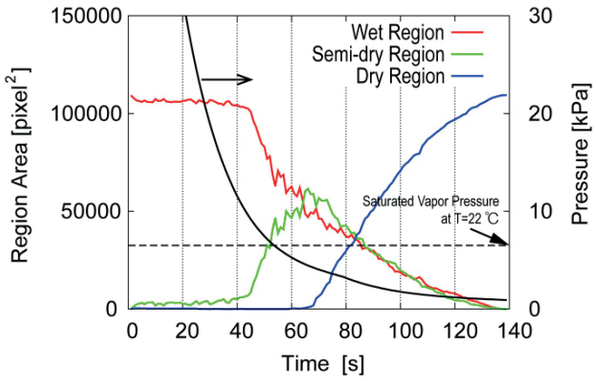

Fig. 6 Area change of three regions during the evaporation; ethanol case. The experiment is done at 22 ℃; the saturated pressure of ethanol at this temperature is $P_s \cong 6.5$ kPa [6].

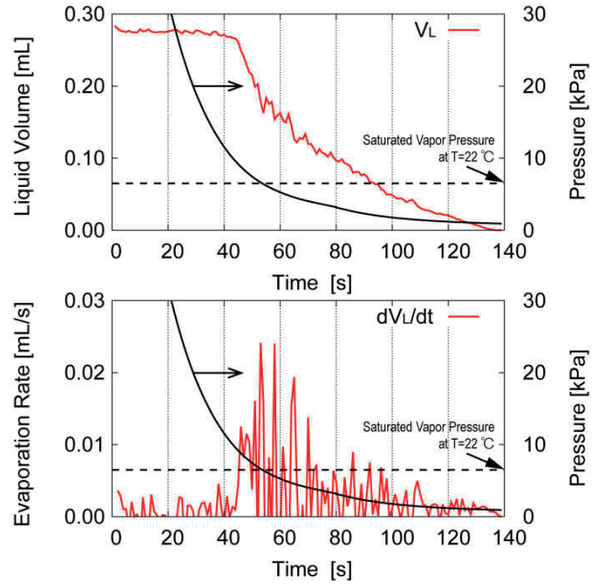

Fig. 7 Liquid volume change and the estimated evaporation rate; ethanol case..

plates. The glass plates sandwiching liquid are placed horizontally without clamping in the same vacuum chamber as in Fig. 1. When the chamber pressure is sufficiently reduced under the saturated vapor pressure, the top plate suddenly jumps up. Typical examples are shown in Fig. 9.

By detecting the position of the top plate with an image processing technique, the jumping height is measured as a function of time. Typical results are shown in Fig. 10 with the chamber pressure. A sudden jump starts when the pressure reaches the saturation

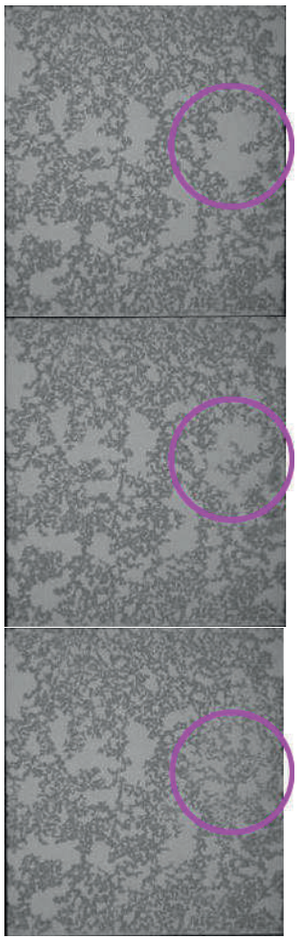

Fig. 8 Example of two-dimensional flush boiling; ethanol case. The three images were taken every 0.2 s. The rapidly changed area is shown by circles.

pressure. In most cases of a single jump, the motion of the top plate is parabolic as a function of time, as shown in Fig. 11 (a), which suggests that a single flush causes this kind of free-jumping. From its maximum height, we can estimate the kinetic energy of each jump, which is found to be corresponding to the phase change free energy which ethanol of about 3 mg releases.

The jumping becomes more frequently at later stage, and finally a quasi-periodic oscillation is observed, as shown in Fig. 11 (b). A typical frequency for the jumping oscillation is 20~30 Hz depending on the experimental conditions. Here we propose a simple explanation for the oscillation based on incomplete condensation of vapor. Consider first ideal gas of temperature T confined in a

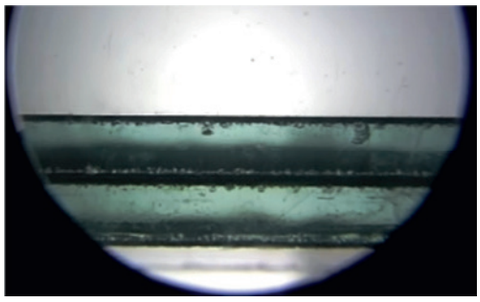

(a) At rest

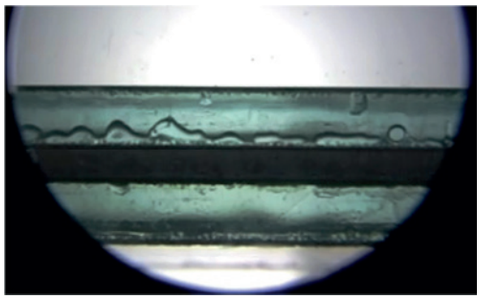

(b) During jump

Fig. 9 Example of top plate jumping under reduced pressure; ethanol case.

cylinder of length L and cross-section area A, which would show harmonic oscillation of frequency

$$f_0 \equiv \frac{1}{2\pi}\sqrt{\frac{pA}{ML}} \tag{1}$$

for small adiabatic volume change, where M is the pressure and m is the mass of the piston, respectively. When the gas is not ideal and vapor condensation takes place, the frequency would reduce, and a rough approximation gives a form

$$f = \sqrt{1-\alpha_c}\cdot f_0 \tag{2}$$

with an apparent condensation coefficient α_c. The oscillation frequency in Fig. 11 (b) leads to a value of $\alpha_c \cong 0.98-0.99$, which seems to give a reasonable explanation.

This jumping behavior strongly depends on the surface roughness as shown in Fig. 12. When both plates are float glass with smooth surface, much fewer but larger jumps are

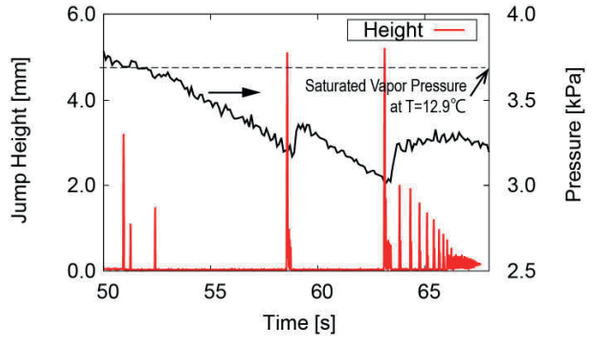

Fig. 10 Example of the jump height data; ethanol case.

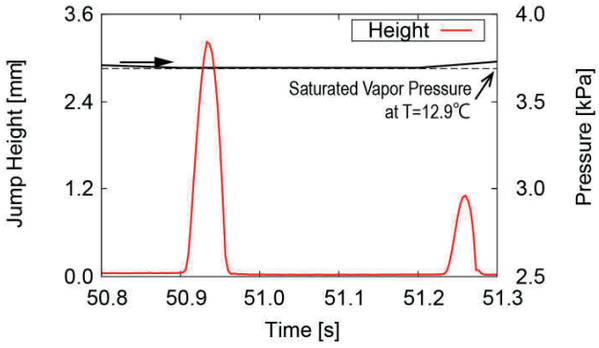

(a) Isolated jump during earlier stage

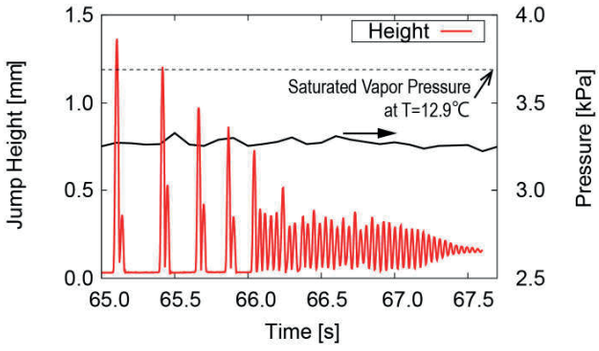

(b) Oscillation at final stage

Fig. 11 Enlarged plot of Fig. 10.

observed; in contrast, incessant isolated jumpings are observed in the case of sand-blasted glass for both plates.

4 Summary

Using two types (float and sand-blasted) of glass plates we carried out visualization experiments of liquid evaporation in thin gaps of 10~50 μm under reduced pressure. For

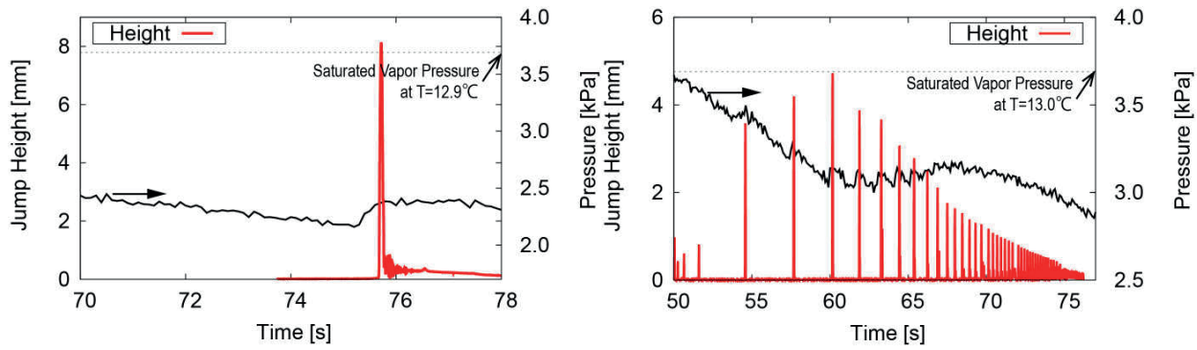

(a) Float glass/Float glass

(b) Sand-blast glass/Sand-blast glass

Fig. 12 Jumping behavior for glass plates with different roughness; ethanol case.

the clamped plate system, three regions are typically observed based on the intensity of transmitted light; completely wet, completely dry, and the half-dark or partially dried areas in between. Complex branching pattern of partially dried area often appears, which seems to be affected by various factors, such as types of working fluid, surface roughness, and dissolved gas. Rapid motions of liquid similar to flush boiling are occasionally seen, which should be important in modeling the evaporation dynamics. When the plates are placed without clamping, the top plate shows occasional jumping motions due to the flush boiling. The height and the frequency depend largely on the surface roughness.

To have better understanding of the mechanism of vapor cleansing for laminated metal plates, quantitative modelling of such quasi two-dimensional fluid phase change is required. There are several relevant control parameters, such as fluid properties (e.g., vapor pressure, viscosity, and surface tension), surface roughness and wettability, and dissolved gases. Detailed investigations with more precise control of experimental conditions (such as the plate temperature and the chamber pressure) are under way.

Acknowledgements

The authors are grateful to Dr. Eiichi Kato and his colleagues at Central Research Laboratory, NEOS Company Ltd., Japan, for stimulating discussion and encouragement. A part of this work is financially supported by JSPS KAKENHI (No. 15K05826).

References

[1] Y. Kuroiwa, “Disposal plant of electric transformers (in Japanese),” *Industrial Machinery*, **7**, pp. 57-61 (2010).

[2] Y. Yasumoto, Y. Okura, M. Matsumoto, “Quasi two-dimensional boiling under reduced pressure,” *Proc. 25th Int. Symp. Transport Phenomena*, 134 (Krabi, 2014).

[3] Y. Yasumoto, Y. Okura, K. Ogawa, M. Matsumoto, “Quasi two-dimensional evaporation and boiling under reduced pressure,” *Proc. 5th Int. Symp. Micro Nano Tech.,* S8-115 (Calgary, 2015).

[4] K. Ogawa, Y. Yasumoto, M. Matsumoto, “Quasi two-dimensional boiling under reduced pressure,” *Proc. 1st Pacific Rim Therm. Eng. Conf.*, 14530 (Hawaii, 2016).

[5] B. Bhushan and Y. Jung, “Micro- and nanoscale characterization of hydrophobic and hydrophilic leaf surfaces,” *Nanotechnology*, 17 (2006) 2758.

[6] D.R. Lide, ed., *CRC Handbook of Chemistry and Physics*, 72nd, CRC Press (Boston, 1992).

5th Micro and Nano Flows Conference
Milan, Italy, 11-14 September 2016

Micro-scale engineered scar-like tissues as in vitro model to investigate fibroblast proliferation and phenotype switch typical of a wound healing process

Chiara Conficconi[1,2]*, Marta Lemme[1,2]*, Paola Occhetta[2], Giulia Cerino[1], Roberta Visone[2], Emanuele Gaudiello[1], Marija Plodinec[3], Alberto Redaelli[2], Marco Rasponi[†2], Anna Marsano[†1]

* Equally contributing authors

[†] Corresponding authors: Marco Rasponi: Tel.:+39 02 2399 3377; Email: marco.rasponi@polimi.it; Anna Marsano: Tel.: +41 (0)61 32 87448; Email: anna.marsano@usb.ch

[1] Departments of Surgery and Biomedicine, University Basel, University Hospital Basel, Basel, Switzerland;
[2] Department of Electronics, Information and Bioengineering, Politecnico di Milano, Milano, Italy
[3] Biozentrum and The Swiss Nanoscience and Pathology Institutes, University of Basel, Basel, Switzerland

Keywords: Micro Fluidic System, Uniaxial Strain, 3D, Engineered Tissue

Introduction

Research on cardiac biology and clinical translation might benefit from the generation of engineered 3D micro-scale cardiac tissues suited to reproduce controlled key native biophysical conditions [1]. In particular, after myocardial infarction, tissue necrosis occurs and a wound healing process takes place to form a dense collagenous scar, which impairs the normal cardiac function. Our aim is to generate a micro-scale engineered scar-like tissue as model for wound healing process to investigate the process to reverse fibroblast switch into myofibroblasts and ultimately control the extracellular matrix deposition. TGFβ1 supplementation is known to both support the switch of cardiac fibroblasts into myofibroblasts at the macro-scale [2]. We hypothesize that combined exposure to TGFβ1 supplementation and physiological mechanical stimulation (as uniaxial strain) regulates fibroblast proliferation and fibroblast-myofibroblast phenotype transition.

Material and Methods

For this purpose, we used a recently developed microfluidic bioreactor capable to apply controlled uniaxial strain to 3D cell-based constructs [3]. Rat cardiac fibroblasts were isolated from 3-day-old neonatal pups expanded in high glucose culture medium supplemented by 10% fetal bovine serum. Cardiac fibroblasts were embedded at the density of 1,45·104 cells/µl in a fibrin gel (composed by 20 mg/ml of fibrinogen and 5 U/ml of thrombin) and cultured for 7 days into the microfluidic devices. In particular, fibroblasts were statically and dynamically (10% of strain and 1 Hz of frequency) cultured, with or without the addition of a specific biochemical cue, the transforming growth factor β1 (TGFβ1). The effect of the different culture conditions on cell phenotype, proliferation and ECM stiffness were investigated through immunofluorescence and optical microscopy, immunofluorescence, and atomic force microscopy (AFM)-based nano-indentation, respectively.

Results

Combined stimulation with TGFβ1 and cyclic strain (10% amplitude at 1 Hz) increased both cell proliferation and percentage of fibroblasts committed towards myofibroblast phenotype (defined as the percentage of smooth muscle α-actin (α-SMA+ positive cells) compared to the static condition without TGFβ1 supplementation. In particular, cell proliferation was statistically different in the static condition without TGFβ1 supplementation (0,95 ± 0,60%,) compared to both the static (3,35 ± 1,19%) and dynamic (3,75 ± 1,33%) condition with TGFβ1 supplementation. A statistically significant increase in α-SMA expression was also found between the static condition without TGFβ1 supplementation (23,92 ± 15,30%), and both the dynamic conditions without and with TGFβ1 supplementation (58,55 ± 8,97% and 56 ± 21,03%, respectively), confirming the key role of the mechanical stimulation. Static culture yielded constructs with a relatively low mechanical stiffness, even in presence of TGFβ1 (~0.7 kPa). Conversely, mechanically stimulated fibroblasts deposited an extracellular matrix with superior Young modulus, and the constructs were similarly stiff in presence (~7 kPa) or in absence (~2 kPa) of TGFβ1 supplementation.

Conclusions

The micro-scale scar-like engineered tissues here generated represents a reliable model to investigate the effects of different molecules/drugs in the phases of proliferation and maturation of wound healing processes not only for cardiac related research but also for other tissue types (e.g. skin, liver).

References

[1] D. T. Y. Huh, G. A. Hamilton, H. J. Kim e D. E. Ingber, «Microengineered physiological biomimicry: Organs-on-chips,» Lab on a Chip, 2012.

[2] R. A. Evans, Y. C. Tian, R. Steadman e A. O. Phillips, «TGF-β1-mediated fibroblast–myofibroblast terminal differentiation—the role of smad proteins,» Experimental Cell Research, 2003.

[3] A. Marsano, C. Conficconi, M Lemme, P Occhetta, E. Gaudiello, E. Votta, G. Cerino, A. Redaelli, M. Rasponi. «Beating heart on a chip: a novel microfluidic platform to generate and assess functional 3D cardiac microtissues». Lab on a Chip, in press.

5th Micro and Nano Flows Conference
Milan, Italy, 11-14 September 2016

On-Chip Magnetic Platform for Single-Particle Manipulation with Integrated Electrical Feedback

Marco MONTICELLI[1,*], Daniela PETTI[1], Edoardo ALBISETTI[1], Marco CARMINATI[2], Giorgio FERRARI[2], Marco SAMPIETRO[2], Riccardo BERTACCO[1]

* Corresponding author: Tel.: +39 02 23991 9668; Email: marco.monticelli@polimi.it
1 Department of Physics, Politecnico di Milano, Italy
2 Department of Electronics Information and Bioengineering, Politecnico di Milano, Italy

Keywords: Lab-on-chip, Microfluidic, Magnetic particles, Electrical detection

Introduction

Single molecule imaging and handling are particularly relevant for in-vitro biological application (e.g. drug delivery studies), because they offer a clear and direct way to investigate functions and dynamics of single biomolecules.
In this paper, we exploit a fully magnetic and electrical system integrated in a microfluidic device to achieve a controlled deliver and detection of single magnetic nano and micro-particles diluited in liquid.

Materials and methods

Our system is based on domain-walls (DWs) displacement by means of external magnetic fields in confined ferromagnetic zig-zag nanostructures, fabricated on-chip, to attract, move [1] and sense [2] particles in suspension over the chip. To this scope, we employed as attracting pole DWs nucleated at the corner of zig-zag structures for particles manipulation and electrical contacts to monitor the DW presence through anisotropic magnetic resistance (AMR) measurements. The chip was fabricated by means of optical and e-beam lithography and lift-off processes. The device was then capped with 35 nm of SiO_2 to preserve the nanostructures from the wet environment. The measurements were performed in a Polydimethylsiloxane cell placed inside a quadrupole electromagnet, in four probe configuration, applying an AC voltage of 50 mV at 50 kHz and through lock-in detection. The movement of the particles suspended in buffer solution was monitored under an optical microscope during the measurement.

Results and Discussion

The controlled motion of the magnetic particle has been achieved by the DW displacement due to the application of a sequence of external magnetic fields parallel to the chip surface (see Fig.1a).
The magnetization of the structure is initialized by a saturating field H_0 (1000 Oe) directed in the negative direction of y-axis; the field H_1 (150 Oe), along the positive direction of y-axis, nucleates a single transverse DW, reversing the magnetization of the injection pad (which is a larger extremity of magnetic conduit) and propagating the DW up to the first corner in the zig-zag. The DW position remains stable after removal of H_1, due to the geometrical constrain at the corner. This is the position at which the DW stray field captures a magnetic particle in suspension. Moreover, with a sequence of external magnetic fields (along the segments direction) H_2 and H_3 (190 Oe), the DW can be displaced along the conduit up to the last corner. In this way, a trapped bead can be dragged over the conduit.

The presence of the magnetic particle over the DW affects the value of the magnetic depinning field, thus allowing the bead detection. In fact, (see inset in Fig.1b), the superparamagnetic bead moment (**μ**) creates a stray field which opposes the external field, causing an increase of the depinning field required to move the DW. In Fig.1b, the variation of the voltage drop across a corner of the zig-zag structure due to the AMR while sweeping the magnetic field (0-300Oe) is used to detect the transit of the particle over the corner. For a bead of 1μm the depinning field variation is 14±3 Oe. In this way, the same magnetic conduit can be employed to accomplish both the functions of particles manipulation and detection.

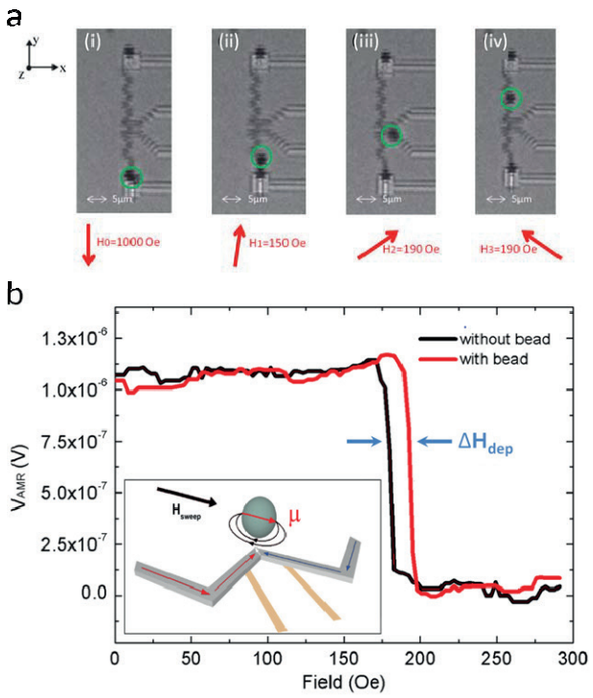

Fig.1 **a** Frames from a video showing the attraction and the manipulation of a single 1μm bead along the magnetic zig-zag conduit. Red arrows represent the direction of the applied magnetic fields. **b** Voltage drop across the zig-zag as a function of the magnetic field for the clean zig-zag (black) and during the transit of the beads (red). In the inset: 3D sketch of the device.

References

[1]M. Donolato et al., *Adv. Mat.* 22, 2706 (2010).
[2]M. Donolato et al., *Nanotechnology* 20, 385501 (2009)

1-D Modelling of Pressure Fluctuation and Flow Reversal during Flow Boiling in a Micro-channel with Vapour Venting Membrane

Ahmed MOHIUDDIN , Sateesh GEDUPUDI *

*Corresponding author: ++91 (0)44 2257 4721; Email: sateeshg@iitm.ac.in
Department of Mechanical Engineering, Indian Institute of Technology Madras, Chennai, India

Keywords: Micro-channel, Flow Boiling, Confined Bubble, Flow Instability, Pressure Fluctuation, Vapour Venting Membrane

The rapid miniaturization of electronic devices and the compactness of thermal equipment necessitate high heat flux removals. Flow boiling in mini/microchannels seems to be a promising method of cooling high heat flux devices. But flow boiling in microchannels encounters problems such as high amplitude local pressure fluctuations, rapid flow reversals and uneven flow distribution between the channels. These lead to local hot spots and thermo-mechanical stresses which may damage a fragile silicon, the commonly used substrate in electronic devices. Researchers have used different techniques to overcome this problem. These include employing the pressure drop elements at the inlet to channels, Kandlikar et al (2006), promoting the bubble formation inside the channels, Agostini et al (2008) and Xu et al (2009). David et al (2011) employed vapour venting membranes to reduce the channel pressure drop and wall temperature.

1-D modeling of local pressure fluctuations and flow reversals during flow boiling in a rectangular micro-channel has been done by Gedupudi et al (2011). They studied the flow reversals caused by condensable vapour due to subcooled boiling in the upstream region (for e.g., preheater) and trapped non-condensable gas at the inlet, and modelled the effect of inlet restriction.

The objective of the present work is to model the effect of vapour venting membranes on local pressure fluctuations and flow reversals caused by the confined bubble growth during flow boiling in a rectangular microchannel. Working fluid is water boiling at atmospheric pressure (channel outlet pressure). Effects of porosity, pore size and thickness of hydrophobic membrane are presented. Figure 1 shows the local pressure fluctuations with membrane (m) and without membrane, considering the condensable vapour in the upstream region, for a 0.38 x 1.5 x 40 mm channel, with nucleation site at 20 mm from the inlet. Heat flux and mass flux are 200 kW/m^2 and 200 kg/m^{2}s respectively. Hydrophobic membrane pore diameter, porosity and thickness are 0.5µm, 0.72 and 65 µm respectively. With membrane, there is a large reduction in the amplitude of local pressure fluctuations, p_1-p_2 (m), across upstream liquid slug, and p_3-p_e (m), across downstream liquid slug. However, the reduction in the plenum pressure fluctuation, p_0-p_e (m), is small. Results are presented for different heat fluxes and mass fluxes.

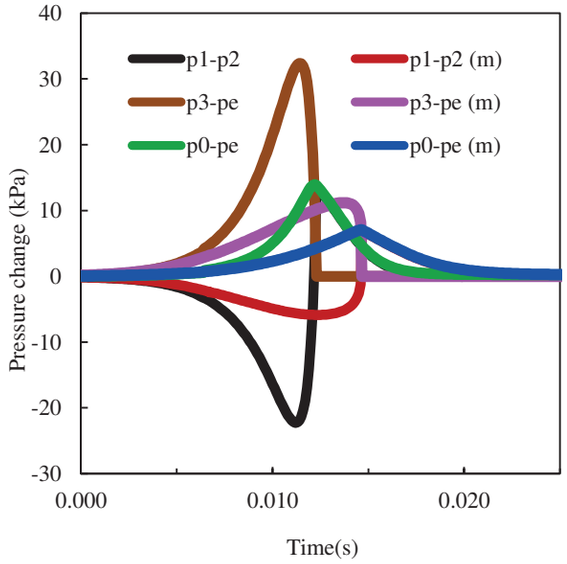

Fig. 1. Local pressure variation with membrane (m) and without membrane.

References

Kandlikar, S.G., Kuan, W.K., Willistein, D.A.,Borrelli, J., 2006. Stabilization of flow boiling in microchannelsusing pressure drop elements and fabricated nucleationsites, J. Heat Transfer 128, 389-396.

Agostini, B., Thome, J.R., Fabbri, M., Michel, B., Calmi, D., Kloter,U., 2008. High heat flux flow boiling in silicon multi-microchannels - Part I: Heat transfer characteristics of refrigerant R236fa, Int. J. Heat Mass Transfer 51 (2008) 5400-5414.

Xu, J., Liu, G., Zhang, W., Li, Q., Wang, B., 2009. Seed bubbles stabilize flow and heat transfer in parallel microchannels, Int. J. Multiphase flow 35, 773-790.

David, M.P., Miler, J., Steinbrenner, J.E., Yang, Y., Touzelbaev, M., Goodson, K.E., 2011. Hydraulic and thermal chanractreistics of a vapor venting two-phase microchannel heat exchanger, Int. J. of Heat and Mass Transfer 54, 5504 – 5516.

Gedupudi, S., Zu, Y.Q., Karayiannis, T.G., Kenning, D.B.R., Yan, Y.Y., 2011. Confined bubble growth during flow boiling in a mini/micro-channel of rectangular cross-section Part I: Experiments and 1-D modeling, Int. J. Thermal Sciences 50, 250-266.

ID 131

Experimental study of the effect of an electrical field on a liquid vapor interface in a narrow channel

Baptiste BLAINEAU [1,*],Sébastien DUTOUR [1],Thierry CALLEGARI [1],Pascal LAVIEILLE [1],Marc MISCEVIC [1], Stéphane BLANCO [1],Yves BERTIN [2]

* Corresponding author: Tel.: +33 (0) 561 556 005; Email: blaineau@laplace.univ-tlse.fr
1 : Université de Toulouse ; UPS, INP ; LAPLACE (LAboratoire Plasma et Conversion d'Energie) ; 118 route de Narbonne, F-31062 Toulouse, France
2 : Université de Poitiers ; Insitut Pprime UPR3346 CNRS – ENSMA, 1 avenue Clément Ader BP 40109 – 86961 Futuroscope Chasseneuil Cedex

Abstract An academic experiment has been set-up to highlight and understand the electro-hydrodynamic effects on the liquid vapor interface. Experimental results on HFE-7000 and HFE-7100 show that it generates a differential pressure about 120 Pa for 2kV/mm, at the interface. It could be used to improve the performance of Capillary Pumped Loops where the pumping is limited by the differential pressure generated by the porous media.

Keywords: Liquid-vapor interface, electro-hydrodynamics

1. Introduction

Many systems used for thermal management process involve liquid-vapor interfaces in very confined spaces. Such configurations induce mainly two kinds of forces: the capillary force and the viscous force. For example, Capillary Pumped Loops and Loop Heat Pipes are highly efficient and self-sufficient heat transfer devices used for electronics cooling. Their pumping limit is known: the maximal differential pressure generated by the porous medium determines the maximal heat flux that the system can carry for a given distance between the heat sources. As a consequence, the system performance is affected during some operating conditions such as sudden change of heat load or in applications where gravity impacts the flow. So to improve the performance of such thermal management systems, it is now considered the use of an auxiliary active pumping system. One option is to use electro-hydrodynamics (EHD) forces that enable to act on a fluid thanks to an electric field. This method needs no moving pieces; it reduces the risk of damage and it is interesting for space application.

2. Background

The electrical force acting on a dielectric fluid is usually formulated in terms of the Korteweg-Helmholtz body force density :

$$\mathbf{f}_{KH} = \rho_E \mathbf{E} - \frac{1}{2} E^2 \nabla \varepsilon + \frac{1}{2} \nabla \left(\rho \frac{\partial \varepsilon}{\partial \rho} E^2 \right) \quad (1)$$

The first term is the well-know strength of Coulomb. Beyond a value of 10^6 V/m for the electric field, charges are generated by species dissociation. These charges will move and bring the liquid with them. Systems based on this phenomenon are called "conduction pump" and they can generate a differential pressure of 320 Pa for an electric field of 3,5 kV/mm with R-123 used as the working fluid [1]. The second term is the dielectrophoresis force induced by polarization effect and linked to the contrast between the permittivity of the liquid and of the vapor. This one acts at the liquid-vapor interface, the differential pressure generated for an electric field of 0,25 kV/mm, is 58 Pa for deionized

water [2]. Before using these strengths in a two phase system to improve the pumping capacity and/or the heat exchange, or to reduce the instabilities, there are some needs to understand and model the complex interactions between the electromagnetism phenomena, the heat transfer at the liquid-vapor interface, and the capillary effects. The last term is the term of electrostriction.

The main purpose of this work is to understand these interactions at this micro-scale thanks to an experiment and check the validity of the models for two-phase heat transfer application.

3. Experimental set-up

An experimental set-up has been built to visualize the behavior of the interface between two vertical electrodes at different potentials. The experiment takes place in a control temperature enclosure. Glass electrodes coated with ITO (Indium Tin Oxide) are used to allow the visualization of the interface. There are 3 different positions for the electrodes that enable to change the gap between the electrodes from 1 to 3 mm. As their width is of 30 mm, we can make the hypothesis that the electric field is homogenous between the electrodes. The maximal voltage applied between the electrodes before flashover follows the Paschen's law. It will depend on the pressure and the distance between the electrodes. We are in pure liquid-vapor system, so it will depend on the temperature.

4. Experimental results

Under the electric field, the liquid rises between the electrodes due to the pressure generated by the electric field. The liquid height has been measured for different temperatures. The final purpose is to apply a heat flux to the electrodes. First results (Figure 1) have been obtained with aluminum electrodes at ambient temperature and without heat flux, for two different fluids (HFE-7000 and HFE-7100). For both, the relative dielectric permittivity is 7.4. For an electric field of 1,5kV/mm, the differential pressure generated is about 50 to 70 Pa (symbols) that agree with models of dielectrophoresis strength available in the literature (dashed line). The relation between the pressure jump and the apply voltage is based on the works of JONES [2] :

$$\Delta P = \frac{\left(\varepsilon_l - \varepsilon_v\right)V^2}{2D^2} \qquad (2)$$

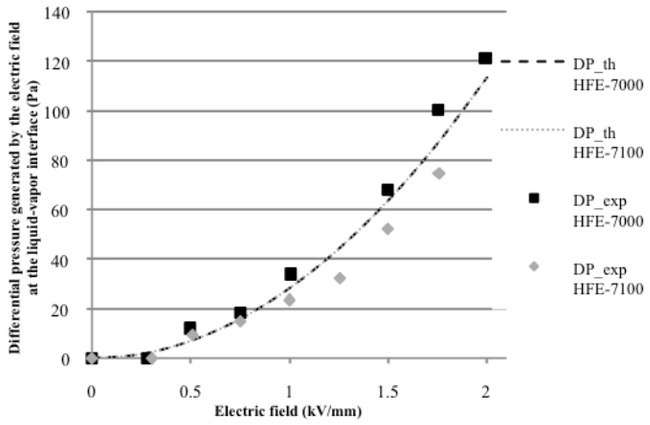

Figure 1 Experimental and theoretical results of differential pressure generated by the electric field at the liquid vapor interface

5. Conclusion

The dielectrophoresis force acts in very located area, on the liquid vapor interface. It has the potential to pump liquid film and could be used in heat pipe for example.

Additional results will be presented for others temperatures. Specific experiments will also been presented when a heat flux is applied on the wall, involving vaporization of the liquid.

6. References

[1] Yinshan FENG and Jamal SEYED-YAGOOBI, Understanding of electrohydrodynamic conduction pumping phenomenon. Physics of fluids, 2432-2441, June 2004

[2] Thomas B. JONES, Frequency-dependent electromechanics of aqueous liquids: Electrowetting and dielectrophoresis. Langmuir, 2813–2818, February 2004

5th Micro and Nano Flows Conference
Milan, Italy, 11-14 September 2016

CFD model of mouse liver microcirculation based on a 3D reconstruction

Monica PIERGIOVANNI[1], Elena BIANCHI[1], Lucia GANZER[2], Giada CAPITANI[1], Irene LI PIANI[1], Matteo IANNACONE[2,3], Luca G. GUIDOTTI[2,3], Gabriele DUBINI[1]

1 Laboratory of Biological Structure Mechanics (LaBS), CMIC, Politecnico di Milano, Milan, Italy
2 Division of Immunology, Transplantation and Infectious Diseases, IRCCS San Raffaele Scientific Institute, Milan, Italy
3 Vita-Salute San Raffaele University, Milan, Italy

Keywords: Liver microcirculation, CFD model, 3D reconstruction

Introduction

The liver is organized in functional units of a hexagonal structure - termed lobules - that are characterized by a rather peculiar blood microcirculation (Fig. 1). Blood enters the liver lobule from branches of both the hepatic artery and the portal vein, flows through a tangled network of sinusoids and exits from the central vein that is positioned at the center of the lobule. A better understanding of the hemodynamics that govern liver microcirculation is relevant to clinical and biological studies aimed at improving our management of liver diseases and liver transplantation.

Most of the fluid dynamic studies reported so far are either focused on the macroscopic vasculature [1] or model the sinusoidal network as a homogeneous porous medium [2, 3], thus missing local information.

Herein, we built a computational fluid dynamic (CFD) model of a 3D sinusoidal network, based on *in vivo* images of the mouse liver.

Materials and methods

The geometry reconstruction was performed with the software Mimics (Materialise, Leuven) from a stack of mouse liver images (0.38×0.38×25 µm) obtained *in vivo* using a 2-photon microscope pumped by two Ti:Sa lasers and one OPO (TriM Scope II, LaVisionBioTec, Germany). Of note, we focused on a lobule inlet (Fig. 1) and on the first branching of the sinusoids.

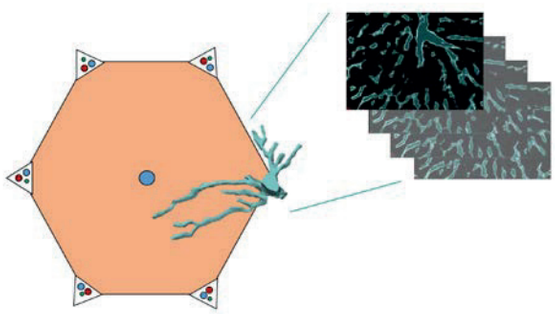

Figure 1 Representation of the liver lobule and sinusoid reconstruction.

The CFD model was developed with Fluent 16.0 (ANSYS Inc., Canonsburg, PA), using a mass flow rate as inlet condition and no slip boundary at the walls. To account for the remaining branches of the sinusoids (that could not be reconstructed because out of the field of view), a lumped parameter model was used to prescribe the correct pressure in each outlet. Blood was represented as a Newtonian fluid.

Results and conclusions

As shown in Fig. 2, the CFD model here proposed can accurately simulate the fluid dynamics in a portion of the sinusoidal network in mouse liver. Mean velocities (100 – 500 µm/s) and mass flow rates (4.5×10^{-3} – 2×10^{-2} µg/s) in each branch are in agreement with literature values both from *in vivo* measurements on rats [4, 5] and from other computational models [6].

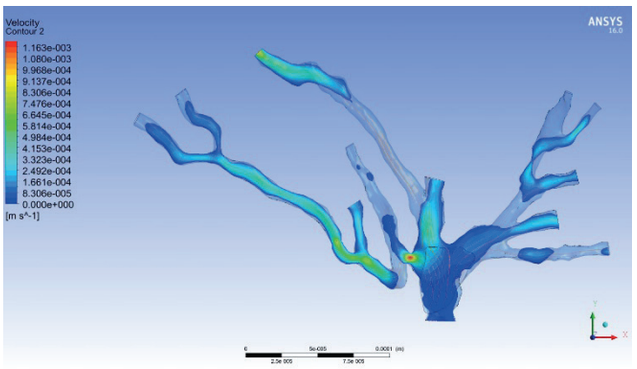

Figure 2 Blood velocity and streamlines in the reconstructed sinusoidal network

The high resolution provided by the 2-photon microscope allows for a detailed reconstruction of a portion of the mouse sinusoidal network. By means of a deeper and larger stack of images, it could be possible to model the fluid dynamics of an entire liver functional unit.

References

[1] S. George *et al*., "Hemodynamics in Normal and Diseased Livers: Application of Image-Based Computational Models", Cardiovasc Eng Technol, 2015;

[2] C. Debbaut *et al*, "A 3D porous media liver lobule model: the importance of vascular septa and anisotropic permeability for homogeneous perfusion", Comput Methods Biomech Biomed Engin, 2012;

[3] A. Bonfiglio *et al*., "Mathematical Modeling of the Circulation in the Liver Lobule", J Biomech Eng, 2010;

[4] R. Maass-Moreno *et al.*, "Distribution of pressure gradients along hepatic vasculature", Am J Physiol, 1997;

[5] K. Nakata *et al.*, "Direct measurement of blood pressures in minute vessels of the liver", Am J Physiol, 1960;

[6] C. Debbaut *et al*., "Perfusion characteristics of the human hepatic microcirculation based on 3D reconstructions and computational fluid dynamic analysis", J Biomech Eng, 2012.

A Review on Slip Models for Gas Microflows Using Perturbation Method

Mohammad S. KHALILI [1,*], Mohsen SAGHAFIAN [1], Ahmad SEDAGHAT [1], Ebrahim SHIRANI [1]

* Corresponding author: Tel.: ++98 (0)372 4525206; Email: ms.khalili@me.iut.ac.ir
1: Department of Mechanical Engineering, Isfahan University of Technology, Iran
saghafian@cc.iut.ac.ir, sedaghat@cc.iut.ac.ir, eshirani@cc.iut.ac.ir

Keywords: Micro Flow, Perturbation Method, Slip Model, Micropoiseuille, Microcouette, Microcavity

1 Introduction and Perturbation Method

A new method for modeling of micro flows is presented in this research. First, the continuum equations of fluid dynamics are developed by using perturbation expansions of the velocity, pressure, density and temperature fields:

$$\phi = \phi_0 + Kn\,\phi_1 + Kn^2\,\phi_2 + Kn^3\,\phi_3 + O(Kn^4) \quad (1)$$

$$\phi = u, v, w,\ p,\ \rho, T$$

Where the no-slip fields are denoted by $\phi_0(\boldsymbol{x},t)$, and corrections to the fields due to different orders of Kn dependence are denoted by $\phi_i(\boldsymbol{x},t)$ (i=1, 2, ...), and also slip fields are denoted by $\phi(\boldsymbol{x},t)$. Subsequently, different orders of equations in dependence of Knudsen number are obtained. Required boundary conditions for solving each order of these equations are obtained by substitution of the perturbation expansions into the general boundary conditions for velocity slip and temperature jump [1-2].

2 Development, Discretization and Solution Algorithm

In the present work, we use three-term perturbation expansions and reach to three order of equations O(1), O(Kn), O(Kn^2) and their boundary conditions. In fact, the equations of O(1) are the no-slip Navier-Stokes equations. Also, the equations of O(Kn) and O(Kn^2) govern the required corrections due to the velocity slip and temperature jump. This set of equations is discretized in two-dimensional state on a staggered grid using the finite volume method.

Total algorithm of solution includes three steps: The first step is solution of the O(1) equations with the O(1) boundary conditions. The second step is solution of the O(Kn) equations with the O(Kn) boundary conditions. This step's boundary conditions are obtained by fitting the first step's fields on the walls. The third step of algorithm is solution of the O(Kn^2) equations with the O(Kn^2) boundary conditions. This step's boundary conditions are also obtained by fitting the first and second step's fields on the walls. A three-part computer program has been produced for solving the set of discretized equations. Each part of this code, solve one order of the equations with the SIMPLE algorithm.

3 Some Micro Flows, Results and Conclusions

At First, incompressible slip micropoiseuille and microcouette flows are solved either analytically or numerically using the perturbation method. Good agreement is found between analytical and numerical results. In Both case, numerical results of the perturbation method deviate from its analytical results by increasing the Knudsen number.

Also, a shear-driven microcavity flow is investigated and its results are compared with those by the DSMC approach [3]. Good agreement is found between the results of two approaches, except near the upper corners of the cavity. This reveals that more corrections are needed in the perturbation method by increasing the Knudsen number.

By combination of two slip coefficients and the two-correction perturbation method, it can be easily used this method in the higher Knudsen numbers. At this study, we also try to evaluate different researcher's slip models [4] and probably to propose more accurate slip coefficients.

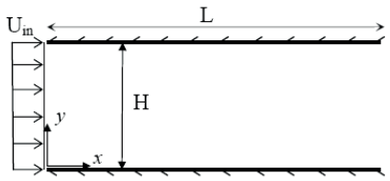

Figure 1. Channel geometry for micro poiseuille flow.

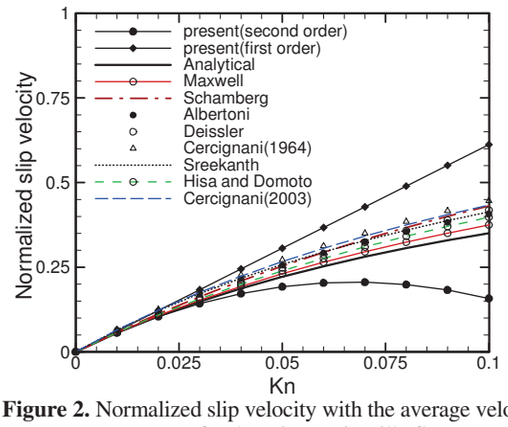

Figure 2. Normalized slip velocity with the average velocity versus Kn for the micro poiseuille flow.

4 Some References

[1] Karniadakis, G., Beskok, A. and Aluru, N., 2005. Microflows and Nanoflows- fundamentals and simulation. SpringerScience and Business Media, Inc., New York.

[2] Khalili, M. S., Saghafian, M., Shirani, E. and Saberian, I., 2011. Modeling of micro flows using perturbation method- 3rd Micro and Nano Flows Conference, Thessaloniki, Greece.

[3] Mizzi, S., Emerson, D. R. and Stefanov, S. K., 2007. Effects of rarefaction on Cavity flow in the slip regime. Journal of Computational and Theoretical Nanoscience, 4(4), 817-822.

[4] Zhang, W. M., Meng, G. and Wei, X., 2012. A review on slip models for gas microflows. Microfluidics and Nanofluidics, 13, 845-882, ISSN 1613-4982.

5th Micro and Nano Flows Conference
Milan, Italy, 11-14 September 2016

1-D Modelling of the Influence of Nucleation Frequency on Pressure Fluctuations and Flow Reversal during Flow Boiling in Rectangular Micro-channels

Mahesh KURUP , Sateesh GEDUPUDI*

* Corresponding author: Tel.: ++91 (0) 44 2257 4721; Fax: ++91 (0)44 22574652; Email: sateeshg@iitm.ac.in
Department of Mechanical Engineering, Indian Institute of Technology Madras, Chennai, India

Keywords: Microchannel, Flow Boiling, Nucleation Frequency, Pressure Fluctuations

Inventions in micro-scale technologies have introduced compact and high power density devices, which dissipate high heat fluxes beyond the scope of conventional heat sinks. Microchannel heat sinks with flow boiling has the potential to cool high heat flux devices. However, confined bubbles in these channels lead to pressure fluctuations, which, in the presence of a common inlet header, trapped non-condensable gases and subcooled boiling in the upstream region, in turn can lead to flow instabilities, causing transient dry-out, local hot spots and thermo-mechanical stresses.

Kew and Cornwell (1996) modeled rapid bubble growth and subsequent pressure fluctuation during flow boiling in tubes. Later, measurements of pressure changes at different locations along the axis of the test section as obtained by Kenning and Yan (2001) were found to be of the same order as those modeled by Kew and Cornwell. Flow reversal due to trapped gases were also noticed during the experiments. Kandlikar et al. (2006) were able to suppress the pressure fluctuation using constriction at the channel inlet and artificial nucleation sites. Thome and DuPont (2007) induced nucleation in microchannels using a micro pulsed heater as a means to stabilize the flow and enhance the heat transfer. Xu et al. (2009) attempted to stabilize flow instabilities in micro-channel using such seed bubbles.

Gedupudi et al. (2011) presented a 1-D model for estimation of the pressure changes and flow reversal considering trapped non-condensible gas at the inlet and condensable vapour due to sub-cooled boiling in the upstream region, for a single bubble in the channel. However, a channel can contain multiple bubbles given the bubble nucleation frequency, nucleation sites at different locations and stabilization techniques. This influences the pressure fluctuation and also flow reversal in the presence of inlet compressibility. In the present study, the above 1-D model is extended to include the effects of nucleation frequency in the channel. Water boiling at 1 atm is considered.

Figure 1 shows a typical effect of bubble nucleation frequency on pressure fluctuation during flow boiling in a microchannel, with bubble incipience from the same nucleation site located at the channel inlet, without inlet compressibility. The channel is 0.375 mm deep, 1.5mm wide and 42mm long. The heat flux and mass flux are 200 kW/m^2 and 700 kg/m^{2}s respectively. As can be seen in the figure, the amplitude of pressure fluctuation decreases with the increase in nucleation frequency. The study presents results for different mass fluxes, heat fluxes and nucleation site locations with and without inlet compressibility.

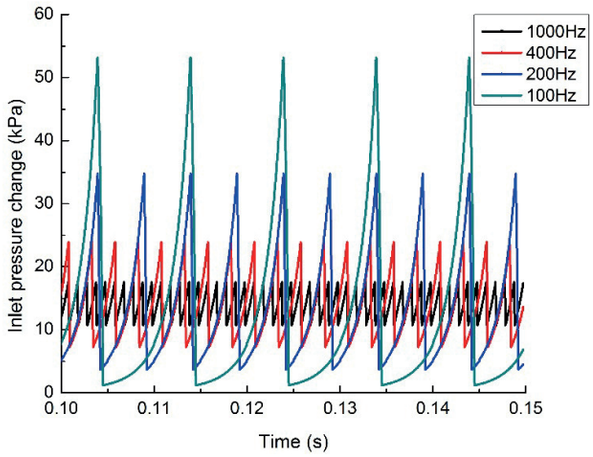

Fig. 1. Effect of bubble incipience frequency on inlet pressure.

References

Kew, P.A., Cornwell, K., 1996. On pressure fluctuations during boiling in narrow channels. In: 2nd European Thermal Sciences and 14th UIT National Heat Transfer Conference 3, 1323-1327.

Kenning, D.B.R., YanY., 2001. Saturated flow boiling of water in a narrow channel: experimental investigation of local phenomena. IChemE Trans. A, Chemical Engineering Research and Design 79, 425-436.

Kandlikar, S.G., Kuan, W.K., Willistein, D.A.,Borrelli, J., 2006. Stabilization of flow boiling in microchannels using pressure drop elements and fabricated nucleationsites, J. Heat Transfer 128, 389-396.

Thome, J.R., Dupont,V., 2007. Heat transfer assembly. European Patent EP 1779052 B1, November 28.

Xu, J., Liu, G., Zhang,W.,Li,Q., Wang,B., 2009. Seed bubbles stabilize flow and heat transfer in parallel microchannels. International J. of Multiph. Flow 35, 773–790.

Gedupudi, S., Zu, Y.Q., Karayiannis, T.G., Kenning, D.B.R., Yan,Y.Y., 2011. Confined bubble growth during flow boiling in amini/micro-channel of rectangular cross-section Part I: Experiments and 1-D modeling. Int. J. Thermal Sciences 50, 250-266.

5th Micro and Nano Flows Conference
Milan, Italy, 11-14 September 2016

ID 140

Steady State and Transient Numerical Simulations of Condensation in Small Diameter Channels

Paolo TONINELLI, Stefano BORTOLIN, Marco AZZOLIN, Davide DEL COL *

* Corresponding author: Tel.: +39 049 8276891; Fax: +39 049 8276896; Email: davide.delcol@unipd.it
Department of Industrial Engineering, University of Padova, Italy

Abstract In the recent years, numerical simulations by means of the Volume of Fluid (VOF) method have become an interesting tool to study two-phase flow with and without phase change. When dealing with small geometries, experimental investigations can be invasive and affect the phenomenon itself and also very expensive and time demanding. However, validation of the numerical simulations by experiments is still a key point to obtain reliable results. The present paper aims at providing an understanding of the annular condensation process inside minichannels at low mass velocities ($G \leq 200$ kg m^{-2} s^{-1}) by means of VOF simulations and experimental heat transfer measurements. Three-dimensional and steady numerical simulations of R134a condensation inside 3.4 mm i.d. circular minichannel have been validated with the experimental data to analyze the influence of liquid film distribution and liquid film flow on the heat transfer coefficient.
Furthermore, since from experimental flow visualizations at these operating conditions it is possible to note the presence of waves at vapour-liquid interface at certain mass fluxes, 2-D axisymmetric and unsteady simulations have been performed to study the waves formation during adiabatic flow inside 3.4 mm and 1 mm i.d circular minichannel.

Keywords: Condensation, VOF simulations, Minichannels, Heat Transfer

1. Introduction

From recent and past literature emerges that correlations originally developed to predict the heat transfer during condensation in convectional channels can be successfully applied also to the minichannel technology at high mass fluxes [1].
At lower mass fluxes the turbulence of the liquid film is negligible and the local heat transfer coefficient is strictly related to the liquid film distribution [2].
In this low mass flux region the predicting procedures may not provide accurate estimations. At these operating conditions, in the literature there are few experimental data for condensation inside single minichannels; the heat transfer is about few watts and the heat transfer coefficient is difficult to measure with low uncertainties. Furthermore, most of the time an "insight view" of the condensation process results experimentally impossible without affecting the phenomenon itself. For this reason it is important to support the experimental investigation with the numerical simulations. With this aim, in present work, the R134a steady annular condensation inside 3.4 mm i.d. minichannel and the unsteady adiabatic annular flow inside 3.4 mm and 1 mm i.d. circular minichannel at low mass velocities have been analyzed by means of VOF simulations, experimental heat transfer measurements and flow visualizations.

2. Steady state numerical simulations

In small diameter channels, the annular flow regime during condensation covers a wide range of vapour qualities. In addition, waves formation at the vapour-liquid interface is reduced if compared to larger diameter channels [3]. As a first step, since the computational effort is lower compared to time-dependent calculations, steady state

numerical simulations are used to investigate annular condensation inside minichannels.
Three-dimensional numerical simulations of R134a condensation have been carried out in a horizontal circular minichannel with an internal diameter D=3.4 mm. Simulations have been performed at 40°C saturation temperature, at a fixed saturation-to-wall temperature difference (T_s-T_w) of 10 K and variable mass fluxes G.
In order to validate the numerical results, experimental data measured during R134a condensation inside a 3.4 mm channel are also reported.

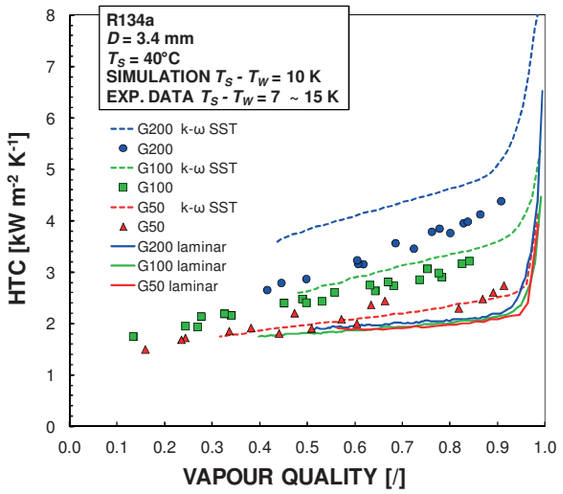

Figure 1. Comparison between experimental and numerical heat transfer coefficient (HTC) during R134a condensation inside 3.4 mm i.d. circular minichannel at 40°C saturation temperature. Mass flux G ranges between 50 kg m^{-2} s^{-1} and 200 kg m^{-2} s^{-1}.

Two different numerical methods have been considered to take into account the occurring or the absence of turbulence inside the liquid film (*k-ω SST* and laminar approach, respectively). As depicted in Fig. 1, for mass velocities G=100 kg m^{-2} s^{-1} and G=200 kg m^{-2} s^{-1} a better prediction of the experimental results can be achieved when the *k-ω SST* turbulence model is used.

3. Waves formation at the vapour-liquid interface

From the experimental visualization performed inside the 3.4 mm minichannel [4], at certain values of mass flux, it can be seen that the liquid interface is irregular with the presence of waves. Steady state simulations cannot account for the presence of waves at the vapour-liquid interface. For this reason, time-dependent numerical simulations have been performed. For computational time saving, a 2-D axisymmetric domain has been considered (zero-gravity). A preliminary result is reported in Fig. 2, where the waves formation during adiabatic flow inside a 3.4 mm and 1 mm i.d. minichannel channel at two different mass fluxes has been analyzed.
The influence of mass flux and tube diameter on the occurrence of interfacial waves has been investigated.

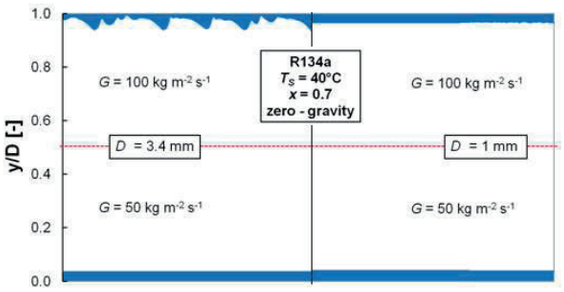

Figure 2. Waves formation at the liquid-vapour interface during R134a adiabatic flow inside a 3.4 mm (left) and 1 mm (right) i.d. circular minichannel, at zero gravity condition and vapour quality x=0.7. Top: G = 100 kg m^{-2} s^{-1}; bottom: G = 50 kg m^{-2} s^{-1}. The ratio y/D is the adimensional channel height.

References

[1] Del Col, D., Bortolato, M., Azzolin, M., Bortolin, S., Condensation heat transfer and two-phase frictional pressure drop in a single minichannel with R1234ze(E) and other refrigerants, *Int. J. Refrig.*, 50, 87–103 (2015).

[2] Liu, N., Li, J., Experimental study on condensation heat transfer of R32, R152a and R22 in horizontal minichannel, *Appl. Therm. Eng.*, 90, 763–773 (2015).

[3] Nema, G., Garimella, S., Fronk, B.M., Flow regime transitions during condensation in microchannel, *Int. J. Refrig.*, 40, 227–240 (2014).

[4] Azzolin, M., Bortolin, S., Del Col, D., Measurements and visualization during condensation inside a 3 mm diameter channel, ICMF-2016 – 9th International Conference on Multiphase Flow May 22nd –27th 2016, Firenze, Italy.

ID 142

5th Micro and Nano Flows Conference
Milan, Italy, 11-14 September 2016

Numerical Study of Heat Transfer Enhancement during Gas-Liquid Taylor Bubble Flow in Mini/Microchannel

Prafulla P. SHEVKAR [1], Manoj K. MOHARANA [2,*]

* Corresponding author: Tel.: ++91 (0)661 246 2533; Fax: ++91 (0)661 247 2926; Email: mkmoharana@gmail.com
1 Graduate Student, Department of Mechanical Engineering, National Institute of Technology Rourkela, Odisha, India
2 Assistant Professor, Department of Mechanical Engineering, National Institute of Technology Rourkela, Odisha, India

Keywords: Taylor bubble flow, microchannel, heat transfer, two-phase flow

Abstract

Taylor bubble flow in microchannel systems play an important role in many industrial applications such as two-phase flow micro heat exchangers, pulsating heat pipes, monolithic reactors, digital microfluidics, microscale mass transfer process, fuel cells, etc. Taylor bubble is formed in capillary tubes when gas-liquid or liquid-liquid flows with particular range of flow rate ratios. In this work, a 3-D numerical study has been carried out using the volume-of-fluid (VOF) method on commercially available Ansys Fluent® for the formation of (i) isolated Taylor bubble, and (ii) a train of Taylor bubbles, in a square channel of side 1.0 mm. At inlet of the capillary tube, gas and liquid flows in co-current flow arrangement neglecting the nozzle thickness. Constant thermo-physical properties are considered for solid and fluid. The flow is hydrodynamically developing at the inlet of the channel. Taylor bubble formed gets stabilized at the entry section of the fluid channel. The Taylor bubble then passes through a square channel (1 mm^2) carved on a solid substrate of size $3 \times 2 \times 30$ mm^3. The flow is hydrodynamically fully developed and thermally developing inside this channel. Constant heat flux is applied on the bottom wall of the substrate (3×30 mm^2), while all other surfaces exposed to the ambient are insulated. To avoid the end effect, the fluid again passes through a capillary tube after it travels the full length of the heated substrate. Thus, three-dimensional Navier-Stokes and energy equations are solved simultaneously. No slip boundary condition is imposed on the inner walls of the channel. Sufficiently fine mesh considered near the boundary to capture liquid film surrounding a Taylor bubble interface near the wall. The liquid film is maintained without its breakup throughout the length of the channel. Grid independence tests are carried out using standard procedure to decide the final mesh size. The method adopted for Taylor bubble formation is validated with existing results.

The objective of this study is to explore heat transfer enhancement due to injection of Taylor bubbles in steady flow, which causes disturbance in the flow field at its head and tail, resulting in mixing in the fluid that shows reduction in wall temperature compared to single phase liquid flow in the channel. The axial variation of bulk fluid temperature shows a footprint of a Taylor bubble at its front end. The average Nusselt number (Nu_{avg}) is calculated based on bulk fluid temperature and average wall temperature of three side walls (except upper wall), which shows increased heat transfer up to 1.2-1.6 times (even more than this) compared to steady single phase liquid flow in the channel. The analysis is carried out for a wide range of capillary numbers (different combination of water and air velocities). It is also attempted to capture the foot print of the bubble. The effect of bubble length and the frequency of bubble occurrence is also studied.

References

[1] Salman, W., Gavriilidis, A., and Angeli, P., 2006, "On the formation of Taylor bubbles in small tubes," Chemical Engg. Science, 61, pp. 6653-6666.

[2] Angeli, P., and Gavriilidis, A., 2008, "Taylor flow in microchannels," In: Li, D., (ed.) Encyclopedia of Microfluidics and Nanofluidics. (1971 - 1976). Springer: New York.

[3] Majumder, A., Mehta, B., and Khandekar, S., 2013, "Local Nusselt number enhancement during gas-liquid Taylor bubble flow in a square mini-channel: An experimental study," Int. J. Thermal Science, 66, pp. 8-18.

[4] Mehta, B., Khandekar, S., 2014, "Measurement of local heat transfer coefficient during gas–liquid Taylor bubble train flow by infra-red thermography," Int. J. Heat Fluid Flow, 45, pp. 41-52.

[5] Gupta, R., Fletcher, D. F., and Haynes, B. S., 2009, "On the CFD modelling of Taylor flow in microchannels," Chemical Engg. Science, 64(12), pp. 2941-2950.

[6] Gupta, R., Fletcher, D. F., and Haynes, B. S., 2010, "CFD modelling of flow and heat transfer in the Taylor flow regime," Chemical Engineering Science 65, pp. 2094–2107.

5th Micro and Nano Flows Conference
Milan, Italy, 11-14 September 2016

ID 143

Pressure Drop Analysis in a Rectangular Microchannel with Staggered Arrangements of Cylindrical Micro Pin Fins

Ali MOHAMMADI [1,*], Ali KOSAR [2]

* Corresponding author: Tel.: ++90 (0)553 1194788; Email: alimohammadi@sabanciuniv.edu
1 & 2: Faculty of Engineering and Natural Sciences (FENS), Mechatronics Engineering Program, Sabanci University, Istanbul, Turkey

Abstract This article presents a computational study on hydrodynamic characteristics of the flow inside a rectangular microchannel with the dimensions of 5000 x 1500 x 100 μm^3 (L x W x H) which includes different staggered arrangements of cylindrical micro pin fins. Three different diameters are considered for micro pin fins which results in three different height to diameter (H/D) ratios of 0.5, 1 and 2. Besides, two different pitch ratios of 1.5 and 3 are considered in the horizontal (S_L/D) and vertical (S_T/D) directions. Thus, totally seven configurations are analyzed using the commercial CFD package of ANSYS v.14.5 software. The simulations are performed for each configuration at four Reynolds numbers of 20, 40, 80 and 120 while a constant heat flux is applied through the bottom surface of the microchannel as well as the liquid interacting surfaces of the micro pin fins. The results showed that a decrease in pin fin diameter (increasing H/D ratio) increases pressure drop and friction factors. Moreover, while utilizing larger S_T/D ratio significantly decreases pressure drop, it has a significant adverse effect on friction factor. Besides, using larger S_L/D ratio results in slightly lower pressure drops and friction factors.

Keywords: Single Phase, Micro Flow, Micro Pin Fins, Staggered, Pressure Drop

1. Introduction

Micro heat sinks are widely used in cooling applications. A common method for achieving heat transfer enhancement is using enhanced surfaces such as micro pin fins. However, this results in higher pressure losses. There are a number of studies to identify the sources of associated pressure loss and to reduce them while maintaining a desirable performance. Kosar et al. [1] experimentally studied the pressure drops in microchannels with different micro pin fin arrangements at Reynolds numbers below 128. Koz et al. [2] did a computational analysis on a single low H/D ratio circular micro pin fin at Reynolds number below 150 with different heat fluxes. In this article, pressure drop and friction factor results of seven staggered arrangements of micro pin fins are presented and the effects of height to diameter ratio (H/D) and different horizontal and vertical pitch ratios (S_L/D and S_T/D) are investigated.

2. Geometrical Modeling:

A 5000 × 1500 × 100 μm^3 (*l x w x h*) rectangular microchannel is modeled with seven different staggered arrangements of circular micro pin fins (MPF) using the same height as h. The specifications of each configuration are presented in Table 1 where L, M and S stand for large, medium and small diameter size. V and H regards to vertical and horizontal directions, and d and s stands for dense and sparse pitch ratios.

Table 1 - Geometrical specifications of configurations

No.	*Name*	*D (μm)*	*H/D*	*S_T/D*	*S_L/D*
1	LV_dH_d	200	0.5	1.5	1.5
2	LV_dH_s	200	0.5	1.5	3
3	MV_dH_d	100	1	1.5	1.5
4	MV_dH_s	100	1	1.5	3
5	MV_sH_d	100	1	3	1.5
6	MV_sH_s	100	1	3	3
7	SV_dH_d	50	2	1.5	1.5

3. Numerical Modeling - Data Reduction:

The simulations are done at four Reynolds numbers of 20, 40, 80 and 120 by specifying the fluid's inlet velocity to the microchannel. The highest Reynolds number corresponds to the inlet velocity of 0.643 m/s. Atmospheric conditions are imposed as the outlet boundary conditions. A constant heat flux of 30 W/cm^2 is applied through the bottom surface and similar heat fluxes are applied through the liquid interacting faces of MPFs. All other surfaces are assumed to be thermally isolated. It is assumed that water remains as liquid at all working temperatures and its thermodynamic properties are set to be temperature dependent. Continuity, momentum and energy equations are solved with the convergence criteria for all residuals to be less than 10^{-5}. Besides, prior to performing the analysis, a grid sensitivity analysis is done and the results of the numerical model is validated using the experimental data of the 2CLD configuration in [3]. Pressure drop and friction factor are obtained using the following expressions:

$$\Delta P = P_{in} - P_{out} \tag{1}$$

$$f = \frac{2\rho\Delta P}{N_{hor.}G^2} \tag{2}$$

where ρ is the fluid's average density, N_{hor} is the number of MPFs in the horizontal direction and G is the mass flux, which is expressed as:

$$G = \frac{\rho Q}{A_{\min}} \tag{3}$$

$$A_{\min} = \frac{S_T - D}{S_T} wh \tag{4}$$

4. Results and Discussion:

Figure 1 shows that the highest pressure drop is obtained in the SV_dH_d configuration which has the smallest diameter size while the lowest pressure drops correspond to the MV_sH_s and MV_sH_d configurations, respectively, which both have larger vertical pitch ratios. The larger horizontal pitch ratio also slightly contributes in decreased pressure drops as can be seen when comparing the MV_sH_s configuration with the MV_sH_d configuration as well as the LV_dH_d configuration with the LV_dH_s configuration.

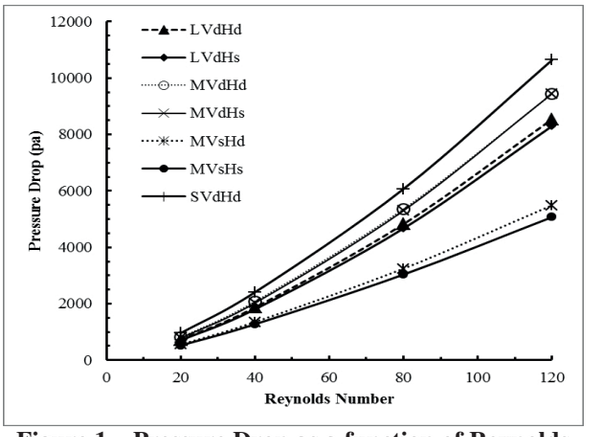

Figure 1 – Pressure Drop as a function of Reynolds

Figure 2 shows that as the diameter increases, friction factor decreases. Also, the larger S_T/D ratio results in significantly higher friction factors. Nevertheless, the larger S_L/D contributes to a decrease in the friction factor.

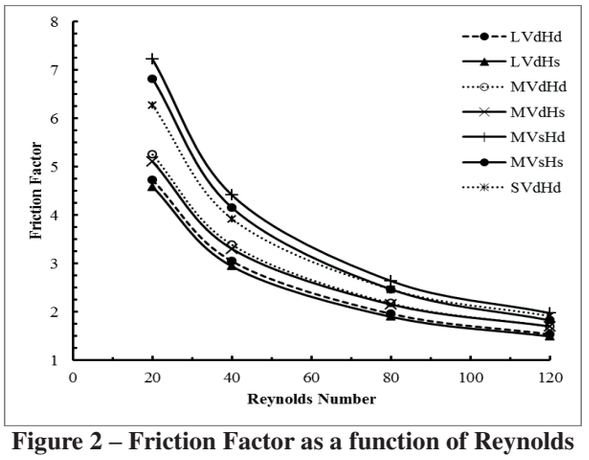

Figure 2 – Friction Factor as a function of Reynolds

References

[1] Koşar, A., Mishra, C., and Peles, Y., 2005, "Laminar Flow Across a Bank of Low Aspect Ratio Micro Pin Fins," J. Fluids Eng., **127**, pp. 419–430.

[2] Koz, M., Ozdemir, M. R., and Koşar, A., 2011, "Parametric study on the effect of end walls on heat transfer and fluid flow across a micro pin-fin," Int. J. Therm. Sci., **50**, pp. 1073–1084.

[3] Kosar, A., and Peles, Y., 2007, "Micro scale pin fin heat sinks -Parametric performance evaluation study," IEEE Trans. Components Packag. Technol., **30**, pp. 855–865.

5th Micro and Nano Flows Conference
Milan, Italy, 11-14 September 2016

Analysis and design of a new micropump doable with a simple micro-fabrication process

Raffaele ARDITO [1,*], Emanuele BERTARELLI [1], Alberto CORIGLIANO [1], Marco FERRERA [2]

* Corresponding author: Tel.: ++39 02 23994272; Email: raffaele.ardito@polimi.it
1 Department of Civil and Environmental Engineering, Politecnico di Milano, Italy
2 ST Microelectronics, Agrate Brianza (MI), Italy

Keywords: Micropump, Orthoplanar valves, MEMS, Multiphysics simulation

Silicon micropumps [1] are the "heart" of active microfluidic systems that allow one to perform precise manipulation of fluids for many applications, e.g. Drug Delivery Systems (DDS), biological fluids handling and thermal management of electronic components. In particular, focus is on the so-called diaphragm displacement micropump, which uses the mechanical oscillation of a thin plate in order to displace fluid. With the recent advancements in microfabrication techniques, pursuing more compact dimensions and enhancing pump performances while lowering power consumption has become a main trend.

This work presents the modelling and the design of a new diaphragm micropump, with the main purpose of achieving good pumping performances along with easy and cheap fabrication. The new device (patent pending, see [2]) is fully compatible with standard micromachining processes customarily adopted in the field of microsystems or microelectromechanical systems (MEMS), hence it can be easily industrialized. The proposed design aims at manufacturing a compact device, which can be easily coupled with the control circuitry and suitable sensors. The research activities have been referred to the geometry and the peculiar features of the device (double-diaphragm symmetric actuation, passive inlet valve, active/passive outlet valve for easy priming), as well as the manufacturing process to be adopted (surface micromachining on two facing wafers). The innovative design intends to solve the following technical problem: to realize a micropump with integrated valves by using two silicon wafers only, without the introduction of materials (e.g. piezoelectric) which are not adopted in the most common MEMS fabrication processes. It is worth noting that previously introduced designs require the stacking of several layers, thus entailing higher production costs and complexity. Moreover, electrostatic actuation is highly compatible with the aforementioned machining techniques, while it does not require the use of external drivers. A double-diaphragm symmetric actuation is introduced, in order to improve the pumping efficiency; to this purpose, the height of the pumping chamber can be freely decided, thus avoiding the problem of small compression ratio shown by previous proposals. The device is endowed with pre-loaded ortho-planar valves: in this way, the leakage problems (typical of flaps valves) are circumvented. We have adopted a passive inlet valve and an active/passive outlet valve for easy priming.

The performances of the proposed design have been evaluated on the basis of multi-physics simulation, carried out by means of the Finite Element method. Moreover, the preliminary parametric analyses have required the development of ad hoc simulation techniques [3], which allowed for the fast execution of different analysis for various geometric configurations. The achieved results revealed the good performances and the reliability of the proposed micropump, also confirmed by some experimental tests on specific parts of the device [4].

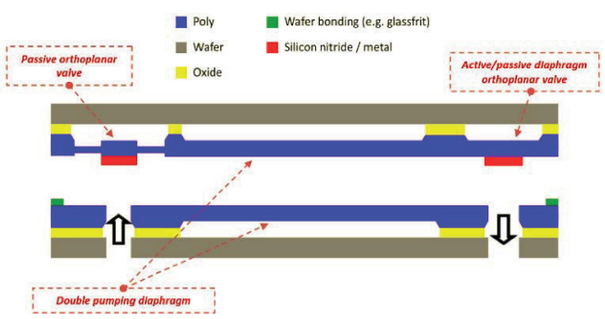

Fig. 1. Scheme of the proposed micropump: cross-section view of the circular pumping chamber with two lateral chambers for hosting the valves.

References

[1] Iverson, B., Garimella, S., 2008. Recent advances in microscale pumping. Microfl. and Nanofluidics 5, 145–174.

[2] Corigliano, A., Ardito, R., Bertarelli, E., Ferrera, M., 2015. Micropompa con attuazione elettrostatica, Italian pending patent n. 102015000030182.

[3] Bertarelli, E., Ardito, R., Corigliano, A., Contro, R., 2011. A plate model for the evaluation of pull-in instability occurrence in electrostatic micropump diaphragms. Int. J. of Appl. Mech. 3, 1-19.

[4] Bertarelli, E., Colnago, A., Ardito, R., Dubini, G., Corigliano A., 2015. Modelling and characterization of circular microplate electrostatic actuators for micropump applications, Proc. 16th Int. Conf. EuroSimE 2015, art. no. 7103121.

5th Micro and Nano Flows Conference
Milan, Italy, 11-14 September 2016

Design and process optimization in microfluidic devices for DNA amplification

Ioanna N. KEFALA, Vasileios E. PAPADOPOULOS, Georgia KAPROU, George KOKKORIS *, Angeliki TSEREPI

* Corresponding author: Tel.: ++30 2106503238; Fax: ++30 210 6511723; Email: g.kokkoris@inn.demokritos.gr
Institute of Nanoscience & Nanotechnology, NCSR "Demokritos", Greece

Keywords: LoC, PCR, isothermal amplification, HDA

A microfluidic device for DNA amplification is a critical component of lab-on-chip (LoC) systems intended for diagnostics. A typical process for DNA amplification is the Polymerase chain reaction (PCR), performed in continuous flow or static chamber microfluidic devices, where the DNA sample flows through three separate zones: Denaturation (92-98 ^{o}C), where DNA bonds are disrupted, annealing (50-60 ^{o}C), where primers denote the part of the DNA chain to be replicated, and extension (68-72 ^{o}C), catalyzed by Polymerase, which replicates the denoted DNA part [1]. Moreover, recent studies in molecular biology have offered isothermal processes for DNA amplification such as loop-mediated isothermal amplification (LAMP), rolling circle amplification (RCA), single stranded displacement amplification (SDA), Recombinase Polymerase amplification (RPA), and Helicase dependent amplification (HDA) [2]. All processes are temperature sensitive and (most of them) are facilitated in microfluidic devices with integrated heating elements.

This work focuses on the design of microfluidic devices fabricated with flexible printed circuit (FPC) or printed circuit board (PCB) technologies which allow integration of the heating elements on the same substrate. Commercial thin polymeric films are used as structural materials for the microfluidic channels, while the integrated metallic layers are used for realizing the resistive microheaters [3].

The objective of this work is the design and the process optimization of DNA amplification devices based on PCR and HDA processes. For the PCR microfluidic device, the focus is on the temperature uniformity of the heated zones and the thermal isolation between them. For the HDA device, the focus is on reaction kinetics. The design and the optimization are performed by a computational study. The mathematical model consists of a detailed 3d model which couples fluid flow, heat transfer, mass conservation of species, and Joule heating equations. The equations are numerically solved by the finite element method implemented by the commercial code COMSOL.

Calculations for the PCR microfluidic device show that the low thermal conductivity and the small thickness of the polymeric films (polyimide in our case) allow for temperature uniformity when the footprint of the device is large enough [3, 4]. However, when the desired device footprint is small, one metallic layer is not enough and multiple metallic layers in a PCB are required to achieve the necessary-for-heating total resistance of the heating elements. The combination of layers with higher thermal conductivity (such as the materials used in PCBs) and the increase of the thickness of the stack make the design a challenging task.

The results in Fig. 1 refer to a case of a continuous flow PCR microfluidic device where an optimization of the distances between the heating elements has been performed; the calculations correspond to the unit cell of the device, where one thermal cycle takes place. Fig 1a shows the fluid temperature at the middle height of the microfluidic channel and Fig. 1b shows the fluid temperature along the channel axis. The optimized distances allow good thermal isolation between the heated zones and the achievement of the desired temperature at each zone.

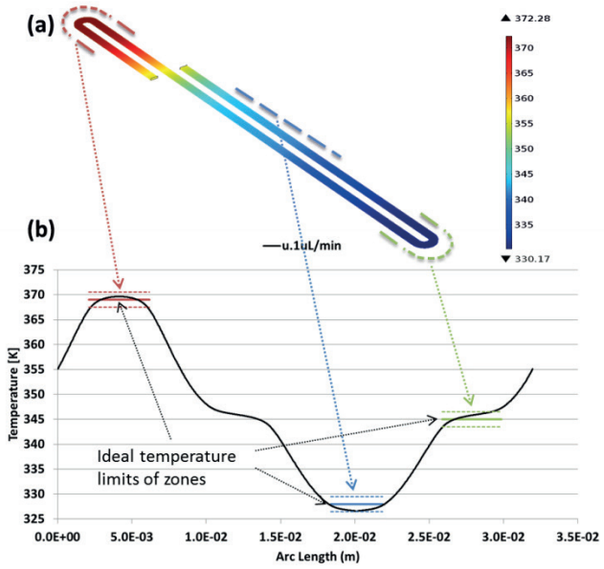

Figure 1. Results for a small footprint continuous flow PCR microfluidic device. (a) Fluid temperature at the mean height of the microfluidic channel. (b) Fluid temperature along the channel axis.

Regarding the microfluidic device for HDA [5], preliminary results on HDA reaction kinetics will be presented.

[1]. Kopp M. U., Mello A. J. d., and Manz A., Science. **280**:1046-1048 (1998)
[2]. Tong Y., Tang W., Kim H. J., Pan X., Ranalli T., and Kong H., Biotechniques. **45**:543-57 (2008)
[3]. Moschou D., Vourdas N., Kokkoris G., Papadakis G., Parthenios J., Chatzandroulis S., *et al.*, Sensors and Actuators B: Chemical. **199**:470-478 (2014)
[4]. Papadopoulos V. E., Kokkoris G., Kefala I. N., and Tserepi A., Microfluidics and Nanofluidics. **19**:867-882 (2015)
[5]. Kaprou G., Papadakis G., Kokkoris G., Papadopoulos V., Kefala I., Papageorgiou D., *et al.*, Proc. Conf. Bio-MEMS and Medical Microdevices II Conference (2015).

Measurement of thermal transpiration flow through a microtube

Jie CHEN, Marcos ROJAS-CARDENAS, Lucien BALDAS, Stéphane COLIN*, Christine BARROT

* Corresponding author: Tel.: ++33 (0)5 61 17 10 95; Email: colin@insa-toulouse.fr
Institut Clément Ader (ICA), Université de Toulouse, CNRS-INSA-ISAE-Mines Albi-UPS, Toulouse France

Keywords: rarefied gas, thermal transpiration

In confined rarefied gases, one can generate a flow by solely applying a tangential temperature gradient along a wall: without any initial pressure gradient, the gas macroscopically moves from the cold to the hot region. This phenomenon is the so-called thermal creep or thermal transpiration effect and it is the main operating principle of the well-known Knudsen compressor, which can generate gas pumping without the need of moving parts [1]. A recent experimental study on thermal transpiration has produced results for some characteristic parameters associated to this phenomenon, such as the thermal molecular pressure difference (TPD) at the final zero-flow stage, the stationary mass flow rate and the characteristic time of the system [2]. However, experimental results on thermal transpiration, especially regarding the thermally driven mass flow rate and characteristic times of the pumping system, are still lacking in the literature. Many important characteristics of this type of flow cannot yet be accurately analyzed.

In this study, a new experimental set-up for investigating a thermal transpiration flow through a single micro-tube is presented (Fig. 1). The experimental apparatus has been designed in order to be adaptable to test other geometries and finally Knudsen compressors, too. The experimental set-up is composed of four main parts: (i) the test section, where the microsystem, such as a micro-tube or a Knudsen pump, can be connected; (ii) the measurement ring section, composed of two reservoirs coupled to capacitance diaphragm pressure gauges (CGA and CGB) and thermocouples (T_A and T_B); (iii) the temperature control system, consisting of a heater made of constantan wire, a Peltier module and its controller, three thermocouples and a power supply; and (iv) the accessories section, composed of a turbomolecular pump, supply gas tanks and the acquisition system. One of the most important features of this set-up is that the tested microsystems are easily interchangeable. Moreover, the independent and punctual temperature control system can provide desired temperatures at any place in the microsystem.

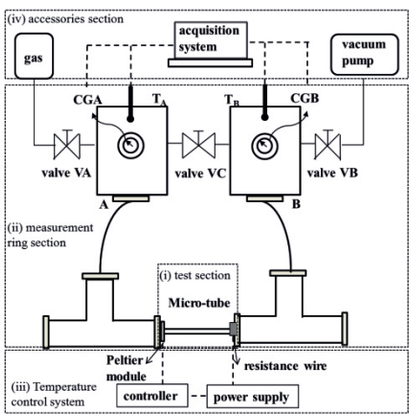

Figure 1: Schematic diagram of the experimental set-up

In order to test our experimental apparatus, a single glass micro-tube configuration has been mounted at the test section. The diameter of the tube is $D = 503.97$ μm and the effective length where the temperature gradient is imposed is $L = 52.01$ mm. One side of the tube is heated at an adjustable temperature while the other side is just cooled by the ambient air. Only a small zone near the hot side of the tube is at a relative high temperature, thus the temperature of both reservoirs can be considered close to the ambient temperature of 298 K, which is the ideal operating temperature of the pressure gauges used here. This configuration should avoid any possible parasite thermal transpiration flows inside theses gauges.

At first, the influence of the rarefaction level of the gas is studied. Figure 2 shows the TPD values obtained in the present study by applying a temperature difference of 45 K to the tube ($T_1 = 295$ K, $T_2 = 340$ K). These values are compared to results reported in [2]. The characteristic time of our experiments is of the order of 20 min, to be compared with the 100 s reported in [2], which provides the possibility of studying the transitional stage more accurately. The great difference between the characteristic times of the two experiments is due to the difference in the tank dimensions of both configurations. The volumes used in our configuration correspond to 5.7 times the volumes employed in [2]. Moreover, the influence of temperature differences and temperature distributions (exponential one and quasi-linear one) along the tube are presented and discussed.

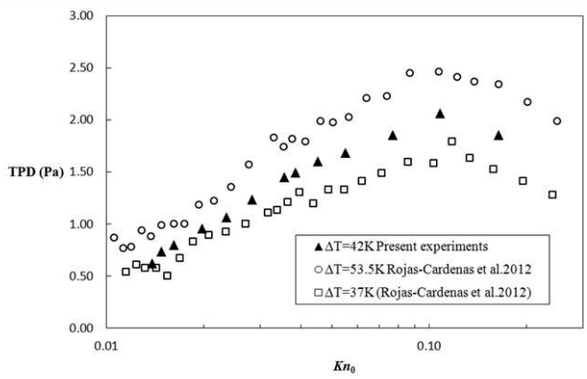

Figure 2: Thermal molecular pressure difference (TPD) versus Knudsen number

References

1. J. Chen, L. Baldas, S. Colin, Numerical study of thermal creep flow between two ratchet surfaces, Vacuum, 109, 294-301, 2014.
2. M. Rojas-Cardenas, I. Graur, P. Perrier, and J.G. Méolans, Time-dependent experimental analysis of a thermal transpiration rarefied gas flow, Physics of Fluids, 25(7), 0720012013, 2013.

5th Micro and Nano Flows Conference
Milan, Italy, 11-14 September 2016

ID 148

Parametrization study of the thermally driven rarefied flow between saw-tooth like surfaces

Giorgos TATSIOS[1,*], Dimitris VALOUGEORGIS[1], Jie CHEN[2], Lucien BALDAS[2], Stephane COLIN[2], Stefan STEFANOV[3]

* Corresponding author: Tel.: ++30 24210 74309; Fax: ++30 24210 74085; Email: tatsios@mie.uth.gr
1 Dept. of Mechanical Engineering, University of Thessaly, Greece
2 Institut Clément Ader (ICA), Université de Toulouse, CNRS-INSA-ISAE-Mines Albi-UPS, Toulouse France
3 Institute of Mechanics, Bulgarian Academy of Science, Bulgaria

Abstract Recently, a novel configuration of a thermally driven pump has been proposed, where the induced net flow in a gas confined between two saw-tooth like isothermal surfaces kept at different temperatures is produced, based on the principal of the thermal-stress flow. Here, the performance of this design is numerically investigated by a parametric study. Simulations are performed via the Shakhov model, solved on a triangular grid to perfectly fit the flow boundaries. The effect of all parameters, including the Knudsen number, the temperature ratio and the geometry, on the flow patterns and net flow rate are examined.

Keywords: Thermally driven flow, Knudsen number, micro-pump, rarefied gas dynamics.

1. Introduction

Based on the principles of the classic Knudsen pump, various configurations of thermally driven gas micro-pumps have been proposed, with most of them relying on the thermal transpiration mechanism. However, in miniature devices, it is hard to maintain the large temperature gradients needed along the pump surfaces. Recently, a novel configuration for a thermally driven pump has been proposed, utilizing the thermal-stress flow in order to induce a net mass flow rate in a gas confined between two saw-tooth like isothermal surfaces kept at different temperatures. This configuration has been numerically investigated in [1] using a hydrodynamic approach and in [2] using the Direct Simulation Monte Carlo (DSMC) method.

In the present work the same setup is simulated via a deterministic approach by the direct solution of the nonlinear Shakhov kinetic model equation. The validity of kinetic modeling is demonstrated by a comparison with corresponding DSMC results and then, a parametrization study is performed to optimize performance design. In general, in low speed flows, kinetic solvers are computationally more effective than the DSMC approach.

2. Flow Configuration

The examined configuration is shown in Fig. 1, where the top and bottom walls are kept at temperatures T_1 and T_2 respectively, ($T_2 > T_1$), which are maintained constant, while periodic boundary conditions are applied at the two side boundaries. Due to the temperature difference two counter-rotating vortices are formed which drive the flow and finally induce a net mass flow rate. A maximum value of the net mass flow rate is observed in the early slip regime [2]. The temperature driven flow is characterized by the Knudsen number Kn (or the rarefaction parameter $\delta \sim 1/Kn$), the temperature ratio, the working gas and the geometrical parameters of the periodic saw-tooth like channels. The effect that each one of those parameters has on the flow is analyzed, in order to fully reveal the advantages and drawbacks of the design. Apart from those operational parameters, the partial momentum and thermal accommodation on the walls is important. Simulations are conducted for

various temperature ratios, corresponding to small, medium and large temperature differences in a wide range of the Knudsen number.

3. Modeling and Results

The flow is modeled by the nonlinear Shakhov model equation, which is solved numerically by the Discrete Velocity Method (DVM) in the velocity space and typical finite differencing in the physical space, using an unstructured triangular mesh to perfectly fit the flow setup boundaries. More importantly, a recently developed algorithm is introduced, to allow the implementation of marching through the physical grid even in the present case of unstructured meshes. Based on this advancement, the simulation is performed, following the particle trajectories in a properly indexed grid, while the method of characteristics is used for the solution of the kinetic equation at each physical element. Based on this development there is no need of matrix inversion in solving the deduced algebraic system in each DVM iteration.

Indicative results are shown in Fig. 1, where streamlines and temperature contours are plotted for $L/d=4$, $l=L/4$, $h/d=1.5$ and $\alpha=0.422\pi$ (these geometrical parameters are defined in Fig. 1a). It is seen that for $\delta=1$ there is a wavy net flow, moving along the center of the channel between the stationary vortices appearing in the lower and upper grooves of the periodic channel. For $\delta=0.5$ the net flow is in the opposite direction and follows a different path. It is moving along the upper part of the cold wall, through the region between the vortices and finally along the hot wall. These routes are shown with red lines in Fig. 1. For $T_1=300\,\mathrm{K}$, $d=1\,\mu\mathrm{m}$ and a width of $20\,\mu\mathrm{m}$ with Ar as the working fluid, the net mass flow rate for $\delta=1$ is of the order of 10^{-13} kg/s, while for $\delta=0.5$ it is one order of magnitude smaller. This analysis is generalized for various values of the involved parameters in an effort to optimize the design.

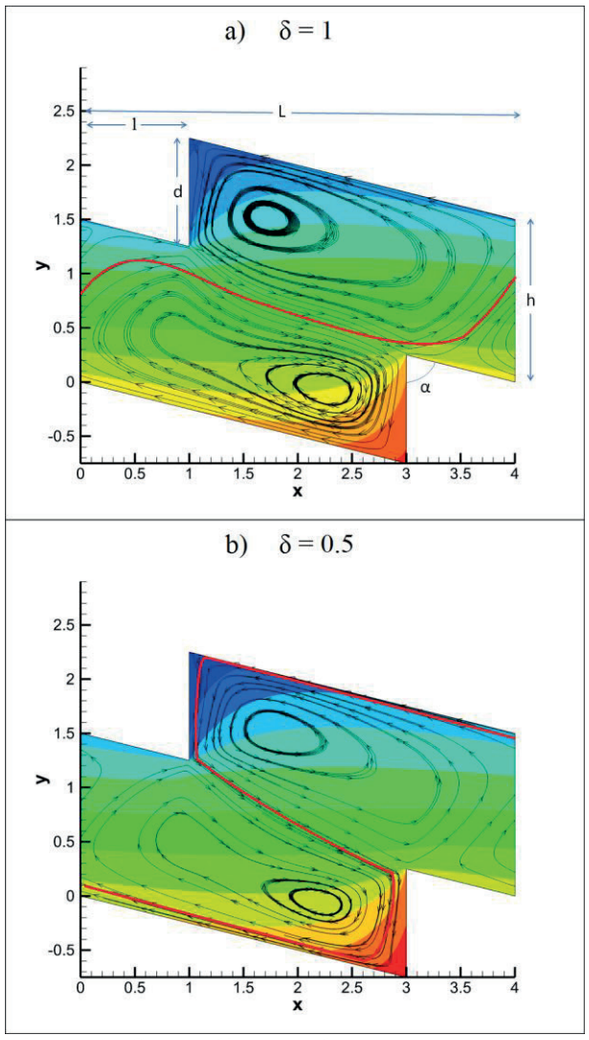

Figure 1: Streamlines and temperature contours for a specific saw-tooth geometry with $T_2/T_1=2$ and $\delta=1$ (top), $\delta=0.5$ (bottom).

Acknowledgments

This research has received funding from the EU Framework Programme Horizon 2020 (MSCA-ITN-2014) under Grant agreement no 643095 (MIGRATE).

References

1. J. Chen, L. Baldas, S. Colin, Vacuum, 109, 294-301, 2014.
2. J. Chen, S. Stefanov, L. Baldas, S. Colin, International Journal of Heat and Mass Transfer, 2016, in press.
DOI: 10.1016/j.ijheatmasstransfer.2016.04.023.

5th Micro and Nano Flows Conference
Milan, Italy, 11-14 September 2016

Cyclic uniaxial strain on 3D microconstructs: a novel heart-on-a-chip platform for the generation of functional cardiac microtissues

Anna MARSANO [1], Chiara CONFICCONI [1,2] , Marta LEMME [1,2], Paola OCCHETTA [2], Emanuele GAUDIELLO [1], Emiliano VOTTA [2], Giulia CERINO [1], Alberto REDAELLI [2], Marco RASPONI [2,*]

* Corresponding author: Tel.: +39 02 2399 3377; Email: marco.rasponi@polimi.it
1: Departments of Surgery and Biomedicine, University Basel, University Hospital Basel, Basel, Switzerland
2: Department of Electronics, Information and Bioengineering, Politecnico di Milano, Italy

Keywords: Heart-on-a-chip, Cardiac tissue engineering, induced Pluripotent Stem Cells

To date, the generation of functional micro-cardiac tissues still remains an open issue. *In vivo*, cardiac cells undergo multiple cues deriving from the local heart tissue "niche", which instructs cells through dynamic biochemical, electrical and mechanical signaling, eventually guiding tissue development and maturation. In particular, cardiomyocytes (CMs) are subjected to periodic contraction/relaxation sequences deriving from the beating of the heart [1,2]. A robust and predictive *in vitro* model of mature cardiac tissues should thus enable the recapitulation of (i) the three-dimensional (3D) architecture of complex cell-cell and cell-extracellular matrix (ECM) interactions and (ii) electro-mechanical stimuli resembling the native myocardial environment, (iii) in the presence of controlled biochemical signals [3].

Materials and Methods

Here, we report a new method to generate mature and highly functional cardiac microtissues within perfused microfluidic devices. To this purpose, an innovative micro-bioreactor for the culture of 3D cell constructs was designed, able to recapitulate the physiological strains experienced by cells in the native myocardium (range 10-15%). Briefly, an array of posts was implemented to confine and culture cell-laden gels, and a pneumatic actuation system was embedded to induce uniaxial cyclic strains to the 3D constructs (generated by neonatal rat or human pluripotent derived cardiomyocytes). The presence of auxiliary channels allowed to perfuse medium during culture, while providing biochemical stimulation and transporting pacing signals during the functional evaluation of tissues.

Results

As shown in the figure, stimulated cardiac constructs expressed higher levels of connexin-43 (Cx43) compared to the 3D static culture condition, suggesting superior electrical connection among neighboring cells and cardiac maturation. Interestingly, stimulated constructs highlighted higher cell viability with respect to control. Moreover, the cyclic mechanical stimulation promoted spontaneous synchronous beating of the constructs, all over their volume. Electric pacing experiments further demonstrated the superior maturation of the stimulated constructs.

Conclusion

We introduced a novel heart-on-a-chip platform able generate functional cardiac microtissues from either neonatal rat or human pluripotent derived cardiomyocytes. This result was achieved through the application of a highly controlled cyclic uniaxial strain to 3D microtissues in culture. The compatibility with electrical pacing makes the platform suitable for both high-throughput pre-clinical drug screenings and physio/pathological states investigations.

References

[1] A. Salameh, A. Wustmann, S. Karl, K. Blanke, D. Apel, D. Rojas-Gomez, H. Franke, F. W. Mohr, J. Janousek and S. Dhein, Circulation research, 2010, 106, 1592-1602.

[2] X. Trepat, L. Deng, S. S. An, D. Navajas, D. J. Tschumperlin, W. T. Gerthoffer, J. P. Butler and J. J. Fredberg, Nature, 2007, 447, 592-595.

[3] H. Parsa, K. Ronaldson and G. Vunjak-Novakovic, Advanced drug delivery reviews, 2015.

Fluid Flow and Heat Transfer of a Non-Newtonian Fluid in a Micro -Annulus in the Presence of Viscous Dissipation

Marco LORENZINI [1,*], Irene DAPRA' [2], Giambattista SCARPI[2]

* Corresponding author: Tel.: ++39 0543 374455; Fax: ++39 0543 374444; Email: marco.lorenzini@unibo.it
1 School of Engineering and Architecture Università di Bologna, Forlì, ITALY
2 Dipartimento di Ingegneria Civile, Chimica, Ambientale e dei Materiali – Bologna, ITALY

Keywords: Micro Flow, Non-Newtonian fluid, annular flow, viscous dissipation

Annular geometries with the inner represent the reference model for a number of technical applications, such as journal bearings, viscometry, drilling etc. The annular gap may be filled by fluids which cannot be modelled as Newtonian, as is the case for emulsions, rather more complex rheological models such as that of Giesekus must be used. In the manufacturing of micro-holes, the desired geometry may be achieved by the use of peck-drilling, which involves the use of an emulsion acting as a coolant. Under these conditions, the rheological and thermal behavior of the cooling fluid is important to correctly set drilling parameters. This work analyzes the fluid dynamical and thermal behavior of a Giesekus fluid in a rotating annulus in the presence of viscous dissipation and non-isothermal flow.

The Giesekus model characterizes a fluid through use of three physical parameters: viscosity, mobility factor and relaxation time. Many previous works have proposed analytical solutions for the velocity profile based on a linear approximation, which makes mathematical treatment easier but restricts the validity of the results to a comparatively small range in the values of the parameters involved. A recent work by Daprà and Scarpi [1] proposed an analytical solution for the flow in an annulus with the inner wall rotating and the outer wall at rest, which takes into account the non-linearity in the constitutive equation for different values of the inner-to-outer-diameter ratio k and wide ranges of the mobility factor α and the Deborah number De, as shown in Fig. 1, for k=0.5 and different values of the De, De=0 corresponding to a Newtonian fluid behavior.

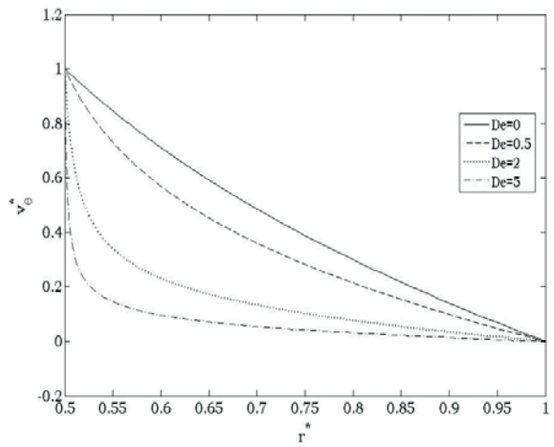

Figure 1 – Velocity profiles in the rotating annulus.

As can be seen from the plot, the velocity gradients for increasing values of De become confined to a short distance from the rotating wall, which modifies the stress distribution and causes a sharp decrease of the friction factor, as exemplified by the ratio of the Poiseuille numbers (related to the Fanning friction factor) Po/Po_N, which is always below unity and decreases as De increases, Po_N being the Poiseuille number for a Newtonian fluid.

The energy equation is also solved accounting for viscous dissipation as embodied by the Brinkman number. Concerning the latter, the classical expression which contains a viscosity independent of the shear rate and is thus inapplicable when Giesekus fluids are involved, as pointed out by Coelho and Faria [2]. As a consequence, a new definition of the Brinkman number for the geometry and fluid involved is given, which is based on the original meaning of the Brinkman number, i.e. the ratio of the work dissipated due to friction to the heat transfer rate at between fluid and walls.

As the velocity profile differs from that of a Newtonian fluid, also the temperature profile is affected: the influence of the Deborah number and mobility factor is investigated and it is found that the increase in De and a abate the maximum temperature significantly, thus allowing higher rotation speeds than in the case of a Newtonian fluid, as seen in Figure 2.

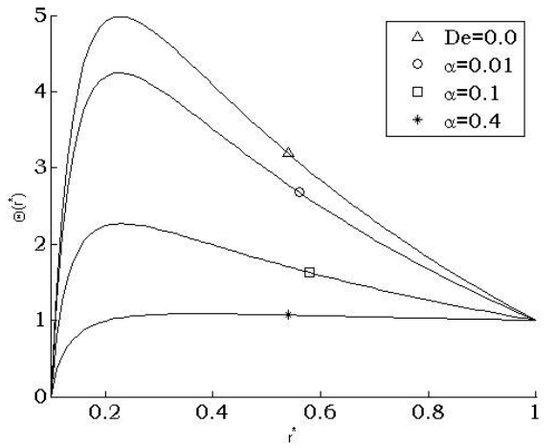

Figure 2 –Non-dimensional temperature profile for different α.

References

[1] I. Daprà, G. Scarpi, Analytical solution for a Couette flow of a Giesekus fluid in a concentric annulus, *Journal of Non-Newtonian Fluid Mechanics*, (223), 221-227, 2015.

[2] P.M. Coelho, J.C. Faria On the Generalized Brinkman Number Definition and Its Importance for Bingham Fluids, *Journal of Heat Transfer* (133), 054505, 2011.

ID 155

5th Micro and Nano Flows Conference
Milan, Italy, 11-14 September 2016

Fluid dynamic modeling of a size-based sorter Lab-on-chip for the inertial trapping of circulating tumor cells

Annalisa VOLPE [1,2,*], Antonio ANCONA [2], Giuseppe PASCAZIO [3]

* Corresponding author: Tel.: ++39 080 5442397; Fax: ++39 080 5442219; Email: annalisa.volpe@ifn.cnr.it
1 Department of Physics, University of Bari, Italy
2 Institute for Photonics and Nanotecnology (CNR), Bari, Italy
3 Dipartimento di Meccanica, Matematica e Management, Politecnico di Bari, Italy

Keywords: Lattice Boltzmann Method, Microfluidic, Circulating Tumor Cells, Particle Trapping, Numerical Simulations

1 Abstract

Presence and frequency of circulating tumor cells (CTCs) in bloodstream of patients with epithelial cancers (carcinomas) is an important intermediate step in cancer metastasis and provides a routinely valuable insights associated with disease stage and treatment evaluations without the inconvenience of obtaining fresh tissue biopsy.
Despite significant clinical relevance, progress on CTCs research is hindered by the lack of efficient and robust CTCs separation techniques due to their extremely rare occurrence (1–100 CTCs per 10^9 blood cells). This, coupled with their highly heterogeneous morphologies and molecular signatures, makes their isolation from blood technically challenging and limits their use as potential cancer biomarkers in clinical cancer management.
The application of microfluidics based technologies for CTCs separation is an attractive tool which not only offers control of the microenvironment during separation but also facilitates integration and automation for high throughput sample processing. Current microfluidic CTCs isolation technologies are primarily based on physical/size based filtration (CTCs have 2-3 times the red blood cell dimensions) [1,2] or immuno-mediated CTCs capture in surface functionalized channels or microstructures [3].
In particular in the last years it has been demonstrated that inertial forces can be exploited for high throughput, size based particle and cell separation. Thanks to a balance of hydrodynamic forces, the particles flowing in a micro-channel can migrate across streamlines to focus at distinct positions. Using expansion-contraction of reservoirs, multiple laminar vortices are generated in the channel expansion. The cell focused in proximity of the wall, larger than a defined cut-off size, are trapped in these vortices and then separated from the other cells [4].
Several groups have investigated how to improve the performance of these completely inertial-based microfluidic devices [1,5].
In this work we study the performance of a completely inertial-based microfluidic device using numerical simulations based on a lattice-Boltzmann method in order to select an appropriate geometry and its effectiveness. A first chosen geometry is shown in Fig. 1. It is based on a straight microchannel, followed downstream by a channel expansion (microchamber) with outlets as a powerful unit for continuous inertial separation.

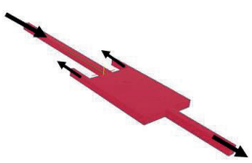

Fig.1: Microfluidic device scheme: the flow enters from the main rectangular cross section channel (on the left of the image). The outflows are located in the other three channels.

The lattice-Boltzmann method (LBM) using the Palabos open-source CFD solver [6] is employed to solve the incompressible, time-dependent Navier-Stokes equations numerically. We employ the Guo off-lattice boundary condition to describe the confining walls. It is noteworthy that such a model allows one to employ a fixed space discretization and geometries described by an STL file, so that the investigation of different geometrical configurations is straightforward.
A constant mass flow is imposed at the inlet by means of a velocity Poiseuille profile and the velocity is exactly zero on the walls.
Firstly, a series of simulations without particles to validate the flow assumption (which predicts that the average flow velocity should be strictly proportional to the applied pressure gradient) have been run.
The influence of the Reynold number (Re) on the stream tracer distribution in the chamber has been studied for different aspect ratios of the outlet channel. In the microchamber the fluid is separated into main flow, sheath flow and vortex. Simulation results show how the boundary of the main flow and the sheath flow change depending on the Re value, thus affecting the sorting efficiency. Whereas, keeping fixed Re, and varying the output pressure (changing the outlet channels aspect ratios), the boundary position is affected.
Afterwards, we simulate the injection of neutrally buoyant particles into the inlet and their interacting with each other and with the fluid flow. The particles motion is governed by the Newton's law, where the force is computed from the relative fluid velocity (with friction) and from the interaction with nearby particles.
Results of these simulations will pave the way towards the design and fabrication of a fully inertial sorting lab-on-chip (LOC) device.

2 References

[1] X. Wang and I. Papautsky, Size-based microfluidic multimodal microparticle sorter, Lab Chip 15, 1350–1359, 2015.
[2] H. W. Hou, M. E. Warkiani, B. L. Khoo, Z. R. Li, R. A. Soo, D. S.W. Tan, W. T. Lim, J. Han, A. Asgar, S. Bhagat, Isolation and retrieval of circulating tumor cells using centrifugal forces Scientific Reports 3, 1259 (2013).
[3] J. P. Gleghorn et al., Capture of circulating tumor cells from whole blood of prostate cancer patients using geometrically enhanced differential immunocapture (GEDI) and a prostate-specific antibody. Lab Chip 10, 27–29, 2010.
[4] Hydrodynamic mechanisms of cell and particle trapping in microfluidics, A. Karimi,1 S. Yazdi,2 and A. M. Ardekani, Biomicrofluidics 7, 021501, 2013.
[5] D. Di Carlo, D. Irimia, R. G. Tompkins, M. Toner, Continuous inertial focusing, ordering, and separation of particles in microchannels. Proc. Natl. Acad. Sci. U. S. A. 104, 18892–18897, 2007.
[6] http://www.palabos.org/

5th Micro and Nano Flows Conference
Milan, Italy, 11-14 September 2016

ID 162

Fundamental Issues Related to Flow Boiling and Two-Phase Flow Patterns in Microchannels - Experimental Challenges and Opportunities

Vladimir V. KUZNETSOV

Tel.: +7 (383)3307121; Fax: +7 (383)3308480; Email: vladkuz@itp.nsc.ru
Kutateladze Institute of Thermophysics SB RAS, Russia

Abstract The characteristics of gas-liquid two-phase flow and the regularities of the heat transfer during flow boiling in non-circular microchannels, resulting from the experimental and theoretical studies, are discussed in this paper. A new approach for prediction of the transition to annular flow is proposed and verified experimentally using the statistical characteristics of the gas-liquid flow. A convective evaporation model for the annular flow with curved and ruptured liquid microfilm is proposed and discussed. Combined model of flow boiling heat transfer for non-circular microchannel and microchannel heat sink unifying the phenomena of nucleate boiling suppression and heat transfer enhancement for extremely thin liquid film is presented. The examples of model validation based on experiments with refrigerants and water are discussed.

Keywords: Flow Boiling, Evaporation, Gas-Liquid Flow Patterns, Non-Circular Microchannel

1. Introduction

In recent years, flow boiling in microchannels has received considerable attention due to its capability for thermal management of microelectronics, compact two-phase cooling systems and micro-evaporators. The present paper is focused at understanding the mechanisms of flow boiling heat transfer in non-circular microchannels in an attempt to identify methods to improve the heat transfer performance. Using dual-beam laser scanning and laser induced fluorescence statistical characteristics of gas-liquid flow are analyzed to identify the flow patterns. The annular flow model for evaporation in non-circular microchannel is presented and discussed including the recent analysis of liquid film rupture and rivulet evaporation. Combined model for calculating of the flow boiling heat transfer in microchannels is proposed and verified experimentally.

2. Gas-Liquid Flow Patterns

2.1 Statistical analysis of the flow

To further explore the scale effects on gas-liquid flow in microchannels, a scaling analysis is presented in this paper to identify the effect of various forces on Taylor flow. Statistical analysis of the duration of gas and liquid phase existence is performed for water-nitrogen flow using the laser flow scanning [1]. It is shown that highest values of the overall variance correspond to the transition to annular flow. An equivalent film thickness approach to the prediction of the transition from Taylor to annular flow is proposed and verified experimentally. For annular flow the film thickness is measured using laser-induced fluorescence and it was shown that capillary forces deform the interface in microchannels. Flow patterns for refrigerants flow boiling at different reduced pressures are discussed also.

2.2 Annular flow model for microchannel

Convective evaporation model at annular flow is of fundamental importance for the prediction of flow boiling in microchannels. The modeling suite for non-circle channel [2] based on the allocation of two zones of the liquid flow: flow in the menisci near the corners and film flow on the channel walls, is modified to account the peculiarities of film flow in rectangular channel and wall roughness effect. Proposed model considers the peculiarities of heat transfer enhancement

after breaking of the evaporating liquid film. It is shown that in vicinity of contact line the interface shape and heat transfer are determined by the capillary forces and evaporation rate. The calculations for adiabatic annular flow show non-uniform liquid film thickness in a channel cross-section and are in agreement with the LIF measurements.

3. Flow Boiling Heat Transfer

The primary objective of this study is presentation of the combined flow boiling model which can predict how the heat transfer coefficient correlates with heat flux, reduced pressure, mass flux and vapor quality. While this problem was addressed in many studies, flow boiling heat transfer in non-circle microchannels still not predicted precisely.

Combined model of the convective evaporation and nucleate boiling, unifying the phenomena of nucleate boiling suppression and heat transfer enhancement at annular flow is based on the regularities of flow boiling heat transfer for refrigerants and water. In experiments, the microchannel plate containing 21 channels with 335x930 μm cross-section is used. For R134a at reduced pressure of above 0.2, the obvious impact of heat flux on the magnitude of heat transfer coefficient is observed [3]. It occurs, when nucleate boiling is the dominant mechanism of heat transfer. For R21 and R141b at reduced pressures less 0.11, the convective evaporation becomes essential at low heat flux and high vapor quality. Nevertheless, nucleate boiling is still dominant mechanism at high heat flux.

To take account of events provided, the multi-scale model based on approach [3] is proposed. Together three mechanisms of heat transfer are considered: two-phase convection, nucleate boiling and heat transport through evaporating liquid film. To predict nucleate boiling deterioration at high vapor quality, the suppression function is applied for liquid film. For non-circular microchannel the suppression function was modified to account the existence of nucleate boiling near the channel corner. For annular flow and inside a bubble the convective evaporation model from 2.2 is used to calculate the heat transport through evaporating film. The interfacial shear stress is calculated according to [4]. Figure 1 presents the calculation of the flow boiling heat transfer for R134a in comparison with the data [3] at a distance of 2.5 mm. The predictions versus measurements are shown also for model [5]. Flow boiling of water at reduced pressure less 0.01 is very different from the above cases.

This study was performed at the Kutateladze Institute of Thermophysics SB RAS by a grant 16-19-10519 from the Russian Science Foundation.

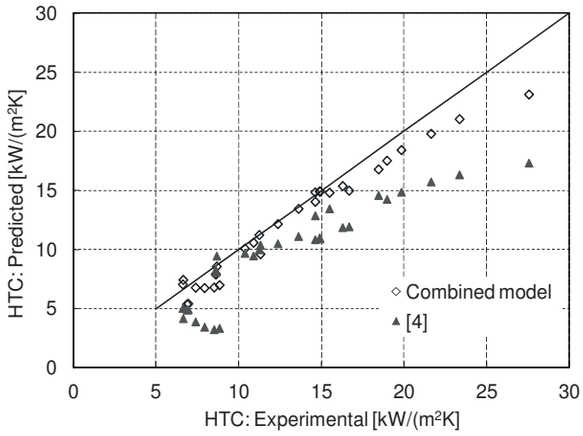

Figure 1. Flow boiling heat transfer results for R134a: predictions versus measurements [3].

References

[1] Kozulin, I. A., Kuznetsov, V. V., 2011. Statistical characteristics of two-phase gas-liquid flow in a vertical microchannel. J. Appl. Mech. Tech. Phys V. 52 (6), 956-964.

[2] Kuznetsov, V.V., Safonov, S.A., 2013. Fluid flow and heat transfer with phase change in minichannels and microchannels. Heat pipes and solid sorption transformations fundamentals and practical applications, ed. L.L. Vasiliev, S. Kakac. CRC Press, Boca Raton, 465-496.

[3] Kuznetsov, V. V., Shamirzaev, A. S., 2014. Flow Boiling Heat Transfer of Refrigerant R-134a in Copper Microchannel Heat Sink. Proceedings of the 4th Micro and Nano Flows Conference UCL, London, paper ID 111.

[4] Asali, J.C., Hanratty, T.J., Andreussi, P., 1985. Interfacial Drag and Film Height for Vertical Annular Flow. AlChE J. 31, 886-902.

[5] Thome, J.R., Dupont, V., Jacobi, A.M., 2004. Heat Transfer Model for Evaporation in Microchannels. Part I: Presentation of the Model. Int. J. Heat Mass Transfer 47, 3375-3385.

ID 163

Nano-PCMs for enhanced Thermal Energy Storage applications

Laura COLLA[1], Laura FEDELE[1], Simone MANCIN[2], Sergio BOBBO[1], Michela ALFÉ[3], Davide ERCOLE[4], Oronzio MANCA[4,*]

* Corresponding author: Tel.: :+39 081 5010217 Fax:+39 081 5010204; Email: oronzio.manca@unina2.it
1 Consiglio Nazionale delle Ricerche -Istituto per le Tecnologie della Costruzione, Padova, IT
2 Dip. di Tecnica e Gestione dei Sistemi Industriali, Università di Padova, Vicenza, IT
3 Consiglio Nazionale delle Ricerche, Istituto di Ricerche sulla Combustione, Napoli, IT
4 Dip. di Ingegneria Industriale e dell'Informazione, Seconda Universita' degli Studi di Napoli Real Casa dell'Annunziata, Aversa, IT

Abstract The present work aims at investigating a new challenging use of aluminium oxide (Al_2O_3) nanoparticles and Carbon black (CB) nano-aggregates to enhance the thermal properties of pure paraffin waxes to obtain a new class of PCMs, the so-called nano-PCMs. The nano-PCMs were obtained by seeding suitable amounts of Al_2O_3 nanoparticles and CB nano-aggregates in a paraffin wax with a melting temperatures of 70 °C to obtain 1%wt dispersions. The thermophysical properties such as specific heat, latent heat, and thermal conductivity were measured to understand the effects of the nanoparticles on the thermal properties of both the solid and liquid PCMs and then compared with the ones obtained for the pure paraffin wax. Finally, a numerical comparison between the use of pure paraffin wax and the nano-PCMs obtained in a typical hybrid water TES was developed and implemented. The modelled hybrid TES is a typical 70 L water tank, where a certain number of pipes filled up with PCMs are located to improve its heat storage capabilities. The results are presented in terms of loading and unloading time, and total amount of energy stored.

Keywords: Nano-Phase Change Materials (nano-PCMs), Thermal Energy Storage (TES), Nanoparticles, Paraffin wax

1. Introduction

A Thermal Energy Storage (TES) systems is a device that permits to storage energy by heating a storage medium. There are two types of TES, sensible TES and latent TES. This latter type has more advantages because the heat stored changes the phase of the base material during the storing and the temperature does not increase. The base material of a latent TES is the Phase Change Material (PCM) that during the solid-liquid phase change process, adsorbs and then releases the heat loads[1]. The common and useful PCMs are the paraffin waxes that presents many desirable characteristics, such as high latent heat, non-toxicity and chemical stability. However, they also have a very low thermal conductivity and therefore, different enhancement are necessary to improve their thermal conductivity, for example by adding nanoparticles to a base PCM [2]. This paper studied the effect of the nanoparticles inside a pure PCM. Two different nano-PCMs are obtained by adding 1.0%wt of Al_2O_3 and CB inside a paraffin waxes with a melting temperature of 70°C (RT70). The thermophysical properties are then experimentally evaluated. Moreover, a numerical analysis is made to evaluate the thermal performance of the nano-PCMs respect to the pure PCM.

2. Preparation of the model

The nano-PCMs are built by seeding suitable amounts of Al_2O_3 nanoparticles and CB nano-aggregates in the RT70 paraffin wax to obtain 1%wt dispersions. The thermophysical properties such as specific heat, latent heat, and thermal conductivity were measured to understand the effects of the nanoparticles on the thermal properties of both the solid and liquid PCMs and they are showed in table 1. A TES is numerically implemented in 3D space as a typical 70 L water tank, filled up with pure paraffin wax or Nano-PCM with 1.0% weight of Al_2O_3 nanoparticles or CB nanoparticles The dimensions of the TES are 120 x 157 x 710 mm but for thermal symmetry the

computational domain is only a part of the whole system as showed in Fig 1.

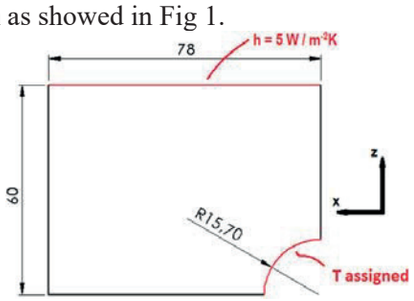

Figure 1: Frontal view of the computational domain with the boundary conditions.

An assigned temperature at 350K on the pipe surface is imposed in order to simulate the heat transfer between the Heat Transfer Fluid and the system during the charging operation while during the discharging phase the temperature is imposed to 300K. A convective heat transfer on the top surface is considered while the other surfaces are adiabatic. The phase change of paraffin wax is modelled with the enthalpy-porosity method [3]. The properties of the materials are listed in the table 1.

Table 1: thermal properties of the materials.

Properties		Pure PCM (RT70)	Nano-PCM Al_2O_3 1.0%wt	Nano-PCM CB 1%wt
Density [kg/m^3]	Solid	880	887	860
	Liquid	770	776	755
Specific heat [J/kg K]	Solid	2052	2060	2057
	Liquid	2692	2336	2628
Thermal Conductivity [W/m K]	Both phases	0.2	0.3671	0.3910
Viscosity [kg/m s]		0.0256	0.0259	0.0263
Thermal expansion factor [1/K]		$1.25*10^{-4}$	$1.22*10^{-4}$	$1.19*10^{-4}$
Latent Heat [J/kg]		$2.5*10^5$	$2.536*10^5$	$2.505*10^5$
T solidus [K]		338	338	338
T liquidus [K]		348	348	348

Figure 2 shows the evolution of the liquid fraction for different materials.

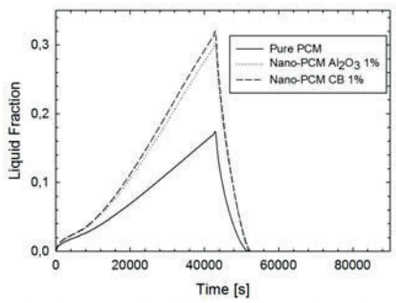

Figure 2: Average liquid fraction vs time for different PCM during the charging and discharging phase.

It can be noted that the discharging phase is faster than the charging phase because of the heat loss on the top surface of the domain.

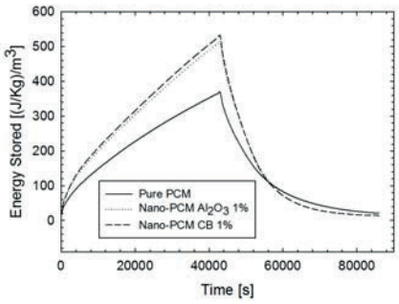

Figure 3: Average energy stored vs time for different PCM during the charging and discharging phase.

In figure 3 the evolution of the average energy stored is depicted; the addition of the nanoparticles leads to an enhancement of the energy stored. Moreover, with the nanoparticles the heat transfer is improved because the evolution of the liquid fraction for the nano-pcm is faster and the energy storage rate is higher than that of the pure paraffin because the thermal conductivity is enhanced.

4. Conclusions

This paper is focused on an experimental and numerical study concerning the use of the nano-PCMs for thermal storage application. Generally, the addition of the nanoparticles leads to an enhancement of the thermal conductivity and latent heat of the pure PCM. Moreover the numerical analysis showed that the nanoparticles improved the heat transfer inside the system and the thermal energy storable.

5. References

[1] Mancin, S., Diani, A., Doretti, L., Hooman, K., Rossetto, L., 2015, "Experimental analysis of phase change phenomenon of paraffin waxes embedded in copper foams", International Journal of Thermal Science, Vol. 90, pp. 79-89.

[2] Kibria, M., A., Anisur, M.,R., Mahfuz,M.,H.Saidur, R., Metselaar I., H., S., C., 2015, "A review on thermophysical properties of nanoparticle dispersed phase change materials", Energy Conversion and Management, Vol. 95 69–89.

[3] Voller, V. R., Prakash, C., 1987, "A fixed grid numerical modelling methodology for convection-diffusion mushy region phase-change problems", International Journal of Heat and Mass Transfer, Vol. 30, pp.1709-1719.

ID 166

5th Micro and Nano Flows Conference
Milan, Italy, 11-14 September 2016

Flow and mass transfer optimization in a biotherapeutic purification device based on nanofibre material

Cesar A. CORTES-QUIROZ [1,*], Alice R. MAZZER [1], Iwan ROBERTS [2], Oliver HARDICK [2], Daniel G. BRACEWELL [1]

* Corresponding author: Tel.: ++44 (0)2076 797745; Fax: ++44 (0)1895 256392; Email: cesar.cortes@ucl.ac.uk
1: Department of Biochemical Engineering, Advanced Centre for Biochemical Engineering, University College London, UK
2: Puridify Limited, UK

Keywords: Liquid Micro Flow, Mass Transfer, Affinity Chromatography, Nanofibre, Biotherapeutic Purification, CFD

A growing market demand of therapeutics is leading the biopharmaceutical industry to produce large batch volumes while reducing processing costs. Thereby downstream processing, which accounts for over 50% of manufacturing costs, requires high throughput operations for rapid bioseparation. Nanofiber adsorbents are an efficient alternative to conventional packed bed format and membrane chromatography. Their fabrication characteristics [1] give small diffusion distances which allow their use at high liquid flow rates without becoming mass transfer limited, while showing superior operating performance in permeability and fouling over conventional adsorbents.

This places significant demands on efficient adsorbent holding device design to avoid loss of resolution due to mixing effects. The performance of adsorbent modules housing porous cast membranes can be enhanced by optimisation [2].

In this study, a new nanofibre technology [3] is implemented in a novel housing for biotherapeutic purification. This is geometrically defined and optimised using computer aided design (CAD) and computational fluid dynamics (CFD) together with experimental flow and bioseparation studies. Experimentally obtained values for pressure drop across the nanofiber bed at different flow rates are used to specify the settings of the numerical model. Prototypes of device designs are fabricated and tested using Akta liquid chromatography systems to validate and improve the models, which in turn describe the fluidic properties and residence time distribution in the devices.

Flow behaviour is evaluated experimentally by passing various solutions through the devices and monitoring the conductivity and/or UV absorbance at the outlet; pulse and transition curves are compared to mass fraction curves generated by CFD. Bioseparation performance is assessed using model proteins such as bovine serum albumin to generate breakthrough curves and perform bind and elute studies. Coomassie stains are utilised to determine the distribution of protein bound to nanofibers in devices loaded with protein and then dismantled.

The optimized design of the nanofibre device resulted in a significantly higher dynamic binding capacity at the 5% breakthrough level, compared to the original prototype. Combining CFD simulation methods with experimental validation efforts was an effective strategy for optimisation of the housing design and nanofibre conformation of a developing purification technology.

References

[1] O. Hardick, B. Stevens, D. G. Bracewell, Nanofibre fabrication in a temperature and humidity controlled environment for improved fibre consistency, J. Mater. Sci. 46 (2011) 3890-3898.

[2] R. Ghosh, T. Wong, Effect of module design on the efficiency of membrane chromatographic separation, J. Membr. Sci. 281 (2006) 532-540.

[3] O. Hardick, S. Dods, B. Stevens, D. G. Bracewell, Nanofiber Adsorbents for High Productivity Downstream Processing, Biotechnology and Bioengineering Vol. 110, No. 4 (2013) 1119-1128.

5th Micro and Nano Flows Conference
Milan, Italy, 11-14 September 2016

ID 167

Scale-out of liquid-liquid flows in small channels

Eduardo GARCIADIEGO ORTEGA, Dimitrios TSAOULIDIS, Panagiota ANGELI*

* Corresponding author: Tel.: +44 (0)2076 793832; Email: p.angeli@ucl.ac.uk
Department of Chemical Engineering, University College London, Torrington Place, WC1E 7JE, London, UK

Abstract Intensification of liquid-liquid processes can lead to sustainable manufacturing and reduced costs. Scale-out (or number-up) is the use of parallel channels to increase throughput in two-phase contacting equipment. The mixture velocity and phase flowrate ratio should be similar in all channels, but channel fabrication tolerances and pressure variations at the channel inlets and outlets can lead to flow maldistribution. Designing around maldistribution will enable high-throughput intensified contactors to be used optimally. This paper proposes the use of flow pattern transition lines together with different scenarios for flow distribution to decide on the best manifold designs. The transition from the plug to the annular pattern during water/kerosene flow was studied experimentally in 2 mm ID FEP channels. Flow distribution in the manifolds and the flow patterns in the contacting channels are currently investigated with high speed imaging.

Keywords: Scale-out, Number-up, Multiphase Flow, Flow maldistribution

1. Introduction

Flow of two immiscible liquids is encountered in a wide range of equipment such as agitated contactors and solvent extraction columns. Operating in small channels can potentially improve mixing, reduce equipment size and enhance heat/mass transfer rates because, among others, of the thin fluidic films formed, high specific interfacial areas and recirculation within the phases. Plug flow (Taylor flow) is one of the most common patterns in millimetric (and smaller) channels consisting of elongated droplets (plugs) of one liquid in the continuum of the other, separated by a thin film from the channel wall. Biswas et al. [1] recently found high mass transfer coefficients during plug flow and low ones in annular flow in 2mm and 6 mm ID channels with a water/acetic acid/toluene system.

To exploit the advantages of small channel systems, high throughputs must be achieved while operating at optimal velocities and flow regimes. The preferred way to achieve this is by using parallel channels, where similar conditions are established in all of them. This approach is called scale-out (or number-up) in contrast to classic scale-up, where the apparatus is made larger for increased throughput. Several examples of scale-out can be found for single-phase reactions in fine chemicals and pharmaceuticals production [2]. There is, however, limited work on the scale-out of immiscible liquid-liquid systems. The main challenge in scale-out is the maldistribution of fluids when they are divided into several channels. Maldistribution in single-phase flows can arise as a result of manufacturing variations in the geometry of the flow distributor and pressure variations along the channel [3]. In two-phase flows, pressure fluctuations during droplet formation at the channel inlet and during exiting will also affect flow distribution in [3].

In the present work, manifolds for two-phase liquid-liquid flows are studied. Information on flow pattern transitions in single channels is used together with different scenarios for flow distribution to decide on the best manifold designs.

2. Experimental set up

The experimental set-up used in the study consists of two syringe pumps (KDS Legato 270) and straight, horizontal, FEP test capillaries with 2 mm ID. Different inlet configurations were tested. These were ETFE T-junctions with through-holes of 1.25 mm (fig. 1A), 0.50 mm (fig. 1B) and a cross with 1.25 mm through-hole (fig.1C). Deionized

water with ink and kerosene (Exxsol D80) were used as test fluids. Flow patterns were observed visually at a distance over 100 L/D from the mixing inlet so the patterns were fully developed. The flow was visualised with a high-speed camera (Photron APX) and illuminated with a 60W continuous arc lamp. Images were acquired at 2000–4000 Hz (depending on the total flow rate).

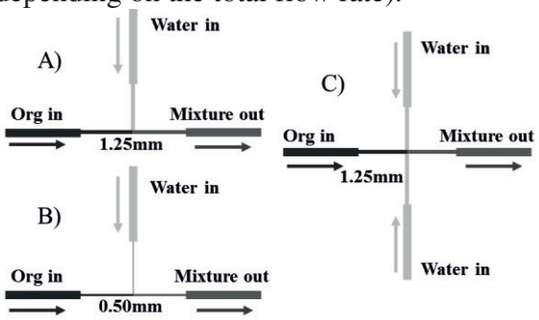

Fig. 1 Schematics of the three inlet configurations used.

3. Results and discussion

Transition lines between Taylor and annular flow are found to be very similar for the three inlet configurations used (fig. 2).

A multichannel contactor can be designed by connecting the side-channels from a water phase manifold and an organic phase manifold as depicted in fig. 3A. Considering flow maldistribution in both single-phase manifolds, four scenarios, shown in fig. 3B, are possible for the two-phase flow in the channels after the single phase flows are brought into contact. In the two-phase flow channels, the superficial velocity of water (U_{wi}) may be different than the design superficial velocity ($\hat{U}_w=Q_w/A_{ch}\times n$). The same applies for the organic phase. In some combinations the mixture velocity is mainly affected, while in others the flow ratio.

To scale-out the liquid-liquid systems, it is desirable to operate at high U_{mix} within the plug flow regime, to maximize throughput. In addition, operating at $U_w/U_o>>1$ reduces the amount of organic solvent required, which can be important for expensive solvents. These conditions imply that the operation point is very close to the flow pattern transition line in fig. 2. Deviations in any given two-phase flow channel from this point would change the flow pattern and affect the mass transfer performance of the whole equipment. For the proper design of manifolds for two-phase flows it is necessary, therefore, to know the flow maldistribution profile in the single phase manifolds [3, 4] and the flow pattern map.

Performance of multichannel contactors using single phase manifolds with 2 to 4 side-channels each is currently being studied. The flow patterns and flow distribution in each two-phase channel will be investigated with high speed imaging.

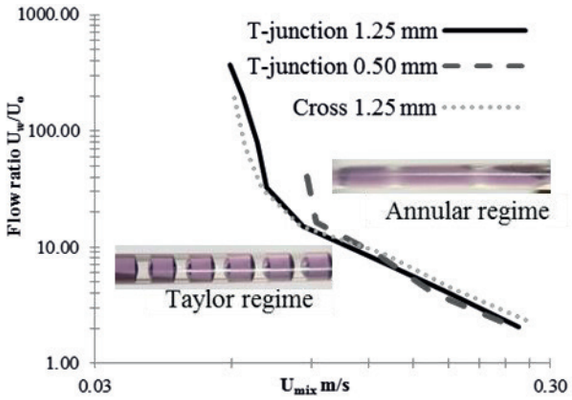

Fig. 2 Flow transition line between Taylor (or plug) flow and annular flow.

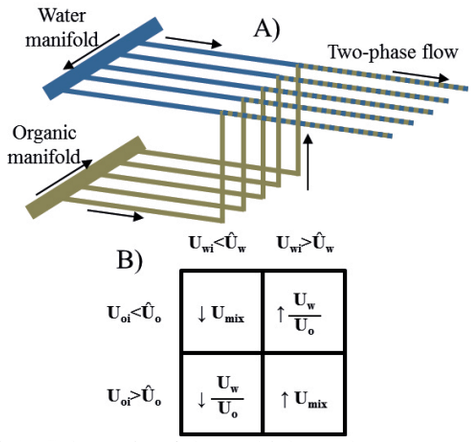

Fig. 3 A) Schematic of the multichannel contactor. B) Matrix of maldistribution possibilities.

4. References

[1] Biswas, K. G., et al., 2015. Mass transfer characteristics of liquid-liquid flow in small diameter conduits. Chem. Eng. Sci. 122, 652-661.
[2] Hessel, V., et al., 2009. Micro Process Engineering: A Comprehensive Handbook. (Vol. 1-3).
[3] Amador, C.; et al., 2008. Design of a mesh microreactor for even flow distribution and narrow residence time distribution. Chem. Eng. J., 135 S259 - S269.
[4] Commenge, J. M., et al., 2002. Optimal Design for Flow Uniformity in Microchannel Reactors. AIChE J., 48(2), 345-358.

5th Micro and Nano Flows Conference
Milan, Italy, 11-14 September 2016

The effect of RBC stiffness on microhemodynamics

Andreas PASSOS [1], Joseph SHERWOOD [2], Efstathios KALIVIOTIS [3], Rupesh AGRAWAL [4], Carlos PAVESIO [5], Stavroula BALABANI [1,*]

* Corresponding author: Tel.: +44 (0)7478343194; Email: s.balabani@ucl.ac.uk
1Department of Mechanical Engineering, University College of London, UK
2 Department of Bioengineering, Imperial College London, UK
3 Department of Mechanical Engineering and Materials Science, Cyprus University of Technology, Cyprus
4 National Healthcare Group Eye Institute, Tan Tock Seng Hospital, Singapore
5 Moorfields Eye Hospital, UK

Keywords: Red blood cells, deformability, aggregation, apparent viscosity, micro particle image velocimetry

The multi-phase nature of blood poses many challenges in the understanding of microvascular flows. Red blood cells (RBCs) deliver oxygen and carbon dioxide to and from body tissues respectively. The ability of RBCs to deform is key to this function as it allows them to flow through microvessels with dimensions smaller than the cells. The morphology and mechanical properties of RBCs such as deformability and aggregability may change in disease (i.e. diabetes, malaria) or the presence of environmental stimuli such as drug therapeutics. These changes affect the rheology and hemodynamics in the microcirculation. Quantifying these changes is a very important step to understand how erythrocyte properties, impact on various pathologies.

In vivo animal studies have shown that reduced RBC deformability increases vascular resistance and the effect depends on the method and extent of RBC rigidification (Pantely et al. 1988; Chien 1987). Numerical studies by Fedosov et al. (2011) have demonstrated up to 50% increase in bulk viscosity with increasing levels of parasitemia i.e. percentage of malaria infected cells, in 20 μm vessel diameters and Ht = 0.45. The velocity in the centre of the capillary was shown (Fedosov 2010) to decrease as the number of malaria stiffened cells increased resulting in lower flow rates. Similar trends have been observed in the 2D simulations of Zhang et al. (2009) for various levels of deformability and aggregation strengths.

Despite recent advances in microfluidic devices for cell deformability characterisation there are no systematic in vitro studies on the effects of RBC deformability on velocity profiles and viscosity. The changes in the velocity profiles reported in the numerical study of Fedosov (2010) are not particularly pronounced considering the markedly increased stiffness that malaria cells exhibit in comparison to healthy cells. Given the wide range of RBC deformability values in pathological states it is important to investigate the microscale behavior of RBC suspensions by systematically varying the cell deformability within the range expected in disease in order to quantify resulting hemodynamic changes.

In the present study preliminary experiments with artificially stiffened RBCs perfused through a straight 50μm square microchannel were conducted in order to assess the role of deformability on hemodynamics and in particular on viscosity, velocity and aggregation characteristics. RBCs were obtained by centrifuging transfusion blood obtained from University College London Hospital (UCLH). Various levels of membrane stiffening were introduced artificially by glutaraldehyde (GA) treatment to the samples. Three fixed samples were prepared by washing RBCs to GA suspended in PBS solutions with concentrations of 0.01%, 0.005%, 0.001%, and an unfixed sample was also prepared and used as control.). Samples with different haematocrit levels (5%, 15%, 25%) were perfused through the microchannels using an Elveflow microfluidic flow controller at flow rates ranging from 20 to 200 channel widths per second. Pressure drop measurements were performed simultaneously in order to determine the apparent viscosity of each sample. A separate set of experiments was also conducted by Dextran 2000 treated samples to induce aggregation and establish the effects of deformability on local aggregation characteristics and their combined effect on haemodynamics.

Quantitative imaging was performed using a Labview driven μPIV system described previously (Sherwood et al. 2014) using LED illumination and RBCs as tracers. The acquired images were processed using MATLAB and JPIV. The effect of stiffening on aggregation was also examined using previously developed imaged based metrics of aggregation (Kaliviotis et al. 2015).

The study is currently been extended to healthy human red blood cells. Our aim is to quantify the extent RBC stifness alters hemodynamics, assess and finetune our methodology before rolling it out to study occular pathologies (Agrawal et al. 2016).

References

Agrawal et al., 2016. Red blood cells in retinal vascular disorders. *Blood Cells, Molecules, and Diseases*, 56(1), pp.53–61.

Chien, S., 1987. Red cell deformability and its relevance to blood flow. *Annual review of physiology*, 49, pp.177–192.

Fedosov., 2010. Multiscale Modeling of Blood Flow and Soft Matter.PhD thesis, Brown University.

Fedosov, D.A. et al., 2011. Multiscale Modeling of Red Blood Cell Mechanics and Blood Flow in Malaria. *PLoS Comput Biol*, 7(12)

Kaliviotis et al., 2015. Quantifying local characteristics of velocity, aggregation and hematocrit of human erythrocytes in a microchannel flow. *Clinical Hemorheology and Microcirculation,* DOI 10.3233/CH-151980

Pantely, G.A. et al., 1988. Increased Vascular Resistance Due to a Reduction in Red Cell Deformability in the Isolated Hind Limb of Swine'. *Microvascular Research*, 35, pp.86–100.

Sherwood et al., 2014. Spatial distributions of red blood cells significantly alter local haemodynamics. *PLoS ONE*. Jun 20;9(6):e100473. doi: 10.1371/journal.pone.0100473

Zhang et al., 2009. Effects of erythrocyte deformability and aggregation on the cell free layer and apparent viscosity of microscopic blood flows. *Microvascular research*, 77(3), pp.265–72.

5th Micro and Nano Flows Conference
Milan, Italy, 11-14 September 2016

Local aggregation characteristics of microscale blood flows

Efstathios KALIVIOTIS [1,*], Joseph SHERWOOD [2], Stavroula BALABANI [3]

* Corresponding author: Tel.: +44 (0)7478343194; Email: e.kaliviotis@cut.ac.cy
1 Department of Mechanical Engineering and Materials Science, Cyprus University of Technology, Cyprus
2 Department of Bioengineering, Imperial College London, UK
3Department of Mechanical Engineering, University College of London, UK

Keywords: Red blood cells, aggregation, image processing, particle image velocimetry

Erythrocyte aggregation (EA) is an important aspect of microvascular flows affecting the flow field and viscosity of blood. Microscale blood flows have been studied extensively in recent years using computational and microfluidic based approaches. However, the relationship between the local structural characteristics of blood and the velocity field has not been quantified. We report simultaneous measurements of the local velocity, aggregation and haematocrit distributions of human erythrocytes flowing in straight and bifurcating microchannels. Experiments were performed using human blood collected from healthy donors following an approved protocol. RBCs were separated, washed and suspended in PBS at a haematocrit of 25% whereas Dextran 2000 at 5mg/ml was added to induce RBC aggregation. The RBC suspensions were perfused through a straight (250 x 50 um) and a T-junction bifurcating PDMS microchannel (100 x 40 um) using a pressure -controlled regulator. The microchannels were placed on an inverted microscope and imaged using brightfield illumination. Acquired images were processed to obtain time-averaged velocity (using PIV algorithms and RBCs as tracers) and haematocrit distributions as described in Sherwood et al. (2012; 2014).

Local aggregation characteristics were firstly determined in the straight microchannel using statistical and edge-detection image processing techniques described in (Kaliviotis et al, 2015) while velocity profiles were obtained using PIV algorithms. Aggregation intensity was found to strongly correlate with velocity distributions. To investigate this further, the edge detection method was subsequently applied to the imaged RBC flows in the bifurcating microchannel and the size and distribution of aggregates through the flow domain were determined for various flow ratios between parent and daughter branch. The results demonstrate the combined effect of haematocrit and velocity distributions on local aggregation characteristics and the potential of various measures of aggregation in characterising the structural properties of blood.

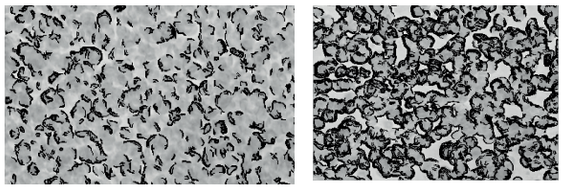

(a) (b)

Figure 1. Edge detection applied to RBC microchannel flow images at a) high shear-b) low shear rates

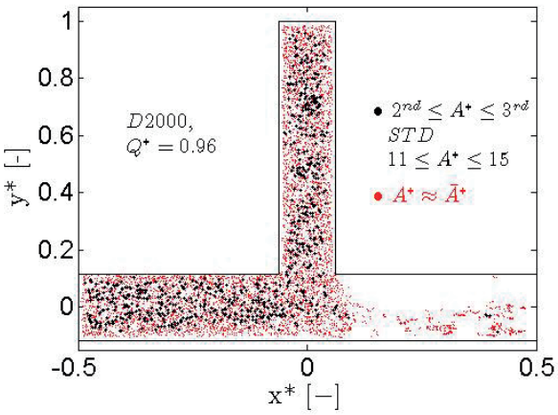

Figure 2. Distribution of aggregates with size A* between the 2nd and 3rd standard deviation for a flow ratios Q*= 0.96 in the left outlet branch of bifurcating microchannel. Aggregates of mean size (Ā*) are also shown for comparison. A*=1 corresponds to 1 RBC.

Kaliviotis et al., 2015. Quantifying local characteristics of velocity, aggregation and hematocrit of human erythrocytes in a microchannel flow. *Clinical Hemorheology and Microcirculation* DOI**:** 10.3233/CH-151980

Sherwood, J., Dusting, J., Kaliviotis, E. and Balabani, S. (2012). The effect of red blood cell aggregation on velocity and cell-depleted layer characteristics of blood in a bifurcating microchannel, *Biomicrofluidics*, 6(2):24119. doi: 10.1063/1.4717755

Sherwood, J., Kaliviotis, E., Dusting, J. and Balabani, S. (2014). Hematocrit, viscosity and velocity distributions of aggregating and non-aggregating blood in a bifurcating microchannel, *Biomech Model, Mechanobiol,* 13, Issue 2, Page 259-273, DOI 10.1007/s10237-012-0449-9.

5th Micro and Nano Flows Conference
Milan, Italy, 11-14 September 2016

The challenge to measure single-phase convective heat transfer coefficients in microchannels

Gian Luca MORINI*

* Corresponding author: Tel.: ++39 (0)51 2093381; Fax: ++39 (0)51 2093296; Email: gianluca.morini3@unibo.it
Dipartimento di Ingegneria Industriale, Alma Mater Studiorum Università di Bologna, Bologna, IT

Keywords: Micro Flow, Experimental techniques, Single-phase Convection, Microfluidics

During the last twenty years a very strong interest on the analysis of forced convection in microdevices has been demonstrated by the large number of papers dealing with this topic appeared in scientific journals as well as by the impressive number of patents presented by researchers and industrial companies involving convective aspects in microdevices [1]. In this period the comprehension of the physical mechanisms of momentum and heat transfer phenomena activated in microfluidic devices has been dramatically increased by the improved capability to make accurate measurements at micrometric scales [2]. In fact, the scientific and industrial interest on microfluidics has stimulated the development of new experimental techniques for the measurement of local velocity, temperature, pressure, flow rates and other measurable quantities in microchannels [3].

In this lecture a critical review of the experimental techniques developed specifically for the investigation of forced convection in microchannels will be presented. The problem of the experimental determination of convective heat transfer coefficients in channels having dimensions lower than 1 mm is discussed by stressing the pro's and con's of each experimental approach [4].

A conclusion of this critical review is that, due to the small dimensions of the observed objects, the development of non-intrusive experimental techniques with a negligible impact on the observed system is very hard. There are two solution to this problem:

- reduce the presence of invasive sensors within the system; in this case the number of observed quantities decreases and from few experimental data one must infer the behavior of the whole system;
- accept the use of invasive experimental techniques in order to obtain more information about the microsystem; in this case the presence of sensors can determine a significant change of the behavior of the system and one must remove the effects due to the experimental techniques in order to know the real behavior of the system.

In the first case it becomes crucial to be able to model numerically the whole system in order to fill the information gap due to the limited number of available measured data.

As an example, in the analysis of forced convection in microchannels a series of practical issues linked to the real geometry of the microchannel, the real thermal boundary conditions imposed experimentally and the presence of micro-fittings and sensors within the test section can have a strong influence on the convective behavior of the system. In this case, only if the few experimental data are coupled to a complete computational thermal fluid-dynamics analysis of the whole tested micro-system it becomes possible to check the physical meaning of the experimental data and improve their interpretation. Conventional CFD codes can help for this [4].

In the second case, it become crucial to be able to model, by using a numerical approach, the disturbances induced by the experimental techniques on the system in order to extract the right values of the observed quantities. Bottom-up numerical approaches (like Molecular Dynamics, Lattice-Boltzmann, Montecarlo or kinetic approaches) can make this job. This means that in Microfluidics invasive experimental techniques must be generally integrated by numerical models in order to obtain an accurate data post processing avoiding wrong interpretations of the measured quantities. In this sense, the numerical models become an integrated part of the experimental technique. This concept will be fully exploited in the paper by considering two techniques for the measurement of local velocity in microdevices: μPIV (micro Particle Image Velocimetry) [5] and MTV (Molecular Tagging Velocimetry) [6].

In addition, this review highlights the presence of specific gaps in the experimental techniques proposed up to now for the analysis of convective phenomena in microchannels with the aim to stimulate and address the research on this topic in the next future.

References

[1] G.L. Morini, Single-phase convective heat transfer in microchannels: a review of experimental results, *Int. J. Thermal Sciences*, 43(7), 631–651 (2004).

[2] S.G. Kandlikar, S. Colin, Y. Peles, S. Garimella, R. F. Pease, J. J. Brandner and D. B. Tuckerman, Heat Transfer in Microchannels — 2012 Status and Research Needs, *J. Heat Transfer* 135(9), 091001 (2013)

[3] G.L. Morini, Y. Yang, H. Chalabi, M. Lorenzini, A critical review of the measurement techniques for the analysis of gas microflows through microchannels, *Exp. Thermal and Fluid Sci.*, 35(6), 849–865, (2011)

[4]] G.L. Morini, Y. Yang, Guidelines for the Determination of Single-Phase Forced Convection Coefficients in Microchannels, *J. Heat Transfer* 135(10), 101004 (2013)

[5] S. Burgmann, N. Van der Schoot, C. Asbach, J. Wartmann and R. Lindken, Analysis of tracer particle characteristics for micro PIV in wall-bounded gas flows, *La Houille Blanche*, 4, 55 – 61 (2011)

[6] F. Samouda, S. Colin, C. Barrot, L. Baldas, J. Brandner, Micro molecular tagging velocimetry for analysis of gas flows in mini and micro systems, *Microsystem Technologies*, 21(3), 527-537 (2015).

ID 171

5th Micro and Nano Flows Conference
Milan, Italy, 11-14 September 2016

μAngelo: 3D Lithography Based on Thermocapillary Sculpting of Nanofilms

Sandra M. TROIAN

Tel.: +1 626.395.3362 Fax: +1 626.395.6106 Email: stroian@caltech.edu URL: www.troian.caltech.edu
T. J. Watson, Sr. Laboratories of Applied Physics, MC 128-95
California Institute of Technology, Pasadena, CA, USA

Keywords: Thermocapillary, Bénard-Marangoni instability, 3D lithography, Thin films, Micro-optics

1. Background

Many systems in nature caused by flows generated by thermal gradients give rise to beautiful pattern formations, perhaps the most famous of which is the Rayleigh-Bénard instability triggered by buoyancy effects. This instability, which occurs in systems ranging in size from millimeters to kilometers and beyond, generates arrays of fluid cells which undergo circular convection. Evaporative remnants of this instability in multicomponent systems can produce spectacular polygonal salt crust formations as seen in the largest salt flat on Earth called the Salar de Uyuni in Bolivia. Once the dimensions of a fluid system are reduced to the micron scale, however, the surface to volume ratio increases tremendously, whereupon surface forces like thermocapillarity become predominant and trigger instabilities such as Bénard-Marangoni flow. In recent years, digital control over thermocapillary forces along an air/liquid interface has led to the development of planar microfluidic devices capable of numerous functions including droplet positioning and registration, routing, coalescence, scission and even mixing [1-2]. In this talk, we focus on even smaller systems sizes of the order of 100 nm or so, to demonstrate how patterned thermocapillary forces can be projected onto the surface of a liquid nanofilm to sculpt material in 3D. Once the driving force is removed, the resulting shapes rapidly solidify *in-situ* forming shapes highly suited to optical applications for spatial beam shaping. We coin this non-contact method of film patterning, μAngelo, and trace its origin to a long standing debate involving spontaneous nanopillar formations in ultrathin films.

2. Electrostatic, Phononic or Thermocapillary Driving Force?

For over 15 years now, researchers have struggled to explain a phenomenon whereby a flat molten polymeric nanofilm exposed to a nearby cooler substrate undergoes spontaneous formation of nanopillars, rings, spirals, chain-like forms, labyrinth and other structures separated by about 1 – 10 microns. Even after solidification, these 3D arrays exhibit ultrasmooth interfaces, which are particularly advantageous for use in optical and photonic systems. Three very different mechanisms have been proposed as the source of instability: (i) electrostatic attraction between the molten film and proximate substrate due to image charge (Chou *et al.* 2002), (ii) radiation pressure from coherent interface reflections of acoustic phonons (Schäffer *et al.* 2003), and (iii) enhancement of film fluctuations by thermocapillary forces (Troian *et al.* 2009 – 2011) [3-5]. Here we demonstrate that the observed instability is likely triggered by long wavelength thermocapillary fluctuations whose growth cannot be suppressed by capillary forces due to the excessively large thermal gradients enforced by experiment. Linear and nonlinear stability analysis of the governing thin film equation indicate there is no critical number for onset of instability and no steady state for systems which are not mass limited. Lyapunov analysis confirms that 3D formations tend to grow toward the cooler target until contact is achieved. Comparison of theoretical predictions with in-house optical microscopy and white light interferometry measurements strongly suggests that the thermocapillary mechanism is indeed predominant. Numerical studies also indicate parameter regimes displaying resonant wavelength behavior leading to uniform peak formations.

3. Fabrication of Microlens Arrays by μAngelo Technique

To capitalize on this finding, we turn toward nonlinear amplification of film deformation by patterned masks of slender pin arrays placed in close proximity and maintained at a cooler temperature than the nanofilm. The resulting temperature distribution projected onto the film surface produces the necessary thermocapillary stress distribution for sculpting desired liquid shapes in 3D. Numerical studies based on finite element simulations are used to tune the amplitude and pitch of the resulting microlens arrays. Scanning white light interferometry of the solidified shapes also helps optimize array parameters for micro-optical applications such as Shack-Hartmann wavefront sensors [6]. We are currently exploring the use of alternative cooled mask patterns to fabricate novel components such as linear waveguides with non-rectangular cross-section. In summary, we hope that our combined studies establish the potential for a new type of 3D lithography based on spatial modulation of surface forces.

Acknowledgements

SMT wishes to thank the students and postdocs who contributed to this work over the years, namely A. Darhuber, M. Dietzel, E. McLeod, K. Fiedler, D. Lim, N. Liu, Y. Liu, Z. Nicolaou and C. Zhou.

References

[1] A. A. Darhuber and S. M. Troian, *Annu. Rev. Fluid Mech.* 37, 425 (2005)
[2] A. A. Darhuber, J. P. Valentino and S. M. Troian, *Lab on a Chip* 10 (8), 1061-1071 (2010)
[3] M. Dietzel and S. M. Troian, *Phys. Rev. Lett.* 103 (7), 074501 (2009) and *J. Appl. Phys.* 108, 074308 (2010)
[4] E. McLeod, Y. Liu and S. M. Troian, *Phys. Rev. Lett.* 106, 175501 (2011)
[5] K. Fiedler and S. M. Troian, submitted to *J. Appl. Phys.* (2016)
[6] D. Lim, K. Fiedler and S. M. Troian, preprint (2016)

5th Micro and Nano Flows Conference
Milan, Italy, 11-14 September 2016

Microfluidic-Enabled Screening of Kidney Organogenesis

Glass, N[1], Takasato, M[2], Xuan Er, P[2], Little, M[2], Wolvetang, EW[1], Cooper-White, J[1,3,4]

* Corresponding author: Tel.: +61 (7) 3346 3858 ; Email: j.cooperwhite@uq.edu.au
1: Australian Institute for Bioengineering and Nanotechnology, The University of Queensland, QLD, Australia
2: Murdoch Children's Research Institute, Melbourne, Vic, Australia
3: CSIRO Manufacturing Flagship, VIC, Australia
4: School of Chemical Engineering, The University of Queensland, QLD, Australia

Keywords: Microbioreactor arrays, factorial, soluble factors, stem cells, kidney.

Introduction:
The differentiation of human pluripotent stem cells (hPSCs) towards kidney is of great interest for developmental biology, toxicology and regenerative medicine. Soluble factor-based methods for directing human embryonic stem cells to produce kidney cell populations, including nephrons and ureteric bud, have recently been reported [1,2]. Here, these current protocols are probed for new insight into the developmental processes driving such development through the use of a microfluidic system and image cytometry in a systematic and quantitative manner. Understanding these pathways provides the necessary insight for the development of novel biomaterial systems that enable directed kidney tissue genesis using 3D printing.

Experimental:
We have investigated this complex differentiation process with several soluble factor perturbations using a 3 by 3 factorial microbioreactor previously developed in the Cooper-White lab [3]. This allowed for 27 unique soluble factor combination inputs. These inputs are then perfused through 10 serial wells allowing for the investigation of potential paracrine and autocrine signalling. This generates 270 unique conditions within the system.

Cells were differentiated towards intermediate mesoderm cell populations (PAX2+), before running several different factors across the microbioreactor array. Initial experiments examined the effect of known signalling pathways on the differentiation of hPSCs towards renal cell populations at day 9 and day 12 time points of the differentiation protocol.

Results and Discussion:
Results confirmed the essential factors for the differentiation towards kidney like cell phenotypes and the condensation of ureteric epithelial cells (GATA3+, ECAD+). This effect was synergistically enhanced in the presence of some of the factors investigated but also gave rise to populations not known to be of renal origin (GATA3+, ECAD-). Early nephrons (WT1+, ECAD+) and metanephric mesenchyme (WT1+ ECAD-) have also been observed to form around the ureteric epithelial structures.

Image cytometry was then performed across the entire device to provide FACs-like data for the population within each well. Examination across the microbioreactor demonstrated that approximately 15% of the cells had formed early nephrons. Further parameters based on clustering structures of cells were also investigated and quantified with respect to soluble factor and paracrine signalling.

Conclusion: This provides a proof of concept for microfluidic-enabled factorial optimisation of directed differentiation into complex structures of the human kidney. Several different cell subtypes of the kidney were identified and quantified in many different conditions, confirming novel developmental pathways that are open to modulation with functionalised biomaterials.

References

[1] Takasato M, Er PX, Becroft M, Vanslambrouck JM, Stanley EG, et al. (2014) Directing human embryonic stem cell differentiation towards a renal lineage generates a self-organizing kidney. Nat Cell Biol 16: 118-126.

[2] Xia Y, Nivet E, Sancho-Martinez I, Gallegos T, Suzuki K, et al. (2013) Directed differentiation of human pluripotent cells to ureteric bud kidney progenitor-like cells. Nat Cell Biol 15: 1507-1515.

[3] Titmarsh DM, Hudson JE, Hidalgo A, Elefanty AG, Stanley EG, et al. (2012) Microbioreactor arrays for full factorial screening of exogenous and paracrine factors in human embryonic stem cell differentiation. PLoS One 7: e52405.

R1234yf condensation inside a horizontal 3.4 mm ID microfin tube

Andrea DIANI [1] , Alberto CAVALLINI [2], Luisa ROSSETTO [3,*]

* Corresponding author: Tel.: +39 049 827 6869; Fax: +39 049 827 6896; Email: luisa.rossetto@unipd.it
1 Department of Industrial Engineering, University of Padova, Italy

Keywords: R1234yf, condensation, microfin tube, heat transfer coefficient, pressure drop.

According to the definition of Qu and Mudawar [1], a mini tube has a hydraulic diameter between 1 and 3 mm. Mini microfin tubes are a smart option to achieve higher heat transfer coefficient compared to smooth tubes. Commercial microfin tubes are now widely implemented for air conditioning and refrigeration systems, with inner diameters ranging approximately between 5 and 10 mm. Mini microfin tubes were initially studied for CO_2 applications, due to CO_2 high working pressure [2, 3], but they are now widening their applications also to traditional refrigeration and air conditioning systems. Recently, mini microfin tubes are becoming a topic of the research community because they can assure higher heat transfer coefficient compared to classical microfin tubes, thus leading to more compact and efficient systems, with a consequent refrigerant charge reduction. Up today, some works on refrigerants two phase flow inside small-sized microfin tubes regard flow boiling [4, 5], but only few works study condensation [6].

This paper explores the heat transfer characteristics of a mini microfin tube during R1234yf condensation. R1234yf is a new eco-friendly refrigerant, with an extreme low GWP (<1). The microfin tube under investigation has an inner diameter at the fin tip of 3.4 mm, apex and helix angle of 43° and 18°, respectively, it has 40 fins along the inner circumference, and each fin is 0.12 mm high.

Tests were carried out in a facility built at the Heat Transfer in Micro Geometries Laboratory of the Department of Industrial Engineering at University of Padova. The facility was designed for pressure drop and either condensation or flow boiling heat transfer measurements. It has a maximum working pressure of 30 bar, and the refrigerant mass flow rate can be varied up to 72 kg h^{-1}.

In the experimental set up, the refrigerant is pumped through a brazed plate evaporator by a magnetically coupled gear pump, at the exit of which it is superheated. Then, the refrigerant is cooled and partially condensed in a pre-condenser: this is a tube-in-tube heat exchanger, where the refrigerant flows in the inner tube and water flows in the annulus. Cold water is supplied in the cold water loop, where it is possible to adjust both the water flow rate and water temperature by means of a chiller. By adjusting the water heat flow rate at the pre-condenser, it is possible to set the vapour quality at the inlet of the test section. The test section is a water-cooled condenser, which permits heat transfer and pressure drop measurements during condensation inside a microfin tube.

The test section is made of a microfin tube around which a smooth copper tube with an inner diameter of 1.9 mm is wrapped. Cold water flows in the wrapped copper tube to remove the heat flow rate from the refrigerant flowing inside the microfin tube. Cold water is supplied by a thermostatic bath. The microfin tube with the wrapped smooth tube is located inside an aluminum housing, filled with tin, to guarantee a thermal contact between the microfin tube and the wrapped tube.

The heat transfer coefficient was defined as:

$$HTC = \frac{q_{water}}{A_D \cdot \left(\bar{t}_{sat} - \bar{t}_{wall}\right)} \quad (1)$$

where q_{water} is the heat flow rate measured on the water side, A_D is the inner area of an equivalent smooth tube with the same inner diameter at the fin tip, whereas $\bar{t}_{sat}$ and $\bar{t}_{wall}$ are the mean saturation and wall temperatures, respectively.

Experimental tests were run at 30 °C of saturation temperature at the inlet of the test section, with mass velocities ranging between 200 to 1000 kg m^{-2} s^{-1} and vapour qualities from 0.1 to 0.9. From the experimental measurements, it was possible to calculate the heat transfer coefficient and frictional pressure drop.

Experimental results show that the heat transfer coefficient increases with vapour quality and mass velocity. Frictional pressure drop increases with mass velocity at constant vapour quality; at constant mass velocity, it increases with vapour quality up to a maximum value, after which it slightly decreases.

The results show the interesting heat transfer capabilities of the mini microfin tube under investigation, as long as the capabilities of the new low GWP refrigerant R1234yf. The combination of mini microfin tube and low GWP refrigerant can lead to eco-friendly air conditioning and refrigeration systems.

References

[1] Qu, W., Mudawar, I., 2004. Measurement and correlation of critical heat flux in two-phase micro-channel heat sinks. Int. J. Heat Mass Tran. 47, 2045-2059.

[2] Gao, L., Honda, T., Koyama, S., 2007. Experiments on flow boiling heat transfer of almost pure CO_2 and CO_2-oil mixture in horizontal smooth and microfin tubes. HVAC&R Res. 13, 415-425.

[3] Dang, C., Haraguchi, N., Hihara, E., 2010. Flow boiling heat transfer of carbon dioxide inside a small-sized microfin tube. Int. J. Refrig. 33, 655-663.

[4] Diani, A., Mancin, S., Rossetto, L., 2014. Flow boiling heat tranfer of R1234yf inside a 3.4 mm ID microfin tube. Exp. Therm. Fluid Sci. 66, 127-136.

[5] Sagawa, K., Jige, D., Inoue, N., Haba, T., 2015. Pressure drop and heat transfer for flow boiling inside horizontal smooth and internally helical-grooved small-diameter tubes. In: Proceedings of the 24th IIR International Congress of Refrigeration. Paper ICR2015-726. Yokohama.

[6] Hirose, M., Ichinose, J., Jige, D., Inoue, N., 2015. Condensation heat transfer and pressure drop of azeotropic mixture refrigerant R32/R1270 inside horizontal small-diameter tubes. In: Proceedings of the 24th IIR International Congress of Refrigeration. Paper ICR2015-702. Yokohama.

ID 174

Convective condensation at small scales: Experimental and analytical advances

Dr. Srinivas Garimella, Hightower Chair in Engineering
Professor and Director, Sustainable Thermal Systems Laboratory
Georgia Institute of Technology
Atlanta, GA 30332
sgarimella@gatech.edu; STSL.gatech.edu

Abstract

Interest in mini- and microscale geometries for the enhancement of heat transfer started in the early 1980s, with a focus on single-phase heat transfer enhancement. The small hydraulic diameters led to high heat transfer coefficients, and also enabled geometries with high surface-to-volume ratios. These two aspects of the move toward smaller hydraulic diameters both led to the reduction of heat transfer resistance (1/hA), in turn enabling high heat transfer rates in small packages. The electronics cooling industry, grappling with the ever increasing heat duties that had to be dissipated from chips, provided the necessary impetus for the further development of high heat flux geometries. Single-phase microscale heat transfer studies then yielded to interest in boiling heat transfer due to the considerably high heat transfer coefficients possible due to phase change. This was especially important to remove the high heat dissipation rates from chips and their accessories constrained to small spaces, and also because this convective resistance from the chip to the coolant formed one of the dominant thermal resistances for heat removal. Interest in condensation at the microscales lagged, however, because in several applications, heat removal is accomplished through rejection to the ultimate heat sink, commonly ambient air, which presents the more significant thermal resistance.

In the early 1980s, with the dual emphases on reducing heat exchanger size due to the increasing demands for smaller vehicles, and the phasing out of refrigerants with CFCs, automotive manufacturers in particular started focusing on a departure from the round tube/flat or wavy fin geometries for condensers. The combination of multi-port microchannel extrusions in rectangular tubes and multilouver fins for the air-side led to the interest in condensation at the small scales. Because the multilouver fins provided higher air-side heat transfer coefficients while also providing 10-20 times the surface area of the tubes, understanding the thermal resistance on the condensation side became more important to the overall heat transfer, and in several cases, could benefit from the higher tube-side heat transfer coefficients possible with smaller hydraulic diameters. The headered arrays of rectangular multiport tubes also offered the opportunity for the optimization of tube-side pass arrangements, with a larger number of tubes per pass near the condenser inlet where the two-phase mixture velocities were high, and gradually decreasing the number of tubes per pass as the liquid fraction increased toward the outlet due to condensation. Automotive condensers saw a relatively quick adoption of these condensers with rectangular tubes containing ports with hydraulic diameters ranging for 400 to 700 μm.

The understanding of condensation phenomena lagged much behind the adoption of the abovementioned microchannel condensers. For the first several years, condenser designs were developed based on extrapolations of the pertinent models and correlations for flow regime transition criteria, pressure drop, void fraction, and heat transfer for larger diameter channels, typically in the 8 – 25 mm range. Furthermore, these extrapolations were necessarily also across working fluids, because much of the literature on flow regimes in large diameter channels was based on air-water mixtures simulating condensing flows, and due to their typical origins in power plant applications, condensing steam. The significant differences in working fluid properties between air-water or steam on the one hand and condensing synthetic refrigerants on the other, in particular the vast differences in vapor-phase densities and surface tension, make such extrapolations largely ineffective in predicting condensation phenomena for these much different fluids. In addition, the relative influence of gravity, shear, viscous forces and surface tension change significantly as hydraulic diameters are reduced.

With the goal of achieving a comprehensive and self-consistent modeling capability for condensation heat transfer in small geometries for a wide range of fluids based on the underlying physics rather than purely empirical correlations, a small but growing research community, including the present author and coworkers, started systematically addressing these condensing phenomena. The emphasis was on understanding the coupled phenomena of flow morphology (i.e., flow regime and void fraction), and momentum, heat and mass transfer. Flow regimes were first investigated in the late 1990s through visualization of the actual condensation process instead of surrogates through innovative test section designs that enabled visual access at the high saturation pressures characteristic of "real world" condensation processes. These experimental investigations clearly documented the decreasing influence of gravity and the dominance of surface tension effects at smaller hydraulic diameters. Annular and intermittent flows were shown to dominate, while the gravity dependent stratified and

wavy flows were largely absent. Flow regime maps and transition criteria based on dimensionless parameters were introduced for a range of synthetic fluids with operating pressures all the way up to close to the critical pressure, in circular and noncircular geometries with D_h as small as 400 μm over a wide range of mass fluxes. These higher pressures are particularly important because almost all the refrigerants that replace the original high ozone depletion potential CFCs, and those that will replace the high GWP HFCs, require operation at much higher pressures for heat rejection.

Mini- and microchannel flow visualization work also revealed new insights on the void fraction during condensation. The knowledge of void fraction is necessary for closure to mechanistic models for determining pressure drops and heat transfer coefficients during convective condensation. Computational tools were developed to extract quantitative information from flow visualization using interface recognition and spline fitting techniques. This allowed the phase distributions in micro- and minichannels to be identified, which, along with idealization and analytical models of the time-averaged interface boundaries, yield the void fractions as well as details of phase distributions across the cross section for a variety of conditions.

Frictional pressure drop during convective condensation has been measured at high resolution across small vapor quality changes, with proper accounting of the contributions due to deceleration of the fluid. For annular flows, some version of two-phase multipliers, but with the corresponding interfacial shear based on measurements at these small scales, have yielded considerable success. For intermittent flows, mechanistic models that account for the pressure drops in the liquid slug, the interfacial shear at the liquid film-vapor bubble interface, and due to the transitions between the vapor bubble region and the liquid slug region fore and aft of the bubble have yielded excellent predictive capabilities. Measurement of condensing heat transfer coefficients poses unique challenges due to inability of direct heat transfer rate measurements, as would be possible by measuring the electrical heat input in boiling experiments. The thermal amplification technique developed by the author, which addresses the coupled conflicting challenges of heat duty measurements and thermal resistance measurement largely independently, has offered the ability to measure these heat transfer coefficients with high accuracy. Heat transfer models, with closure based on the underlying void fraction and pressure drop models, and that account for conjugate heat transfer behavior in the channel walls, are yielding a unified, consistent picture of all relevant phenomena during condensation of refrigerants in mini and microchannels.

Attention in recent years has turned to the investigation of condensation of multi-constituent zeotropic mixtures of fluids, e.g., ammonia-water, and hydrocarbons. The zeotropic nature of these mixtures present new challenges due to the introduction of temperature and concentration gradients and coupled heat and mass transfer resistances in liquid and vapor phases. These phenomena present new measurement and modeling challenges. The author and his coworkers have investigated these coupled phenomena for several mixtures ranging from near-azeotropic to high zeotropic, and characterized the applicability of engineering approximations such as the Silver-Bell-Ghaly method, as well as the more rigorous non-equilibrium methods that explicitly address the relevant resistances in the two phases. In addition, maps for the applicability of these two methods have been developed, and influence of working fluid-to-coolant temperature differences in determining heat transfer coefficients have been measured and modeled. Research is also underway to address the issue of maldistribution in multiple parallel channels more typical of actual condensers and the limitations they pose in benefitting from the advantages of high heat transfer coefficients at the small scales. A thorough understanding of the drivers for maldistribution at the inlet and outlet headers and across the channels themselves is leading to preliminary passive solutions for minimizing maldistribution and mitigating its effects.

Challenges remain. As the hydraulic diameter continues to decrease, the capability of optical techniques to characterize flow phenomena reaches its limits, generating the need for alternative measurement techniques. At such small scales, the heat transfer coefficients continue to rise, while due to the low mass flow rates per channel, the heat duty that must be measured decreases drastically, making the measurement of heat transfer coefficients particularly challenging, especially for condensation in contrast with boiling. Furthermore, with the increasing interest in binary fluid mixture condensation, it is particularly important that novel techniques for measuring local surface and fluid temperatures be developed without affecting flow phenomena, so that the corresponding analytical models can be validated at the local levels. The influence of surface tension over these ranges of mixtures, operating conditions, and geometries also requires more rigorous modeling than has been possible thus far. These challenges provide rich opportunities and a roadmap for the investigation of convective condensation heat transfer for a wide range of applications such as electronics cooling, automotive and residential air-conditioning and refrigeration systems, small-scale portable cooling and heating systems, and medical devices.

ID 175

Spontaneous capillary flow limit in diverging open U-grooves and suspended channels

J. Berthier[1], K. Brakke[2], D. Gosselin[1], F. Navarro[1], E. Berthier[3]

[1]Department of Biotechnology, CEA-Leti
University Grenoble Alpes F-38000 Grenoble, F-38054, Grenoble, France.
[2] Mathematics Department, Susquehanna University, Selinsgrove, PA 17870, USA.
[3] Tasso Inc., Seattle, WA, 98119, USA

Introduction: Due to their compactness and independence of exterior energy sources, capillary microsystems are increasingly used in many different scientific domains, from biotechnology to biology, chemistry, energy and space [1-4]. Obtaining a capillary flow depends on channel geometry and contact angle. A general condition for the establishment of a spontaneous capillary flow in a uniform cross section channel has already been derived from Gibbs free energy [5]. In this work, we consider spontaneous capillary flows (SCF) in linearly diverging open U-grooves and suspended channels, and we show that they do not flow indefinitely but stop at some location in the channel. Using Gibbs free energy, we derive the expression that determines the location where the flow stops. The theoretical approach is verified by using the Surface Evolver numerical program [6] and checked by experiments.

Theory: First, let us recall the condition for SCF in a uniform cross section channel. The morphology of the free interface is such that it evolves to reduce the Gibbs free energy G

$$dG = \gamma\, dA - p\, dV < 0 \ . \tag{1}$$

By definition SCF occurs in a capillary where the upstream pressure is null, and SCF occurs as long as the pressure (p<0) at the flow front is smaller than that of the reservoir (p~0). In the case of a U-groove or suspended channel, using Young's law, it can be shown that equation (1) can be cast in the form

$$\frac{dA_{LG}}{dA_{SL}} < \cos\theta\,, \tag{2}$$

where θ is the contact angle, A_{LG} the liquid-gas surface area, and A_{SL} the liquid-solid surface area. Let us now consider a diverging open U-groove, or a diverging suspended channel, as shown in figure1. Assume an infinitesimal progression dx of the front of the fluid. For the U-groove, one finds the approximate condition for which the SCF continues

$$\frac{w}{h} < \frac{2\left(\cos\theta - \sin\alpha\right)}{\cos\alpha\left(1-\cos\theta\right)}, \tag{3}$$

and for the suspended channel

$$\frac{w}{h} < \frac{\cos\theta - \sin\alpha}{\cos\alpha} \ . \tag{4}$$

Clearly, when α=0, the two expressions reduce to the well-known uniform cross section expressions.

Numerical approach: The location where the flow stops can be determined using Surface Evolver [6]. The free surface is characterized by its surface tension, while the triple line is determined by Young's constraints. Figure 2 shows the aspect of the liquid surface at the location where it stops.

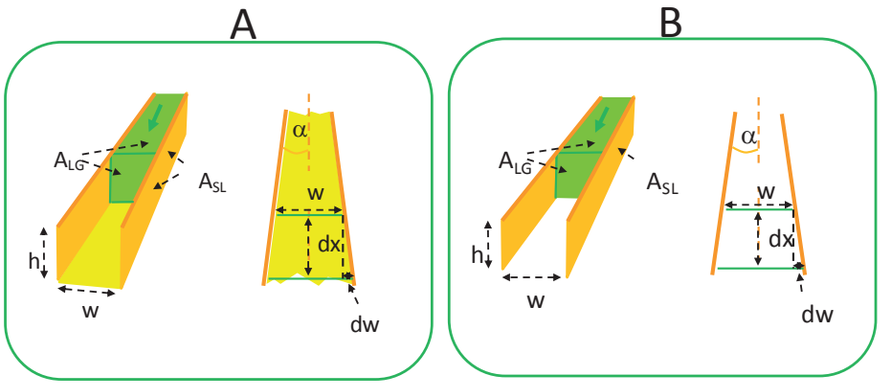

Fig.1. A: U-groove; B: suspended channel. Left: perspective sketch of the channel; right: top view.

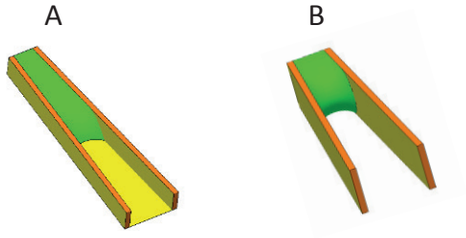

Fig.2. Evolver prediction of the stopping of the SCF: A, U-groove, B, suspended channel.

Experimental approach: Suspended channels of different diverging angle α have been designed in a PMMA plate. Their diverging angles have been designed so that the flow reaches the extremities for contact angles of 30, 40, 50 60 and 70°. Large widths at the extremity correspond to small contact angles, and conversely. Experiments have been performed with tinted water in hydrophilically treated PMMA channels, and mineral oil and not-treated PMMA channels (figure 3).

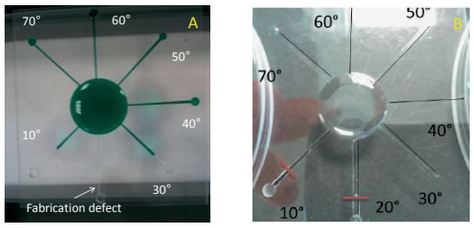

Fig.3. Radial suspended channels and central reservoir (A) PMMA hydrophilic treated device: colored water penetrates unto the extremity of the 40° channel, but not to the extremity of the 30° channel; (B) PMMA non hydrophilic treated device: mineral oil has a contact angle with PMMA comprised between 20 and 30°

Conclusion: SCF in a diverging channel does not flow indefinitely. It stops when the cross section becomes larger than a threshold depending on the geometry and contact angle. Expressions for this limit have been derived for U-grooves and suspended channels.

References

[1] C.D. Chin, Sau Yin Chin, T. Laksanasopin, S.K. Sia, Chapter 1: Low-Cost Microdevices for Point-of-Care Testing, in Point-of-Care Diagnostics on a Chip, eds. D. Issadore and R.M. Westervelt, Springer-Verlag Berlin Heidelberg 2013.
[2] L. Gervais, E. Delamarche, Toward one-step point-of-care immunodiagnostics using capillary-driven microfluidics and PDMS substrates. Lab. Chip **9**, 3330–3337, 2009.
[3] J.P. McHale, S.V. Garimella, Heat transfer in trapezoidal microchannels of various aspect ratios, Int J Heat Mass Trans. **53**, 365–375, 2010.
[4] M. Conrath, P. J. Canfield, P. M. Bronowicki, M. E. Dreyer, M.M. Weislogel, and A. Grah, Capillary channel flow experiments aboard the International Space Station, Phys. Rev. E **88**, 063009, 2013.
[5] J. Berthier, K. Brakke, E. Berthier, A general condition for spontaneous capillary flow in uniform cross-section microchannels, Microfluid Nanofluid **16**, 779–785, 2014.
[6] K.A. Brakke, The Surface Evolver, Experimental Mathematics **1**(2), 141-165, 1992.

ID 176

Thread-based microfluidics: spontaneous capillary flow in homogeneous and heterogeneous microfiber bundles

K.A. Brakke[1], D. Gosselin[2], E. Berthier[3], J. Berthier[2]

[1] Mathematics Department, Susquehanna University, Selinsgrove, PA 17870, USA.
[2] Department of Biotechnology, CEA-Leti
University Grenoble Alpes F-38000 Grenoble, F-38054, Grenoble, France.
[3] Tasso Inc., Seattle, USA

Introduction: Thread-based microfluidics has recently seen important developments in the domain of portable diagnostic systems [1-4], smart bandages [5] and tissue engineering [6-8]. Threads consist of fibers of natural origin—such as cotton or cellulose—or of artificial origin such as polymers, aligned or twisted together (fig.1). Wetting properties of the fibers are necessary to obtain wicking. In the case of aqueous liquids, either the fibers are naturally hydrophilic—like cotton or cellulose—or they are hydrophilically treated—like polymeric fibers which are treated by plasma O_2—in order to obtain a capillary flow.

Wicking of threads has been investigated in the literature, either in the case of solitary fibers [9], or from a global, average standpoint [10]. However, a detailed approach of the different flow regimes is still missing. In this work, we investigate theoretically [11,12] and numerically with the software Surface Evolver [13] the capillary flow patterns in homogeneous and heterogeneous fiber bundles (fig.2).

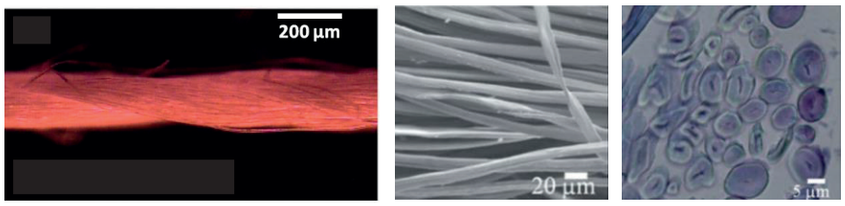

Fig.1. Different types of yarns: left, plasma O2 treated polymeric fibers; middle, cotton fibers; right, cross section of a

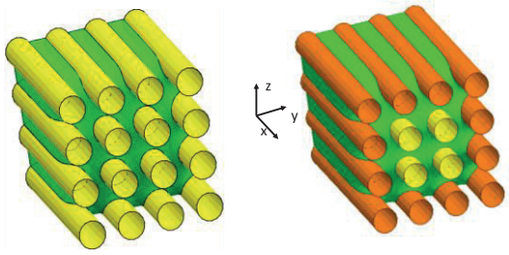

Fig.2. Homogeneous and heterogeneous fiber bundles.

Theory and numerical approach: Spontaneous capillary flow is determined by the generalized Cassie equation [11,12]

$$\sum_i p_{w,i} \cos\theta_i + p_F \cos\pi > 0\,, \qquad (1)$$

where the notations $p_{w,i}$ correspond to the wetted parts of the perimeter in a cross section, p_F is the unwetted (free) perimeter, and θ_i are the contact angles. In the case of a homogeneous fiber bundle, relation (1) leads to a condition of the type $A\cos\theta + B\sin\theta > D$, where A, B and D are parameters depending on the fiber spacing and arrangement. The case of a heterogeneous bundle is far more complicated. Considering a bundle where the outer ring has a different contact angle than that the inner fibers, different flow patterns are predicted. Figure 3 shows the liquid in a cross section of the bundle depending on the compactness of the bundle (ratio between rod radius and rod center distance) and the contact angles of the inner and outer rings.

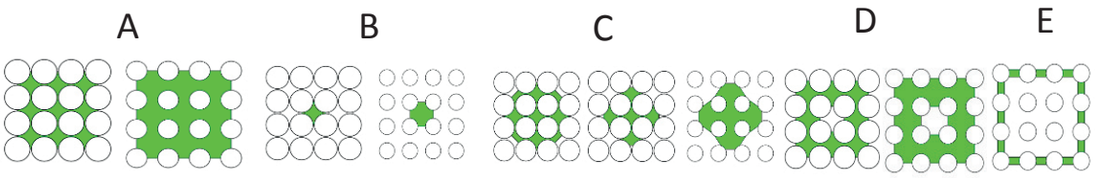

Fig. 3. Different flow patterns depending on the compactness of the bundle and contact angles.

For a given compactness ratio, flow diagrams can be plotted as functions of the two contact angles, showing the domains corresponding to the different patterns: all wetted (case A in figure 3), center only (case B in figure 3), wonky corners (case C in figure 3), all outer (case D in figure 3), outer ring (case E in figure 3) (fig.4).

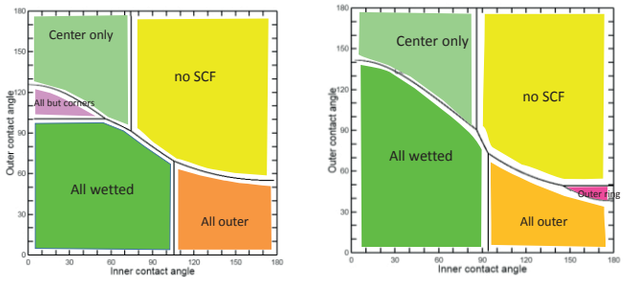

Fig.4. Phase diagram for a square and a round fiber bundle.

Experimental work: At the present time, there is no experimental work directly related to the present approach. However, some very recent experiments using threads to separate plasma from whole blood are showing many similarities with our approach [14] (fig.5). Further experimental work is needed.

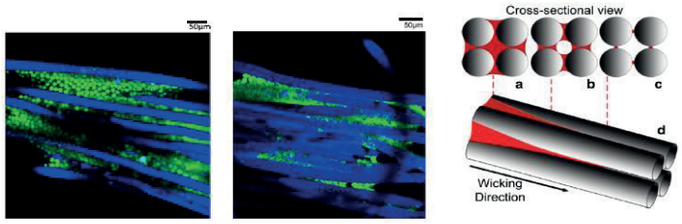

Fig.5. Left and middle: RBCs blocked or not in a parallel fiber bundle (depending on the fiber coating); right: sketch of fibers wicking by Nilghaz et al. [14]

References

[1] R. Safavieh, M. Mirzaei, M. A. Qasaimeh, D. Juncker, Yarn-based microfluidics: from basic elements to complex circuits, Thirteen International Conference on Miniaturized Systems for Chemistry and Life Sciences, November 1-5, 2009, Jeju, Korea.
[2] X. Li, J. Tian, W. Shen, Thread as a versatile material for low-cost microfluidic diagnostics, ACS Applied Materials and Interfaces, **2**(1), 1-6, 2010.
[3] M. Reches, K.A. Mirica, R. Dasgupta, M.D. Dickey, M.J. Butte, G.M. Whitesides, Thread as a matrix for biomedical assays, ACS Applied Materials and Interfaces, **2**(6), 1722-1728, 1010.
[4] A. Nilghaz, D. R. Ballerini, and W. Shen**,** Exploration of microfluidic devices based on multi-filament threads and textiles: A review, Biomicrofluidics **7**(5), 051501, 2013.
[5] D. Sharp, The development of smart-bandage technologies, Thesis at Nottingham Trent University, 2009.
[6] C.D. Young, J.R. Wu, T.L. Tsou, High-strength, ultra-thin and fiber-reinforced pHEMA artificial skin, Biomaterials **19**(19), 1745-52, 1998.
[7] A. Tamayol, M. Akbari, N. Annabi, A. Paul, A. Khademhosseini, D. Juncker, Fiber-Based Tissue Engineering: Progress, Challenges, and Opportunities, Biotechnology Advances, Biotechnol Adv. **31**(5): 669–687, 2013.
[8] T.V. Chirila, An overview of the development of artificial corneas with porous skirts and the use of PHEMA for such an application, Biomaterials **22**(24), 3311-3317, 2001.
[9] D. Quéré, Fluid coating on a fiber, Annu. Rev. Fluid Mech., **31**, 347–84, 1999.
[10] D.R. Ballerini, Xu Li, Wei Shen, Flow control concepts for thread-based microfluidic devices. Biomicrofluidics, **5**, 014105, 2011.
[11] J. Berthier, K.A. Brakke, The physics of microdroplets, Scrivener-Wiley Publishing, 2012.
[12] J. Berthier, K. Brakke, E. Berthier, A general condition for spontaneous capillary flow in uniform cross-section microchannels. Microfluid. Nanofluid. **16**(4), 779-785, 2014.
[13] K.A. Brakke, The Surface Evolver, Experimental Mathematics **1**(2), 141-165, 1992.
[14] A. Nilghaz, D.R. Ballerini, L. Guan, L. Li, W. Shen, Red blood cell transport mechanisms in polyester thread-based blood typing devices, Anal. Bioanal. Chem. on line, July 2015.

5th Micro and Nano Flows Conference
Milan, Italy, 11-14 September 2016

An integrated microfluidic digital PCR system for alginate droplet formation, efficient direct PCR amplification and imaging

Lijun Li[1], Linfen Yu[1]*, Tianzhun Wu[1]

* Corresponding author: Tel.: +086 (755)86585206; Fax: +086 (755)86392299; Email: lf.yu@siat.ac.cn
1 Shenzhen institute of Advanced Technology, Chinese Academy of Science, Shenzhen, China

Keywords: microfluidic , digital droplet, PCR, alginate beads

Microfluidic based digital PCR (dPCR) enables precise, highly sensitive absolute quantification for nucleic acids without the need for standard curves [1]. For example, by segregating single DNA molecules in individual water-in-oil emulsion droplets, emulsion PCR (ePCR) offers the advantage of massively parallel clonal amplification of DNA templates, which allows the identification and quantization of rare mutant gene within a large population [2, 3] and enables new generation of ultra-high throughput DNA sequencing technologies [4]. More recently, microfluidic microdroplet technology has been exploited to perform PCR in droplets because of its unique features. It can prevent crossover contamination and PCR inhibition, is suitable for single-cell and single-molecule analyses, and has the potential for system integration and automation. Although significant advances have been made in developing droplet-based microfluidic PCR devices, most of them were still cannot integrate droplet formation, PCR amplification, and fluorescent signal detection into one machine. An ideal microfluidic system with implemented on-chip PCR function should be fully autonomous, easy for non-experts to use, and has complete protocol integration. In this paper, we developed a high throughput technology enabling formation and encapsulating PCR sample into solid alginate bead, locating the beads into individual chambers, which allow the on-chip PCR amplification and fluorescent imaging. We demonstrate an integrated and automatic digital PCR system, making it a promising platform for many single copy genetic studies. This platform will also greatly improve our understanding of disease pathophysiology and diagnosis.

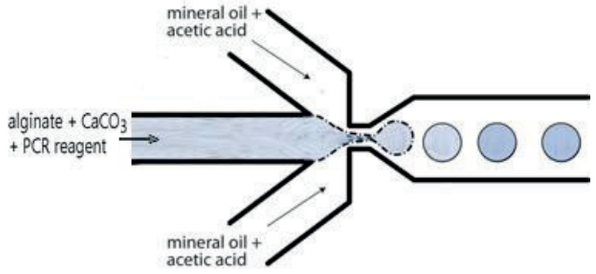

Fig1. Formation of alginate PCR beads. Flow focusing using two dispersed phases and one immiscible continuous phase forms alginate PCR beads. The first dispersed phase consisted of PCR smaples suspended in alginate precursor solution and insoluble calcium carbonate particles. The immiscible continuous phase was mineral oil containing acetic acid. In this internal gelation method, acid diffuses into the alginate precursor solution, and releases Ca^{2+} ions from the $CaCO_3$ particles. The alginate crosslinks in the presence of Ca^{2+} to give a gel.

1. Droplet formation

The microfluidic chips were fabricated in PDMS using standard soft lithographic techniques[5]. High aspect ratio features were first patterned using SU-8 3050 (MicroChem Corporation, USA) photoresist on a silicon substrate. These features later defined the microchannels and inlet/outlet reservoirs. The SU-8 and silicon structure served as the mold master, onto which poly-(dimethylsiloxane) (PDMS) (Sylgard 184, Dow Corning, USA) was poured. PDMS was cured at 80℃ for 1h, then the PDMS structure was peeled off the mold master.The PDMS channel was bonded to a glass substrate on which a thin layer of PDMS was spin-coated and cured, so that all four interior walls of the microfluidic channel would have the same surface properties. This method improves the reliability of entirely wetting the channel interior by the continuous oil phase during flow focusing, and reduces the formation of jets instead of droplets during the flow focusing step. The schematic of the droplet-based microfluidic device is shown in Fig. 1. The alginate encapsulated PCR droplet was formed on the microfluidic chip using multiple inlet flows in a flow focusing geometry as shown in Fig. 1. The water dispersed phase (1) consisted of alginate precursor, PCR reagent, insoluble calcium carbonate particles, potassium chloride and sodium chloride dispersed in solution. The immiscible continuous phase (2) was mineral oil containing 2μL/mL acetic acid and 2.5% Span 80 (Sigma-Aldrich Co. LLC.). The outlet of chip flows to the collection vial, where gel beads were collected. The alginate powder (Sigma-Aldrich Co. LLC. A2033) was dissolved in sterile water and stirred overnight. Powder of $CaCO_3$ particles (J.T. Baker@1301-01) was dissolved and sonicated in sterile water at the concentration of 2 M. The final concentration of $CaCO_3$ in alginate solution was 40 mM, The final concentration of potassium chloride and sodium chloride is respectively 7mM and 75mM. Alginate gels via calcium-mediated crosslinking. Calcium, bound in the insoluble form of $CaCO_3$, is mixed into an ungelled alginate solution of high or neutral pH. When the pH is lowered, the acid reacts with the calcium carbonate to release water, CO_2 and Ca^{2+}, initiating alginate gelation. Na^+ and K^+ avoid the inhibition of alginate to PCR amplification. Here, the oil phase is acidified, and as the alginate droplets spend more time in the oil, more acid will diffuse into the alginate, causing Ca^{2+} release and alginate gelation. Once gelled, the beads can be collected in a parallel of trapping chambers, which can be located for downstream PCR amplification and fluorescent imaging analysis.

2. Droplet trapping

In this paper, we designed a high-throughput droplet trapping

matrix as shown in Fig 2. There are totally 62 parallel rows with 95 U-shaped microsieves in each row. Each micro-sieve is semicircular with a 20 um apertures. To increase the throughput of trapping efficiency and reduce the clogging, we utilized a continuous and orthogonal flow based on the microseives structure. Specially, the beads are generated and flow horizontally from left to right into the microfluidic matrix, and simultaneously a constant vertical pressure was applied to push up the beads to allow them travel diagonally up into the microseives. With the continuous flow, each micro-sieve will efficiently retain an alginate bead and achieve an 86.15 % of trapping rate. The redundant beads were flushed out of the channel through the outlet.

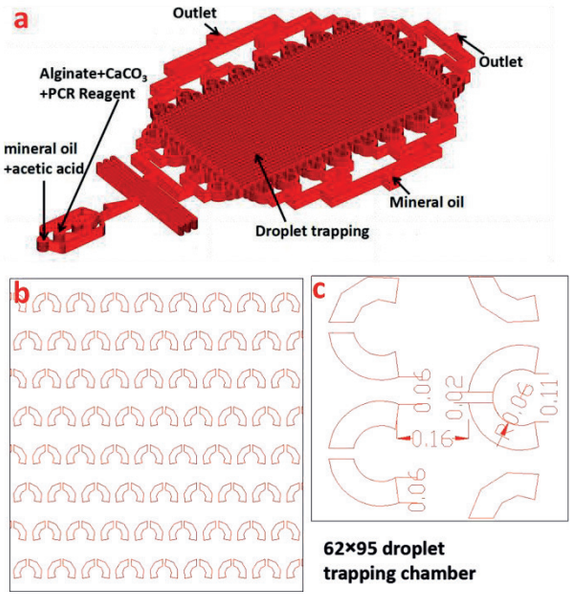

Fig 2. (a) Illustration of digital droplet PCR microchip. (b) the image of micro-sieve structure for beads trapping. (c) the dimension of micro-sieve structure.

3. Droplet PCR and Imaging

Although microfluidic droplet-based PCR reaction has been developed and commercialized by Bio-Rad, and Rain Dance Company, they cannot integrate droplet formation, PCR amplification, and fluorescent signal detection into one machine. In this paper, we developed a promising platform which enables integration of droplet formation, PCR amplification and signal detection. We designed an integrated chip and further investigated the capability of this system for encapsulation of alginate beads carrying PCR reagent, and applied it for H7N9 amplification and image. Fig 3a showed the high efficient beads capture, which could reach 86.15 percent (1950 alginate beads counted). Microfluidic flow focusing produces alginate beads with good size uniformity. The hydrogel alginate beads exhibited a narrow size distribution with CV of 0.08 (Fig. 3b). The average alginate bead diameter was 84.53 μm (equivalently 0.32 nL). The alginate bead structure assists in maintaining spherical droplet and bead shape. Figure 3c exhibited fluorescent microscope image of alginate beads after amplification from H7N9 template. The PCR amplification occurred within the alginate beads. A reverse transcription PCR (RT-PCR) thermocycler used cycling protocol: a reverse transcriptionan step at 42 ℃ for 25 minutes, and then a initial denaturation step at 95 ℃ for 3 minutes, 40 cycles of denaturation (95 ℃ for 8 s), annealing and extension (60 ℃ for 35 s), and a final step hold on 4 ℃. After RT-PCR we photographed fluorescent microscope image (Fig.3c). We can see that RT-PCR could successfully react in the alginate beads on the chip. The integrated and automatic system will be a potential new tool for gene diagnosis, single-cell analysis, drug efficacy and prognosis.

4. Conclusions

This droplet based microfluidic system integrating a droplet formation and a droplet trap array is described for encapsulating PCR reagent into a parallel series of alginate beads. The concept of using alginate microspheres as nanoliter-scale reactors for PCR is relatively new. This method enables highly efficient DNA amplification and high throughput fluorescent imaging. This platform has the benefit of scaling of dimensions that enables controlled and precise droplet generation and rapid trapping beads into individual chambers, on-chip PCR amplification and fluorescent imaging which make it a promising, and ideal platform for many biological applications, especially for single cell genetic analysis.

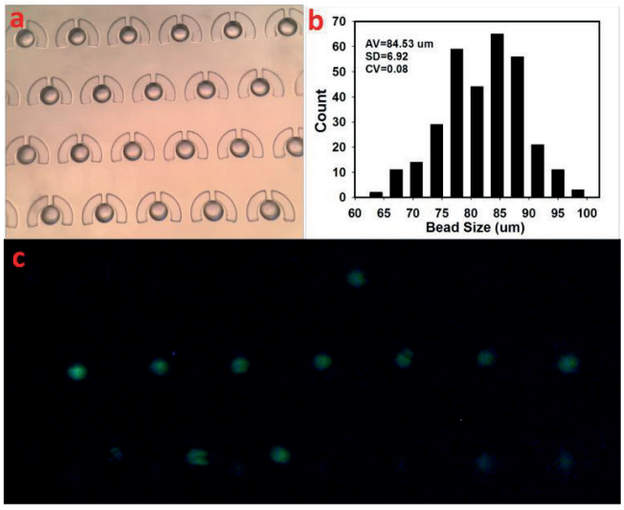

Fig 3. (a) Image of 62×95 array droplets encapsulated into the U-shaped microsieves. (b) Size distribution of the alginate beads. (c) Fluorescent microscope image of alginate beads after amplification from H7N9 template.

5. Acknowledgment

This work is supported by NSFC (No. 51475451), Guangdong Innovative and Entrepreneurial Research Team Program (No. 2013S046), Shenzhen Peacock Plan and Shenzhen Scientific Research Plan (JC201105201157A).

6. References

[1] Nakano M, Komatsu J, Matsuura S I, et al. Single-molecule PCR using water-in-oil emulsion. Journal of Biotechnology, 2003, 102(2):117-124.

[2] Pekin D, Skhiri Y, Baret J C, et al. Quantitative and sensitive detection of rare mutations using droplet-based microfluidics. Lab on A Chip, 2011, 11(13):2156-66.

[3] Zhang Y, Jiang H R. A Review on Continuous-flow microfluidic PCR in droplets: advances, challenges and future. Analytica Chimica Acta, 2016.

[4] Jacobs B K, Goetghebeur E, Clement L. Impact of variance components on reliability of absolute quantification using digital PCR. Bmc Bioinformatics, 2014, 15(1):3419-3420.

[5] Whitesides G M, Ostuni E, Takayama S, et al. Soft lithography in biology and biochemistry. Annual Review of Biomedical Engineering, 2001, 3(1):335-373.

5th Micro and Nano Flows Conference
Milan, Italy, 11-14 September 2016

Dynamics of Droplets Evaporating on Structured Surfaces

Gail DUURSMA [1,*], Coinneach Mackenzie-Dover[1], Nathan WEST [1], John CHRISTY [1], Khellil SEFIANE [1]

* Corresponding author: Tel.: ++44 (0)131 6504868; Fax: ++44 (0)131 6506551; Email: gail.duursma@ed.ac.uk
1: School of Engineering, The University of Edinburgh, Edinburgh, UK

Keywords: Evaporation, Sessile droplets, Contact lines, Hydrophobicity

Wetting phenomenon plays a crucial role in a wide range of technological applications. Spreading of liquids on solids involving phase change is encountered in many areas ranging from biological systems to industrial applications. Ring formation from evaporating droplets and its use for thin films coating, and DNA chains elongation using a drying sessile droplet are examples of new developments and interest in the understanding of the pinning process of evaporating droplets. Previous studies have sought to understand the fundamentals of this process (for example [1-3]), yet the effect of surface structure and roughness remains to be fully elucidated. In recent investigations it has been shown that on real surfaces evaporating droplets tend to remain pinned to the solid surface, implying that the base of the droplet remains constant while evaporation takes place. The dynamics of the contact line is an important phenomenon as it controls the evaporation rate. It has been shown that as far as the droplet is pinned the evaporation rate is constant and almost proportional to the droplet radius. After the depinning the evaporation rate deviates from this trend [1].

Many descriptions of the evaporation of a sessile droplet have been reported, including the work of Hu and Larson [2] and Pickenett and Bexon [3]. On ideal surfaces the contact angle remains constant and the base of the droplet decreases, ideal system having no hysteresis.

On real surfaces two stages are observed. In the first stage, the contact angle decreases while the contact line holds its original position - this corresponds to a droplet with a fixed or pinned contact line. In this case the liquid must flow radially outward for the contact line to maintain its position, and the contact angle decreases with time as volume decreases because of evaporation. This first stage is responsible for the ring formation in drying droplets investigated by Deegan *et al.* [1]. When the contact angle reaches a critical value, the droplet depins and the second stage of evaporation starts. In this stage the contact line recedes while the contact angle remains constant, Pickenett and Bexon [3]. For the first stage, a model of local mass flux droplet evaporation has been proposed. Real surfaces are usually rough and contaminated because of defects, thus pinning is mostly observed.

In the present study we fabricated an array of structured surfaces on silicon wafers, Figure 1. Each square contains a grid of uniformly spaced pillars, with each square having a different spacing, from 5 – 100 microns. This allows testing in the same conditions.

The experiments consisted of depositing water droplets on structured surfaces and recording the evaporation process. Using FTA200 software, droplet profile evolution in time data, such as radius, volume, contact angle and height of the sessile droplet, were extracted. Lifetimes of droplets depended on intial contact angle as expected (not shown). Using data of the radius and contact angle evolution, the time of depinning was determined. This corresponds to the moment the base radius of the droplet start to recede.

Using a force balance near the contact line the depinning force is estimated as follows [4]:

$$F_{depinning} = \gamma\left(\cos\theta_{depinning} - \cos\theta_{initial}\right) \qquad (1)$$

The magnitude of the depinning force as a function of the structures spacing is plotted in Figure 2. The results show a lower region where the depinning force decreases with spacing. Above a certain threshold spacing, however, the depinning force is constant and independent of pillar spacing.

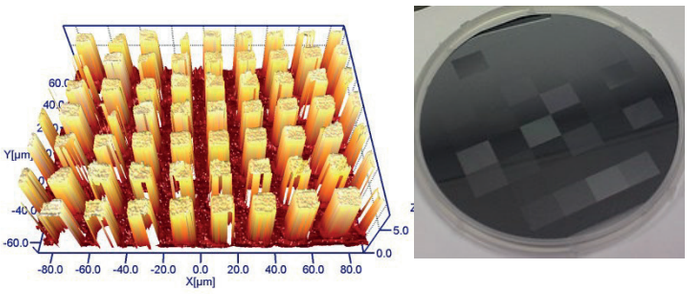

Figure 1 – Structured surfaces.

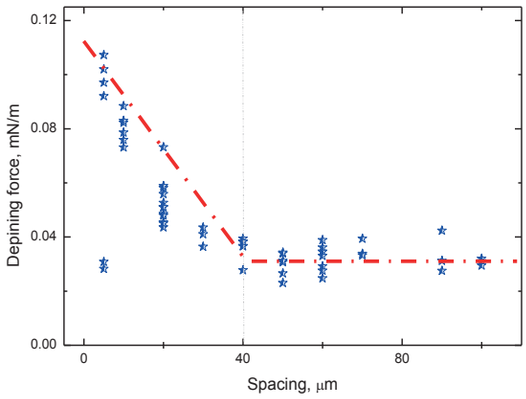

Figure 2 – Calculated depinning force vs. spacing.

These results are fundamental to understanding the effect of roughness on contact line dynamics and further work on quanitifying the trend for small spacings will be undertaken.

References

1. Deegan, R., *Pattern formation in drying drops*. Phys Rev E, 1998. 61(1): pp. 475-485.
2. Hu, H. and R.G. Larson, *Evaporation of a Sessile Droplet on a Substrate*. Journal of Physical Chemistry B, 2002. 106: pp. 1334-1344.
3. Pickenett, R. and R. Bexon, *The Evaporation of Sessile or pendant Drops in Still Air*. Journal of Colloid and Interface Science, 1977, 61(2): pp. 336-350.
4. DeGennes, P., *Wetting: statistics and dynamics.* Rev. Mod. Phys., 1985. 57: pp. 827-863.

ID 181

5th Micro and Nano Flows Conference
Milan, Italy, 11-14 September 2016

Cooling Process of Nanofluid in a Cavity Submitted to Non-isothermal Heating

ARROUB Ismail[1], BAHLAOUI Ahmed[*1], RAJI Abdelghani[2], HASNAOUI Mohamed[3], NAÏMI Mohamed[2]

* Corresponding author: Tel.:+212 5 23 42 46 85; Fax: +212 5 23 42 45 97; Email: bahlaoui75@yahoo.fr

[1] Interdisciplinary Laboratory of Research in Sciences and Technologies (LIRST), Physics Department, Polydisciplinary Faculty, Sultan Moulay Slimane University, Béni-Mellal, Morocco

[2] Laboratory of Flows and Transfers Modelling (LAMET), Physics Department, Faculty of Sciences and Technics, Sultan Moulay Slimane University, Béni-Mellal, Morocco

[3] Laboratory of Fluid Mechanics and Energetics (LMFE), Unit Affiliated to CNRST (URAC 27), Physics Department, Faculty of Sciences Semlalia, Cadi Ayyad University, Marrakech, Morocco

Keywords: Mixed convection, nanofluid, linearly varying heating, suction, ventilated cavity.

1. Introduction

Mixed convective heat transfer is an important phenomenon in many engineering applications for example cooling of electronic components, nuclear energy, solar energy, transportation, building heating and lubrication technologies. However, low thermal conductivity of conventional fluids such as water, oil and ethylene glycol is the primary limitation on the enhancement of heat transfer performance in such engineering applications. In order to achieve a better performance on the heat transfer, highly conductive nanoparticles are suspended in base fluid; the resulting fluid is called nanofluid. This technique was developed by many researchers as Choi [1] who suggested that the addition of nanoparticles into the base convective fluid increases its thermal conductivity and therefore substantially enhances its heat transfer characteristics. In the recent years many works have investigated numerically the enhancement of mixed convection heat transfer utilizing nanofluids. In this perspective, Talebi et al. [2] studied numerically mixed convection flows in a square lid-driven cavity utilizing nanofluid. Their results showed that at a given Reynolds and Rayleigh numbers, solid concentration has a positive effect on the heat transfer enhancement. Concerning the same problem, Chamkha and Abu-Nada [3] investigated steady laminar mixed convection flow in single and double-lid square cavities filled with water-Al_2O_3 nanofluid. They found that significant heat transfer enhancement is obtained due to the presence of nanoparticles which is accentuated by increasing the nanoparticle volume fractions. More recently, mixed convection of nanofluids in ventilated cavities has been also the object of interest. In this context, Shahi et al. [4] conducted a numerical study of mixed convection flows of Cu-water nanofluid in a vented square cavity submitted to an imposed heat flux. The results presented indicate that the increase in solid concentration leads to an augmentation of the average Nusselt number at the heat source surface and, at the same time, to a decrease of the average bulk temperature. A similar problem was treated numerically by Mahmoudi et al. [5] with imposed temperature for different locations of inlet and outlet ports. The authors reported that, in the presence of nanoparticles, the bottom-top configuration was the most efficient (in terms of heat transfer improvement) compared to the remaining configurations considered in this study. In addition, the least effects accompanying the increase in solid concentration were observed in the case of top-top configuration.

The aim of the current study is to simulate numerically mixed convection heat transfer characteristics of water-based Al_2O_3 nanofluid flowing through a rectangular cavity with suction. The consequence of varying the Reynolds number, Re, the nanoparticles concentration, ϕ, and the mode of heating on the hydrodynamic and thermal characteristics have been investigated and discussed.

2. Problem Definition

A schematic diagram of the studied configuration is shown in Fig. 1. It consists of a ventilated horizontal rectangular cavity having an aspect ratio A = 2 and heated from its lower wall with a linearly increasing or decreasing hot temperature profile (Fig. 2) while the remaining boundaries are insulated. The physical system is subjected to an external flow which passes through the cavity by suction. The water-alumina nanofluid enters into the cavity from the bottom opening located in left vertical wall and leaves from the upper opening of the opposite vertical one. The inlet and outlet ports have a constant dimensionless height, B = 1/4.

3. Results and Discussion

In this section, the Rayleigh number was kept at a constant value ($Ra = 10^6$). In Fig. 3, we illustrate the evolution of the average Nusselt number versus the Reynolds number for both heating modes and various values of ϕ. As expected, the results presented indicate that for both heating modes, Nu increases with the increase of Re and ϕ. However, the rate of increase of the dimensionless heat transfer with ϕ is manifestly limited for low values of Re, particularly for the case of increasing temperature profile. For a fixed value of Re, it is seen that the decreasing heating mode is more efficient to heat removal compared to the other heating mode, either with or without the presence of nanoparticles. The comparative thermal efficiency is amplified (in favor of the decreasing temperature profile) with the increase of Re. Finally, it should be recalled that the suction mode has led to periodic solutions in the case of increasing temperature profile for Re ranging from 200 to 600. The upper limit of Re depends on ϕ.

Variations of the average temperature $\overline{T}$ of the fluid within the cavity are plotted versus Re in Fig. 4 for both increasing and decreasing heating modes and various values of ϕ. As can be seen, for the decreasing case, the average temperature $\overline{T}$ decreases drastically by increasing Re. This tendency is explained by the fact that the heat released by the hot wall is driven outwardly from the cavity by the growing effect of the forced flow which leads to a better cooling of the cavity. In the case of an increasing temperature

profile, the parameter $\overline{T}$ increases slightly with Re until reaching a maximum value for a critical value of Re ranging in [600, 700] which strongly depends on ϕ. This trend is attributed to the assisting flows of natural and forced convections due to the competition between them. Above this threshold the evolution is reversed and is characterized by a clear decrease of $\overline{T}$ with Re as a consequence of the forced flow predominance which favors the heat evacuation through the outlet. For a fixed value of Re, it is found that the mean temperature increases with the solid volume concentration for the two heating modes. Moreover, it is retained from this figure that the decreasing heating mode involves globally to a better cooling inside the cavity since the related values of $\overline{T}$ are weaker in comparison with the increasing heating one, if we except the case corresponding to weaker values of Re ($Re \leq 400$) for which the increasing heating gives the most cooling efficiency.

4. Conclusion

A numerical analysis has been performed to study the laminar two-dimensional mixed convection flow of Al_2O_3-water nanofluid in a horizontal vented enclosure heated from below and cooled by an external flow. The obtained results show that the suspended nanoparticles contribute substantially to improve the heat transfer exchanged between the active wall and the nanofluid and to an increase of the average temperature of the fluid either in the case of increasing or decreasing heating modes. On the other hand, it is to remember that the decreasing heating mode gives a better thermal efficiency than the increasing heating mode by leading to more heat transfer across the cavity even with or without the presence of nanoparticles. In addition, it is found that a better cooling of the cavity is generally reached by applying the decreasing heating (for moderate and high values of Re) since these cases lead to lower values of the mean temperature.

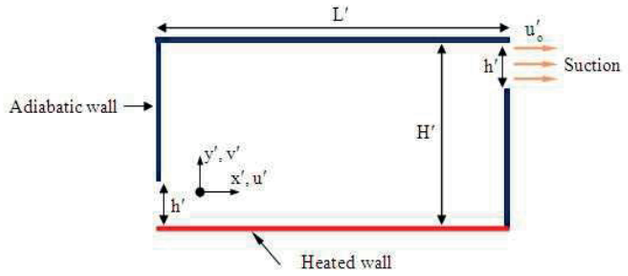

Figure 1: Studied configuration

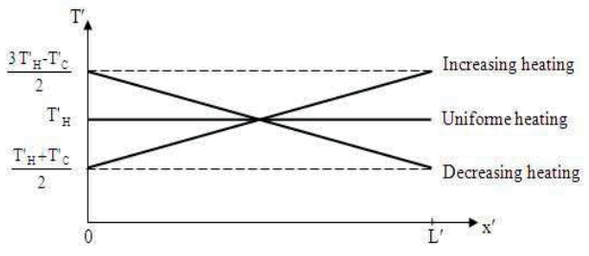

Figure 2: Imposed temperature profiles on the heated wall

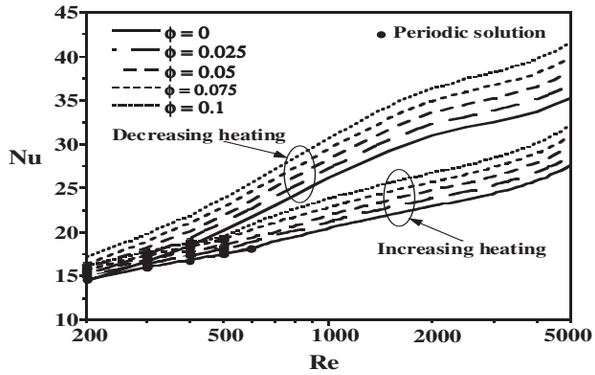

Figure 3: Variations, with Re, of the average Nusselt number, Nu, for different values of ϕ in both increasing and decreasing heating cases.

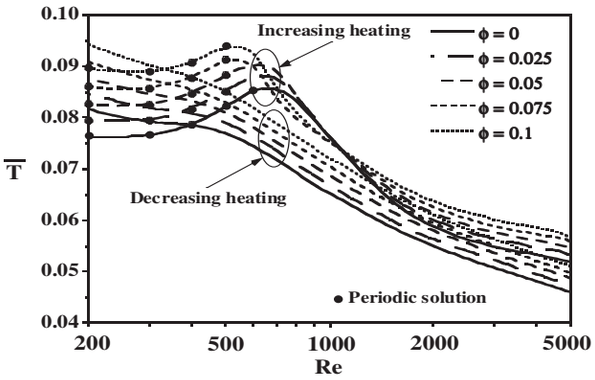

Figure 4: Variations, with Re, of the mean temperature, $\overline{T}$, for different values of ϕ in both increasing and decreasing heating cases.

References

[1] U.S. Choi, Enhancing thermal conductivity of fluids with nanoparticles, ASME Fluids Engineering Division 231 (1995) 99-103.

[2] F. Talebi, A.H. Mahmoudi, M. Shahi, Numerical study of mixed convection flows in a square lid-driven cavity utilizing nanofluid, International Communications in Heat and Mass Transfer 37 (2010) 79-90.

[3] A.J. Chamkha, E. Abu-Nada, Mixed convection flow in single- and double-lid driven square cavities filled with water-Al_2O_3 nanofluid: Effect of viscosity models, European Journal of Mechanics B/Fluids 36 (2012) 82-96.

[4] M. Shahi, A.H. Mahmoudi, F. Talebi, Numerical study of mixed convective cooling in a square cavity ventilated and partially heated from the below utilizing nanofluid, International Communications in Heat and Mass Transfer 37 (2010) 201-213.

[5] A.H. Mahmoudi, M. Shahi, F. Talebi, Effect of inlet and outlet location on the mixed convective cooling inside the ventilated cavity subjected to an external nanofluid, International Communications in Heat and Mass Transfer 37 (2010) 1158-1173.

5th Micro and Nano Flows Conference
Milan, Italy, 11-14 September 2016

Accelerating a multiscale fluidic model with Gaussian processes

David STEPHENSON [1,*], James R. KERMODE [2], Duncan A. LOCKERBY [1]

* Corresponding author: Email: david.stephenson@warwick.ac.uk
1 School of Engineering, University of Warwick, Coventry, UK
2 Centre for Predictive Modelling, University of Warwick, Coventry, UK

Abstract We present a hybrid continuum-atomistic scheme which combines molecular dynamics (MD) simulations with on-the-fly machine learning techniques for the accurate and efficient prediction of multiscale fluidic systems. Using a Gaussian process as a surrogate model for the computationally expensive MD simulations, we employ Bayesian inference to predict the system behaviour at the atomistic scale, purely from consideration of the macroscopic inputs and outputs. Whenever the uncertainty of this prediction is greater than a predetermined acceptable threshold, a new MD simulation is performed to continually augment the database, which is never required to be complete. This provides a substantial enhancement to the current generation of hybrid methods which often require many similar atomistic simulations to be performed, with information wastefully discarded after it is used once. We apply our hybrid scheme to nano-confined unsteady flow through a high-aspect-ratio converging-diverging channel for a range of uncertainty thresholds and initial databases. For low thresholds, our hybrid solution is highly accurate - within the thermal noise of a full MD simulation. As the uncertainty threshold is raised, the accuracy of our scheme decreases and the computational speed increases, enabling the compromise between precision and efficiency to be tuned. The speed-up of our hybrid solution (over a full MD simulation) ranges from an order of magnitude, with no initial database, to cases where an extensive initial database ensures no new MD simulations are required.

Keywords: Multiscale modelling, Machine learning, Hybrid methods, Micro/nanofluidics, Molecular dynamics

There are numerous applications in fluid dynamics where atomistic information is required to capture non-continuum/non-equilibrium phenomena, but the macroscopic flow develops over much larger length and time scales: for example, pumping technology that exploits thermal creep in a rarefied gas [1]; and high-throughput nanotube membranes for salt water desalination [2]. The multiscale nature of these systems leads to a dual requirement for capturing the local atomistic-scale interactions and the macro-scale fluid response. The complexity of the flow necessitates modelling with atomistic resolution, but the state-of-the-art techniques, e.g. molecular dynamics (MD) [3], are extremely computationally expensive. This limits their application to small system sizes, typically ~100 nm^3, and short simulation times, typically ~100 ns, rendering many important engineering problems intractable, and limiting possibilities for comparison with experiments.

Hybrid methods provide a promising framework for simulating such systems, by combining a continuum solution (here, the unsteady 1D equations for mass and momentum conservation) with atomistic solver subdomains (here, MD) and exploiting scale-separation, where it exists, to obtain a highly accurate, yet efficient, solution. In our example system (see Fig. 1a), the flow is highly multiscaled, as scale separation exists in the streamwise direction, but not in the transverse (wall-to-wall) direction, owing to non-continuum effects (e.g. molecular layering and velocity slip) persisting over the entire cross section. There has already been extensive research into hybrid methods (e.g. see recent review [4]); however, despite much progress, a

common flaw of hybrid methods is that, often, repetitious atomistic simulations are performed - i.e. information is used once, then wastefully discarded, despite configuration conditions remaining similar.

Here we propose an enhancement to hybrid methods, by modelling a database of MD simulations with a Gaussian process (GP) and using Bayesian inference to predict the output of new system configurations. When the posterior variance (uncertainty) of this prediction is above a given threshold (i.e. when the system configuration is not well represented in the database), a new MD simulation is performed on-the-fly to augment the database, whose completeness is never required. Thus, as the database grows, progressively fewer MD simulations are necessary, because 'new' system configurations are more rarely encountered. This ensures near-optimal information efficiency, drastically reducing the computational cost, and potentially enabling the simulation of systems previously considered prohibitively large.

We apply our hybrid scheme to nano-confined unsteady flow through a high-aspect-ratio converging-diverging channel, and make comparisons to the full MD simulations of Borg et. al. [5] for a range of uncertainty thresholds and initial databases. The macroscopic inputs for the MD subdomain simulations (or GP surrogate model) are channel height, density, and external force; and the macroscopic outputs of the simulations/GP regression are pressure and mass flow rate. For low uncertainty thresholds, our hybrid solution is highly accurate, with errors within the range of thermal noise from a full MD simulation.

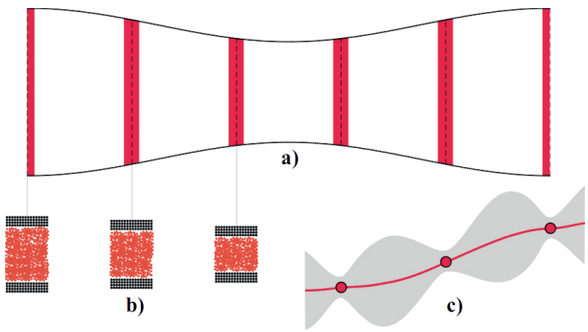

Fig. 1. Schematics of **a)** a multiscaled converging-diverging channel, **b)** the molecular subdomain decomposition, and **c)** the representation of the Gaussian-process predictive model.

As the uncertainty threshold is raised, the error increases to up to 2.5x the MD simulation noise; however, the computational speed-up over a full MD simulation also increases. When starting from an empty database, raising the uncertainty threshold for mass flow rate from 0.1 ng/s to 0.9 ng/s increases speed-up from 12.3x to 69.3x. Thus, the choice of threshold is a trade-off between the required accuracy and computational efficiency.

We demonstrate the computational benefit of creating an initial database to train our predictive model, by estimating the expected range of inputs. This enables more predictions to be made via interpolation between training data points, leading to fewer MD simulations performed on-the-fly. While maintaining the same level of accuracy, starting with a modest initial database covering just a few data points can result in a speed-up of 30.5x the full MD simulation for an uncertainty threshold of 0.1 ng/s.

We also show how existing databases can be built upon (while never needing to be fully complete) to rapidly obtain high resolution hybrid solutions - i.e. cheaply add more MD subdomains at locations of interest - or to model different flow fields effectively instantly - i.e. no new MD simulations are required.

References

1) Patronis, A., Lockerby, D.A., 2014. Multiscale simulation of non-isothermal microchannel gas flows. J. Comput. Phys. 270, 532-543.

2) Ritos, K., Borg, M.K., Lockerby, D.A., Emerson, D.R., Reese, J.M., 2015. Hybrid molecular-continuum simulations of water flow through carbon nanotube membranes of realistic thickness. Microfluid. Nanofluid. 19, 997-1010.

3) Allen, M.P., Tildesley, D.J., 1987. Computer Simulation of Liquids. Clarendon Press.

4) Mohamed, K.M., and Mohamad, A.A., 2009. A review of the development of hybrid atomistic-continuum methods for dense fluids. Microfluid. Nanofluid. 8, 283-302.

5) Borg, M.K., Lockerby, D.A., Reese, J.M., 2015. A hybrid molecular–continuum method for unsteady compressible multiscale flows. J. Fluid Mech. 768, 388-414.

5th Micro and Nano Flows Conference
Milan, Italy, 11-14 September 2016

High-accuracy particle sizing in sheath less microfluidic impedance cytometry

Federica CASELLI [1,*], Paolo BISEGNA [1]

* Corresponding author: Tel.: ++39 06 72597096; Email: caselli@ing.uniroma2.it
1 Department of Civil Engineering and Computer Science, University of Rome Tor Vergata, Italy

Keywords: Microfluidics, Electric impedance, Lab on chip, Single-cell analysis

Microfluidic impedance cytometry is a lab-on-chip technology offering a simple, non-invasive, label-free method for counting, identifying and monitoring cellular function at the single-cell level [1]. Impedance-based microfluidic systems are used to discriminate between WBCs in a differential count; to detect parasite-infected RBCs; to analyze viability of yeast and bacteria. Single-cell electrical phenotyping by means of multifrequency analysis enables tumor cell classification in mice. Other applications include examination of on-target and off-target effects during drug screening on a mixed cell population, or characterization of stem cells for therapeutic use.

The working principle of a typical impedance cytometer is quite simple (Fig. 1). Two pairs of facing microelectrodes are integrated into the wall of a fluid-filled microchannel. An AC excitation signal is applied to the top electrodes, and the differential current flowing through the bottom electrodes is measured. When a cell passes through the electrode region, a variation of the differential current, depending on cell dielectric properties, is recorded. However, the measured impedance signal also depends on the position of the cell between the electrodes [2], i.e. the trajectory of the cell as it flows through the channel (Fig. 2). This is because the electric field in the channel is not uniform, and is one of the fundamental limiting issues for the application of microfluidic impedance cytometry.

To obtain high quality (low CV) data, nearly all cytometers use some form of cell focusing. Typically, hydrodynamic focusing is adopted, like sheath flow or inertial focusing. However, the former increases the complexity of the layout and control for microfluidic devices and consumes additional fluid, while the latter requires high flow-rates that may induce stress in the cell, and restricts simultaneous measurement of heterogeneous populations. Other approaches proposed in the literature (e.g., dielectric focusing, DEP-inertial microfluidics) present similar limitations.

In this work, an original approach to overcome the aforementioned issue is described [3]. The transit times of cells through the device using two simultaneous current measurements, a transverse current and an oblique current, are recorded. Their ratio gives a new metric, used to estimate the position of the cell trajectory through the microchannel, and thus to compensate for the position-dependent variation of impedance. The new technique is developed and validated using numerical modelling. Then, it is applied to experimental impedance data relevant to a mixture of beads with different diameters. As a result, the position-dependent variation of impedance is completely eliminated, i.e. all particles of a given size show the same corrected impedance, irrespective of their trajectory through the channel. The method gives a Coefficient of Variation in (electrical) radius of particles of 1% for a sheath less configuration, independently of flow rate.

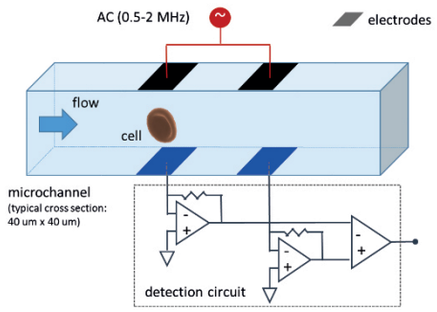

Fig. 1 Schematic of a typical microfluidic impedance cytometer (parallel-facing electrode design).

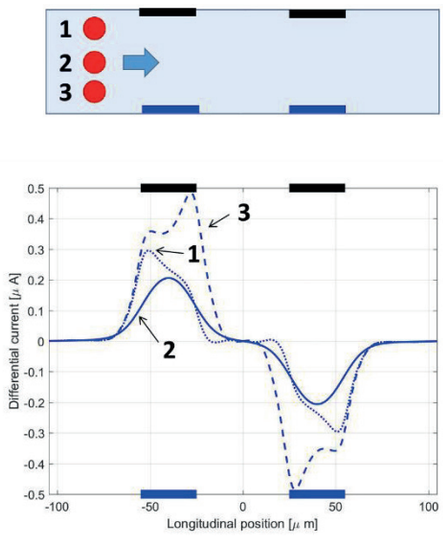

Fig. 2 Positional-dependence of the measured impedance signal. The experimental traces are relevant to equal-size spherical particles traveling in the center of the channel (2) or near the top (1) or bottom (3) electrodes.

Acknowledgment

This work was supported by the Scientific Independence of Young Researchers Programme, SIR 2014, RBSI14TX20-MUSIC Project.

References

[1] K.C. Cheung, M.Di Berardino, G. Schade-Kampmann, M. Hebeisen, A. Pierzchalski, J. Bocsi, A. Mittag and A. Tarnok, Microfluidic impedance-based flow cytometry, *Cytometry, Part A*, 77A, 2010.

[2] D. Spencer and H. Morgan, Positional dependence of particles in microfludic impedance cytometry, *Lab Chip*, 11, 2011.

[3] D. Spencer, F. Caselli, P. Bisegna, and H. Morgan, *submitted.*

5th Micro and Nano Flows Conference
Milan, Italy, 11-14 September 2016

Pool Boiling Enhancement on Nanostructured Copper Oxide Surfaces Prepared by Wet Chemical Method with Various Hydrophilicity

Amir M. GHEITAGHY [1,2*], Seyyede SH. TABATABAE [1], Hamid SAFFARI [1]

* Corresponding author: Tel.: ++98 (0)2177 240540; Fax: ++98 (0)2177 240488; Email: a_m_gheitaghy@mecheng.iust.ac.ir, a. mirzagheytghi@tudelft.nl
1 School of Mechanical Engineering, Iran University of Science and Technology, Iran
2 Electronic Components, Technology and Materials, Delft University of Technology, Netherlands

Abstract Surface hydrophilicity effect on pool boiling heat transfer enhancement was experimentally investigated. Various treatment time in wet chemical method were used to vary the hydrophilicity of the copper surface by modifying surface topography and chemistry. Experimental results show that critical heat Zux (CHF) values are higher in the hydrophilic surfaces. Investigation of bubble dynamics show why the heat transfer coefficient (HTC) not significantly improved in comparison of polished copper surface.

Keywords: Pool boiling, Hydrophilic, Copper oxide, Wet chemical.

1. Introduction

Pool boiling heat transfer is an effective mechanism for removing a high heat flux in low surface temperature at several engineering and industrial Eelds such as power plants, electronic cooling, and power generation. Recent advances on changing the surface energy of the heater surface have opened up new opportunities for enhancing the pool boiling by changing the contact angle (CA) through the implementation of nanostructures on the heater surface. It is well known that the CHF decreases dramatically on hydrophobic surfaces, whereas hydrophilic surfaces exhibit higher HTC as well as higher CHF values [1].

A variety of work has reported in regards to induction of hydrophilicity. Takata et al. [2] fabricated a photo induced superhydrophilic surface for pool boiling test. Nam et al. [3] fabricated superhydrophilic surface by generating needle shaped copper oxide nanostructures on microposts using electrochemical deposition. Chen et al. [4] reported a superhydrophilic surface made by electroless etching of nanowire arrays on Si and Cu substrate can be increased the CHF by more than 100%. Kwark et al. [5] fabricated nanoporous coating by boiling a copper substrate in ethanol based nanofluid.

This study applies the wet chemical method in three treatment time of 30, 60, and 180 min to grow the copper oxide on copper surface. Morphology and hydrophilicity of fabricated hydrophilic surfaces are determined with SEM and CA measurement. Pool boiling experiment is done to investigate the effect of hydrophilicity on bubble dynamics and performance of surfaces.

2. Experiment

2.1. Sample fabrication method

Copper has relatively poor surface wettability and hydrophilic treatments with wet chemical method was selected here. The procedures were as follows: a) polishing the surface with sandpaper and then cleaning the sample in acetone and ethanol at 25ŁC for 5min, with the assistance of ultrasonication, b) preparation of a solution of 5gr/L NaOH with 1gr/L $K_2S_2O_8$ mixed at a preset temperature in the ionized water tank, c) immersion of and holding the sample in the solution for a certain length of time, d) taking out the sample and rinsing it with de-ionized water and acetone, and e) air drying the sample [6].

3. Results and Discussion

3.1. Morphology and characteristics

Fig. 1 shows the surface condition of untreated sample and treated samples in different time steps. With increasing the immersion time, the copper color convert to black due to formation of copper oxide.

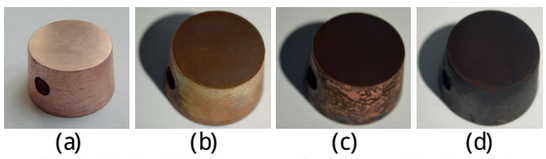

(a) (b) (c) (d)

Fig. 1. Hydrophilic copper surfaces treated in chemical solution (a) 0 min; (b) 30 min; (c) 60 min; (d) 180 min.

Fig. 2 shows the SEM photo of the treated and untreated copper surfaces. The untreated surface of the copper looks smooth with some sand paper crashes, while that of the hydrophilic surface is rougher, implying that cupric oxide is formed on the surface. Carey [12] stated that both chemical components and roughness affect the wetting properties of a surface, and the rougher the surface, the better the wettability will be. Also, the copper oxide has an inherent hydrophilic chemical property.

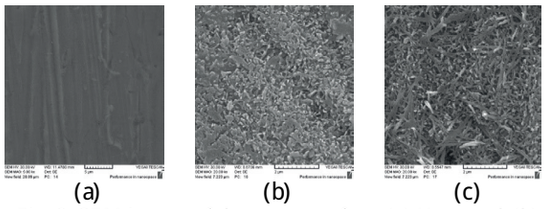

(a) (b) (c)

Fig. 2. SEM images of the copper surface; (a) Untreated; (b) Treated for 60min; (c) for 180min in chemical solution.

Table. 1 summarizes the advancing, receding and static CAs measured on each sample after the solution treatment for different treating time steps. The data support that a longer treating time tend to yield a smaller contact angle. Fig. 3 demonstrate the measured contact angles for one sample.

Table. 1. Contact angles and roughness of samples for different treatment time steps

treatment time (min)	::	:;	:a	R_a
0	75	64	83	0.15
30	34	30	44	0.18
60	22	18	30	0.23
180	<10	<10	<10	0.35

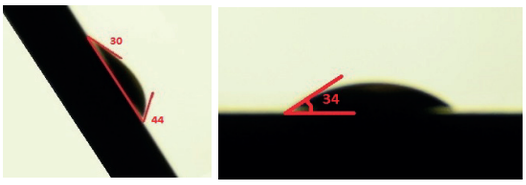

Fig. 3. Measurement of the static and dynamic contact angle for the sample prepared at 30 min.

3.2. Pool boiling curves

Fig. 4 plots the boiling curves of heat Zux value against the wall superheat for different treatment times. The hydrophilic surface with contact angle of 22ł had a larger CHF than the other surfaces. However, CHF of 30 min treated sample was in order of polished surface but in lower wall superheat and the HTC was more than all samples. Fig. 5 shows the bubble dynamic in nucleate pool boiling on surfaces. By increasing the hydrophilicity, nucleation site on surface decreased and bubble have to nucleate on edge of sample.

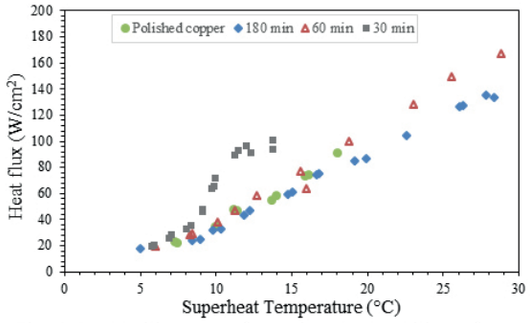

Fig. 4. Pool boiling curve for various hydrophilic surfaces.

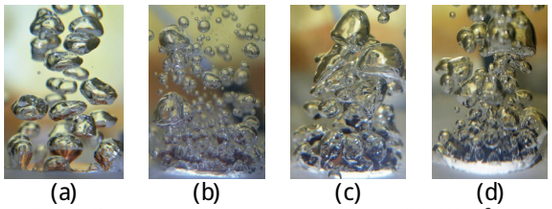

(a) (b) (c) (d)

Fig. 5. Bubble dynamics in heat flux about 30 W/cm^2 for various hydrophilic surfaces.

4. Conclusion

Copper surfaces with different hydrophilicity were fabricated with wet chemical method as heating surfaces to investigate the effect on pool boiling heat transfer enhancement. The CHF value increased 90% in superhydrophilic copper surface and HTC value increased 80% in hydrophilic surface with 30min treatment time.

4. References

[1] S. G. Kandlikar, A Theoretical Model to Predict Pool Boiling CHF Incorporating Effects of Contact Angle and Orientation, J. Heat Trans., vol. 123, pp. 1071¯1079, 2001.

[2] Y. Takata et al., Pool Boiling on a Superhydrophilic Surface, International J. Energy Research, vol. 27, pp. 111¯119, 2003.

[3] Y. Nam et al. Fabrication and Characterization of the Capillary Performance of Superhydrophilic Cu Micropost Arrays, J. Microelectromechanical Sys., vol. 19, no. 3, pp. 581-588, 2010.

[4] R. Chen et al., Nanowires for Enhanced Boiling Heat Transfer, Nano Let., vol. 9, no. 2, pp. 548-553, 2009.

[5] S.M. Kwark, et al., Effects of Pressure, Orientation, and Heater Size on Pool Boiling of Water with Nanocoated Heaters, Int. J. Heat Mass Transfer, vol. 53, no. 23-24, pp. 5199-5208, 2010.

[6] J. Min et al., Hydrophilic Treatment and Performance Evaluation of Copper Finned Tube Evaporators, App. Ther. Eng. 31, 2936-2942, 2011.

5th Micro and Nano Flows Conference
Milan, Italy, 11-14 September 2016

Effect of Nanostructure in Microporous Surfaces on Pool Boiling Augmentation

Amir M. GHEITAGHY [1, 2*], Hamid SAFFARI [1], Kouchi ZHANG [2]

* Corresponding author: Tel.: ++98 (0)2177 240540; Fax: ++98 (0)2177 240488; Email: a_m_gheitaghy@mecheng.iust.ac.ir, a. mirzagheytghi@tudelft.nl
1 School of Mechanical Engineering, Iran University of Science and Technology, Iran
2 Electronic Components, Technology and Materials, Delft University of Technology, Netherlands

Abstract Porous micro/nanostructures electrodeposited in various electrolyte temperature on copper to investigate the saturated pool boiling enhancement of distilled water in atmospheric pressure. Surface structure topography and capillary performance were compared to investigate their relation to pool boiling performance. Scanning Electron Microscopy (SEM) shows that the micro-clusters have nanostructures from cubic at 5 łC to dendritic at 60 łC electrolyte temperature. The experimental results of pool boiling heat transfer indicated that the critical heat flux (CHF) increased with surface capillarity performance. Electrodeposited porous surface in hot electrolyte shows the highest CHF and heat transfer coefficient (HTC) of the 124 W/cm^2 and 17 W/cm^{2}K, respectively which is 50% and 270% higher than that of plain surface. However the two-step electrodeposition used in fabrication of surfaces, but the mechanical strength of layer need improvement by annealing.

Keywords: Pool boiling, Micro/nanostructure, Copper, Electrodeposition.

1. Introduction

Pool boiling heat transfer on micro and nanostructured surfaces has attracted much research interest in recent years due to high HTC and CHF. Several study was conducted to change the effective parameters of surface roughness, wettability, and porosity for optimized pool boiling performance [1]. Experimental results show that hydrophilic porous surfaces have best performance in enhancing the boiling curve [2]. Several manufacturing techniques proposed to develop porous surfaces such as sintering, electrodeposition, soldering, binding, spray painting, alloy¯dealloying, and unidirectional solidiEcation [3]. Electrochemical deposition employed in the present work is simple, inexpensive, well controlled, and reproducible to large scale area. However, reaching to an optimized structure with high mechanical stability using electrodeposition method for pool boiling applications needs more research.

In this paper, two-step electrochemical deposition of copper is used in various electrolyte temperature to fabricate the hydrophilic porous surfaces with different micro/nanostructures.

2. Experimental Method

2.1. Sample fabrication method

Electrodeposition is an electrochemical process of ion reduction at the cathode by passing direct current through the solution (galvanostatic). Circular polished copper with diameter of 22 mm was used as the cathode and a copper cylinder with larger area was used as the anode. The two electrode surfaces were fixed parallel at a 30 mm distance in the stationary solution. Two-step electrochemical deposition is carried out in an electrolyte solution of $CuSO_4$(0.4M)+H_2SO_4(1.5M), subjected to high current density (600mA/cm^2) for a short time (100sec) followed by lower current density (60mA/cm^2) for a longer time (2500sec) at different temperatures of 3, 25, and 60 éC.

2.2. Pool boiling experiment

Pool boiling experiment is done by experiment setup presented in [4] with water in atmospheric pressure on three electrodeposited samples and polished copper to investigate the effect of micro/nanostructures on pool boiling performance.

3. Results and Discussion

3.1. Morphology and characteristics

Fig. 1. shows the different magnification SEM pictures of electrodeposited copper surface morphology under three electrolyte temperatures. For the surface prepared in cold temperature of 5éC, nanocube grains clustered to form a nonuniform biporous interconnected structure. As

the electrolyte temperature increases to 60éC, the grains turned to dendritic branches and the clusters connected more uniformly to form a hole with diameter of about 100ı m.

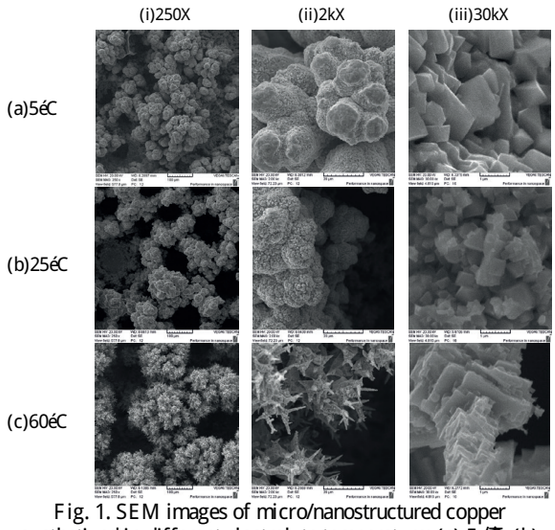

Fig. 1. SEM images of micro/nanostructured copper synthetized in different electrolyte temperature: (a) 5 ‡, (b) 30 ‡, and (c) 60 ‡.

The selected frames of the capillary rate-of-rise experiment has been shown in the Fig. 2 to compare the capillary performance in three samples.

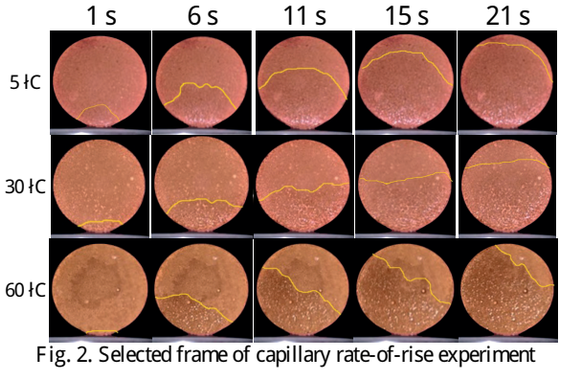

Fig. 2. Selected frame of capillary rate-of-rise experiment

Fig. 3. Shows the similarity between hydrogen bubble template in electrodeposition process and vapor bubble in pool boiling experiment on electrodeposited copper.

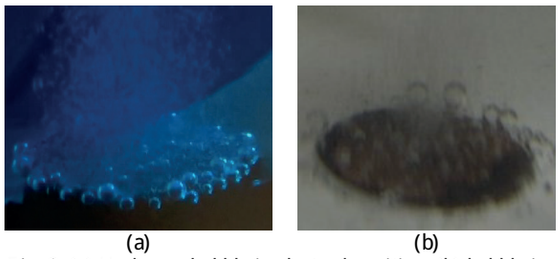

(a) (b)

Fig. 2. (a) Hydrogen bubble in electrodeposition, (b) bubble in pool boiling

3.2. Pool boiling curves

Fig. 3. demonstrates the lower boiling incipience temperature and higher HTC and CHF of micro/nanostructured surfaces rather than the plain surface and also Ref [5]. The porous surface electrodeposited in high electrolyte temperature reach the maximum CHF of 124 W/cm^2 and the best HTC of 17 W/cm^{2}K that was over 1.5 and 3.7 times that of the plain surface, respectively. However, the mechanical stability of this porous surface need improvement. The surface prepared at 5 ‡ destroyed during the pool boiling experiment.

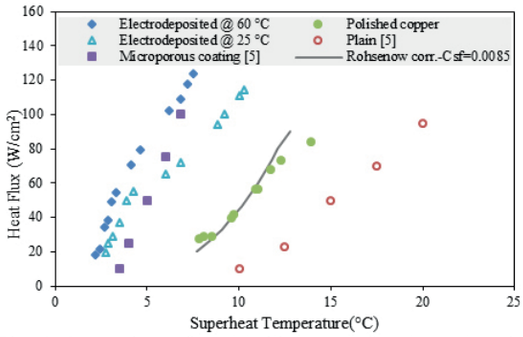

Fig. 4. Comparison of pool boiling curve for electrodeposited samples and polish copper with Ref [5]

4. Conclusion

An experimental study has been made to investigate pool boiling heat transfer performance of electrodeposited porous surfaces that fabricated in electrolyte temperature of 5, 30, 60éC. However, better HTC and CHF was observed in porous samples rather than plain and other surfaces, but these fragile structures need more structural improvement. Dendritic nanobranch in micropores of sample prepared at 60éC, was caused better capillary and pool boiling performance.

4. References

[1] D.E. Kim et al., Review of boiling heat transfer enhancement on micro/nanostructured surfaces, Exp. Therm. Fluid Sci., 66 (2015) 173-196.
[2] H. O'Hanley et al., Separate effects of surface roughness, wettability, and porosity on the boiling critical heat flux, App. Phys. Let., 103 (2013) 024102.
[3] Patil C.M., Kandlikar S.G., Review of the Manufacturing Techniques for Porous Surfaces Used in Enhanced Pool Boiling, Heat Trans. Eng., 35 (2013) 887-902.
[4] A. M. Gheitaghy et al., Investigation Pool Boiling Heat Transfer in U-shaped Mesochannel with Electrodeposited Porous Coating, Exp. Therm. Fluid Sci., 76 (2016) 87-97.
[5]J. H. Kim et al., Microporous coatings to maximaize pool boiling heat transfer of saturated R-123 and water, J. Heat Trans., 137, 8 (2015) 81501-7.

Numerical simulation of electroosmotic/pressure driven nanofluid flow in a microchannel using the lattice Poisson-Boltzmann method

Mohammad KALTEH*, Mohammadreza AKEF

* Corresponding author: Tel.: +98 1333690485 (3078); fax: +98 1333690273.
E-mail address: mkalteh@guilan.ac.ir
Department of Mechanical Engineering, University of Guilan, P.O. Box 3756, Rasht, Iran

Abstract In this paper, electroosmotic/pressure driven nanofluid flow in a horizontal microchannel with constant surface electric potential is investigated for two-dimensional, laminar, incompressible and steady conditions. To do this, the Poisson-Boltzmann method is used to determine the electric potential and velocity distributions. At first, the numerical results are compared with analytical solutions for special cases and a good agreement is obtained. The results show that with increasing the nanoparticles volume fraction, the mass flow rate increases in low velocity scale ratios and decreases in large amounts of that for specified pressure gradient and electric field.

Keywords: Electroosmotic flow; Pressure driven flow; Nanofluid;Lattice Poisson-Boltzmann method

1. Introduction

In a rather new method, the fluid motion is made by employing the traveling dissolved ions that is called Electro-Osmotic Flow (EOF). In an electroosmotic micropump the fluid is transferred by an external electric field with no need for any mechanical parts. Therefore, these micropumps can be managed easier than the mechanical micropumps [1].
Pressure gradient and electroosmotic forces or their combination may be used to generate the fluid flow in microchannels. The flow rate induced by electroosmotic force is usually small, and therefore even a small pressure gradient applied along a microchannel may cause velocity distributions and corresponding flow rates that deviate from the purely electroosmotic flow [2].

2. Problem definition

The EOF by pressure driven studied in this paper is an electrolyte flow through a two-dimensional microchannel with length L=30 μm and height H=6 μm. The upper and lower plates of the microchannel are kept at a constant electric potential ζ. The nanofluid motion is caused by pressure gradient and also the external electric field with strength E_x, which is applied by use of an Anode and a Cathode placed at the two ends of the microchannel.

3. Governing equations

By using Boltzmann approximation governing equations are Poisson, continuity and momentum equations:

$$\nabla^2\Psi = -\frac{\rho_e}{\varepsilon_{nf}} \tag{1}$$

$$\nabla.\boldsymbol{u} = 0 \tag{2}$$

$$\rho_{nf}(\boldsymbol{u}\,.\,\nabla\boldsymbol{u}) = -\nabla P + \mu_{nf}\nabla^2\boldsymbol{u} + \rho_e E_x \tag{3}$$

Where ρ_e is the net electric charge density and using Boltzmann approximation can be defined as:

$$\rho_e = -2Zen_{i\infty}\sinh\left(\frac{Ze\Psi}{k_B T_0}\right) \tag{4}$$

2.1 Nanofluid Thermophysical Properties

The following models are used to estimate the nanofluid density, specific heat and dynamic viscosity, respectively [3,4]:

$$\rho_{nf} = \rho_f(1-\varphi) + \rho_s\varphi \tag{5}$$

$$(\rho C_p)_{nf} = \left(\rho C_p\right)_f(1-\varphi) + \left(\rho C_p\right)_s\varphi \tag{6}$$

$$\frac{\mu_{nf}}{\mu_f} = 1 + 2.5\varphi + 6.5\varphi^2 \tag{7}$$

Where φ isvolume concentration. For electric

permittivity of nanofluid Doyle and Jacobs model [5] is used:

$$\left[\frac{\left(\varepsilon_{nf}/\varepsilon_f\right)-1}{\left(\varepsilon_{nf}/\varepsilon_f\right)+2}\right]=\varphi\left[1+(\frac{\varphi}{\phi_c})(\frac{1}{\phi_c}-1)\right] \quad (8)$$

where ϕ_c (=0.63) is an empirical constant.

3. Numerical method

In this study, the Lattice Poisson-Boltzmann method is used to solve the governing equations.

$$h_i(\boldsymbol{X}+\boldsymbol{e_i}\delta_{t,h}\,,t+\delta_{t,h})-h_i(\boldsymbol{X}\,,t\,)=-\frac{1}{\tau_h}$$
$$[h_i(\boldsymbol{X}\,,t\,)-h_i{}^{eq}(\boldsymbol{X}\,,t)]+\left(1-\frac{0.5}{\tau_h}\right)\delta_{t,h}\omega_i\frac{\rho_e}{\varepsilon_{nf}} \quad (9)$$

$$f_i(\boldsymbol{X}+\boldsymbol{e_i}\delta_t\,,t+\delta_t)-f_i(\boldsymbol{X}\,,t\,)=$$
$$-\frac{1}{\tau_f}[f_i(\boldsymbol{X}\,,t\,)-f_i{}^{eq}(\boldsymbol{X}\,,t)]+\delta_t F_i \quad (10)$$

The Zou and He method [6] to impose the velocity boundary conditions and Wang et al. method [7] for internal electric potential boundary conditions are used in the current study.

4. Results

Figure (1) shows the mass flow rate variation of electroosmotic and pressure driven nanofluid flow at different nanoparticle voulme fraction and velocity scale ratios.

The results show that with increasing the nanoparticles volume fraction, the mass flow rate increases in low velocity scale ratios (ratio of the reference velocity for pure pressure driven flow to reference velocity of the pure electroosmotic flow) and decreases in large amounts of that for a specified pressure gradient and electric field.

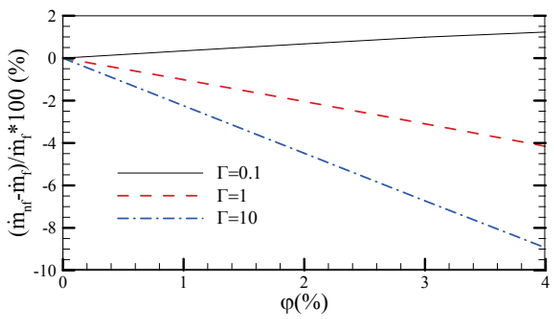

Fig. 1. Variation of mass flow rate in terms of nanoparticle volume fraction at different value of velocity scale ratios.

3. References

[۱] A. Alizadeh, J. K. Wang, S. Pooyan, S. A. Mirbozorgi, M. Wang, (2013), "Numerical study of active control of mixing in electro-osmotic flows by temperature difference using lattice Boltzmann methods", Journal of Colloid and Interface Science, Vol. 407, pp. 546–555.

[2]C. H. Chen, "Fully-developed thermal transport in combined electroosmotic and pressure driven flow of power-law fluids in microchannels", International Journal of Heat and Mass Transfer, Vol. 55, pp 2173–2183, 2012.

[3] S.M. Aminossadati, A. Raisi, B. Ghasemi, (2011), "Effects of magnetic field on nanofluid forced convection in a partially heated microchannel", International Journal of Non Linear Mechanics, Vol. 46, pp. 1373–1382.

[4] C. T. Nguyen, F. Desgranges, G. Roy, N. Galanis, T. Mare, S. Boucher, H. A. Mintsa, (2007), "Temperature and particle-size dependent viscosity data for water-based nanofluids – Hysteresis phenomenon", International Journal of Heat and Fluid Flow, Vol. 28, pp. 1492–1506.

[5] W. Doyle, I. Jacobs, (1990), "Effective cluster model of dielectric enhancement in metal-insulator composites", Phys Rev B, Vol. 42, pp. 9319–9327.

[6] Q. Zou, X. He, (1997), "On pressure and velocity boundary conditions for the lattice Boltzmann BGK model", Phys. Fluids, Vol. 9, pp. 1591–1598.

[7] J. Wang, M. Wang, Z. Li, (2006), "Lattice Poisson–Boltzmann simulations of electro-osmotic flows in microchannels", Journal of Colloid and Interface Science, Vol. 296, pp. 729–736.

Investigating the electroosmotic/pressure driven nanofluid flow in a microtube using the lattice Poisson-Boltzmann method

Mohammad KALTEH*, Sina GHADAMKHEYR

* Corresponding author: Tel.: +98 1333690485 (3078); fax: +98 1333690273.
E-mail address: mkalteh@guilan.ac.ir
Department of Mechanical Engineering, University of Guilan, P.O. Box 3756, Rasht, Iran

Abstract In this study, the velocity field of mixed electroosmotic and pressure driven flow of a nanofluid (aluminum-oxide), has been investigated in a horizontal microtube with homogeneous surface electrical potential. The flow has been considered two-dimentional, laminar, incompressible, and hydrodynamicaly developed. The electrical potential and velocity distribution of nanofluid has been obtained numerically by the axisymmetric lattice Poisson-Boltzmann method. The effect of different parameters such as surface zeta potential, electric field strength, ionic molar concentration, ratio of pressure gradient to electroosmotic force, nanoparticle volume fraction and diameter on the velocity field has been investigated. In this research, the velocity scale ratio parameter (ratio of the reference velocity for pure pressure driven flow to reference velocity of the pure electroosmotic flow (Γ)) is used to represent the numerical results. The results show that at low velocity scale ratios, the mass flow rate increases with increase in nanoparticles volume fraction and at high velocity ratios, decreases with increase in nanoparticles volume fraction.

Keywords: Microtube, Electroosmotic Flow, Nanofluid, Axisymmetric Lattice Poisson-Boltzmann method

1. Introduction

Recently, the microfabrication technology has led to a rapid development of microelectromechanical systems (MEMS) and lab-on-a-Chip devices [1]. For liquid flow at microscale, one of the most important surface effects is electrokinetic effect. In this study we focus on one of the electrokinetic effects named as electroosmosis. Maynes and Webb [2] analytically solved pure electroosmotic flow at low zeta potential. Tang et al. [3] numerically investigated the effect of non-Newtonian fluid on pure electroosmotic flow in a microtube.

2. Macroscopic equations

Consider an incompressible Newtonian aqueous electrolyte with ions continuously distributed in the whole microtube of radius R=2 μm and length L=20 μm. The electric potential ϕcan be described by the following Poisson equation in the cylindrical coordinate system:

$$\nabla^2\phi(r) = \frac{1}{r}\frac{d}{dr}\left(r\frac{d\phi}{dr}\right) = -\frac{\rho_e(r)}{\epsilon_r\epsilon_0} \quad (1)$$

where $\rho_e(r)$is the net charge density at a point distance r from the axis and can be expressed by considering Boltzmann approximation:

$$\rho_e = -2zq_e n^\infty \sinh\left(\frac{zq_e\phi(r)}{k_BT}\right) \quad (2)$$

Substituting Eq. 2 into Eq. 1 yields the nonlinear PB equation:

$$\frac{d^2\phi(r)}{dr^2} = \frac{2n^\infty q_e z}{\varepsilon_r\varepsilon_0}\sinh\left(\frac{zq_e\phi(r)}{k_BT}\right) \quad (3)$$

When an external electric field and pressure gradient is applied along the axial direction, the motion of aqueous electrolyte is governed by the Navier–Stokes equations, which can be reduced to the following equation with assuming a fully developed flow:

$$\rho\left(\frac{\partial u_x}{\partial t}\right) = -\frac{\partial p}{\partial x} + \mu\left[\frac{1}{r}\frac{\partial}{\partial r}\left(r\frac{\partial u_x}{\partial r}\right)\right] + \rho_e(r)E_x \quad (4)$$

3. Boundary Conditions

The boundary conditions on $\phi(r)$and $u_x(r)$ are, as follows:

$$\left.\frac{d\phi(r)}{dr}\right|_{r=0} = 0 \qquad \phi(r)|_{r=R} = \zeta \quad (5)$$

$$\left.\frac{du_x(r)}{dr}\right|_{r=0} = 0 \qquad u_x(r)|_{r=R} = 0 \quad (6)$$

4. Nanofluid properties

The density, dynamic viscosity and relative permittivity of nanofluid can be calculated, as follows:

$$\rho_{nf} = \rho_f(1-\varphi) + \rho_s\varphi$$
$$\frac{\mu_{nf}}{\mu_f} = 1 + 2.5\varphi + 6.5\varphi^2$$
$$\left[\frac{\left(\varepsilon_{nf}/\varepsilon_f\right) - 1}{\left(\varepsilon_{nf}/\varepsilon_f\right) + 2}\right] = \varphi\left[1 + (\frac{\varphi}{\phi_c})(\frac{1}{\phi_c} - 1)\right] \quad (7)$$

4. Numerical method

In this study, the Zhou's axisymmetric lattice Boltzmann method [4] is employed to solve the velocity field and Li's method [5] to solve the electrical potential field.

4. Conclusions

Figure (1) shows the mass flow rate variation of electroosmotic and pressure driven flow of nanofluid by increasing the volume fraction of nanoparticles from 0 to 5% at different velocity scale ratios.

The results show that the mass flow rate at low velocity scale ratios increases slightly with increase in nanoparticles volume fraction and at high velocity ratios decreases with increase in volume fraction. For example when the velocity scale ratio is zero, by increasing the nanoparticle volume fraction from 0 to 5% the mass flow rate increases 6.02% but when the velocity scale ratio becomes 10 the mass flow rate decreases 11.15%.

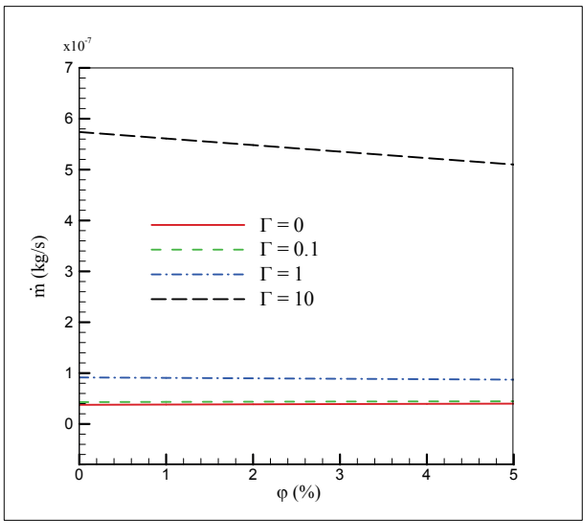

Fig. 1. Variation of mass flow rate in terms of nanoparticle volume fraction at different values of velocity scale ratios.

5. References

[1] D. Q. Li, *Electrokinetics in Microfluidics* Elsevier Academic, Boston, 2004.

[2] D. Maynes, B.W. Webb, (2003), ‘‘Fully developed thermal transport in combined pressure and electroosmotically driven flow in microchannels’’, ASME J. Heat Transfer, Vol.125, pp. 889–895.

[3] G.H. Tang, X.F. Li, W. Q. Tao, (2010), ‘‘Microannular flow with the axisymmetric lattice Boltzmann method’’, Journal of Applied Physics, Vol. 108, pp. 114903.

[4] J. G. Zhou, (2008), ‘‘Axisymmetric lattice Boltzmann method’’, Physical Review E, Vol. 78, pp. 036701.

[5] Q. Li, Y. L. He, G. H. Tang, and W. Q. Tao, (2009), ‘‘Lattice Boltzmann model for axisymmetric thermal flows’’, Physical Review E, Vol. **80**, pp. 037702.

5th Micro and Nano Flows Conference
Milan, Italy, 11-14 September 2016

Experimental Investigation of Thermal Performance of an Aluminum-Grooved Micro Heat Pipe

Hossein ALIJANI[1], Barbaros CETIN[1,*], Zafer DURSUNKAYA[3]

[*]Corresponding author: Tel.: +90 (312) 290 2108; Fax: +90 (312) 266 4126
Email: barbaros.cetin@bilkent.edu.tr
[1]Microfluidics & Lab-on-a-chip Research Group, Mech. Eng. Dept., Bilkent University, Ankara, Turkey
[2]Mech. Eng. Dept., Middle East Technical University, Ankara, Turkey

Abstract As the electronic components get more and more miniaturized, their thermal management becomes more and more challenging. High heat flux and requiring no moving parts are of benefits that has brought micro-grooved heat pipes as an effective heat removal method, to researchers' attention in recent years. In current study, thermal performance of an array of 50 micro-grooved heat pipes fabricated on aluminum and filled with DI water is experimentally investigated; temperature distribution along the heat pipes is read and reported under different operating conditions.

Keywords: Micro-grooved heat pipes, Aluminum, Heat Transfer

1. Introduction

Heat pipes, as an efficient heat removal component, provide the benefits of higher thermal conductivity, compared to the material fabricated of, and considerable heat flux, while not requiring a significant/substantial temperature gradient between heat source and heat sink [1, 2]. As another advantage over conventional methods, they can transfer large amounts of heat "through a small cross-sectional area over a considerable distance with no additional power input to the system" [3]. First proposed by Cotter [4], micro heat pipes (MHPs), in particular, have the advantage of being adaptable in electronic cooling applications [3], where the available space is as small as electronics components; being able to protect the electronic components against sustaining damage due to insufficient heat removal [5], employing them for thermal management purposes in electronic industry has become of research interest in recent years.

In current study, thermal performance of a hermetically sealed array of 50 micro-grooved heat pipes on an aluminum piece filled with DI water as working fluid, covered with a transparent layer of plexiglas, is presented. Temperature distribution along the grooves and working pressure is reported; thermal resistance of the micro heat pipe and its effective thermal conductivity is calculated; moreover, the operation of the micro-grooves is visualized.

2. Experimental Setup

2.1. Materials

The setup includes an array of 50 grooves 200μm×200μm in cross-section and 75mm in length, spaced 200μm from each other, on the bottom of a 2.5mm sink in a piece of aluminum (80mm×159mm×5mm) fabricated by micro-machining. On the outside wall of the aluminum, 5 holes are drilled evenly spaced to place type T thermocouples to read the temperatures. A piece of Plexiglas sheet (80mm×159mm×9mm) covers the aluminum piece by 6 screws. Plexiglas's transparency enables the visualization of the working area during phase change heat transfer operation. In addition, three holes are drilled on the plexiglas sheet for evacuation, pressure reading, and filling the MHP. Perfectly sealed by two o-rings (Viton, durometer A75), the space between the aluminum and plexiglas is defined as our system in this context.

DI water is chosen as the working fluid due to its superior thermodynamic properties within the planned operating conditions. To prevent dissolved air in the water from entering the system, DI water is degassed under 2×10^{-1} Torr vacuum for 30 minutes prior to charge the system.

Two thermoelectric heater/cooler units are used in the experiments, each can work as either cooler or heater by switching their positive and negative inputs. Their input power can be set by adjusting their input current and multiply it by the

corresponding voltage.

The vacuum pump used in the experiments is able to evacuate the system down to 2×10^{-1} mbar.

To achieve uniform heat transfer, silicone thermal grease was applied in any possible contact, such as peltiers' surfaces and thermocouple holes.

A programmable micro syringe pump is utilized to charge the MHPs with a desirable amount of working fluid via capillary tubes; the accuracy of its volume measurements is 0.1μL.

Figure 1 shows all the components of the setup before assembly.

2.2. Experimental method

The schematic procedure of evacuating and charging the MHPs is depicted in Figure 2. As the very first and crucial step, the system is put under 5×10^{-2} Torr vacuum for two hours, ensuring all materials degassed; during this step, valves V1 and V2 is opened, and V3 is on plugged mode. Subsequent to evacuation, to fill the MHPs, valves V1 and V2 are closed and V4 is connected to V3 (V3 is also used to refill the syringe pump from the water reservoir, when it gets drained out). The amount of filling water is chosen as much as the volume of all grooves in total, considering 50% excess for condensed water at the sidewalls and corners of the sink in aluminum. When the grooves were filled with the proper amount of the working fluid, V4 is put on plugged mode again and the MHP is ready to be examined.

Heating and cooling is started to perform at this point by means of two thermoelectric heater/cooler units placed underneath the MHP; while one plays as heat source and the other as heat sink. During operation, the temperature is measured along the grooves, working pressure is recorded, and the phase change heat transfer, after reaching steady state condition, is visualized.

References

[1] S. Taze, B. Cetin and Z. Dursunkaya, "Multi-physics modeling of silicon micro-grooved heat pipe," in *8th International Conference on Computational Heat and Mass Transfer*, Istanbul, Turkey, 2015.

[2] C. W. Chan, E. Siqueiros, J. Ling-Chin, M. Royapoor and A. P. Roskilly, "Heat utilisation technologies: A critical review of heat pipes," *Renewable and Sustainable Energy Reviews,* vol. 50, pp. 615-627, 2015.

[3] A. Faghri, "Heat Pipes: Review, Opportunities and Challenges," *Frontiers in Heat Pipes,* vol. 5, no. 1, 2014.

[4] T. P. Cotter, "Principles and Prospects for Micro Heat Pipes," in *International Heat Pipe Conference*, Tsukaba, Japan, May 14-18, 1984.

[5] S. Lips, F. Lefèvre and J. Bonjour, "Nucleate boiling in a flat grooved heat pipe," *International Journal of Thermal Sciences,* vol. 48, p. 1273–1278, 2009.

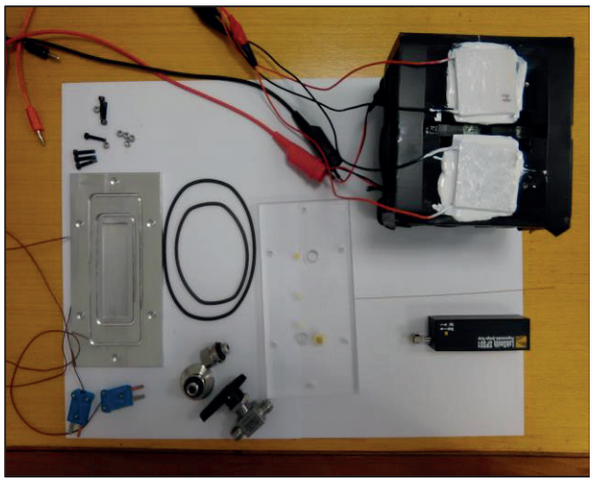

Figure 1. Disassembled components of the MHP

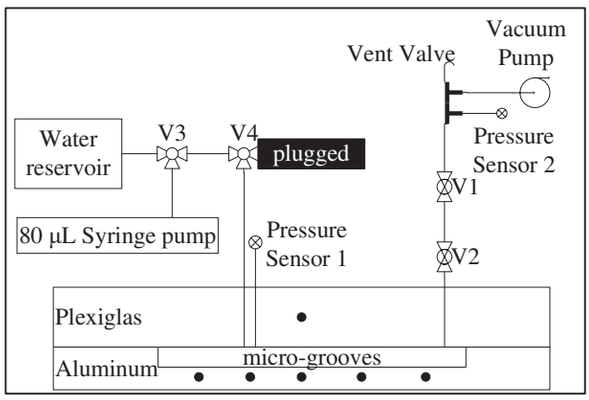

Figure 2. Schematic diagram of the charging of the MHP. Black-filled circles are the place of thermocouples

5th Micro and Nano Flows Conference
Milan, Italy, 11-14 September 2016

Development of "*Evanescent Wave for a Chip*" for Distribution Measurements of Physical Quantities in the Vicinity of Liquid-Solid Interface

Atsuhisa UCHIGASAKI [1,*], Maho URUSHIDANI [1], Yohei SATO [1]

* Corresponding author: Tel.: +81 (0)45 566 1740; Fax: +81 (0)45 566 1720;
Email: uchigasaki@tfe.sd.keio.ac.jp
1: Department of System Design Engineering, Faculty of Science and Technology, Keio University, Japan

Abstract
A novel compact illumination device for total internal reflection fluorescence microscopy, "*Evanescent wave for a chip*" was developed. Based on the concept of complete readiness and usability, a laser system and mirrors were fixed thereby removing complex optics from the measurement. Owing to the mirrors fixed at an optimal angle, without any adjustment, laser beam was introduced into the slide glass to generate total internal reflection at the interface of the glass and fluid. Therefore, evanescent wave was generated and fluorescent dye in the vicinity of slide glass, i.e. channel wall were excited. For quantitative measurements in solution, calibration measurements for fluorescent intensity on pH and temperature were conducted. In addition, a simultaneous measurement for the velocity and pH distribution of the solution was conducted by using a 3-CCD camera to evaluate the utility of the device in more complex measurements of near wall flow fields. Since this device is able to excite fluorescent dyes only in a region close to a cell-substrate interface, collagen beads with a fluorescent dyes, which mimic the cell were observed. Elimination of background fluorescence from the outside of the focal plane achieved a significant improvement of the signal-to-noise ratio. These results show that the device has a rich potential to be used for investigations of themofluid and biological phenomena in the vicinity of an interface of microfluidic devices.

Keywords: Lab on a Chip, Evanescent Wave, Scalar Quantities, Nano-LIF

1. Objective

The influence of channel surface on distribution of velocity, concentration, pH, and so on in microchannel plays an important role in performance of micro- and nanofluidics. Measurements using evanescent wave in which it decays exponentially from the wall is one of the most powerful method to investigate the physical quantities in the vicinity of channel surface. Numerous methods have been developed to use evanescent wave for measurements. However, most of methods tend to get complicated and limited further development in measurements. The objective of this study is to develop a built-in device, which easily generates an evanescent wave in the vicinity of liquid-solid interface.

2. Development of Built-in Device

Kazoe & Sato [1] have developed a two-prism system for generating the evanescent wave in order to investigate the zeta-potential distribution in the vicinity of solid-liquid interface of micro channel wall and the fluid. The present study proposes a compact and built-in device called "*Evanescent wave for a chip* (herein after referred to as *EvaChip*)" illustrated in Fig. 1., which overcomes the shortcomings found in Kazoe & Sato's experiments. *EvaChip* is made from acrylic using micro-machining technique and mirrors were attached to the bottom side of *EvaChip* thereby removing complex optics from the system. A small optically pumped semiconductor laser (488 nm or 532 nm) was amounted vertically to introduce a laser beam into *EvaChip* for total internal reflection. Fluorescent dye injected into microchannel placed on top of *EvaChip* was illuminated by the evanescent wave. Its intensity was captured by a 3-CCD and an EM-CCD camera through the objective lens and filters.

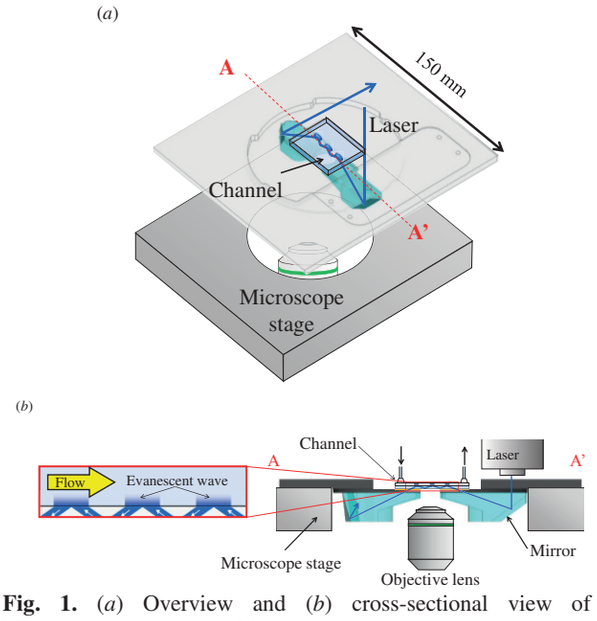

Fig. 1. (*a*) Overview and (*b*) cross-sectional view of "*Evanescent wave for a chip*".

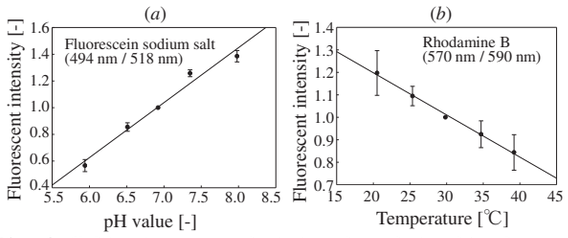

Fig. 4. Calibration curve depicting the relationships between the fluorescent intensity and (*a*) pH and (*b*) temperature.

3. Results and discussions

3.1 pH and temperature measurements

Prior to applying *EvaChip* to mixing flow fields, calibration curves depicting relationships between pH and temperature to the intensity from fluorescent dyes were obtained. Fluorescent sodium salt and Rhodamine B was used as fluorescent dyes for the pH and temperature measurement, respectively. For pH measurement, phosphate buffer solution (PBS) with 5 different pH values were used. I-shaped channel was used for pH calibration experiment. Temperature controlled water was flown from the thermostat chamber to heat the Rhodamine B solution through BK7. Figs. 4(*a*) and 4(*b*) show calibration curves for pH and temperature, respectively. Both curves indicate linear relationships, which are consistent with the experimental results of Kazoe & Sato [1].

3.2 Simultaneous measurement of pH and velocity

Considering more complex measurement fields, simultaneous measurement of pH and velocity at mixing flow field was conducted. A T-shaped channel, as illustrated in Fig. 5, and PBS at different pH (5.89 and 8.16) were prepared. Both fluorescent sodium salt, which has green emission wavelength, and fluorescent particles with red emission wavelength were mixed into PBS. Solutions were injected into the inlets at 190 μL/min by a syringe pump. The evanescent wave spot was adjusted to a junction area of the channel and both dye and particles were excited. Two different emission lights were captured by red and green elements of 3-CCD camera respectively at the same time as shown in Fig. 6. LIF was conducted by measuring the fluorescent intensity of green emission light and using the calibration curve shown in Fig. 4(*a*). PIV was conducted by measuring the red emission light. Thus pH and velocity were quantitatively visualized the mixing process in the vicinity of liquid-solid interface, simultaneously. Fig. 7 shows the pH and velocity distribution in the vicinity of interface. The result indicates that it is quite easy to obtain the special distribution of scalar quantities using *EvaChip*.

3.3 Observation of collagen beads

In anticipation of biological use of *EvaChip*, observation of collagen beads with an EM-CCD camera was carried out. This study was conducted to compare the difference between the volume and evanescent wave illumination. Collagen beads with the diameter of approximately 20 μm were prepared to mimic the cell. The fluorescent dye with excitation wavelength of 488 nm was mixed in the beads. Illumination was captured by an EM-CCD through 20× objective lends. In case of the volume illumination, as shown in Fig. 8(*a*), a large volume of beads were excited in the depth direction which lower the SN ratio. Fig 8(*b*) shows the evanescent wave illuminated beads. Contrary to the case of the volume illumination, illuminated area of beads became drastically small and high SN ratio was achieved by *EvaChip*. This is because the penetration depth of evanescent wave conducted by *EvaChip* was approximately 80 nm and only the bottom of the beads were illuminated. This result indicates the potential capacity of applying *EvaChip* to not only fluidic dynamics but also biological region.

4. Conclusions

Velocity, temperature and pH of channel surface play a significant role in characterizing the flow in micro channels. The system presented is a powerful and simple method to investigate the above-mentioned physical quantities in the vicinity of liquid-solid interface. Owing to its simplicity, *EvaChip* is able to use without any skill and the study revealed that it is capable of measuring highly complex flow field. The possibility of applying *EvaChip* to biological region in the future work was also indicated by the study.

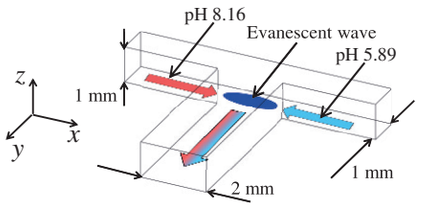

Fig. 5. Schematic of the T-shaped channel for the two-dimensional pH distribution measurement.

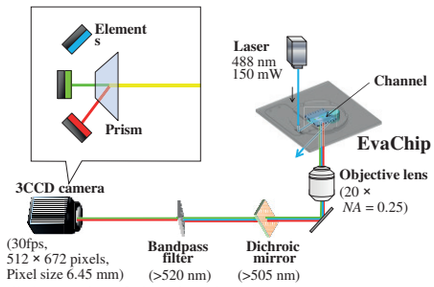

Fig. 6. Schematic of the simultaneous measurement system.

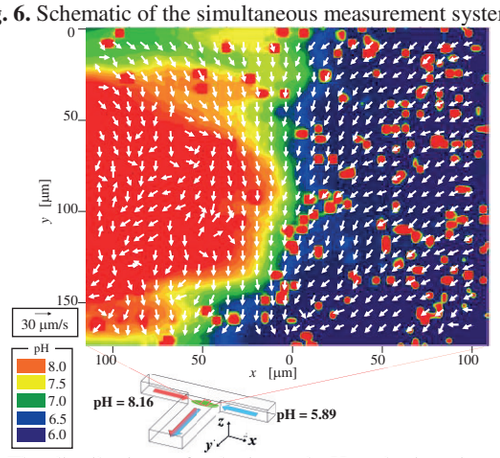

Fig. 7. The distributions of velocity and pH at the junction area of the T-shaped channel.

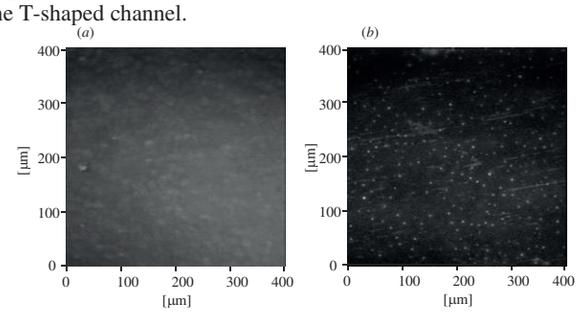

Fig. 8. Picture of (*a*) collagen beads by volume illumination and (*b*) collagen beads by evanescent wave.

Acknowledgments

This work was supported by a Grant-in-Aid for Scientific Research (A) (No. 26249022 and No. 15H02223) from the Japan Society for the Promotion of Science, and Program for the Advancement of Next Generation Research Projects from Keio University.

References

[1] Kazoe, Y., Sato, Y., 2007. Effect of Ion Motion on Zeta-Potential Distribution at Microchannel Wall Obtained from Nanoscale Laser-Induced Fluorescence. Anal. Chem., 79, 6727-6733.

Measurement of Molecular Diffusion in the Vicinity of Liquid-Solid Interface by Total Internal Reflection Raman Imaging

Masaharu KINOSHITA [1,*], Tetsuro TATEISHI [1], Reiko KURIYAMA [2], Yohei SATO [1]

* Corresponding author: Tel: +81 (0)45 566 1740; Fax: +81 (0)45 566 1720;
Email: kinoshita@tfe.sd.keio.ac.jp
1 Department of System Design Engineering, Faculty of Science and Technology, Keio University, Japan
2 Department of Mechanical Engineering Science, Graduate School of Engineering, Kyoto University, Japan

Abstract The present study proposes total internal reflection (TIR) Raman imaging for measurement in the vicinity of liquid-solid interface. This measurement technique was applied to the near-wall illumination by the evanescent wave to the Raman scattering. Raman scattering emitted from molecules in the vicinity of a channel surface was two-dimensionally captured by an EM-CCD camera through bandpass filters. Since the intensity of Raman scattering is proportional to the number of illuminated molecules, the Raman images can be converted into the concentration distributions via calibration curves. With this technique, concentration distributions of D_2O and H_2O in a D_2O/H_2O mixing field in a T-shaped microchannel were visualized. Concentration measurement of NH_4Cl in a mixing field of NH_4Cl deuterium oxide solution was also carried out. The measurement resolution in the depthwise direction was approximately 90 nm and 100 nm in the mixing fields of D_2O/H_2O and NH_4Cl deuterium oxide solution, respectively. The concentration distributions of D_2O, H_2O and NH_4Cl were visualized in the vicinity of liquid-solid interface. These results imply that the TIR Raman imaging has a potential to evaluate the molecular diffusion under electrochemical influence from a channel surface.

Keywords: Molecular Diffusion, Raman Imaging, Evanescent Wave Illumination, Liquid-solid Interface

1. Introduction

In micro- and nanoscale channels, flow structures are influenced significantly by interfaces owing to the large surface-to-volume ratio [1]. In the space of 10^1–10^2 nm from a channel surface, the flow structure is different from the bulk due to the electrochemical effect of the channel surface [2]. For more advanced analysis systems, it is necessary to understand the flow structure in the vicinity of the interface. However, the flow structure is not elucidated because a measurement method whose resolution exceeds the diffraction limit is not established. The objective of this study is to develop a non-intrusive technique for measurement in the vicinity of liquid-solid interface using the TIR and the Raman imaging.

2. Experimental setup and procedure

The intensity of the Raman scattering increases linearly with concentration. The concentration distributions of D_2O, H_2O and NH_4Cl were visualized in mixing fields of D_2O/H_2O and D_2O/NH_4Cl deuterium oxide solution by detecting the intensity of Raman scattering. The measurement system is illustrated in Fig. 1. In order to capture the Raman scattering from target molecules selectively, the bandpass filters which pass each Raman band of D_2O, H_2O and NH_4Cl were prepared. Raman spectra of the samples were shown in Figs. 2 (*a*) and 2 (*b*). TIR Raman scattering from the target excited by the evanescent wave was captured by an EM-CCD camera through the bandpass filter. The intensity of the detected TIR Raman scattering was converted into the near-wall concentration via pre-obtained calibration curves. In this study, the measurement resolution in the depthwise direction was determined by the penetration depth of the evanescent wave.

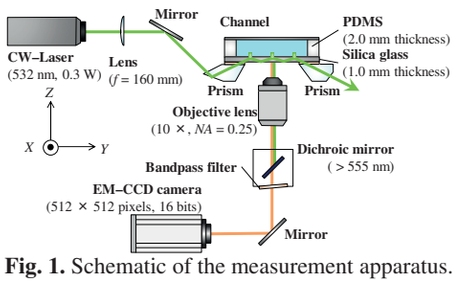

Fig. 1. Schematic of the measurement apparatus.

(*a*)

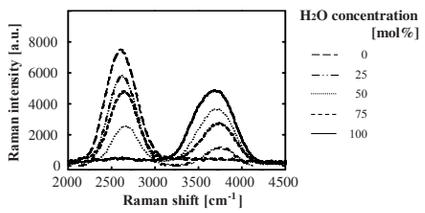

(*b*)

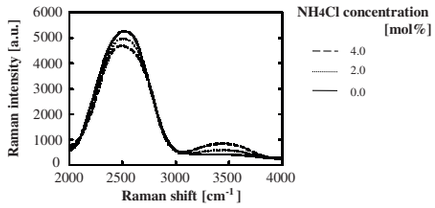

Fig. 2. Raman spectra of (*a*) D_2O/H_2O and (*b*) NH_4Cl deuterium oxide solution.

3. Results and discussions

Near-wall concentration measurement was performed in non-uniform mixing flow fields in a T-shaped microchannel. Fig. 3 shows top views of the T-shaped microchannel and the measurement area.

3.1. Mixing field of D_2O/H_2O

3.1.1. Calibration experiment

Prior to the measurement of the near-wall concentration distributions, the Raman scattering from D_2O/H_2O mixtures was measured with various mixing rate in order to obtain a relationship between Raman intensity and concentration. Fig. 4 shows the calibration curves for D_2O and H_2O. Linear relationships between the Raman intensity and concentration were confirmed.

3.1.2. Near-wall concentration measurement

The visualization of the concentration distributions was performed. The measurement resolution in the depthwise direction was approximately 90 nm. D_2O and H_2O were injected at constant flow rate of 2.0 μL/min from inlets A and B of the T-shaped microchannel, respectively. The calibration curves for D_2O and H_2O were applied to each Raman image captured at the junction area. Figs. 5 (*a*) and 5 (*b*) depict the two-dimensional concentration distributions of D_2O and H_2O in the T-shaped microchannel, respectively.

3.2. Mixing field of NH_4Cl deuterium oxide solution

3.2.1. Calibration experiment

In order to obtain a relationship between the Raman intensity and concentration, Raman scattering from NH_4Cl deuterium oxide mixtures was measured. Fig. 6 shows the calibration curve for NH_4Cl. A linear relationship between Raman intensity and concentration was confirmed.

3.2.2. Near-wall concentration measurement

The visualization of the concentration distribution was performed. The measurement resolution in the depthwise direction was approximately 100 nm. NH_4Cl deuterium oxide solution, which contains 4.0 mol/L of NH_4Cl were injected at constant flow rate of 2.0 μL/min from inlets A and B of the T-shaped microchannel, respectively. The calibration curve for NH_4Cl was applied to the Raman image captured at the junction area. Fig. 7 depicts the two-dimensional concentration distribution of NH_4Cl in the T-shaped microchannel.

4. Conclusions

The present study proposes the total internal reflection Raman imaging for the measurement in the vicinity of liquid-solid interfaces. The main accomplishments of this work are summarized below.

(1) The linear relationships between the Raman intensity and the concentrations were confirmed by the calibration experiment.

(2) Near-wall concentration distribution measurements were performed by detecting the intensity of Raman scattering and applying the calibration curves to the Raman images. The non-uniform concentration distributions of H_2O, D_2O, and NH_4Cl were visualized at the evanescent spot, respectively.

Acknowledgments

This work was supported by a Grant-in-Aid for Scientific Research (A) (No. 26249022 and No. 15H02223) from the Japan Society for the Promotion of Science, Keio Gijuku Academic Development Funds, and Program for the Advancement of Next Generation Research Projects from Keio University.

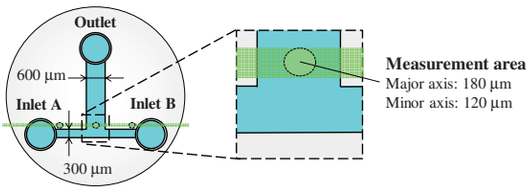

Fig. 3. Top views of the T-shaped microchannel and the measurement area.

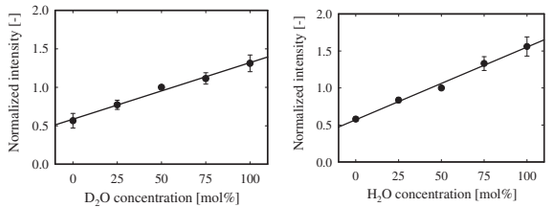

Fig. 4. Calibration curves for (*a*) D_2O and (*b*) H_2O.

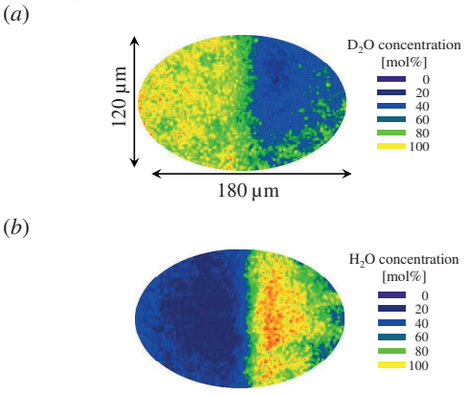

Fig. 5. Two-dimensional concentration distributions of (*a*) D_2O and (*b*) H_2O in the T-shaped microchannel.

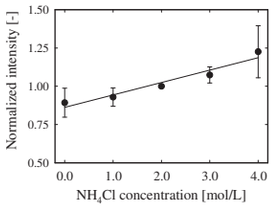

Fig. 6. Calibration curve for NH_4Cl in NH_4Cl deuterium oxide solution.

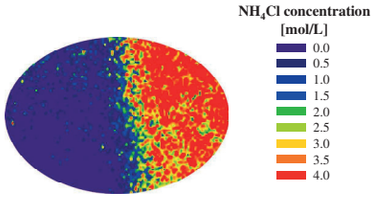

Fig. 7. Two-dimensional concentration distribution of NH_4Cl in the T-shaped microchannel.

References

[1] Kazoe Y., Miyakawa S., Miki N. and Sato Y., 2009, Fluorescence imaging technique of surface electrostatic potential using evanescent wave illumination, Appl. Phys. Lett., 95, 234104 (3pp).

[2] Tsukahara T., Mawatari K. and Kitamori T., 2010, Integrated extended-nano chemical systems on a chip, Chem. Soc. Rev., 39, pp. 1000-1013.

5th Micro and Nano Flows Conference
Milan, Italy, 11-14 September 2016

Experimental Investigation of Supersonic Two-Dimensional Free Microjets

Vladimir M. ANISKIN [1,3*], Anatoliy A. MASLOV [1,2], Sergey G. MIRONOV [1,2], Ivan V. TIMOFEEV [2]

* Corresponding author: Tel.: +7 (383) 3308528; Fax: +7 (383) 3307268; Email: aniskin@itam.nsc.ru
1 Khristianovich Institute of Theoretical and Applied Mechanics SB RAS, Novosibirsk, Russian Federation
2 Novosibirsk State University, Novosibirsk, Russian Federation
3 Institute of Thermophysics, Novosibirsk, Russian Federation

Abstract The work is devoted to experimental investigation of the structure of two-dimensional supersonic underexpanded microjets. The characteristic size of micronozzles ranges from 175 to 22.3 microns. The working gas is air at room temperature. The Reynolds number ranges from 600 to 10,000 The first shock cell size of the jet and the average shock cell size are determined and approximation dependences are offered. The supersonic core length (the distance from the nozzle exit to the point on the jet axis, where the velocity reaches the local speed of sound) of two-dimensional supersonic underexpanded microjets is determined.

Keywords: Micronozzle, Supersonic microjet, Pitot microtube, Laminar-turbulent transition

1. Introduction

Due to the considerable capabilities of the microfluidic device applications there is an interest in the study of the gas flow on the microscale. Regard it as a gas flow in microchannels, and the exhausting of gas from micron-sized holes. Depending on the pressure at the inlet of the hole, the jet can be subsonic or supersonic. Subsonic and supersonic microjets may find their applications in macroflows control, in noise reduction systems, in jet cooling systems.

There is no studies on the structure of two-dimensional supersonic microjets, except [1], which presented some of the data for only one Reynolds number and for one prechamber pressure.

There are a number of works considering the structure of two-dimensional supersonic macro jets [2-4].

However, we could not find any data on the supersonic core length of a two-dimensional supersonic macrojets in the available literature.

The aim of this study is to determine the main characteristics of supersonic underexpanded air microjets.

2. Micronozzles

Based on the technology developed in [5], two-dimensional micronozzles were made. Figure 1 shows the SEM images of some of them.

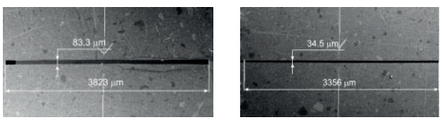

Fig.1. SEM images of micronozzle exit sections

3. Experiment

The experiments of studding the structure of microjets were performed using Pitot microtube, hot-wire anemometer and by Shadow flow visualization method.

The Pitot microtube was made of glass, an outer diameter of 40 μm, internal diameter of 20 μm. Hot-wire probe has a diameter of 5 μm and a length of 0.7 mm. During the experiments, the jet blew the central part of the hot-weir probe.

From the flow visualization photographs and the pressure distribution along the jet axis the first shock cell and the average shock cell

sizes of the jets were determined. Average shock cell size was determined by the size of the second, third and fourth shock cells (if they were visible).

The supersonic core length is determined from the pressure distribution on the jet axis.

Figure 2 shows, as an example, the flow visualization of the jets escaping from the nozzles with the height of 175 microns at different pressures in the settling chamber. Sawtooth structure in the photographs is a scale element.

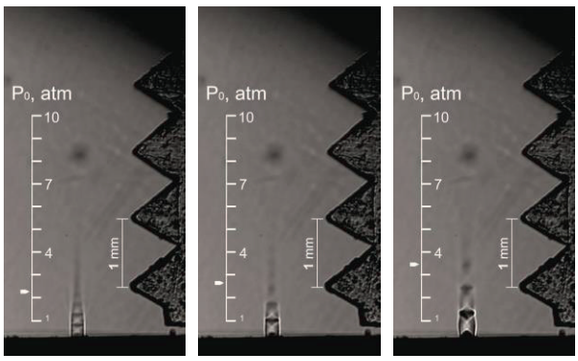

Fig.2. Flow visualization of supersonic two-dimensional underexpanded microjets

From the flow visualization photographs and the pressure distribution along the jet axis the first shock cell and the average shock cell sizes of the jets were determined. The results for the first shock cell are shown in Fig. 3.

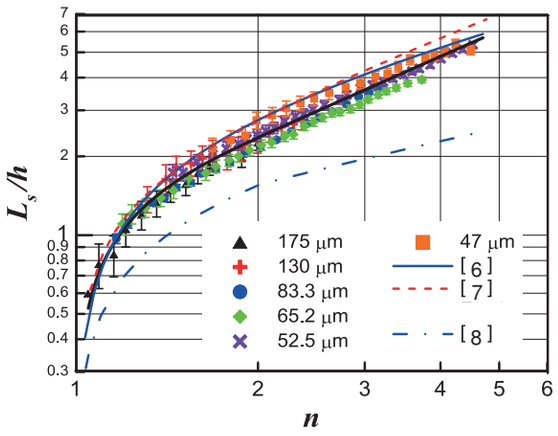

Fig. 3. The first shock cell size of the jets

4. Conclusions

On the basis of studies of the structure of two-dimensional supersonic microjets it can be done the following conclusions:

- the first shock cell and the average shock cell sizes of the microjets are determined and approximation dependences are offered;
- the supersonic core length is defined. It is shown that for some jets there is a long supersonic core length mode. An increase of supersonic core length are shown for jets issuing from the nozzle with the height less than 50 microns at moderate jet off-design value (n <1,5);
- it is shown that the supersonic core length increases due to the laminar-turbulent transition in the mixing layer of microjets.

4. Acknowledgement

The study was supported by the Russian Science Foundation (project No. 16-19-10675).

5 References

[1]Aniskin, V.M., Mironov, S.G., Maslov, A.A. (2012). The structure of supersonic two-dimensional and axisymmetric microjets. *Int. J. Microscale and Nanoscale Thermal and Fluid Transport Phenomena*., 3, 1, 49-59.

[2]Sheeran, W.J., Dosanjh, S. (1968). Observations on Jet Flows from a Two-Dimensional, Underexpanded, Sonic Nozzle. *AIAA Journal.*, 6, 540-542.

[3]Werle, M.J., Shaffer, D.G., Driftmyer, R.T. (1970). Free jet Terminal Shocks. *AIAA Journal*., 8, 2295-2297.

[4]Addy, A.L. (1981). Effects of Axisymmetric Sonic Nozzle Geometry on Mach Disk Characteristics. *AIAA Journal*., 19, 1, 121-122.

[5]Aniskin, V.M., Mironov, S.G., Maslov, A.A. (2013). Investigation of the structure of supersonic nitrogen microjets. *Microfluidics and Nanofluidics*., 14, 3, 605-614.

[6] Kashimura H., Masuda Y., Miyazato Y., Matsuo K. (2011). Numerical Analysis of Turbulent Sonic Jets from Two-Dimensional Convergent Nozzles, *J. Termal Science*, 20, 2, 133-138.

[7]Tam C.K.W. (1988). The Shock Cell Structure and Screech Tone Frequencies of Rectangular and Non-Axisimmetric Supersonic Jets, *J. Sound and Vibration*, 121-1, 135-147.

[8]Love E.S. at al. Experimental and Theoretical Studies of Axisymmetric Free Jets. (1959). *NASA Technical Report.*. R-6, 1-292.

5th Micro and Nano Flows Conference
Milan, Italy, 11-14 September 2016

Measurements of micro-mushroom patterns in a magnetic micromixer

F. Gökhan ERGİN [1,*]

* Corresponding author: Tel.: +45 4457 8173; Fax: +45 4457 8001; Email: gokhan.ergin@dantecdynamics.com
1 Product Manager, Dantec Dynamics, Skovlunde, DK

Keywords: MicroPIV, Adaptive PIV, magnetic micromixer, local contrast normalization, difference of Gaussian filter, front detection

Fingers and mushroom patterns are common features at the interface of surface instabilities. These can be observed in different scales: large-scale examples are the remnants of supernova explosions, (Fig. 1a), nuclear detonations (Fig. 1b), hot gas and ash produced by volcanic eruptions (Fig. 1c). Smaller scale examples can be produced at home using 2 liquids with different densities (Fig. 1d). These patterns are often described by the Rayleigh-Taylor Instability (RTI), where a heavy fluid is above a lighter fluid in the presence of a gravitational field. Similar patterns can be produced with other mechanisms, as long as one fluid is forced to penetrate into another across a flat interface. For example if magneto-hydrodynamic forces are used the instability is called Magnetic Rayleigh-Taylor Instability (MaRTI).

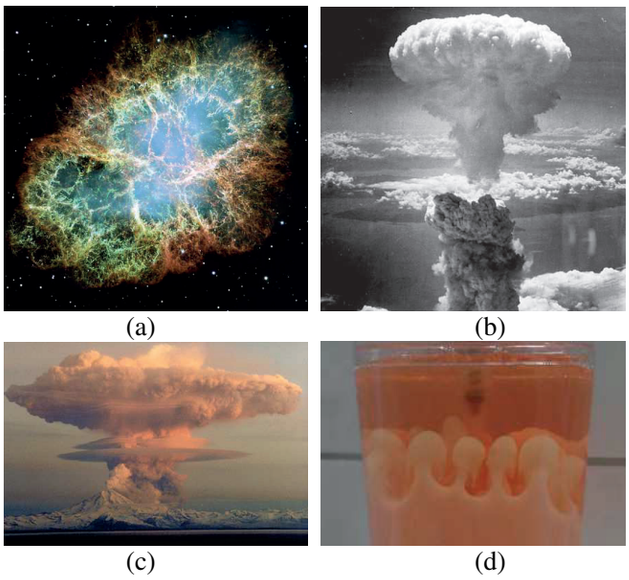

(a) (b) (c) (d)

Figure 1 Examples of finger and mushroom formations observed in nature. (a) Crab nebula (b) Nuclear explosion (c) 1990 Redoubt volcano (d) Two liquids with different densities in a glass container. Image credits: Wikipedia commons

Recently, MaRTI has been the subject of several experimental studies in micro scale, where a magnetic fluid and water was forced to penetrate into each other using an electromagnet [1-5]. The first quantitative velocity field was measured using MicroPIV in combination with image pre-processing functions, such as contrast normalization and Gaussian difference filters [1]. A successful model was developed for the magnetic microconvection problem [2] based on the experimental results. In order to understand the reasons behind the formation of these finger and mushroom patterns the flow field information and the interface front is required simultaneously [3]. Time-resolved information on velocity and interface location revealed the well-known finger and mushroom patterns typical to this instability in Ref. 4 where an uncertainty analysis of the measurement was also reported [4]. Modal analysis of the MaRTI instability was performed using Proper Orthogonal Decomposition (POD) and Oscillating Pattern Decomposition (OPD) [5]. In this study we revisit the data acquired in Ref. 4 and focus on an individual finger turning into a mushroom.

MicroPIV technique has great potential in providing multi-parameter information in microfluidics research on mixing and the details of the experimental setup can be found in Ref. 4. Briefly, the Hele-Shaw cell was constructed using two cover glasses separated with a 127-µm-thick Parafilm. A magnetic fluid and deionised water was brought into contact in the cell with a relatively flat interface. Then the Hele-Shaw cell was placed in the center of the electro-magnet and the magnetic field was applied before pure solvent was mixed in the magnetic fluid. The magnetic forces were produced using an electromagnet, which produced a magnetic field strength of 1.8 mT in the central part of the coil. Both phases were seeded with 1µm Nile-red fluorescent particles with the same seeding density. Experiments are performed using a MicroPIV system consisting of an inverted fluorescence microscope, a high quantum efficiency PIV camera, a pulsed LED illumination device, a synchronization box and a system controller. Image recording, image pre-processing, MicroPIV analysis, vector processing and graphical display of results were performed using the DynamicStudio software.

In Ref. 4 both the velocity and the interface information are extracted from a sequence of time-resolved particle images. Planar velocity measurements are obtained using an adaptive cross-correlation algorithm, where particle image contrast was enhanced using image pre-processing. The use of image pre-processing functions proved to be essential: First, local contrast normalization and difference of Gaussian filters are used to enhance the particle image contrast [1]. Second, interface location is estimated using Prewitt edge detection filter together with a combination of standard image processing functions [3].

It was found that only some of the fingers turn into mushroom patterns in the presence of counter-rotating vortex system [4]. The fingers oriented in the horizontal plane (against the flow) tend to produce some mushroom patterns. On the other hand, the fingers located at the top and bottom of the FoV oriented vertically (perpendicular to the flow direction) are simply convected towards left under the influence of the main flow of the water phase. In particular, one horizontal finger close to the middle of the FoV in Fig. 8k to 8o in Ref. 4 gradually changes into a mushroom shape (Fig. 2). The thickness of the finger in Fig. 2a is approx 120µm, and this gradually turns into a mushroom shape with a size of approx 195µm (Fig 2c). The size of the transforming finger at each time step is shown next to each subfigure and the velocity vectors are placed every 20µm in Fig. 2. To the authors knowledge this is the smallest mushroom pattern measured as a result of a RTI, where quantitative flow field and interface information is available simultaneously. Motion of raw particle images, time resolved velocity field, POD-filtered flow field and the interface are available in Ref. 6. When the average flow velocity is subtracted, a counter-rotating vortex system is observed with the center of the vortex system coinciding with the centerline of the growing finger. In fact, the observed counter-rotating vortex system in the plane is the cross-sectional view of a toroidal vortex in three dimensions.

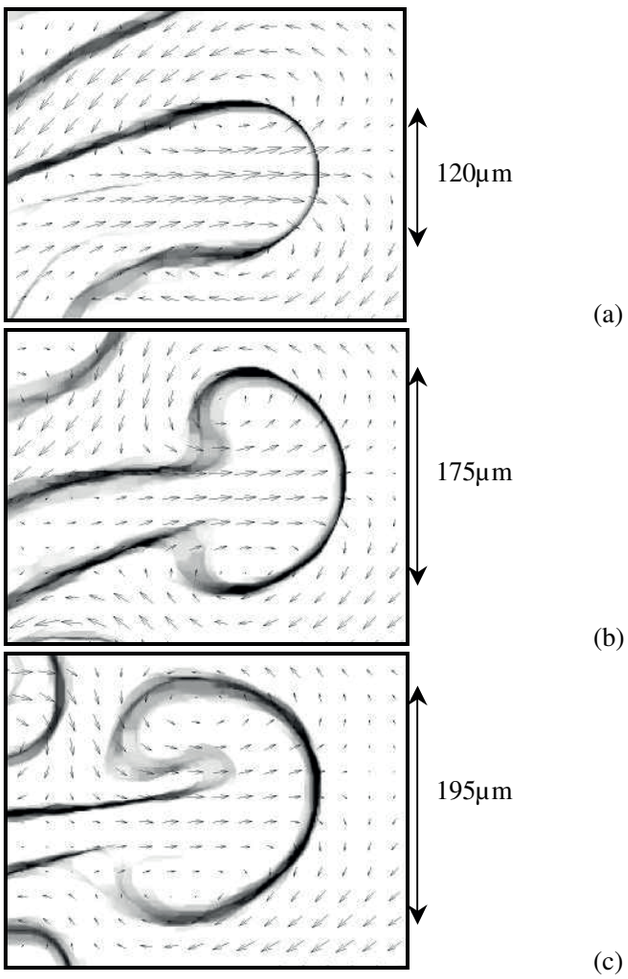

Figure 2 Flow field around an individual finger turning into a mushroom. (a) t=12.5 s (b) t=15 s (c) t=17.5 s

REFERENCES

[1] Ergin FG, Watz BB, Erglis K and Cebers A "Poor-contrast particle image processing in Micro scale mixing" Proc. ASME ESDA 2010; 10th Biennial Conference on Engineering Systems Design and Analysis, Istanbul, Turkey (2010)

[2] Erglis K, Tatulchenkov A, Kitenbergs G, Petrichenko O, Ergin FG, Watz BB, and Cebers A, "Magnetic field driven micro-convection in the Hele-Shaw cell" *J. Fluid Mech.* **714** (2013) 612–633.

[3] Ergin FG, Watz BB, Erglis K and Cebers A "Planar velocity & concentration measurements in a magnetic micromixer with interface front detection" Proc. PIV13; 10th International Symposium on Particle Image Velocimetry, Delft, The Netherlands (2013)

[4] Ergin FG, Watz BB, Erglis K and Cebers A "Time-resolved velocity measurements in a magnetic micromixer" *Exp. Therm. Fluid. Sci.* **67** (2015) 6-13

[5] Ergin FG, Watz BB, Erglis K and Cebers A "Modal analysis of magnetic microconvection" *Magnetohydrodynamics* **50** (2014) 339-352

[6] Microfluidics application example – Modal analysis of magnetic microconvection: http://www.dantecdynamics.com/microfluidics-category/modal-analysis-in-a-micromixer

5th Micro and Nano Flows Conference
Milan, Italy, 11-14 September 2016

Fabrication of nanoporous membranes through silicon templates : two different approaches

Stefano S.G: VARRICCHIO*, Niccolò PIACENTINI, Arnaud BERTSCH, Philippe RENAUD

* Corresponding author: Tel.: ++41 (0)21 693 65 81; Email: stefano.varricchio@epfl.ch
Microsystems Laboratory 4, École Polytechnique Fedérale de Lausanne (EPFL), Switzerland

Abstract We present here a novel approach to fabricate nanoporous membranes based on the use of sacrificial template structures to individually define pore parameters such as geometry, shape, and placement. Based on this rationale two different nano-fabrication methods were developed; one resulting in conical multilayered nanopores arrays with openings with critical dimensions down to 60 nm; and a second one resulting in high aspect ratio nanopores with diameters down to 17 nm and 1 µm length. The presented methods are relevant for the fields of nanofabrication and nanofluidics since they extend the shapes, geometries and materials into which nanoporous membranes can be obtained.

Keywords: Nanofluidics, Nanopores, Membranes, Sacrifical templates, High aspect ratio

The question of designing and fabricating well controlled solid-state nanoporous membranes made of different materials still remains a bottleneck that impedes the development of nanofluidics and its potential applications [1-2]. Controlling individual pore parameters such as dimension, shape, placement as long with the material at the liquid-solid interface is of fundamental importance depending on the application targeted. Furthermore until now only few materials were used to create nanopores (and nanochannels in general) because of the difficulty to fabricate device in exotic materials.

Here we propose two different fabrication methods for nanoporous membranes based on the same rationale, which is relying on the fabrication of sacrificial templates to define the pore geometrical parameters, depositing the material for the membrane around the template and finally selectively remove the template to release the pores. The difference between the two approaches presented lies in the method used to deposit the membrane material. A directional deposition (evaporation) on the templates results in multilayered and conical nanopores whereas a conformal deposition (sputtering or CVD) results in high aspect ratio pores made of the same material (Figure 1.A). The templates used in both processes are etched into bulk Silicon through e-beam lithography followed by SF_6/C_4F_8 based dry etching (HARSiN [3]). This way high aspect-ratio structures with critical dimensions sown to 25 nm and about 1 µm high were obtained as visible in Figure 1.B.

The method relying on directional deposition through evaporation allows to obtain multilayered nanoporous membranes with and unprecedented freedom in the choice of materials resulting in the possibility to control the pore material (and thus the surface charge properties) along the pore axis. Similar results were obtained in the past with FIB milling but the presented method is less time consuming, and has no material re-deposition inside the nanopore. A limitation of the process arises from the deposition and its lateral growth of material on top of the template which creates a "cap" (as visible in figure 2.A). This shadows the deposition at the base of the template, and results in a conical nanopore which angle is material dependent. Membranes made of alternated layers of

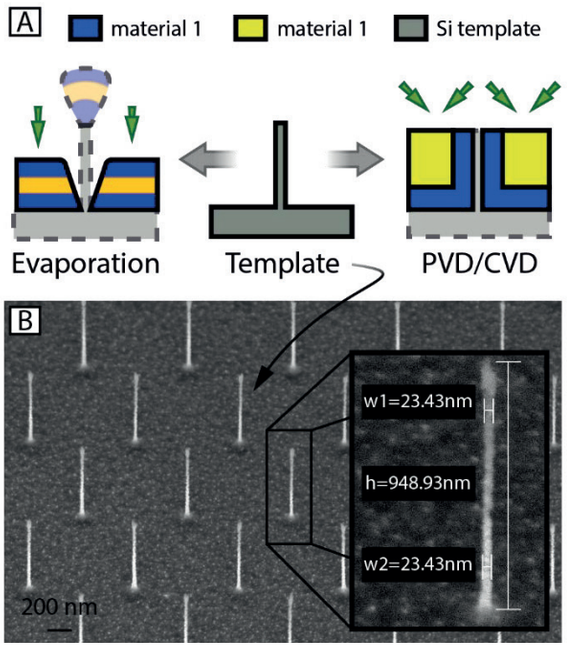

Fig 1.A: - Schematic representation of the fabrication concept presented
Fig 1.B: SEM image of an array of templates

SiO2 and Pt (1x and 3x Pt layers) were successfully fabricated with critical dimensions down to about 60nm (Figure 2.A) [4]. The integrity of the membranes was proved through electrical measurements during which a slight current rectification effect was observed due to the conic shape of the nanopores [5].

The second process presented consists in using conformal deposition techniques (sputtering or CVD) to deposit the thin films composing the membrane on the template structure. The planarization of the sample until the templates emerges from the surrounding material and their consequent selective removal finally reveals the pore (Figure 1.A). As shown in figure 1.A on the right, two stacked materials can be used to fabricate the membranes. The blue layer is the material that will be the pore surface once the pore released, or "pore material"; the yellow layer is a "supporting material" that has no active function but to support the membrane. With this method nanopores are thus made of the same material (i.e. the pore material), and have a shape which is the negative of the template. This way membranes with PECVD amorphous carbon (figure 2.B) or sputtered Platinum as pore material and low temperature SiO_2 (LTO) as supporting material were fabricated with high aspect-ratio pores (typically length=1µm for Ø≤20nm). SEM inspection of the membranes shows the absence of defects or collapse of the membrane after pore release.

These fabrication methods are therefore very similar in concept but results in devices with different properties. The method based on evaporation gives the possibility to fabricate multilayered nanopores which is not possible with the other method. On the other hand the method based on conformal deposition can be used to obtain smaller nanopores compared to the evaporation-based one (15nm vs. 60nm), with high aspect ratios (up to 1:50). Such approach may be especially useful since long nanopores can be fabricated in any material that can be conformally deposited in thin film and which adhere to the templates, since only a thin layer of membrane material is needed. A thick supporting layer can then be used to sustain the membrane and get micrometer-long pores without the need to deposit micrometers of the material of interest.

Compared to other fabrication technologies for solid-state nanoporous membranes, the presented templated technology allows fabrication of devices with high aspect ratio nanopores in a wide variety of materials without the need to further modify the process, it is compatible and integrable with other micro-machining processes (such as micro-channel fabrication), it results in membranes with nanopores defined individually by design and it allows the fabrication of nanofluidic chips at wafer-scale.

The presented methods can therefore boost the study of nanofluidics and extend its applications to new fields by facilitating the fabrication of nanodevices, widening the choice of materials, and lowering the technical bottlenecks actually limiting its development.

References

[1] Bocquet et al., Lab Chip, vol. 14, no. 17, 2014.
[2] Napoli, et al., Lab Chip, vol. 10, no. 8, 2010.
[3] C. Hibert et al., MNE 2005: Proceedings.
[4] Varricchio et al., Nanoscale, vol. 7, no. 48, 2015.
[5] Cervera et al., J. Chem. Phys., vol. 124, no. 10, 2006.

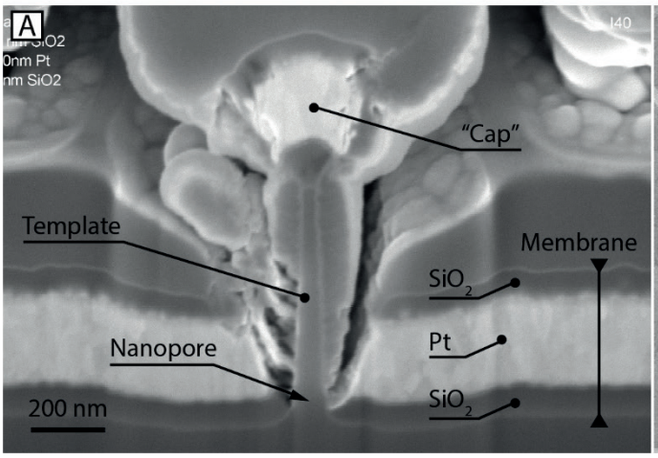

Fig 2.A: FiB cross section of a 3 layers membrane obtained through evaporation method, before template removal. The shown pore dimension is about 80nm, the cone angle is 29°. Note, the image is tilted 45° so the vertical dimension appears to be shorter than it is in reality.

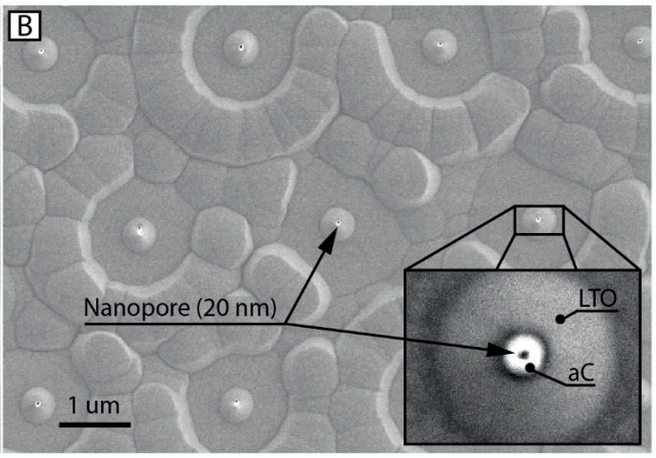

Fig 2.B: Top-view of a nanopore obtained through conformal deposition, after template removal. The pore diameter is 17nm for a length of 850nm. The apparent corrugation of the surface is due to the suboptimal planarization process and was measured to be less than 20nm.

5th Micro and Nano Flows Conference
Milan, Italy, 11-14 September 2016

TEM Study on Phase Change in a Nano Liquid Cell

Yoko TOMO [1], Koji TAKAHASHI [1,2*], Takashi NISHIYAMA [1,2], Tatsuya IKUTA [1,2], Yasuyuki TAKATA [2,3]

* Corresponding author: Tel.: +81-92-802-3016; Fax: +81-92-802-3017; Email: takahashi@aero.kyushu-u.ac.jp
1 Department of Aeronautics and Astronautics, Kyushu University Fukuoka, Japan
2 International Institute for Carbon-Neutral Energy Research (WPI-I2CNER), Kyushu University Fukuoka, Japan
3 Department of Mechanical Engineering, Kyushu University Fukuoka, Japan

Abstract Transmission electron microscope (TEM) is used as an experimental method of bubble nucleation at the initial stage of boiling, which is not understood sufficiently because it is difficult to observe the bubble at nanometer scale. We developed a nano liquid cell, whose tiny gap was filled with pure water. When the water was irradiated by TEM electron beam at high magnification mode, nanobubbles generated and grew due to phase change. In this paper, we introduce the fabrication technique of the nano liquid cell and the dynamic behavior of nanobubbles.

Keywords: TEM, nanobubble, nano liquid cell, electron beam, boiling

1. Introduction

Boiling is one of the most effective heat transfer methods due to its high heat transfer coefficient. Therefore, boiling heat transfer has a variety of applications in technological and industrial engineering. The complicated boiling mechanism has been investigated by many researchers but the bubble nucleation at the initial stage of boiling is still veiled. The major reason is that there had been no experimental method to observe the bubble nucleation at nanometer scale. Nanobubbles were reported observable by atomic force microscopy and the freeze-fractured replica method [1]. However, these methods can't reveal the mechanism of nanoscale phase change sufficiently. On the other hand, newly-developed techniques represented by MEMS have enabled us to make a nano liquid cell for observing the nanobubbles by using transmission electron microscope (TEM) [2–6]. In this study, we aimed to reveal the mechanism of bubble nucleation and phase change in nanoscale by using TEM.

For TEM observation, we prepared liquid cells by using the commercially-available microchip (Structure Prove. Inc., West Chester, PA, USA) which is 3.0 mm x 3.0 mm x 200 µm Si (100) substrate with Si_3N_4 membrane window. The thickness, length, and width of the window are 50 nm, 500 µm, and 500 µm respectively. Two microchips were bonded each other to sandwich a spacer of 40 nm-thick Pt and 8 nm-thick Ti films, which were fabricated by physical vapor deposition. Finally, two Si_3N_4 membrane windows are set face to face with a gap of ca. 50-300 nm as shown in Fig.1. This nano-gap was filled with pure water and the leakage of water was prevented by epoxy resin.

JEM-3200FSK was used for our *in situ* TEM observation, which is operated at 300 kV with emission current of 108 µA. The bright-field screen-image of TEM of water in the cell was recorded by a CCD camera and a high-speed video (FASTCAM Mini AX50, Photron.

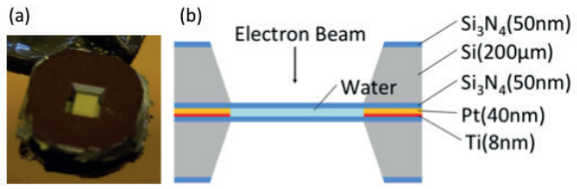

Figure1. (a) Image of a fabricated nano liquid cell. (b) Schematic of the cell filled with water.

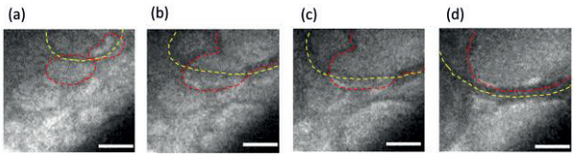

Figure2. Snapshots of nanobubbles, captured at (a) 0 s, (b) 2.4 s, (c) 3.4 s, (d) 5.4 s. Onset time of nucleation was undetermined. Scale bars show 15 nm.

Tokyo, Japan) at 250 frames per second. Its image resolution was 256 x 256.

2. Results and discussion

Bubble formation was found only in the electron-irradiated area in the cell and the generated bubbles continued growing when we observe it at high magnification mode (80k-200k). Soon after we started to observe in the nanochannel at 200k magnification, nanobubbles generated on both Si_3N_4 membranes and grew. Their initial diameters were 5-10 nm. When a nanobubble touched another one, which was as large as it, it coalesced with the other one slowly. On the other hand, when a nanobubbles touched another one, which was larger or smaller than it, it didn't coalesce. Continuing to irradiate electron beam at high magnification mode, new nanobubbles are generated in thin water films between nanobubbles one after another. In addition to the growth of nanobubbles, we observed nanobubbles disappearing. When the TEM magnification was shifted to low magnification (5k-50k). The generation and growth of nanobubbles were induced by electron beam irradiation. However, the shape of nanobubbles were not perfect circles, which suggests that heterogeneous nucleation occurs dominantly in comparison with homogeneous nucleation. Moreover, the minimum diameter of nanobubbles was ca. 5 nm, which is supposed to be the critical bubble nucleation radius under the current condition.

Acknowledgement

This work was partially supported by JSPS KAKENHI and CREST, JST. TEM observations were performed at the Ultramicroscopy Research Center, Kyushu University.

References

[1] T. Uchida, S. Oshita, M. Ohmori, T. Tsuno, K. Soejima, S. Shinozaki, Y. Take, and K. Mitsuda, "Transmission electron microscopic observations of nanobubbles and their capture of impurities in wastewater.," *Nanoscale Res. Lett.*, vol. 6, no. 1, p. 295, 2011.

[2] J. M. Grogan, N. M. Schneider, F. M. Ross, and H. H. Bau, "Bubble and pattern formation in liquid induced by an electron beam.," *Nano Lett.*, vol. 14, no. 1, pp. 359–64, 2014.

[3] T.-W. Huang, S.-Y. Liu, Y.-J. Chuang, H.-Y. Hsieh, C.-Y. Tsai, Y.-T. Huang, U. Mirsaidov, P. Matsudaira, F.-G. Tseng, C.-S. Chang, and F.-R. Chen, "Self-aligned wet-cell for hydrated microbiology observation in TEM.," *Lab Chip*, vol. 12, no. 2, pp. 340–7, 2012.

[4] N. De Jonge, W. C. Bigelow, and G. M. Veith, "Atmospheric Pressure Scanning Transmission Electron Microscopy," pp. 1028–1031, 2010.

[5] T. J. Woehl, K. L. Jungjohann, J. E. Evans, I. Arslan, W. D. Ristenpart, and N. D. Browning, "Ultramicroscopy Experimental procedures to mitigate electron beam induced artifacts during in situ fluid imaging of nanomaterials," *Ultramicroscopy*, vol. 127, pp. 53–63, 2013.

[6] D. Shin, J. B. Park, Y. Kim, S. J. Kim, J. H. Kang, B. Lee, S.-P. Cho, B. H. Hong, and K. S. Novoselov, "Growth dynamics and gas transport mechanism of nanobubbles in graphene liquid cells.," *Nat. Commun.*, vol. 6, p. 6068, 2015.

5th Micro and Nano Flows Conference
Milan, Italy, 11-14 September 2016

Microfluidic Characterisation of Ultralow Interfacial Tension Droplets by Thermal Capillary Wave Analysis

Guido G. Bolognesi [1,*], Yuki SAITO [1], Arwen I. I. Tyler [2], Andrew D. WARD [2], Colin D. BAIN [3], Oscar CES [1]

* Corresponding author: Tel.: ++44 (0) 20 7594 1173; Email: g.bolognesi@imperial.ac.uk
1 Department of Chemistry, Imperial College London, UK
2 Central Laser Facility, STFC, UK
3 Department of Chemistry, Durham University, UK

Abstract Measurements of the mechanical properties for heptane droplets in AOT-NaCl aqueous solutions were performed in a microfluidic device through the analysis of the thermal capillary waves. After generation in a flow focusing junction device, the droplets were collected in an observation chamber chip fitted with a thermal control unit. Subsequently, the droplet interfacial tension was lowered down to ultralow values (<1μN/m) by approaching the microemulsion phase inversion temperature. In this regime, the Fourier spectrum of the stochastic droplet interface displacement could be measured through bright-field video microscopy and a contour analysis technique. The droplet interfacial tension γ together with the surfactant film bending rigidity κ were hence obtained by fitting the experimental results to the prediction of a theoretical model. Compared to existing tensiometry techniques, our contactless all-optical approach has several advantages, including fast measurement, easy implementation, cost-effectiveness, reduced amount of liquids, and integration into lab-on-a-chip devices.

Keywords: Interfacial Tensiometry, Microemulsions, Droplet Microfluidics, Thermal Capillary Waves

1. Introduction

Surfactant-oil-water microemulsions with ultralow interfacial tensions (ULIFT) are used in several important applications in oil industry (e.g. enhanced oil recovery) and environmental protection (e.g. oil pollution remediation). More recent applications of these systems include flow actuation in micron-sized liquid channels created by light,[1] optical sculpture of micron-sized droplets[2] for the synthesis of asymmetric solid particles[3] and optical generation and manipulation of nanofluidic networks.[4]

Current ultralow interfacial tensiometry techniques (e.g. spinning droplet method, relaxation time method, etc.) require dedicated apparatus and cannot be integrated into lab-on-a-chip devices with multiple functionalities. To this end, a microfluidic ultralow interfacial tensiometry method, based on the analysis of the trajectories of magnetic particles crossing a flat liquid interface, has been recently introduced[5]. However, the pre-calibration of the particle magnetic susceptibility, the risk of interface contamination caused by these magnetic probes, and the requirements of low viscosity contrast between the liquid phases limit the applicability of this method. Furthermore, none of the mentioned methods can measure the bending rigidity of the fluid-fluid interface.

In this research, we present a microfluidic technique for the measurement of the ultralow interfacial tensions as well as the surfactant film bending rigidity for micron-sized droplets through the analysis of the thermal capillary waves.

2. Methods and Materials

A monodisperse population of heptane droplets in Aerosol OT surfactant NaCl-water solutions were generated in a flow focusing junction device[6] and, subsequently, transferred in an observation chamber (ObC) chip for analysis (Figure 1a). The ObC chip was fitted

with a temperature control system to lower the droplet interfacial tension γ down to ultralow values (< 1 μN/m) by approaching the microemulsion phase inversion temperature. Under these conditions, the stochastic displacement of the droplet interface position[7] are on the order of 100 nm so they could be measured by standard bright-field digital video microscopy. The droplet interface profile was measured via image processing analysis implemented in Python.

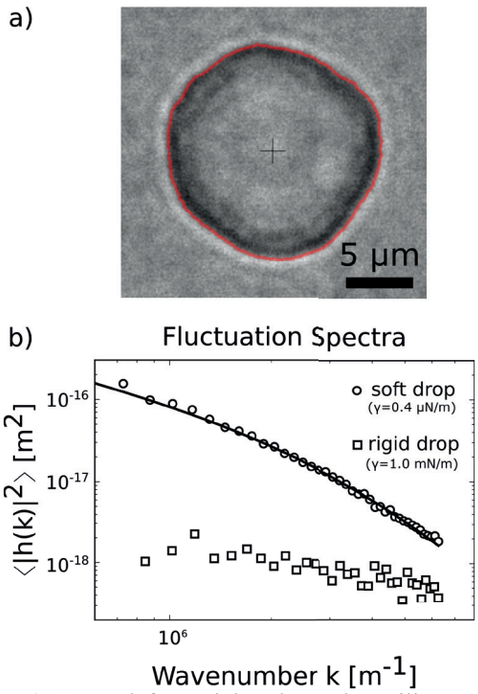

Fig 1 a) Drop deformed by thermal capillary waves together with the measured interface profile. b) Fluctuation spectra for `soft' and `rigid' drops.

3. Results and Discussion

Figure 1 shows the micrograph of a deforming heptane droplet in 50 mM NaCl and 2 mM AOT water solution at 26.3°C together with the measured droplet interface profile. The latter can be denoted as $h(x)$, with $x = R\,\vartheta$, R the droplet radius and ϑ the azimuthal angle. By calculating the discrete Fourier transform of $h(x)$ and averaging the result over hundreds of frames, the experimental fluctuation spectrum $\langle|h(k)|^2\rangle$ was obtained. By fitting this spectrum to the prediction of a capillary wave model,[8] both γ and κ were measured.

Figure 2 shows the experimental spectrum and the best-fitting curve for a 'soft' droplet. The best-fitting parameters are $\gamma = 0.4$ μN/m and κ = 4.0 k_bT for the interfacial tension and bending rigidity, respectively. The accuracy of our interface tracking method can be assessed by analysing a 'rigid' droplet with an interfacial tension of ca. 1 mN/m. Since the corresponding interface fluctuations - on the order of few nm - are inaccessible to our optical system, the resulting spectrum provides a measure of the measurement noise level in the Fourier domain (Fig 1b).

We analysed the droplet interfacial properties under varying conditions of temperature and salinity level. The variance of the fluctuation amplitude was observed to scale linearly with the ratio between the thermal energy k_bT and γ, as expected. A positive correlation between γ and κ was also found, hence suggesting a possible dependence of γ on the spatial wavenumber.

This technique[9] will prove very useful for the rapid characterization of microemulsions as well as other ULIFT systems (e.g. phase-separated colloid-polymer solutions, all-aqueous polymer solutions), provided that the interface fluctuation amplitudes can be detected by an optical microscope and an appropriate capillary wave model is used.

References

[1] J.-P. Delville et al. *J. Opt. A: Pure Appl. Opt.* **2009**, 11, 034015.
[2] A.D. Ward et al. *Chem. Commun.* **2006**, 4515–4517.
[3] A. D. Ward et al. **2012,** US Patent 8,183,540.
[4] D.A. Woods et al. *Soft Matter* **2011**, 7, 2517−2520 ; G. Bolognesi, et al. *SPIE Microtechnologies. 2015*; 95200B
[5] S. S. Tsai et al. *Lab on a Chip* **2013**, 13, 119-125.
[6] G. Bolognesi et al. *RSC Adv.* **2015**, 5, 8114−8121.
[7] D. G. Aarts et al. *Science* **2004**, 304, 847-850.
[8] W. Helfrich et al. *Nuovo Cimento D* **1984**, 3, 137
[9] G. Bolognesi et al. *Langmuir* **2016,** DOI: 10.1021/acs.langmuir.5b04702.

5th Micro and Nano Flows Conference
Milan, Italy, 11-14 September 2016

Structural optimization of microjet array cooling system

Tomasz MUSZYNSKI [1*], Dariusz MIKIELEWICZ [1],

* Corresponding author: Tel.: ++48 58 347-24-57; Fax: ++48fax: 58 347-28-16; Email: Tomasz.Muszynski@pg.gda.pl,
1: Gdansk University of Technology, Faculty of Mechanical Engineering, Department of Energy and Industrial Apparatus Narutowicza 11/12, 80-233 Gdansk, Poland

Abstract The single phase heat transfer from an upward facing, horizontal copper surface to arrays of impinging water jets was experimentally investigated. Square nozzles arranged in four different geometries were used. Additionally for set of two jets array geometry was varied by adjusting nozzle to nozzle distance. The area averaged heat transfer coefficient was fund to be a strong function of working fluid mass flux and array geometrical aspect ratio. The authors proposed empirical correlation to describe and optimize microjet structural configuration.

Keywords: microjets, heat transfer coefficient, heat transfer intensification,

1. Introduction

Liquid jet impingement is one of the most effective means of achieving very high convection coefficients, especially when the coolant undergoes phase change. Choice of jet configuration is based on several practical considerations including operating environment, coolant compatibility, and, of course, heat dissipation and surface temperature. The jet typically impinges the heat–dissipating surface through a circular or a rectangular orifice. The convection coefficient is highest in the impact zone below the orifice and diminishes away from the impact zone. The average heat transfer coefficient for a large surface can be increased substantially and the surface temperature rendered more uniform by using multiple jets.

While jets can demand higher coolant flow rates than competing high performance cooling schemes, they do offer significant advantages. For example, compared to micro-channel flow, they facilitate the removal of very high heat fluxes with relatively modest pressure drops. They are also highly adaptable to cooling multiple devices in a compact package,ensure temperature uniformity when using multiple confined jets, and are applicable to both terrestrial and microgravity environments, as well as can endure the severe body forces induced by military aircraft maneuvers.

Overall methods to intensify the heat exchange in channels using passive techniques have been presented in the work of Gupta [1] and Webb [2]. Stone [3] worked on intensifiction of heat transfer in compact heat exchangers.

Present study shows results of steady state heat transfer experiments, conducted for single phase cooling in order to obtain wall temperature and heat fluxes.

Optimization of heating module may considerably improve energy savings in these systems. On the other hand, improved efficiency leads to reduced exchanger size, thus significantly reduces its manufacturing cost, and annual energy expenditures related to pumping. The transferred heat and the pressure drops have been investigated. The heat transfer performance for various jet geometries and dimensions has been obtained. The effects of pitch, angle and jet number on temperature has been studied.

2. Test setup

Present study shows results of steady state heat transfer experiments, conducted for single phase cooling in order to obtain wall temperature and heat fluxes. Fig. 1 shows the schematic diagram of the test section. It consisted of the probe, fluid supplying system,

the measuring devices and DC power supply. Working fluid was fed to the nozzle from a supply tank, which also serves as the pressure accumulator. The water pressure in the test section was raised by air compressor. Desired fluid flow rate was obtained by sustaining the constant pressure of fluid with a proper use of flow control valve. In order to reduce pressure drop necessary to create a steady laminar jet, nozzle was 2mm long. Due to low volumetric flow rate of coolant it was measured at inlet and outlet from the cooling chamber with a graduated flask.

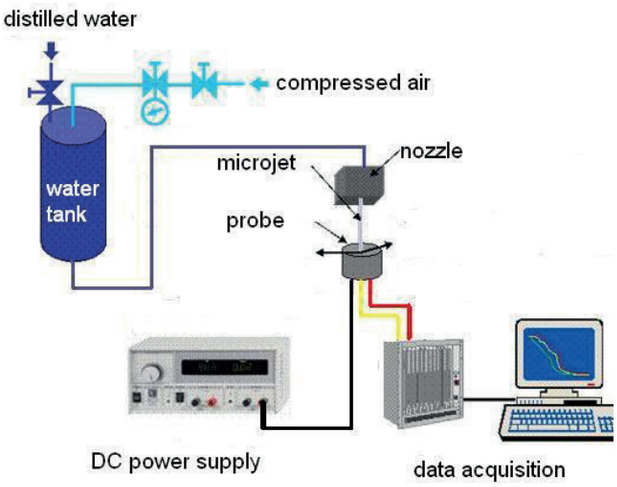

Fig.1. The schematic diagram of test section

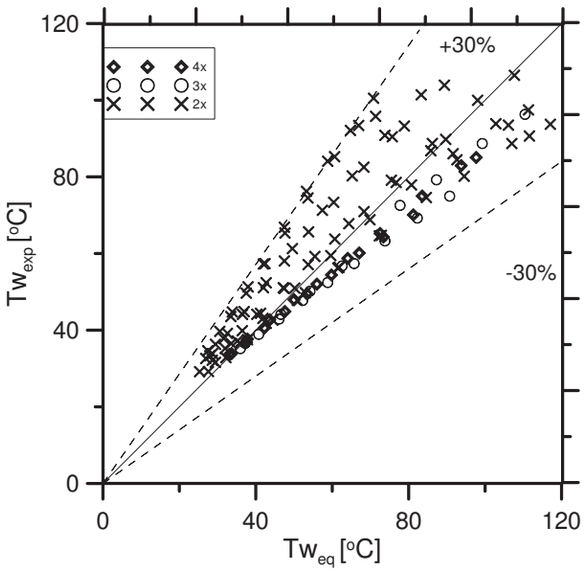

Fig. 2. Experimentally obtained and predicted values of cooled surface temperature

Liquid distribution of microjets on cooled surface is influenced by presence of the neighboring jets. Thus a number of adjoining and similar impingement cells are formed. The experimental setup is aimed at reproducing the conditions of CPU cooling. The effect of nozzle array geometry on the heat transfer characteristics was further investigated by experimental runs, conducted with arrays consisting of 2, 3, 4 and 5 nozzles. Nozzle pitch was modified in range from 1 to 5 mm.
Sample experimental results are depicted on figure 2.

3. Conclusions

The experimental research of single phase heat transfer due to impingement of microjet array of water was studied on a specially designed rig. Systematic data on wall temperature, and dissipated heat has been collected, which enabled development of empirical correlation for Nusselt number.
A simple form of distribution of wall temperature and cooling fluid temperature obtained in analytical model is of a great value when the sensitivity tests are to be carried out. That will enable, for example the optimization of parameters consisting for the method of cooling. The model is quite general and its further modifications are possible when some of the assumptions are relaxed. The performance of presented model depends very strongly on the distribution of heat transfer coefficient. More experiments on the structure of a single microjet are needed which will confirm the heat transfer coefficient correlation presented in the paper.

REFERENCES

[1] Gupta A., Uniyal M.: Review of heat transfer augmentation through different passive intensifier methods. IOSR Journal of Mechanical and Civil Engineering, vol. 1, pp. 14-21, 2012.
[2] Webb R. L.: Principles of enhanced heat transfer. Wiley-Interscience, New York, 1994.
[3] Stone. K.M.: Review of literature on heat transfer enhancement in compact heat exchangers. Air Conditioning and Refrigeration Center Technical Reports, 1996.

5th Micro and Nano Flows Conference
Milan, Italy, 11-14 September 2016

Heat transfer optimization in compact air heat exchanger

Tomasz MUSZYNSKI [1], Slawomir M. KOZIEL [2,3],

* Corresponding author: Tel.: ++48 58 347-24-57; Fax: ++48fax: 58 347-28-16; Email: Tomasz.Muszynski@pg.gda.pl,
1: Gdansk University of Technology, Faculty of Mechanical Engineering, Department of Energy and Industrial Apparatus Narutowicza 11/12, 80-233 Gdansk, Poland
2: School of Science and Engineering, Reykjavik University, Menntavegur 1, 101 Reykjavik, Iceland
3: Faculty of Electronics, Telecommunications and Informatics, Gdansk University of Technology, 80-233 Gdansk, Poland E-mail: Koziel@ru.is,

Abstract Two-dimensional numerical investigations of the fluid flow and heat transfer have been carried out for the laminar flow of the louvered fin-plate heat exchanger, designed to work as an air-source heat pump evaporator. The transferred heat and the pressure drop predicted by simulation have been compared with the corresponding experimental data taken from the literature. Two dimensional analyses of the louvered fins with varying geometry have been conducted. Simulations have been performed for different geometries with varying louver pitch, louver angle and different louver blade number. Constant inlet air temperature and varying velocity ranging from 2 to 8 m/s was assumed in the numerical experiments. The air-side performance is evaluated by calculating the temperature and the pressure drop ratio. Efficiency curves are obtained that can be used to select optimum louver geometry for the selected inlet parameters. The maximum heat transfer improvement interpreted in terms of the maximum efficiency has been obtained for the louver angle of 16 degrees and the louver pitch of 1.35 mm. The presented results indicate that varying louver geometry might be a convenient way of enhancing performance of heat exchangers.

Keywords: air side heat transfer, heat exchangers, heat transfer intensification,

1. Introduction

Heat exchangers play an important role in almost every engineering system [1], [2]. Their primary purpose is heat transfer between two working fluids such as air, refrigerants, water, glycols, etc. [1]. For example, air-to-refrigerant exchangers are used in refrigeration and air conditioning [3], automotive [4], as well as heat pump industry [5]. One of the most important design challenges for this type of devices is improvement of their efficiency, especially the heat transfer rate [6]. In compact heat exchangers, thermal resistance is generally dominant on the air side and may account for over 80% of the total thermal resistance. The air-side heat transfer surface area is up to 10 times larger than the water-side one. However, water-side heat transfer coefficient is approximately 50 times higher than air-side one. Thus, the air-side thermal resistance turns out to be higher by a factor of five. Consequently, any improvement in the heat transfer on the air side improves the overall performance of the heat exchanger. Louvered fins are frequently used on the air side of air conditioning evaporators and other heat exchangers to enhance the overall heat transfer rate. The louvers act to interrupt the air flow and create a series of thin boundary layers which have lower thermal resistance than the thick boundary layers on the plain fins.

Optimization of heat exchanger geometry may considerably improve energy savings in these systems. On the other hand, improved efficiency leads to reduced exchanger size, thus significantly reduces its manufacturing cost, and annual energy expenditures related to pumping. In this study, a numerical simulation of the air-side heat transfer and flow characteristics of the louvered fin-and-plate heat exchanger. The transferred heat and the pressure drops have been investigated.

2. Modeling

Louvered plate fins are frequently used on the air side of air conditioning evaporators and other heat exchangers to enhance the overall heat transfer rate. Figure 1 shows the overview of a multi-louvered plate heat exchanger. The following parameters are considered: louver angle, louver pitch and the number of louvers. Table 1 presents a list of all geometrical parameters used in calculations. The schematic diagram of the louvered fin-and-tube heat exchanger is shown in Fig. 1

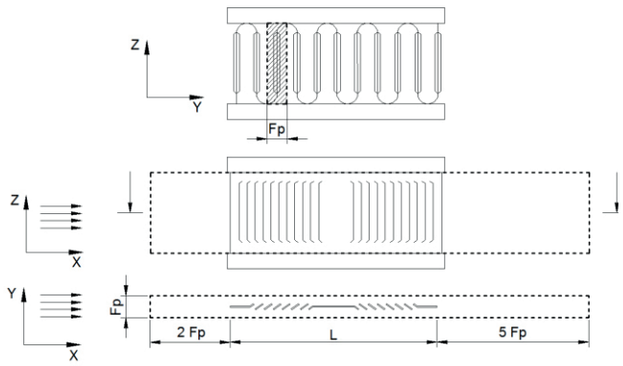

Fig. 1. Schematic of louvered fins-plate heat exchanger

Table 1. Geometrical and working parameters of the evaporator of the air source heat pump

Parameter	Dimension
Fin thickness F_t	0.1 mm
Louver no.	6 - 8
Fin pitch F_p	2 mm
Louver pitch L_p	0.9 – 1.4mm
Louver angle	10 - 70
Fin length L	36.6mm
Louver width H	6.53 mm
Inlet air velocity	2 - 8 m/s

A simple method of selecting the optimal geometry can be formulated as follows. The pressure drop is a function of the friction factor based on the fin surface condition and position. The power required to move the fluid across the bank is often a major operating expense and is directly proportional to the pressure drop. Overall efficiency of the heat exchanger can be expressed as a ratio of the pumping power to the transferred heat:

$$\eta = \frac{\dot{Q}_{ex}}{P_p} = \frac{\rho \cdot c_p \cdot \Delta T}{\Delta P} \qquad (1)$$

3. Conclusions

A parametric variation of the geometry provides a map to find a desired configuration for which the heat transfer to the pressure drop ratio attains its maximum. Furthermore, for each louver blade number and air inlet velocity, a region with a local maximum of efficiency can be found. Among all considered geometry parameters, the louver angle of 16 degrees yields the maximum efficiency for all considered combinations of the flow rate and the louver pitch.

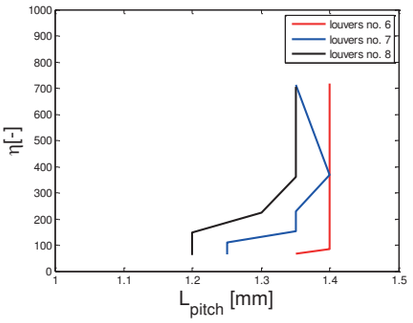

Fig. 2. Maximum efficiency as a function of frontal louver pitch for selected geometries.

REFERENCES

[1] Rohsenow, Warren M.; Hartnett, James P.; Ganic, Ejup N. Handbook of heat transfer applications. New York, McGraw-Hill Book Co., 1985, 973

[2] Cengel, Yunus A., and Michael A. Boles. Thermodynamics: an engineering approach. Vol. 5. New York: McGraw-Hill, 2011.

[3] Kandlikar, S. G. Two-phase flow patterns, pressure drop, and heat transfer during boiling in minichannel flow passages of compact evaporators. Heat Transfer Engineering, 2002, 23.1: 5-23.

[4] J.P. Rugh, J.T. Pearson, S. Ramadhyani, A study of a very compact heat exchanger used for passenger compartment heating in automobiles Compact Heat Exchangers for Power and Process Industries, ASME Symp. Ser. (2nd edn), HTD-Vol. 201, ASME, New York (1992), pp. 15–24

[5] Hepbasli, Arif, and Yildiz Kalinci. "A review of heat pump water heating systems." Renewable and Sustainable Energy Reviews 13.6 (2009): 1211-1229.

[6] T.A. Cowell, A general method for the comparison of compact heat transfer surfaces J. Heat Transfer, 112 (1990), pp. 288–294

5th Micro and Nano Flows Conference
Milan, Italy, 11-14 September 2016

Heat transfer enhancement in microjet heat exchanger

Tomasz MUSZYNSKI [1*], Rafal ANDRZEJCZYK [1],

* Corresponding author: Tel.: ++48 58 347-24-57; Fax: ++48fax: 58 347-28-16; Email: Tomasz.Muszynski@pg.gda.pl,
1: Gdansk University of Technology, Faculty of Mechanical Engineering, Department of Energy and Industrial Apparatus Narutowicza 11/12, 80-233 Gdansk, Poland

Abstract The article presents experimental studies on a compact heat exchanger with heat transfer intensification by means of impinging microjets. The pursuit to provide high performance of heat exchangers is a response to the demand both in economics and in the universal tendency to miniaturization of industrial equipment. This paper presents the design and tests of a prototype, microjet heat exchanger. The modular design of the heat exchanger allows to change its geometrical dimensions, as well as changing the heat exchange membrane material. The study of heat transfer in water-water flow, allows to determine the heat transfer efficiency, the characteristics of heat transfer, and the heat transfer coefficient values.

Keywords: microjets, heat exchangers, heat transfer intensification,

1. Introduction

Achieving the technological control on the micoscale heat and energetic installations and making them high- efficient is the challenge of 21st century. This direction of development has been delineated by the general trend towards miniaturization and by the expected widespread. The main elements of such systems must be highly compact and highly efficient heat exchangers. Regarding to that fact one of the technical problems associated with the heat removal in refrigeration and air-conditioning is an installation of high-performance heat exchangers i.e. evaporator, condenser or regenerative heat exchanger. Striving to ensure high performance of these elements is today a source of universal trend both to the miniaturization of these devices for both industrial and domestic applications, while maintaining the highest possible size to thermal energy ratio. As is well known, in recuperators heat transfer coefficient have decisive influence their efficiency. Overall heat transfer coefficient depends mainly on the lower value of HTC from working media. It is therefore most significant to improve the heat transfer with special attention on the side of the medium with lower heat transfer coefficient.

The article presents experimental studies on a compact heat exchanger with heat transfer intensification by means of impinging microjets. The pursuit to provide high performance of heat exchangers is a response to the demand both in economics and in the universal tendency to miniaturization of industrial equipment. This paper presents the design and tests of a prototype, microjet heat exchanger. The modular design of the heat exchanger allows to change its geometrical dimensions, as well as changing the heat exchange membrane material. The study of heat transfer in water-water flow, allows to determine the heat transfer efficiency, the characteristics of heat transfer, and the heat transfer coefficient values.

2. Test setup

Present study shows results of steady state heat transfer experiments, conducted for single phase cooling in order to obtain working fluids temperatures and heat fluxes. It consisted of the heat exchanger, fluid supplying system, the measuring devices, constant temperature bath and chiller. Cold working fluid was fed by a pulsation free gear pump from a supply tank. Desired fluid flow rate was obtained by means of power inverter and flow control valve. Detailed view of heat exchanger module is

presented in Figure 1.

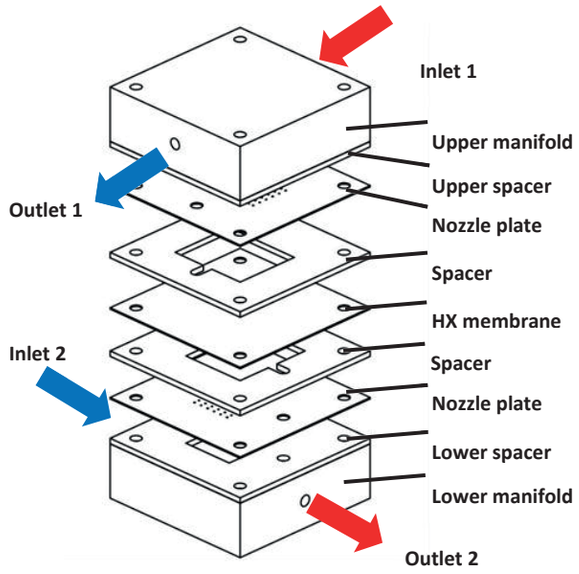

Fig. 1. Schematic of microjet HX

In order to validate the applicability of experimental correlations to design and build microjet heat exchangers experimental results were compared to literature correlations for impinging jets heat transfer.

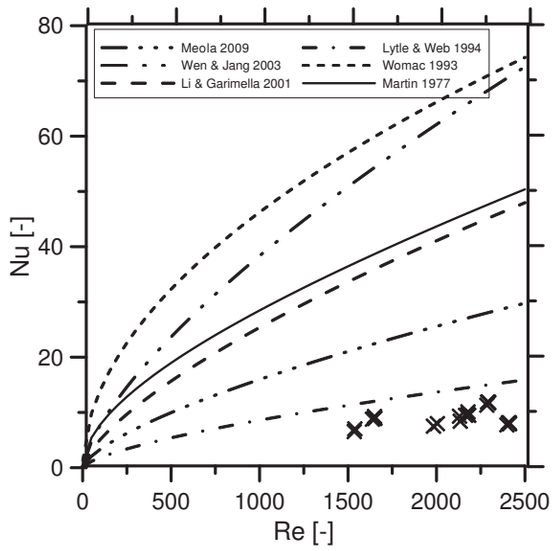

Fig. 2. Comparison between predicted and experimental average Nusselt numbers for 4x0.6mm geometry.

3. Conclusions

A prototype heat exchanger was built and tested. It incorporates very effective method of enhancing the heat transfer by means of impinging microjets. Modular configuration allows to carry out a series of tests with various working fluids, for both single phase and convective heat transfer and two phase boiling/condensation flow. The research allows the determination of the heat exchanger thermal performance, and to determine the usefulness of the intensification of heat exchange method in the refrigeration and air conditioning systems. Tested design has a great number of potential applications in a variety of machines and devices.

The Wilson plot method was successfully applied to determine the heat transfer coefficients in the laminar and transition flow regimes of a liquid-to-liquid heat exchanger. The heat exchanger is capable of exchanging 800W of thermal energy at LMTD of 60 K. The obtained overall heat transfer coefficient reaches over 10000 W/m2K.

REFERENCES

[1] Womac, D. J., Incropera, F. P., and Ramadhyani, S., 1994, “Correlating Equations for Impingement Cooling of Small Heat Sources With Multiple Circular Liquid Jets,” ASME J. Heat Transfer, 1162, pp. 482–486.

[2] Martin, H. Heat and Mass Transfer between Impinging Gas Jets and Solid Surfaces (1977) Advances in Heat Transfer, 13 (C), pp. 1-60.

[3] Li C-Y, Garimella S. V. Prandtl-number effects and generalized correlations for confined and submerged jet impingement International Journal of Heat and Mass Transfer, Volume 44, Issue 18, September 2001, Pages 3471-3480

[4] Wen MY, Jang KJ (2003) An impingement cooling on a flat surface by using circular jet with longitudinal swirling strips. Int J Heat Mass Transf 46:4657–4667

[5] Meola C. A New Correlation of Nusselt Number for Impinging Jets Heat Transfer Engineering, 30(3):221–228, 2009

[6] D. Lytle, B.W. Webb, Air jet impingement heat transfer at low nozzle–plate spacings, Int. J. Heat Mass Transfer 37 (1994) 1687–1697.

5th Micro and Nano Flows Conference
Milan, Italy, 11-14 September 2016

Improvement of thermosyphon performance by wall wettability modification

Rafal ANDRZEJCZYK [1*],Tomasz MUSZYNSKI [1],

* Corresponding author: Tel.: ++48 58 347-24-57; Fax: ++48fax: 58 347-28-16; Email: Rafal.Andrzejczyk@pg.gda.pl,
1: Gdansk University of Technology, Faculty of Mechanical Engineering, Department of Energy and Industrial Apparatus, Narutowicza 11/12, 80-233 Gdansk, Poland

Abstract Paper presents experimental investigations of passive heat elements such as thermosyphons, in use in domestic building applications, as in sidewalk deicing fig. 1. Main goal of this article is to find the best working fluid to utilize low grade ground heat source, instead of high temperature heat source. The paper presents an experimental test rig which was constructed to carry out investigations of two phase thermosiphon with new generation of refrigerants as working fluids. Sample experimental results are presented. Experimental data for acetone and HFE7100 were gathered. Conducted experimental research, will be used to verify the applicability of the existing correlations describing heat transfer coefficient for two-phase thermosyphons.

Keywords: heat transfer intensification, effectiveness, minichannels, number of transfer unit, helical coil,

1. Introduction

For the past many years, two-phase passive heat transfer devices like heat pipes and thermosyphons have played an important role in a variety of engineering heat transfer systems, ranging from electronics thermal management to heat exchangers and reboilers.
Currently available technologies for internally heating bridge decks consist primarily of three types of systems: electrical, hydronic, and heat pipe. In the electrical system, heat is produced by a current flow in an insulated metallic cable mounted within a bridge deck. Typically, the cable is laid out in a corrugated pattern to provide uniform heat distribution across the surface. The cable transfers heat to the surrounding material when it warms up due to the passage of an electrical current. These heating cables have been used on projects that comprise pavements, sidewalks etc.
Some research projects were conducted on using alternative energy sources to eliminate icing or frost on roadways and bridges. The heat is provided by GSHP in order to prevent icing on pavements and bridges. Some researchers studied the process of snow melting on pavements through solar collection by experiments and numerical simulation Many researchers have performed extensive experimentation and numerical analysis on thermosyphon to study the thermal characteristics and performance of the thermosyphon system. Yang and Chang [1] conducted experimentation on reciprocating tilted thermosyphon. Rahimi et al. [2] studied the effect of the condenser and evaporator resurfacing on overall performance of the thermosyphon. It was found that making the evaporator more hydrophilic and condenser more hydrophobic, the thermal performance increased and thermal resistance decreased in comparison to conventional thermosyphon. Literature review shows that not many studies in open literature carried out experiments improvement of two-phase thermosyphon by surfaces modifications

2. Test setup

The paper presents the investigation to find best suited surfaces wettability modification to improvement of two- phase thermosyphon. Authors shown their own experimental test rig, fig.1 which was constructed to carry out investigations of two phase thermosyphon with new generation of refrigerants as working fluids.

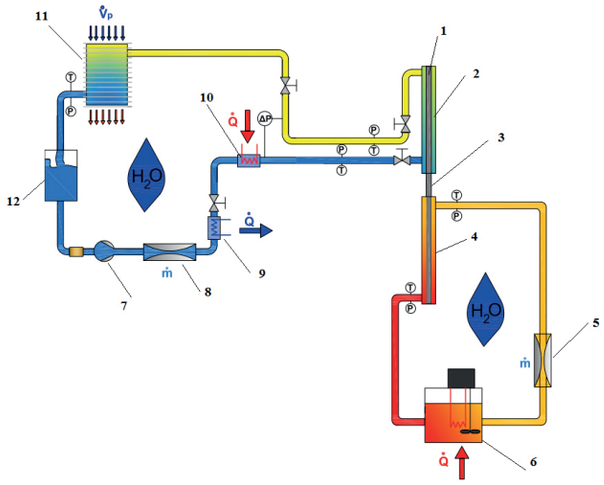

Fig.1 Experimental facility: 1 – thermosiphon, 2- cooling section, 3- adiabatic section, 4 – heating section, 5- ultrasonic flow meter, 6 – ultrathermostatic bath, 7 – nonpulsation gear pump, 8- corriolis mass flow meter, 9 – chiller, 10 – electric heater, 11 – heat sink, 12 – fluid thank

The considered element here is the heat pipe, having an internal diameter of 6 mm, the outer of 10 mm, made of stainless steel. The total length of the pipe is 2 m, but heat is supplied to the length of 0.5 m. There is also a 1 m long adiabatic section and cooling section over a length of 0.5 m. For the winter conditions temperature changes along with the depth , however, it is assumed that the temperature at the depth where the pipe is inserted (the part where heat is transferred) should range from 5C to 8C.

Fig. 2 shows the comparative results of transferred heat in thermosyphon with acetone HFE7100 and R365mfc.

Lowest thermal performance obtained with HFE7100 as the working fluid. Similar results were obtained for R365mfc as a medium. Best performance was observed for acetone. In general, thermal performance slightly rises with rising source temperature.

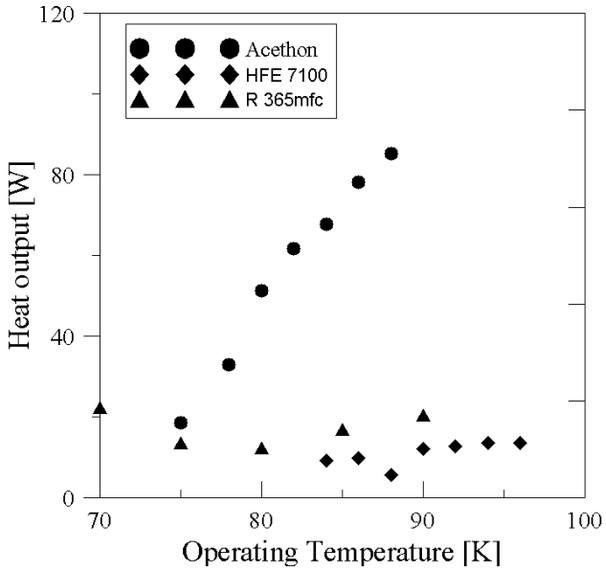

Fig. 2. Effect of operating temperature and fluid properties on transferred heat

3. Conclusions

A two-phase gravity assisted thermosyphon was designed, fabricated and tested with three refrigerants. Baseline thermal performance was obtained with HFE7100 as the working fluid. In general, it is observed that thermal performance slightly rises with rising source temperature. Maximum performance was observed for acetone while minimum was for HFE7100.Further investigations are needed in order to develop correlations to predict the heat transfer coefficients and performance of the termosyphone.

REFERENCES

[1] T. L.Yang and S. W. Chang, “Heat transfer in tilted reciprocating anti-gravity open thermosyphon,” International journal of heat and mass transfer, vol. 52, pp. 880-893, 2009

[2] M. Rahimi, K. Asgary, S.Jesri, “Thermal characteristics of a resurfaced condenser and evaporatorclosed two-phase thermosyphon”, International Communications in Heat and Mass Transfer, vol. 37, pp. 703-710, 2010.

5th Micro and Nano Flows Conference
Milan, Italy, 11-14 September 2016

Heat transfer intensification in vertical shell -and coil heat exchangers; exergy and NTU analysis

Rafal ANDRZEJCZYK [1*],Tomasz MUSZYNSKI [1],

* Corresponding author: Tel.: ++48 58 347-24-57; Fax: ++48fax: 58 347-28-16; Email: Rafal.Andrzejczyk@pg.gda.pl,
1: Gdansk University of Technology, Faculty of Mechanical Engineering, Department of Energy and Industrial Apparatus, Narutowicza 11/12, 80-233 Gdansk, Poland

Abstract In helical coil centrifugal force are acting on the moving fluid due to the curvature of the tube results in the development. It has been long recognized that the heat transfer in helical tube is much better than the straight ones because of the occurrence secondary fluid flow in planes normal to the main flow inside the helical structure. Helical tubes show great performance in heat transfer enhancement, while the uniform curvature of spiral structure is inconvenient in pipe installation in heat exchangers.
Authors have presented their own construction of shell and tube heat exchanger with intensified heat transfer. The purpose of this article is to assess the influence of the surface modification over the performance coefficient and effectiveness. The experiments have been performed for the steady-state heat transfer. Experimental data points were gathered for both laminar and turbulent flow, both for co current and counter current flow arrangement. To find optimally heat transfer intensification on the shell-side authors used NTU analysis.

Keywords: heat transfer intensification, effectiveness, minichannels, number of transfer unit, helical coil,

1. Introduction

Striving to ensure high performance of the heat exchangers, nowadays is a source of universal trend both to the miniaturization of these devices for both industrial and domestic applications, while maintaining the highest possible size to thermal energy ratio. As is well known, that in recuperators heat transfer coefficient have decisive influence on their efficiency. Overall heat transfer coefficient, depends mainly on the lower value of HTC from working media [1]. It is therefore most significant to improve the heat transfer with special attention on the side of the medium with lower heat transfer coefficient [2].
Helical coils are widely used in applications such as heat recovery systems, chemical processing, food processing, nuclear reactors, and high-temperature gas cooling reactors. Helical coils have been widely studied both experimentally [3] and numerically [4].
The purpose of this article is to assess the influence of the surface modification over the performance coefficient and modified effectiveness of vertical helical coiled tube heat exchangers. The calculations have been performed for the steady-state and the experiments were conducted for both laminar and turbulent flow inside and outside the coil. In spite of numerical and experimental studies which have been carried on in relation to tube-side heat transfer coefficient, there are not many investigations on the shell-side heat transfer coefficient. Going through existing literature, it has been shown that there are a luck of investigations on the heat transfer coefficient of this kind of heat exchanger considering the different surfaces modifications. To find optimal heat transfer intensification on the shell-side authors used exergy and NTU analysis.

2. Test setup

Present study shows results of steady state heat transfer experiments, conducted for single phase cooling in order to obtain working fluids temperatures and heat fluxes. It consisted of the heat exchanger, fluid supplying system, the measuring devices, constant temperature bath

and chiller. Cold working fluid was fed by a pulsation free gear pump from a supply tank. Desired fluid flow rate was obtained by means of power inverter and flow control valve. Detailed view of heat exchanger coil is presented in Figure 1.

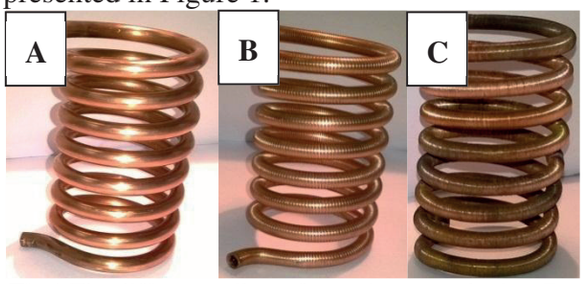

Fig.1 The different coils surfaces: A – smooth pipe, B - normal thread fins, C – extra-fine thread

In order to validate the applicability of experimental correlations to design and build microjet heat exchangers experimental results were compared to literature correlations for heat transfer.

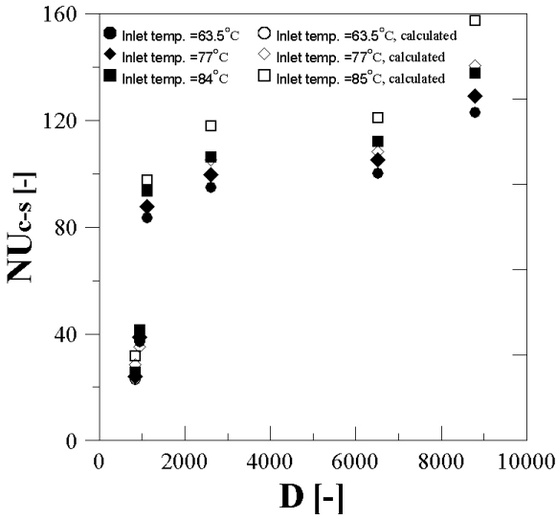

Fig.2 Variation of Nusselt number with Dean number for different fluid inlet temperature in case of non-modified surface: at left side for shell side, at right for coil side

3. Conclusions

Authors presented and successfully implemented, a simple mathematical methodology to model a shell and coil heat exchanger. In this paper, results show comparison between helically coiled heat exchanger with surface modification by means of microfins. During the experiments the mass flow rate in the inner tube and the annulus were both varied, both the counter and parallel flow configuration was tested. The experimental values of heat transfer coefficient have been obtained by the Wilson plots method.

It was observed that the overall heat transfer coefficient increases with increase in the inner-coiled tube Dean number for a constant flow rate in the annulus region. Similar trends in the variation of overall heat transfer coefficient were observed for different flow rates in the annulus region for a constant flow rate in the inner-coiled tube. It was shown that obtained average Nusselt numbers for the shell side have increased with surface modifications.

The literature predictions for hydrodynamics and fully developed heat transfer were in good agreement with experimental results. The agreement with the numerical and experimental predictions of Nusselt number values was well within 30%.

As was expected based on presented above facts the heat exchanger with surface modification on average has larger effectiveness from all of considered constructions.

REFERENCES

[1] T. Muszynski, R. Andrzejczyk, Heat transfer characteristics of hybrid microjet – Microchannel cooling module, Applied Thermal Engineering 93 (2016) 1360–1366

[2] T. Muszynski, R. Andrzejczyk, Applicability of arrays of microjets heat transfer correlations to design compact heat exchangers, Applied Thermal Engineering (2016), http://dx.doi.org/doi: 10.1016/j.applthermaleng.2016.01.120

[3] Rozzi, S., Massini, R., Paciello, G., Pagliarini, G., Rainieri, S., Trifiro, A., Heat treatment of fluid foods in a shell and tube heat exchanger: Comparison between smooth and helically corrugated wall tubes, J. Food Eng. 79, 249-254, 2007..

[4] J.S. Jayakumar, S.M. Mahajani, J.C. Mandal, P.K. Vijayanb, Rohidas Bhoia, Experimental and CFD estimation of heat transfer in helically coiled heat exchangers, Chemical Engineering Research and Design 86, 221–232, 2008

5th Micro and Nano Flows Conference
Milan, Italy, 11-14 September 2016

Asphaltene aggregation and deposition in transparent T-shaped micro-channel

Afshin GOHARZADEH*, Yougong ZHUANG, Yap Yit FATT

* Corresponding author: Tel.: +971 (2) 6075 396; Fax: +971 (2) 6075 200; Email: agoharzadeh@pi.ac.ae

Department of Mechanical Engineering, The Petroleum Institute, Abu Dhabi, UAE

Abstract This paper focuses on experimental investigation of asphaltene aggregation and deposition in a transparent T-shaped micro-channel. The dissolved asphaltenes from the crude oil are precipitated using N-heptane in the micro-channel at room temperature and standard atmospheric pressure. Asphaltene particles aggregate and deposit gradually on the surface of micro-channels. The growth of asphaltene deposits along the mixing line of crude oil and N-heptane is visualized. It is observed that asphlatene particles deposit in both longitudinal and transverse directions of the flow mixture. The dynamic of deposit front is studied for two flow rate ratios of crude oil and N-heptane. Obtained experimental results provide useful information on the behavior of asphaltene deposition and are helpful in developing and validating numerical models.

Keywords: asphaltene deposition, flow visualization, T-shaped micro-channel

1. Introduction

In the process of oil production, transportation and refinery, asphaltene deposition is a recurring problem, especially for wide utilization of enhanced oil recovery (EOR) technologies. Deposition of precipitated asphaltene particles can cause formation damage in reservoirs, blockage in wellbores or even problem in separators, pumps, pipelines, heat exchangers and other equipment [1]. Recently microfluidic experiments have provided precise control of fluid conditions and offered the opportunity to characterize the asphaltene deposition in microscale. With the decrease of channel dimensions, the interaction between asphaltene particles and channel walls become significant [2-5]. Over the last two decades, several experimental studies in microscale have been focused on characterizing asphaltene deposition in both stainless steel capillary tubes [6-10] and transparent glass capillary tubes or micro-channels [11-14]. These above experimental studies used flow visualization techniques to understand the asphaltene deposition process quantitatively at fully developed flow regions. Several predictive models were developed to estimate the amount of asphaltene deposit in micro-scale systems. However, the process of asphaltene aggregation and deposition at the inlet of micro-mixer devices remains unclear. Therefore, this study focuses on the asphaltene aggregation and deposition process at the mixing area of a T-shaped micro-channel where both crude oil and N-heptane are interacting. In a transparent T-shaped micro-channel, the mixing area is visualized and asphaltene aggregation and deposition is quantified.

2. Experimental Setup

The experimental setup consists of a T-shaped micro-channel (Figure 1), a dual-drive syringe pump having two glass syringes, a collection tank and a microscope for flow visualization.

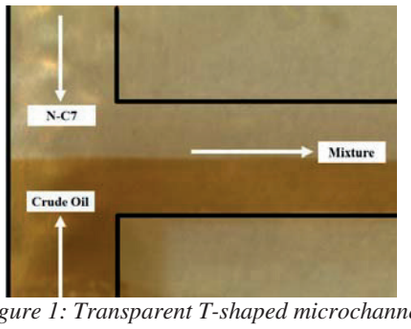

Figure 1: Transparent T-shaped microchannel

The horizontal T-shaped micro-channel has the depth of 20 μm. The syringe pump (Cole-Parmer with 106.6 mL/min maximum flow rate) is used to generate a mixing working fluid flowing at a designed flow rate. Both fluids (Crude oil and N-heptane) were injected

in the test section and mixed at a T-Junction area. The ratio of working fluids including crude oil and N-heptane is controlled by flow rates via the syringe pump. The temperature of the working fluids is at a constant temperature of 21°C.

3. Results

Experiments in terms of different flow rate ratios of crude oil and N-heptane were conducted. The flow rate ratios (crude oil:N-heptane) in these experiments were 1:9 and 2:8 respectively. The dynamic of asphaltene aggregation and deposition front is studied during 60 minutes with images recorded every 2 minutes (Figure 2). It is observed that asphaltene aggregates and deposits in x-direction at the interface between crude oil and N-Heptane. For a constant flowrate ratio of crude oil and N-heptane, asphaltene aggregates and deposits also in y-direction (perpendicular to the flow direction).

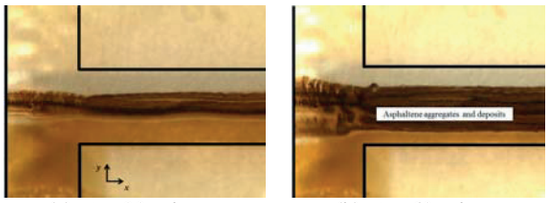

(a) t = 30 min. (b) t = 60 min.

Figure 2: Asphaltene deposition at the T-Junction

For both flow rate ratios, the region of asphaltene deposit in y-direction is measured every 2 minutes and reported in figure 3. After 60 minutes, asphaltene deposits in y direction increase up to 1.2 mm for both conditions, covering approximately 60% of the micro-channel. The slopes of the curve representing the velocity of deposit front is approximately 0.02 mm/min.

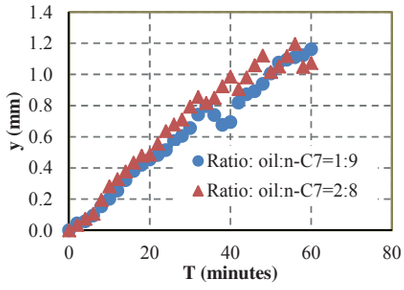

Figure 3: Thickness of asphaltene deposit area vs time.

4. Conclusions

In this study, experimental investigations of asphaltene deposition were carried out in the laboratory conditions using transparent T-shaped micro-channels. N-heptane induced asphaltene precipitation and subsequent deposition were obtained and quantified based on image processing method. The effect of flow rate ratio of crude oil and n-heptane is studied. It was observed that the result using ratio of 1:9 (crude oil to n-C7) is similar to that using 2:8 ratio. In the 60 minutes asphaltene deposits in y direction increase up to 1.2 mm for both conditions, covering appropriately 60% of the micro-channel. Future work will be focused on the influence of type mixing geometry (Y-shaped) and type of crude oil on the dynamic of asphlatene front deposition.

References

1. Akbarzadeh, K., Eskin, D., Ratulowski, J., and Taylor, S., *Energ. Fuel.,* vol. 26, no. 1, pp. 495-510, 2012.
2. Jensen, K.F., *Chem. Eng. Sci*. 56, 293–303, 2001.
3. Schneider, M. H., Sieben, V. J., Kharrat, A. M., and Mostowfi, F., *Anal. Chem*., vol. 85, no. 10, pp. 5153-5160, 2013.
4. Hu, C., Morris, J. E., and Hartman, R. L., *Lab Chip,* vol. 14, no. 12, 2014.
5. Seifried, C.M., Boek, E.S., Crawshaw, J.P., Al Lawati, S., *SPE 166289*, 2013.
6. Broseta, D., Robin, M., Savvidis, T., Féjean, C., Durandeau, M., and Zhou, H., *SPE-59294-MS*, 2000.
7. Wang, J., Buckley, J. S., and Creek, J. L., *J. Dispersion Sci. Technol.,* vol. 25, no. 3, pp. 287-298, 2004.
8. Nabzar, L. and Aguiléra, M., *Oil & Gas Science and Technology-Revue de l'IFP,* vol. 63, pp. 21-35, 2008.
9. Jamialahmadi, M., Soltani, B., Müller-Steinhagen, H., and Rashtchian, D., *Int. J. Heat Mass Transfer,* vol. 52, no. 19, pp. 4624-4634, 2009.
10. Hoepfner, M., Limsakoune, V., Chuenmeechao, V., and Maqbool, T., Fogler, H., *Energ. Fuel.,* vol. 27, pp. 725-735, 2013.
11. Boek, E. S., Ladva, H. K., Crawshaw, J. P., and Padding, J. T, *Energ. Fuel.,* vol. 22, no. 2, pp. 805-813, 2008.
12. Boek, E. S., Wilson, A. D., Padding, J. T., Headen, T. F., and Crawshaw, J. P, *Energ. Fuel.,* vol. 24, pp. 2361-2368, 2009.
13. Lawal, K. A., Crawshaw, J. P., Boek, E. S., and Vesovic, V., *Energ. Fuel.,* vol. 26, no. 4, pp. 2145-2153, 2012.
14. Zhuang, Y.G., Goharzadeh, A., Yap, Y.F., Chai, J.C., Mathew, N., Lin, Y.J.N., Vargas, F., Biswal, S.L., *J. Petrol Sci. Eng.,* vol 145, pp. 77-82, 2016.

5th Micro and Nano Flows Conference
Milan, Italy, 11-14 September 2016

Synthesis, characterization and functionalization of carbon nanotubes to produce stable nanofluids

Letícia R. OLIVEIRA[1], Enio P. BANDARRA FILHO [2, *]

* Corresponding author: Tel.: ++55 (34) 99944 3351; Fax: ++55 (34) 3239 4022; Email: bandarra@mecanica.ufu.br
1,2 Mechanical Engineering School, Federal University of Uberlandia, BR

Abstract Stable nanofluids were prepared by dispersing carbon nanotubes (MWCNT) functionalized in water without the addition of any surfactant and the viscosity and thermal conductivity properties investigated experimentally. The nanofluids were produced by the two-step method with volumetric concentrations of 0.02% to 0.2% by dispersion of nanoparticles previously functionalized by acid treatment. The characterization was done by X-ray diffraction (XRD) and high-resolution transmission electron microscopy (TEM). The thermal conductivity and viscosity are measured in the 20-50°C range. The results indicated an increase in thermal conductivity, and the positive addition of these nanoparticles in water for producing nanofluids. Moreover, functionalization by acid treatment facilitated the water dispersion stability improves long-term nanofluids.

Keywords: Nanofluids, Carbon nanotubes, Functionalization, Thermal conductivity, Viscosity

1. Introduction

Nanofluids are colloidal dispersions of nanoparticles in a host fluid and plays a crucial role in the development of new technologies, which could be applied in many industrial areas. However, development of heat transfer fluids with improved thermal conductivity has become more and more critical to the performance of energy systems [1].

Nanofluids offer stable dispersions for long periods and exhibit a greater thermal conductivity than that of the host fluid [2]. The big challenge of synthesis stable nanofluids is to prevent sedimentation of nanoparticles while keeping their size and optimal concentration in the base liquid. For this, ultrasonic agitation and/or mechanical stirring are the widely used techniques for breaking the large agglomerates into smaller pieces, and to ensure good dispersion of particles in the liquid.

Multi-walled carbon nanotubes (MWCNTs) have attracted substantial interest since 1991 due to their unique [3]. To enhance or change the properties of MWCNTs, nanotubes have been treated using different methods, like acid functionalizing, coating, doping or filling pristine nanotubes, thereby obtaining a so-called nanohybrid [4].

In this work, we investigated the thermal performance such as thermal conductivity of nanofluids MWCNT-COOH and dynamic viscosity. The characterization of carbon nanotubes was toke by scanning electron microscope (SEM) and X-ray diffraction (XRD).

2. Experimental methodology

2.1 Functionalization acid

MWCNTs with diameters of 8-15 nm, length 10-50 micrometers 95% purity, 230 m^2/g of specific surface area were bought of Nanostructured & Amorphous Materials Inc. Nitric and sulfuric acids were obtained from Synth. In a mixture of 3: 1 (H_2SO_4/HNO_3) were added 15 g of MWCNTs. This mixture was under agitation magnetic for about 16h. Then the nanotubes were washed with deionized water until the pH~7.

2.2 Preparation of the nanofluid and characterization

The nanofluids were prepared by two-step method is homogenized in a high-pressure

homogenizer for 30 minutes at 400 bar. Nanofluids were produced MWCNT-COOH in distilled water in volumetric concentrations of 0.02%, 0.08%, 0.1% and 0.2%. The characterization of MWCNTs-COOH was made by XRD and TEM images. Therefore, we have done the thermal conductivity measurements and viscosity dynamic for these nanofluids.

3. Results and discussion

Fig. 1 shows the patterns of X-ray diffraction (XRD) to the pure MWCNT and after acid functionalization. For the analysis of the diffraction patterns, it is possible to observe a difference in the peaks, which indicates the functionalization.

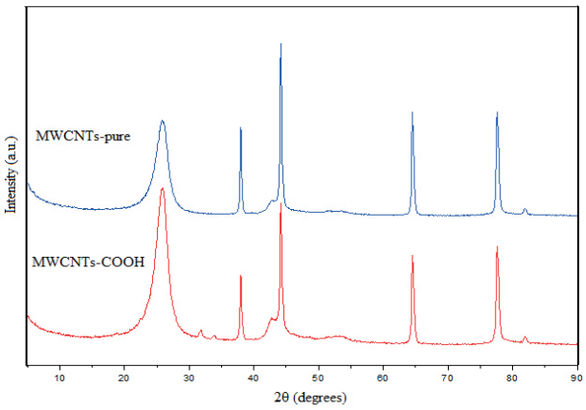

Fig. 1. XRD patterns for pure MWCNT and after acid functionalization.

Fig. 2 shows images of the MWCNTs. Is possible to observe the nanoparticles dimensions and the shape.

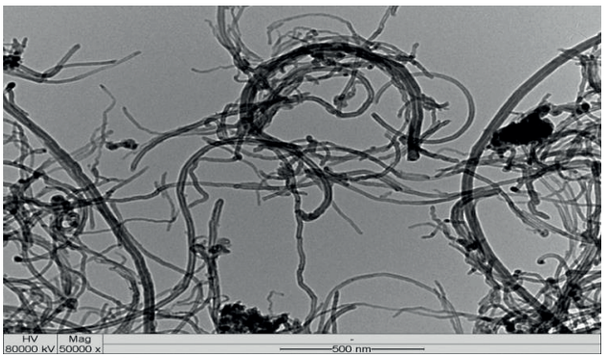

Fig. 2. Nanoparticle images obtained through transmission electron microscope (TEM).

Dynamic viscosity measurements were performed for temperature of 20-50 °C. Fig. 3 shows the relative viscosity values measured for different temperatures. We observed viscosity increase with increasing volume fraction of nanoparticles, and this is in agreement with the literature.

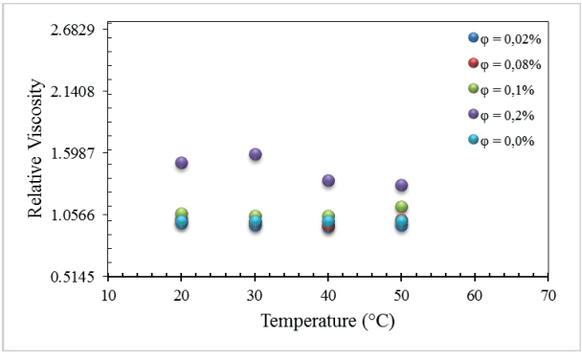

Fig. 3. Relative viscosity for different temperature and volumetric concentration.

Fig. 4 shows the relative values of thermal conductivity, being observed an increase with respect to pure water.

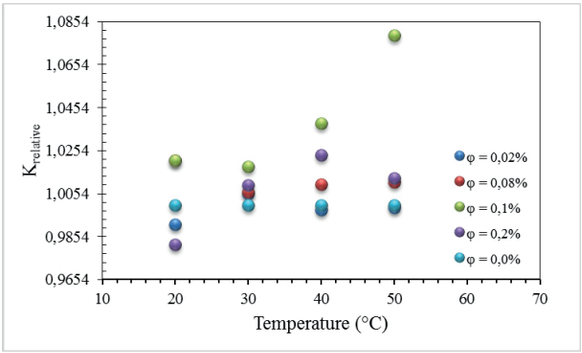

Fig. 4. Relative thermal conductivity for different temperature and volumetric concentration.

4. Conclusion

The acid functionalization was effective and allowed the synthesis of stable nanofluids with an increase in thermal conductivity with increasing volume fraction without increasing considerably the viscosity.

References

[1] LotfizadehDehkordi B et al (2013) Investigation of viscosity and thermal conductivity of alumina nanofluids with addition of SDBS. Heat Mass Transf 49(8):1109–1115.
[2] S.U.S. Choi (Enhancing thermal conductivity of fluids with nanoparticles), Proceedings of the 1995 ASME International Mechanical Engineering Congress and Exposition, 231, ASME, 1995, pp. 99–105.
[3] S.M. Abbasi et al. Ceramics International 39 (2013) 3885–3891.
[4] Dominik Eder, Carbon nanotube – inorganic hybrids, Chemical Review 110 (2010) 1348–1385.

5th Micro and Nano Flows Conference
Milan, Italy, 11-14 September 2016

Study of the phase separation effect in capillary-size micro-channels

Adlan MERLO [2,1*], Paul DURU [1,2], Sylvie LORTHOIS [2,1]

* Corresponding author: adlan.merlo@imft.fr
1 Université de Toulouse; INPT, UPS; IMFT (Institut de Mécanique des Fluides de Toulouse), France
2 CNRS; IMFT; Toulouse, France

Abstract It has been known for more than 50 years that the distribution of red blood cells (RBCs) in microvessel networks is highly heterogeneous. Yet, the phase separation effect (PS), i.e the non-proportional distribution of RBCs between the two daughter branches of a simple divergent bifurcation, is still poorly understood especially when RBC concentration (tube hematocrit) reaches high values (> 20%) and when vessel diameter is close to that of RBCs' (~8µm), as often encountered in microcirculation. The most commonly used PS law has been empirically derived *in vivo* by Pries et al. [1] but its validity has been recently questioned [2]. Therefore, experimental data obtained in controlled conditions are needed. We have designed squared micro-channel bifurcations, with side ranging from 5 to 20 microns, and adapted the injection geometry. Associated to a new method for the measurement of high tube hematocrit values, this allows for an *in vitro* systematic investigation of the parameters influencing the PS (tube hematocrit, confinement, bifurcation geometry). Our results are compared with Pries' PS law.

Keywords: Microcirculation, Red Blood Cells, Phase Separation Effect

1. Introduction

RBCs carry oxygen throughout the whole body. Exchanges with the tissues take place mainly in networks of capillary or slightly larger vessels, which diameters are comprised between ~3µm and ~20µm. At rest, RBCs have a biconcave shape of ~8µm in diameter and a thickness of ~2µm. They are able to deform enough to squeeze into the tiniest capillaries. Capillary vessels form dense, complex 3D networks [3]. RBC distribution within these structures exhibits strong spatio-temporal heterogeneities [4,5]. To better understand that behavior, one needs to understand what happens in the simplest component of a network: one simple divergent bifurcation. RBCs split in a non-proportional fashion between the two daughter branches, with respect to total flow fractionation [1]. This phenomenon, called phase separation (PS), is influenced by numerous parameters: RBC to mother branch diameter ratio, daughters to mother diameter ratio, daughters to mother branch flow rate ratio, concentration of RBCs (tube hematocrit) in the mother branch, and the hematocrit profile within this branch [1]. Yet, no study of the PS has been conducted in such small vessels, in controlled conditions, as pointed out in recent numerical works investigating the distribution of RBCs in realistic or simplified microvascular networks [2,5]. Therefore our aim is to provide reference *in vitro* experimental data of PS in channels of diameters close to that of the RBCs.

2. Material and Methods

2.1 RBCs suspensions and microfluidic chips

RBCs are centrifugated from whole human blood, washed and suspended in a density-matching solution [6].

Microfluidic chips are fabricated by multiple mask soft lithography, resulting in squared cross-sections of 5, 10 or 20 microns for the channels in the bifurcation, with an improved injection geometry. The chips are composed of a PDMS matrix bounded on a glass slide for microscopic observation and channels enclosure. Different pressure values are imposed at inlet and outlets, thus enabling

to control the flow rate partition between both daughter branches, with a good stability over long periods of time (~45min) and for a wide range of tube hematocrits (~1.5 to ~30%).

2.2 Tube hematocrit and velocity profiles

When a dilute suspension of RBCs flows in a channel, one can count them to obtain a mean hematocrit value. However, this gives no information about the hematocrit profile and it is most often impossible to proceed that way as hematocrit increases. Studies have taken advantage of the Beer-Lambert law [7]. To implement this method, a rigorous and tedious calibration is needed [7]. We have developed a simpler calibration using glass chambers with calibrated thickness of 10 and 20 microns (Leja slides). The idea is to relate the precisely known hematocrit of a prepared RBC suspension to the mean temporal attenuation of light in the depth of the chamber over a group of pixels. For that purpose, a drop of ~2µl is put at the entrance of the chamber which immediately fills by capillarity. After filling, due to lateral migration in the depth of the chamber, RBC distribution is not uniform throughout the chamber. Being of weakly inertial nature, this effect has been counteracted by partially filling its outlet with viscous oil prior to injection. As a consequence, the filling speed was tremendously lowered, allowing to achieve the uniform RBC distribution needed to perform calibration. We found a linear relation between hematocrit and light intensity reduction, up to a plateau value. The linear coefficient is proportional to the chamber depth. Calibration was performed with the same microscope and objectives as the ones used for the PS study in micro-channels.

Velocity profiles have been obtained using the dual slit method [6]. This method, based on temporal correlation between grey levels profiles across the channel, yields the maximal velocity profile of the RBCs, when implemented as shown in [6].

3. Results

To validate the above methods, we quantified the apparent deviation to mass conservation due to experimental uncertainties and demonstrated values below 15% for all our experimental conditions. Figure 1 displays the results obtained in a symmetric T-shaped bifurcation, with three branches of equal side length (10µm), for dilute (1.5%) and concentrated (25%) suspensions. As in [1], the RBC flow fraction entering one of the daughter branches is plotted against the total blood flow fraction entering that branch. The results obtained are consistent with Pries' PS law when the parameters are rescaled to take into account the difference in size between human and rat RBCs [3]. A systematic analysis of the influence of hematocrit, absolute flow rate in the inlet branch and bifurcation geometry on the parameters of this law is under progress.

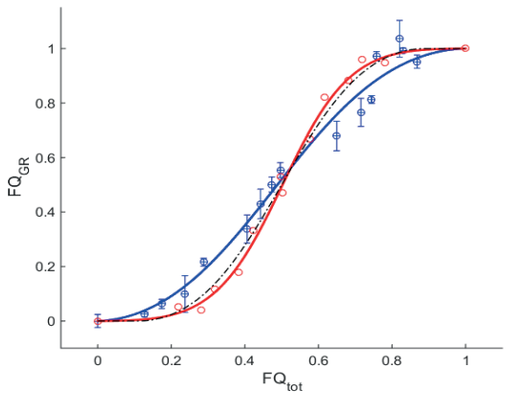

Fig. 1. PS in a 10µm symmetric T-shaped bifurcation. Mean tube hematocrit in mother branch: ~1.5% (red) ~25% (blue). Error-bars : apparent deviation to mass conservation (not shown in red for clarity). Continuous lines: least-squares fits to Pries' PS law. Discontinuous line : Prediction from Pries PS in 10 µm-diameter vessels in the limit of small hematocrits.

References

[1] Pries et al., Microvascular Res. **38**, 81-101, 1989
[2] Gould and Linninger, Microcirculation **22**, 1-18, 2015
[3] Lorthois et al., Neuroimage **54**, 1031-1042, 2011
[4] Desjardins et al., Neurobiol. Aging **37**, 1947-1955, 2014
[5] Obrist et al., J. Royal Soc. Interface **368**, 2897-2918, 2010
[6] Roman et al., Microvascular Res. **84**, 249-261, 2012
[7] Pries et al., Am. J. Physiol. **245** (Heart Circ. Physiol. **14**), H167-H177, 1983

5th Micro and Nano Flows Conference
Milan,Italy, 11-14 September 2016

Simulation of Bio-Particle Separation Using Inertial Microfluidics in a Spiral Microchannel for Biomedical Applications

Reza RASOOLI , Onur Kaan KARAOĞLU, Barbaros ÇETIN*
* Corresponding author: Tel.: +90 (312) 290-2108; Fax: +90 (312)266-4126
Email: barbaros.cetin@bilkent.edu.tr, barbaroscetin@gmail.com
Microfluidics and Lab-on-a-chip Research Group, Mechanical Engineering Department
İhsan Doğramacı Bilkent University 06800 Ankara Turkey

Abstract Particle manipulation in microfluidic channels is an important problem since it is the basis of many microfluidics technologies for biomedical applications. Particle manipulation can accomplished by means of many different techniques such as hydrodynamic, electrokinetic, magnetic and etc. Hydrodynamic techniques are the most promising ones among them since it just uses the flow field which leads to a passive manipulation without any need for additional equipment. Particle separation based inertial microfluidics is a passive manipulation procedure which has many advantages such as high throughput, simple structure, label free and so forth. In the present study, the particles equilibrium focusing has been investigated for a spiral microchannel using force balance integration method. Particles with different sizes and initial positions has been released and the equilibrium position has been obtained for each particle using different.

Keywords: Inertial microfluidics, Secondary flow, Inertial migration, Particle separation, Equilibrium position

1. Introduction

Microfluidic field has most often connected to the assumption for the negligible inertia. This assumption occurs when the Reynolds number is very small. In this case, the Stokes equation is the governing equation for the system. For the microfluidic systems with high flow velocity, the Reynolds number is not small and thus neglecting inertia effects is no longer correct. Inertial microfluidics is a subclass of hydrodynamic-based manipulation techniques in which the manipulation of the particles achieved using the finite Reynolds number (1-100) nature of the flow field. Particles in inertial microfluidics experience an inertial lift force which consists of four forces: Magnus force [1], Saffman force, wall-induced lift force and shear gradient lift force. Sum of all these four forces is considered as the net inertial lift force. There are some studies for the net inertial lift forces in literature [2-4]. One of the most important application of inertial microfluidic and inertial migration is the particle manipulation and separation [5]. Straight and curved microchannels has been widely exploited for bio-particle separation [6-9]. Spiral microchannel is of significant interest due to its great capability in particle separation. For this purpose, many studies has been done to assess the efficiency of spiral microchannel both experimentally and numerically [9],[10]. Typically, the design of the inertial microfluidic platform is performed by the flow field simulations. A rigorous modeling of the particle motion is a key point to further improve the performance of inertial microfluidic devices. In this study, a point particle approach is implemented for the prediction of the performance of an inertial microfluidics based devices. The main purpose of the present study is to implement and compare different models available in the literature for the net inertial lift force acting on the particle in a spiral microchannel. The flow field was simulated using COMSOL Multiphysics software and the force balance integration was performed using the MATLAB link of the COMSOL.

2. Formulation and Force Elements

The Newton's second law was implemented to track the particles using force elements acting

on the particles. For a spiral channel, the Newton's second law can be written as:

$$u_{pr}{}^{k+1} = u_{pr}{}^{k} + \left[\frac{1}{M_p}\sum F_r{}^{k} + \frac{(u_{p\theta}{}^{2})^{k}}{r^{k}}\right]\Delta t \quad (1)$$

$$u_{p\theta}{}^{k+1} = u_{p\theta}{}^{k} + \left[\frac{1}{M_p}\sum F_\theta{}^{k} - \frac{(u_{p\theta}u_{pr})^{k}}{r^{k}}\right]\Delta t \quad (2)$$

$$u_{pz}{}^{k+1} = u_{pz}{}^{k} + \left[\frac{1}{M_p}\sum F_z{}^{k}\right]\Delta t \quad (3)$$

where the superscript k+1 shows the values at the next step. Similarly, the forces can be expressed as:

$$F_D = \frac{1}{2}\pi R_p{}^{2} C_D \rho_f (u_f - u_p)^2 \quad (4)$$

$$F_L = \frac{\rho_f U_{max}{}^{2} D_p{}^{4}}{D_h{}^{2}} C_l(r,z) \quad (5)$$

where the u_p, F_D, F_L, C_D, C_l and M_p are particle velocity, drag force, net lift force, drag coefficient, lift coefficient and particle's mass respectively. Drag coefficient is taken from [11] and lift force from [2-4]. Asmolov [2] obtained the net inertial lift force on a spherical particle in a two dimensional poiseuille flow for Reynolds numbers up to 1500. Hood [3-4] used a numerical asymptotic method to calculate the net inertial lift force and lateral velocity of spherical particles in 3 dimensional poiseuille flow both in square and rectangular channel with aspect ratio of 2.

3. Results and Discussion

Formulation first was verified for microchannel with square and rectangular (AR=2) cross section both for straight and spiral shapes (figs 1 and 2). Finally, the simulation was performed for the spiral channel of our interest with rectangular cross section with width and height of 600 and 70 µm respectively. Particles with size of 8 and 16 µm were considered. The hollow circles, solid circles and dashed lines show the initial position, equilibrium position and trajectories of particles. Volumetric flow rate of 24 ml/h and zero gauge pressure were assigned for the inlet and outlet respectively. In figure 2, lift force was taken from straight channel with the same aspect ratio. In figure 3, which is the rectangle of AR=9, there is not any data available in the literature for the lift force and the lift force in straight channel of AR=2 was used. A stretch was made for the data to fit the aspect ratio of the channel.

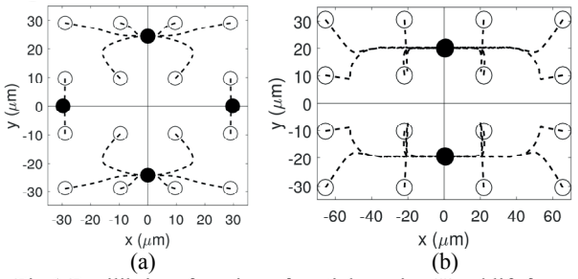

(a) (b)

Fig.1:Equilibrium focusing of particles using Hood lift force in :(**a**)square straight channel, (**b**) rectangle AR=2 straight channel

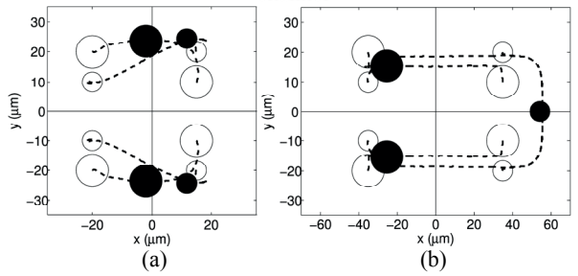

(a) (b)

Fig.2: Equilibrium focusing of particles using Hood lift force in :(**a**) square spiral channel, (**b**) rectangle AR=2 spiral channel

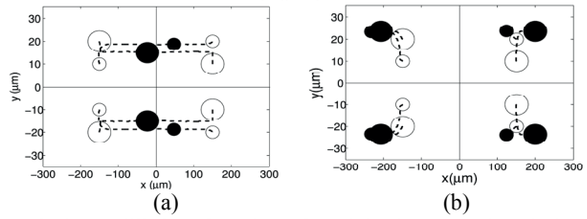

(a) (b)

Fig.3: Equilibrium focusing of particles in rectangle spiral with AR=9 using: (**a**) Hood inertial force, (**b**) Asmolov inertial force

References

1. Rubinow and J. B. Keller, J. Fluid Mech., 1961, 11, 447-459.
2. E. S. ASMOLOV, J. Fluid Mech., 1999, 381, 63-87.
3. Hood, Kaitlyn, et al. arXiv preprint arXiv:1509.01643 (2015).
4. Hood, Kaitlyn, Sungyon Lee, and Marcus Roper. J. Fluid Mech765 (2015): 452-479.
5. Çetin, B., Özer, M. B., & Solmaz, M. E. (2014). Biochem.Eng.J, 92, 63-82.
6. Hur, Soojung Claire, et al. PLoS One 7.10 (2012): e46550.
7. Mach, A. J., & Di Carlo, D. (2010). Biotech.Bioeng, 107(2), 302-311.
8. Bhagat, A. A. S., Kuntaegowdanahalli, S. S., & Papautsky, I. (2008). Lab Chip, 8(11), 1906-1914.
9. Sun, Jiashu, et al. Lab chip 12.20 (2012): 3952-3960.
10. Sun, Jiashu, et al. Biomicrofluidics 7.1 (2013): 011802.
11. Morsi, SAj, and A. J. AlexanderJ. Fluid Mech 55.02 (1972): 193-208.

Experimental Analysis of Droplet Formation in a Micro Cross-Junction

Behnam ROSTAMI [1,*], Beatrice PULVIRENTI [1], Giacomo PUCCETTI [1], Gian Luca MORINI [1]

* Corresponding author: Tel.: ++39 (0)5120 90541; Fax: ++39 (0)5120 90544; Email: behnam.rostami2@unibo.it
1 DIN – Alma Mater Studiorum Università di Bologna, Laboratorio di Microfluidica, Via del Lazzaretto 15/5, Bologna 40131, Italy

Abstract In this paper the mechanism of the formation of water droplets in silicone oil within commercial micro cross-junctions is investigated experimentally. By varying the inlet flow rate of both fluids, the breakup of the water droplets in silicone oil (W/O) is investigated and compared for two different geometries of the cross-junction in order to highlight the role of the channel geometry on the droplet production. The images of the droplets have been obtained via a high-speed camera, connected to an inverted microscope. The procedure of water phase contour detection is based on Matlab Image Toolbox scripts.

Keywords: Micro Cross-Junction, Droplet Formation, Size Effect, Two-Phase Flow

1. Introduction

In the last years, several microdevices have been developed for the production of droplets and emulsions, which have a large use in many fields, especially in the field of drug delivery [1-2]. Cross-junction droplet generators are examples of flow-focusing devices, widely used for droplet-based microreactors and chemical synthesis. Based on the experimental observations collected in the last years, a complete control over the two-phase flow behavior, by these devices, requires a detailed understanding of the bubble or droplet formation mechanisms. In this work, two different cross-sections (*Dolomite Micro-fluidics Co.*) obtained as intersection of two stadium-shaped glass microchannels, have been studied in order to check the influence of the geometry of the junction on the droplet characteristics. The cross-junction #1, shown in Figure 1a, is characterized by a cross section restriction at the junction in which the width of the channel goes from W_w=300 µm down to W_j=105 µm. The *restriction ratio* which can be defined as the ratio of these two parameters ($R=W_j/W_w$) is equal to 0.35. The height of the channels (H) is equal to 100 µm. The *aspect ratio*, *i.e.* the ratio between the channel height and width, is equal to A_j=0.95 at the junction and A_w=0.33 out of the junction region. The cross-junction #2, shown in Figure 1b, has a width W_j=195 µm at the junction and a width W_w=390 µm out of it; the height of the channels is equal to 190 µm. For the cross-junction #2 the *restriction ratio* is equal to R=0.5 while the channel aspect ratio is equal to A_j=0.97 and A_w=0.49.

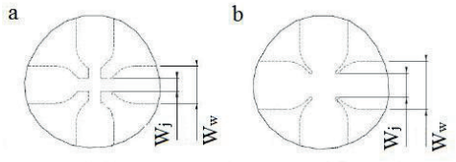

Figure 1: Sketch of the tested cross-junctions: the cross-junction #1 (a) and #2 (b)

In the experimental tests, the de-ionized water is used as the dispersed phase and silicone oil, (υ=20 cSt and ρ=0.95 g/ml (*Sigma-Aldrich*)) as the continuous phase. The experimental setup is based on an inverted microscope illuminated from the bottom and top of the microdevice. In order to acquire the images, the microscope is connected to a high-speed camera.
During the experimental tests, the flow rates of the dispersed (Q_d) and continuous (Q_c) phases have been changed to observe the effect of the flow rate ratio ($\alpha=Q_d/Q_c$) ranging between 0.1 and 0.5; for each fixed value of α, different tests characterized by a Capillary number linked to the continuous phase (Ca_c) ranging

between 0.004 up to 0.01 have been conducted. The acquired images have been post-processed to follow the evolution of the water droplet interface within the cross-junction by using a series of Matlab Image Toolbox [3].

2. Results

Figure 2 confirms that the quality of the typical images is very good, as underlined by the well-defined contours of the water droplets and of the channel walls.

Figure 2: The formation of the water droplet

In order to compare the effect of the geometry of the two cross junctions on the water droplet size, in Figure 3 the droplet interface position obtained by using both the cross-junctions is figured for the same value of α (=0.40) and Ca_c (=0.004); the displacement of the droplet during a time interval (Δt) of 0.002 s is shown.

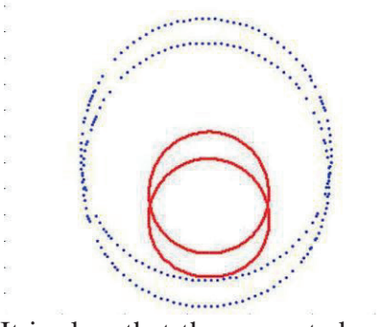

Figure 3: Water droplets obtained for α=0.40 and Ca_c=0.004 with the cross-junction #1 (red solid line) and #2 (blue dot line).

It is clear that the generated water droplets are characterized by a very different diameter. By defining the mean diameter of the water droplet as $D = \sqrt{D_h D_v}$, with D_h and D_v being the horizontal and vertical diameters, a non-dimensional diameter of the droplet can be introduced as $D^*=D/H$. In Figures 4 and 5 the trend of D^* is given as a function of α for values of Ca_c ranging between 0.004 and 0.01. It is obvious that the results obtained for the cross-junction #2 tend to be in a good agreement with the scaling law ($D^*=\varepsilon+\omega\alpha$) [4] for the squeezing regime. On the contrary, for the cross-junction #1 some discrepancy can be seen, especially for low Ca_c (<0.006).

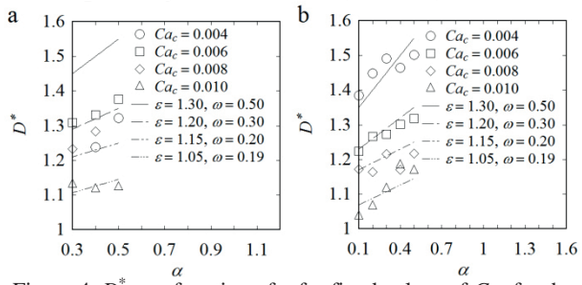

Figure 4: D^* as a function of α for fixed values of Ca_c for the cross-junction #1 (a) and #2 (b)

This observation is corroborated by Figure 5 where a non-monotonic trend of D^* as a function of Ca_c (in disagreement with the scaling laws) is demonstrated for the cross-junction #1 for all the values of α when Ca_c is reduced.

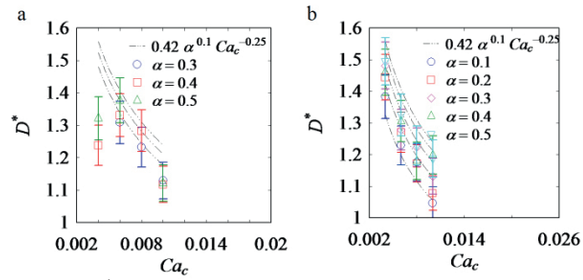

Figure 5: D^* as a function of Ca_c for the cross-junction #1 (a) and #2 (b)

It may be easily understood that it is impossible to use the same scaling law for the both cross-junctions, which confirms the fundamental role of the geometry on the droplet formation and its influence on the droplet features can be accounted for by changing the coefficients used in the scaling law. However, more experimental data are needed in order to clarify this aspect.

References

[1] C.-X. Zhao, Multiphase flow microfluidics for the production of single or multiple emulsions for drug delivery, *Advanced Drug Deliery Reviews* **65** (2013), 1420-1446.

[2] C.-X. Zhao, A.P.J. Middelberg, Two-phase microfluidic flows, *Chemical Engineering Science* **66** (2011), 1394-1411.

[3] B. Pulvirenti, B. Rostami, G. Puccetti, G.L. Morini, Determination of droplet contours in liquid-liquid flows within microchannels, *Journal of Physics: Conference Series* **655** (2015) 012028.

[4] J. Xu, S. Li, J. Tan, G. Luo, "Correlations of droplet formation in T-junction microfluidic devices: From squeezing to dripping," *Microfluidics and Nanofluidics* **5** (2008), 711-717.

5th Micro and Nano Flows Conference
Milan, Italy, 11-14 September 2016

Velocity measurements in an Omega-micromixer using Stereo-MicroPIV

F. Gökhan ERGİN [1,*]

* Corresponding author: Tel.: +45 4457 8173; Fax: +45 4457 8001; Email: gokhan.ergin@dantecdynamics.com
1 Product Manager, Dantec Dynamics, Skovlunde, DK

Keywords: MicroPIV, Stereo MicroPIV, Image calibration, omega micromixer

Mixing is often enhanced in the presence of three-dimensional (3D) flow structures such as vortices. In micro scales the initiation of such 3D microstructures is often suppressed because of the low Reynolds number inherent to micro scale flows. Passive, omega-shaped serpentine micromixers have the potential to induce three- dimensional rotating flow structures around sharp corners and thereby enhance mixing efficiency.

Experiments are performed on the flow through an omega micromixer in order to check the presence of micro scale vortices. The microchannel features a simple Omega shape with several 90-degree corners (Fig. 1). The channel height and width is 1mm, which is rather large compared to what can be achieved with current micro-manufacturing techniques. This is intentional in order to perform measurements at different channel depths and construct the time-averaged 3D flow field in the future campaigns. In the current study results from a single measurement plane (center-plane) is reported.

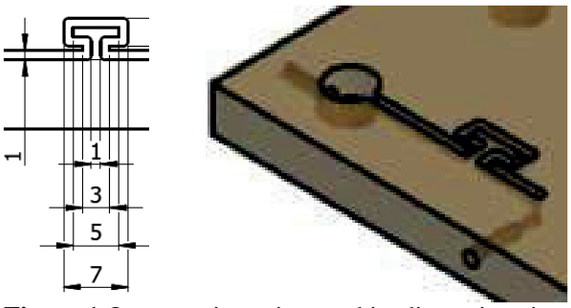

Figure 1 Omega-micromixer and its dimensions in mm

Stereoscopic MicroPIV technique [1,2] has received increased attention recently, as it can provide the necessary multiple-component velocity information in micromixers in micron scale resolution. Experiments are performed to measure all three velocity components in the middle plane of the microchannel, at the sharp corners. The experimental setup includes a Leica fluorescence stereomicroscope, 2x PlanApochromatic common main objective, a custom-built micro image calibration kit (Fig. 2), laser and LED illumination, and a checkerboard calibration plate (Fig. 3). The selected microscope and objective configuration can produce a stereoscopic half-angle of ~23 degrees in water (full angles 46 degrees), and this means that the uncertainty of the off-axis velocity component is expected as 2.4 times that of the in axis velocity components [3].

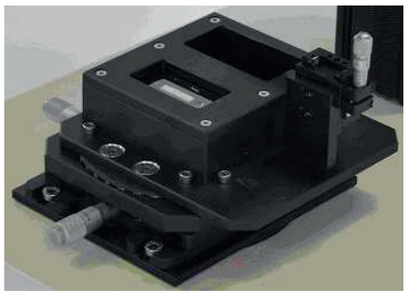

Figure 2 Stereoscopic image calibration kit

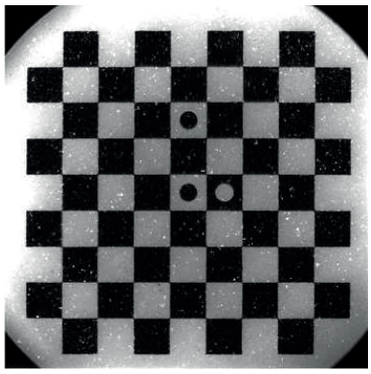

Figure 3 View of the checkerboard calibration target. Each square edge dimension is 100µm.

Stereoscopic image calibration in a microchannel is simply difficult, if not impossible. In order to achieve an accurate representation of the object space in 3D, a dedicated image calibration kit is used, which consists of a checkerboard calibration target, a calibration pool and a microstage to traverse the target in the calibration pool. The cover glass of the calibration pool and of the microchannel are the same material simulating similar optical conditions during calibration and measurements. The calibration target includes two checkerboard patterns for 1mm and 0.5mm object size. The larger pattern is used to match the channel dimension. Carefully placed circular markers allow an unambiguous definition of the planar coordinate axes. During calibration, a pulsed mono- chromatic LED device is used for illumination, which proves useful in obtaining calibration images with good contrast. The calibration is performed (i) by imaging the checkerboard pattern in known positions within the depth of field (ii) by computing mapping function for the 3D space using a 3rd order polynomial function used by Soloff et al [4] and (iii) by performing calibration refinement. The depth of field is adjusted by closing the aperture of the zoom optics of the stereomicroscope.

A depth calibration is also performed for accurate positioning of the measurement plane in the microchannel. The depth calibration, stereoscopic calibration and experiments are performed at 5x system magnification, which resulted in a Field of View of 3mm x 3mm. During depth calibration and measurements the aperture was fully open producing a 16µm field depth (important for depth calibration) and 99µm correlation depth (important for experiments). During calibration the iris diaphragm was only 2/3 open, producing a field depth of 32µm. Five calibration images were used at h=400µm, 450µm, 500µm, 550µm and 600µm. The average reprojection error for left and right cameras were found as <0.2pixels.

A high precision syringe pump with a linear step resolution of 12 nm is used to deliver the distilled water seeded with 1µm-diameter Nile-red fluorescent particles. The flow rate accuracy and reproducibility are given as ±0.35% and ±0.05% respectively. The syringe pump can drive two syringes simultaneously and the flow rate is adjustable between 1.6 pl/min to 300 ml/min using different syringe sizes. High quality airtight glass syringes are used to generate a smooth flow during the measurements. A flow rate of 15ml/min produced an expected average velocity of 250mm/s. (Re = 250)

During measurements, pulsed illumination at 532nm from a 60mJ/pulse dual-cavity Nd:YAG laser is delivered to the microscope using a liquid light guide and imaging is performed using two FlowSenseEO 4Mpix PIV cameras. Planar three component velocity measurements are computed by combining the 2D2C velocity field information from each camera, and refined image calibration information. Contrast of raw particle images was enhanced by performing a background subtraction using minimum pixel value found in the ensemble. An ensemble masking technique is also applied.

It was challenging to find intricate flow details when the complicated flow field was observed using the 2D viewer. 3D views of the results indicate that micro-vortex systems are present close to the corners of the omega-micromixer (Fig. 4). These small-scale vortices are only recognizable using a 3D viewer and from a particular angle.

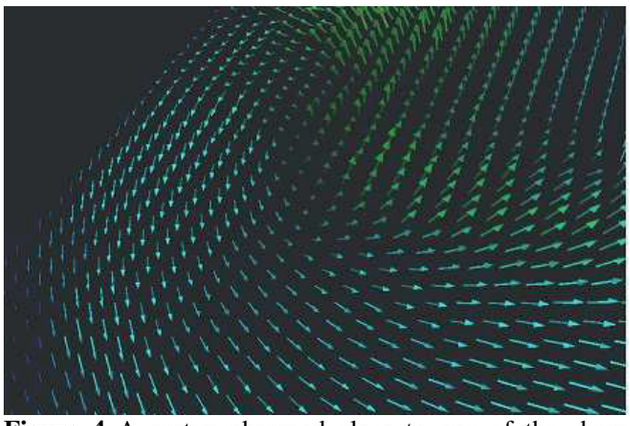

Figure 4 A vortex observed close to one of the sharp corners in the simple omega-micromixer. Colors indicate the magnitude of the velocity vector.

REFERENCES

[1] Lindken, R., Westerweel, J., & Wieneke, B. (2006). Stereoscopic micro particle image velocimetry. *Experiments in Fluids*, 41(2), 161-171.

[2] Brede, M., Witte, M., & Leder, A. (2006) Stereo-Micro PIV measurements of the three-dimensional separated flow in the wake of a backward facing step. Proc. 13th Int Symp on Applications of Laser Techniques to Fluid Mechanics.

[3] Prasad, A.K., Stereoscopic Particle Image Velocimetry. (2000) *Experiments in Fluids*, 29, 103-116.

[4] Soloff, S.M., Adrian R.J., & Liu Z.-C. (1997) Distortion compensation for generalized stereoscopic particle image velocimetry. *Meas. Sci. Tech. in Fluids*, 8, 1441-1454.

5th Micro and Nano Flows Conference
Milan, Italy, 11-14 September 2016

Accurate and Inexpensive Thermal Time-of-Flight Sensor for Measuring Refrigerant Flow in Minichannels

Allison J. MAHVI [1,*], Bachir EL FIL [1], Srinivas GARIMELLA [1,*]

* Corresponding author: Tel.: +1 404 894 7479; Fax: +1 404 894 8496; Email: sgarimella@gatech.edu
1 Sustainable Thermal Systems Laboratory, Georgia Institute of Technology, Atlanta, USA

Abstract A new thermal time-of-flight sensor is developed to measure the flow rate of subcooled refrigerant in minichannels. The flow meter measures refrigerant velocities using a small heater and two downstream thermocouples. The heater is pulsed to achieve a temperature rise in the fluid, with the time for the temperature fluctuation to reach the downstream thermocouples recorded. The design of the flow meter and its experimentally validated uncertainties are presented. Additionally, the results are compared with predictions of an analytical model.

Keywords: Thermal flow meter, Time-of-flight, Refrigerant, Minichannel

1. Introduction

In recent years, there has been considerable interest in developing sensors that can accurately measure flow rates in mini- and micro- channels for applications such as compact heat exchangers and lab on a chip (LOC) devices. Thermal flow meters are inexpensive and can be arranged in compact configurations, making them a good candidate for minichannel applications.

This paper discusses the development of a thermal time-of-flight sensor designed to measure flow rates of subcooled refrigerants in minichannels. This work focuses on flow rates commonly seen in heat exchangers with 1-mm diameter channels.

2. Novel Flow Meter Design

The flow meter proposed in this study consists of a small heater and two downstream thermocouples. The heater is a 100 Ohm film resistor connected to a variable power supply through a MOSFET that can be turned on and off using a control system developed in LabVIEW 2014. The components are mounted inside a 4.83-mm diameter channel. The flow meter is activated by supplying between 16 and 24 volts to the heater for one second. The heater locally increases the temperature of the surrounding fluid, which is then transported downstream with the flow. The flow rate is determined by measuring the time lag between the heater pulse and the peak temperature rise at the downstream thermocouples.

3. Experimental Approach

A test facility was constructed to measure refrigerant flow rates through a 1-mm diameter channel. The facility circulates R134a and measures the flow rate with the proposed thermal flow meter and a high-accuracy Coriolis flow meter. Data are collected for refrigerant mass fluxes in the minichannel between 29.1 and 583 kg m^{-2} s^{-1}, corresponding to velocities in the flow meter between 1 and 20 mm s^{-1}.

The flow meter was calibrated by collecting 50 repeated data points at velocities between 1 and 20 mm s^{-1} at intervals of 1 mm s^{-1}. The time differences between when the heater was turned on and when the maximum temperature was detected by the thermocouples were recorded and averaged. The calibration results are shown in Figure 1. The calibration data were used to calculate the fluid velocity for all subsequent data sets using logarithmic interpolation.

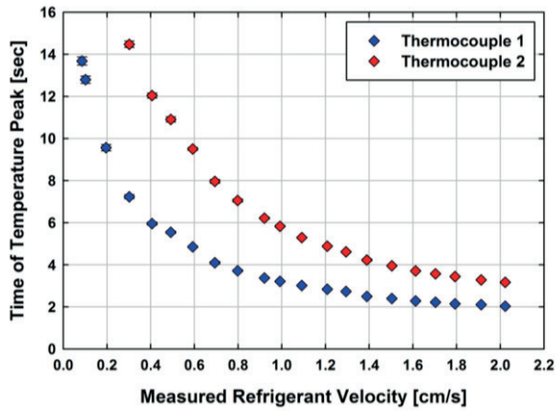

Figure 1: Results for calibration data set

4. Analytical Model

An analytical model was developed for the proposed flow sensor using the one-dimensional advection diffusion equation shown in Equation 1.

$$\frac{\partial T}{\partial t} + \overline{U}\frac{\partial T}{\partial x} = \alpha \frac{\partial^2 T}{\partial x^2} \qquad (1)$$

This partial differential equation was transformed using Equation 2 to obtain a governing equation in the form of the diffusion equation, as suggested by Mojtabi and Deville [1].

$$T(x,t) = y(x,t) \cdot \exp\left[\frac{\overline{U}}{2\alpha}x - \frac{\overline{U}^2}{4\alpha}t\right] \qquad (2)$$

The simplified governing equation was solved using the Laplace Transform method.

5. Results and Discussion

Three data sets were collected to validate the operation of the proposed flow meter. After steady state was achieved, ten consecutive measurements were taken at each velocity using the thermal flow meter. The control system recorded the time at which the peak temperature occurred for each thermocouple and averaged the results over the ten measurements. The velocity results from the three runs are shown in Figure 2. The flow meter was able to measure 93.3% of the collected data within ±5%, with an absolute average deviation (ADD) of 1.96%.

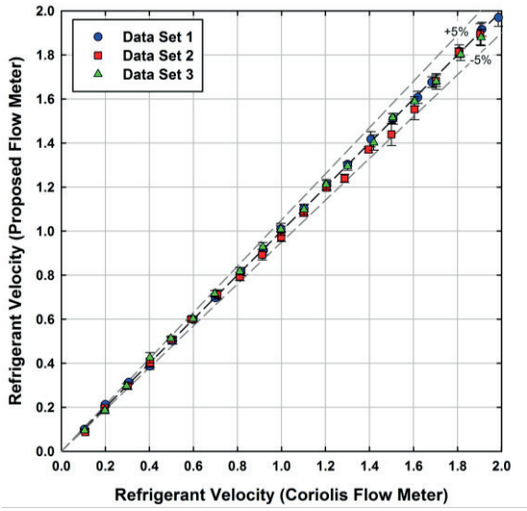

Figure 2: Comparison of the refrigerant velocity using the proposed thermal flow meter and the high-accuracy Coriolis sensor

The results from the analytical model were also compared with the calibration data set. The model was able to predict the time at which the peak temperature occurred with an ADD of 8.14%.

6. Conclusion

A new thermal time-of-flight sensor was developed to measure flow rates common in minichannel heat exchangers. The flow rate of R134a was experimentally measured using a high-accuracy Coriolis flow meter and the proposed sensor. The thermal flow meter was calibrated and additional data sets were collected to verify its operation. The sensor was able to measure 93.3% of the collected data within ±5%. Additionally, a closed-form analytical solution was developed, which can be used optimize the thermal flow meter in future design iterations. The model can predict the flow meter performance with an ADD of 8.14%.

7. References

1. Mojtabi, A., and Deville, M. O., 2015, "One-Dimensional Linear Advection-Diffusion Equation: Analytical and Finite Element Solutions," *Computers & Fluids*. **107**: pp. 189 - 195.

5th Micro and Nano Flows Conference
Milan, Italy, 11-14 September 2016

High Pressure Condensing Refrigerant Flows through Microchannels Part 1: Pressure Drop Models

Brendon L. KEINATH [1], Srinivas GARIMELLA [2,*]

* Corresponding author: Tel.: +1 404 894 7479; Fax: +1 404 894 8496; Email: sgarimella@gatech.edu
1 ExxonMobil Upstream Research Company, USA
2 Sustainable Thermal Systems Laboratory, Georgia Institute of Technology, Atlanta, USA

Abstract A multi-regime pressure drop model for condensing fluids in small diameter channels is presented. Pressure drop measurements were conducted on condensing R404A in circular channels (D = 0.508, 1.00, 3.05 mm) over the entire quality range. Saturation temperatures were varied from 30 to 60°C, and mass fluxes from 200 to 800 kg m^{-2} s^{-1}, to evaluate their effect on pressure drop. The saturation temperatures investigated here correspond to reduced pressures of $0.38 < P_r < 0.77$. The pressure drop models are developed using a microchannel flow regime map [1] and the void fraction models presented by the authors in previous work [2]. The resulting model predicts 85.5% of the data within ±25%.

Keywords: Pressure drop; Condensation; Refrigerants; Microchannels

1. Introduction

Pressure drop in two-phase flow through macrochannels has been extensively studied for several fluids, including refrigerants. Although many classical correlations are widely used for macrochannels, their predictive abilities are often poor when extrapolated for use in smaller diameter channels. In recent years, some research has focused on the effects of tube diameter on two-phase pressure drop. This work includes models that make modifications to classical correlations [3] and multi-regime models that pay special attention to the liquid-vapor interactions in each regime [4].

2. Experimental Approach

Two separate experimental facilities, one for large (D = 3.05 mm), and one for small (D = 0.508 and 1.00 mm) channels, were used to obtain pressure drop measurements for refrigerant R404A over a range of mass fluxes and saturations temperatures. The test section in both facilities was a counter-flow tube-in-tube condenser. The test section coolant flow rate is controlled to achieve a change in quality of ~0.15 across the test section.

3. Pressure Drop Model

The pressure drop model developed here is a multi-regime, semi-mechanistic model that requires prediction of the flow regime and void fraction. The Nema *et al.* [1] flow regime map is used to determine the appropriate pressure drop formulation. The majority of the data collected in this study are predicted to be in the annular or wavy flow regimes, with a few data points collected in the intermittent regime.

3.1 Annular and Wavy Regime

The annular regime was observed to have a liquid film around the entire circumference of the tube and a fast moving vapor core. An important parameter affecting pressure drop is interfacial shear, which is taken into account in this model through the interfacial friction factor concept used by Garimella *et al*. [4]. The interfacial friction factor (f_i) for the annular flow regime was found to depend on the Martinelli parameter, liquid Reynolds number, liquid Capillary number, void fraction and density ratio, as shown in Equation 1.

$$\frac{f_i}{f_l} = A \cdot X^b \cdot \mathrm{Re}_{l\alpha}^c \cdot \left(\frac{Ca_l}{1-\alpha}\right)^d \left(\frac{\rho_l}{\rho_v}\right)^e \qquad (1)$$

The coefficients in the equation depend on whether the liquid film is laminar or turbulent. For laminar liquid films, A = 0.0007, b = 0.48,

c = 0.91, d = -0.258, and e = 0.1, while for turbulent liquid films, A = 1.72, b = 0.43, c = -0.164, d = 0.07, and e = 0.5.

For the wavy flow regime, in which there is a significant stratified liquid pool, gravitation forces are dominant compared to surface wave dampening. In this case, the modified Froude number replaces the capillary number. The resulting interfacial friction factor for wavy flows is shown in Equation 2.

$$\frac{f_i}{f_l} = A \cdot X^b \cdot \mathrm{Re}_{l\alpha}^c \cdot Fr_{\mathrm{mod}}^d \left(\frac{\rho_l}{\rho_v}\right)^e \qquad (2)$$

For laminar liquid films, A = 0.0001, b = 0.477, c = 1.057, d = 0.064, and e = 0.6717, while for turbulent liquid films, A = 1.634, b = 0.49, c = -0.2, d = -0.039, and e = 0.614.

3.2 Intermittent Regime

The pressure drop in the intermittent regime is modeled by dividing the two-phase flow into two distinct regions: a film/bubble and a liquid slug region. The pressure drop is modeled for a unit cell consisting of a single vapor bubble and liquid slug. The total pressure drop within a unit cell is due to the sum of the pressure drop in the film-vapor bubble region, the liquid slug, and the transitions between the film/bubble and slug region.

In the present study, only four out of all of the data points were predicted by the Nema *et al.* [1] flow regime map to be in the intermittent regime. It was found that using a model specific to the intermittent flow regime for predicting pressure drop instead of using the annular/wavy model described above yields only a small improvement in accuracy. The marginal improvement in accuracy therefore does not warrant the added complexity of an additional, dedicated intermittent flow model.

3.3 Summary of Predictions

The pressure drop predictions using the models described above are compared with the measured values in Figure 1. The model is able to predict values and trends of the pressure drop for each tube diameter and saturation temperature well, with 85.5% of the data predicted within ±25% and an absolute average deviation of 12.7%.

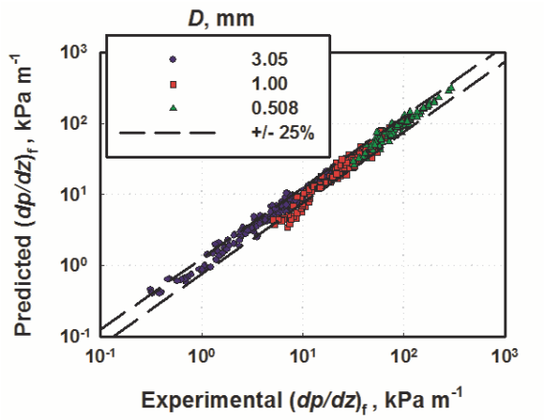

Figure 1: Frictional pressure gradient predictions categorized by tube diameter.

4. Conclusion

A comprehensive, multi-regime pressure drop model for condensing refrigerant R404A through circular tubes with diameters ranging from 0.508 to 3.048 mm over a wide range of reduced pressures ($0.34 < P_r < 0.77$) was developed. The pressure drop model was based on the previous framework of Garimella et al. [4]. The model was in good agreement with the data and predicts 85.5% of the data within ±25%.

5. References

1. Nema, G., Garimella, S., and Fronk, B. M., 2014, "Flow Regime Transitions During Condensation in Microchannels," *International Journal of Refrigeration*. **40**: pp. 227-240.
2. Keinath, B., and Garimella, S., 2016, "Measurement and Modeling of Void Fraction in High Pressure Condensing Flows through Microchannels," *Heat Transfer Engineering*. **37**(13-14).
3. Tran, T. N., Chyu, M. C., Wambsganss, M. W., and France, D. M., 2000, "Two-Phase Pressure Drop of Refrigerants During Flow Boiling in Small Channels: An Experimental Investigation and Correlation Development," *International Journal of Multiphase Flow*. **26**(11): pp. 1739-1754.
4. Garimella, S., Agarwal, A., and Killion, J. D., 2005, "Condensation Pressure Drop in Circular Microchannels," *Heat Transfer Engineering*. **26**(3): p. 28.

5th Micro and Nano Flows Conference
Milan, Italy, 11-14 September 2016

High Pressure Condensing Refrigerant Flows through Microchannels Part 2: Heat Transfer Models

Brendon L. KEINATH [1], Srinivas GARIMELLA [2,*]

* Corresponding author: Tel.: +1 404 894 7479; Fax: +1 404 894 8496; Email: sgarimella@gatech.edu
1 ExxonMobil Upstream Research Company, USA
2 Sustainable Thermal Systems Laboratory, Georgia Institute of Technology, Atlanta, USA

Abstract A multi-regime heat transfer model for condensing refrigerants in microchannels is presented. Heat transfer coefficients were measured during condensation of R404A in circular channels (D = 0.86, 1.55, 3.05 mm) over the entire quality range. The saturation temperature was varied from 30 to 60°C, and mass flux from 200 to 800 kg m^{-2} s^{-1}, to evaluate their effects on condensation heat transfer coefficient. The heat transfer model is developed using the Nema *et al.* [1] flow regime map and the void fraction model presented by the authors in previous work [2]. The resulting model predicts 93.6% of the data within ±25%. Data from condensing ammonia [3] and carbon dioxide [4] are also compared with the model predictions. The model exhibited good agreement with these data also, predicting 84.8% and 97% of the data within ±25%, respectively.

Keywords: Heat transfer coefficient, Condensation, Microchannels, Refrigerants

1. Introduction

It is well known that flow mechanisms affect heat transfer during condensation. Several studies have investigated the characteristics of condensation heat transfer in macrochannels (D_h > 3 mm), but studies for condensation in smaller diameter mini- and microchannels have lagged behind.

This paper builds upon the results from related work by the authors on flow regimes, void fractions, and pressure drop during condensation of R404A in small diameter tubes at high reduced pressures, and presents a multi-regime heat transfer model.

2. Heat Transfer Model

The condensation data from the present study were compared with the predictions of correlations from the literature. While some of the models are able to predict the measured heat transfer coefficients for some geometries and operating conditions, in general, they do not follow the observed trends. The majority of the data from this study (65%) are in the annular flow regime, while the remaining data are in the wavy flow regime [1]. Therefore, a regime-specific set of models was developed to calculate heat transfer coefficients in small diameter tubes.

2.1 Annular Flow Model

The annular flow model is based on the two-phase multiplier approach of Thome *et al.* [5]. The film thickness is assumed to be uniform around the entire tube and is deduced from the void fraction model previously developed by the authors [2]. The film Nusselt number depends on the liquid Reynolds and Prandtl numbers coupled with a two-phase multiplier, ϕ. Significant disturbances at the vapor-liquid interface influence heat transfer throughout the condensation process. These disturbances are mainly due to the difference in phase velocities. Therefore, it is assumed that the two-phase multiplier is dependent on this difference. A regression analysis was conducted to develop the Nusselt number correlation shown in Equation 1.

$$Nu = 0.0049\,\mathrm{Re}_l^{0.8} \cdot \mathrm{Pr}_l^{0.4}\left[1+\left(\frac{U_v}{U_l}\right)^{0.69}\right] \qquad (1)$$

2.2 Wavy Flow Model

Heat transfer in the wavy flow regime is typically addressed by considering two regions of the flow: the liquid film and the stratified pool. The overall Nusselt number can then be predicted as a function of the film and pool components.

The film contribution is determined analytically, assuming negligible shear at the vapor-liquid interface, which yields the film Nusselt number shown in Equation 2.

$$Nu_{film} = \left(\frac{1.93}{\theta}\right)\left(Ra\left[\frac{1}{Ja_l}+1\right]\right)^{1/4} \quad (2)$$

The contribution of the liquid pool is approximated using a two-phase multiplier applied to a single-phase turbulent correlation. Again, a regression analysis was used to determine the empirical constants, resulting in the correlation shown in Equation 3.

$$Nu_{pool} = 0.0066 \cdot \mathrm{Re}_l^{0.8}\,\mathrm{Pr}_l^{0.4} \cdot \left[1+\left(\frac{x}{1-x}\right)^{0.74}\left(\frac{\rho_l}{\rho_v}\right)^{1.51}\right] \quad (3)$$

2.3 Summary of Predictions

This heat transfer model predicts 93.6% of the data within ±25%, with an absolute average deviation of 11.4%. In addition to comparing the model predictions with the data from the present study, the applicability of the model was also evaluated for data on different fluids, as shown in Figure 1. The model was able to predict 84.8% of the heat transfer coefficients of condensing NH_3 in a circular microchannel (D = 1.435 mm) within ±25%. The present model was also adapted for rectangular geometries and was able to predict 97% of condensing CO_2 data in rectangular channels with hydraulic diameters ranging from 100 to 160 μm within ±25%.

3. Conclusions

Heat transfer coefficients for condensing R404A in small diameter channels were obtained over a wide range of saturation temperatures and mass fluxes. A comprehensive, multi-regime heat transfer model was developed for condensing fluids in microchannels. The model was able to predict 93.6% of the R404A data, 84.8% of the ammonia data from Fronk and Garimella [3], and 97% of the carbon dioxide data from Fronk and Garimella [4] within ±25%.

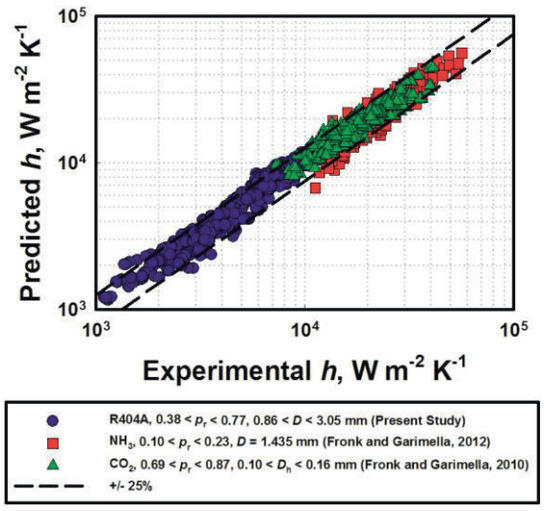

Figure 1: Heat transfer coefficient predictions for R404A, NH_3 and CO_2

4. References

1. Nema, G., Garimella, S., and Fronk, B. M., 2014, "Flow Regime Transitions During Condensation in Microchannels," *International Journal of Refrigeration*. **40**: pp. 227-240.
2. Keinath, B., and Garimella, S., 2016, "Measurement and Modeling of Void Fraction in High Pressure Condensing Flows through Microchannels," *Heat Transfer Engineering*. **37**(13-14).
3. Fronk, B. M., and Garimella, S., 2012, *Heat Transfer and Pressure Drop During Condensation of Ammonia in Microchannels*, in *3rd Micro/Nanoscale Heat & Mass Transfer International Conference*, ASME, Atlanta, GA.
4. Fronk, B. M., and Garimella, S., 2010, *Measurement of Heat Transfer and Pressure Drop During Condensation of Carbon Dioxide in Microscale Geometries*, in *International Heat Transfer Conference 14*, Washington, D.C.
5. Thome, J. R., El Hajal, J., and Cavallini, A., 2003, "Condensation in Horizontal Tubes, Part 2: New Heat Transfer Model Based on Flow Regimes," *International Journal of Heat and Mass Transfer*. **46**(18): p. 3365.

Deformability and size based capsule sorting

Doriane VESPERINI [1], Nadège MUNIER [1], Pauline MAIRE [1], Anne-Virginie SALSAC [1], Anne LE GOFF [1,*]

* Corresponding author: Tel.: +33 (0)3 44 23 79 55; Fax: +33 (0)3 44 23 79 42; Email: anne.le-goff@utc.fr
[1] BioMécanique et BioIngénierie (UMR, CNRS 7338), Université de Technologie de Compiègne - Sorbonne Universités, France

Keywords: Microfluidic, Capsule stiffness, Deformability, Separation

1 Introduction

Circulating tumor cell (CTCs) isolation from whole blood samples is a promising technique for early cancer detection. Microfluidics presents many advantages for cancer diagnosis applications, such as small reaction volumes and high sensitivity. Antibodies-based microfluidic systems have demonstrated their ability to detect circulating tumour cells [1], but remain an expensive method. Since cancer is known to modify mechanical properties of cells, abnormal stiffness could be used as a criterion to detect and isolate pathological cells due to the reorganisation of their cytoskeleton [2]. Depending on their type, blood cells have different mechanical properties that may be altered by diseases. These properties govern essential physiological behaviours such as margination [3]. Due to their mechanical properties, CTCs follow the walls of the vessels, and can crawl through the endothelium, which favors metastasis development [4]. Dupin et al. have shown that varying mechanical properties of objects in a suspension can alter their flow [5]. The experimental validation is not trivial because of the lack of homogeneous population of micro-objects with well-controlled mechanical properties. While size-based microfluidic sorting has already been studied extensively [6], the concept of sorting based on deformability has emerged more recently and is very promising. In a recent numerical study, Zhu et al. [7] proved the feasibility of sorting elastic capsules based on their deformability and membrane elasticity by flowing them past a channel-centred obstacle.
We have created and experimentally studied a microfluidic device whose geometry is inspired from the simulation of Zhu et al. [7]. This device consists of a straight rectangular microchannel including a semi-cylindrical obstacle at its end, and of a subsequent divergent chamber. We propose to determine the sorting capabilities of the device by using biomimetic models of cells, consisting of artificial microcapsules made of a thin elastic membrane around a liquid droplet. Between pillar and wall, capsules are confined and deformed by the flow. After the obstacle, the divergent shape of the chamber allows to separate streamlines. Our objective is to determine trajectories of capsules as a function of their confinement in the gap (size) and of their mechanical properties (stiffness).

2 Material and Methods

The device represented in figure 1, is fabricated in PDMS with standard soft lithography protocols [8], and sealed on a glass slide. Sealing the two surfaces together is realized activating them in a vacuum oxygen plasma chamber.
The channel leading to the obstacle is rectangular (width = 200 µm; depth = 170 µm). Upstream of this main channel a flow focusing module is added in order to align capsules with the channel centerline. The obstacle consists of a semi-cylindrical pillar (Figure 1 (b) diameter = 100 µm, depth = 170 µm – see Figure 1b). At the end of the diverging section, capsules may be oriented towards different outlets.
Microcapsules have previously been fabricated by colleagues from the Université de Reims Champagne-Ardenne following [9], by first creating an emulsion between a solution of ovalbumin and an oil phase and by cross linking the proteins at the drop interface.

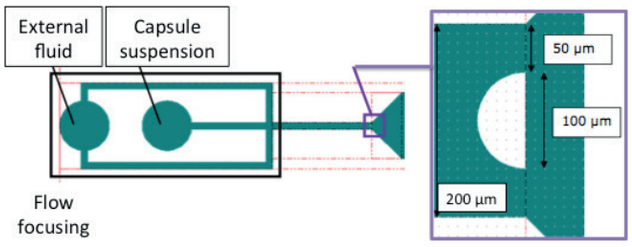

Figure 1 (a) Outline of a microfluidic device, with a flow-focusing entrance. (b) Focus on the obstacle located at the end of the straight channel. Channel width is 200 µm, its depth is 170 µm, and the obstacle is semi-cylindrical and centred in the channel.

Parameters such as gelation duration, emulsification speed and pH, can be varied in order to control the capsule size and membrane properties. Treating them with ethanol or diamide increases capsule stiffness. In order to determine their shear modulus G_s, capsules are forced to flow though a narrow cylindrical microchannel. Their deformed shape is recorded and compared with a library of numerical profiles in order to identify G_s by inverse analysis [10]. Prior to treatment, capsules have a shear modulus $G_s \sim 30$ mN/m. After ethanol treatment, capsules are so stiff that their profile does not even match with the extreme cases in the database. From this we can conclude that $G_s > 300$ mN/m
Experiments are performed at 20°C, which guarantees a constant dynamic viscosity μ of the suspending fluid (glycerol or concentrated sugar solution). The same fluid is used to suspend the capsules and to focus them on the obstacle suspension. To control the fluid pressure, the microfluidic device inlets are connected with thin capillaries to a pressure controller (MFCS Fluigent), which can reach 7 bars. A high-speed camera (Photron SA3) mounted onto an inverted microscope monitors capsule deformation.

3 Results

Capsule trajectories are determined by tracking the position of the center of mass. We find that the trajectories of the capsule mass center are linear after the obstacle; this allows to select different populations of capsules in the channel outlets.
The capsule flow and deformation are governed by the elastic capillary number $Ca = U\mu/G_s$, a non-dimensional number that compares the viscous forces exerted onto the capsules to the elastic forces in the membrane. The capsule diameter D and mean velocity U are measured from the recordings obtained prior to the obstacle.
To obtain the same Ca with less viscous fluids, the only possibility we have is to increase the flow speed, since we have no control on the capsule shear modulus G_s once they are fabricated.

3.1 Size-based capsule sorting

The flow of non-treated polydisperse capsule populations through the device has been studied. We reach low Ca conditions at low pressures (400 mbars for the capsules flow and 1000 mbars for the external flow), or when water or sugar syrup are used as

suspending/external fluids. Following capsules of different sizes in the divergent, we noticed that larger capsules are deflected further from the horizontal axis, defining a larger angle ß between their trajectory and the channel axis.

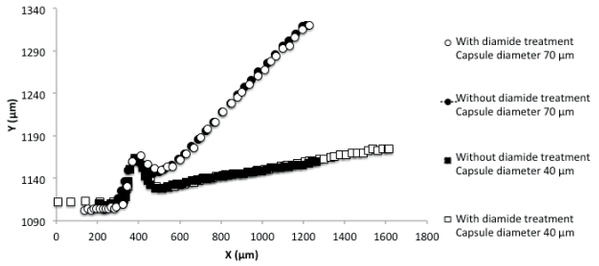

Figure 2 Trajectories of soft capsules of diameters 40 µm (squares) and 70 µm (bullets) at low flow rate in sugar syrup. Full symbols: no treatment. Hollow symbols: diamide treatment.

Figure 2 represents experimental trajectories of capsules of two different sizes, with or without diamide treatment. In this regime, we find that, regardless of their rigidity, small capsules remain close to the axis while larger ones drift away at larger angles in the divergent. Large capsules have a center of mass more distant from the obstacle than small capsules. In brief, the further the streamline is from the pillar, the larger the deflection. Thus, under these flow conditions; capsule size has a strong impact on the trajectory, while no effect of capsule stiffening is observed.
These results indicate that, in this regime, the device is capable of sorting objects according to their size whatever their mechanical properties**,** as a standard pinched flow fractionation device [11].

3.2 Deformability-based capsule sorting

At high pressures (large *Ca*), size is no longer the only parameter influencing separation: mechanical properties, which have a negligible effect at low capillary number, now also impact trajectories (Figure 3). In order to achieve deformability based sorting, the viscous shear stress acting on the capsules is increased compared to the previous situation. In figure 3, we show that in the presence of high viscous forces, trajectories can be even more affected by changes in deformability than by size. Stiffer capsules keep following the same trajectory as in the previous case but softer capsules do not. The softer the capsule, the closer the pathline is from the horizontal axis.

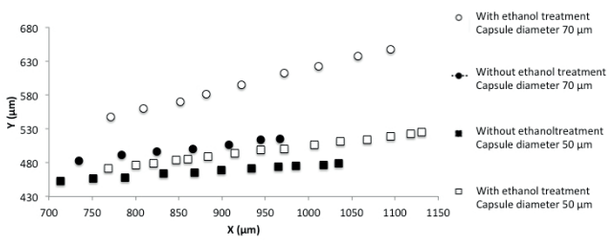

Figure 3 Focus on the linear part of the trajectory, for capsules of diameter 50 µm (squares) and 70 µm (bullets), at high flow rate in glycerol. Full symbols: no treatment. Hollow symbols: ethanol treatment.

In general, the study shows that the larger and stiffer the capsules are, the more deviated the trajectories are from the horizontal axis. This phenomenon initiates the possibility to sort capsules populations that are heterogeneous in size and mechanical properties and to collect them in different outlets after sorting.
As size remains the most important sorting parameter, we propose a two-step sorting technique, using first size-based separation at low shear rates, and then deformability-based sorting for the capsules in the desired size range.

3.3 Off-centred influence on capsule trajectory

The centering of capsules has a strong influence on their trajectories, whether the capillary number is high or low. That is the reason why a flow focusing is important to pinch the internal capsule flow. By tuning the pressure of the capsule suspension flow for a fixed pressure of the external fluid (Figure 1a), we can control the width of the core capsule flow. When the internal pressure is much lower than the external one, a precise centering of capsule flow on the obstacle is possible, which enables deformability-based sorting. But it is at the cost of a low throughput. Increasing the internal pressure at constant external pressure allows for a larger capsule throughput, but off-centred soft capsules may end up being sorted as stiff ones. We have found that an internal-to-external pressure ratio of 0.4 offered in our case a good balance between accuracy and capsule throughput, but this ratio must be tuned depending on the size and deformability distribution of the capsule suspension, and the desired level of precision for each sorted population.

4 Conclusions

We have demonstrated that capsule sorting based on deformability and size can be achieved experimentally by using the same device at different flow rates. The present device allows separating and collecting capsules in different outlets after sorting. It is based on the particle ability to deform around an obstacle and to follow different trajectories depending on its size and stiffness. In the case of a polydisperse suspension where both size and mechanical properties vary, the system can be used in two steps. A deformability-based sorting at high flow rate can follow a previous size-based separation at low flow rate, in the desired size range. This is the proof that we have developed a versatile multipurpose sorting microsystem based on a really simple design.

Acknowledgment

The authors would thank F. Edward-Levy and co-workers (ICMR laboratory, Université de Reims Champagne-Ardenne) for the fabrication and donation of microcapsules.

References

[1] S. Nagrath, M. Toner et al. *Nature* (2007)
[2] S. Suresh, *Acta Materialia* (2007)
[3] P.A. Aarts, S.A. van der Broek, G.W. Prins, G.D. Kuiken, J.J. Sixma, R.M. Heethaar, *American Heart Association* (1988)
[4] J. Condeelis, J.E. Segall, *Nature* (2003)
[5] M.M. Dupin, I. Halliday, C.M. Care, L. Alboul, L.L. Munn, *Physical Review* E 75, 066707 (2007)
[6] C.Wyatt Shields IV, C.D. Reyes, G.P. Lopez, *The Royal Society of Chemistry* (2015)
[7] L. Zhu, C.Rorai, D. Mitra, L. Brand. *Soft Matter* 10 (2014): 7705-7711.
[8] G.M. Whitesides, E. Ostuni, S. Takayama, X. Jiang, D.E. Ingber, *Annual Review Biomedical Engineering* (2001)
[9] M.-C. Andry, F. Edwards-Levy, M.-C. Levy. *Int. J. Pharm.* 128 (1996): 197-202.
[10] T.-X. Chu, A.-V. Salsac, E. Leclerc, D. Barthès-Biesel, H. Wurtz, F. Edwards-Lévy. J. *Coll. Interf. Sci.* 355 (2011): 81-88.
[11] M. Yamada, M. Nakashima, M. Seki, *Analytical Chemistry* (2004)

Analyzing a single deformable cell in an inclined centrifuge microscope: a numerical study

Arash Alizad Banaei [1,*], Jean Christophe Loiseau [1], Luca Brandt [1]
Suguru Miyauchi [2], Toshiyuki Hayase [2]

* Corresponding author: Tel.: +46 8 790 71 62; Fax: +46 8 796 98 50; Email: arash2@mech.kth.se
1 Linnè FLOW Centre and SeRC, KTH Mechanics, Stockholm, Sweden
2 Institute of Fluid Science, Tohoku University, Japan

Abstract The motion of a cell (consisting of a droplet enclosed within a thin elastic membrane) in an inclined centrifuge microscope has been studied numerically using the immersed boundary method. The cell is set into motion due to centrifugal force and eventually reaches a steady translational velocity. The larger the inclination of the microscope with respect to the horizontal axis, the smaller is this translational velocity. Comparisons with previous 2D numerical results and experimental works show a qualitative agreement.

Keywords: Centrifugal Microscope, Deformable Cell, Neo Hookean membrane

1. Introduction

Endothelial Glycocalyx layer (EGL) is a layer of fiber-like structures on the membrane of endothelial cells. Interactions between this glycocalyx and red blood cells (RBC) typically occur in blood vessels having a diameter smaller than the characteristic diameter of RBC. Inclined centrifuge microscope can be used to elucidate these intricate interactions. The key features of such observations is the equilibrium state reached by the cell when subject to the centrifugal force. It is characterized by a given deformation of the cell and a steady translational velocity of its center of mass. This steady state depends on the cell's characteristics, on the plate above which it moves, as well as on the angular speed and inclination of the plate. Oshibe et al. [1] have studied numerically the frictional characteristics of concave and biconcave rigid particles subjected to an inclined centrifugal force. Qualitative agreements with the experimental work of Kandori *et al.* [2] have been obtained.

The goal of the present research is to extend the work of Oshibe et al. [1] to the motion of a single deformable cell and to provide qualitative and quantitative comparisons with previous numerical and experimental works.

2. Governing equations and numerical methods

Figure 1 depicts a schematic of the inclined centrifuge microscope considered. A cell, initially spherical, is set into motion due to the application of a centrifugal force. The dynamics of the fluid are governed by the Navier-Stokes equation:

$$\left(\frac{\partial U}{\partial t} + U.\nabla U\right) = -\nabla P + \frac{1}{Re}\nabla^2 U + \left(\frac{Ta}{Re^2}\right)^{\frac{1}{4}} I(x)n + \frac{1}{We}f_e \quad (1)$$

where Re, Ta and We are the Reynolds, Taylor and Weber numbers, respectively. $I(x)$ is an indicator function, while n is the support vector of the centrifugal force and f_e is the elastic force exerted by the membrane onto the fluid. The fluid-structure interaction is treated using the immersed boundary method [3].

The computational domain is a 10×5×5 box (based on the initial diameter of the cell). No slip boundary conditions are used for walls, while periodicity is imposed in the other two directions. Spatial discretization of the NS equations relies on second order central

differences, while the membrane's equation is discretized using spherical harmonics. The pressure equation is solved using a FFT-based Poisson solver. Finally, temporal integration is performed using a semi-implicit scheme.

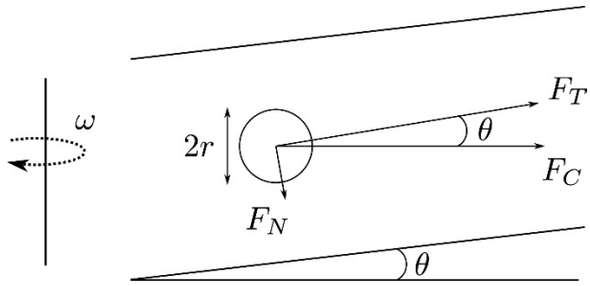

Figure 1. Schematic of the geometry considered.

3. Results

Simulations are carried out for three different angles: θ=20°, 30° and 40°. Reynolds, Taylor and Weber numbers are set to 1.6×10^{-3}, 1.16×10^{6} and 4.8×10^{-4} respectively. Figure 2 depicts the position and deformation of the cell at various instants of time for θ=20°. It can be observed that it slowly approaches the wall. The time evolution of its streamwise velocity is depicted on figure 3. After some transient, this tangential velocity eventually tends towards a steady value. This value then depends on the inclination angle of the plate. As the inclination increases, the tangential velocity of the cell decreases. This results from the force balance: increasing the inclination of the plate causes an increase of the normal component of the centrifugal force, so does the friction force exerted by the wall onto the cell. On the other hand, this decreases the tangential component of the centrifugal force exerted onto the cell, thus further decelerating it.

The motion of a single cell in an inclined centrifuge microscope has been studied numerically. The translational velocity of the cell as well as its final shape is dependent on the angle of the plate. Preliminary comparisons with experimental results (not shown) yield to qualitative agreements for inclination angles θ<45°. However, in order to correctly resolve the very thin layer of fluid in-between the cell and the wall as the inclination angle become larger (θ>45°), a local mesh refinement approach is currently being under development.

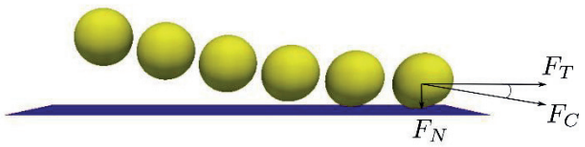

Figure 2. Position and deformation of the cell at different instants of time (θ=20°).

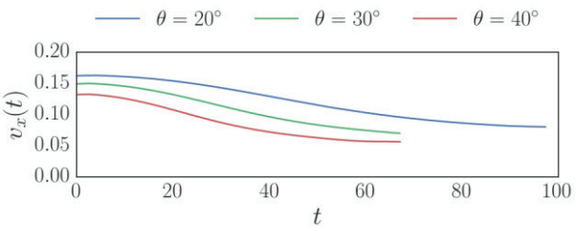

Figure 3. Time history of the cell's streamwise position and velocity.

References

[1] Oshibe, T. Hayase, T. Funamoto, K and Shirai, A., 2014. Numerical Analysis for Elucidation of Nonlinear Frictional Characteristics of a Deformed Erythrocyte Moving on a Plate in Medium Subject to Inclined Centrifugal Force, J. Biomech Eng-T ASME, DOI: 10.1115/1.4028723.

[2] Kandori, T. Hayase, T. et.al, 2008. Frictional Characteristics of Erythrocytes on Coated Glass Plates Subject to Inclined Centrifugal Forces, J. Biomech Eng-T ASME, DOI: 10.1115/1.2948420.

[3] Peskin, C. S., 2002. The immersed boundary method, Acta Numerica, DOI: 101017/ S09624929020000

5th Micro and Nano Flows Conference
Milan, Italy, 11-14 September 2016

A Novel De-noising Scheme For Effective Extraction of Ensemble Solution From Nano/Microfluid Simulations

Małgorzata J. ZIMOŃ[1,2*], Robert PROSSER [1], David R. EMERSON[2]

* Corresponding author: Email: malgorzata.zimon@stfc.ac.uk
1 School of Mechanical, Aerospace and Civil Engineering, The University of Manchester, M13 9PL, UK
2 Scientific Computing Department, STFC Daresbury Laboratory, WA4 4AD, UK

Abstract Filtering of particle-based simulation data can lead to reduced computational costs and enable more efficient information transfer in multi-scale modelling. In this presentation we will introduce a new processing approach capable of reducing correlated numerical noise. We show that the method referred to as ldWienerChop can capture the structures of nano-flow systems. In addition, a combination of this algorithm with proper orthogonal decomposition for time-dependent measurements is discussed.

Keywords: Nano Flow, Noise Reduction, Wavelet Transform, Singular Value Decomposition

1. Introduction

Particle-based methods are indispensable to resolve accurately the dynamics at the atomistic scale and are widely used to model nano/microfluid flows (e.g. confined in channels such as nanotubes). In addition, information obtained from molecular simulations forms the basis of new emerging hybrid multi-scale modeling strategies [1] for physical and biological applications. A critical aspect of particle schemes is their substantial noise, which corrupts the instantaneous measurements of the observables. The uncertainty in the results arises from disturbances caused e.g. by additional forcing terms such as thermostats. Extracting the genuine information from the molecular data is rendered challenging due to the often correlated nature of the corrupting fluctuations. Traditional statistical averaging over a very large number of samples can improve the quality of results but only at significant computational expense. Multi-scale modelling strategies to couple molecular simulations to continuum dynamics require smooth gradients and precise particle distributions, but long averaging periods can result in bottlenecks in the intra-scale communication. Obtaining accurate approximations of the ensemble-averaged quantities is particularly problematic for unsteady simulations. Therefore, there is a growing need for robust de-noising approaches in molecular simulations, which provide approximations to the ensemble solution, but without the concomitant computational expense. A novel algorithm has been proposed that combines the strengths of wavelet transforms with singular value decomposition. It is shown that the method is a useful alternative to statistical averaging and outperforms techniques such as wavelet thresholding [2] alone in removing low-frequency noise. A successful application to stationary and unsteady fluid simulations performed with molecular dynamics and dissipative particle dynamics is presented.

2. Methododology

Wiener filters have been used in a range of applications, such as signal detection and noise reduction, as they offer an optimal estimation analysis of time series. However, the main practical problem in their implementation is that a desired signal needs to be known *a priori*. Ghael [3] proposed a straightforward estimate of the signal and noise by using wavelet transforms. Wavelet-based empirical Wiener filtering (WienerChop) performs two wavelet transforms (*WT*) in order to estimate

the filter parameters, a noise variance with a signal prior, and perform de-noising. To improve the performance of the method in cases when the data is corrupted with correlated noise, we propose to implement a level-dependent wavelet-based Wiener filter, ldWienerChop. In the wavelet domain, a noisy signal $f(t) = f_t(t) + f_n(t)$ is defined as a set of coefficients $f^w = f_t^w + f_n^w$, consisting of an underlying true structure, $f_t^w = WT(f_t(t))$, and noisy details, $f_n^w = WT(f_n(t))$. In the new approach, an approximation of the signal's coefficients $\tilde{f}_t^{w1}$ is obtained in the wavelet space by level-dependent thresholding [5]. After filtering, the data is reconstructed, and a second transform (WT_2) is performed to estimate noise levels at each resolution, σ_n. Afterwards, the signal prior in WT_2 and the noise variances are used to construct the wavelet-based Wiener filter given as

$$W_{Chop} = \frac{f_t^{w21}}{f_t^{w21} + \sigma_n^2} . \quad (1)$$

In Eq. (1), the superscript $w21$ indicates that WT_2 was applied to the signal estimate obtained from WT_1, $f_t^{w21} = WT_2(\tilde{f}_t(t))$. The WT_2 of the original signal, $f^{w2} = WT_2(f(t))$, allows to filter the coefficients. In addition, to improve information extraction from data-sets, we propose to apply the ldWienerChop filter on dominant singular vectors obtained from proper orthogonal decomposition (POD) [6].

3. Results

Study on synthetically generated data showed that the new method outperforms decimated wavelet thresholding and POD in filtering data corrupted with low frequency noise. Results on molecular dynamics measurements also confirmed benefits of applying the new approach. We considered an oscillating flow in a converging-diverging channel described in [6]. The channel was divided into $N = 200$ sub-domains in order to extract smooth mass-flow rates with POD or statistical averaging. However, with our new approach only $N = 1$ measurement was enough to obtain a satisfactory result (see Fig. 1), recovering higher signal-to-noise ratio, SNR = 30.21 dB than the other methods. During the presentation, an application of coupled POD and ldWienerChop filter will be shown on time and space-varying measurements. Further improvements including processing of scaling function coefficients will be discussed.

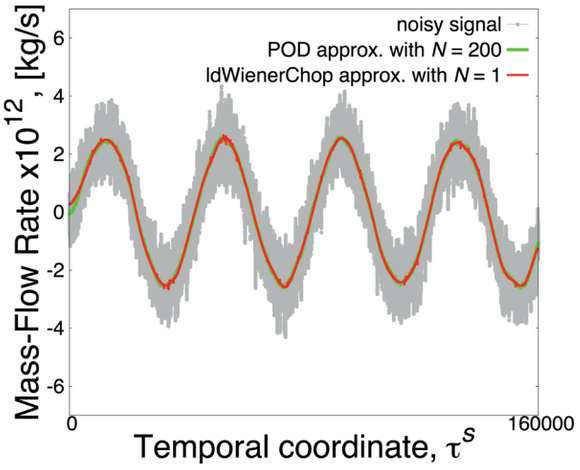

Figure 1: Result of applying POD and ldWienerChop to the mass-flow rate measurements with SNR = 10.33 dB from the MD simulation of a periodically-pulsating channel flow; level-dependent wavelet thresholding alone obtained SNR = 26.83 dB.

References

[1] K. M. Mohamed, A. A. Mohamad, A review of the development of hybrid atomistic–continuum methods for dense fluids, Microfluidics and Nanofluidics 8 (3) (2010) 283–302.

[2] D. L. Donoho and J. M. Johnstone. Ideal spatial adaptation by wavelet shrinkage. *Biometrika*, 81(3):425–455, 1994.

[3] S. P. Ghael, A. M. Sayeed, R. G. Baraniuk, Improved wavelet denoising via empirical Wiener filtering, in: Optical Science, Engineering and Instrumentation'97, International Society for Optics and Photonics, 389–399, 1997.

[4] I. M. Johnstone, B. W. Silverman, Wavelet threshold estimators for data with correlated noise, Journal of the Royal Statistical Society: series B (statistical methodology) 59 (2) (1997) 319–351.

[5] L. Grinberg, Proper orthogonal decomposition of atomistic flow simulations, Journal of Computational Physics 231 (16) (2012) 5542–5556.

[6] M. K. Borg, D. A. Lockerby, J. M. Reese, A hybrid molecular–continuum method for unsteady compressible multiscale flows, Journal of Fluid Mechanics 768 (2015) 388–414.

5th Micro and Nano Flows Conference
Milan, Italy, 11-14 September 2016

Investigation of elasticity in micromixing of low viscosity emulsions

Valentina PREZIOSI [1], Giovanna TOMAIUOLO [1], Sergio CASERTA [1,2*] , Stefano GUIDO [1,2]

* Corresponding author: Tel.: ++39 0817682261; Fax: ++39 0812391800; Email: sergio.caserta@unina.it
[1] Dipartimento di ingegneria chimica, dei materiali e della produzione industriale, Napoli, Italy
[2] Consorzio Interuniversitario Nazionale per la Scienza e Tecnologia dei Materiali, INSTM, Napoli, Italy

Abstract This study is focused on the development of low viscosity emulsions and on the investigation of their elasticity on emulsion formation. Non-Newtonian continuous phases made of two different molecular weight Polyacrylamide in water plus glycerol solutions were used. While, as Newtonian continuous phase, a water plus glycerol solution showing the same viscosity as the non-Newtonian one was prepared and as dispersed phase silicon oil was used. Visualization of these emulsions flowing through a micromixer was useful in order to extract quantitative information of their behavior, such as the velocity profile and droplets' size distribution. The formation of a droplet-rich core and of a droplet-devoid wall region was observed, and significantly enhanced by matrix elasticity. These effects lead to the accumulation of larger droplets around the center of the channel, while smaller droplets are pushed toward the periphery. The velocity profiles for the Boger continuous phase were flat in the droplet-rich core, thus suggesting that the confined emulsions behave as a Bingham fluid. Then the formation of vortex upstream of a divergent-convergent configuration has been shown as the wall migration effect, which drives droplets away from the walls and toward the center of the microcapillary investigated.

Keywords: Mixing, non-Newtonian, Boger fluids, Microfluidics

1. Introduction

Liquid-liquid mixing is a common industrial practice, widely used in a variety of application, ranging from polymer synthesis and processing to biotechnology. Despite the extensive literature available on the topic, liquid-liquid mixing is still one of the most difficult and least understood mixing problems, especially when one of the two phases shows a non-Newtonian behavior; in fact the case of a Newtonian drops, in terms of deformation, relaxation and breakup in a Newtonian fluid has been extensively studied, both numerically and experimentally as in the pioneering works of Taylor [1], Grace [2] and Rallison [3] but most of the fluids used in the industries show non-Newtonian behavior. It is also well known that the viscoelasticity of one of the phases can prevent the break-up of a single drop in a controlled flow as studied by Guido [4] and Sibillo [5], but very little is known about the mixing of non-diluted emulsion, when one or both the liquid phases show non-Newtonian behavior. A comprehensive characterization of liquid-liquid mixing in these systems is still missing and their application is based more on intuition and vendors claims than on scientific data.

Moreover since non-Newtonian fluids can have elastic behavior and at the same time exhibit nonlinear viscous effects like shear-thinning of the viscosity, it is particularly difficult to study viscoelastic flows in isolation from other effects. However, there's a class of viscoelastic fluids, known as Boger fluids[6], in which the viscosity is nearly constant with the shear rate. These fluids are particularly important because they enable elastic effects to be probed separately from shear thinning effects; comparing the viscosity behavior of a Boger fluid flow with that of a Newtonian fluid allows one to assess the influence of elasticity.

In the present work the setup of a microsystem for the formation of emulsions made of silicon droplets as dispersed phase and as continuous phase a Newtonian and non-Newtonian matrix

has been performed. Then the effect of elasticity on liquid-liquid mixing comparing fluid dynamic behavior of Newtonian droplets in a Newtonian and non-Newtonian matrix has been analyzed.

2. Results

2.1 Materials and methods. In order to investigate the effect of matrix elasticity, three different model systems were used in the experiments. As a continuous Newtonian reference fluid, a system made of water and glycerin (79.74% wt). For simplicity this fluid will be referred in the paper as NF. In order to increase the elasticity and then to study the viscoelastic effect on mixing efficiency a polymer is added to the water plus glycerin solution, by forming low viscosity fluids that were used as continuous phase and indicated as LE (low elasticity) and HE (high elasticity). The dispersed phase is a blend of 0.02 Pa·s and 0.01 Pa·s Newtonian silicon oil in order to maintain the same viscosity of the suspending fluid of 0.05 Pa·s.

Fig. 1 shows a scheme of the experimental set-up.

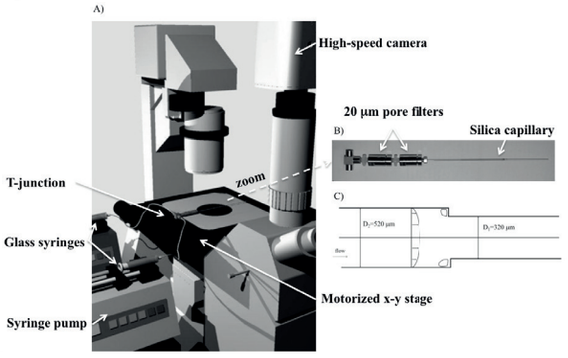

Figure 1: A) Drawing of the experimental set-up; B) Picture of the mixing set-up; C) Schematic diagram of the contraction geometry with two silica capillaries, D_1=320 µm and D_2=520 µm.**The reagents were injected into the microsystem with two glass syringes by placed on syringe pumps. The syringes are connected by plastic tubes to a stainless steel T-junction of 1 mm, where a premix of the phases takes place, and then the device is connected to two stainless steel frits in 20 µm porosity, that is where the efficient mixing occurs.**

In all the experiments presented, a wall depletion layer from the wall, with significant differences among the fluids, was observed as observed in Fig. 2. The visual trend is that the more elastic is the matrix, the wider is the depletion layer.

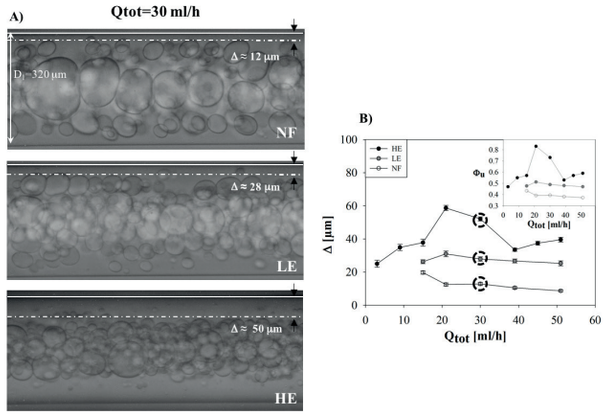

Figure 2: A) Wall depletion layer of NF (upper), LE (middle) and HE (lower) as continuous phases, at 30 ml/h.. B) Wall depletion layer as a function of total flow rate for the three matrix fluids.

3. Conclusions

In this work, we present results from the direct visualization of confined flow of low viscosity biphasic liquids. The influence of matrix elasticity on fluid dynamic behavior of low viscosity emulsion was performed. Moreover, in all the experiments, a droplet-free layer can be observed close to the wall, while smaller droplets are marginated in an intermediate region. The effect of elasticity is to enhance the size of the droplet-free region. This result was qualitatively discussed in terms of the flow-induced forces acting on the droplets. The results could be relevant for the design of mixers and emulsification systems based on confined flow.

References

[1] G.I. Taylor, Proc Roy Soc A, 146 (1934) 501-522.
[2] H.P. Grace, Chem Eng Comm, 14 (1982) 52.
[3] J. Rallison, Annual Review of Fluid Mechanics, 16 (1984) 45-66.
[4] S. Guido, M. Simeone, F. Greco, Journal of Non-Newtonian Fluid Mechanics, 114 (2003) 65-82.
[5] V. Sibillo, M. Simeone, S. Guido, Rheologica acta, 43 (2004) 449-456.
[6] D.F. James, Boger Fluids, in: Annual Review of Fluid Mechanics, Annual Reviews, Palo Alto, 2009, pp. 129-142.

Determining Transport Properties by Molecular Dynamics

Angelo DAMONE [1], Pietro POESIO [1,*]

* Corresponding author: Tel. : +390303715646 ; Email: pietro.poesio@unibs.it
1: Department of Industrial and Mechanical Engineering, University of Brescia, IT

Abstract : The knowledge of the transport properties of liquids is important to design new processes and devices in the oil, chemical, and biotechnological industries. The use of Molecular Dynamics in the calculation of transport properties has increased in last years, and in this job are shown numerical methods for estimation of transport properties applied to real liquids, particularly we focus the attention on the study of thermal conductivity of complex mixtures such as water and triethylamine which have potential applications in heat exchange inside electronic circuits.

Keywords : Molecular Dynamics, Numerical Simulation, Liquid Systems, Transport Properties

1. Introduction

The knowledge of the transport properties of liquids is important to design new processes and devices in the oil, chemical, and biotechnological industries. The aim of this work is to estimate these properties using Molecular Dynamics simulations. Our calculation starts from atomistic liquids, which are modeled by Lennard-Jones potential interactions, and extends to real liquids such as water, carbon tetrachloride, and complex mixtures of liquids, as water and triethylamine. The values of transport properties are obtained by Green-Kubo method, which uses the auto-correlation function of the stress tensor to estimate the shear viscosity and the average of heat flux auto-correlation function to compute the thermal conductivity.

2. Simulation Details

All simulations were performed with a cubic simulation box using the minimum number of molecules [1-3] and periodic boundary conditions were applied. For each liquid appropriate models were used to describe the inter-molecular and intra-molecular interactions, i.e. for the water molecules we have employed the TIP4P/2005 model [4]; for the other liquids we employed the optimized potential for liquid simulation (OPLS-AA) for all atom interactions [5] including Lennard-Jones, charge, bond, angle, and dihedral interactions. The simulations are performed by imposing the NVT ensemble for Lennard-Jones liquids, water and carbon tetrachloride, while for the water-triethylamine mixture we used the NPT ensemble to compute the phase diagram. A Nosè-Hoover thermostat is used to bring the system at required temperature.

3. Results

We performed MD simulations of atomistic liquid using the Lennard-Jones parameters of Argon: σ = 3.4 Å, ε/k = 120 K where k is the Boltzmann constant. The numerical value of shear viscosity and thermal conductivity provided by this simulation are 0.219 mPa•s and 0.127 W/(m•K), respectively. A NVT ensemble is used with temperature of 94.4 K and density of 1.374 g/cm^3. The experimental values of shear viscosity and thermal conductivity for this system are 0.197 mPa•s and 0.115 W/(m•K), respectively [6]. Calculations of shear viscosity for two real liquids, one polar liquid, such as water, and one non-polar liquid, such as carbon tetrachloride (CCl_4) are also carried out.

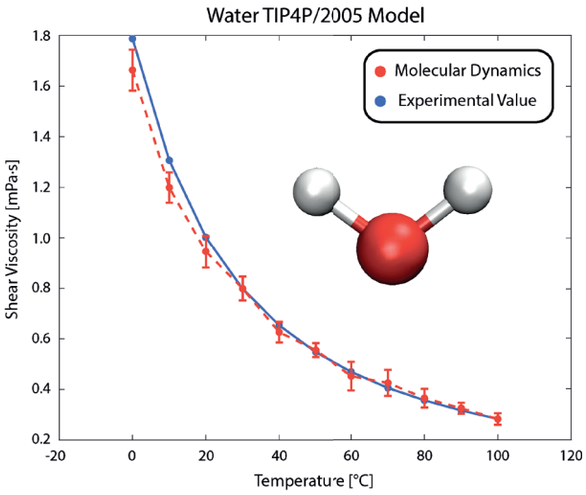

Figure 1. Comparison between MD simulation and experimental values [7] for water shear viscosity as function of temperature

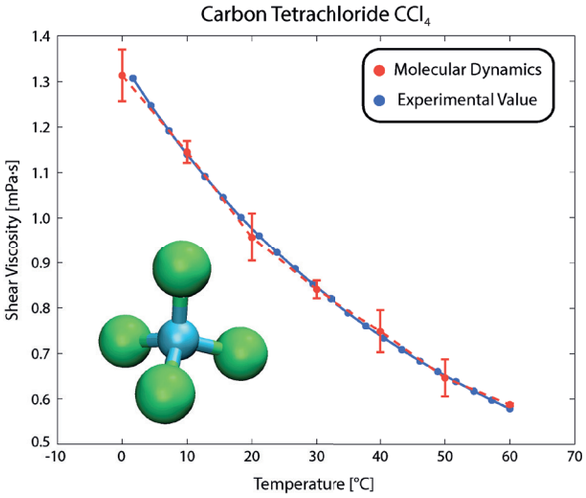

Figure 2. Comparison between MD simulation and experimental values [7] for CCl_4 shear viscosity as function of temperature

Studies about shear viscosity were carried out at different temperatures for both liquids and, as shown in Fig. (1) and Fig. (2), a good agreement with experimental values of shear viscosity taken from literature [7] is observed.
An important study include the calculation of transport properties for complex liquids such as mixture of water and triethylamine ($C_6H_{15}N$), which have potential applications in heat exchange inside electronic circuits. We perform simulations at different temperature with different chemical composition of water and triethylamine in mole fraction. Following results concerning the thermal conductivity are shown Fig. (3) .

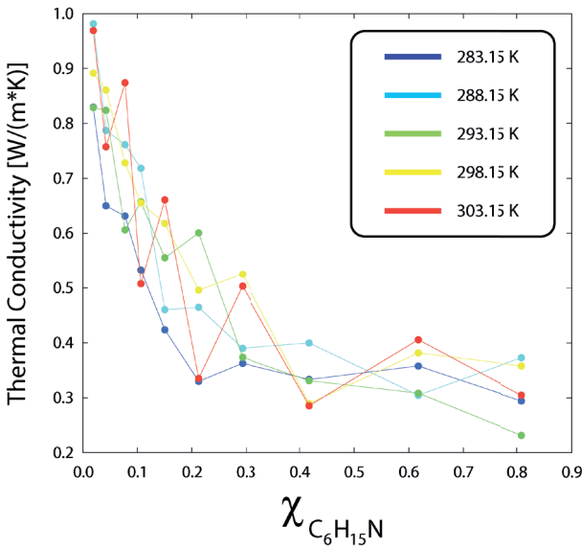

Figure 3. Thermal Conductivity of water-triethylamine mixtures at different temperatures and mole fractions

In this work, it is proved how the Molecular Dynamics can be used to calculate the transport properties of complex real liquids and allow to study the behavior of these liquids under different condition of temperature and chemical composition.

4. References

[1] Chen, T. ; Smit, B. ; Bell, A. T. ; J. Chem. Phys. **2009**, 131, 246101.
[2] Hess, B. ; J. Chem. Phys. **2002**, 116, 209-217.
[3] Yeh, I. C. ; Hummer, G. ; J. Phys. Chem. B **2004**, 108, 15873-15879.
[4] Abascal, J. L. F. ; Vega, C. ; J. Chem. Phys. **2005**, 123, 34505.
[5] Jorgensen W.L., Maxwell D.S., Tirado-Rives J. ; J. Am. Chem. Soc. **1996**, 118 (45): 11225-11236.
[6] S.H. Lee ; D.K. Park ; D.B. Kang ; Bull. Korean Chem. Soc. **2003**, Vol. 24, No. 2.
[7] Lide, D. R. ; CRC Handbook of Chemistry and Physics, 70th ed. **1990** CRC Press: Boca Raton, FL.

ID 222

ABSTRACT

Atomically controlled electrochemical reaction for cost-effective and high-throughput fabrication of nanopores in 2D materials

Prof. A. Radenovic, EPFL – Dr. G. Turri, Namiki Precision Jewels LTD

Solid state nanopore based bio-sensing is emerging as a rapid single molecule detection and manipulation technique [1, 2]. Conceptually, a single nanometer size aperture located on a membrane can detect electrophoretically driven biomolecules translocation in a high throughput manner, revealing localized information of the analyte. However, the formation of single nanopores relies heavily on expensive instrumentation, i.e., Transmission Electron Microscope (TEM) and well trained TEM users, which renders it still confined to laboratory use. Atomically thin nanopore membranes, graphene [4] and molybdenum disulphide (MoS_2) [5, 6], have drawn much attention due to their unprecedented single nucleotide resolution, which holds promise as a candidate for so called 3rd generation DNA sequencers. Dielectric breakdown has been demonstrated as a facile method to make individual nanopores on silicon nitride membranes (10-30 nm thick) without the need for TEM [7, 8]. ***This can dramatically reduce the cost of device fabrication and scale up the production of devices.*** However, if the same methodology of nanopore fabrication is applied to the membranes made in 2D materials, we observe that the mechanism that governs the pore formation is not dielectric breakdown but **electrochemical reaction** that occurs once the transmembrane potential exceeds oxidation voltage. Inspired by the dielectric breakdown nanopore fabrication in thick nitride membranes, we are developing with our technology partner Namiki Precision, a feedback controlled ***electrochemical reaction (ECR) method of making individual nanopores and nanopore arrays in 2D materials, which can be readily accessible for commercialization.***

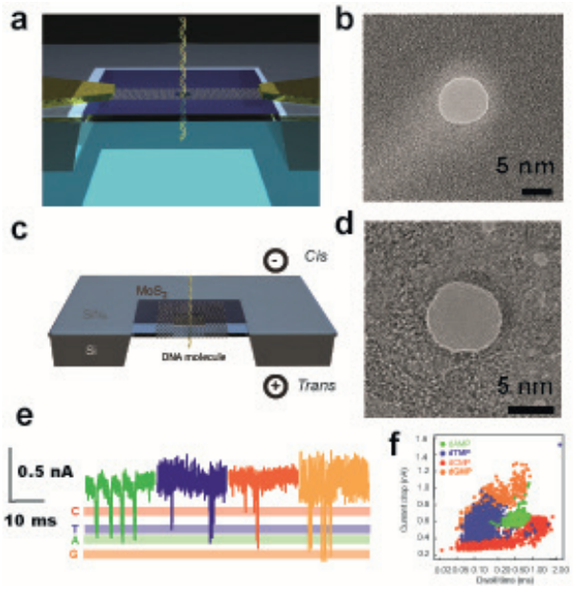

Figure 1. Highlight's of our previous and current research nanopores in 2D materials. **(a)** Graphene nanoribbon supported on SiN membranes for simultaneously recorded ionic current and electrical current. **(b)** A TEM image of nanopore drilled by focused electron beam. **(c)** Freestanding MoS_2 nanopore membrane. **(d)** Atomically resolved TEM image of MoS_2 nanopore. Taken from [3] **(e)** Current trace for dAMP (green), dCMP (red), dTMP (blue), and dGMP (orange). **(f)** Scatter plots of nucleotide translocation events, showing distinguished current drops and dwell times. Taken from [5].

References

1. Branton, D., et al., *The potential and challenges of nanopore sequencing.* Nature Biotechnology, 2008. **26**(10): p. 1146-1153.
2. Dekker, C., *Solid-state nanopores.* Nature Nanotechnology, 2007. **2**(4): p. 209-215.
3. Liu, K., et al., *Atomically thin molybdenum disulfide nanopores with high sensitivity for DNA translocation.* ACS nano, 2014. **8**(3): p. 2504-11.
4. Garaj, S., et al., *Graphene as a subnanometre trans-electrode membrane.* Nature, 2010. **467**(7312): p. 190-U73.
5. Feng, J., et al., *Identification of single nucleotides in MoS2 nanopores.* Nat Nano, 2015. **advance online publication**.
6. Liu, K., et al., *Atomically Thin Molybdenum Disulfide Nanopores with High Sensitivity for DNA Trans location.* Acs Nano, 2014. **8**(3): p. 2504-2511.
7. Kwok, H., K. Briggs, and V. Tabard-Cossa, *Nanopore Fabrication by Controlled Dielectric Breakdown.* Plos One, 2014. **9**(3).
8. Feng, J., et al., *Electrochemical reaction in single layer MoS2: nanopores opened atom by atom.* Nano letters, 2015.

5th Micro and Nano Flows Conference
Milan, Italy, 11-14 September 2016

Active Micro-Mixer for Biomedical Applications

Simone FERRARI [1], Gabriele DUBINI [1], Luca CORTELEZZI [2,3,*]

* Corresponding author: Tel.: ++1 514 3986299; Fax: ++1 514 3987365; Email: luca.cortelezzi@mcgill.ca
1 Dipartimento di Chimica, Materiali ed Ingegneria Chimica "G. Natta". Politecnico di Milano, Italy
2 Department of Mechanical Engineering, McGill University, Montreal, Canada
3 Dipartimento di Scienze e Tecnologie Aerospaziali, Politecnico di Milano, Italy

Keywords: Micro-mixer, mixing, microfluidic, CFD.

Introduction

Rapid mixing of two or more fluids is critical in many integrated microfluidic systems for biomedical, chemical and biological applications. Micro-mixers are generally classified in two main categories: passive or active [1]. In general, passive micro-mixers rely entirely on molecular diffusion to induce mixing is long thin channels or network of channels, whose geometry is specifically designed to increase the interface separating the fluids to be mixed. Active micro-mixers, in general, substantially enhance mixing by maximizing stretching and folding of the mixture through the action of appropriate actuators that intelligently modify the time evolution of the hydrodynamic field [2, 3].

Modeling and Simulations

The aim of the present work is to design an active micro-mixer suitable for a wide range of biomedical/bioengineering applications and potentially assimilable in a Lab-on-Chip [4]. Figure 1 shows the geometry of the micro-mixer. The two fluids to be mixed are injected through three inlet micro-channels of width 100μm. In the central channel is injected the medication (e.g. dopamine, strontium ranelate, etc.) at constant flow rate, while in the lateral channels is injected, at a time-dependent flow rate [5, 6, 7], the carrier solution (e.g. distilled water). The constant flow from the main channel merges with the time-dependent flows from the optimally oriented lateral channels at the entrance of a cylindrical mixing chamber (diameter 1000μm), where their interaction creates a sequence of lamellae of different concentration [2]. The circular geometry of the mixing chamber favors the expansion of the flow and the stretching of the lamellae. A cylindrical obstacle of optimal size (diameter 400μm) is positioned in the mixing chamber to split the incoming flow and enhance the folding of the lamellae. Furthermore, this obstacle reduces the volume of the mixing chamber and, therefore, reduces the time needed to reach the regime operating conditions. Finally, the mixture exits through a microchannel of width 100μm.

We model the two fluids to be mixed as incompressible, viscous and having physical properties similar to water, with the only difference being the value of the passive scalar (e.g. concentration of a tracer, temperature) they transport. The time evolution of the hydrodynamic field is governed by continuity and Navier-Stokes equations, while the time evolution of the concentration field is governed by the advection-diffusion equation. We assume the gradients of concentration field to be small enough so that the problem is one-way coupled, i.e. the time--evolution of the hydrodynamic field governs the evolution of the scalar field, while the evolution of the scalar field does not affect the evolution of the hydrodynamic field.

We make the problem dimensionless by defining as characteristic length the width (200μm) of the entrance to the mixing chamber, as characteristic time the inverse of the frequency of forcing and as characteristic velocity the fluid velocity in the main channel. Therefore, our results are parametrized in terms of Reynolds (***Re***), Strouhal (***St***) and Peclèt (***Pe***) numbers.

We discretize and solve the governing equations using a Finite Volume Method. The computational domain is discretized with an unstructured (free) mesh generated using the solid modeler ICEM (Ansys, Canonsburg, PA, USA). The numerical simulations of the flow were performed using the commercial FVM software Ansys Fluent 14 (Ansys, Canonsburg, PA, USA).

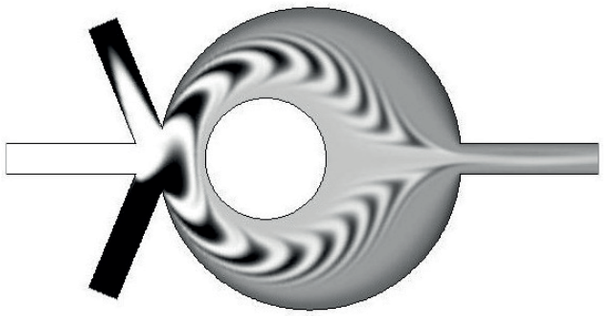

Figure 1 Scalar concentration field at dimensionless time 119.6 when **Re**=2, **St**=0.8 and **Pe**=10^4.

Results

We quantify the mixing efficiency, *M*, of our device by using a weighted form of the variance of the concentration field [5] measured at a cross-section of the exit micro-channel near the outlet and averaged over a period of forcing. We characterize the mixing performance of our device in terms of Reynolds, Strouhal and Peclèt numbers [8].

Firstly, we studied how the mixing performance depends on the Reynolds number at dimensionless time 119.6, when the micro-mixer operates at regime conditions. For the range $0.2 \leq \boldsymbol{Re} \leq 20$ ($\boldsymbol{St}$=0.8 and $\boldsymbol{Pe}$=10^4), we observe two peaks, one at $\boldsymbol{Re}$=2 (M=91.4%) and the other at $\boldsymbol{Re}$=15 (M=91.3%), separated by a region of lower performance ($\boldsymbol{Re}$=5, M=73%), see figure 2 (top). The error bars indicate the the maximum and minimum values of the scalar variance over a period of forcing. The averaged results are linearly interpolated with a dashed line to improve the readability of the plot. The low mixing performance at $\boldsymbol{Re}$=5 is due to the transition between two different regimes: a purely laminar

regime at ***Re***=2 and a regime involving recirculation vortices at ***Re***=15. Quite surprising is the size of the error bars, which one would expect to decrease as mixing efficiency increases. In reality the trend is opposite, the value of the concentration oscillates substantially less, around ±0.5%, when the mixing performance is lower, around 75%-80%, than when it is higher, around 90%, where the amplitude of the oscillations are about ±3%. This can be explained by recognizing that the flow within the mixing chamber can be subdivided in three distinct, but equally important, flows: the region where the lamellae are convected, stretched and folded and the two regions along the outer wall of the mixing chamber and along the wall of the cylindrical obstacle, see figure 1. These three flows contribute almost equally to the flow in the outer channel. The poor performance at ***Re***=5 is mainly due to the fact that the concentrations of the two wall-flows are different. Ironically, at ***Re***=5 the lamellae are thinner and more equally spaced than in the other cases (***Re***=2 and ***Re***=15), inducing therefore a lower level of oscillations in the concentration of the outflowing mixture.

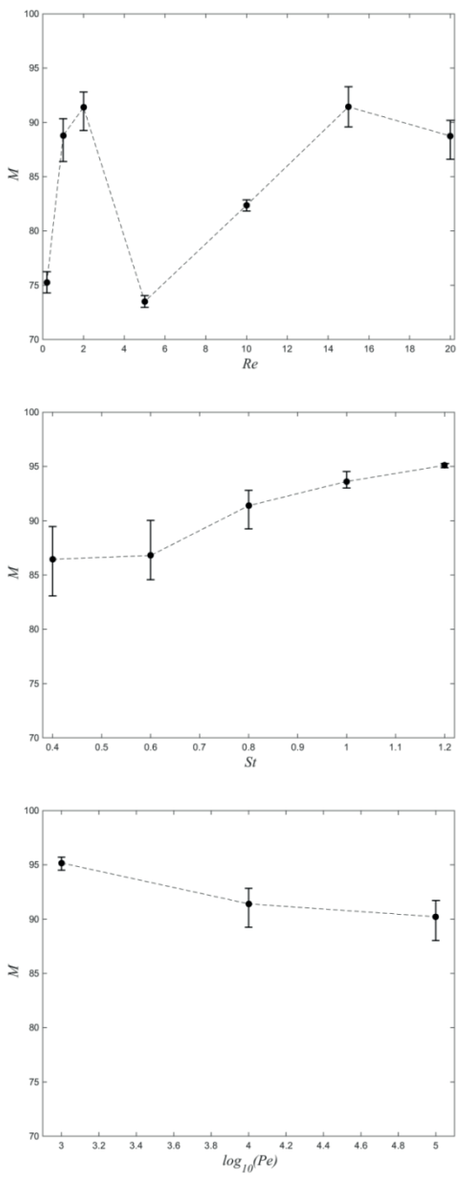

Figure 2 Mixing efficiency versus Reynolds (top), Strouhal (center), and Peclèt (bottom) numbers at dimensionless time 119.6.

Secondly, we studied how the mixing performance depends on the Strouhal number. For the range $0.4 \leq \boldsymbol{St} \leq 1.2$ (***Re***=2 and ***Pe***=10^4), at dimensionless time 119.6, the mixing efficiency increases almost linearly from M=85% at ***St***=0.8 to M=95% at ***St***=1.2 with a weak inflection at ***St***=0.8 where M=92%, see figure 2 (center). The trend of the mixing efficiency versus Strouhal number clearly indicates that the mixing efficiency increases as the frequency of forcing increases. The error bars show that the fluctuation in concentration at the outlet decrease substantially as the Strouhal number increases. Therefore, one would be tempted to increase the forcing frequency as much as possible in order to improve the mixing performance and the reduce fluctuations of the concentration field. However, this come at high price because the power input required will also grow considerably. A more sophisticated approach is to optimize mixing at lower frequency, where the power input required is low [2, 3].

Finally, we studied how the mixing performance depends on the Peclèt number. For the case $10^3 \leq \mathbf{Pe} \leq 10^5$ (**Re**=2 and **St**=0.8), at dimensionless time 119.6, the mixing efficiency decreases weakly nonlinearly from M=95% at **Pe**=10^3 to M=90% at **Pe**=10^5, where the performance is still robust, see figure 2 (bottom). Obviously, the mixing performance of our device improves and the fluctuations of concentration decrease, both monotonically, as the Peclèt number decreases.

Conclusions

We presented a novel, compact, active micro-mixer able to process volumes of fluid in the range $10^{-9} \div 10^{-6}$ liters. The micro-mixer has a simple geometry to facilitate its manufacturing and assimilation in LoC and other platforms, a sort of one-size-fits-all. The micro-mixer produces rapid mixing due to its active actuation system that produces lamellae of alternate concentrations and its geometry that favors the folding and stretching of the lamellae. The micro-mixer has a mixing efficiency above 90% for a wide range Strouhal and Peclèt numbers. Its performance it is not uniform in terms of Reynolds number due to the transition between two different mixing regimes at ***Re***=2 and 15. However, the performance can be easily made uniform by operating the mixer at higher Strouhal numbers where is needed.

References

[1] Nguyen N-T, Wu Z, Micromixers – a review, Journal of Micromechanics and Microengineering, 15, R1-R16 (2005)

[2] Gubanov O, Cortelezzi L, Towards the design of an optimal mixer, J. Fluid Mech., 651, 27--53 (2010)

[3] Gubanov O, Cortelezzi L, On the cost efficiency of mixing optimization, J. Fluid Mech., 692, 112--136 (2011)

[4] Mark D, Haeberle S, Roth G, von Stetten F, Zengerle R, Microfluidic lab-on-a-chip platforms: requirements, characteristics and applications, Chemical Society Reviews, 39, 1153-1182 (2010)

[5] Glasgow I, Aubry N, Enhancement of microfluidic mixing using time pulsing, Lab on a Chip – Miniaturisation for Chemistry and Biology, 3, 114-120 (2003)

[6] Müller SD, Mezić I, Walther JH, Koumoutsakos P, Transverse momentum micromixer optimization with evolution strategies, Computers and Fluids, 33, 521-531 (2004)

[7] Sun C-L, Sie J-Y, Active mixing in diverging microchannels, Microfluidics and Nanofluidics, 8, 485-495 (2010)

[8] Glasgow I, Lieber S, Aubry N, Parameters influencing pulsed flow mixing in microchannels, Analytical Chemistry, 76, 4825-4832 (2004)

5th Micro and Nano Flows Conference
Milan, Italy, 11-14 September 2016

ID 224

Transient Flow Boiling Local Heat Transfer in a Multi-Microchannel Evaporator under a Heat Flux Disturbance

Houxue HUANG*, Nicolas LAMAISON, John R. THOME

* Corresponding author: Tel.: +41 (0)2169 36853; Fax: +44 (0)2169 35981; Email: houxue.huang@epfl.ch
Laboratory of Heat and Mass Transfer, École Polytechnique Fédérale de Lausanne (EPFL), Switzerland

Abstract Multi-microchannel evaporators are often used to cool down electronic devices subjected to continuous heat load variations. However, so far, rare studies has addressed the transient flow boiling local heat transfer data occurring in such applications. The present paper introduces and compares two different data reduction methods for transient flow boiling data in a multi-microchannel evaporator. The transient test of heat disturbance from 20 to 30 W cm^{-2} was conducted in a multi-microchannel evaporator using R236fa as working fluid. The test section was 1 cm^2 in size and had 67 channels, each having a cross-sectional area of 100x100 μm^2. The evaporator's backside temperature was obtained with a fine-resolution infrared camera at a frequency of 60Hz. The first method consisted of solving a 3D inverse heat conduction problem by using a TDMA method with base temperature and heat flux known, combined with a Newton-Raphson iteration on the footprint temperature. Once the solution for the inverse problem was converged at each time step, a local energy balance was used to attain the footprint heat flux, which was further utilized by the fin equations for obtaining the local wall heat transfer coefficient. The second method considered only 2D conduction with the LSODE (Livermore Solver for Ordinary Differential Equations) semi-implicit solver. This method used a numerical dynamic PI controller on the heat transfer coefficient boundary so that the latter was corrected at each time step based on the difference between the calculated and experimentally measured base temperature. It is shown that both methods yielded an initial sharp increase of the heat transfer coefficient followed by a smooth decrease to the steady-state value after the heat flux disturbance was applied. The first method was more accurate since exact solution was obtained at each time step. The second one reduced the computational time significantly but led to an approximated solution with, for example, a lower magnitude sharp increase of the heat transfer coefficient obtained.

Keywords: Flow boiling local heat transfer, multi-microchannel evaporator, heat flux disturbance, dynamic data processing

1. Introduction

Multi-microchannel evaporators with two-phase flow boiling provide promising potential for cooling high heat flux devices, such as high performance CPUs, GPUs and advanced military avionics. The multi-microchannel evaporators usually experience heat load disturbances in time during operation due to the variation in the heat generation from the cooled devices. This requires the two-phase cooling system to response swiftly while avoiding a big variation in the evaporators' base temperature, which will inevitably cause the undesired thermal stress or fatigue for the micro-evaporators, thus severely threatening the operation safety of the two-phase flow cooling system. The micro-evaporators' base temperature variation is depending on the flow boiling local heat transfer coefficients, therefore, the study of which is of practical importance for implementing the two-phase cooling system with multi-microchannel evaporators. However, the studies dealing with such a topic in the literature are few.

ID 226

5th Micro and Nano Flows Conference
Milan, Italy, 11-14 September 2016

Advancements in electrical-based techniques on chip for single-cell level analytics

Carlotta GUIDUCCI [1,*]

* Corresponding author: Tel.: ++41 (0)21 37813; Fax: ++41 (0)21 31105; Email: carlotta.guiducci@epfl.ch
1 Institute of Bioengineering and Institute of Electrical Engineering, Ecole polytechnique fédérale de Lausanne, CH

Keywords: Lab-on-chip, biosensors, microelectrodes, impedance flow-cytometry

Integrating biosensors and signal processing circuits will enable a new generation of biochips, providing addressing, measurement and elaboration functions on the same system. Potential applications for such multi-functional systems range from genetic arrays to personalized medicine-based tests, to cells manipulation and sensing. The main advantages of integrated electronics in biochip arrays have been shown in some recent successful applications. For instance, a fully-electronic system is now available for DNA sequencing [1], which enables fast read-out of large number sites and fluorescence-free protocols. In a different domain, researchers have demonstrated long-term observation of neural networks on chips integrating stimulation and elaboration circuitry and analog to digital conversion, providing fast sampling of low-amplitude signals from cells [2]. Moreover, in the framework of DNA analytics, we contributed to the development of the first fully-electronic integrated system for the label-free detection of DNA hybridization [3].

Major challenges in the development of biosensors on chip arise from reliability in a liquid environment. We contributed to the field by showing the superior performance of insulating material for surface passivation such as SU-8 and parylene and introducing new processing solutions for the enhanced stability of microelectrode features for electrical and electrochemical sensing on chip [4].

Integrated microelectrode technologies play a crucial role in lab-on-chip development since electric fields can be effectively used to sense, manipulate and move molecules and cells at the microscale. Nevertheless, high-throughput implementations of already assessed techniques are constrained by the design limitations entailed by planar electrodes in microfluidic configurations. These could be overcome by vertical electrodes, either integrated in micro-channel sidewalls or as free-standing structures. We proposed a new approach to achieve arrays of singularly-addressable vertical elements generating highly-confined electric fields for sensing or actuation [5 6]. Our approach is based on the conformal coating of passive cores with metal layers, defining electrodes in microfluidic channels with high aspect-ratio and vertical uniformity. This method achieves high electrodes density, granting high conductivity of both connections and metal sidewalls with no need for electroplating. The resulting vertical electrodes span the full height of the microfluidics, generating homogeneous fields along the z-axis of the channel.

Leveraging the technological advancement achieved, we are developing a label-free high-throughput on-chip systems for single-cell level discrimination and observation. In particular, we target the analysis of cells in flow, in a configuration where a large number of suspended cells flow through a chip and each cell is sampled by means of distributed non invasive sensors integrated in microchannels. Sensors have to be multiple and to be arranged in a wide channel to avoid clogging and cell damage by shear stress.

Our sensors can successfully discriminate cell types such as activated T cells, with the aim of identifying rare activated cells in human samples and isolate them for successive expansion. This system is presently based on two layers of metal and can be integrated with TSVs and IC for larger parallelism using the technology described in [7].

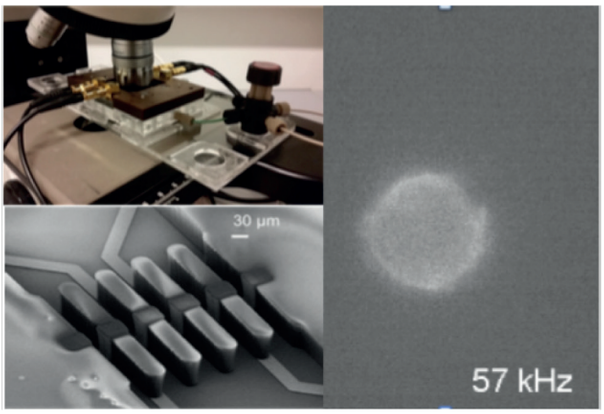

Figure 1. (Top left) Observation of single cells on the lab-on-chip system by high-resolution microscopy; (Right) Neuroblastoma cell observed on the chip during electrorotation experiments; (Bottom left): 3D microelectrodes integrated with microfluidics and SU-8 passive structures for impedance flow-cytometry.

References

1. Rothberg, J. M. *et al.* An integrated semiconductor device enabling non-optical genome sequencing. *Nature* **475,** 348–352 (2011).
2. Müller, J. *et al.* High-resolution CMOS MEA platform to study neurons at subcellular, cellular, and network levels. *Lab Chip* **15,** 2767–2780 (2015).
3. Stagni, C. *et al.* CMOS DNA Sensor Array With Integrated A/D Conversion Based on Label-Free Capacitance Measurement. *IEEE Journal of Solid-State Circuits* **41,** 2956–2964 (2006).
4. Temiz, Y., Ferretti, A., Leblebici, Y. & Guiducci, C. A comparative study on fabrication techniques for on-chip microelectrodes. *Lab Chip* **12,** 4920–4928 (2012).
5. Kilchenmann, S. C., Rollo, E., Bianchi, E. & Guiducci, C. Metal-coated silicon micropillars for freestanding 3D-electrode arrays in microchannels. *Sensors and Actuators, B: Chemical* **185,** 713–719 (2013).
6. Kilchenmann, S. C., Rollo, E., Maoddi, P. & Guiducci, C. Metal-Coated SU-8 Structures for High-Density 3-D Microelectrode Arrays. *J. Microelectromech. Syst.* 1–7 doi:10.1109/JMEMS.2016.2539000
7. Temiz, Y., Guiducci, C. & Leblebici, Y. Post-CMOS Processing and 3-D Integration Based on Dry-Film Lithography. *IEEE Trans. Compon., Packag. Manufact. Technol.* **3,** 1458–1466 (2013).

A Novel Chip Design with Side-channel Pre-alignment for Particle Sorting

S. XIONG[1], Y. Y. CHEN[1, 2], L. Lei[1], L. K. Chin[1], H.Y. WANG[2], M. HILL[3] and A. Q. LIU[1*]

*Corresponding author: Email: eaqliu@ntu.edu.sg
1 School of Electrical and Electronic Engineering, Nanyang Technological University, Singapore
2 Department of Engineering and System Science, National Tsing-Hua University, Hsinchu, Taiwan
3 Engineering Sciences, University of Southampton, Southampton, UK

Abstract This paper demonstrates particle sorting by using a novel chip, in which particles are accoustically pre-aligned with the side-channels. Tunable pressure nodal position is achieved by changing the liquid filling in the side channels. The relationship among the pressure nodal positions, particle separation distance and liquid properties are discussed. The sorting of 5-μm and 7-μm particles are experimentally demonstrated with a 2-time increase of the separation distance. It shows a high potential for different microbial sorting in drinking water monitoring and cancer cell diagnosis.

Keywords: Acoustofluidic, Particle sorting, Per-alignment, Liquid tunable

Acoustofluidic chip based particle manipulation has been widely applied in microbial and cell separation, which is critical in various fields of research, including drinking water quality analysis and disease diagnosis [1, 2]. In this paper, two side-channels are used to acoustically pre-align the particles, which offer a promising approaching to enhance the sorting efficiency and resolution.

Figure 1 shows the schematic illustration of the chip, which consists of one main microchannel and two side-channels. Two piezoelectric transducers (PZT) are attached below the chip, which generate a standing wave with two pressure nodes in the pre-alignment region, and a standing wave with single pressure node in the separation region, respectively. When the particles pass through the region with the side-channels, they are pre-aligned and pushed close to the side walls. Thereafter, the particles are deflected and sorted in the separation region according to their intrinsic acoustic properties.

Figure 2 shows the cross-sectional views of the pre-alignment and separation regions with different designs. The pre-alignment with side-channels (Fig. 2b, c) has longer nodal distance compared with the normal one (Fig. 2a), resulting in a longer separation distance between different particles (Fig. 2e). In addition, the position of the pressure node is controllable by changing the liquid in the side-channels (Fig. 2b, c). The acoustic pressure and the position of the nodes are simulated as shown in Fig. 3.

Figure 4 shows the silicon/glass microfluidic chip. The pre-alignment region is actuated at a frequency of 2.16 MHz and the separation region is actuated at 1.853 MHz. When different liquids are injected into the side channels, the positions of pressure nodes are tuned accordingly. Figure 5 shows that the nodal distance is increased from 250 μm to 320 μm when the injected liquid is changed from glycerin to acetone. On the contrary, the nodal distance for normal pre-alignment without side-channels is fixed at 187.5 μm.

Figure 6 shows the separation of 5-μm and 7-μm polystyrene particles after pre-alignment. The maximum separation distance between the two sizes of particles is increased by two-folds when using the pre-alignment with side-channels instead of the normal one.

In conclusion, a novel chip for particle sorting is designed, fabricated and tested. The tunable position of pressure nodes and increased separation distance indicate a robust sorting performance in the future detection applications.

References

[1] T. Laurell, F. Petersson and A. Nilsson, Chem. Soc. Rev., 2007, 36, 492-506.

[2] M. Antfolk, C. Antfolk,H. Lilja, T. Laurella and P. Augustsson, Lab Chip, 2015, 15, 2102–2109.

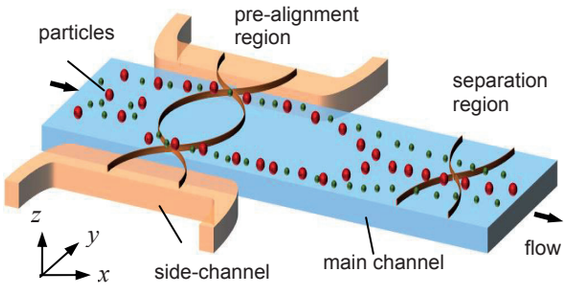

Figure 1: Schematic illumination of the acoustofluidic chip for particle sorting

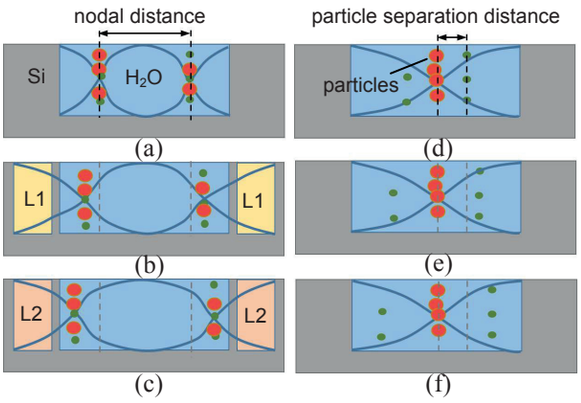

Figure 2: Different designs of (a)-(c) pre-alignment regions and (d)-(f) the corresponding separation regions

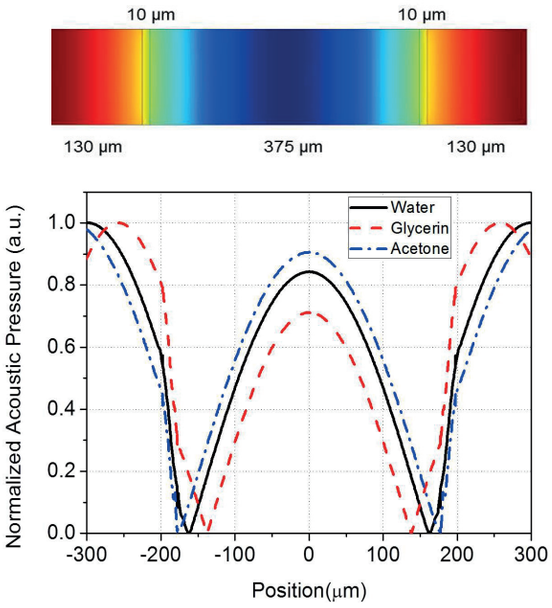

Figure 3: Simulation of the acoustic pressure amplitude with different liquids in the side-channels

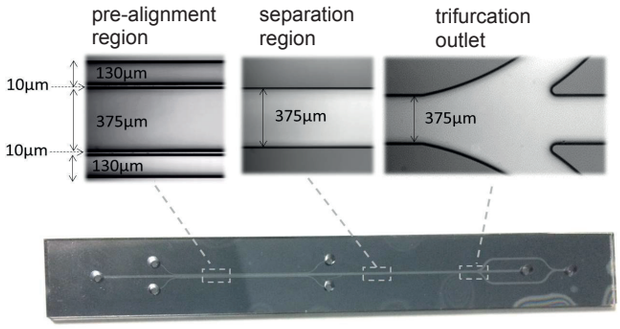

Figure 4: Photographs of the fabricated chip

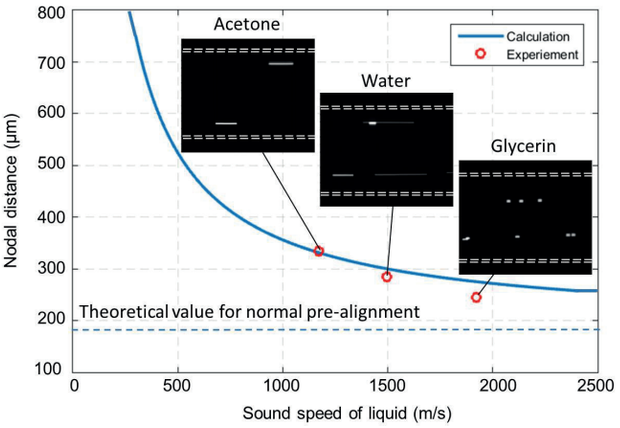

Figure 5: Relation between the nodal distance and the sound speed of liquid in the side channels

(a)

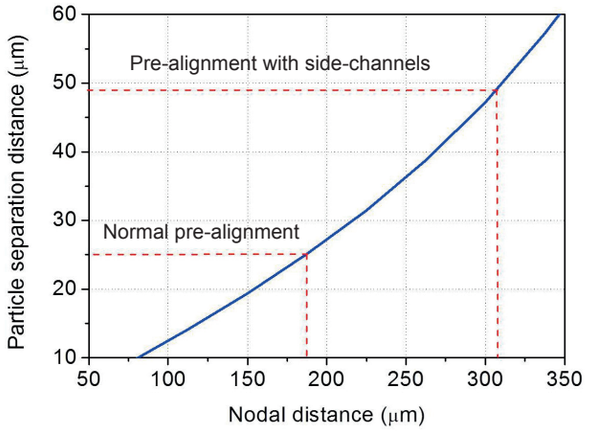

(b)

Figure 6: (a) Separation of 5-μm and 7-μm particles after pre-alignment. (b) Relation between the particle separation distance and the nodal distance

5th Micro and Nano Flows Conference
Milan, Italy, 11-14 September 2016

High-throughput Pre-concentration for Bacteria using Acoustofluidic Chip

Y. Y. CHEN[1, 2], S. XIONG[1], L. Lei[1], L. K. Chin[1], H.Y. WANG[2], M. HILL[3] and A. Q. LIU[1]*

*Corresponding author: Email: eaqliu@ntu.edu.sg
1 School of Electrical and Electronic Engineering, Nanyang Technological University, Singapore
2 Department of Engineering and System Science, National Tsing-Hua University, Hsinchu, Taiwan
3 Engineering Sciences, University of Southampton, Southampton, UK

Abstract This paper demonstrates the pre-concentration of bacteria in a cost-effective acoustofluidic chip. The chip assembled by a glass coverslip and a glass slide offers a high throughput and high recovery performance. More than 80% of 0.75-μm latex microparticles and *Bacillus subtilis* can be focused within the acting distance of 25-μm from the reflector. It shows a high potential to develop a disposable device for drinking water monitoring and food inspection.

Keywords: Acoustofluidics, Thin-reflector resonator, Pre-concentration

Recently, a microfluidic system associated with acoustophoresis (named as acoustofluidics) has received a lot of interest and been widely applied in particle manipulation and cell separation, which is a critical technique in many areas such as biomedical research and drinking water monitoring [1]. In this study, a cost-effective acoustofluidic chip was demonstrated for concentrating *Bacillus subtilis*. It is one of the indicator organisms as a surrogate in drinking water monitoring.

Figure 1 shows the acoustofluidic chip design, which consists of the following layers: a transducer (PZT), a carrier layer, a fluid layer and a reflector layer. Since the thickness of each layer is relatively thin as compared to the wavelength, the node of the quarter standing wave is at the reflector layer. Bacteria in the fluid layer are attracted towards the node and pushed to the fluid/reflector interface by acoustic force. Therefore, bacteria-rich flow can be collected from the top outlet.

The acoustofluidic chip was assembled by a glass coverslip (reflector layer) and a glass slide (carrier layer) which were bonded by double-sided tapes as shown in Fig. 2. It was actuated at a frequency of 1.25 MHz. Figure 3 and Figure 4 show the cross-sectional distribution of the latex microparticles (diameter is 0.75-μm) without and with acoustophoresis in the chip, respectively. After actuated by acoustophoresis, most of the 0.75-μm microparticles can be focused in the distance of 25-μm from the reflector.

Figure 5 shows the recovery of microparticles at different total flow rates and actuated voltages. At a certain voltage, the recovery of microparticles decreases as the total flow rate increases. When the total flow rate was increased to 250 μL/min, the recovery was dramatically decreased to 57% under 15 V and 20 V, but slightly decreased to 70 % under 25 V. Therefore, increasing actuated voltage can enhance the recovery of microparticles.

Figure 6 shows the distributions of particles and *Bacillus subtilis* at different vertical positions. More than 75% of 0.75-μm particles were focused in the distance of 15-μm from the reflector. However, only 53% of bacteria was in the same region. It indicates that bacteria with lower cell density are relatively difficult to be focused by acoustophoresis. However, more than 80% of bacteria in the distance of 25-μm from the reflector still can be collected from the outlet since the height of ladder in the channel is 60-μm, which is larger than the focusing thickness.

In conclusion, a cost-effective acoustofluidic chip for bacteria pre-concentration is designed and demonstrated with a high throughout of 250 μL/min and high recovery of 80%. It shows a high potential as a rapid screening tool for bacterial inspection.

References

[1] D. Carugo, T. Octon, W. Messaoudi, A. L. Fisher, M. Carboni, N. R. Harris, M. Hill and P. Glynne-Jones, Lab Chip, 2014, 14, 3830-3842.

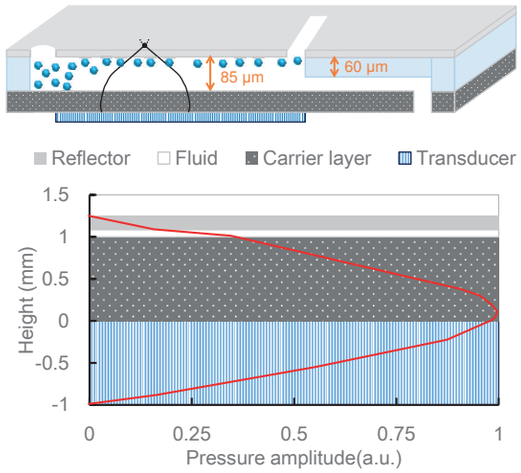

Figure 1. Schematic of cross-section in the acoustofluidic chip.

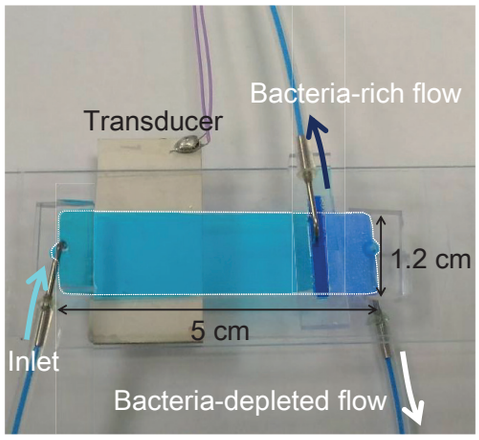

Figure 2. Fabricated acoustofluidic chip.

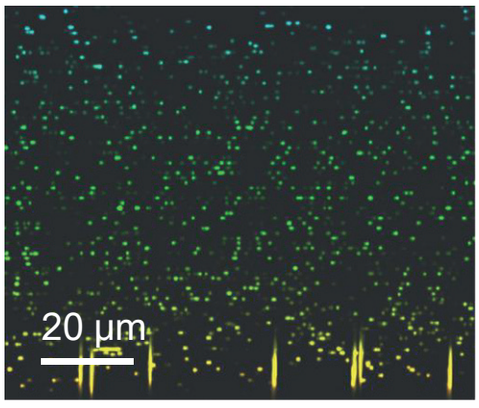

Figure 3. Confocal microscopic image of particle distribution without acoustic focusing.

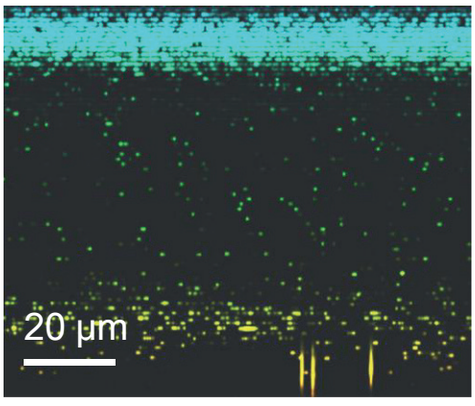

Figure 4. Confocal microscopic image of particle distribution under acoustic focusing.

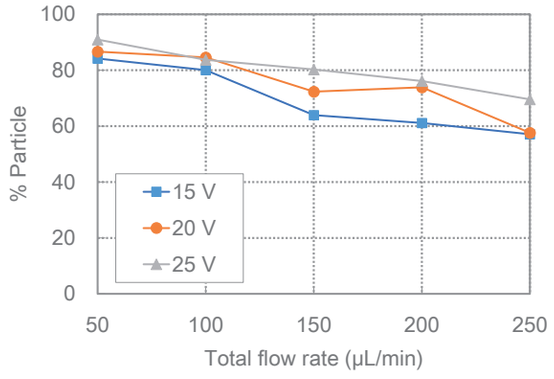

Figure 5. Recovery of 0.75-μm latex particles at different total flow rates and voltages, when the flow rate of bacteria-rich stream was kept at 20 μL/min.

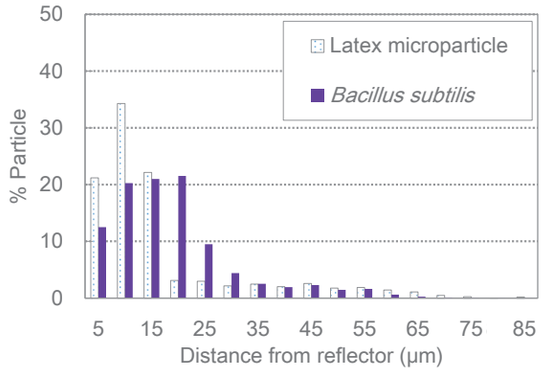

Figure 6. Particle distribution of 0.75-μm latex particles and Bacillus subtilis at different vertical positions.

5th Micro and Nano Flows Conference
Milan, Italy, 11-14 September 2016

Simulation of R134a Flow Boiling in Microchannels

Rahim JAFARI [1,*]

* Corresponding author: Tel.: +90 312 586 8761; Fax: +90 (312) 586 80 91; Email: rahim.jafari@atilim.edu.tr
1 Department of Automotive Engineering, ATILIM University, Kızılcaşar Mahallesi, İncek, Ankara, Turkey

Keywords: Microchannel, Boiling, Mixture model

Fabrication of integrated circuits with higher performance is now possible owing to novel manufacturing techniques. The main obstacle in achieving such high performances with more compact and functional devices is the dissipation of heat due to the increased power density. International Technology Roadmap for Semiconductors predicts maximum heat flux of 108 W/cm^2, maximum junction temperature of 85ºC, and an extreme ambient temperature of 45ºC for desktop personal computers in 2016 [1]. It may be inferred from this trend that the difference between junction and ambient temperatures is decreasing, and the heat flux is increasing. Additionally, the average power density for specialty applications such as laser diode arrays, phased array radar systems and power electronics, raised over 1000 W/cm^2 [2,3]. Hence the conventional air cooling systems, which are currently preferable and commercial to save the costs, seem to be unsatisfactory to overcome this challenge.

The heat transfer coefficient in microchannels with single phase flow is quite high due to the small hydraulic diameter. Because of the coolant's latent heat, the heat transfer coefficient for flow boiling in microchannels is even higher. Additionally, the axial wall temperature maintains much uniform close to the coolant's saturation temperature.

There are many numerical studies in the literature which have been carried out to examine flow boiling in microchannels. Common methods in the literature are based on the tracking of the interface between the liquid and vapor phases. Level-set method, phase-field method, Lattice-Boltzmann method and Arbitrary Lagrangian-Eulerian method are techniques which track the interface of two separated phases of vapor and liquid. These methods have been employed to model different types of boiling flows as bubbly flow, slug flow, annular flow and film boiling in microchannels.

Although the modeling of the two-phase flow with evaporation is a difficult issue due to the complexity of the non-linear set of equations that governs the two-phase flow, the interfacial discontinuity and deformation, and mass transfer between the vapor and the liquid phases, it results unique data compared to those for experimental tests.

On the other hand, while the foregoing numerical methods provide precise information about the hydrodynamics and heat transfer of boiling in microscale, they are restricted to confined geometries as a few bubbles due to computational time and cost. Therefore, an alternative numerical method which is computationally cheaper than the aforementioned methods is required to simulate an extensive domain of microchannels heat sinks.

Mixture models [4] are macroscopic two-phase flow models which follow the average phase concentration, volume fraction, instead of the interface explicitly. Furthermore, one single momentum equation is defined to solve the mixture velocity, and both phases share the same pressure field. Hence, considerably smaller numbers of variables are solved comparing the other multiphase models.

In the present study, a mixture model is utilized to investigate the hydrodynamics and heat transfer of saturated R134a boiling in microchannels. The heat transfer coefficient, vapor quality and pressure drop are obtained which are desired results of flow boiling in microchannel heat sinks need carrying out experiments to be determined.

[1] Roadmap, I., International Technology Roadmap for Semiconductors, 2006 Semiconductor Industry Association, 2009, http://www.itrs.net/ Last visited on August 30, 2015

[2] S. Krishnan, S. Garimella, G. Chrysler and R. Mavajan, Towards a thermal Moore's law, IEEE Transactions on Advanced Packaging 30(3)462-474, 2007

[3] D. C. Price, A review of selected thermal management solutions for military electronic systems, IEEE Transactions on Components and Packaging Technologies 26(1)26-39, 2003

[4] C. Crowe, M. Sommerfeld, and Y. Tsuji, *Multiphase Flows with Droplets and Particles,* CRC Press, 1998

5th Micro and Nano Flows Conference
Milan, Italy, 11-14 September 2016

Evaporator Surface Modification Using Super Ice-Phobic

Mohammad Reza Heravi[1,*], Mohammad Matin Nejatbakhsh[2], Arash Babaee[3]

* Corresponding author: Tel.: +98 (0)9227039417; Fax: - ; Email: heravi1378@gmail.com

1,2,3 Mofid high school of Tehran, Iran

Keywords: Evaporator, super ice-phobic, surface, freeze, Nano scratches.

Evaporator by creating the cold and sending it to the refrigerator and absorbing the heat from the refrigerator environment that is the refrigerators main task but due to freeze moisture on the surface of the evaporator, efficiency of this piece is reduced greatly and apply the heat to solve this problem as well as follow to damage to the surface.[1] According to test conducted, this method is based on the creation of the Nano scratches on various surface that this scratches are 3 to 4 times increase based on the properties[2] of the surface tension of water that prevent to sit water on the surface that will not be possible to allowed to sit on the evaporator's Aluminium surface.

During the activities on this project, hydrophobia sol includes kinds of organic and mineral materials such as Cobalt chloride, Colin chloride was obtained after preparations using vacuum and magnetic and by utilizing from homogenizing method. The results show that it coated on surface of evaporator. The results show that due to the hydrophobic property created prevented of creation ice crystals on the surface, so that to prevent formation Moisture and water droplets on the surface also that was prevented waste of energy particularly in the evaporator and continuing the activity changing in the DuPont material by utilizes some carbohydrates to needs for to improve the project as a result, the angle of droplets of water than the initial state increased about 70 to 90 degrees.

Organic matter in the structure of the material as well as with regard to the large contact area of matter on surface increases the adhesion and durability.[3] but it will not penetrate the main surface and the Aluminium surface of the evaporator only including layer that is separate but coherent and also therefore moisture around the evaporator does not get the ability to penetrate and reach the evaporator.

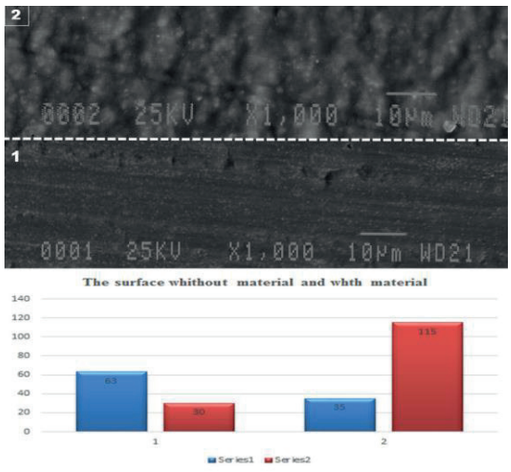

Fig 1. Comparison the surface without material and with material. General order (blue Column) and about Angle drops of water on surface (red Column) According to SEM and CA tests.

References

[1] Antoine Lacroix. Dr. James F. Manwell. Wind Energy: Cold Weather Issues - Contents lists available at ScienceDirect - University of Massachusetts at Amherst. June 2000. p.p 12-19

[2] S.J. Monte, G. Sugerman, Titanate coupling agents — current applications, presented at the 110th Meeting of the Rubber Division, Am. Chem. Soc. (1976)p.p 38–44.

[3] J.-M. Wang, L.-D. Wang, L. Feng, One-step fabrication of fluoropolymer transparent films with super hydrophobicity by dry method, J. Appl. Polym. Sci.120. (2011) p.p. 524–529

5th Micro and Nano Flows Conference
Milan, Italy, 11-14 September 2016

Graphene Powder Processing For Water Solar Distillation using Nanofluids

Nadhira Laidani[1,*], Francesca Marchetti[1], Hafeez Ullah[1, 2], Marina Scarpa[2], Cecilia Ada Maestri[2], Said Makhlouf[3], Gloria Gottardi[1], Ruben Bartali[1], Victor Micheli[1]
* Corresponding author: Tel.: ++39 0461 314 453; Email: laidani@fbk.eu
[1] Fondazione Bruno Kessler, Materials & Systems Centre, Trento, Italy
[2] University of Trento, Department of Physics, Trento, Italy
[3] University Mouloud Maameri, Tizi-Ouzou, Algeria

Abstract: Recently graphene and graphene-based hybrid materials have attracted much attention due to outstanding chemical and physical properties. Thanks to their high thermal conductivity graphene-based nanomaterials constitute excellent candidates for water-based nanofluids. This class of new materials can be beneficially exploited in water purification technologies using renewable energy. Solar distillation efficiency to produce clean water can be improved through the use of nanofluids.
In this work we studied the plasma route processing effects of graphene powders in terms of ability to produce graphene-water based nanofluids. The powders were treated by radio-frequency sputtering by which metal oxide and silicon oxide were deposited onto the surface of the graphene powders, forming hybrid graphene-inorganic nanomaterials in order to enhance the solubility in water. The surface modification was studied by means of x-ray photoelectron spectroscopy and transmission electron microscopy. The graphene based materials suspension stability in water and the surface wettability were studied by means of UV-Vis. spectrophotometry and contact angle measurement respectively. Preliminary results showed a significant improvement of the graphene solubility in water by the plasma treatment.

Keywords: graphene-based material; dispersion; nanofluid; sputtering.

Access to clean water, suitable for human consumption and domestic uses, is increasingly becoming the most important issue facing people around the world. Worldwide drought and desertification are expected to increase the problem [1].
Current water purification methods employ chemically intensive treatment that is relatively expensive and not translatable to the non-industrial world. The latest trends consist of shifting from electrical and fossile energy use of the so-called thermal technologies for water purification to renewable energy use, including the various membrane technologies. However, these technologies are of relatively high costs and complexity of installation and exploitation and not suitable for the remote and the arid regions where electrical facilities are hardly applicable, but with plenty of solar energy.
Clean water production for drinking purposes by means of solar distillation of brackish water is an attractive technology, using cost-free solar energy. The solar energy can be used for distillating water in devices named “solar stills”. The direct solar distillation for desalination is the most appropriate for a large use by non-industrial communities, for lower costs, simplicity of construction and installation, self-operation and low need of maintenance. However, this technology has to overcome a serious obstacle related to the relatively low productivity. In this regard, in order to fully exploit the low cost and use of free and renewable energy as the solar one, solutions should be found for an advancement of the technology and an improvement of the process yield. This imperatively implies the development of new materials and new design of the devices. By now, the approach aimed to the optimization of the technology was based on the re-design of the devices structures and the improvement of their thermal efficiency. The development of new materials has much less been investigated and, in the case of nanomaterials, very scarcely associated to such approaches, leaving a large margin for further development of the solar stills for an efficient and economical application. In this context, nanofluids proved to be efficient in considerably enhancing thermal conductivity

and heat transfer. Nanofluids are expected to exhibit superior evaporation rate compared with conventional water.

This work consists of developing advanced materials, based on graphene-inorganic oxide hybrid nanopowders, to increase water heating and evaporation effect. In this regard, graphene nanofluids have outstanding properties such as high heat transfer ability with thermal conductivity values in the range 2000-5000 W/(mK) at room temperature. However to fully exploit these characteristics in order to use graphene in water-based nanofluids, its hydrophobicity should be overcome. Different methods may be followed to stabilize the graphene particles dispersion in water, among which the use of surfactants. However surfactants may decrease the thermal conductivity of the nanofluids and new routes are being explored [2 and references therein].

In this work, the results of the graphene powder processing by plasma route will be presented to enhance its solubility in water. The powder consisted of 1.6 nm thick flakes of graphene of 10 mm of average lateral size. Hybrid nanomaterials were obtained by decoration of the graphene flakes with transition-metal oxide and SiO_2 clusters by means of RF sputtering. A sample holder stage designed to move the powder during the plasma processing was used to achieve a uniformity of treatment of the powders. A transmission electron microscopy image of a treated particle is given in Fig. 1, which shows graphene flakes decorated by niobium oxide particles.

The effect of the oxide amount and coverage on the graphene-oxide hybrid surface wettability was studied by means of contact angle measurement in water.

In order to be employed as fluid material, the hybrid powders were tested for their suspension stability in water. The latter was measured over time by Uv-Vis. spectrophotometry, in particular by optical absorbance measurement of the supernatant liquid in the acquous solution.

Preliminary results showed a beneficial effect of the plasma treatment on the graphene solubility in water, as shown in Fig.2.

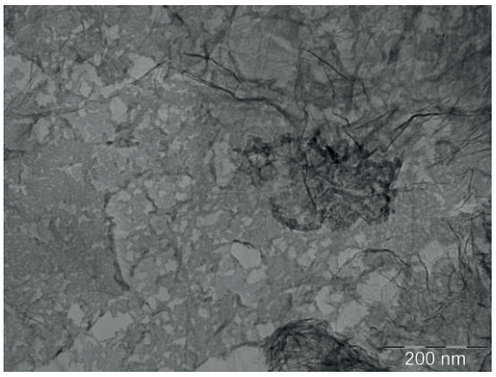

Fig.1: TEM image of graphene (light areas are uncoated) decorated with RF sputtered niobium oxide (dark areas).

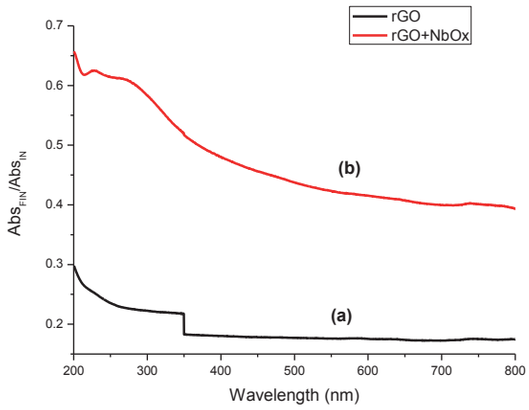

Fig.2: Normalized absorbance spectra, for graphene powder (a) and after NbOx decoration (b), upon dispersion in distilled water following a 60 min sonication. The spectra were acquired after 4 days monitoring and the graphene amount was of 0.01 wt.%.

References:

[1] Velmurugan V, Srithar K, Renewable Energy and Sustainable Energy, No.15 8 2011) 1294.

[2] E. Sadeghinezhad, M. Mehrali, R. Saidur, M. Mehrali, S. T. Latibari, A. R. Akhiani, H. S. C. Metselaar, Energy Conversion and Management 111 (2016) 466.

Acknowledgments: The research leading to these results has received funding from "Ministero degli Affari Esteri e della Cooperazione Internazionale, Direzione Generale per la Promozione del Sistema Paese" in Italy.

Hybrid Numerical Simulations of Digital Rock from Pore Scale to Darcy scale

Moussa TEMBELY[1*], Ali AlSUMAITI[1], Khurshed RAHIMOV[1], Mohamed Soufiane JOUINI[2],
E-mail: mtembely@pi.ac.ae
1 Department of Petroleum Engineering, Petroleum Institute, Abu Dhabi, UAE
2 Department of Mathematics, Petroleum Institute, Abu Dhabi, UAE

Abstract In this paper we report a numerical simulation of the flow properties at both pore-scale and Darcy scale, by direct modeling of the 3D micro-CT images using a Finite Volume Method (FVM). The model is first validated against 2 benchmark samples, namely Fontainebleau sandstone and Grosmont carbonate. Then the model is favorably compared to a Lattice Boltzmann(LB) method. The numerical model is based on the resolution of the steady-state Navier-Stokes equations in conjunction with an adaptive mesh technique used to generate the mesh along with the appropriate boundary conditions to compute the permeability. After validation, the model is applied to an actual reservoir rock carbonate from the Middle East using both the FVM and LB methods. In order to upscale the permeability a new Darcy simulator is used based on the FVM and taking as input a more general permeability tensor field. Finally, using the result by the upscaling simulator a scaling argument is derived to infer on the permeability of multiple concentric rectangles textures.

Keywords: Digital Rock Physics, Porous Media, Finite Volume Method, Lattice Boltzmann Method

1. Introduction

Understanding reservoir rock and fluid properties is essential for applications such as oil and gas industry, water management, hydrology, and geosciences. Oil exploration and production in conjunction with the prospective impact on the environment is highly related to the fluid flowing inside the highly complex geometry of the rock. In order to optimize reservoir management, the fluid flow processes in porous media should be investigated through a multiscale approach ranging from the field to the core level, down to the pore scale. One of the most important petro-physical properties for reservoir rock is the permeability, which is function of the complex microstructure of the rock, fluid properties (density, viscosity) and parameters (velocity). Since no simple universal correlation exists for the permeability, an accurate and efficient numerical tool to predict the permeability is highly desirable.

Using the micro-CT 3D images, numerical simulation has been applied to perform the pore-scale imaging modelling ranging from the finite difference method [1], finite element method [2], and more recently finite volume method approach [3] applied to one sample without full validation nor upscaling.

In the present paper, we use a finite volume method (FVM) coupled with an adaptive meshing technique to perform the pore scale simulation from the micro-CT images of samples from both the literature and our own carbonate reservoir sample. As the segmentation is crucial, we explore its effect on the numerical simulation. In addition, we will assess the effect of the boundary conditions, namely periodic and non-periodic, on the permeability computation. Besides, we performed simulation based on the LB method for comparison and validation in addition to the results in the literature. Finally, we developed a new Darcy simulator based on the FVM capable of performing the upscaling from the results at the pore-scale model. This model serves to establish an analytical expression for the permeability of a multiple concentric rectangles textures.

2. Governing Equations

2.1 Pore-scale model

The continuity and momentum equations to be numerically solved in the finite volume method (FVM) formulation expresses as follows:

$$\nabla.\mathbf{V} = 0 \tag{1}$$

$$\rho\mathbf{V}\nabla\mathbf{V} = -\nabla p + \rho\boldsymbol{g} + \nabla.\left(\mu\nabla\mathbf{V}\right) \tag{2}$$

where $\mathbf{V}$ is the fluid velocity vector, and $\boldsymbol{g}$ denotes the gravity, while the fluid is assumed incompressible of density ρ, viscosity μ.

A non-slip boundary condition (Fig. 1) is applied at the top and bottom of the micro-plug sample for the computation of the permeability. After solving the fluid equation, the permeability can be computed following Darcy's law as follows:

$$K_l = \frac{\mu L Q_l}{A_o \Delta P} \tag{3}$$

where A_o is the outlet surface area of the sample and Q the flow rate computed by integration from the outlet as $Q_l = \int_{Ao} V dA$.

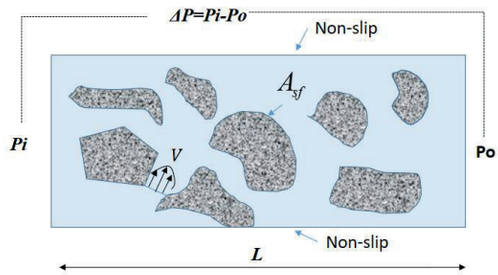

Fig. 1. Illustration of the flow configuration at pore scale.

2.2 Darcy scale model

The Darcy scale model is deduced from the Darcy's law in combination with the continuity equation. Hence following Darcy's law, the velocity is proportional to the pressure loss through the permeability tensor $\boldsymbol{K}_l(x,y,z)$:

$$U = \frac{\boldsymbol{K}_l}{\mu}.\nabla p \tag{4}$$

Applying the continuity equation, one obtains:

$$\nabla.\left(\boldsymbol{K}_l.\nabla p\right) = 0 \tag{5}$$

where the global permeability $\boldsymbol{K}_G$ is deduced through the global flow rate, $Q_G = \int U dA$, similarly to Eq. (3).

3. Numerical simulation and results

In order to run the simulation, the segmented image is meshed using SnappyHexMesh/C++ code to perform an Adaptive meshing technique, through refinement and adjustment to fit onto the provided geometries of the rock; the addition of the boundary layers' cells near the solid surface is also performed for better accuracy (Fig. 2).

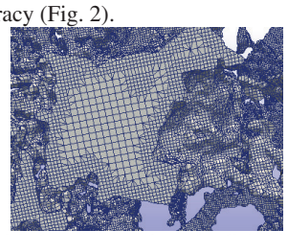

Fig. 2. Adaptive Mesh at the pore from the digital image of the rock.

Finally, the governing equations are implemented in OpenFOAM/C++ opensource code. The SIMPLE algorithm is used to calculate the pressure and velocity fields using a Generalized Geometric-Algebraic Multi-Grid (GAMG) solver in conjunction with a Gauss Seidel smoother. The convergence criteria set for the pressure and velocity fields is of the order of 10^{-8}. The simulations are run in parallel using a domain decomposition method.

3.1 Pore-scale model

We consider for validation purpose of our model 2 rocks sample from the literature, the Fontainebleau sandstone and Grosmont carbonate [2]. We perform our simulation on these 2 samples on the 3 axis X, Y, Z (Fig. 3). The boundary condition applied is the non-slip boundary condition at the sides of the sample similarly to the experimental conditions. The use of the explicit jump stokes method in [2] which results in a periodic boundary conditions on all sides of the samples leads to a higher value of the permeability as shown in [3]. We summarize our FVM and LBM (using Palabos library) simulation results on Z-axis in Table 1 along with the relative errors.

Table **1**

Sample Name	Voxel size (µm)	Image size (XxYxZ)	FVM	LBM	%
Fontainebleau Sandstone	7.5	288x288x300	1614	1610	0.2%
Grosmont Carbonate	2.02	400x400x400	217	214	1.4%

The anisotropy illustrated by the permeability tensor of the Fontainebleau sandstone results in

$$K_{Fontainebeau} = \begin{pmatrix} 1551 & 0 & 0 \\ 0 & 1313 & 0 \\ 0 & 0 & 1614 \end{pmatrix}$$

From which we can deduce the anisotropy ratio R, $R=K_{min}(K_{max}\ K_{int})^{-1/2}=0.83$, for the Fontainebleau sandstone while the carbonate anisotropic ratio is found to be about 0.68, consistent with the values in the literature for these types of rock.

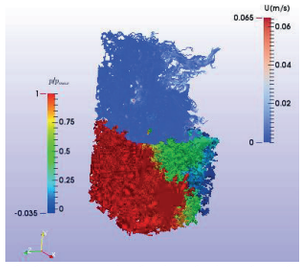

Fig 3. Results of the numerical simulation by the Finite Volume Method of the carbonate Grosmont on the Z-axis. The streamlines are shown at the top of the carbonate for clarity.

3.2 Darcy scale model

In addition to the pore-scale model, we implement a Darcy simulator based on the FVM accounting for the permeability as a tensor field by solving Eq. (4-5).

3.2.1 Validation

We validate the model by comparing it with the layered vertical and horizontal configuration, which theoretical expression is given by Eq.(6):

$$K_H = \frac{(L_1K_1 + L_2K_2 + L_3K_3 + L_4K_4)}{L_T} \quad K_V = \frac{L_T}{L_1/K_1 + L_2/K_2 + L_3/K_3 + L_4/K_4} \quad (6)$$

The relative error between the numerical and the theoretical permeability (Eq.6) matched at less than 0.001 %.

3.2.2 Applications

After determing the permeability by direct numerical simulation, the upscaling of the the permeabilty is performed on the Middle East reservoir carbonate as illustrated in Fig 4 below.

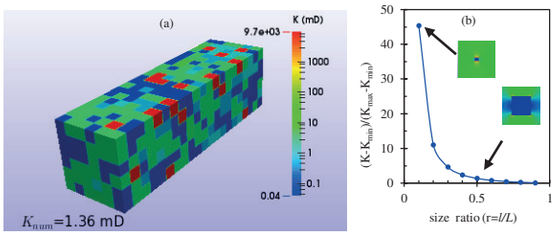

Fig. 4. (a) Permeability upscaling of a carbonate subdivided into 6x6x21 (b) average permeability for varying concentric rectangle size

Finally, using the Darcy scale model, a recursive relation for the permeability for a given concentric rectangle texture is found after some algebraic manipulations:

$$K_{1\ldots-n} = \frac{ck_n r_{n-1}^{\ \alpha} + K_{1\ldots-(n-1)}}{1 + cr_{n-1}^{\ \alpha}} \quad (7)$$

Where $K_{1\ldots-n}$, and r_n are the permeability and radius of the n^{th} concentric rectangle, respectively; while c and α are the 2 parameters of the correlations (Fig 4b).

Acknowledgements

Authors gratefully acknowledge the financial support from ADNOC and TOTAL under the Digital Rock Physics(DRP) project.

Reference

[1] P. Mostaghimi, M. J. Blunt, B. Bijeljic, Computations of Absolute Permeability on Micro-CT Images, *Mathematical Geosciences*, 45(1), pp 103-125, 2013.

[2] Andrä H., Combaret N., Dvorkin J., Glatt E., Han J., Krzikalla F., Lee M., Madonna C., Marsh M., Mukerji T., Ricker S., Saenger E.H., Sain R., Saxena N., Wiegmann A. and Zhan X., 2013: Digital rock physics benchmarks - Part II: Computing effective properties, *Computers & Geosciences* 50, 33–43, 2013. See supplements at https://github.com/fkrzikalla/drp-benchmarks

[3] R. Guibert, M. Nazarova, P. Horgue, G. Hamon, P. Creux, G. Debenest, Computational Permeability Determination from Pore-Scale Imaging: Sample Size, Mesh and Method Sensitivities, *Transp. Porous Med*, 107:641-656, 2015.

5th Micro and Nano Flows Conference
Milan, Italy, 11-14 September 2016

Magnetic nanofluids help improve the efficiency of solar thermal collector

Mustafa Alsaady[1, 2], Rong Fu[1], Yuying Yan[1],

* Corresponding author: Tel.: ++44 (0)1159513168; Fax: ++44 (0)1159513159; Email: yuying.yan@nottingham.ac.uk
[1]*Fluids & Thermal Engineering Research group, Faculty of Engineering, University of Nottingham, UK*
[2]*Chemical Engineering department, Faculty of Engineering, University of Jeddah, Saudi Arabia*

Keywords: Magnetic nanofluids, Ferrofluids, Solar energy, Parabolic trough

Abstract

The paper reports the authors' recent work relating to the use of magnetic nanofluids (ferrofluids) in a direct absorption solar thermal collector with parabolic trough to enhance thermal efficiency compared to conventional solar collectors. Ferromagnetic nanoparticles dispersed in common heat transfer fluids (or base fluids) exhibit better thermos-physical properties compared to the base fluids. By applying an appropriate level of magnetic intensity and magnetic field direction, the thermal conductivity of the ferrofluid is increased higher than conventional nanofluids. Moreover, the ferrofluids exhibit good optical properties. The ferrofluids absorb most of solar radiation at the depth of 10 mm. The design of ferrofluids based concentrating solar collector is different from conventional solar collectors. External magnetic source is installed to alter the thermos-physical properties of the fluid, and the absorber tube does not have selective surface allowing ferrofluids to absorb the incoming solar irradiance directly.

In the present study, an experimental investigation of the performance of direct absorption solar collector using ferrofluids as absorber is carried out. Various nanoparticle concentrations ranged from 0 to 1vol% at the operational temperatures between 19°C and 40°C were used. The results show that using ferrofluids as a heat transfer fluid increases the efficiency of solar thermal collectors. The heat flux from radiation was absorbed by the body of nanofluids in the DAC collectors instead of by the top surface for coating ones. Increasing particles concentration can increase the efficiency of the collector. In the presence of external magnetic field, the solar collector efficiency increases to the maximum, 25% higher than conventional parabolic trough. At higher temperatures, the ferrofluids show much better efficiency than convectional heat transfer fluid. The ferrofluids show better heat transfer coefficient and decreases the surface temperature of the absorber. Ferromagnetic particles build a chain-like structure in the presence of external magnetic field allowing faster heat transfer throw conduction. The heat transfer coefficient increases when the magnetic field is parallel to flow direction. The study has indicated that nanofluids, even of low-content, have good absorption of solar radiation, and can improve the outlet temperatures and system efficiencies.

The schematic of the experimental setup is shown in Fig. 1. Fig. 2 shows the result of Fe_3O_4-water ferrofluids 0.05vol% with applied magnetic field. The efficiency increases with increasing the magnetic field intensity when the orientation of the magnetic field is parallel to the direction of the flow. The maximum efficiency of 30%, 35%, and 40% for 3.14mT, 6.28mT, and 10.47mT, respectively. Water was also used with external magnetic field. There is no effect of magnetic field on the measurements.

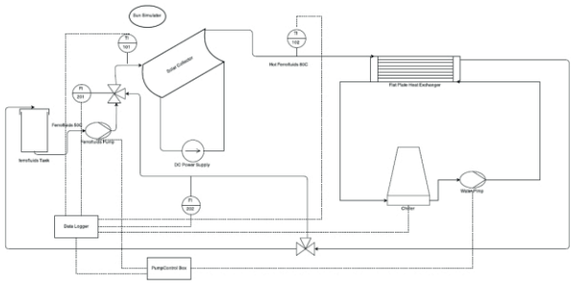

Figure 1 Schematic and photograph of the experimental setup

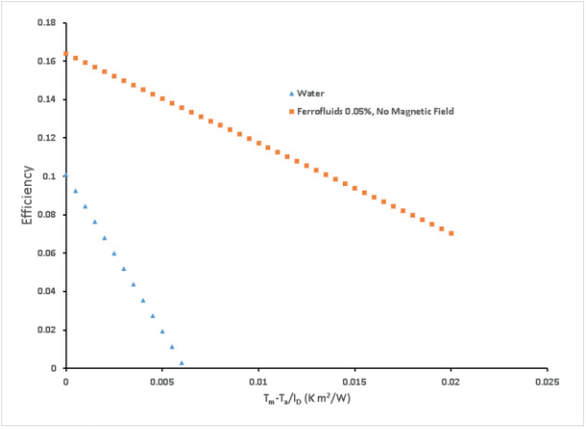

Figure 2: Thermal efficiency of parabolic trough with water and ferrofluids without applying external magnetic

Inserita Pagina Bianca

la scritta non verrà stampata